General Analysis of Breed-and-Burn Reactors and Limited-Separations Fuel Cycles

by
Robert C. Petroski

B.S. Nuclear Engineering & Engineering Physics
University of California, Berkeley, 2006
M.S. Nuclear Science and Engineering
Massachusetts Institute of Technology, 2008

Submitted to the Department of Nuclear Science and Engineering
in Partial Fulfillment of the Requirements for the Degree of

Doctor of Philosophy in Nuclear Science and Engineering
at the
Massachusetts Institute of Technology

February 2011

Signature of Author_____
Robert Petroski
Department of Nuclear Science and Engineering
December 16, 2010

Certified by_____
Professor Benoit Forget
Assistant Professor of Nuclear Science and Engineering
Thesis Supervisor

Certified by_____
Doctor Charles Forsberg
Executive Director, MIT Nuclear Fuel Cycle Project
Thesis Reader

Accepted by_____
Professor Mujid S. Kazimi
TEPCO Professor of Nuclear Engineering
Chairman, Department Committee on Graduate Students

General Analysis of Breed-and-Burn Reactors and Limited-Separations Fuel Cycles

by
Robert C. Petroski

Submitted to the Department of Nuclear Science and Engineering
in Partial Fulfillment of the Requirements for the Degree of
Doctor of Philosophy in Nuclear Science and Engineering

February 2011

ABSTRACT

A new theoretical framework is introduced, the "neutron excess" concept, which is useful for analyzing breed-and-burn (B&B) reactors and their fuel cycles. Based on this concept, a set of methods has been developed which allows a broad comparison of B&B reactors using different fuels, structural materials, and coolants. This new approach allows important reactor and fuel-cycle parameters to be approximated quickly, without the need for a full core design, including minimum burnup/irradiation damage and reactor fleet doubling time. Two general configurations of B&B reactors are considered: a "minimum-burnup" version in which fuel elements can be shuffled in three dimensions, and a "linear-assembly" version composed of conventional linear assemblies that are shuffled radially.

Based on studies of different core compositions, the best options for minimizing fuel burnup and material DPA are metal fuel (with a strong dependence on alloy content), the type of steel that allows the lowest structure volume fraction, and helium coolant. If sufficient fuel performance margin exists, sodium coolant can be substituted in place of helium to achieve higher power densities at a modest burnup and DPA penalty. For a minimum-burnup B&B reactor, reasonably achievable minimum DPA values are on the order of 250-350 DPA in steel, while axial peaking in a linear-assembly B&B reactor raises minimum DPA to over 450 DPA. By recycling used B&B fuel in a limited-separations (without full actinide separations) fuel cycle, there is potential for sodium-cooled B&B reactors to achieve fleet doubling times of less than one decade, although this result is highly sensitive to the reactor core composition employed as well as thermal hydraulic performance.

Acknowledgments

I would like to thank my thesis supervisor Ben Forget for being a great person to work for, and my thesis reader Charles Forsberg for his enthusiastic support of my research. Thanks to Professor Driscoll for being a great resource whenever I had questions. Thanks very much to my coworkers at TerraPower for their strong encouragement, diverse knowledge, and permission for me to use their vast computing resources. I am grateful for the funding supplied for this project from TerraPower, a Nuclear Regulatory Commission fellowship, and an Areva fuel cycle study fellowship. Most of all, thanks to my friends and loved ones everywhere for making this entire process worthwhile.

For my parents

Table of Contents

List of Figures

List of Tables

Nomenclature

ΔA: Total neutron absorptions per unit volume (mol/cm^3) (Equation 2.1-1)
$\overline{\Delta A}$: Volumetric average of ΔA (mol/cm^3)
ΔN: Neutron excess, i.e. net neutron absorptions/productions per unit volume (mol/cm^3) (Equation 2.1-3)
$\overline{\Delta N}$: Volumetric average of ΔN (mol/cm^3)
ΔN_{adj}: Adjusted neutron excess, equal to neutron excess with neutron absorptions scaled by k_{eq} or $\overline{k_{eq}}$ (Equation 2.4-7)
ΔN_{adj2}: Twice-adjusted neutron excess, incorporates neutron losses to axial leakage for use in analyzing linear-assembly B&B reactors (Equation 6.4-13)
ΔP: Total neutron productions per unit volume (mol/cm^3) (Equation 2.1-2)
$\overline{\Delta P}$: Volumetric average of ΔP (mol/cm^3)
ϕ: Scalar neutron flux (#/cm^2/s)
Σ_a: Total macroscopic neutron absorption cross section, including fission (cm^{-1})
Σ_f: Total macroscopic fission cross section (cm^{-1})
ν: Average number of neutrons per fission (#)
$\overline{\nu}$: Average number of neutrons per fission, averaged over the entire core (#)
AIROX: Atomics International Reduction and Oxidation process
B&B: Breed and Burn
BOC: Beginning Of Cycle
BOEC: Beginning Of Equilibrium Cycle
dA: Differential unit of total neutron absorptions ΔA, equal to $\phi\Sigma_a dt$ (mol/cm^3)
dN: Differential unit of neutron excess ΔN, equal to dP minus dA (mol/cm^3)
dP: Differential unit of total neutron productions ΔP, equal to $\phi\nu\Sigma_f dt$ (mol/cm^3)
D_{fuel}: Equilibrium cycle feed fuel discharge rate (m^3/y)
DPA: Displacements Per Atom, a measure of radiation induced material damage, which depends on total fluence, fluence spectrum, and the material being irradiated
DUPIC: Direct Use of PWR spent fuel In CANDU process
EFPD: Effective Full Power Day, equal to total energy divided by reactor rated power
EFPY: Effective Full Power Year, equal to total energy divided by reactor rated power
EOC: End of Cycle
EOEC: End of Equilibrium Cycle
Equilibrium cycle feed fuel: Feed fuel that undergoes the equilibrium cycle depletion history
f: Fraction of total starter fuel requirement needed for starting up a new B&B reactor; affects performance of advanced B&B fuel cycle options
F_{av}: Total amount of available starter fuel in a reactor fleet, i.e. starter fuel that has undergone the cooling/processing time t_c
F_{tot}: Total amount of starter fuel in a reactor fleet
f'_{axial}: Cumulative conditional probability over a material's depletion that a neutron produced in the material is lost to axial leakage, provided it is not lost to control or radial leakage (Equation 6.4-12)
$\overline{F'_{axial}}$: Conditional probability over a cycle that a neutron is lost to axial leakage, provided it is not lost to control or radial leakage (Equation 6.4-11)

$\overline{F_{ctrl}}$: Ratio of neutrons absorbed in control to neutrons absorbed in fuel over a cycle (Equation 6.4-2)

$\overline{F_{leakage}}$: Ratio of neutrons lost to leakage to neutrons absorbed in fuel over a cycle (Equation 6.4-2)

FIMA: Fissions per Initial heavy Metal Atom, a unit of burnup

IHM: Initial Heavy Metal; i.e., the amount of heavy metal present before any depletion; for reused fuel, IHM is defined to be the heavy metal present in the original fuel rather than for the reused fuel

Infinite reactor doubling time: Doubling time computed from a one-dimensional infinite slab model, can be scaled by radial power peaking factor to obtain realistic reactor doubling times

k_{eq}: Ratio of total neutrons produced to total neutrons absorbed in fueled regions (k_{fuel}) in equilibrium state of a continuous system

$\overline{k_{eq}}$: Neutron-absorption weighted average of k_{fuel} over an equilibrium cycle (Equation 2.3-14)

$\overline{k_{eq2}}$: Similar to $\overline{k_{eq}}$, but factoring in axial neutron leakage for analysis of linear-assembly B&B reactors (Equation 6.4-6)

$\overline{k_{fuel}}$: Neutron-absorption weighted average of k_{fuel} over a cycle (Equation 2.4-12)

$\overline{k_{fuel2}}$: Similar to $\overline{k_{fuel}}$, but factoring in axial neutron leakage for analysis of linear-assembly B&B reactors (Equation 6.4-6)

k_{unc}: Uncontrolled (all rods out) k-effective (Equation 2.2-1)

$k_{unc\text{-}eq}$: Uncontrolled (all rods out) k-effective at reactor equilibrium state

k_{∞}: Ratio of neutron production to absorption rates in a material's infinite-medium spectrum (equal to infinite-medium k-effective)

k'_{∞}: Ratio of neutron production to absorption rates in a material's local spectrum (Equation 2.1-4)

LBE: Lead Bismuth Eutectic

Linear-assembly B&B reactor: B&B reactor with conventional axially-connected assemblies, in contrast to a minimum-burnup B&B reactor

Minimum-burnup B&B reactor: B&B reactor capable of fuel shuffling in all three dimensions, allowing burnup gradients in all directions to be flattened

MOC: Middle Of Cycle

MOEC: Middle Of Equilibrium Cycle

Neutron excess curve: Plot of ΔN or ΔN_{adj} vs. ΔA for a composition

$P_{reactor}$: Total reactor power (MW)

$\overline{Q}$: Average energy per fission, averaged over the entire core (MeV)

R_0: Total number of operating B&B reactors in a fleet at time zero

R_{eq}: Total number of equilibrium cycle B&B reactors in a fleet

R_{tot}: Total number of operating B&B reactors in a fleet

t_c: Cooling and processing time, i.e. the length of time between when feed fuel is discharged and when it can be reused as starter fuel (y)

t_{cycle}: Length of a reactor cycle (y)

t_e: Reactor fleet e-folding time, i.e. how long it takes for R reactors to expand into $R*e$ reactors (y) (Equation 4.4-14)

t_{feed}: Time required to generate amount of burnup contained in equilibrium cycle (y)

t_s: Spawning time, i.e. time required for an equilibrium cycle reactor to produce enough starter fuel to start a new reactor, equal to $V_{starter}/D_{fuel}$ (y)

$t_{starter}$: Starter fuel burn time, time required to completely burn $V_{starter}$ volume of starter fuel (y)

t_{tr}: Transition time, equal to the sum of $t_{starter}$ and t_{feed}, corresponds to the minimum duration of the transition stage and when feed fuel can be discharged at the equilibrium cycle rate D_{fuel} (y)

t_{tsb}: Total starter fuel burn time, time required to burn $V_{starter}$ volume of fuel from zero burnup to the starter discharge burnup, equal to $t_s + t_{starter}$ (y)

SWU: Separative Work Unit, a unit of enrichment work

Thought experiment B&B reactor: Idealized B&B reactor with continuously flowing fuel and no control or leakage, described in Subsection 2.2.1

Transition feed fuel: Feed fuel that does not undergo the equilibrium cycle depletion history, i.e. feed that participates in the transition stage of a reactor

Transition: The stage of reactor operation between startup and when the equilibrium cycle state is established

$\dot{V}$: Fuel volumetric flow rate in continuous thought experiment B&B reactor (m^3/y)

$V_{starter}$: Amount of fuel required to establish desired equilibrium cycle (m^3) (Equation 2.4-19)

Y: Asymptotic ratio of equilibrium cycle reactors to total reactors (R_{eq}/R_{tot}) in the baseline fuel cycle (Equation 4.4-8)

1. Introduction

The goal of this thesis is to broadly characterize the breed-and-burn reactor concept and its role in an advanced nuclear infrastructure using limited-separations processes. Such an infrastructure has the potential to greatly extend uranium resources while minimizing the need for enrichment and fuel processing.

The present global nuclear infrastructure is based almost entirely on light water reactor (LWR) technology, in either a once-through fuel cycle (e.g. in the United States) or in a closed fuel cycle using chemical reprocessing (e.g. in France). One disadvantage of an LWR nuclear infrastructure is that it uses uranium inefficiently: LWRs fission less than 1% of mined natural uranium, because they primarily burn uranium-235, which only makes up 0.71% of natural uranium ore. At current usage rates, known reserves of economically extractable uranium resources would run out in less than a century [IAEA, 2010a], and substantial growth of the nuclear energy industry could cause these resources to only last several decades. Once economically extractable resources are depleted, reactors would have to be fueled using uranium from lower grade ores, which would increase extraction and fuel cycle costs. Using reprocessing to recycle used nuclear fuel in LWRs can improve fuel utilization by only about one quarter (assuming all of the plutonium in used fuel can be recycled and burned).

A second disadvantage of an LWR nuclear infrastructure is that it requires uranium enrichment to increase the concentration of uranium-235 to the ~4% needed for LWR fuel. One byproduct of the enrichment process is a significant amount of depleted uranium; i.e. leftover uranium in which the fraction of uranium-235 is less that 0.71%, typically 0.2 or 0.3%. The major disadvantage of the enrichment process is its associated proliferation risk. The spread of enrichment technology makes it possible for nations with the technology to produce highly enriched uranium suitable for a nuclear weapon, with over 80% uranium-235 by weight.

One way to dramatically extend uranium resources and reduce the need for uranium enrichment is through the use of fast breeder reactors. Fast breeder reactors are able to produce fissile fuel by "breeding" plutonium-239 from uranium-238 (which comprises the other 99.3% of natural uranium). Like uranium-235, plutonium-239 is "fissile", meaning it is capable of sustaining a nuclear chain reaction. The defining characteristic of a breeder reactor is that it is capable of producing more fissile fuel than it consumes. Therefore, a breeder reactor could in principle be used to convert up to 100% of natural uranium into usable fissile fuel, increasing uranium resource utilization by two orders of magnitude. Such an increase would allow nuclear energy to sustain world energy demand for millennia. Furthermore, newly bred fissile fuel can be used in place of enriched uranium, reducing or even eliminating the need for enrichment. Analogously, fast or thermal breeder reactors can be used to convert thorium into fissile uranium-233.

A conventional breeder reactor configuration contains "seed" or "driver" fuel with a high enough concentration of fissile material (typically 10-20%) to sustain a chain reaction. The seed fuel is surrounded by or interspersed with natural or depleted uranium "blanket" fuel, which are specialized low-power fuel assemblies consisting almost entirely of uranium-238. As the reactor generates power, neutrons produced in the seed fuel are absorbed in uranium-238 present in both the seed and blanket fuel, producing plutonium-239. To make new fuel from the produced

plutonium, portions of the seed and blanket fuel are periodically taken out of the core (on the order of once or twice a year) to undergo reprocessing. Reprocessing chemically separates the fissile plutonium from uranium and accumulated fission products, allowing new seed fuel to be made from the extracted plutonium. Eventually, enough new seed fuel can be produced to start up a new breeder reactor.

The primary disadvantage of a conventional breeder reactor infrastructure is the need for reprocessing. Reprocessing is very expensive both monetarily and politically because it involves handling highly radioactive material, and the plutonium extracted during reprocessing can also be used as material in a nuclear weapon. Therefore, even though reprocessing can be used to offset the need for enrichment, it too constitutes a significant proliferation risk.

The goal of this research is to study a new type of fuel cycle: one consisting of breed-and-burn (B&B) reactors in a limited-separations fuel cycle. This fuel cycle is of interest because once it is established, it is capable of operating without requiring any uranium enrichment or chemical reprocessing capability. This is potentially a tremendous advantage, because both enrichment and reprocessing are associated with sizeable costs and proliferation risks. In particular, by eliminating the need for both enrichment and reprocessing at once, a fuel cycle using B&B reactors avoids the two major pathways for acquiring nuclear weapon materials, permitting a reactor infrastructure with minimal weapons production capability. At the same time, a B&B reactor fuel cycle can achieve very high uranium utilization rates (upward of 40% of natural uranium, more than an order of magnitude higher than LWRs). Through the use of a limited-separations fuel cycle, it is possible to take the fuel discharged from a B&B reactor and use it to start up additional B&B reactors, resulting in a reactor infrastructure that can exponentially expand to meet growing energy demand without requiring additional fissile input.

1.1 Description of breed-and-burn reactor concept

Breed-and-burn reactors (also known as convert-and-burn or traveling wave reactors) are reactors that are able to operate using primarily fertile fuel as reload fuel, such as low-enriched uranium, natural or depleted uranium, used LWR fuel, or thorium. This fuel would ordinarily contain too little fissile material to be able to sustain a chain reaction, but in a B&B reactor, fissile material is first bred into the fuel by neutrons produced in the reactor. The resulting bred fuel is then directly burned in the same reactor to sustain the chain reaction and supply neutrons for breeding additional fuel.

Figure 1.1-1 shows a schematic illustration of a B&B reactor with three fuel zones. In the figure, fresh fertile feed fuel is loaded into the outermost zone. As the reactor operates, neutrons produced in the power producing central region are absorbed in the feed fuel, breeding it into usable fissile fuel. Each cycle, the most highly burned fuel in the center is discharged, and the outer fuel zones are shuffled inward to replace the discharged fuel. Adding fresh feed fuel to the outermost zone restores the original state of the reactor. The figure gives an example of a reactor operating in an "equilibrium cycle"; i.e. when the state of the reactor is the same from cycle to cycle.

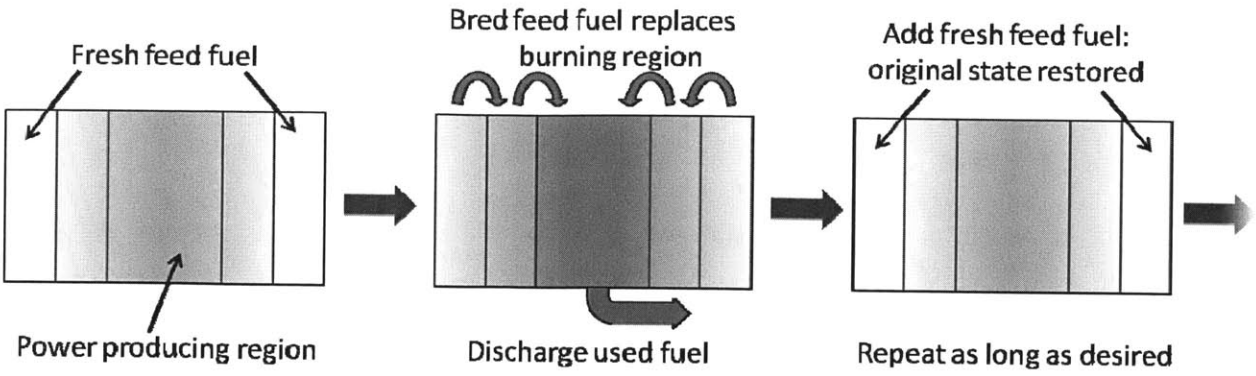

Figure 1.1-1. Schematic diagram of three-zone equilibrium cycle B&B reactor

A B&B reactor differs from a conventional "seed-and-blanket" breeder reactor configuration in two important ways. First, in a seed-and-blanket configuration, breeding occurs in specialized blanket assemblies, which are typically configured to maximize the fuel volume fraction by reducing the amount of coolant present. In a B&B reactor, the breeding and burning regions share the same fuel geometry, since fuel is directly transferred from one region to another. Second, to utilize the bred fuel in a seed-and-blanket configuration, the blanket fuel undergoes chemical reprocessing to separate fissile plutonium-239 or uranium-233, which is then incorporated into newly fabricated seed fuel. In a B&B reactor this intermediate reprocessing does not occur, so no separated plutonium is created.

Unless fission products and fissile elements can be separated from fuel during reactor operation, B&B reactors need to operate with either a fast or mixed (i.e. fast in some regions and thermal/epithermal in others) neutron spectrum. In a thermal spectrum, breeding is less effective because fewer neutrons are produced per absorption in fuel. Also, fission products have much higher absorption cross sections in a thermal spectrum and would quickly poison the reactor.

Initially, a B&B reactor is started using external fissile fuel (such as enriched uranium, plutonium from used LWR fuel, or used fuel from another B&B reactor), which in this thesis is referred to as "starter fuel". The starter fuel allows initial criticality and begins breeding in the reload fuel, called "feed fuel". After sufficient feed fuel is bred, the original starter fuel can be completely replaced with the bred feed fuel, and an equilibrium cycle state can be established that can operate indefinitely on just feed fuel.

1.1.1 Motivation for breed-and-burn reactors

The primary advantage of B&B reactors is that they create their own usable fuel: by breeding then burning its own fissile fuel, a B&B reactor requires less fissile input over its lifetime than other reactors. This advantage is illustrated in Table 1.1-1, which shows representative fissile loadings and fuel burnup values for an LWR, conventional fast reactor, and B&B reactor. The table shows that while LWRs and conventional fast reactors require regular input of fissile reload fuel, B&B reactor are in principle capable of using fertile-only feed fuel (depleted uranium, thorium) as reload fuel.

Table 1.1-1. Representative fuel fissile content and burnup for different reactor options

Reactor type	LWR	Conventional fast reactor	Breed-and-burn reactor
Initial fuel fissile content	4%	10-20%	10-20%
Reload fuel fissile content	4%	10-20%	0-5%
Average fuel burnup (MWd/kg)	45	>50	>150

As a B&B reactor operates and burns more feed fuel, its average fuel enrichment asymptotically approaches that of its feed fuel, which can be as low as 0%. At the same time, B&B reactors achieve fast-reactor fuel utilization rates, and can fission in excess of 15% of the heavy metal atoms loaded into the core. Even in a B&B reactor that uses low-enrichment uranium as feed, the combination of low enrichment and high burnup translates into a *quantitative* reduction in fuel cost: it would require less uranium and less enrichment/reprocessing to produce a given amount of energy in a B&B reactor than in an LWR or non-B&B fast reactor. In the case of a B&B reactor that can run on natural or depleted uranium, there would also be the *qualitative* advantage of eliminating the requirement for additional fissile fuel after startup, which has positive implications for both proliferation resistance and energy security.

Another advantage of B&B reactors is that the fuel bred in them is neutronically capable of reaching extremely high burnup. Upwards of 40% of initial heavy metal atoms (~400 MWd/kg) in fertile-only fuel can be fissioned with the fuel still having positive reactivity (i.e. the fuel is still able to sustain a chain reaction). This allows the bred fuel in a B&B reactor to be reused for a variety of purposes, without needing to undergo chemical reprocessing. Fuel discharged from a B&B reactor can be used to start up additional B&B reactors, or to start up other conventional fast reactors, such as "nuclear-battery" type small modular reactors. Higher burnup also means that fuel discharge can occur further in the future, so costs associated with fuel handling after discharge are smaller on a net present value basis. Higher burnup also reduces the decay heat of fuel at discharge (i.e., short term decay heat) per unit energy produced, since fission products generated earlier in the fuel's life have had additional time to decay.

The converse to achieving very high burnup is the primary disadvantage of B&B reactors: they require higher levels of fluence and burnup to operate than non-B&B reactors. LWRs and conventional fast reactors have fuel that starts with positive reactivity, so they are in principle capable of operating at arbitrarily low burnup (although it is generally also desirable to achieve high burnup in these reactors). Unlike other reactors, B&B reactors have a neutronic limit on *minimum* burnup. B&B reactor feed fuel starts with negative reactivity which increases as it is burned (then decreases again at high burnup). Therefore, a B&B reactor must burn its fuel past a certain minimum burnup value to maintain criticality. The lower the starting enrichment of the feed fuel, the higher the minimum burnup needed. For a B&B reactor to be able to use natural or depleted uranium as feed fuel, the fuel would need to be irradiated past existing knowledge limits on cladding fluence (~4e23 /cm^2 fast (> 0.1 MeV) fluence, or ~200 displacements per atom). Therefore, these knowledge limits will need to be extended in the future in order to enable the full advantages of B&B reactors. Even with higher cladding fluence limits in the future, peak fluence will likely continue to constrain B&B reactor performance. At the same time, high burnup also means that fuel performance characteristics, such as fuel-clad chemical interaction and fuel-clad mechanical interaction, will be a more significant issue for B&B reactors.

Related to high burnup and fluence is fuel residence time: the fuel must spend a long time in the core before it is discharged. This makes fuel more susceptible to slow-acting fuel failure modes, like creep (the gradual deformation of cladding under stress) and wastage (chemical reactions between the fuel and clad that deteriorate the cladding). A long fuel residence time means that feed fuel must be purchased a long time before it begins generating power, which imposes an economic penalty due to cost compounding with time. One other disadvantage of a long residence time is that an irradiation program to test fuel performance would likely require a similarly long amount of time.

Finally, B&B reactors need to have additional space in the core for feed fuel, so that the feed can absorb neutrons being produced in the power-producing region of the core. This feed fuel produces only a small amount of power, which reduces the average power density of the core. Therefore, for a given reactor power level, a B&B reactor would have a much larger fueled area than a standard fast reactor core of the same composition. Partly compensating for this, a B&B reactor would require less shielding since the feed fuel would act as a shield. A larger core would require a larger reactor vessel and would have an impact on plant capital cost.

1.1.2 Previous studies of breed-and-burn reactors

The possibility of a breed-and-burn reactor was first proposed in 1958 by Feinberg [Feinberg, 1958]. Since that time, there have been an assortment of breed-and-burn reactor designs and studies, each considering different choices of fuel, structure and coolant. These designs can be broadly grouped into two classes: designs with standard core configurations and those with non-standard core configurations. Here a standard core configuration is defined as a core composed of conventional linear assemblies, with fuel management accomplished by shuffling these fuel assemblies during refueling outages. A non-standard core configuration consists of other core options, including monolithic unshuffled cores and online refueling designs such as pebble-bed reactors.

For B&B reactors with standard core configurations, the first set of studies were performed at Brookhaven National Laboratory [Fischer, 1979] in collaboration with MIT [Loh, 1980] on the Fast-Mixed-Spectrum Reactor (FMSR); both sodium- and gas-cooled versions were examined. A related design was investigated at MIT [Atefi, 1979], but it includes fissile driver fuel regions in addition to breed-and-burn blanket regions, so it is effectively a hybrid between a B&B reactor and a conventional seed-blanket fast reactor. A lead-cooled design with a standard core configuration was investigated by Toshinsky, beginning in 1997 [Toshinsky, 1997, 2000]. More recently, a gas-cooled B&B reactor design was developed at MIT [Yarsky, 2005], which uses low (5%) enrichment uranium fuel as feed, in order to stay within current knowledge limits on material fluence.

Another active area of B&B reactor studies has been for reactors with monolithic unshuffled cores, in which a nuclear breed-burn wave travels through the fuel. In such a reactor, breeding occurs in fresh fuel at the front of the wave, which travels forward and burns the newly bred fuel as burned fuel is left behind. The appeal of such systems is highlighted in a 1995 Teller paper [Teller, 1996], which introduces a concept for a completely autonomous gas-cooled thorium-burning B&B reactor. A similar concept, the CANDLE reactor (Constant Axial shape of

Neutron flux, nuclide number densities and power shape During Life of Energy producing reactor) has been studied by Sekimoto [Sekimoto, 2001]. Several variants of the CANDLE reactor concept have been developed, such as an LBE-cooled version [Yan, 2007]. A pebble-bed B&B reactor was also proposed around the same time as the CANDLE reactor [Ryu, 2000].

A number of papers have been written on the mathematical theory behind nuclear breed-burn waves traveling through unshuffled cores [van Dam, 1998, 2000, 2003, Chen, 2005, Fomin, 2008], but these are not centered on any particular core design. The papers by van Dam formulate mathematical descriptions of the shape, velocity, and flux distributions of breed-burn waves. The paper by Chen discusses the effects of transverse buckling in a finite size breed-burn wave. The paper by Fomin discusses the initiation of breed-burn waves in a realistic finite geometry.

While unshuffled B&B reactors may have practical advantages over shuffled configurations, they suffer from worse neutron economies because there is inevitably neutron leakage "backwards" into the already-burned fuel. As a result, such reactors would require even higher burnup and fluence than their shuffled counterparts, so it is likely that they would be implemented further in the future than more conventional B&B designs. Because of this disadvantage, unshuffled B&B reactors are not included in this study.

The findings in this thesis qualitatively agree with the findings in previous studies of B&B reactors, especially in identifying the high burnup and fluence required for sustained operation. However, because of the differences in the assumptions used in the different studies, this study does not attempt to directly reproduce their previously obtained results.

Currently, there are two projects aimed at commercializing B&B reactor technology. First is the sodium-cooled Traveling Wave Reactor (TWR) being developed by TerraPower LLC. At the time of writing, a 3000 MWt, 1150 MWe TWR conceptual design has been completed, using a standard shuffled core configuration [Ahlfeld, 2009]. Second is the helium-cooled Energy Multiplier Module (EM^2) being developed by General Atomics. Their design is a 500 MWt, 240 MWe all-ceramic reactor using spent LWR fuel (converted to carbide) as fuel and silicon carbide structural material. The EM^2 core configuration uses axially-stacked blocks of plate-type fuel [Schleicher, 2009].

1.2 Description of limited-separations fuel cycles

A limited-separations fuel cycle is a fuel cycle that recycles fuel without subjecting it to full reprocessing, i.e. chemical separation of actinides. In a limited-separations process, fuel cladding can be replaced but there is no separation of the actinides from each other or from most of the fission products. Examples of limited-separations processes to reuse fuel include direct reuse with no processing, heat treating, physical recladding, fuel recasting/refabrication, and melt processing. Processes that change the fuel form through oxidation and reduction, such as AIROX (Atomics International Reduction Oxidation) would also be considered limited-separations processes, since they do not involve actinide separation chemistry.

Limited-separations fuel cycles share some of the features of both open and closed fuel cycles. They are similar to closed fuel cycles in that a given piece of fuel can be used in more than one reactor. At the same time, they are not properly "closed" because there are no closed loops in which fuel can be repeatedly processed and burned. Like in an open fuel cycle, a limited-separations fuel cycle has a straight path from initial fuel production to disposal: e.g. PWR to CANDU to disposal in the DUPIC (Direct Use of PWR spent fuel in CANDU) fuel cycle. Therefore, limited-separations fuel cycles can be considered a type of modified open fuel cycle.

1.2.1 Motivation for limited-separations fuel cycles

The important factor that distinguishes a limited-separations fuel cycle from a closed fuel cycle with full chemical reprocessing is that there is no means within a limited-separations process to separate bred fissile material from predominantly fertile fuel (i.e. separating plutonium-239 from uranium or uranium-233 from thorium). This distinction is important because it means that there is no way to re-engineer a limited-separations process to yield weapons-usable material. Therefore, limited-separations fuel cycles confer a significant proliferation advantage over closed fuel cycles that use actinide separations. Second, limited-separations processes, especially simpler ones that only involve physical processing, are likely to cost less, require less time, and produce less radioactive waste than processes involving chemical separation of actinides, which would translate to reduced fuel cycle costs.

Compared to a once-through fuel cycle, a limited-separations fuel cycle increases fuel utilization, since fuel can be reused before disposal. More importantly, a limited-separations fuel cycle allows reactors to be started without using fuel from an enrichment or reprocessing plant. This is extremely valuable when used in combination with B&B reactors that can breed usable fissile fuel from fertile-only feed. By linking B&B reactors in a limited-separations fuel cycle, it is possible to establish an exponentially growing reactor infrastructure that requires only depleted or natural uranium as input, with no capability to produce weapons-usable material via enrichment or reprocessing. The only other fuel cycle capable of functioning without enrichment or reprocessing is an unenriched CANDU-style fuel cycle, i.e. a once-through cycle that burns natural uranium using thermal reactors. The chief disadvantage of such a fuel cycle is low uranium utilization (<1% of natural uranium). In contrast, B&B reactors are able to achieve fast-reactor uranium utilization rates (>10% of natural uranium, more than an order of magnitude higher than LWRs and CANDUs), and using a limited-separations fuel cycle can increase fuel utilization to even higher (~40%) levels.

The disadvantage of a limited-separations fuel cycle compared to a closed cycle with full actinide recycling is that the fuel derived from limited-separations processes is not as potent or customizable as that created via reprocessing. This is because without using chemical processes to separate actinides, some fission products will remain in the fuel and act as parasitic absorbers. Also, with limited-separations processes, fertile feedstock (Th, U-238) can be added to fuel but not removed, so there is no way to increase the potency of the fuel (which is the same reason proliferation resistance improves). Also, while limited-separations processes are likely to cost less to implement than full chemical reprocessing, it would be more difficult for them to compete with the cost of a once-through cycle, since at the present enriched uranium fuel is relatively inexpensive, making up only a small fraction of the total cost of nuclear electricity.

1.2.2 Previous studies of limited-separations fuel cycles

One of the best known examples of a limited-separations fuel cycle is the DUPIC (Direct Use of PWR spent fuel in CANDU) fuel cycle, which has been investigated extensively by the Korea Atomic Energy Research Institute with Atomic Energy of Canada Limited and the U.S. State Department [Choi, 2001]. In the DUPIC process, used LWR fuel is ground up (which releases some volatile fission products) and then repressed into fuel pellets for use in a CANDU fuel bundle. This type of reuse is possible because CANDU reactors are able to run on fuel with a low fissile content. Studies of the DUPIC process have included creating a conceptual design for a DUPIC plant and forming cost estimates for the DUPIC fuel cycle.

Another set of limited-separations processes involves oxidizing and reducing fuel to remove volatile fission products. Examples of such processes include AIROX (Atomics International Reduction Oxidation), CARDIO (Carbon Dioxide Oxidation), CARBOX (Oxidation Carbothermic Reduction Process), and OREOX (Oxidation and Reduction of Oxide Fuel) [Plaue, 2003]. These processes, sometimes referred to as "dry reprocessing," can be used to refabricate ceramic fuels and potentially to change fuel types (e.g. change oxide fuel into carbide). The purpose of these processes is generally to condition used LWR fuel for reuse, which also requires that additional enriched uranium is added to the processed fuel.

For limited-separations processes involving metal fuel, there is experience at the EBR-II Fuel Cycle Facility with melt refining of fuel [Hesson, 1963]. In the melt refining process, cladding is cut from the fuel and the fuel is melted in a crucible. This releases volatile fission products (Br, Kr, Rb, Cd, I, Xe, Cs) and causes reactive fission products (Sr, Y, Te, Ba, Am, Th, and rare earth elements) to form oxides with the crucible. The molten fuel is then recast into fuel pins to be reused in the same reactor or another reactor. The purpose of the EBR-II Fuel Cycle Facility was to demonstrate that metal fuel could be remade in this manner then reused in a reactor.

Relatively few studies have considered linking B&B reactors in a limited-separations fuel cycle. The MIT study of a gas-cooled B&B reactor [Yarsky, 2005] did investigate the possibility of putting fuel bred in a B&B reactor through an AIROX process so that it could be reused in an LWR. Other than this, the majority of B&B reactor studies have assumed a once-through cycle, and none so far have investigated using burned B&B fuel to start up additional B&B reactors.

1.3 Objectives of present study

The goal of this thesis is to investigate a wide range of possible B&B reactor types and configurations and compare their performance. This general approach is taken because currently, the fluence required for a B&B reactor to burn natural or depleted uranium as feed is greater than the current knowledge limit on material fluence. Any single design is therefore speculative at best until data for higher fluences exists; it may be either too optimistic (assumes fluences that cannot be achieved) or too conservative (doesn't take full advantage of achievable fluence). Furthermore, it is premature to select a given design without knowing how one's design parameters affect reactor and fuel cycle performance. In addition to comparing reactor types, this thesis investigates the potential performance of a limited-separations fuel cycle, and what

kind of impact reactor design has on fuel cycle performance. To accomplish these goals, new methods to analyze B&B reactors are developed, which can also aid in future studies of B&B reactor designs.

Previous studies of B&B reactors have generally focused on developing one or two point designs and evaluating their performance. While the specific reactor designs developed in these studies are well characterized, one downside of these point design studies is that they do not directly consider the effect of different possible design decisions, such as choosing a different fuel, structure, or coolant material. For example, in the MIT gas-cooled B&B reactor study, it is not explicitly shown how large a neutronic benefit is gained by using a gas coolant relative to using sodium or lead, and how this neutronic benefit compares to the neutronic differences between different fuel types. Meanwhile, it is not possible to directly compare the results of different reactor studies because they all involve different reactor configurations, assumptions, and analysis techniques. By developing and applying a set of methods for analyzing a wide variety of B&B reactor types, this thesis allows quantitative and consistent comparisons of different B&B reactor options to be performed.

1.3.1 Breed-and-burn reactor analysis objectives

An important goal of this thesis is to characterize different reactor options in terms of their suitability for B&B operation using natural or depleted uranium. These reactor options include different coolant, structure, and fuel materials, as well as different geometric configurations. For reactor coolants, the primary fast reactor coolants will be considered: sodium, lead, lead-bismuth eutectic (LBE), helium, and CO_2. For structural material, three types of steel (HT9, T91, and oxide dispersion strengthened or ODS) are considered, as well as silicon carbide, a ceramic. For fuels, a variety of compound fuels (UC, UN, UO_2,U_3Si_2, UP, US, USe, UTe, UCO, and UAl_2) and uranium alloy metal fuels (U-2Zr, U-10Zr, U-2Mo, U-4Zr-2Nb, U-7Nb, and U-9Mo) will be evaluated, as well as thorium metal. In addition to comparing different core materials, the effects of varying the relative amounts of coolant, structure, and fuel will also be examined.

Two different configurations are investigated because of the significant differences in behavior between the two. First is a configuration in which reactor fuel elements can be freely shuffled in three dimensions. This would correspond to a core composed of stacked prismatic blocks (like a prismatic VHTR core), a core with a CANDU-like configuration, or a pebble-bed core. Such a core configuration is special because the ability to shuffle in all dimensions means that it is possible to even out burnup gradients, so that all fuel can be discharged at a uniform burnup. As a result, such reactors are able to minimize the fluence and burnup needed for B&B operation, and are referred to in this thesis as "minimum-burnup" B&B reactors. The other configuration considered is a core composed of conventional axially-connected assemblies that are shuffled in two dimensions; i.e. the standard arrangement used in LWRs and most fast reactors. This type of core, referred to as a "linear-assembly" core in this thesis, is qualitatively different from a minimum-burnup configuration because axial gradients are able to develop along the assembly. It is worth considering linear-assembly cores because they do not require the innovative engineering that would be needed to develop a minimum-burnup system.

Notably, one configuration that is not considered in this thesis is an unshuffled core with a breed-burn wave propagating through it. While such a configuration may have operational advantages, its neutron economy is impaired by the fact that neutrons are lost leaking "backwards" into the already burned part of the fuel. This means that such reactors require even higher fluences and would be less suitable than a shuffled reactor for use in a limited-separations fuel cycle.

One of the important goals of this analysis is to evaluate how different core compositions and configurations compare in terms of minimum fluence for B&B reactors, since this influences which types of cores are closest to implementation. Another important parameter to calculate is the amount of starting fuel required to produce a desired B&B equilibrium cycle. Other important items to investigate include the effect of different equilibrium cycle shuffling paths, the size requirement for B&B reactor cores, and the effects of varying cycle length. Simple thermal hydraulics calculations will be used to examine the tradeoff between having more fuel (better neutronics) and having more coolant (higher power densities).

1.3.2 Limited-separations fuel cycle analysis objectives

Another primary goal of this thesis is to examine the ability for B&B reactors in a limited-separations fuel cycle to allow a sustainable, scalable reactor infrastructure. An important metric is the reactor fleet doubling time, which determines the ability of the fuel cycle to meet the growing demand for electricity, especially the growing demand for carbon-free electricity. The achievable fleet doubling time is evaluated as a function of reactor type, the fluence/DPA limit in effect, as well as what types of limited-separations processes are used. Other fuel cycle results of interest are the degree of uranium utilization, the amount of fuel processed and disposed, and the compositions of the fuel during processing and disposal. Different B&B reactor fuel cycle options are also identified and characterized.

1.3.3 Methods development objectives

Because the goal of this thesis is to investigate a wide range of possible B&B reactors, using a conventional reactor-analysis approach (modeling an entire reactor, determining starting enrichments and shuffling sequences, and repeating for each composition) would be impractical. Therefore, a large part of this thesis is devoted to developing a set of methods that are useful for analyzing B&B reactors, in particular ones that allow such analyses to be greatly simplified. These methods are centered on an idea called the "neutron excess concept." The neutron excess concept focuses on the evolution of materials' depletion quantities over their lifetime in a reactor. These depletion quantities include quantities such as the total number of neutrons absorbed or produced by a given volume of material. This approach is useful because of three reasons: first, neutron excess quantities are closely related to reactor k-effective; second, certain neutron excess quantities are conserved in critical reactor; and third, these quantities can be easily estimated using greatly simplified models, thus allowing a large number of reactor compositions to be evaluated.

The overall goal is to develop methods that can be used to form realistic estimates of the relationships between burnup/fluence, reactivity, cycle length, and losses to either leakage or control. These methods need to be applicable for analyzing both minimum-burnup and linear-

assembly core configurations. While designed for investigating a broad range of different reactor types, the B&B reactor analysis methods developed in this thesis should also be useful for detailed design and analysis of B&B reactors in the future.

Chapter 2 of this thesis discusses the theory of the neutron excess concept and its applications for analyzing B&B reactors, primarily focusing on applications for the "minimum-burnup" B&B configuration, which allows fuel shuffling in three dimensions. Chapter 3 gives examples of using the neutron excess concept and shows how simplified reactor models can be used to approximate the neutron excess results of realistic systems. Chapter 4 investigates the possibility of linking multiple B&B reactors in a limited-separations fuel cycle, and describes how the doubling time of such a fuel cycle can be calculated from reactor parameters. Chapter 5 performs a comparison of different B&B core composition options, using the ideas developed in Chapters 2 through 4. Chapter 6 examines the more complex case of "linear-assembly" B&B reactors, which use conventional axially-connected assemblies. Chapter 7 discusses the broader implications of B&B reactors and limited-separations processes, and Chapter 8 gives a concluding summary of the major results in this thesis.

2. Breed-and-Burn Reactor Analysis Methods

This chapter introduces several B&B reactor analysis methods, based on a newly developed idea: the "neutron excess" concept. Chapter 3 provides examples of how these methods are applied, and shows how simplified models can be used to accurately estimate neutron excess evolution in realistic systems.

Conceptually, the neutron excess concept is a method of keeping track of neutron gains and losses within the materials in a core, and relating these quantities to the excess reactivity of the reactor. The neutron excess method is useful because neutron gains and losses as a function of material fluence are easy to estimate using simple zero-dimensional and one-dimensional models. Application of the neutron excess method can be used to form accurate estimates of both the minimum fluence/burnup and the required amount of starter fuel for a given B&B reactor, which are both important design parameters.

Section 2.1 defines the neutron excess quantities and gives schematic figures for how they evolve with fluence for B&B reactor feed fuel. Section 2.2 describes how the neutron excess quantities relate to uncontrolled k-effective in an idealized "thought experiment" B&B reactor. Section 2.3 shows how the neutron excess concept applies to more realistic cases with non-uniform burnup and finite cycle lengths. Section 2.4 describes how the neutron excess concept can be used to compute the amount of starter fuel required to start up a desired equilibrium cycle. Section 2.5 gives a brief summary of different possible uses for the neutron excess concept.

2.1 Definition of neutron excess quantities

The basic idea of the neutron excess concept is to take the neutron absorption and production rates in a material and integrate them over time to yield intrinsic quantities for that material. Integrating the neutron absorption rate of a material over time yields the total number of neutrons absorbed by that material over time, which is termed ΔA. Integrating the neutron production rate of a material over time yields the total number of neutrons produced by that material, termed ΔP. The difference between ΔP and ΔA is the net number of neutrons produced or absorbed by that material, termed ΔN, which is referred to as the *neutron excess* of a material. A negative neutron excess means that a material as absorbed more neutrons than it has produced, while a positive neutron excess means that a material is a net producer of neutrons. Together, ΔA, ΔP and ΔN are termed *neutron excess quantities*, and have units of number of neutrons per unit volume (e.g. mol/cm^3). They are defined in Equations 2.1-1 through 2.1-3:

$$\Delta A = \int_{t=0} \phi \Sigma_a dt \tag{2.1-1}$$

$$\Delta P = \int_{t=0} \phi \nu \Sigma_f dt \tag{2.1-2}$$

$$\Delta N = \Delta P - \Delta A = \int_{t=0} \phi (\nu \Sigma_f - \Sigma_a) dt \tag{2.1-3}$$

In the above equations, ϕ is the neutron flux experienced by a material in neutrons/cm^2/s, Σ_a is the total macroscopic neutron absorption cross section of the material (including fissions) in cm^{-1}, Σ_f is the total fission cross section of the material, and ν is the average number of neutrons produced per fission. Each of the integrals in Equations 2.1-1 through 2.1-3 is taken starting from t=0, i.e. at reactor startup when all fuel is fresh. The neutron excess quantities for fresh or unirradiated materials are defined to be zero. Neutron excess quantities change with increasing burnup or fluence, since as materials are burned further they continue to absorb and produce neutrons.

The values of Σ_a and $\nu\Sigma_f$ depend on the neutron spectrum experienced by the material, so how neutron excess quantities evolve depends on both the initial material composition and the spectral history it undergoes. In a hard spectrum B&B reactor, the neutron spectrum is fairly uniform, which means that it is straightforward to estimate neutron excess quantities using approximate spectra taken from simple models.

In the above discussion, a "material" can be any homogenized combination of different materials, such as fuel, structure, coolant, control, and void. In this thesis, such a combination is referred to as a "core composition," and a core composition containing fuel is also called a "fuel composition." In a fast reactor, the neutron mean free path is generally many times larger than the size of the individual fuel pins or coolant channels, so it is an accurate assumption to treat a given assembly design as a homogenized composition with the same material ratios. Fuel compositions are also referred to as simply "fuel" in this thesis, when distinguishing them from regions of the core without fuel, such as control or shield assemblies.

2.1.1 Definition of k'_∞

Another useful quantity related to the neutron excess quantities is k'_∞ (k-infinity prime), which is the ratio of neutron production and absorption cross sections in a core composition, as defined in Equation 2.1-4. These cross sections are flux-weighted according to the spectrum experienced by the material, so they are proportional to the rates of neutron production and absorption.

$$k'_\infty = \frac{\nu\Sigma_f}{\Sigma_a} \tag{2.1-4}$$

This definition for k'_∞ is similar to the usual definition for k_∞ (without the prime superscript), which is the ratio of the neutron production to absorption cross sections of a material in an infinite medium. The difference between k'_∞ and k_∞ is that k'_∞ is evaluated using the local spectrum experienced by the material, rather than using the material's infinite-medium spectrum. Following from Equation 2.1-4, a k'_∞ greater than unity means that a material is a producer of neutrons, while a k'_∞ less than unity means that a material is a neutron absorber.

The definitions for neutron excess quantities can be rewritten using the definition of k'_∞, as shown in Equation 2.1-5 and 2.1-6:

$$\Delta P = \int \phi \nu \Sigma_f dt = \int k'_\infty \phi \Sigma_a dt \qquad \frac{dP}{dA} = k'_\infty \tag{2.1-5}$$

$$\Delta N = \Delta P - \Delta A = \int \phi (\nu \Sigma_f - \Sigma_a) dt = \int (k'_\infty - 1) \phi \Sigma_a dt \qquad \frac{dN}{dA} = k'_\infty - 1 \tag{2.1-6}$$

As shown in the above equations, k'_∞ relates the rate of change of the different neutron excess quantities. Unlike the neutron excess quantities, which are integrated over the history of a fuel irradiation, k'_∞ is an instantaneous quantity at a particular point in an irradiation. As such, k'_∞ is sensitive to the current flux spectrum that a material is experiencing, and is a useful quantity for understanding differences in how the neutron excess quantities evolve.

2.1.2 Schematic figures for neutron excess evolution

Figure 2.1-1 shows a schematic of how the neutron excess ΔN evolves with increasing fluence for a primarily fertile B&B feed fuel composition (consisting of fuel, structure, and coolant). In region I, between points A and B, the fuel is a neutron absorber; it produces *less* than one neutron on average for each neutron absorbed. In region II, between points B and D, the fuel has enough fissile material bred in it to become a neutron producer; it produces *more* than one neutron on average for each neutron absorbed. In region III, the accumulation of fission products and depletion of actinides causes the fuel to become an absorber again. Two additional points, C and E, are marked where neutron excess is equal to exactly zero. As will be discussed in Section 2.2, a feed fuel composition must have a net *positive* neutron excess for a B&B reactor to operate in an equilibrium cycle with *k*-effective greater than unity, so points C and E mark the minimum and maximum fluence/burnup achievable by that fuel composition. For a B&B feed fuel composition, point E typically occurs at very high levels of burnup (>40% Fissions per Initial Metal Atom, or FIMA).

Figure 2.1-2 gives a corresponding diagram for the other two neutron excess quantities: the total number of neutrons absorbed (ΔA) and produced (ΔP). The ΔA curve is nearly linear with fluence, while the slope of the ΔP curve varies as the fissile concentration rises and then falls. Figure 2.1-2 shows that the fraction of total neutron absorptions/productions that count toward the total neutron excess is quite small, since ΔA and ΔP follow each other quite closely over a large range of fluence.

To aid understanding of Figure 2.1-1, Figure 2.1-3 gives the corresponding k'_∞ evolution for the same composition. When k'_∞ is lower than unity, the fuel is a neutron absorber and neutron excess decreases. When k'_∞ is greater than unity, the fuel is a neutron producer and neutron excess increases. Figure 2.1-3 explicitly shows how initially fertile feed fuel in a B&B reactor becomes a producer of neutrons.

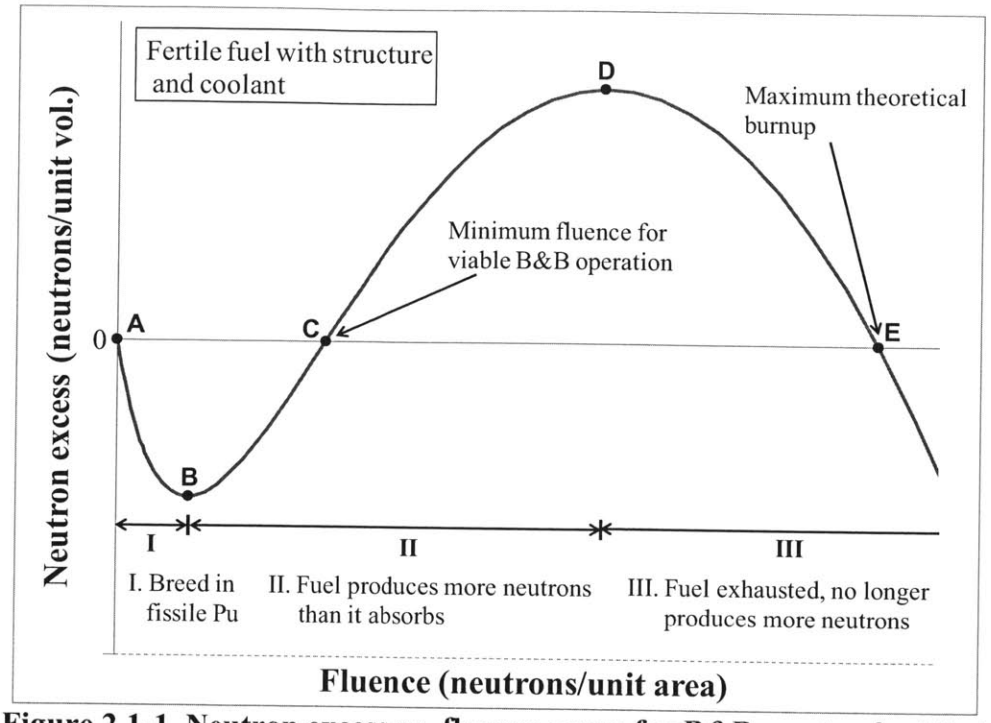

Figure 2.1-1. Neutron excess vs. fluence curve for B&B reactor feed fuel

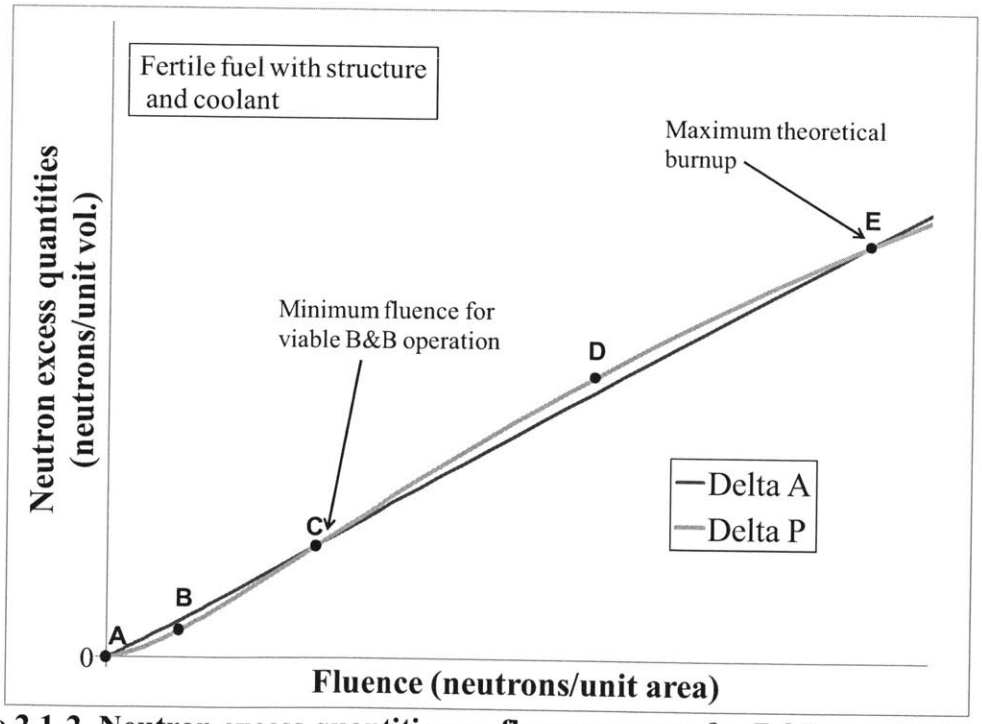

Figure 2.1-2. Neutron excess quantities vs. fluence curves for B&B reactor feed fuel

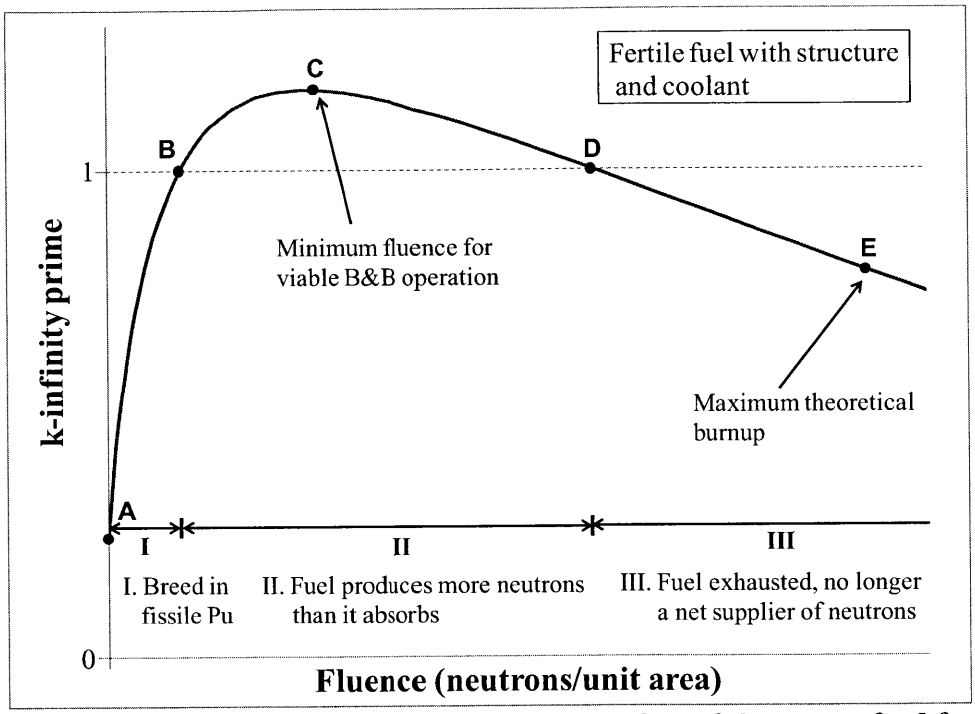

Figure 2.1-3. *k*-infinity prime vs. fluence curve for B&B reactor feed fuel

2.2 Relationship between neutron excess quantities and *k*-effective in an ideal B&B reactor

To understand how neutron excess quantities are related to a core's *k*-effective, it is useful to first consider the case of a simple idealized B&B reactor with constant operating characteristics and no neutron losses to leakage or control. This ideal case is referred to as the "thought experiment" B&B reactor. In addition to being simple to analyze, the thought experiment reactor also represents a neutronic performance limit for B&B reactors, since no neutrons are lost to un-fueled regions.

2.2.1 Description of "thought experiment" B&B reactor.

The "thought-experiment" picture of a breed-and-burn reactor consists of a sphere divided into many arbitrarily thin equal-volume spherical shells. There is a constant volume flow of feed material ($\dot{V}$) from the exterior of the sphere to its center; material is constantly being discharged from the center, while the exterior is replenished with the chosen feed material (this feed material is the chosen feed fuel composition, for example depleted uranium in a U-Zr alloy, with steel clad and sodium coolant). The sphere is producing a constant power (P) in its central burning region, with a flux and power distribution determined by solving the neutron transport equation for the materials in the model. The sphere is assumed to be large enough that essentially all neutrons leaking from the central burning region are captured by neutron-absorbing feed fuel, so neutron leakage is negligible. Materials are depleted as they flow inwards according to the calculated flux.

Independent of the starting configuration of the sphere, the system will eventually reach a steady state that only depends on the ratio of power to volume flow rate. There is some sensitivity to the absolute value of power, because radioactive decay introduces some time dependence, but for the range of specific power of interest to reactor applications, no major isotopes have decay rates comparable to their transmutation rates[1]. This steady state will have a constant uncontrolled *k*-effective, constant flux, power, and burnup distributions, and a fixed discharge burnup equal to the ratio of power to heavy-metal mass flow rate. Since material is continuously flowing, the steady state can be thought of as an equilibrium cycle in the limit of zero cycle length and zero reactivity swing. This type of idealized reactor is referred to in this thesis as a "continuous" system, as opposed to a more realistic "discrete" system with discrete fuel elements and finite cycle length.

2.2.2 Derivation of reactivity-burnup relationship

The reactivity relation for the idealized "thought experiment" reactor is given by Equation 2.2-1; its uncontrolled *k*-effective is equal to the instantaneous neutron production rate over the neutron absorption rate over the entire volume of the system. This is an *uncontrolled k*-effective because it is assumed that there are no neutron absorptions in control; if there were, an additional control absorption rate term would be added to the denominator. For simplicity only fission and total absorption terms are shown.

$$k_{unc} = \frac{neutron\ production\ rate}{neutron\ absorption\ rate} = \frac{\int dV \phi \nu \Sigma_f}{\int dV \phi \Sigma_a} = \frac{\int dV \phi \Sigma_a k'_\infty}{\int dV \phi \Sigma_a} \tag{2.2-1}$$

Using the definitions of neutron excess quantities in Equations 2.1-1 through 2.1-3, it is possible to rewrite the *k*-effective expression in Equation 2.2-1 when the reactor is at equilibrium. This is done by picturing the reactor as a control volume for each of the neutron excess quantities. For a control volume, the rate of change of a quantity in the control volume is equal to the creation/destruction rate of that quantity in the control volume, added to the net flow of that quantity into or out of the control volume. This relationship is written conceptually in Equation 2.2-2; the quantity can be any extensive property such as mass, enthalpy, or the neutron excess quantities. Writing the control volume relationship for ΔA and ΔP yields equations 2.2-3 and 2.2-4:

$$\begin{aligned} &Rate\ of\ change\ of\ quantity\ in\ control\ volume = \\ &\quad Creation\ rate\ in\ volume + Net\ flow\ in - Net\ flow\ out\ of\ volume \end{aligned} \tag{2.2-2}$$

$$\frac{d}{dt}\int dV \Delta A = \int dV \phi \Sigma_a + \dot{V}\,\Delta A_{charge} - \dot{V}\,\Delta A_{discharge} \tag{2.2-3}$$

$$\frac{d}{dt}\int dV \Delta P = \int dV \phi \nu \Sigma_f + \dot{V}\,\Delta P_{charge} - \dot{V}\,\Delta P_{discharge} \tag{2.2-4}$$

---

[1] The isotope which introduces the largest dependence on absolute power is plutonium-241, which has a 14.3 year half life. A "slower" low power system will have less Pu-241 than a "faster" high power system and therefore have slightly lower reactivity. Generally very little Pu-241 is produced in the hard spectrum of a B&B reactor, so the effect on reactivity is very small, less than 100 pcm.

When the thought experiment B&B reactor is at equilibrium, the left-hand sides of these equations are zero, since there is no accumulation or loss of neutron excess quantities in a steady-state system. The first terms on the right-hand side are the neutron absorption/production rates in the system, the same terms as in Equation 2.2-1. The second right-hand-side terms are the rates that neutron excess quantities flow into the system, which are by definition zero for the fresh feed fuel entering the system. The third right-hand-side terms are the rates at which neutron excess quantities leave the system via fuel being discharged.

Equations 2.2-3 and 2.2-4 can be simplified by taking out the terms equal to zero for the equilibrium thought experiment reactor, yielding Equations 2.2-5 and 2.2-6. These equations show that the total neutron absorption and production rates in the reactor are equal to the rate that ΔA and ΔP are discharged from the reactor. Substituting these two expressions into Equation 2.2-1 gives an expression for the uncontrolled equilibrium state k-effective ($k_{unc\text{-}eq}$) in terms of the neutron excess quantities of the discharged fuel, shown in Equation 2.2-7.

$$\int dV \phi \Sigma_a \Big|_{eq} = \dot{V} \Delta A_{discharge} \tag{2.2-5}$$

$$\int dV \phi \nu \Sigma_f \Big|_{eq} = \dot{V} \Delta P_{discharge} \tag{2.2-6}$$

$$k_{unc-eq} = \frac{\int dV \phi \nu \Sigma_f}{\int dV \phi \Sigma_a} = \frac{\dot{V} \Delta P_{discharge}}{\dot{V} \Delta A_{discharge}} = \frac{\Delta P}{\Delta A}\Big|_{discharge} = \left(\frac{\Delta N}{\Delta A} + 1 \right)\Big|_{discharge} \tag{2.2-7}$$

Equation 2.2-7 shows that equilibrium state k-effective depends on the neutron excess quantities of the discharged fuel, which in turn depend on the burnup of the discharged fuel. Equation 2.2-7 shows that $k_{unc\text{-}eq}$ is greater than one when the neutron excess (ΔN) of the discharged fuel is positive; i.e. when the net number of neutrons produced by the feed fuel composition is greater than zero. This makes intuitive sense because a system would not be able to maintain critical operation if each piece of feed material was a net absorber of neutrons. This minimum burnup requirement that $\Delta N > 0$ is equivalent to the minimum burnup expression obtained from using a linear reactivity model formulation [Yu, 2002], which integrates fuel reactivity as a function of burnup instead of integrating neutron absorption and production rates.

The advantage of expressing reactor k-effective as a function of neutron excess quantities is that neutron excess quantities for realistic three-dimensional systems are simple to estimate using simple one-dimensional and even zero-dimensional models, which is discussed further in Chapter 3. This is because the neutron excess quantities depend only on the neutron spectra experienced over fuel irradiation, which do not vary greatly in a hard-spectrum B&B reactor. Since neutron excess quantities in a B&B can be easily estimated using 1D models, accurate estimates of equilibrium cycle k-effective can be made without needing to construct detailed 3D reactor models.

2.2.3 Schematic figures for reactivity-burnup relationship

As shown by Equation 2.2-7, the uncontrolled equilibrium k-effective of the thought experiment B&B reactor is equal to the ratio of ΔN to ΔA for the discharged feed fuel plus one. A schematic plot of ΔN to ΔA corresponding to Figure 2.1-1 is given in Figure 2.2-1; such a plot is referred to as a "neutron excess curve." The curve looks extremely similar to that in Figure 2.1-1 because ΔA varies approximately linearly with fluence.

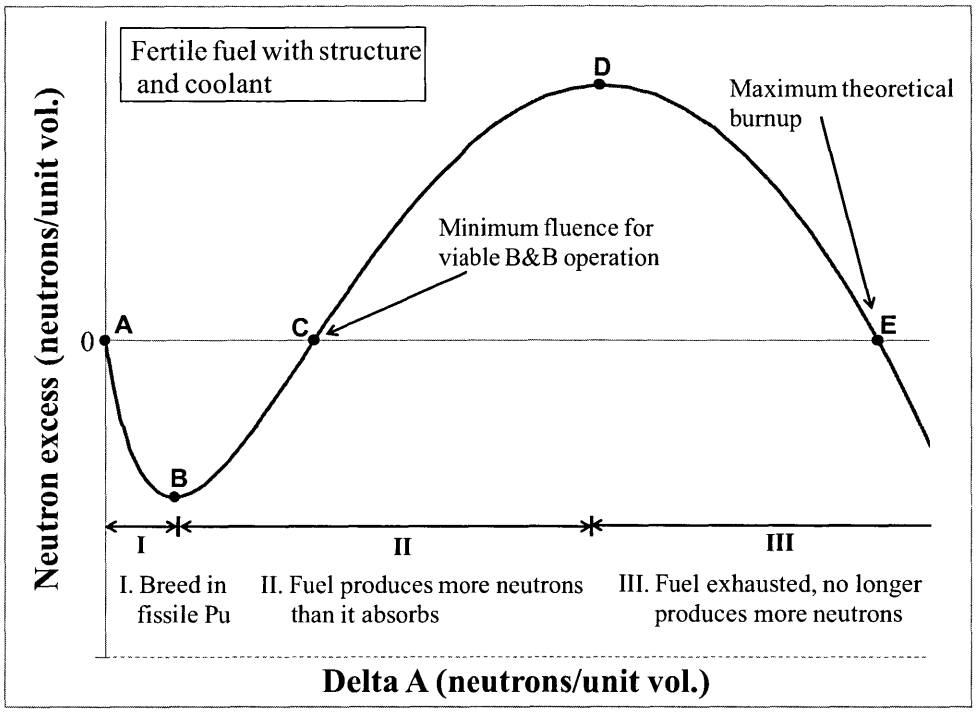

Figure 2.2-1. Neutron excess curve (ΔN as a function of ΔA)

Using Equation 2.2-7, the points on a neutron excess curve can be converted into uncontrolled equilibrium k-effectives ($k_{unc\text{-}eq}$). Figure 2.2-2 plots the $k_{unc\text{-}eq}$ values corresponding to the neutron excess curve in Figure 2.2-1 as a function of total fluence. It is also possible to plot $k_{unc\text{-}eq}$ as a function of burnup or material damage (e.g. displacements per atom, discussed in Chapter 5) instead of fluence. The relationship between equilibrium discharge burnup/fluence and equilibrium k-effective is referred to as the "reactivity-burnup" relationship.

As shown in the figure, points C and E (where neutron excess is zero) correspond to where equilibrium k-effective is exactly unity. Point C represents the minimum burnup/fluence for the "continuous" thought experiment B&B system, and sets a lower bound on the minimum required burnup/fluence in a realistic "discrete" B&B system. Finding the minimum burnup/fluence for a B&B reactor is important, because one of the primary technical challenges for B&B reactors is the high fluence experienced by the fuel and structural materials. The thought experiment B&B reactor is able to minimize burnup because it satisfies several criteria. First, neutron leakage is eliminated by surrounding the core with a thick blanket of absorbing feed fuel. Second, neutron losses to control are minimized by operating the reactor at a constant uncontrolled k-effective. Third, at equilibrium, all the feed fuel is discharged with a uniform burnup, so there is no burnup

peaking. Section 2.3 discusses how deviations from these criteria in more realistic systems affect the reactivity-burnup relationship.

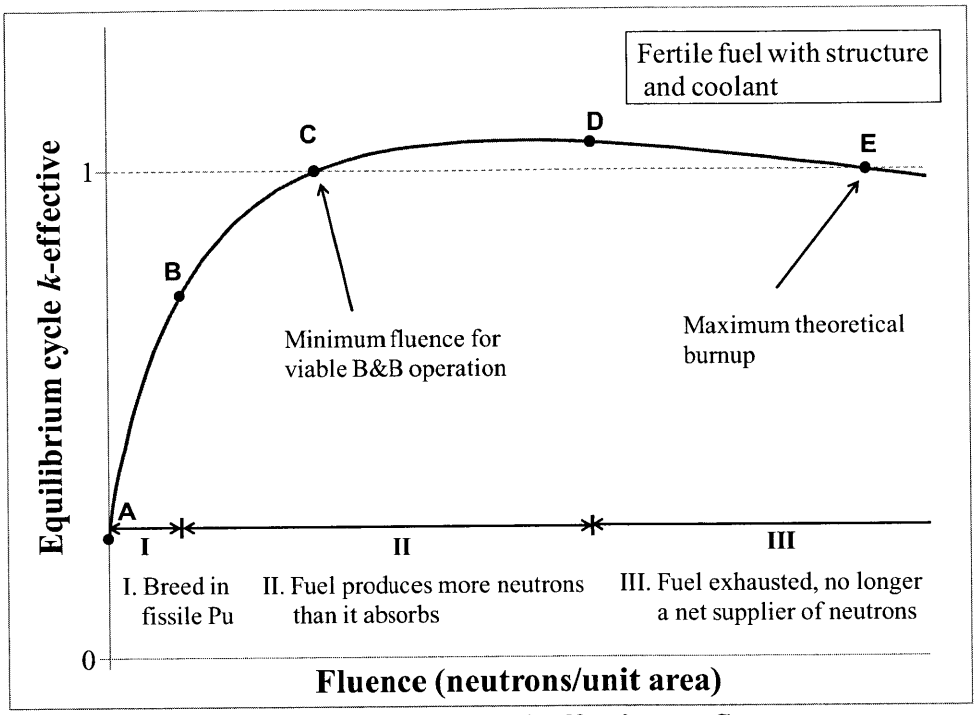

Figure 2.2-2. Equilibrium cycle *k*-effective vs. fluence curve

2.3 Reactivity-burnup relationships for realistic minimum-burnup B&B reactors

A realistic B&B reactor would be different from the ideal thought-experiment B&B in several significant ways. First, a real reactor would have some neutron losses to "leakage", i.e., some neutrons would be absorbed in un-fueled regions. While leakage from the periphery of the core can be minimized by including a thick blanket of absorbing feed fuel, it would be difficult to prevent neutron absorptions in interstitial un-fueled positions, such as control positions. Also, the requirement that the reactor be controlled means that there would be some neutron losses to control as well. How to treat losses to control and leakage is discussed in Subsection 2.3.1.

Instead of constantly flowing fuel elements like in the idealized thought-experiment B&B reactor, real reactor systems use discrete fuel elements that are periodically reshuffled at discrete moments in time. They have finite cycle lengths with uncontrolled *k*-effectives that vary over each cycle, as well as burnup, power, and flux distributions that also vary with time. In a B&B reactor with discrete fuel elements, an equilibrium cycle can still be established, but instead of having constant operating parameters as in the continuous case, its operating parameters will change from the beginning of cycle to end of cycle, and then be reset to their beginning of cycle values by fuel shuffling. With discrete fuel elements, it also becomes possible for burnup gradients to develop in the fuel, so that not all the fuel is discharged at a uniform burnup. The effects of finite cycle length and non-uniform burnup are discussed in Subsection 2.3.2.

In this section, it is assumed that the B&B reactor is composed of fuel elements that can be shuffled in all three dimensions; i.e. it is a "minimum-burnup" B&B reactor. Being able to shuffle in three dimensions allows burnup gradients in the fuel to be flattened in all directions. A B&B reactor using axially-connected linear assemblies would develop significant axial burnup gradients, and tools for analyzing these "linear-assembly" B&B reactors are presented in Chapter 6.

2.3.1 Using k_{fuel} to account for losses to control and leakage

So far, all the expressions given for k-effective have been for the *uncontrolled* k-effective in an "ideal" system with no neutron losses to leakage or control. In a realistic system, control is needed to keep k-effective at unity during operation, and some neutron leakage will occur either into un-fueled positions inside the core or through the outer surface of the core. Equation 2.3-1 gives the relation for k-effective in a system with losses to leakage and control:

$$k = \frac{\textit{neutron production rate}}{\textit{neutron absorption rate}} = \frac{\int_{fuel} dV \phi \nu \Sigma_f}{\int_{fuel} dV \phi \Sigma_a + \int_{ctrl} dV \phi \Sigma_a + \int_{leakage} dV \phi \Sigma_a} \tag{2.3-1}$$

The numerator in Equation 2.3-1 only has one term since neutrons are only produced in fueled regions. The denominator has three terms, corresponding to the different places neutrons can be absorbed: in the fuel, in control, or in leakage regions. Here "leakage region" is defined as any region without fuel or control, such as an un-fueled assembly position (e.g. a material test assembly or gas expansion module) or anything physically outside the fueled region of the core (e.g. reflector, shield, gas plena, or core vessel).

The equation relating uncontrolled k-effective and neutron excess quantities developed in the previous section (Equation 2.2-7) is based on the reactivity relation for the ideal system given in Equation 2.2-1. The difference between Equation 2.2-1 and the more realistic Equation 2.3-1 is that Equation 2.3-1 explicitly includes terms for neutron absorptions in leakage and control. In order to derive a reactivity-burnup relationship for Equation 2.3-1, it is useful to first define a new quantity k_{fuel}, equal to the total neutron production rate in fuel divided by the total neutron absorption rate in fuel, as shown in Equation 2.3-2:

$$k_{fuel} \equiv \frac{\int_{fuel} dV \phi \nu \Sigma_f}{\int_{fuel} dV \phi \Sigma_a} \tag{2.3-2}$$

The quantity k_{fuel} is defined at every time during reactor operation, and the value of k_{fuel} during equilibrium is referred to as k_{eq}. With k_{eq} being defined as the ratio of neutron production to absorption in just the fuel, the same derivation used in Subsection 2.2.2 can be applied to k_{eq} to obtain a relationship between k_{eq} and neutron excess quantities, given as Equation 2.3-3:

$$k_{eq} = \left.\frac{\Delta P}{\Delta A}\right|_{discharge} = \left.\left(\frac{\Delta N}{\Delta A} + 1\right)\right|_{discharge} \tag{2.3-3}$$

This equation is identical to Equation 2.2-7, except the uncontrolled equilibrium cycle k-effective ($k_{unc\text{-}eq}$) has been replaced by k_{eq}, the equilibrium cycle value of k_{fuel}.

The physical meaning of k_{fuel} can be more clearly seen if the numerator in Equation 2.3-2 is replaced with neutron absorption rates, using the substitution in Equation 2.3-1. This is given in Equation 2.3-4:

$$k_{fuel} = k \frac{\int_{fuel} dV\phi\Sigma_a + \int_{ctrl} dV\phi\Sigma_a + \int_{leakage} dV\phi\Sigma_a}{\int_{fuel} dV\phi\Sigma_a} \tag{2.3-4}$$

Equation 2.3-4 shows that k_{fuel} increases with the fraction of neutron absorptions occurring in control and leakage. Therefore, if more neutrons are lost to control and leakage in the equilibrium state, then k_{eq} increases, which raises the required fluence and burnup to achieve that k_{eq}, as shown in Figure 2.2-2. The lowest k_{eq} can be is unity, if there are no neutron losses at all to control and leakage. Minimizing losses to control can be accomplished by reducing reactivity swing, such as by using shorter cycle lengths. Losses to leakage can be minimized by using a thick blanket of feed fuel around the core and minimizing the number of interstitial un-fueled positions (such as control rod positions) inside the core.

There are two ways to evaluate the k_{fuel} of a reactor. First, one can model control explicitly (varying the amount of control to keep k-effective equal to unity), and input the applicable absorption rates into Equation 2.3-4 to compute k_{fuel}. A simpler approximate method is to construct a model without control, and assume that the relative number of absorptions in fuel and leakage regions remains the same as in the controlled case. In such a case, the uncontrolled k-effective (k_{unc}) of the model is equal to the expression for k-effective in Equation 2.3-1 with the control absorption term removed, as shown in Equation 2.3-5:

$$k_{unc} = \frac{neutron\ production\ rate}{neutron\ absorption\ rate} = \frac{\int_{fuel} dV\phi\nu\Sigma_f}{\int_{fuel} dV\phi\Sigma_a + \int_{leakage} dV\phi\Sigma_a} \tag{2.3-5}$$

Using Equation 2.3-5 to substitute the neutron production term in Equation 2.3-2 yields Equation 2.3-6 for k_{fuel}:

$$k_{fuel} = k_{unc} \frac{\left(\int_{fuel} dV\phi\Sigma_a + \int_{leakage} dV\phi\Sigma_a\right)}{\int_{fuel} dV\phi\Sigma_a} \tag{2.3-6}$$

Using a calculation for uncontrolled k-effective to compute k_{fuel} is an approximation because the neutron absorption rates in fuel and leakage regions would be different in a model with control explicitly modeled. This is a reasonable approximation for reactors in which the presence of control does not greatly shift the flux distribution. This approximation is used through the remainder of this thesis, since explicitly modeling control introduces additional complexity and isn't critical to the idea being studied. Notably, in cases in which the leakage probability approaches zero, then k_{fuel} can be approximated simply as k_{unc}, i.e. the measured k-effective of an uncontrolled model. Also, if k_{fuel} is known (by applying the neutron excess concept, e.g. through using Equation 2.3-4), then Equation 2.3-6 can also be used to determine the maximum leakage fraction that allows a target value for k_{unc}.

The quantity k_{fuel} is useful because it associates all the neutron absorptions in a system (in fuel, leakage, and control) with the neutron absorptions in the fuel alone. Section 2.4, which discusses how to compute the starter fuel requirement of a B&B reactor, will show how k_{fuel} can be used to simplify the neutron excess balance equations in such a calculation.

2.3.2 Effect of finite cycle length and non-uniform burnup

With a finite cycle length, the reactor would not be at a fixed steady state, so there would no longer be a single value for k_{eq} and Equation 2.2-7 would not apply. To obtain an equivalent expression in the case with finite cycles, Equations 2.2-3 and 2.2-4 (the control volume equations for neutron excess quantities) are first integrated over one equilibrium cycle, giving Equations 2.3-7 and 2.3-8. Since it is no longer being assumed that the entire system is composed of a fuel composition (i.e. there are regions without fuel present in the core, such as interstitial control positions), the volume integrals have been rewritten to explicitly include only the fueled regions.

$$\int_{cycle} dt \left(\frac{d}{dt} \int_{fuel} dV \Delta A \right) = \int_{cycle} dt \left(\int_{fuel} dV \phi \Sigma_a + \dot{V} \Delta A_{charge} - \dot{V} \Delta A_{discharge} \right) \tag{2.3-7}$$

$$\int_{cycle} dt \left(\frac{d}{dt} \int_{fuel} dV \Delta P \right) = \int_{cycle} dt \left(\int_{fuel} dV \phi \nu \Sigma_f + \dot{V} \Delta P_{charge} - \dot{V} \Delta P_{discharge} \right) \tag{2.3-8}$$

The left-hand side term in each equation is the change in the total amount of a neutron excess quantity in the fuel from cycle to cycle. For an equilibrium cycle, these terms are zero, since after each equilibrium cycle the reactor is reset to the same state as in the previous cycle. On the right-hand side, the neutron excess quantities of the input feed fuel are also zero, since they are defined to be zero for fresh fuel. Omitting these zero terms and rearranging yields Equation 2.3-9 and 2.3-10. In these equations, the time integral over the volume discharge rate is rewritten as a volume integral over the fuel discharged in one equilibrium cycle.

$$\int_{eq-cycle} dt \left(\int_{fuel} dV \phi \Sigma_a \right) = \int_{\substack{eq-cycle \\ discharge}} dV \Delta A_{discharge} \tag{2.3-9}$$

$$\int_{eq-cycle} dt \left(\int_{fuel} dV \phi \nu \Sigma_f \right) = \int_{\substack{eq-cycle \\ discharge}} dV \Delta P_{discharge} \tag{2.3-10}$$

To relate the neutron excess quantities in Equations 2.3-9 and 2.3-10 to equilibrium cycle k-effective, Equation 2.3-2 for k_{fuel} is first rearranged then integrated over one equilibrium cycle, which yields Equation 2.3-11. Dividing each side by the number of neutrons absorbed in a cycle results in Equation 2.3-12.

$$\int_{eq-cycle} dt \left(k_{fuel} \int_{fuel} dV \phi \Sigma_a \right) = \int_{eq-cycle} dt \left(\int_{fuel} dV \phi \nu \Sigma_f \right) \tag{2.3-11}$$

$$\frac{\int_{eq-cycle} dt \left(k_{fuel} \int_{fuel} dV \phi \Sigma_a \right)}{\int_{eq-cycle} dt \left(\int_{fuel} dV \phi \Sigma_a \right)} = \frac{\int_{eq-cycle} dt \left(\int_{fuel} dV \phi \nu \Sigma_f \right)}{\int_{eq-cycle} dt \left(\int_{fuel} dV \phi \Sigma_a \right)} \tag{2.3-12}$$

The terms on the right-hand side of Equations 2.3-11 and 2.3-12 can be substituted with neutron excess quantities by applying Equations 2.3-9 and 2.3-10, resulting in Equation 2.3-13:

$$\frac{\int_{eq-cycle} dt \left(k_{fuel} \int_{fuel} dV \phi \Sigma_a \right)}{\int_{eq-cycle} dt \left(\int_{fuel} dV \phi \Sigma_a \right)} = \frac{\int_{\substack{eq-cycle \\ discharge}} dV \Delta P_{discharge}}{\int_{\substack{eq-cycle \\ discharge}} dV \Delta A_{discharge}} \tag{2.3-13}$$

The left-hand side of Equation 2.3-13 is k_{fuel} averaged over an equilibrium cycle, with the average being weighted by the total number of neutron absorptions. This average equilibrium cycle k_{fuel} is referred to as $\overline{k_{eq}}$, with the bar denoting that it is an averaged quantity. The quantity $\overline{k_{eq}}$, defined explicitly in Equation 2.3-14, is the discrete-cycle analogue to k_{eq} for continuous systems.

$$\overline{k_{eq}} \equiv \frac{\int_{eq-cycle} dt \left(k_{fuel} \int_{fuel} dV \phi \Sigma_a \right)}{\int_{eq-cycle} dt \left(\int_{fuel} dV \phi \Sigma_a \right)} \tag{2.3-14}$$

Meanwhile, the right-hand side of Equation 2.3-13 corresponds to the neutron excess quantities of the discharged fuel. Since both neutron excess quantities are being integrated over the same volume, they can be replaced with volumetric averages ($\overline{\Delta A}$ and $\overline{\Delta P}$) taken over the discharged fuel. Making these substitutions in Equation 2.3-13 results in Equation 2.3-15:

$$\overline{k_{eq}} = \left.\frac{\overline{\Delta P}}{\overline{\Delta A}}\right|_{discharge} = \left.\left(\frac{\overline{\Delta N}}{\overline{\Delta A}} + 1\right)\right|_{discharge} \tag{2.3-15}$$

Equation 2.3-15 is similar to Equation 2.3-3 for a continuous system, except with volumetric averages of neutron excess quantities and the averaged $\overline{k_{eq}}$ instead of k_{eq}. As given in Equation 2.3-14, $\overline{k_{eq}}$ is a neutron-production-weighted average of the k_{fuel} over an equilibrium cycle. For a constant power level (or an integral over total energy instead of time), the integrals in Equation 2.3-14 can be rewritten in terms of the total power $P_{reactor}$, by converting between the number of neutrons absorbed to the number of fissions, as shown in Equation 2.3-16 and 2.3-17:

$$\int_{fuel} dV\phi\Sigma_a = \frac{\int_{fuel} dV\phi\nu\Sigma_f}{k_{fuel}} = \frac{\frac{\bar{\nu}}{\bar{Q}}\int_{fuel} dV\phi Q\Sigma_f}{k_{fuel}} = \frac{\bar{\nu}P_{reactor}}{\bar{Q}k_{fuel}} \tag{2.3-16}$$

$$\overline{k_{eq}} = \frac{\int dt\left(\frac{\bar{\nu}P_{reactor}}{\bar{Q}}\right)}{\int dt\left(\frac{\bar{\nu}P_{reactor}}{\bar{Q}k_{fuel}}\right)} \cong \frac{\int dt}{\int dt\left(\frac{1}{k_{fuel}}\right)} \tag{2.3-17}$$

In Equation 2.3-17, it is assumed that the average number of neutrons per fission ($\bar{\nu}$) and average energy per fission ($\bar{Q}$) averaged over the core do not change appreciably over the cycle of interest, so those terms can be pulled out of the integral and canceled. Equation 2.3-17 shows that the average k_{eq} can be approximated as the harmonic mean of k_{fuel} over an equilibrium cycle. For a small change in k_{fuel} over a cycle, the harmonic mean can be approximated as the arithmetic mean, and for a roughly linear reactivity swing, can be further approximated as the middle of cycle value of k_{fuel}.

This is not an immediately intuitive result: the middle-of-equilibrium-cycle k_{fuel} is a function of the neutron excess quantities of the discharged fuel, which is taken out of the reactor at the end of a cycle. When the reactor is in a middle-of-equilibrium-cycle state, the ΔA of the most depleted fuel is still less than $\Delta A_{discharge}$, but the reactivity at that point still depends on $\Delta A_{discharge}$.

2.4 Determining the starter fuel requirement of a B&B reactor

Determining the minimum starter fuel inventory of a B&B reactor is fundamentally different from determining fissile requirements for both LWRs and standard fast reactors. In typical reactors, fissile loading is tailored to achieve a particular cycle length, and loss of neutrons due to leakage and absorptions requires the continued replenishment of fissile fuel. In a B&B reactor, leakage can be reduced to any level desired through absorptions in the subcritical feed, and

neutrons absorbed in feed serve as an investment toward later reactivity instead of a loss. For B&B reactors operating on fertile-only feed, the starting fissile requirement is a one-time requirement, since they do not require fissile refueling to stay critical. This section discusses how the neutron excess concept can be used to determine how large this one time starter fuel requirement is for a desired equilibrium cycle.

Two new terms are introduced in this section. First, the "transition" stage of a B&B reactor's life is defined as the time between when the reactor is started with an initial load of fissile fuel and when it reaches its equilibrium cycle. Correspondingly, the "transition feed fuel" is defined as feed fuel which has participated in the transition stage, as opposed to "equilibrium cycle feed fuel" which undergoes the equilibrium cycle shuffling sequence and depletion path.

As discussed in Section 2.1, the neutron excess (ΔN) is defined as the net number of neutrons per unit volume produced or absorbed by a given material, as defined in Equation 2.1-3. For a critical system, the rates of neutron production and absorption are equal, so neutron excess is conserved, stemming from the criticality relation:

$$k = 1 = \frac{\int dV \phi \nu \Sigma_f}{\int dV \phi \Sigma_a} \tag{2.4-1}$$

$$\int dV \phi \left(\nu \Sigma_f - \Sigma_a \right) = 0 \tag{2.4-2}$$

$$\int dV \frac{d\Delta N}{dt} = \frac{d}{dt} \int dV \Delta N = 0 \tag{2.4-3}$$

The volume integrals in Equations 2.4-2 and 2.4-3 are taken over any volume that absorbs neutrons, including fueled regions, control elements, and leakage regions outside the core. The fact that neutron excess is conserved can be used to calculate how much starter fuel is required to start a given B&B equilibrium cycle. Conceptually, this is done by comparing the amount of positive neutron excess provided by the starter fuel and balancing that with the negative neutron excess contained in the equilibrium cycle, while also accounting for neutron absorptions in control and leakage.

To perform such a neutron excess balance calculation, the quantity k_{eq} is used to define a new neutron excess quantity, the "adjusted neutron excess" ΔN_{adj}. Subsection 2.4.1 defines ΔN_{adj} and derives the neutron excess balance equation for a simple continuous system with constant equilibrium cycle k_{fuel}. Subsection 2.4.2 gives the derivation for a more general finite-cycle case, in which k_{fuel} can change over an equilibrium cycle. Subsection 2.4.3 shows how the neutron excess balance equations can be used to compute the starting fuel requirements of a desired B&B equilibrium cycle.

2.4.1 Case with constant equilibrium cycle k_{fuel} and definition of ΔN_{adj}

First, a case is considered in which a hypothetical B&B equilibrium cycle has a constant value for k_{fuel}, which was designated k_{eq} in Subsection 2.3.1. Such a case represents the (unrealistic) limit in which at equilibrium, the cycle length is shortened to zero, so there is no cycle reactivity

swing. During the equilibrium cycle, k_{fuel} is equal to k_{eq}, so one can substitute k_{fuel} with k_{eq} in the definition of k_{fuel} (Equation 2.3-2) and rearrange to yield:

$$\int_{fuel} dV\left(\phi\nu\Sigma_f - k_{eq}\phi\Sigma_a\right) = 0 \tag{2.4-4}$$

The neutron absorption and production rates in Equation 2.4-4 can be expressed as time derivatives of neutron excess quantities:

$$\int_{fuel} dV\left(\frac{d\Delta P}{dt} - k_{eq}\frac{d\Delta A}{dt}\right) = 0 \tag{2.4-5}$$

Bringing the time derivative outside the volume integral yields:

$$\frac{d}{dt}\int_{fuel} dV\left(\Delta P - k_{eq}\Delta A\right) = \frac{d}{dt}\int_{fuel} dV\left(\Delta N_{adj}\right) = 0 \tag{2.4-6}$$

$$\Delta N_{adj} \equiv \int_{t=0} dt\phi\left(\nu\Sigma_f - k_{eq}\Sigma_a\right) = \Delta P - k_{eq}\Delta A \tag{2.4-7}$$

Equation 2.4-6 introduces a new quantity ΔN_{adj}, called the "adjusted neutron excess", which is defined in Equation 2.4-7. The definition for ΔN_{adj} resembles that for the normal neutron excess (ΔN), except that neutron absorptions are weighted by the constant term k_{eq}. Unlike the normal neutron excess, the adjusted neutron excess is only defined for fueled regions in the core. By weighing neutron absorptions in fuel by k_{eq}, ΔN_{adj} implicitly accounts for the neutron absorptions occurring outside of fuel (i.e., in control and leakage regions). In the remainder of this paper, ΔN_{adj} is also referred to as just "neutron excess" for simplicity, in places where the "adjusted" connotation is evident.

Equation 2.4-6 states that when k_{fuel} equals k_{eq}, the total adjusted neutron excess ($\int_{fuel} dV\Delta N_{adj}$) of a system is constant. This is the same as Equation 2.4-3, except restated in terms of ΔN_{adj}, which allows the volume integral to be performed over fueled regions only.

Once the equilibrium cycle is established, k_{fuel} by definition equals k_{eq}, so the total ΔN_{adj} of the system becomes constant. In addition, if the system is designed such that its k_{fuel} equals k_{eq} over the entire life of the reactor (i.e. from startup through transition to the equilibrium cycle), then the total ΔN_{adj} is constant and equal to zero over the life of the system (since ΔN_{adj} by definition starts at zero for fresh fuel).

If one removes the assumption that k_{fuel} is constant over the life of the reactor (i.e., if it varies during the transition from startup to the equilibrium cycle), then one can rearrange Equation 2.3-2 in a similar manner as Equation 2.4-4, but without substituting k_{fuel} with k_{eq}:

$$\int_{fuel} dV\left(\phi \nu \Sigma_f - k_{fuel}\phi\Sigma_a\right) = 0 \tag{2.4-8}$$

Shifting the k_{fuel} term to the right-hand side and subtracting a $k_{eq}\phi\Sigma_a$ term yields Equation 2.4-9:

$$\int_{fuel} dV\left(\phi \nu \Sigma_f - k_{eq}\phi\Sigma_a\right) = \int_{fuel} dV\left(k_{fuel}\phi\Sigma_a - k_{eq}\phi\Sigma_a\right) \tag{2.4-9}$$

$$\frac{d}{dt}\int_{fuel} dV\left(\Delta N_{adj}\right) = \left(k_{fuel} - k_{eq}\right)\frac{d}{dt}\int_{fuel} dV\Delta A \tag{2.4-10}$$

Equation 2.4-10 is equivalent to Equation 2.4-9, except written in terms of neutron excess quantities. The left side of Equation 2.4-10 is the time rate of change of the total amount of adjusted neutron excess in the system. Because the time rate of change of the total ΔA in the right-hand-side term is always positive, when k_{fuel} is higher than k_{eq}, the total adjusted neutron excess in a system increases. A higher k_{fuel} means that there are more neutron absorptions in leakage and control, so the fuel has to supply additional neutron excess.

To obtain the total adjusted neutron excess contained in a system, one can integrate Equation 2.4-10 over time to yield Equation 2.4-11, where the time integral is taken from the startup of the reactor:

$$\int_{fuel} dV\left(\Delta N_{adj}\right) = \int_{t=0} dt\left(\left(k_{fuel} - k_{eq}\right)\frac{d}{dt}\int_{fuel} dV\Delta A\right) \tag{2.4-11}$$

Equation 2.4-11 shows that if k_{fuel} is greater than k_{eq} during the transition to the equilibrium cycle, then the total adjusted neutron excess would be positive, meaning that additional fissile fuel would be needed to supply excess neutrons. Conversely, if k_{fuel} is lower than k_{eq}, then the total adjusted neutron excess decreases, reducing the fissile requirement.

2.4.2 Case with varying equilibrium cycle k_{fuel}

In a realistic reactor with finite cycle length, k_{fuel} will vary over an equilibrium cycle as the uncontrolled k-effective (i.e. amount of control required) varies over a cycle. In such a case, it is useful to first define a cycle-averaged value for k_{fuel}:

$$\overline{k_{fuel}} \equiv \frac{\int_{cycle} dt\left(k_{fuel}\int_{fuel} dV\phi\Sigma_a\right)}{\int_{cycle} dt\left(\int_{fuel} dV\phi\Sigma_a\right)} \tag{2.4-12}$$

Here, the definition for $\overline{k_{fuel}}$ is a neutron-absorption weighted average, the same as the definition of $\overline{k_{eq}}$ given in Equation 2.3-14. The difference between the two is that $\overline{k_{fuel}}$ can be calculated

for any cycle, while $\overline{k_{eq}}$ is defined for an equilibrium cycle. Likewise, $\overline{k_{fuel}}$ can be approximated as the harmonic mean of k_{fuel} over a cycle, or as the middle of cycle k_{fuel} if there is only a small change in k_{fuel} over the cycle.

Using the definition of $\overline{k_{fuel}}$ in Equation 2.4-12, it is possible to derive an expression analogous to Equation 2.4-11 but for discrete cycles. First, Equation 2.4-8 is rearranged and integrated over one cycle to yield:

$$\int_{cycle} dt \int_{fuel} dV\left(\phi \nu \Sigma_f\right) = \int_{cycle} dt \left(k_{fuel} \int_{fuel} dV\left(\phi \Sigma_a\right) \right) \tag{2.4-13}$$

The right-hand side of Equation 2.4-13 is equal to the numerator in Equation 2.4-12, allowing it to be rewritten as:

$$\int_{cycle} dt \int_{fuel} dV\left(\phi \nu \Sigma_f\right) = \overline{k_{fuel}} \int_{cycle} dt \int_{fuel} dV\left(\phi \Sigma_a\right) \tag{2.4-14}$$

Subtracting a $\overline{k_{eq}} \int_{cycle} dt \int_{fuel} dV\left(\phi \Sigma_a\right)$ term from each side yields Equation 2.4-15:

$$\int_{cycle} dt \int_{fuel} dV\left(\phi \nu \Sigma_f - \overline{k_{eq}} \phi \nu \Sigma_a\right) = \left(\overline{k_{fuel}} - \overline{k_{eq}}\right) \int_{cycle} dt \int_{fuel} dV\left(\phi \Sigma_a\right) \tag{2.4-15}$$

$$\int_{fuel} dV\left(\Delta N_{adj}\right)\Big|_{cycle} = \left(\overline{k_{fuel}} - \overline{k_{eq}}\right) \left(\int_{fuel} dV\left(\Delta A\right) \right)\Big|_{cycle} \tag{2.4-16}$$

Equation 2.4-16 is equivalent to Equation 2.4-15, except written in terms of neutron excess quantities. In Equation 2.4-16, the vertical bar denotes total change over a cycle, i.e. the value of a quantity at the end of a cycle minus the value at the beginning of a cycle. The left side of Equation 2.4-16 is the change in the total amount of adjusted neutron excess over a cycle. Since there is no single value of k_{eq} for a case with discrete cycles, ΔN_{adj} is defined using $\overline{k_{eq}}$ in place of k_{eq}.

As with the continuous case, when $\overline{k_{fuel}}$ for a cycle is greater than $\overline{k_{eq}}$, the total adjusted neutron excess in a system increases, with the converse being true as well. When $\overline{k_{fuel}}$ equals $\overline{k_{eq}}$, such as over an equilibrium cycle, then total adjusted neutron excess is conserved; i.e. it has the same value at the beginning and the end of the cycle. Summing Equation 2.4-16 over all cycles from reactor startup gives an expression for the total adjusted neutron excess in a system:

$$\int_{fuel} dV\left(\Delta N_{adj}\right) = \sum_{cycles} \left(\left(\overline{k_{fuel}} - \overline{k_{eq}}\right) \left(\int_{fuel} dV\left(\Delta A\right) \right)\Big|_{cycle} \right) \tag{2.4-17}$$

2.4.3 Computing Starting Fuel Requirements

Equation 2.4-17 can be used to form an estimate of the minimum fissile requirement for a desired equilibrium cycle. From examining an equilibrium cycle, parameters such as peak feed discharge burnup, minimum reactivity, reactivity swing, and minimum core size can be measured. Other parameters, such as reactivity coefficients, can also be calculated based on the equilibrium cycle state. For the purposes of computing the needed amount of starter fuel, another significant parameter that can be measured is the total ΔN_{adj} of the feed fuel in the equilibrium cycle. This value does not change from cycle to cycle once the equilibrium cycle is established, because the right-hand side in Equation 2.4-17 is zero over an equilibrium cycle. Let one assume that the average k_{fuel} for the transition cycles is approximately equal to that of the desired equilibrium cycle, which is reasonable because it is desirable to have the same minimum reactivity and reactivity swing over the life of the reactor. Under this assumption, it follows from Equation 2.4-17 that the total system ΔN_{adj} is equal to zero at the beginning and end of each cycle. Therefore, the total ΔN_{adj} of the feed fuel in the equilibrium cycle (which is negative) must be balanced by the positive ΔN_{adj} of the starter fuel, and any contribution from feed fuel that occurs during the transition period:

$$\int_{eq-cycle} dV\left(\Delta N_{adj}\right) + \int_{\substack{starter \\ fuel}} dV\left(\Delta N_{adj}\right) + \int_{\substack{transition \\ feed\ fuel}} dV\left(\Delta N_{adj}\right) = 0 \tag{2.4-18}$$

In Equation 2.4-18, the leftmost term can be measured directly from the equilibrium cycle of interest, by summing over the adjusted neutron excess of all the fuel contained in the equilibrium cycle. If the transition feed fuel is discharged at the same burnup as the equilibrium cycle feed fuel, then its contribution to the total neutron excess will be small, since its neutron excess will be similar to that of equilibrium cycle feed fuel, which is zero by definition. Small deviations from zero arise due to different spectral histories for the transition feed fuel and the equilibrium cycle feed fuel. As shown in Chapter 3, these are generally positive because transition feed fuel is bred in the harder neutron spectrum present around the starter fuel. Since the third term in Equation 2.4-18 is small, the first and second terms must essentially cancel each other out, meaning that the positive adjusted neutron excess of the starter fuel must equal the negative adjusted neutron excess contained in the equilibrium cycle. To find the amount of starter fuel needed, one would divide the total neutron excess needed by the average neutron excess per unit volume of the starter fuel used:

$$V_{starter} = \frac{\int_{\substack{starter \\ fuel}} dV\left(\Delta N_{adj}\right)}{\overline{\Delta N}_{\substack{starter \\ fuel}}} \cong \frac{-\int_{eq-cycle} dV\left(\Delta N_{adj}\right)}{\overline{\Delta N}_{\substack{starter \\ fuel}}} \tag{2.4-19}$$

The actual neutron excess obtained from a unit of starter fuel depends on its specific depletion history, which would be obtained by explicitly modeling the transition from startup to the desired equilibrium cycle. Designing and modeling such a transition is a complex fuel management problem, which makes it difficult to analyze a variety of starter fuel options. Fortunately, neutron excess is straightforward to estimate using simple models, such as by making an infinite-medium depletion approximation, which is described in detail in Section 3.3. The estimate is

made by performing an infinite-medium depletion calculation to the burnup/fluence limit of the starter fuel and measuring the resulting neutron excess. With this result, an estimate for the needed quantity of starter fuel can be made by dividing the total neutron excess contained in the equilibrium cycle by the average neutron excess predicted by the infinite-medium model.

If cycle-averaged k_{fuel} deviates from its equilibrium cycle value during the transition to the equilibrium cycle, the needed ΔN_{adj} is adjusted either upward or downward, as shown on the right-hand side of Equation 2.4-20, which matches the right-hand side of Equation 2.4-17. As a consequence, it is desirable to minimize excess reactivity during transition to reduce neutron losses to control and therefore lower the needed amount of starter fuel.

$$\int_{eq-cycle} dV\left(\Delta N_{adj}\right) + \int_{\substack{starter \\ fuel}} dV\left(\Delta N_{adj}\right) + \int_{\substack{transition \\ feed\ fuel}} dV\left(\Delta N_{adj}\right) = \sum_{\substack{transition \\ cycles}} \left(\left(\overline{k_{fuel}} - \overline{k_{eq}}\right) \left(\int_{fuel} dV(\Delta A) \right) \Bigg|_{cycle} \right) \quad (2.4\text{-}20)$$

Section 3.4 provides a concrete example of how Equation 2.4-20 can be used to estimate the needed amount of starter fuel for a desired equilibrium cycle, and verifies the accuracy of using a simple infinite-medium depletion to approximate the neutron excess obtainable from a chosen starter fuel.

2.5 Summary of neutron excess concept capabilities

This chapter describes the theoretical foundation of the neutron excess concept. Based on the neutron excess quantities for B&B reactor feed fuel, it is possible (using Equation 2.3-15) to determine the average equilibrium cycle k_{fuel} as a function of fuel discharge burnup, where k_{fuel} corresponds to the uncontrolled k-effective of a reactor when the leakage probability approaches zero. Such a relationship is useful for determining the minimum burnup and fluence required for B&B reactor operation, which is an important parameter since fluence and burnup limits are constraining in B&B reactor designs. Sensitivity to factors such as average k-effective and leakage probability can be evaluated.

In addition to evaluating k_{fuel} as a function of burnup or fluence, the neutron excess concept can also be used to determine the adjusted neutron excess "cost" of an equilibrium cycle, which factors into the amount of starter fuel required to initiate that equilibrium cycle (via Equation 2.4-19). This can be used to compare different equilibrium cycle configurations to determine which requires the least amount of starter fuel per unit power. Knowing the neutron excess quantities for a composition of starter fuel allows one to compute the amount of starter fuel required to establish a given equilibrium cycle, and different starter compositions can be compared in terms of how much neutron excess they generate. Knowing how much starter fuel is required to start up a given B&B reactor design allows fuel cycle calculations to be made, as is done in Chapter 4. Finally, Equation 2.4-20 describes how changes in k_{fuel} impact the neutron excess requirement of an equilibrium cycle, which allows one to evaluate the effect of reactivity deviations. For example, one can determine how much extra starter material would be required to allow an extra 1% uncontrolled reactivity over a one year period.

The discussion so far has assumed that some knowledge of neutron excess quantities is known in advance, allowing the described calculations to be performed. The advantage of using the neutron excess quantities is that they can be readily estimated using simple models, and that the results from these simple models correspond very well to those in more realistic models of B&B reactors. Chapter 3 gives examples of simple and more realistic models of B&B reactors and demonstrates how the ideas of the neutron excess concept are applied.

3. Applying the Neutron Excess Concept

The usefulness of the neutron excess concept described in Chapter 2 stems from the fact that neutron excess quantities for realistic systems can be accurately estimated using greatly simplified models. This chapter gives examples of how neutron excess evolves in models with different configurations, ranging from extremely simple (infinite-medium depletion) to fairly realistic (blocks shuffled in three dimensions). This chapter also considers some more general issues related to B&B reactor design, such as cycle reactivity swing and reactor size.

Section 3.1 presents a one-dimensional infinite-slab model of a B&B reactor, which gives a simple illustration of how the neutron excess equations in Section 2.3 can be applied. Section 3.2 introduces models with different geometries and shuffling sequences and compares the neutron excess evolution of their feed fuel. Section 3.3 considers a couple of topics outside the neutron excess concept and explains how the reactivity swing and reactor size can be characterized for B&B reactors.

Section 3.4 describes the infinite-medium depletion approximation, which is useful for determining the minimum burnup/fluence required for a given B&B core composition. Section 3.5 gives an example transition model which shows an equilibrium cycle being established, and demonstrates how the required amount of starter fuel is calculated. Section 3.6 gives an example of how different starter fuel compositions can be compared using the infinite-medium depletion model. Section 3.7 gives examples of realistic three-dimensional B&B reactors and compares their equilibrium cycle performance. Finally, Section 3.8 summarizes the important findings in this chapter.

3.1 Description of infinite slab example models

To study different aspects of B&B reactors, including the burnup-reactivity relationships discussed in Section 2.3, a simple one-dimensional model of a B&B reactor was constructed. Unlike the idealized "thought-experiment" reactor, the model has a planar rather than a spherical geometry, and discrete zones instead of a continuous flow of material. Nevertheless the model is nearly ideal in that there are no neutron losses to leakage or control, and burnup is homogenized within each zone so that fuel is discharged at a uniform burnup.

The models in this section were run using MCNPXT, a version of MCNPX-CINDER90 modified by TerraPower LLC to improve performance and parallelization and to add additional features specific to B&B reactors [Ellis, 2010]. MCNPX [Hendricks, 2008] is a stochastic neutron transport code, and CINDER90 [Wilson, 1995] is a transmutation code that models nuclide depletion and decay. A predictor-corrector method is used with the two codes to perform transport/depletion calculations. A combination of ENDF-B/V and ENDF-B/VII cross section libraries [Chadwick, 2006] was used. For the purposes of this chapter, the code and cross section libraries used to perform transport and depletion calculations are of secondary importance, since the same conclusions can be drawn provided a consistent methodology is used across the different types of runs.

3.1.1 Convergent infinite slab model geometry and composition

First, a simple infinite slab model is considered, which is called the "convergent infinite slab model," so named because fuel is convergently shuffled to the center of the model. The geometry modeled is a series of 5 cm thick infinite-slabs. The 5 cm dimension is chosen to properly resolve the compositional and flux gradients present in the problem. Fifty slabs are modeled with a reflective boundary condition at one end and a vacuum boundary condition at the other, as illustrated in Figure 3.1-1. Fresh feed fuel is fed in from the vacuum boundary and shuffled toward a power producing region in the middle. Feed fuel therefore becomes progressively more burned as it converges toward the center, and the most highly burned fuel is discharged from the center. Three time steps per cycle are modeled, one at the beginning of cycle, one at the middle of cycle, and one at the end of cycle. For the cycle lengths considered, the results do not depend on the number of time steps used, even if only one time step is modeled per cycle. Shuffling between the end of one cycle and the beginning of another is assumed to be instantaneous.

The composition assumed for each slab is 50% by volume uranium fuel (density 19 g/cc), 30% sodium coolant (0.83 g/cc) and 20% iron structure (7.8 g/cc). This is an approximation to an actual sodium-cooled core composition, with volume fractions resembling those found in the BOR-60 reactor [IAEA, 2010b]. A more realistic core composition would include alloying elements in the fuel uranium and structural iron, as well as account for space in the fuel region that is used for bond material. However, the composition analyzed is of secondary importance since the goal of these example models is to establish a set of general conclusions that would also apply to more realistic compositions.

To demonstrate that an equilibrium cycle B&B configuration can be established for this geometry and composition, the problem is first modeled with the following enrichment profile:

Zones 1-4: 15% enrichment
Zones 5-7: 8% enrichment
Zones 8-50 and additional feed fuel: 0.3% U-235 depleted uranium

Here the zones are numbered sequentially from the reflective boundary in the center. The 0.3 enrichment in the outer zones is meant to represent the enrichment of depleted uranium tails from the enrichment process. The model is run at a total power of 120 MW/m^2 and a cycle length of 450 days. After five cycles, the fuel zones are shuffled by discharging zone 1 (the innermost zone), replacing each zone n with the composition in zone $n+1$, then replacing zone 50 with fresh feed fuel (i.e. depleted uranium). This shuffling scheme is repeated at every cycle thereafter. The resulting uncontrolled k-effective evolution for this case is shown in Figure 3.1-2. The first several shuffles remove initially present enriched fuel, driving reactivity down, but even when all the starting fissile material is removed at cycle 12, sufficient additional fissile material has been bred in the depleted feed fuel to maintain criticality.

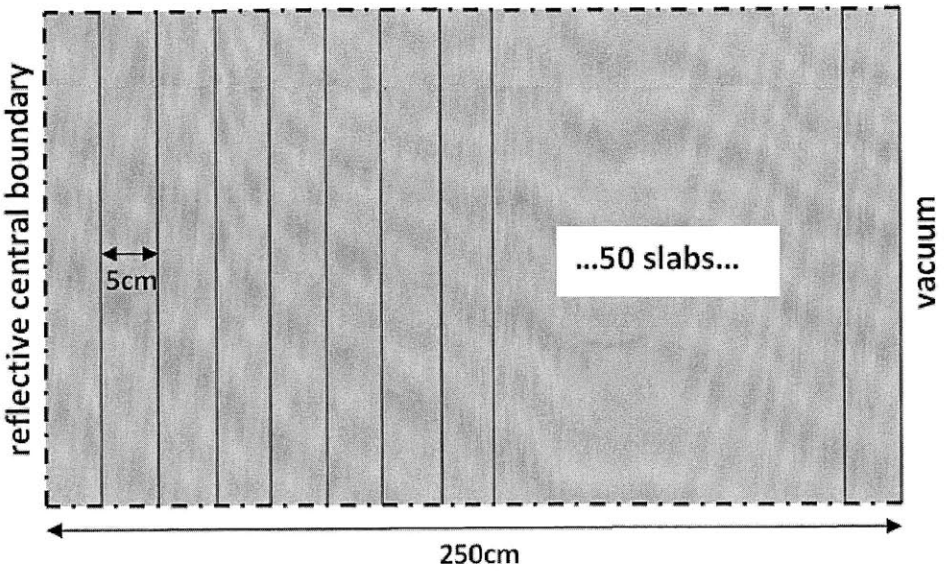

Figure 3.1-1. Geometry for convergent infinite slab model

Figure 3.1-2 shows that with repeated shuffling, the model converges onto an equilibrium cycle with a constant BOEC *k*-effective of about 1.02. In the equilibrium cycle state, the burnup, flux, and power distributions all assume constant shapes from cycle to cycle, as seen in Figures 3.1-3 through 3.1-5. What these equilibrium cycle distributions look like depends only on the feed fuel composition, equilibrium shuffling pattern, and discharge burnup; there is no dependence on the starting fuel configuration or initial shuffling steps.

This equilibrium cycle state does not depend strongly on absolute power and cycle length, only their ratio. This example model can be run at half the cycle length and twice the power (yielding the same energy per cycle), and achieve essentially the same equilibrium cycle conditions. If one were to ignore the effect of radionuclide decay, core materials would see the same neutron environment and undergo the same transmutations, producing the same equilibrium cycle. With the effect of radionuclide decay, only nuclides with decay times between their neutron transmutation times and residence time would exhibit time dependent behavior. Nuclides with decay half lives much shorter than their fast-reactor transmutation half lives would decay before they get transmuted, while nuclides with decay half lives much longer than the reactor residence time are effectively stable. As mentioned in an earlier footnote (in Subsection 2.2.1), the nuclide with the greatest effect on power dependence is plutonium-241, but it is built up at a small enough concentration that the effect is less than 0.1% in *k*-effective.

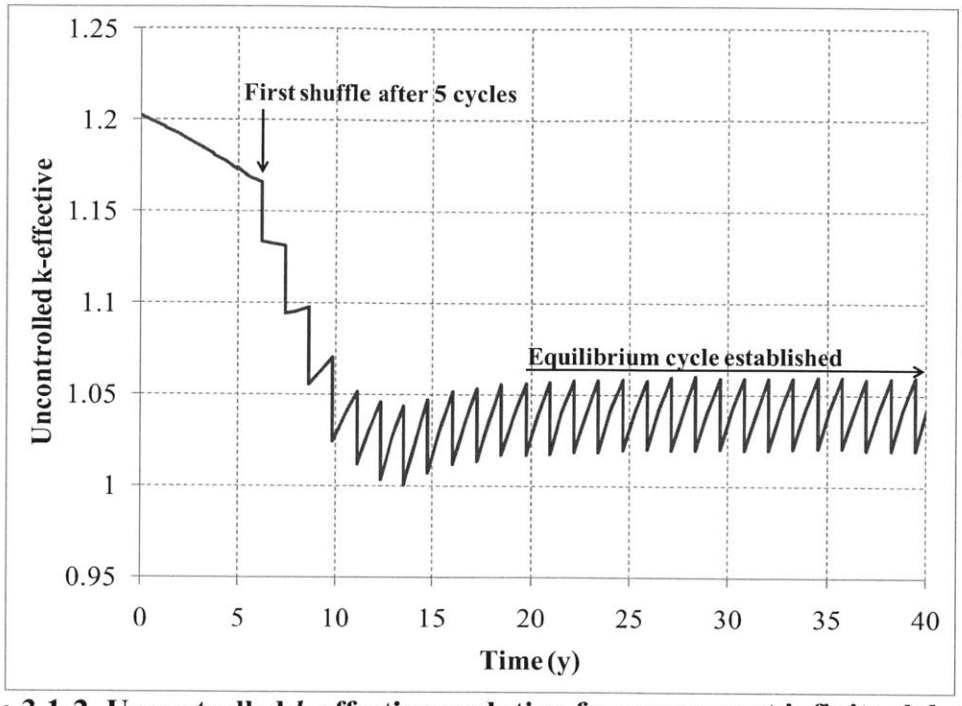

Figure 3.1-2. Uncontrolled *k*-effective evolution for convergent infinite slab model

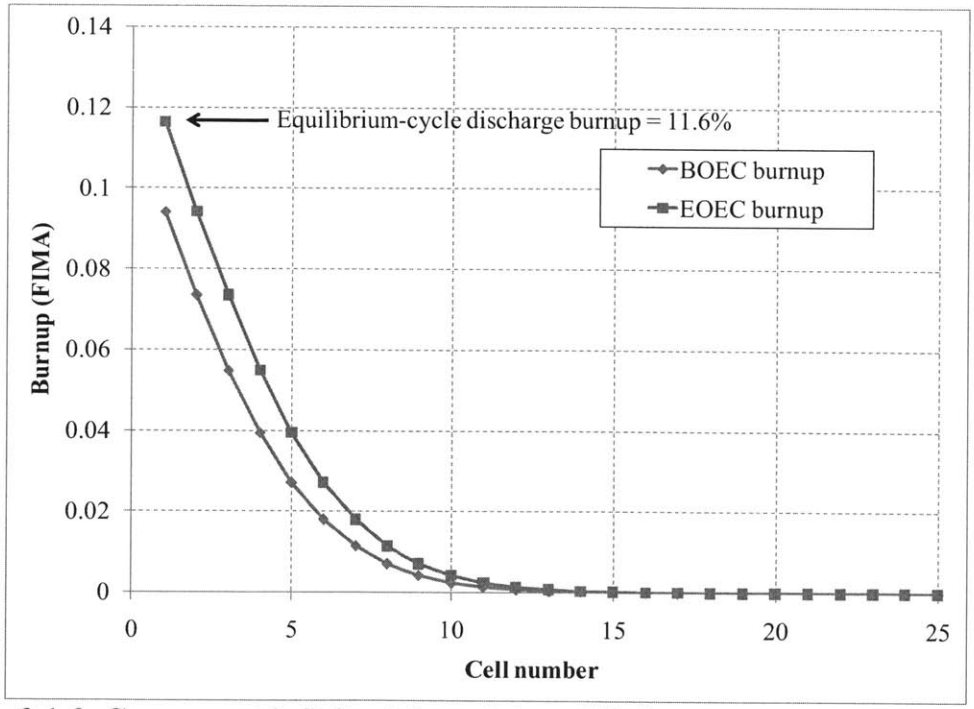

Figure 3.1-3. Convergent infinite slab model equilibrium cycle burnup distribution

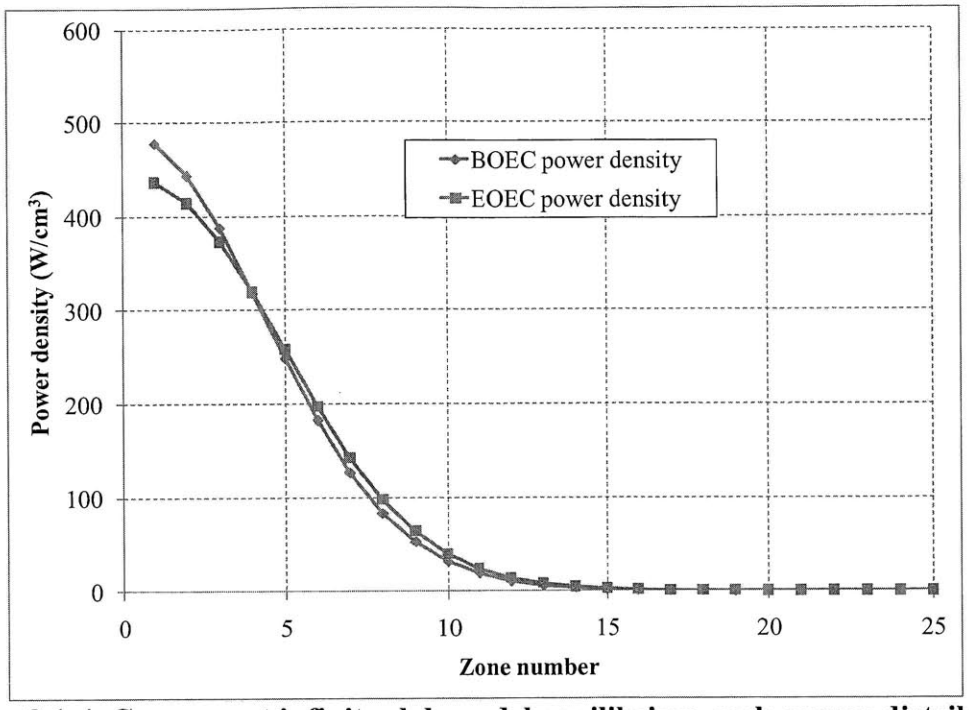

Figure 3.1-4. Convergent infinite slab model equilibrium cycle power distribution

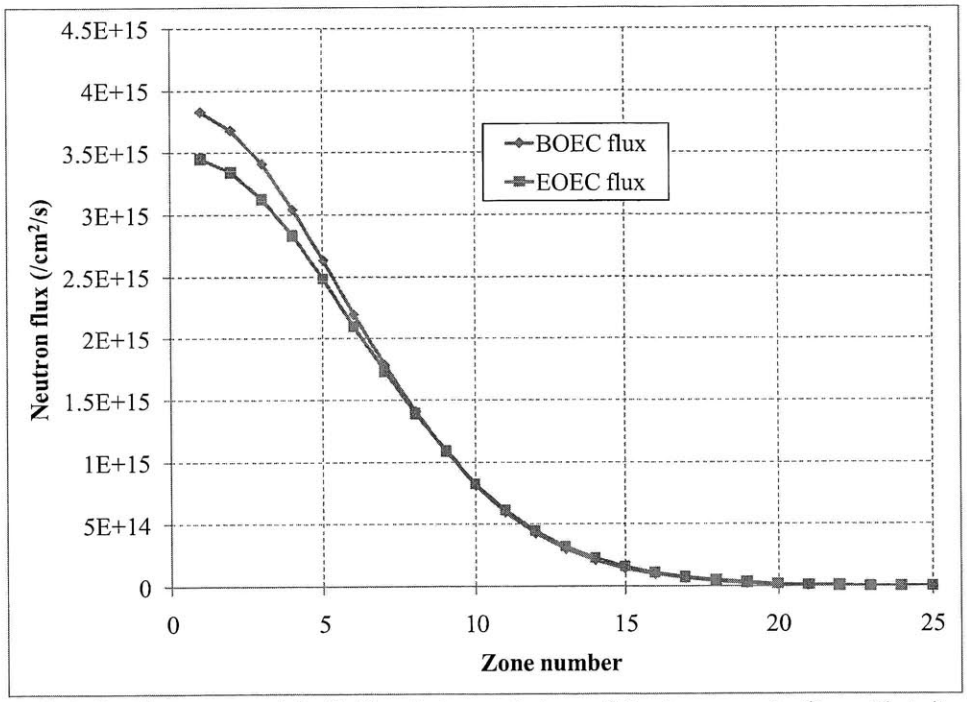

Figure 3.1-5. Convergent infinite slab model equilibrium cycle flux distribution

Because of the insensitivity to power level, the equilibrium cycle state effectively only depends on the ratio of the power level to the cycle length, which determines the discharge burnup. In the equilibrium cycle, the rate of burnup accumulation (through fissions) is equal to the rate of burnup removal (through discharging spent fuel). The average equilibrium cycle discharge

burnup is therefore the ratio of the energy per cycle divided by the amount of heavy metal discharged per cycle. In the convergent infinite slab model this is:

Energy per cycle = 120 MW*450 days = 54,000 MWd/cycle
HM per cycle = (100 cm)^2*5 cm*9.5 g/cc = 475 kgHM/cycle
Equilibrium cycle discharge burnup = 54,000 MWd/475 kgHM = **113.7 MWd/kgHM**
= **11.6% FIMA**

Values for discharge fast fluence or material damage can also be obtained from the model. This amount of burnup corresponds to a total fast fluence (>0.1 MeV) of 6.3E23 /cm^2, and 255 displacements per atom (DPA, a measure of irradiation damage on materials) when calculated using DPA cross sections for HT9 stainless steel. Chapter 5 provides a more in depth description of DPA and how DPA values are calculated.

This simple example method of initiating the equilibrium cycle state is suboptimal in terms of fissile resource usage. First, Figure 3.1-6 shows the discharge burnup of the first 30 zones in the convergent infinite slab model. The discharge burnup of the starting fissile fuel varies from 11.6% to 16.6%, which means that some fissile fuel is either being underutilized, or some is being overutilized by being burned past its permitted burnup limit. Meanwhile, Figure 3.1-2 shows that the model begins with significant excess reactivity, which according to the conclusions from Section 2.4 means that a reduction in starting fissile inventory is possible. Section 3.4 gives an example of a transition sequence that has a uniform starter fuel burnup and minimizes excess reactivity in the transition cycles.

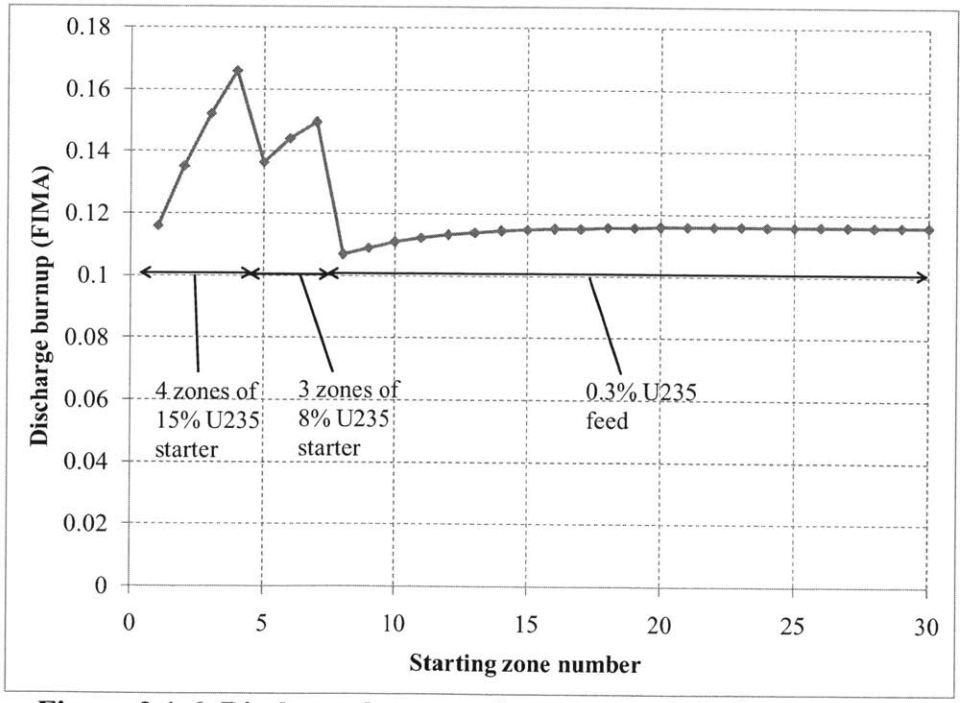

Figure 3.1-6. Discharge burnup of convergent infinite slab model

Figure 3.1-7 gives a plot of the neutron excess quantities of the equilibrium cycle feed fuel in the convergent infinite slab model. The curve shows the evolution of the neutron excess (ΔN) as a

function of the number of neutrons absorbed (ΔA); this type of curve is referred to in this thesis as a "neutron excess curve". As Equation 2.3-3 states, the average k_{fuel} of the equilibrium cycle is given by one plus the slope of the line through the endpoint of the neutron excess curve. Since this is an uncontrolled model with no leakage, k_{fuel} is equivalent to the measured k-effective (as seen in Equation 2.3-6). Therefore, based on Figure 3.1-7, the predicted average equilibrium cycle k-effective is 1.041, which exactly matches the reactivity measured in the model as shown in Figure 3.1-2. Being able to determine reactivity in this way is useful because it is possible to use the neutron excess curves from simple models (such as this infinite slab model) to approximate the neutron excess curves of more realistic reactor configurations. More examples of neutron excess curves from different models are provided in the following sections.

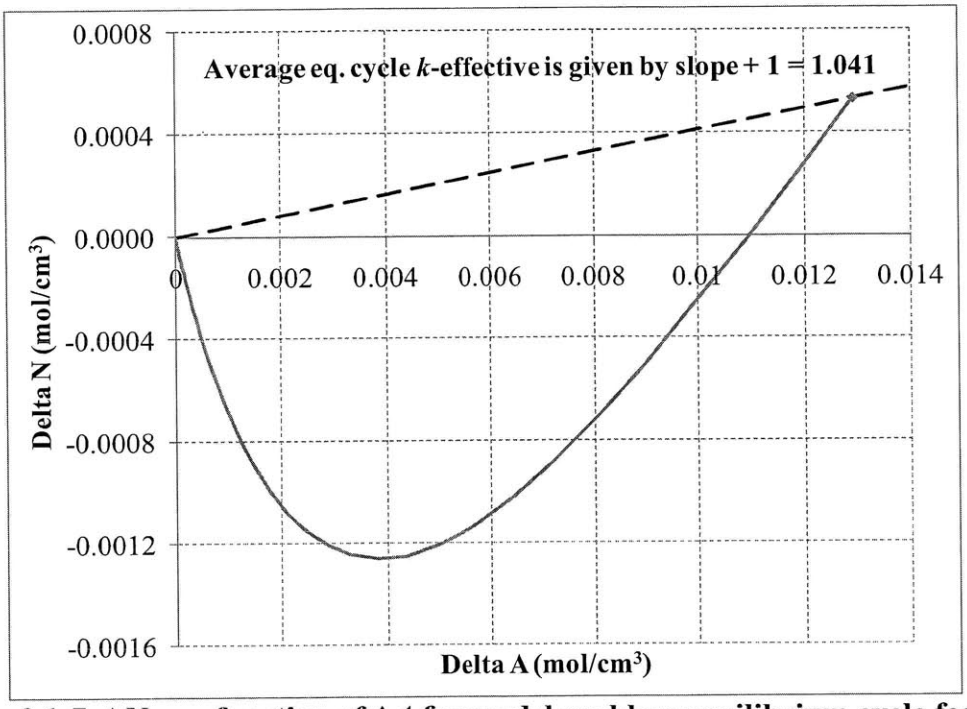

Figure 3.1-7. ΔN as a function of ΔA for model problem equilibrium cycle feed fuel

3.1.2 Example models with different cycle lengths

Additional infinite slab models were constructed with 1 cm and 2 cm slab thicknesses, to compare to the 5 cm convergent infinite slab model. In each case, as before, each slab is moved stepwise toward the center, with the centermost slab discharged and a fresh slab added to the outside. The net volume flow rate and power were kept constant at 5 cm per 450 days and 120 MW/m^2 respectively. As a result, the 1 cm, 2 cm, and 5 cm slab problems have cycle lengths of 90, 180, and 450 days respectively. The zones are assumed to deplete uniformly according to the average flux experienced in each zone. In each case, the initial starting fuel consists of 20 cm of 15 at% enriched fuel, followed by 15 cm of 8 at% enriched fuel (16 cm in the 2 cm slab case), and the rest being 0.3 at% enriched feed fuel. Shuffling begins after 2250 days, using the equilibrium cycle shuffle scheme at each cycle.

The k-effective evolution for these cases is given in Figure 3.1-8. From the figure, one sees that the overall reactivity evolution is similar in each case, but with the shorter cycle length cases

having smaller reactivity swings. Each case settles into an equilibrium cycle by about year 20. A detail of the *k*-effective evolution during the equilibrium cycle is given in Figure 3.1-9; there is a slight statistical scatter ($\sigma = 0.0005$) due to the stochastic method used. The equilibrium cycle reactivity rises over a cycle and drops after each shuffle, resulting in a characteristic sawtooth shape. Table 3.1-1 lists the equilibrium cycle BOEC, MOEC, and EOEC *k*-effectives, as well as the neutron-absorption weighted average *k*-effective $\overline{k_{eq}}$ (defined in Equation 2.3-14) for each case. As shown in Figure 3.1-9, the MOEC *k*-effectives are very close to values of $\overline{k_{eq}}$, which equal 1.041 in each case. Table 3.1-1 also shows that the average rate of change in *k*-effective is the same for each case, so the total change in *k*-effective over a cycle is proportional to the cycle length.

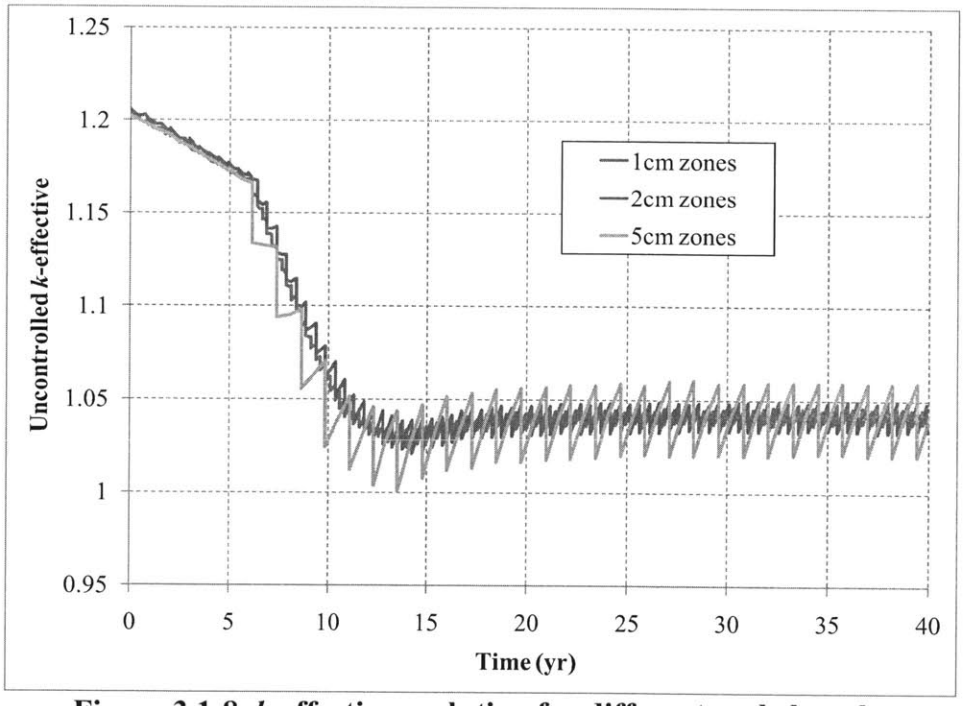

Figure 3.1-8. *k*-effective evolution for different cycle lengths

Table 3.1-1. Equilibrium cycle reactivity parameters for different zone size/cycle lengths

	1 cm zones	2 cm zones	5 cm zones
BOEC k-effective	1.038	1.033	1.021
MOEC k-effective	1.042	1.042	1.042
EOEC k-effective	1.045	1.049	1.059
$\overline{k_{eq}}$	1.041	1.041	1.041
Cycle length (days)	90	180	450
Cycle reactivity swing	0.008	0.016	0.039
Reactivity swing relative to 1 cm case	1.00	2.01	5.04

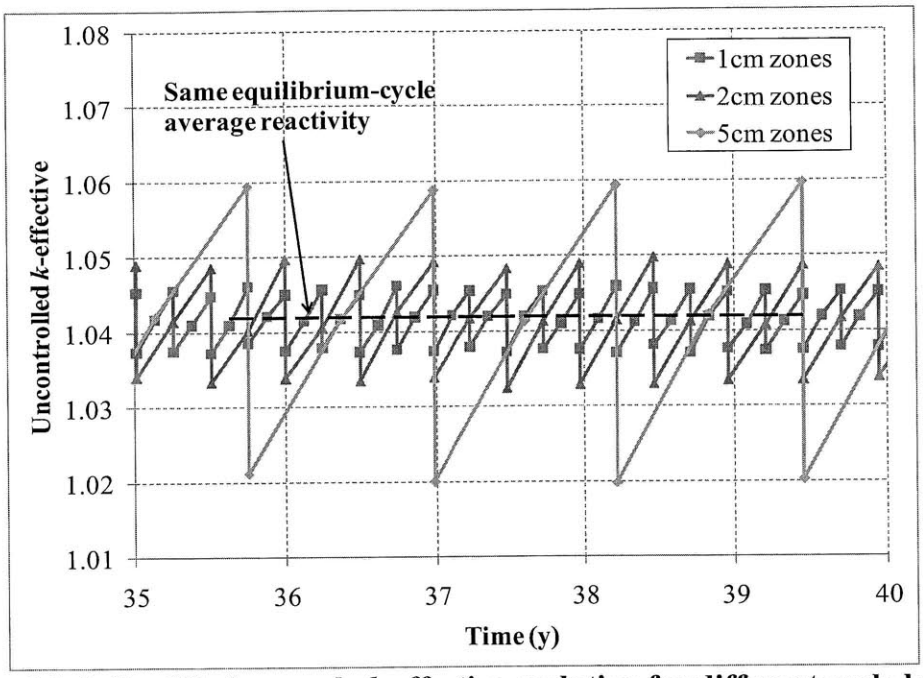

Figure 3.1-9. Equilibrium cycle *k*-effective evolution for different cycle lengths

The neutron excess curves for the three cases with different cycle lengths are shown in Figure 3.1-10. As the figure shows, the three curves all lie exactly on one another, so the neutron excess quantities do not depend on the cycle length of the model. This is explained by the fact that each model has essentially the same burnup and flux distributions, so the fuel evolves in the same manner in each case. As a consequence, the endpoint of each neutron excess curve is the same, and each case has the same discharge burnup and equilibrium cycle average *k*-effective, as given in Table 3.1-1.

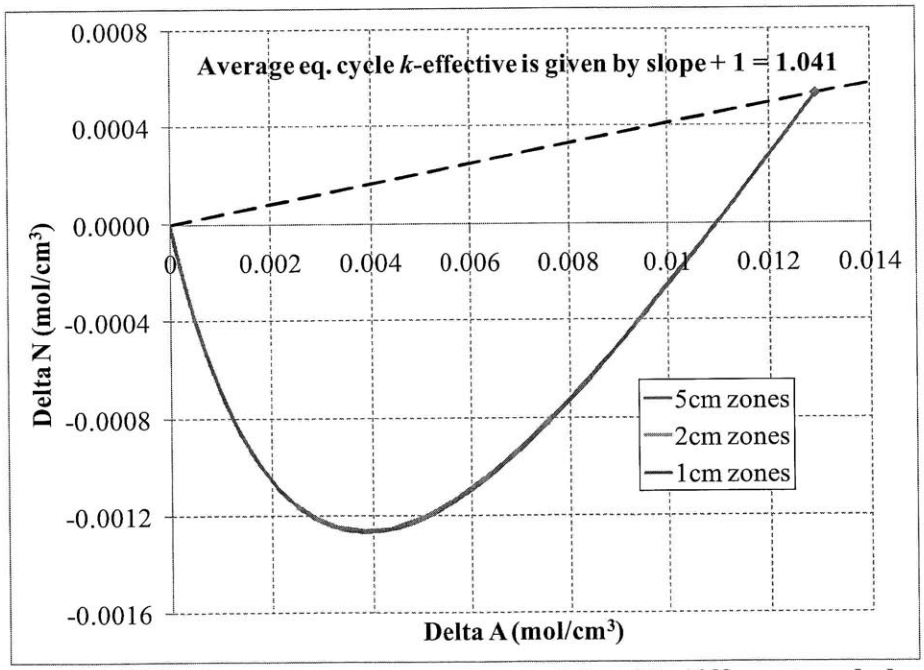

Figure 3.1-10. Neutron excess curves for models with different cycle lengths

3.1.3 Effect of burnup discharge distributions

All the examples so far have had a uniform discharge burnup, i.e. all feed fuel during the equilibrium cycle is assumed to exit at a fixed burnup level after undergoing an identical fuel history. In realistic reactor systems, uneven distributions in burnup arise for several reasons. First, fuel shuffling typically moves around batches of fuel assemblies, rather than moving every assembly by one space incrementally each cycle. As a result, each assembly in a batch encounters a slightly different fuel history, and may be discharged at a slightly different burnup. Second, gradients in a flux distribution can result in uneven burnup within a fuel assembly. For axially-segmented fuel assemblies that can be rearranged both axially and radially in a core (i.e., a minimum-burnup B&B reactor), these burnup gradients can be flattened in all three dimensions by appropriately repositioning fuel assemblies in locations where flux gradients run counter to their burnup gradients. For assemblies that are a single piece in the axial dimension, this flattening can only be done along the horizontal dimensions, by appropriately rotating the assembly during fuel shuffling. The inability to rearrange assemblies axially can result in a highly peaked axial burnup distribution, which is considered in Chapter 6. This subsection gives an example having a fairly uniform discharge burnup distribution, corresponding to a distribution that would arise in a minimum-burnup B&B reactor.

The example case considered is similar to the 5 cm infinite slab problem, but with each 5 cm slab resolved into 5 separately depleting 1 cm zones. The problem is run at the same constant power and cycle length. At the end of each cycle, the five innermost zones are discharged, and each zone n is replaced by the material in zone $n+5$. This results in five slightly different fuel histories, one for fuel that passes through zones 1, 6, 11, 16, ... 5n+1, one for fuel that passes through zones 2, 7, 12, 17, ... 5n+2, and so on. The k-effective evolution of this finely resolved problem is given in Figure 3.1-11 along with that from the original 5 cm zone model. It lies exactly on top of the k-effective curve from the original model with 5 cm zones, showing that modeling depletion homogenously has a minimal effect on measured k-effective.

The neutron excess curves for the five depletion histories in the 1 cm zone case are shown in Figure 3.1-12. The fuel histories lie on top of each other but have different endpoints corresponding to differences in discharge burnup; even though the *average* discharge burnup is still 113.7 MWd/kg, the *peak* burnup is now 122.5 MWd/kg. According to Equation 2.3-15, the average k_{fuel} (equal to k-effective in this uncontrolled model) minus one is equal to the ratio of the *average* discharge ΔN to the *average* discharge ΔA, which is the slope of the line through the centroid of the endpoints in Figure 3.1-11. For a small spread in discharge burnup, this centroid lies very close to the ΔN curve for the average burnup, i.e.:

$$\overline{k_{eq}} = \frac{\overline{\Delta N(burnup)}}{\overline{\Delta A(burnup)}} + 1 \cong \frac{\Delta N(\overline{burnup})}{\Delta A(\overline{burnup})} + 1 \qquad (3.1\text{-}1)$$

This approximation is appropriate for differences in burnup over which the ΔN curve is approximately linear, such as the difference in burnup across the width of an assembly or within an axially-segmented fuel element. One implication of Equation 3.1-1 is that to minimize peak burnup in a B&B reactor, it is desirable to minimize the burnup peaking factor of the discharged fuel, since the equilibrium cycle k-effective depends on the *average*, not the peak burnup.

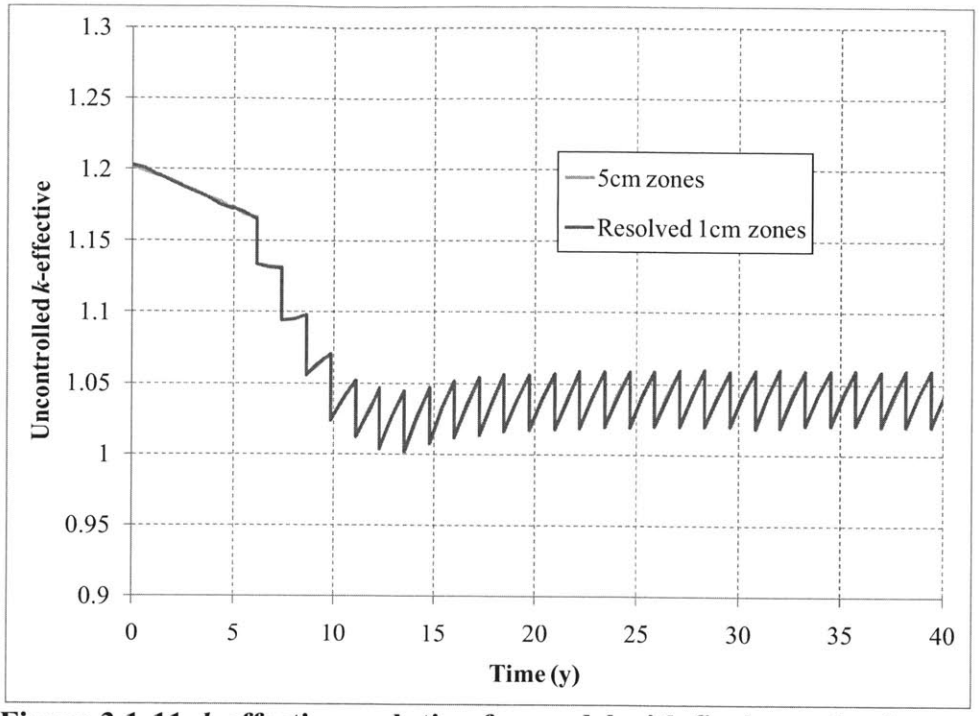

Figure 3.1-11. *k*-effective evolution for model with finely resolved zones

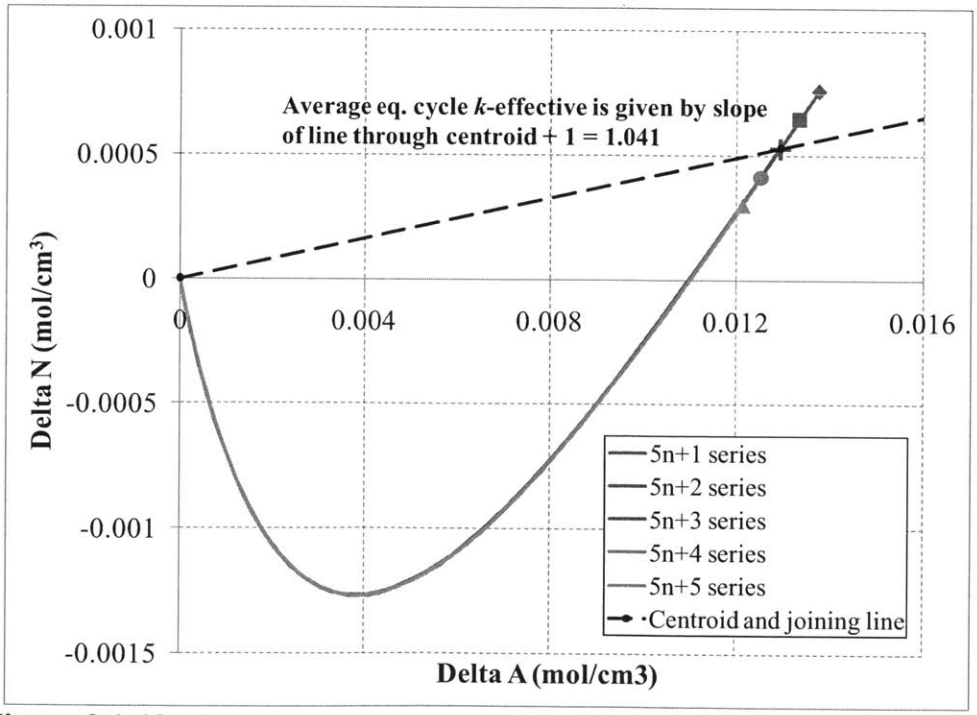

Figure 3.1-12. Neutron excess curves for model with finely resolved zones

The approximation in Equation 3.1-1 does not hold if the spread in ΔA is large for the collection of histories in question. For example, in a linear fuel assembly in which the axial ends are burned much less than the axial center, the equilibrium cycle reactivity would not be the same as if the assembly had burned uniformly to the same average burnup. The average burnup

approximation would apply to the radial distribution in such an assembly; i.e. one could assume that each assembly burns evenly in a radial direction and arrive at the same equilibrium cycle reactivity. However, in such a case a pin peaking factor would need to be applied to the assembly average peak burnup to determine the peak pin burnup in the assembly.

3.2 Effect of geometry and shuffling sequences

Section 2.3 discusses some basic ways in which the neutron excess concept can be applied to non-ideal systems with discrete fuel elements, and Section 3.1 showed some infinite slab models that confirmed the ideas developed in Section 2.3. However, while an infinite slab model is simple and illustrative, it bears fairly little resemblance to a realistic reactor model. In order for the infinite slab models in Section 3.1 to be useful as a design tool, it must be possible to relate its results to those from models with more realistic geometries. This section discusses some alternative geometry models and also investigates the effect that different equilibrium cycle shuffling sequences have on the evolution of neutron excess quantities.

3.2.1 Burnup-reactivity relationships for different geometry models

In addition to the infinite plane model, three other geometries were modeled: two more one-dimensional models (cylindrical shell and spherical shell), and one three-dimensional model (stacked cubes). The cylindrical shell model consists of 100 cylindrical shells that are infinite in the z direction, each with area 400π cm^2. The outer radius of the innermost and outermost shells are 20 cm and 200 cm respectively, and the equilibrium cycle shuffle sequence also consists of removing the center zone and marching every other zone inwards. The spherical shell model consists of 216 spherical shells each with volume $256000\ \pi /3$ cm^3, so the inner and outer spheres have radii of 40 cm and 240 cm respectively, and also uses a convergent shuffling sequence.

The three-dimensional cube model consists of 343 cubes (7 x 7 x 7) making up an octant of a larger cube (i.e., the boundaries around one corner are reflective, while the other three are vacuum boundaries). Each cube has 30 cm sides. As with the other cases, the equilibrium shuffle sequence consists of removal of the central cube (the cube adjacent to all three reflective boundaries) and moving all the other cubes sequentially according to their distance from this cube. Like the spherical shell model, the cube model also occupies a finite volume of space; in addition, each of the fuel elements is the same shape, so the cube model could in principle be built and have its fuel shuffled. The relatively large size of these models (e.g. the 4.2 m cube) is simply to ensure that leakage is essentially zero; however this does not mean that an actual reactor requires such a size to have negligible leakage (B&B reactor size is discussed in Section 3.3). The material composition assumed for each model is the same as in the infinite slab model: 50 volume % depleted uranium metal fuel, 30% sodium coolant and 20% iron structure.

The neutron excess curves for the four different geometries considered are plotted in Figure 3.2-1, for the same equilibrium cycle discharge burnup of 113.7 MWd/kgHM. The figure shows that there are only minor variations in the curves between the different geometries, and furthermore since the endpoints all coincide, each curve has the same discharge $\Delta N/\Delta A$ ratio and the same equilibrium cycle average k-effective of 1.041. Even though the four different models have

markedly different burnup, flux, and power distributions, the fact that the fuel evolves in a similar manner in each case means that they all share the same reactivity-burnup relationship. Thus, the use of neutron excess quantities allows a very simple model such as 1D infinite slabs to predict the *k*-effective of a realistic 3D model.

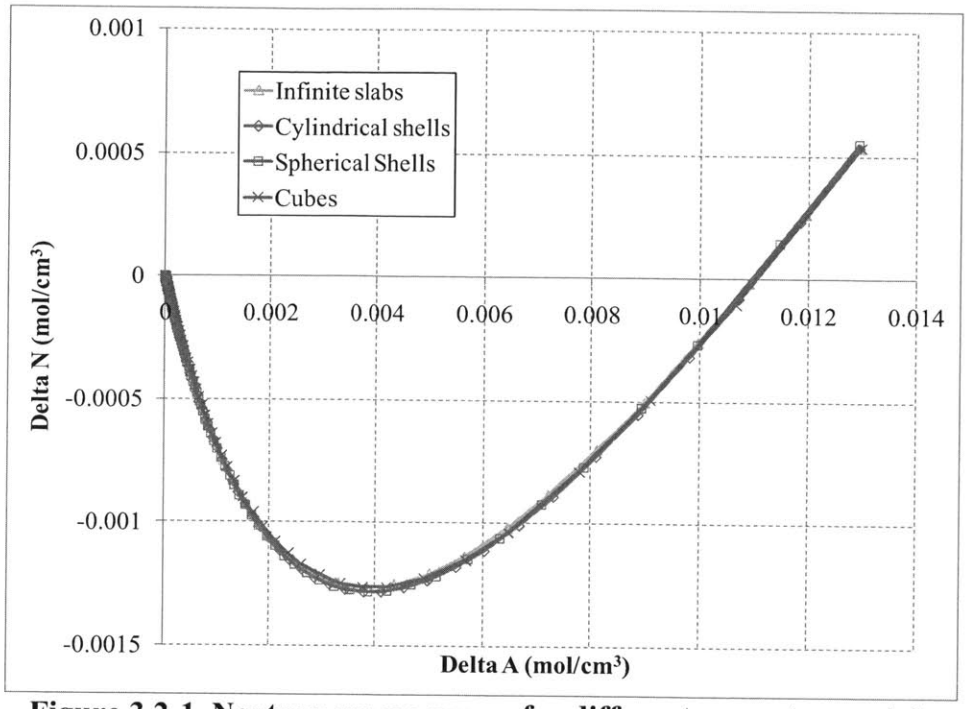

Figure 3.2-1. Neutron excess curves for different geometry models

3.2.2 Effect of different shuffling sequences in an infinite slab model

All the models considered so far have shuffled fuel convergently toward a central discharge point. This shuffling scheme concentrates bred fuel in the center, and as Figure 2.3-4 previous showed, this causes the power distribution to be highly peaked. Using a different equilibrium cycle shuffling scheme can be used to shape the power distribution and achieve other desirable effects, such as minimizing the cycle reactivity swing.

Fuel management is one of the most challenging topics in the design and understanding of B&B reactors, simply because of the enormous number of possible fuel management schemes. Even considering just equilibrium cycles, a reactor with N zones will have $N!$ different possible shuffling paths through it. To further complicate matters, B&B reactors generally have higher values of N than conventional fast reactors. This is because breed-and-burn reactor feed fuel (particularly fertile-only feed) needs to have longer residence times in order to allow for the breeding of fissile material. Since the number of batches N goes as fuel residence time divided by cycle length, a B&B reactor with a standard cycle length but a higher fuel residence time will contain more fuel batches.

The number of possible shuffling patterns increases tremendously when one considers permutations of fuel assemblies within a zone and the possibility of multiple shuffling paths. Each shuffling option yields a reactor with different performance characteristics. There are

many important reactor operating parameters that can be used in evaluating an equilibrium cycle shuffling arrangement in a B&B reactor. These include:

1) Middle of cycle (average) *k*-effective
2) Minimum *k*-effective and reactivity swing
3) Number of shuffling operations per cycle
4) Peak burnup, DPA, and fluence experienced
5) Power peaking factors (both radial and volumetric)
6) Change in power distribution over a cycle
7) Minimum size required to support breed and burn operation
8) Feed fuel residence time
9) Fissile requirement to initiate a given equilibrium state

Many of these parameters are related; for example, fuel residence time is proportional to reactor size and inversely proportional to total power, which in turn depends on the power peaking factors. Evaluating these performance parameters for the tremendous number of available shuffling schemes is computationally prohibitive, and because they generally do not vary in easily predictable manners, it becomes a very difficult problem to determine the optimal shuffling scheme for a system. For example, past work on B&B reactors has applied genetic algorithms to optimize two parameters, peaking factor and reactivity swing [Toshinsky, 2000]. Even though this work used a highly simplified model with 14 fuel zones, the resulting shuffling schemes were very complicated.

This subsection examines a number of one-dimensional equilibrium cycle shuffling sequences to determine their effect on the nine parameters listed above, and Section 3.7 examines a number of realistic three-dimensional sequences. Reactivity swing, minimum size, and feed fuel residence time are investigated in Section 3.3, and an example for computing an equilibrium cycle's fissile requirement is given in Section 3.5.

Example shuffling cases in the infinite slab model

Ten different shuffling patterns were investigated in the 5 cm infinite slab model. A summary of the different sequences is given here, with more details and results given in Appendix A.1. The most important analysis and results are presented in this subsection.

Sequence 1: Simple inward convergent shuffling; fuel is sequentially shuffled inward. Results in the most highly peaked power and flux distributions.

Sequence 2: Fuel is sequentially shuffled inward to zone 11, and then skips to zone 1 and sequentially shuffled back out to zone 10; this is referred to as a "convergent-divergent" sequence. Results in a flattened smoothly varying power distribution.

Sequence 3: Fuel is sequentially shuffled inward to zone 21, skips to zone 10, inwardly shuffles to zone 1, then skips back out to zone 11, where it is outwardly shuffled to zone 20 and discharged. Results in a still flatter power distribution than Sequence 2.

Sequence 4: Fuel is shuffled inward through alternate zones starting from zone 20, then partly-bred fuel is shuffled back outward to the lower power feed region. This places the most burned fuel in a softer spectrum.

Sequence 5: Fuel is shuffled inward through alternate zones starting from zone 20, the partly-bred fuel is then sent back outward for another inward pass. This moves the fuel from a hard to a soft spectrum halfway through depletion.

Sequence 6: Fresh fuel spends one cycle in the high-flux centermost zone, then is shuffled all the way outward and convergently shuffled back to the center, so that partly bred fuel acts as the surrounding blanket.

Sequence 7: Similar to Sequence 6, except fresh fuel spends two cycles in the two centermost zones before being shuffled convergently.

Sequences 8, 9, and 10: Each of these sequences begins with convergent shuffling up to zone 21, after which fuel is shuffled through one of three random permutations of the first 20 zones. These sequences test whether the conclusions reached can be generalized to arbitrary shuffling patterns.

These different sequences were selected to explore a range of different equilibrium cycle behaviors. Total power (120 MW/m^2) and cycle length (450 days) were kept constant, so the average discharge burnup of 113.7 MWd/kg is the same in each case.

Figure 3.2-2 shows the end of equilibrium cycle power distributions for selected shuffling sequences, with sequence 1 being the original convergent shuffling sequence. The figure shows that a great deal of control over the equilibrium cycle power distribution can be achieved simply by changing the equilibrium cycle shuffling sequence. Importantly, changing the shuffling sequence can be used to flatten the power distribution and allow higher power operation. The ability to control the power distribution in this manner allows B&B reactors to be designed with different sizes and power levels, an idea that is explored further for more realistic 3D systems in Section 3.7 and Appendix 4.

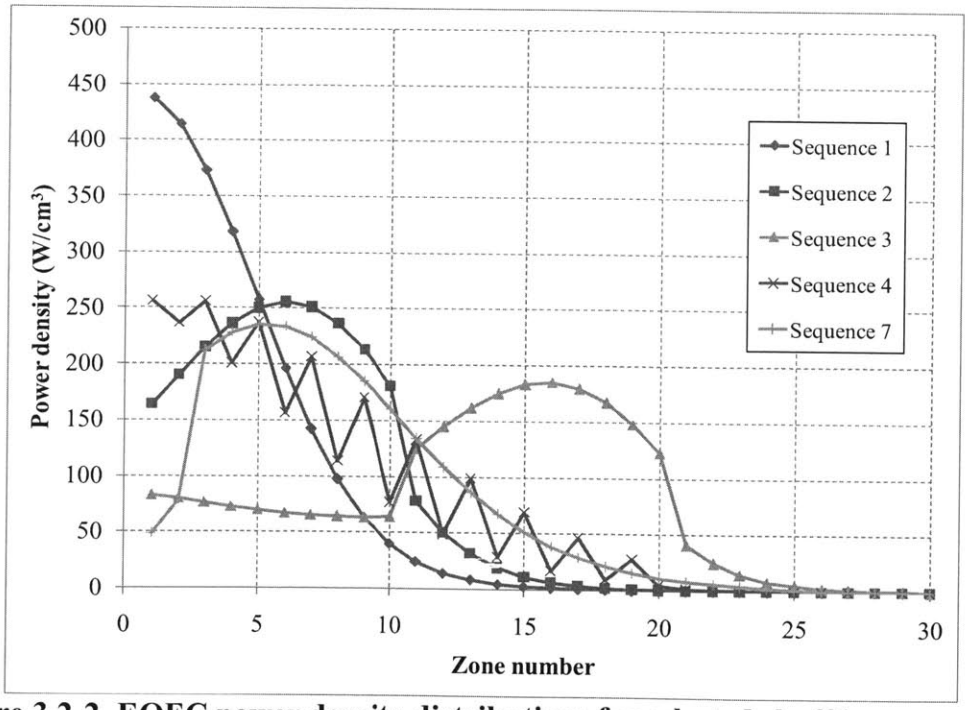

Figure 3.2-2. EOEC power density distributions for selected shuffling sequences

One important point to note is that it is in principle possible to establish any given equilibrium cycle configuration using only fresh fuel. This can be done by simulating equilibrium cycle conditions by using the correct distribution of fissile fuel and absorbers that simulate the presence of fission products, then immediately adopting the equilibrium cycle shuffling scheme. This equilibrium cycle simulating approach has been used to design startup sequences for the CANDLE B&B reactor [Sekimoto, 2010], which shows that *k*-effective can be made to deviate a very small amount from the equilibrium cycle value. The downside to taking this approach is that it causes starter fuel to be discharged early (starting with the first cycle), before it reaches its fuel burnup limit, so there is suboptimal usage of fissile fuel. Section 3.5 gives two examples of other ways to initiate an equilibrium cycle that use shuffling to achieve near optimal utilization of fissile starter fuel.

The most important result from the different shuffling sequences is how their average equilibrium cycle *k*-effectives compare to one another. The equilibrium cycle *k*-effective data for each sequence is given in Table 3.2-1. The table shows that the average k_{eq} for the different sequences range from 1.027 (sequence 4) to 1.041 (sequence 1). This is a remarkably close agreement considering the extremely different power, flux, and material distributions in each of the different cases. The MOEC *k*-effectives are very close to average k_{eq} in each case, differing by at most 0.2%.

Table 3.2-1. Equilibrium cycle *k*-effectives for different shuffle sequences (± 0.001)

Sequence #	1	2	3	4	5	6	7	8	9	10
BOEC *k*-effective	1.021	1.016	1.028	1.002	1.008	1.012	1.018	1.009	1.016	1.021
MOEC *k*-effective	1.042	1.039	1.039	1.029	1.034	1.036	1.036	1.032	1.034	1.035
EOEC *k*-effective	1.059	1.058	1.048	1.051	1.054	1.055	1.052	1.051	1.049	1.049
Δ*k*-effective	0.038	0.042	0.020	0.049	0.046	0.043	0.034	0.042	0.033	0.028
$\overline{k_{eq}}$	1.041	1.038	1.038	1.027	1.032	1.035	1.035	1.031	1.033	1.035

The similarity between the average equilibrium cycle *k*-effective of the different cases can be explained by looking at their respective feed fuel neutron excess curves, shown in Figure 3.2-3. The endpoints of all the curves lie within a small range, resulting in the average *k*-effectives differing by less than 1.5% across all cases. There is a larger variation between the different curves around the minima of the curves at a ΔA of 0.004 mol/cm^3, but this gets mostly canceled out by the endpoint. Sequences 1, 2, 3, 6, and 7 all display similar neutron excess evolutions, sequences 4 and 5 diverge the most from the simple convergent case, and the sequences 8, 9, and 10 (which were randomly generated) fall in between these two groups.

The differences between the neutron excess curves in Figure 3.2-3 can be explained by looking at the feed fuel k'_∞ evolution for the different sequences. The quantity k'_∞ was defined in Equation 2.1-4, and is the ratio of neutron production to absorption in a material, corresponding to one plus the derivative of the neutron excess curve. The value of k'_∞ for a material depends on both the material composition and what spectrum it is placed in. The k'_∞ curves for shuffling sequences 1, 4, and 5 are shown in Figure 3.2-4. In the figure, the curve for sequence 5 gives the

best evidence that neutron spectrum plays an important role: moving the fuel zone from a fast spectrum at the midplane (zone 2) to a softer spectrum far from the midplane (zone 19) causes the $k_{\infty}^{'}$ of the fuel to change from 1.13 to 0.92 (at ΔA of about 0.055), even though the composition of the fuel does not change.

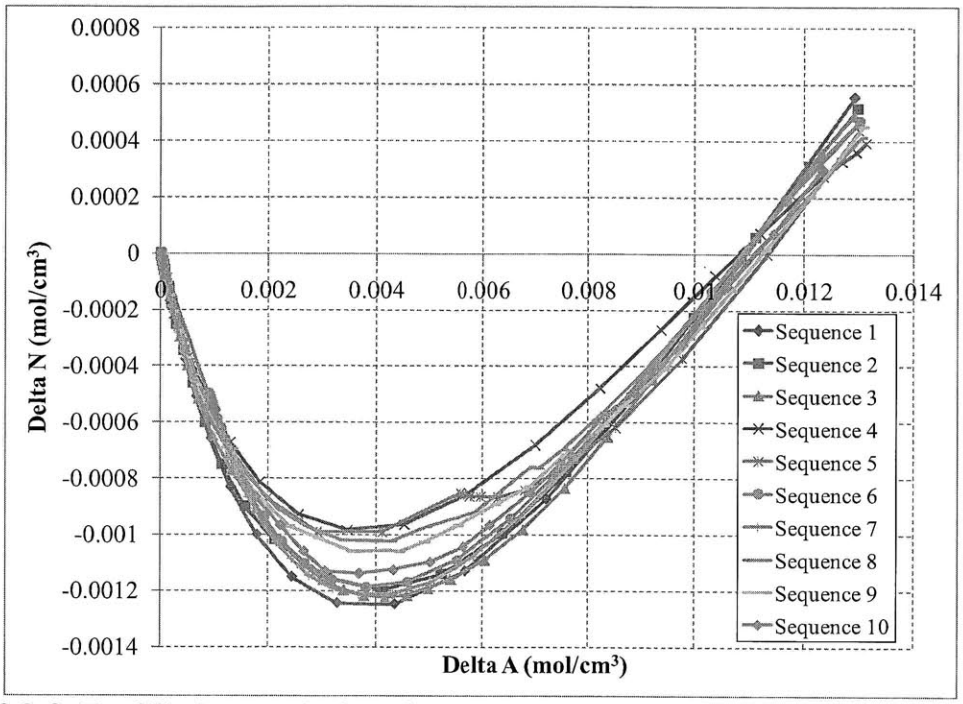

Figure 3.2-3. Equilibrium cycle feed fuel neutron excess curves for different shuffling sequences

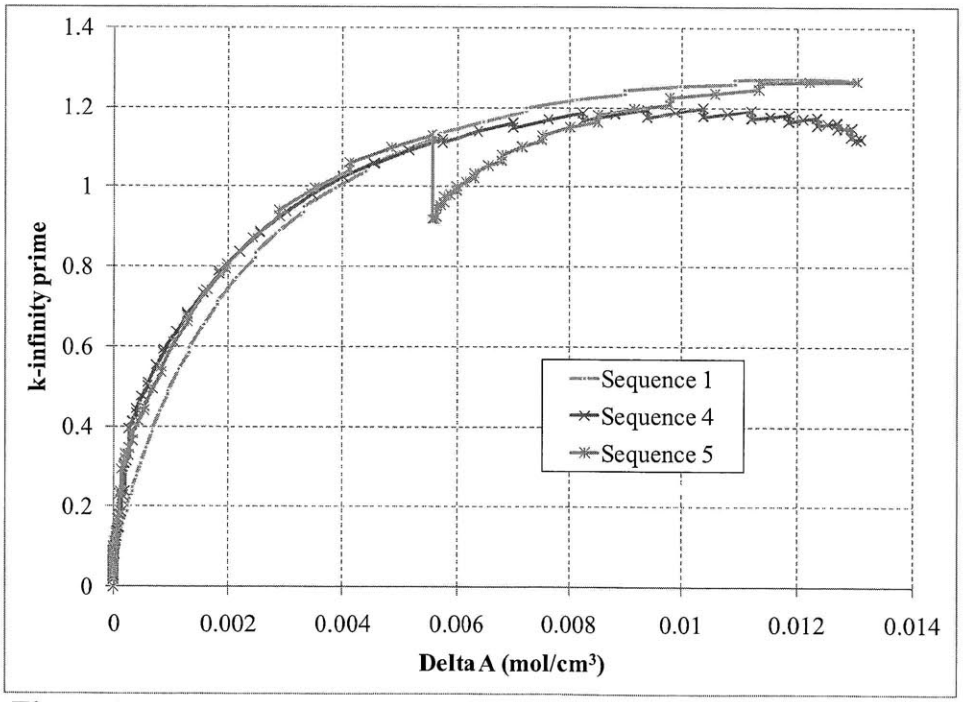

Figure 3.2-4. Neutron excess curves for different shuffling sequences

Even though differences in neutron spectra cause the different k'_∞ curves to have different shapes, the average value of each curve is roughly equal, causing the neutron excess curves to have roughly the same endpoint and resulting in about the same average reactivity. The reason the k'_∞ curves average to roughly the same value is because decreases in k'_∞ due to a softer spectrum are offset by increases in k'_∞ where the spectrum is harder. This occurs because the flux-averaged equilibrium cycle neutron spectrum is weakly dependent on shuffling path; i.e. changing the shuffling path will not raise or lower the average neutron energy in a system significantly. This is expected in a fast system because the average scattering cross section is much higher than the average absorption cross section. For example, at the midplane of the convergent infinite slab model, the total macroscopic elastic scattering cross section is 0.31 cm^{-1}, 36 times higher than the total absorption cross section of 0.0087 cm^{-1}. As a result, each neutron scatters dozens of times on average before being absorbed, and the average neutron energy is primarily a function of how much scattering takes place, which does not change significantly with fuel depletion. Changes in absorption cross section that accompany fuel depletion are small and have only a minor effect on the overall neutron spectrum. This behavior can be observed by plotting the fluence spectra of the discharged fuel for the different shuffling sequences, as done in Figure 3.2-5.

The data for Figure 3.2-5 are for the 63 energy group structure used in Cinder90. The curves lie almost exactly on one another, with small differences in the low energy region, where fluences are about 4 orders of magnitude below the peak fluence. Overall, the fluence spectra match extremely well; Table 3.2-2 shows that the fast fluence fraction (>0.1 MeV) in the different shuffling sequences matches to within 0.2%. The sequences with lower average *k*-effective (e.g. sequence 4) have slightly higher total fluences. This is because fuel in those sequences experiences a softer spectrum later in life, reducing the average fission cross section and increasing the total fluence needed to produce the desired discharge burnup.

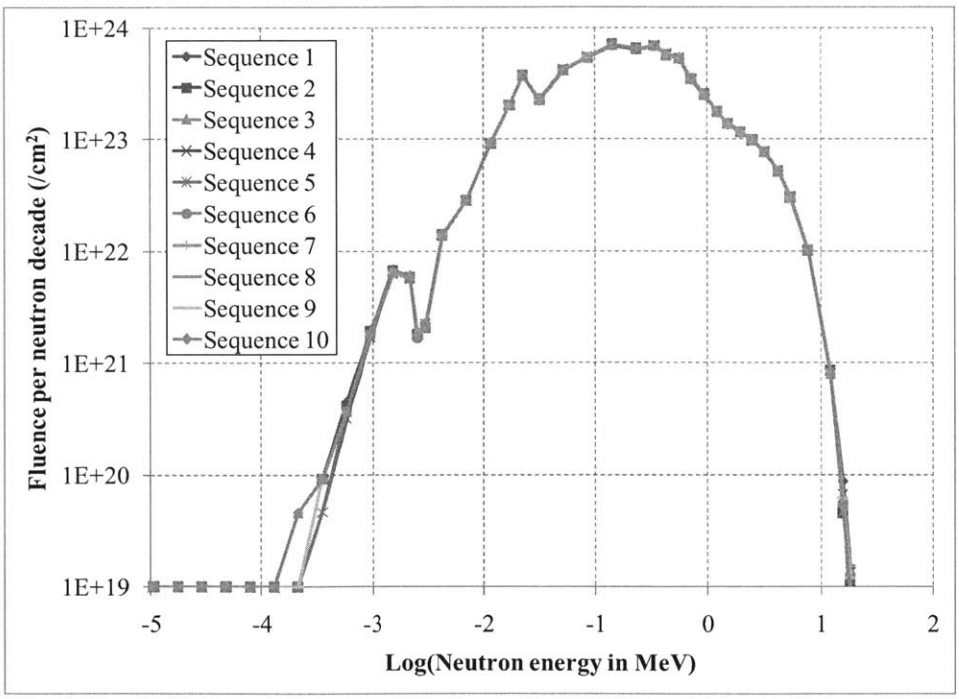

Figure 3.2-5. Neutron fluence spectra for different shuffling sequences at discharge

Table 3.2-2. Discharge fluence for different shuffle sequences

Sequence #	1	2	3	4	5	6	7	8	9	10
Total fluence	9.761E +23	9.792E +23	9.878E +23	9.938E +23	9.875E +23	9.837E +23	9.824E +23	9.925E +23	9.876E +23	9.852E +23
Fast fluence (>0.1 MeV)	6.523E +23	6.546E +23	6.605E +23	6.652E +23	6.609E +23	6.577E +23	6.569E +23	6.639E +23	6.607E +23	6.590E +23
Fast fluence fraction	0.6682	0.6684	0.6687	0.6693	0.6693	0.6686	0.6686	0.6690	0.6690	0.6689

Figure 3.2-6 shows how the neutron spectrum changes as a function of ΔA as feed fuel passes through the reactor. The curves in this figure resemble the k'_∞ curves in Figure 3.2-4 because k'_∞ depends on the local spectrum encountered. The change in ΔA over a cycle is smaller when the neutron spectrum is soft, because the flux is lower in softer-spectrum regions (conversely, the flux is the highest where the neutron spectrum is hardest because that's where fission occur). For sequence 1, the neutron spectrum becomes harder as the fuel is depleted since the fuel is shuffled convergently inward. In comparison, the fuel in sequence 4 experiences a harder spectrum at the beginning of its depletion and a softer one at the end, because in that sequence, fuel is first shuffled to the center then back out toward the periphery. The soft neutron spectrum at the very end of its depletion explains why sequence 4 has the lowest equilibrium cycle k-effective. The soft neutron spectrum results in additional absorptions in actinides and fission products, which has a more detrimental effect at the end of depletion because the fission product concentration is high and additional bred Pu-239 is not fissioned. Sequence 5 displays a softer spectrum in the middle of its depletion and has an equilibrium cycle k-effective between those of sequences 1 and 4.

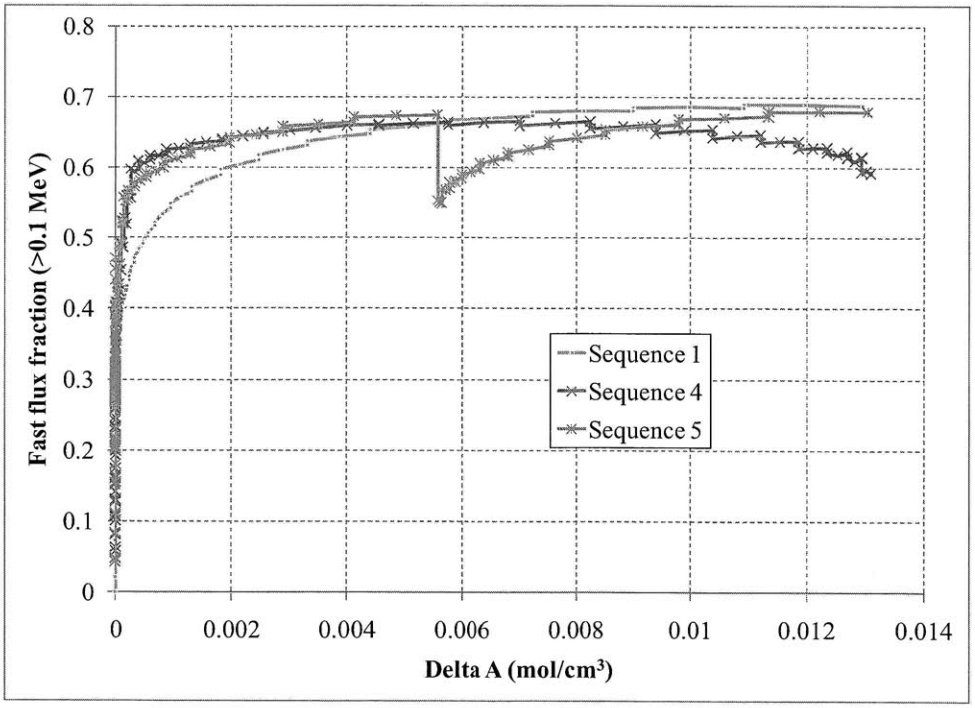

Figure 3.2-6. Fast flux fraction as a function of total neutrons absorbed

A few conclusions can be drawn from the analysis in this subsection. First, changing the equilibrium cycle shuffling path of a B&B reactor is extremely useful for setting the power distribution to a desired shape and size. Second, shuffling sequences have a small effect on average equilibrium cycle reactivity, since the fuel in each shuffling sequence experiences the same overall fluence spectrum. To maximize *k*-effective, convergent shuffling works best since it exposes the most burned fuel to the hardest neutron spectrum in the reactor. Conversely, putting the most-burned fuel into the softer spectrum at the periphery of the reactor, like with sequence 4, reduces the average *k*-effective. Fortunately, it is possible to use shuffling to produce a flattened power distribution without paying a large penalty in reactivity; for example shuffling sequences 2 and 3 significantly flatten the power distribution with only a minimal reduction in average *k*-effective. In addition to the 1D shuffling sequences considered here, Section 3.7 introduces several more realistic 3D shuffling sequences, which also support the conclusions drawn here.

3.3 Breed-and-burn reactor size and reactivity swing

In addition to neutron excess evolution, two other important reactor parameters that depend on equilibrium cycle shuffling sequence are reactor size and reactivity swing. Even though these parameters are not directly related to the neutron excess concept, they both display behaviors that are unique to B&B reactors. Subsection 3.3.1 discusses what sets the minimum size of a B&B reactor and a method of approximating it, and Subsection 3.3.2 considers the related parameter of fuel residence time. Subsection 3.3.3 discusses how different shuffling sequences affect cycle reactivity swing and what strategies can be used to minimize reactivity swing.

3.3.1 B&B reactor size

All the models of B&B reactors considered so far have included very large regions of absorbing feed fuel, in order to guarantee that effectively zero neutrons escape from the fueled region. Having this large subcritical region means that much of it sees effectively zero flux, since there is an exponential attenuation of neutrons with distance through the feed. Therefore, much of this excess feed blanket region can potentially be removed without having a detrimental effect. To examine this possibility in the convergent infinite slab model, the model was rerun with different numbers of fuel zones, retaining the vacuum outer boundary condition. The discharge burnup in each case is kept constant at 113.7 MWd/kgHM. Results for beginning, middle, and end of equilibrium cycle *k*-effectives are given in Figure 3.3-1.

Figure 3.3-1 shows that there is an asymptotic value of k-effective for a very thick blanket region. As the size of the blanket region is reduced, *k*-effective first gradually declines and then steeply drops, eventually decreasing at a rate greater than 1% per 5 cm. Below 15 fuel zones (a half-thickness of 75 cm), there is so much leakage that the equilibrium cycle is no longer critical (BOEC *k*-effective <1). This exponential relationship between k-effective and size is unique to B&B reactors. In a fast reactor that is enriched throughout, the size-reactivity relationship depends on the geometric buckling of the reactor, a term that's inversely quadratic with size. In a fast reactor with a breeding blanket, the blanket thickness affects the breeding ratio but has a minimal effect on core k-effective. However, in a B&B reactor, neutrons absorbed in the

breeding region contribute directly to future reactivity, so leakage from the breeding region affects the equilibrium cycle *k*-effective.

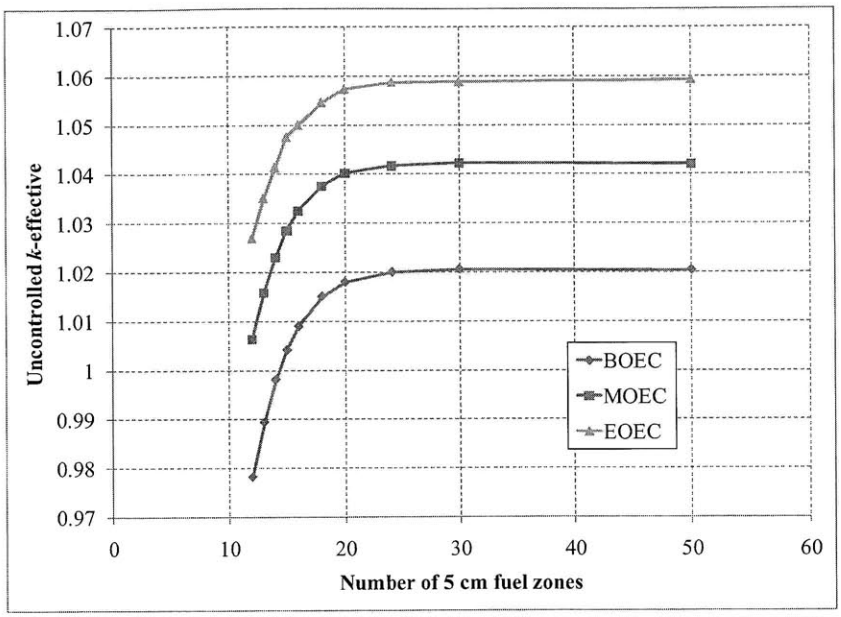

Figure 3.3-1. Equilibrium cycle *k*-effective vs. size for convergent infinite slab model

Since the equilibrium cycle feed fuel is discharged at the same burnup in each case, the discharge composition for each case yields a similar ratio of $\Delta N/\Delta A$, meaning that the average value of the k_{fuel} over an equilibrium cycle is about the same for each reactor. As shown in Equation 2.3-6, k_{fuel} can be related to the uncontrolled *k*-effective (k_{unc}); rearranging Equation 2.3-6 to solve for k_{unc} yields Equation 3.3-1:

$$k_{unc} = k_{fuel} \frac{\int_{fuel} dV \phi \Sigma_a}{\left(\int_{fuel} dV \phi \Sigma_a + \int_{leakage} dV \phi \Sigma_a \right)} \qquad (3.3\text{-}1)$$

Equation 3.3-1 shows that the difference between k_{unc} and k_{fuel} increases with increased neutron leakage. With a very thick blanket, leakage is essentially zero, so k_{unc} equals k_{fuel}. If one knows the fraction of neutrons leaking from the fuel, then one can subtract this leakage fraction from the expected k_{fuel} to obtain a predicted *k*-effective for the case with leakage.

Conveniently, neutron leakage can be estimated accurately from a model with a thick feed blanket (referred to as a "thick-blanket model"). This is done simply by calculating what fraction of neutrons is *not* absorbed within the fueled region of interest in a thick-blanket model. This approach works because the shape of the flux distribution does not change greatly when outer feed blanket elements are removed. To illustrate this, Figure 3.3-2 shows the measured MOEC *k*-effective for different size models compared to a prediction made from the thick-blanket model. The predicted curve is generated by multiplying the asymptotic *k*-effective by the fraction of neutrons that are absorbed within the first *n* zones at the middle of an equilibrium

cycle. The curve is able to accurately predict the onset and magnitude of the drop off in *k*-effective.

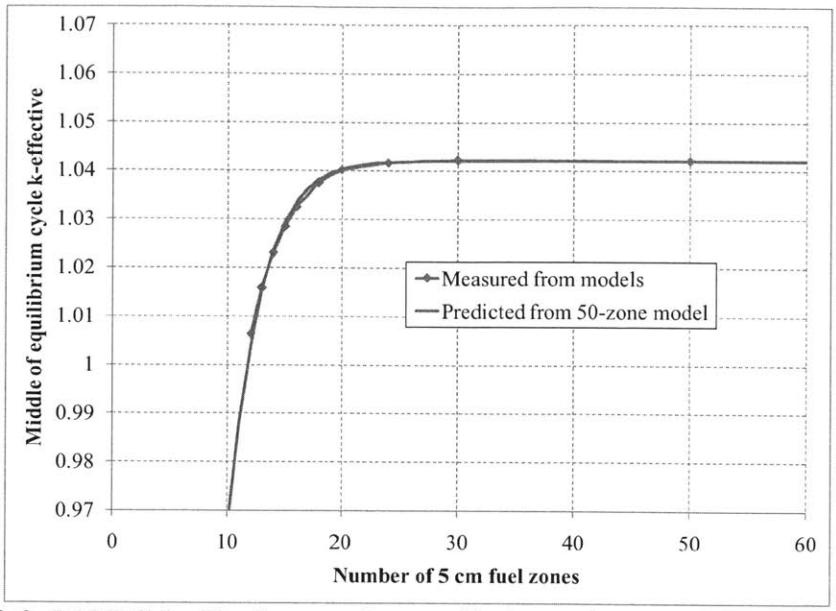

Figure 3.3-2. MOEC *k*-effective vs. size prediction using the thick-blanket model

Since deviations of *k*-effective from the asymptotic value arise due to leakage, they can be reduced by replacing the vacuum boundary condition with a reflector. The reflector in this case is assumed to be a 50%-50% mix of sodium and iron by volume; other reflector compositions (e.g. Zr or MgO filled fuel pins) can be used as well. Results from the cases with a reflector are given in Figure 3.3-3. One sees that the *k*-effectives differ from their asymptotic values by about 50% less than in the vacuum boundary cases. The size of this reduction can be varied by using reflectors with different neutron albedos.

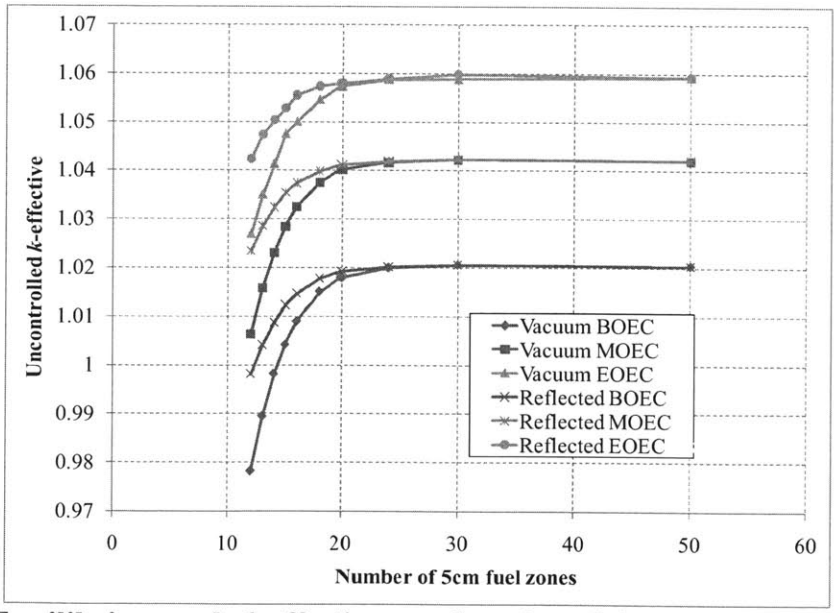

Figure 3.3-3. Equilibrium cycle *k*-effective as a function of size with and without reflector

It is also of interest to consider how beginning-of-equilibrium-cycle k-effective varies with model size, since the minimum k-effective at the beginning of cycle dictates whether reactor operation is possible. A prediction for BOEC k-effectives can be made using neutron absorption rates from a thick-blanket model, as was done for MOEC k-effectives. This prediction is shown in Figure 3.3-4 along with measured results in the vacuum boundary case. Note that in the BOEC case, the prediction slightly over-predicts the measured k-effectives. This is because the smaller-sized cases have a slightly larger reactivity swing than the large cases, because fresh feed fuel is exposed to a higher neutron flux and gains reactivity more quickly (reactivity swing is discussed further in Subsection 3.3.3). Nevertheless, the predicted BOEC k-effective is able to fairly accurately determine the onset and approximate magnitude of the deviation of k-effective from its asymptotic value.

The ability to predict the equilibrium cycle k-effectives for different sized systems from a single thick-blanket model is important because it allows one to avoid constructing and running multiple different sized models to determine how k-effective changes. The choice of what size to select depends on the design goals of the system in question, but there are particular sizes that one would likely want to avoid. First, the reactivity return on increasing the thickness of the feed blanket region becomes smaller the thicker the blanket becomes, eventually yielding nearly no increase with increased thickness. Second, it is also desirable to avoid the steep drop off in reactivity that occurs at lower sizes, since at those sizes higher fuel burnup would be required to maintain critical operation. Since early generations of B&B reactors will likely focus on having efficient neutron economies in order to minimize burnup and DPA, reactor sizes in this thesis are chosen by determining the size cutoff that would result in only a 0.5% loss of neutrons with no reflector present. The addition of a reflector would cause the actual impact on k-effective to be smaller than 0.5%. Using this criterion, the size of the 1D convergent infinite slab model is 85 cm on each side of the midplane, or about 17 zones.

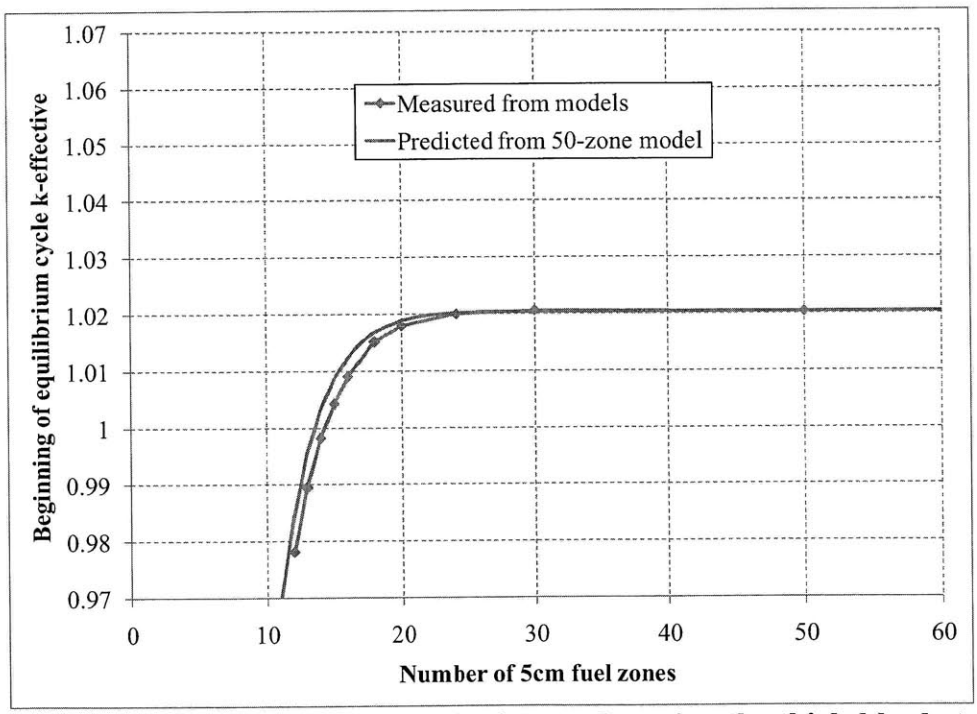

Figure 3.3-4. Prediction of BOEC k-effective vs. size using the thick-blanket model

The method of predicting minimum reactor size by using a thick-blanket model can be generalized to different configurations. For example, Figure 3.3-5 shows the size-reactivity relationship for an infinite slab model using equilibrium shuffling sequence number 2 (described in Appendix A.1). Such a configuration is larger than the convergent shuffling case, being subcritical under 18 zones (vs. 15) and losing more than 0.5% of its neutrons at sizes under 20 zones (vs. 17). It also shows a steeper drop off in *k*-effective as size is reduced, since the distribution of neutron absorptions is less centrally peaked. Predictions from a thick-blanket model are similarly successful in being able to determine at what size *k*-effective begins to decrease.

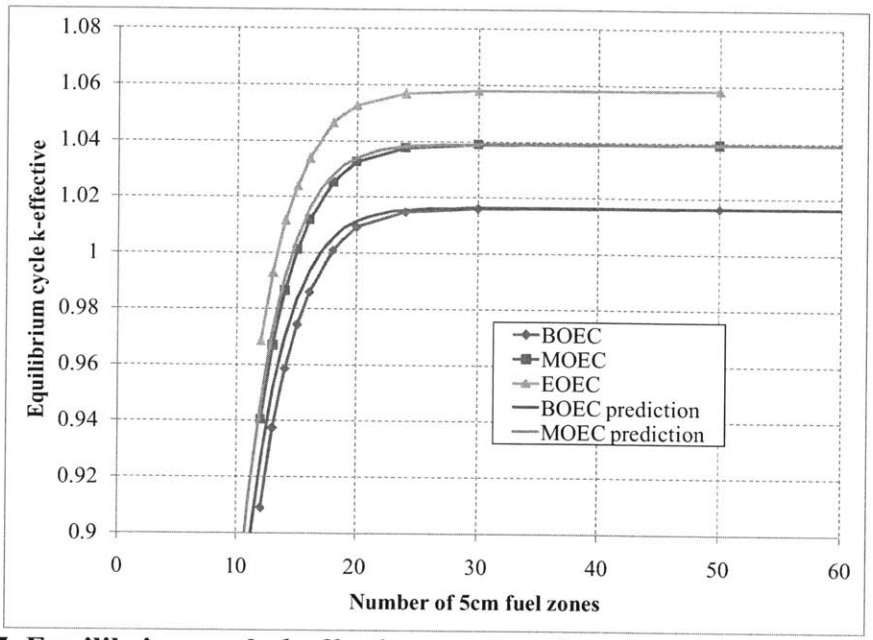

Figure 3.3-5. Equilibrium cycle *k*-effective as a function of model size, with predictions (shuffling sequence 2)

3.3.2 B&B reactor fuel residence time

A parameter that depends on core size is the feed fuel residence time during the equilibrium cycle. Assuming a peak power density of 480 W/cm^3 for the one-dimensional models, the fuel residence time in the baseline model is 17 cycles, or about 21 years, since the minimum size is 17 zones and one zone is shuffled with each 450-day cycle. Residence time can have an effect on fuel performance, the decay heat at discharge, as well as fuel cycle economics. It is desirable to reduce the size of the core and feed fuel residence time to reduce the amount of fuel that needs to be fabricated when the reactor is started. Table 3.3-1 gives the size and residence time results for the ten different infinite slab shuffling sequences investigated, using the 0.5% neutron absorption criteria for determining size. An exponential interpolation between zones is performed to obtain a more exact size in which 99.5% of all neutron absorptions occur, which explains why the size results are not exact multiples of 5 cm. In Table 3.3-1, total power is scaled so that each shuffling sequence has the same peak power density of 480 W/cm^3.

Table 3.3-1. Equilibrium cycle parameters for different shuffle sequences

Sequence #	1	2	3	4	5	6	7	8	9	10
Total power (MW/m^2)	60.0	107.0	143.9	112.5	73.4	94.8	117.3	121.7	142.8	145.9
Size (cm) (0.5% loss to leakage)	85	100	143	117	107	110	122	120	134	137
Average power (W/cm^3)	70	107	100	96	69	86	96	101	107	107
Residence time (y)	21.1	13.8	14.7	15.3	21.5	17.1	15.4	14.7	13.8	13.8

Table 3.3-1 shows that there is an inverse correlation between total power and residence time: the higher total power (lower peaking) systems tend to have higher average power and therefore shorter residence times. Sequences 1 and 5 use principally convergent shuffling and have highly peaked power distributions; as a result they have the lowest average power and the longest residence times.

The reason higher power systems tend to have shorter residence times is because the minimum size of the different sequences is largely determined by the width of the feed fuel region needed to absorb leakage neutrons, which is approximately the same in each case. Low power (highly peaked) systems have smaller power producing regions, so the ratio of feed fuel blanket to power producing region is larger, reducing the average power. Meanwhile, a higher power system will have a larger power producing region while having about the same sized breeding region, which raises the average power and reduces fuel residence time. This is an important conclusion for B&B reactors: higher power systems minimize the fraction of the core devoted to a feed fuel blanket, which allows them to have higher average power. Chapters 4 and 6 will discuss how for realistic three-dimensional systems, the benefit of using higher power systems extends to improving B&B fuel cycles as well.

3.3.3 Cycle reactivity swing

In addition to having different average equilibrium cycle k-effectives, the different shuffling sequences examined in Section 3.2 also have different cycle reactivity swings, as shown in Table 3.2-1. Cycle reactivity swing is important because reactor performance is constrained by minimum cycle k-effective, which is a function of both cycle average k-effective (which can be estimated using the neutron excess concept) and how much k-effective changes over a cycle. In the case of an equilibrium cycle B&B reactor, it is possible to derive an expression for the rate of change in k-effective in terms of how flux is distributed across fresh and bred fuel. This provides a qualitative understanding of what B&B configurations are best at minimizing cycle reactivity swing.

Instead of using the expression for k-effective in Equation 2.2-1, the expression for uncontrolled reactivity in Equation 3.3-2 is used instead, because the approximately constant denominator simplifies taking a derivative. The denominator is equal to the total neutron production rate, which in a B&B reactor is almost exactly proportional to the total power production rate, which is assumed to be constant. The relationship between reactivity and k-effective and their

derivatives is summarized in Equation 3.3-3. For a k-effective close to unity, the time derivative of reactivity and k-effective are approximately equal.

$$\rho_{unc} = \frac{neutron\ production\ rate - neutron\ absorption\ rate}{neutron\ production\ rate} = \frac{\int dV \phi \Sigma_a (k'_\infty - 1)}{\int dV \phi \nu \Sigma_f} \tag{3.3-2}$$

$$\rho_{unc} = \frac{k_{unc} - 1}{k_{unc}} \qquad \frac{d\rho_{unc}}{dt} = \frac{1}{k_{unc}^{\ 2}} \frac{dk_{unc}}{dt} \qquad \frac{dk_{unc}}{dt} = \frac{1}{(1-\rho_{unc})^2} \frac{d\rho_{unc}}{dt} \tag{3.3-3}$$

Taking the derivative of Equation 3.3-2 with respect to time yields Equation 3.3-4, where it has been assumed that the denominator is constant with time:

$$\frac{d\rho_{unc}}{dt} = \frac{\int dV \left[\frac{d(\phi \Sigma_a)}{dt} (k'_\infty - 1) + \phi \Sigma_a \frac{dk'_\infty}{dt} \right]}{\int dV \phi \nu \Sigma_f} \tag{3.3-4}$$

In the numerator of Equation 3.2-3, the bracketed term has two components. The first term is the contribution to reactivity swing due to the flux distribution shifting, and the second term is the contribution due to materials properties (i.e., k'_∞) changing. By comparing the BOEC and EOEC states for the different shuffling sequences, one can determine the relative magnitudes of these two contributions over an entire cycle. Results from such a comparison are given in Table 3.3-2. The contribution due to changing materials is obtained by computing the hypothetical k-effective that would result if one used the *BOEC* neutron absorption distribution and the *EOEC* material k'_∞ distribution. The opposite calculation (using *BOEC* material k'_∞ and *EOEC* absorption distribution) is used to obtain the contribution due to changes in the flux/absorption distribution.

Table 3.3-2. Equilibrium cycle k-effectives for different shuffle sequences (± 0.001)

Sequence #	**1**	**2**	**3**	**4**	**5**	**6**	**7**	**8**	**9**	**10**
Δk-effective	0.040	0.042	0.021	0.050	0.049	0.043	0.033	0.042	0.032	0.028
Δk due to material changes	0.053	0.045	0.027	0.046	0.051	0.048	0.040	0.041	0.033	0.032
Δk due to flux dist. changes	-0.014	-0.004	-0.007	0.003	-0.003	-0.007	-0.008	-0.001	-0.003	-0.004
% due to material changes	132%	106%	130%	92%	105%	111%	119%	99%	105%	111%
% due to flux dist. changes	-36%	-11%	-35%	6%	-6%	-15%	-24%	-2%	-9%	-13%

In Table 3.3-2, the changes in k-effective over a cycle do not exactly match those of Table 3.2-1; this is because Table 3.3-2 uses results from a single cycle calculation while Table 3.2-1 averages over the results from many equilibrium cycles and has less statistical modeling error. Also, the two contributions to Δk-effective do not sum to exactly 100% because they do not add linearly. Generally, changes in the flux distribution tend to *reduce* the reactivity swing, since the

flux distribution tends to move toward less reactive fuel that is being bred up. Meanwhile, changes in materials properties dominate the change in reactivity (this is a standard conclusion for other reactors as well).

Since the most important contributor to Δk-effective is changes in materials, one can make an approximation and assume that the neutron absorption rate is invariant with time over a cycle, which makes the first term in the bracketed expression of Equation 3.3-4 equal to zero. This is a reasonable approximation provided that the distribution of neutron absorptions does not change rapidly. With this approximation, the rate of change of k-effective can be written:

$$\frac{d\rho_{unc}}{dt} \cong \frac{\int dV \phi \Sigma_a \frac{dk'_\infty}{dt}}{\int dV \phi \nu \Sigma_f} = \frac{\int dV (\phi \Sigma_a)^2 \frac{dk'_\infty}{dA}}{k_{unc} \int dV (\phi \Sigma_a)} \tag{3.3-5}$$

$$\frac{dk_{unc}}{dt} \cong k_{unc} \frac{\int dV \left[\phi \Sigma_a \frac{dk'_\infty}{dA} \right] (\phi \Sigma_a)}{\int dV (\phi \Sigma_a)} \tag{3.3-6}$$

In Equation 3.3-5, the term dA is used, which is a differential unit of neutron absorption, and is defined: $dA = \phi \Sigma_a dt$. Equation 3.3-6 uses the expression in 3.3-3 to rewrite the reactivity derivative as a k-effective derivative. By grouping the terms as shown, one sees that the rate of change in k-effective is equal to the *neutron absorption weighted average* of the term in brackets, which is the rate of change of k'_∞ vs. ΔA (i.e. the derivative of the type of curve shown in Figure 3.2-4) multiplied by the neutron absorption rate. Equation 3.3-6 shows that a very important factor is the flux distribution: if there is a relatively high flux in low-burnup fuel (where the quantity dk'_∞/dA is the greatest) then reactivity swing will be higher, and vice versa.

Based on just the flux distribution factor, one would expect that the convergent shuffling pattern (sequence 1) would have the smallest reactivity swing, since its flux distribution is centered on the bred fuel and very low in the fresh fuel. However, Table 3.3-2 shows that four other sequences have smaller reactivity swings. The reason for this is due to the flux term inside the brackets in Equation 3.3-6: a system with a higher absolute flux will have a higher reactivity swing rate. Sequence 1 has the spatially smallest flux and power distributions (see Figure 3.2-2), so for a fixed reactor power it has higher absolute fluxes than all the other sequences, resulting in a higher reactivity swing rate.

More realistically, different shuffling sequences would be bounded by a peak power constraint, which would also set a bound on the magnitude of their fluxes. To incorporate this effect, Table 3.3-3 gives the relative reactivity swing of the different sequences as both a function of energy and time, where the relative power of the different sequences has been scaled by setting a fixed power density limit of 480 MW/cm^3.

In Table 3.3-3, the "unit energy" is the energy in a modeled cycle, i.e. 54,000 MWd. After scaling the shuffling sequences to all have the same peak power density of 480 W/cm^3, the sequences with the lower power peaking have higher relative power and are able to complete a

54,000 MWd cycle more quickly. To obtain Δk-effective per unit time, Δk-effective per unit energy is multiplied by the relative power (here "unit time" is 450 days, the original cycle length).

Table 3.3-3. Δk-effectives for different shuffle sequences (± 0.001)

Sequence #	1	2	3	4	5	6	7	8	9	10
Δk-effective per unit energy	0.038	0.042	0.020	0.049	0.046	0.043	0.034	0.042	0.033	0.028
Modeled peak power density (W/cm^3)*	480	269	200	256	392	304	245	237	202	197
Relative peak power density	1.00	0.56	0.42	0.53	0.82	0.63	0.51	0.49	0.42	0.41
Total power (MW)	60.0	107.0	143.9	112.5	73.4	94.8	117.3	121.7	142.8	145.9
Relative power	1.00	1.78	3.20	1.88	1.22	1.58	1.95	2.03	2.38	3.23
Δk-effective per unit time	0.038	0.075	0.048	0.092	0.056	0.068	0.066	0.085	0.079	0.068

*For a total modeled power of 60 MW

Scaled in this manner, sequence 1 is in fact shown to have the most gradual reactivity swing per unit time, while sequences which shuffle low-burnup fuel into high flux regions (e.g. sequences 2, 4, and 8) have rapid reactivity swings. Therefore, to minimize reactivity swing *per unit time* and maximize cycle length, a shuffling sequence should be designed to avoid having low burnup feed in high flux regions of the core. Meanwhile, having large, flat power and flux distributions decreases the reactivity swing *per unit energy*, so higher power systems are not penalized by having shorter cycle lengths.

3.4 Infinite-medium depletion approximation

Section 3.2 discusses how the neutron excess quantities evolve in very similar manners for models with different geometries and different shuffling sequences, which in turn means that these different configurations have a similar relationship between average equilibrium cycle k-effective and discharge burnup. This section shows how an even simpler model, an infinite-medium depletion model, produces a similar neutron excess curve and therefore can be used as an extremely fast way to produce estimates for equilibrium k-effective.

In the discussion about different one-dimensional shuffling sequences, one conclusion was that the equilibrium cycle average k-effectives fall within a small band because the total discharge fluence experienced has the same spectrum for each sequence, and differences in reactivity could be explained by the distribution of different spectra over the fuel's depletion. Sequences in which fuel experiences a harder spectrum toward the end of its irradiation (e.g. sequence 1) have slightly higher equilibrium cycle k-effectives, while those in which fuel experiences a softer spectrum toward the end of its irradiation (e.g. sequence 4) have lower equilibrium cycle k-effectives. Random-permutation sequences have a fairly uniform spectrum throughout the mixing region, resulting in k-effectives between the two extremes.

Instead of modeling a full geometry with different spectra in different regions, one approximation is to model an infinite medium of feed material and allowing that to deplete in its self-consistent infinite-medium spectrum: this is called the "infinite-medium depletion approximation". Modeling an infinite-medium depletion provides a value for ΔN and ΔA at every value of burnup, allowing an estimate of average k_{eq} as a function of burnup to be made by applying Equation 2.3-3. Plotting the fluence spectrum experienced in the infinite-medium case alongside the fluence spectra experienced in cases with different shuffling sequences (from Subsection 3.2.2) for the same discharge burnup yields the curves in Figure 3.4-1. Table 3.4-1 compares the fast fluence fractions of the different models. Meanwhile, Figure 3.4-2 and Table 3.4-2 show the corresponding fluence spectra and fast fluence fractions for models with different geometries from Subsection 3.2.1.

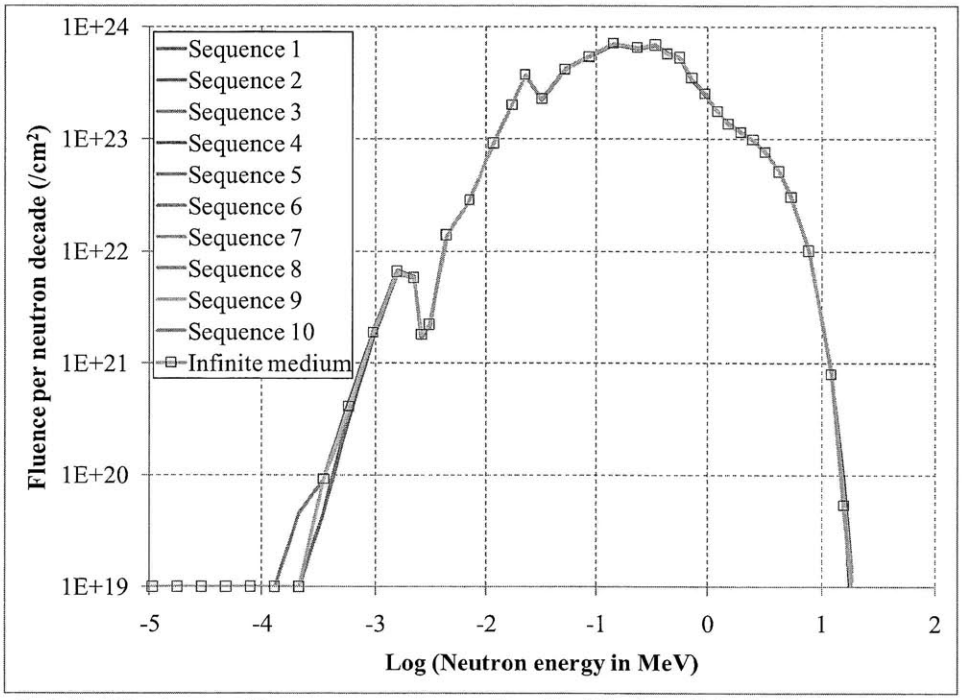

Figure 3.4-1. Discharge fluence spectrum for shuffled and infinite-medium models

Table 3.4-1. Discharge fluence for different shuffle sequences and infinite-medium model

Sequence #	1	2	3	4	5	6	7	8	9	10	Inf. m
Total fluence	9.761E +23	9.792E +23	9.878E +23	9.938E +23	9.875E +23	9.837E +23	9.824E +23	9.925E +23	9.876E +23	9.852E +23	9.875E+ 23
Fast fluence (>0.1 MeV)	6.523E +23	6.546E +23	6.605E +23	6.652E +23	6.609E +23	6.577E +23	6.569E +23	6.639E +23	6.607E +23	6.590E +23	6.605E+ 23
Fast fluence fraction	0.6682	0.6684	0.6687	0.6693	0.6693	0.6686	0.6686	0.6690	0.6690	0.6689	0.6689

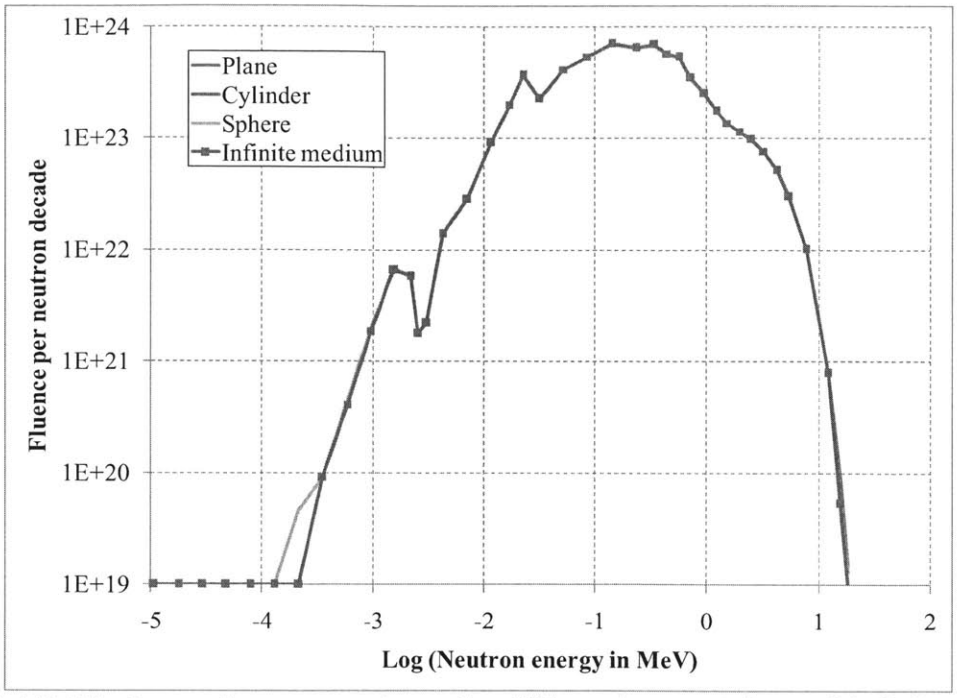

Figure 3.4-2. Discharge fluence spectrum for different geometries and infinite-medium model

Table 3.4-2. Discharge fluence for different geometries and infinite-medium model

Geometry	Infinite slabs	Cylinders	Spheres	Infinite medium
Total fluence	9.761E+23	9.755E+23	9.733E+23	9.875E+23
Fast fluence (>0.1 MeV)	6.523E+23	6.521E+23	6.602E+23	6.605E+23
Fast fluence fraction	0.6682	0.6685	0.6680	.6689

The two figures and tables show that the fluence spectrum for the infinite-medium approximation matches those of the cases with different geometries and shuffling sequences. This is again because in a fast system, the total scattering cross section is much larger than the total absorption cross section, so the neutron spectrum is primarily determined by the numbers of scattering events experienced. In the shuffled systems, this results in a segregation of harder spectrum regions near where fissions were occurring, and softer spectrum regions farther from where neutrons were generated. In the infinite-medium model, there is a uniform spectrum everywhere, and the harder and softer spectra become mixed together to form an intermediate average spectrum. The fast flux fraction as a function of ΔA is shown in Figure 3.4-3 for the infinite-medium depletion approximation and for several of the 1D shuffling sequences.

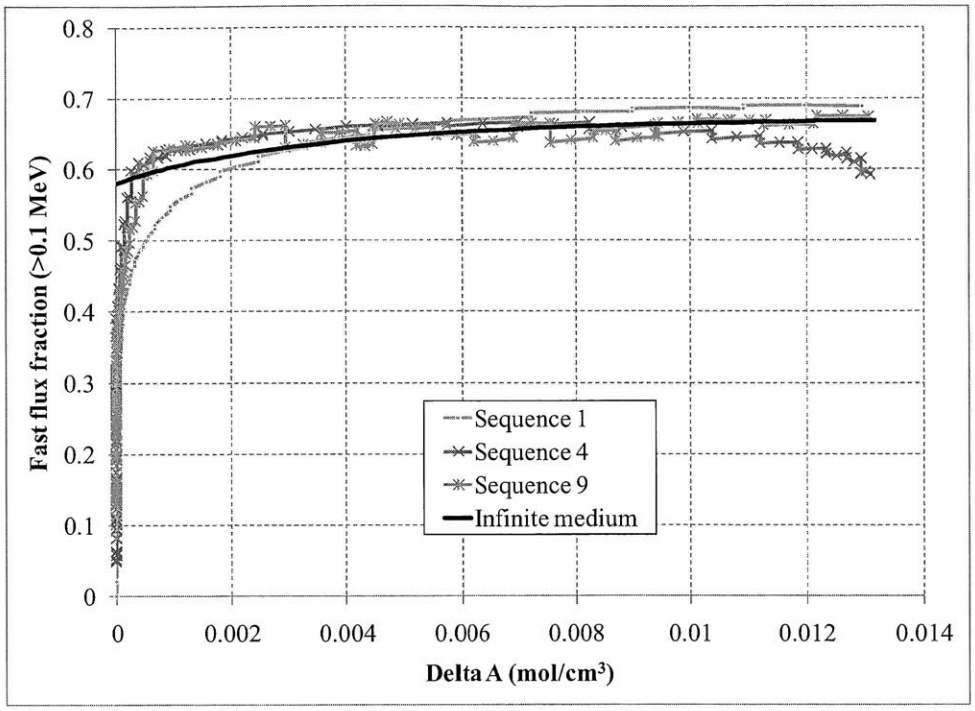

Figure 3.4-3. Fast flux fraction over material depletion for infinite-medium model

Figure 3.4-3 shows that the infinite-medium spectrum has an intermediate hardness over its entire depletion, lying in between sequence 1 and sequence 4 which experience harder spectra at the end and beginning of their respective irradiations. The fast flux fraction for the infinite-medium depletion more closely resembles that of sequence 9, which randomly mixes fresh and depleted fuel. Because the infinite-medium depletion approximation and the various models all experience the same fluence spectrum, the neutron excess curves of the various models have endpoints that all fall near the infinite-medium neutron excess curve, as shown in Figures 3.4-4 and 3.4-5. In particular, the infinite-medium neutron excess curve agrees very well with those from well-mixed cases using random shuffling (shuffling sequences 8, 9, and 10).

As a result of the agreement between the neutron excess curves of the 1D models and the infinite-medium depletion result, the infinite-medium depletion approximation does a good job of estimating the average equilibrium *k*-effective of the shuffled cases. Figure 3.4-4 shows that the infinite-medium depletion approximation predicts a k_{eq} of 1.032, which is within 1% of all the average k_{eq} values in Table 3.2-1 for the different shuffling sequences.

In Figure 3.4-5, which compares the infinite-medium depletion approximation to several convergently shuffled cases, one sees that the infinite-medium result first has a higher neutron excess than the convergent models at low ΔA, then has less neutron excess at higher ΔA. The reason for this behavior is because the infinite-medium depletion has a medium-hardness spectrum throughout, while the convergent case starts with a softer spectrum then ends with a harder one (as shown in Figure 3.4-3). The net result is that the infinite-medium depletion approximation is always slightly conservative for convergent shuffling; it under-predicts the convergent shuffling *k*-effective by about 1%. However, the shape of the infinite-medium neutron excess curve allows it to be useful for predicting *k*-effective over a large range of burnup. Figure 3.4-6 compares the neutron excess curve obtained from the infinite-medium depletion

alongside those from three convergent 1D models with different equilibrium cycle discharge burnup. Even though the infinite-medium result falls slightly lower than the endpoints of the neutron excess curves from the three 1D models, it does so consistently in each case and does a good job of predicting the endpoints of the three different curves.

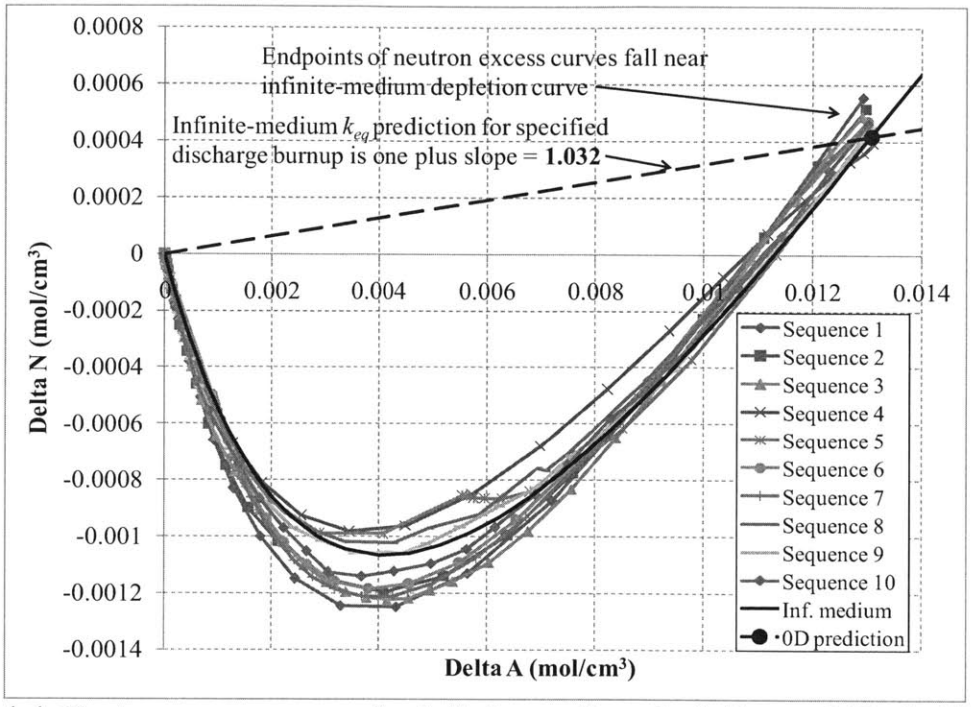

Figure 3.4-4. Neutron excess curves for infinite-medium depletion and 1D shuffling cases

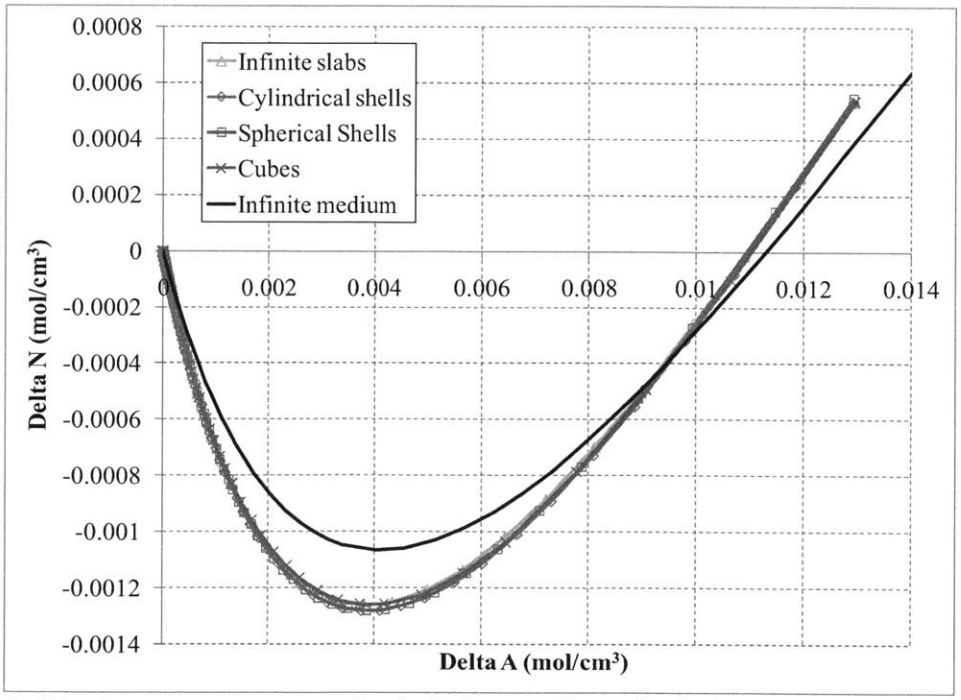

Figure 3.4-5. Neutron excess curves for infinite-medium depletion and different geometries

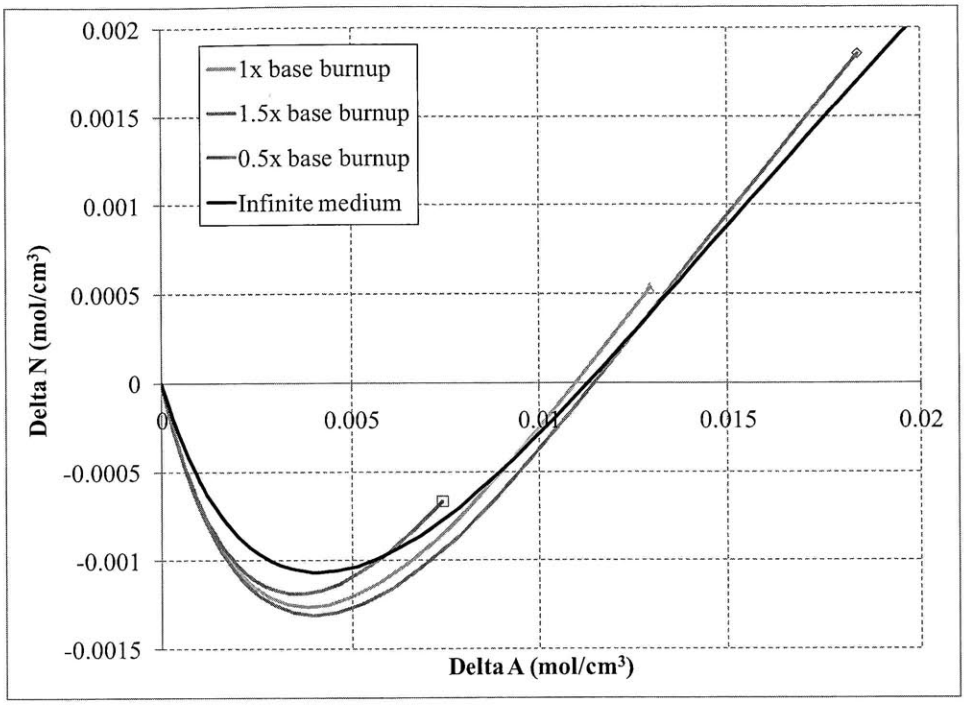

Figure 3.4-6. Infinite-medium and different burnup 1D model neutron excess curves

Figure 3.4-7 explicitly shows how the infinite-medium depletion approximation performs at predicting average k_{eq} as a function of burnup. The points in the figure are measured k-effectives from the different convergently shuffled 1D models. The infinite-medium depletion approximation does a very good job of predicting k-effective for the different models across a very large range of burnup and k-effective. Because the models are convergently shuffled, the infinite-medium depletion approximation prediction is slightly conservative, by about 0.8% in all cases. The predicted result would be more accurate for more complex shuffling sequences that are not strictly convergent. Most importantly, the infinite-medium prediction does a very good job of estimating the minimum burnup required for critical operation. This fact is exploited later in Chapter 5, where the infinite-medium depletion approximation is used to rapidly evaluate a large number of fuel, coolant, and structural material options.

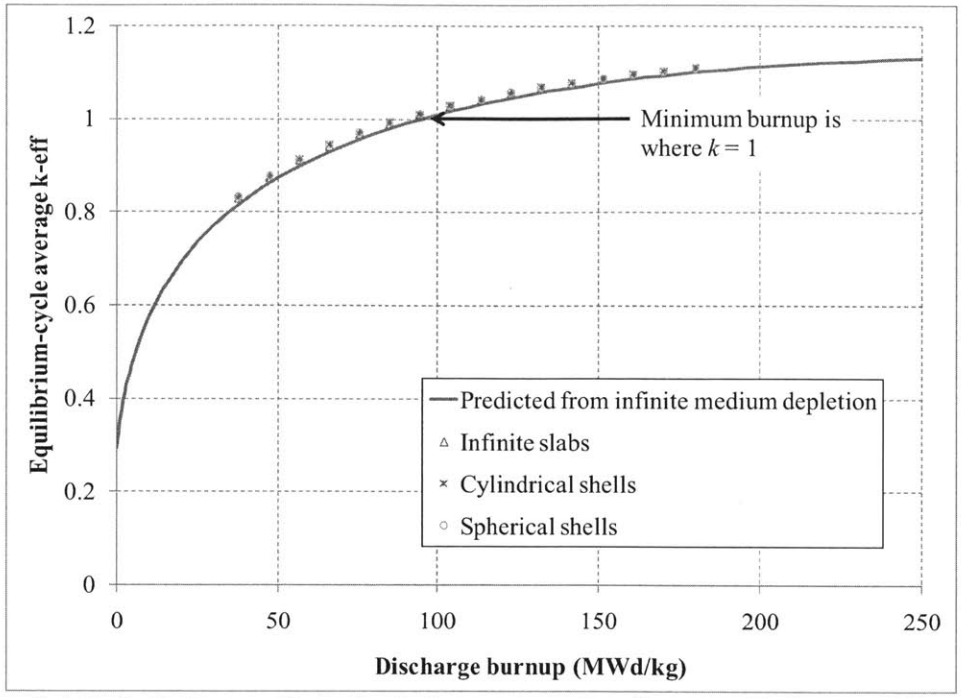

Figure 3.4-7. Infinite-medium depletion approximation prediction vs. 1D models

3.5 Example starter fuel calculation and transition model

Section 2.4 used the neutron excess concept to derive a set of equations that can be used to calculate the amount of starter fuel required to initiate a given equilibrium cycle. This section gives an example of such a calculation. Subsection 3.5.1 describes the targeted equilibrium cycle state. Subsection 3.5.2 calculates the amount of starter fuel required by applying the equations in Section 2.4 and using an infinite-medium depletion calculation for the selected starter fuel. Subsection 3.5.3 presents an explicitly modeled transition sequence that shows how the equilibrium cycle can be produced from starter fuel; this model is referred to as "example transition model." Subsection 3.5.4 compares the results from the example transition model to the predictions made in Subsection 3.5.2. Finally, Subsection 3.5.5 describes the results from a second transition model that uses discharged feed fuel from one B&B reactor to start up a new B&B reactor.

3.5.1 Equilibrium cycle description

The target equilibrium cycle in this example uses the example core composition (50% U, 20% Fe, 30% Na by volume) and the 5 cm infinite slab geometry. The feed material is depleted uranium with 0.3 mol% U-235. The equilibrium cycle shuffling sequence is a convergent-divergent pattern with the discharge zone being the eighth zone from the center: i.e. fuel is first shuffled sequentially from zone 50 to zone 9, skips from zone 9 to zone 1, then is shuffled sequentially from zone 1 back out to zone 8, where it is discharged. Convergent-divergent shuffling schemes are an interesting class of equilibrium shuffle sequences because they can effectively flatten the power distribution while retaining high reactivity and a small change in power distribution over an equilibrium cycle. The power level and cycle length are chosen to be 60 MW/m^2 and 900

days respectively (this is half the power and twice the cycle length of the earlier models, but the results do not depend on the absolute power level), which corresponds to an output burnup of 11.6% FIMA.

The equilibrium cycle configuration can be formed by starting from any starting fuel configuration and repeatedly applying the equilibrium cycle shuffling sequence until an equilibrium state develops. The resulting equilibrium cycle burnup, power, and flux distributions are shown in Figures 3.5-1 through 3.5-3. The power shape in seen in Figure 3.5-2 is a result of zones one through eight having the most Pu-239 bred in them, which causes the flux and power to concentrate there.

Values for uncontrolled equilibrium cycle *k*-effectives are given in Table 3.5-1. Since no control is modeled, it is assumed that these values for *k*-effective are approximately equal to the k_{fuel} of a controlled system. The small number of zones in the burning region of this simple equilibrium cycle as well as the relatively low burnup result in a fairly large reactivity swing, nearly 5%.

Table 3.5-1. Uncontrolled *k*-effective values for convergent-divergent equilibrium cycle

BOEC *k*-effective	1.014
MOEC *k*-effective	1.039
EOEC *k*-effective	1.060
Cycle reactivity swing (Δk-effective)*	0.047
$\overline{k_{eq}}$	1.0375

*the last significant digit does not add exactly due to rounding

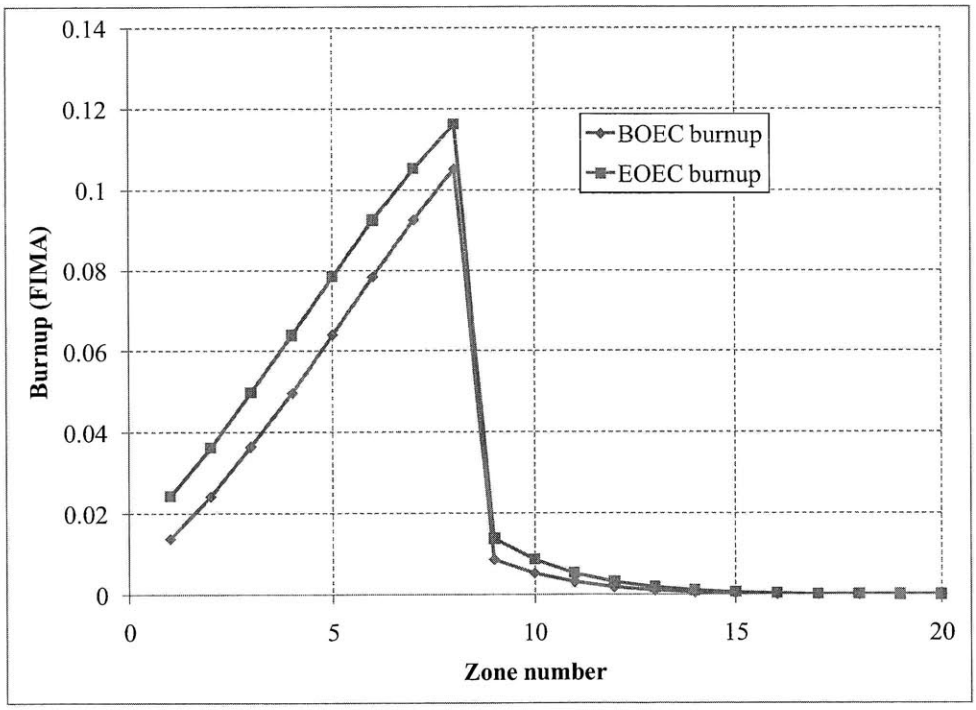

Figure 3.5-1. Equilibrium cycle burnup distributions

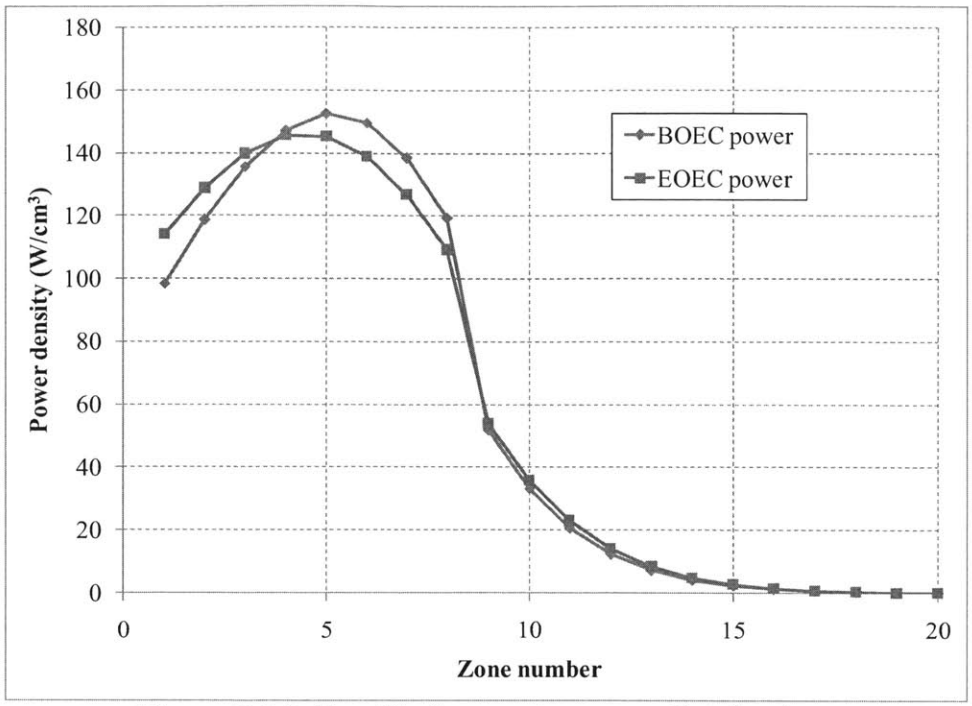

Figure 3.5-2. Equilibrium cycle power distributions

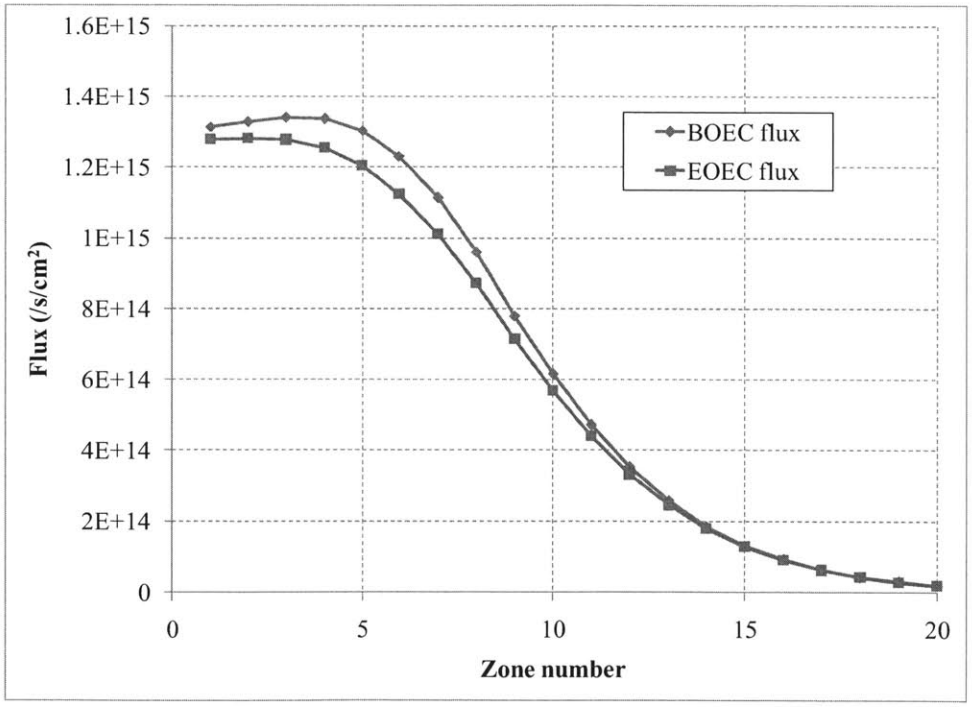

Figure 3.5-3. Equilibrium cycle flux distributions

The equilibrium cycle values for ΔN and ΔN_{adj} as a function of feed fuel burnup are plotted in Figure 3.5-4. The value of ΔN is positive for fuel nearing discharge, which is necessary because a fraction of neutrons are absorbed in control (these control absorptions are virtual, since control is not explicitly modeled). The model size is large enough that there are effectively no losses due to leakage. Accounting for losses to control yields the ΔN_{adj} curve, which is computed

according to Equation 2.4-7, using the value of $\overline{k_{eq}}$ given in Table 3.5-1. The discharge value of ΔN_{adj} is zero, so as the equilibrium cycle proceeds and more discharged feed fuel is created, the total value of ΔN_{adj} in the system does not change. This is illustrated in Figure 3.5-5, which shows the value of ΔN_{adj} as a function of zone index during the equilibrium cycle. Because the fuel has a zero ΔN_{adj} at discharge, the total ΔN_{adj} contained in the equilibrium cycle is the same at the beginning of cycle and end of cycle.

3.5.2 Estimating the needed amount of starter fuel

By integrating ΔN_{adj} of Figure 3.5-5 over all cells, one obtains the total ΔN_{adj} of the chosen equilibrium cycle: –6.20E-02 mol/cm^2. For total ΔN_{adj} to be conserved (Eq. 3.5-13), a positive contribution of 6.20E-02 mol/cm^2 is needed either from feed fuel burned past the breakeven burnup of 11.6%, or from enriched starter fuel. It is assumed that feed fuel cannot be burned much beyond this breakeven value, which is reasonable if one wishes to minimize burnup and cladding fluence. Therefore, nearly all the excess neutrons must come from the starter fuel. For the example transition model, the starting fissile fuel is assumed to be 20 cm (4 zones) of 15% enriched material, with the same composition (U, Fe, and Na) as the feed fuel. The ΔN and ΔN_{adj} of the starter fuel as a function of burnup are estimated by burning an infinite medium of starter fuel, with the results show in Figure 3.5-6. Dividing the required neutron excess (6.20E-02 mol/cm^2) by the amount of feed fuel (20 cm), yields the needed neutron excess per unit of feed fuel (3.10E-03 mol/cm^3), which from Figure 3.5-6 corresponds to an average burnup in the starter fuel of 12.3%. Note that in this case, a given amount of starter fuel was assumed and the needed burnup estimated, but it is equally possible, and usually more practical, to choose a starting fuel composition and for a given burnup limit determine what volume of starting material is needed.

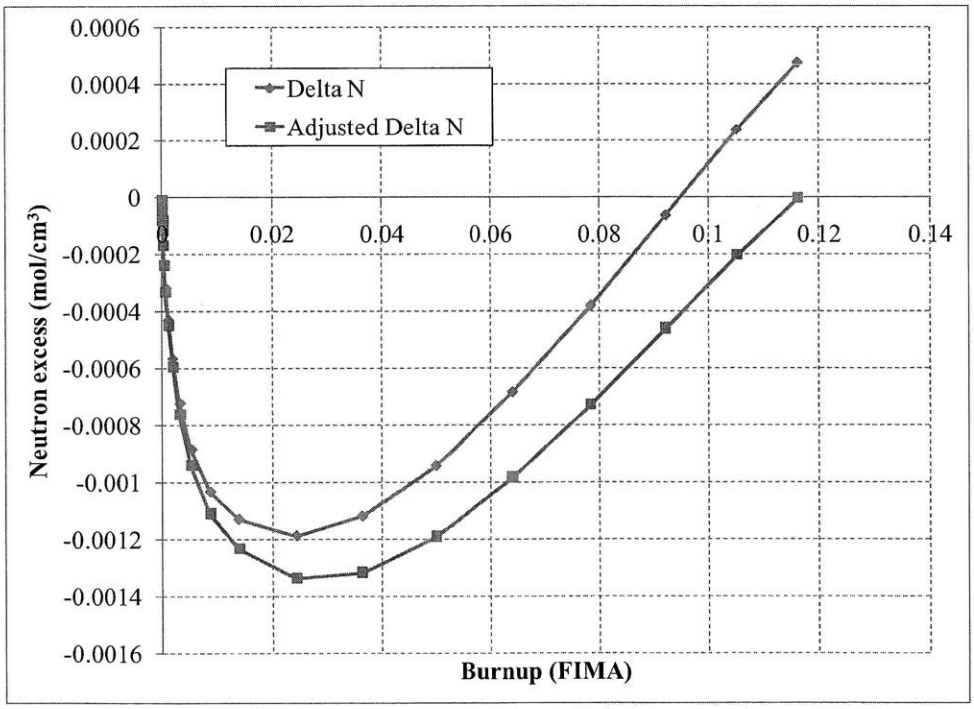

Figure 3.5-4. Neutron excess of equilibrium cycle feed fuel

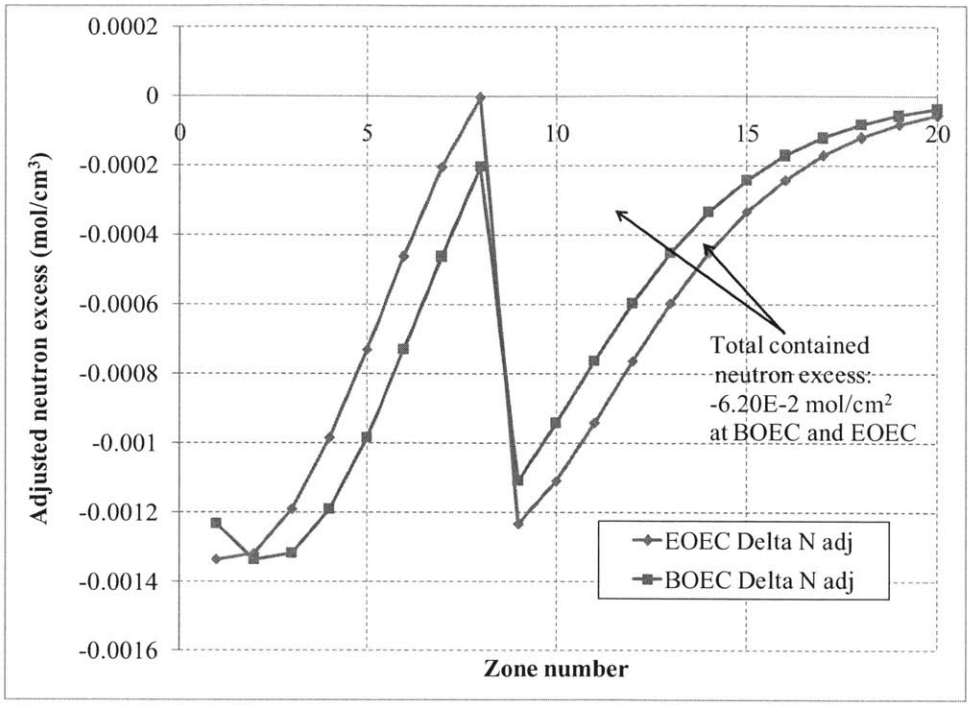

Figure 3.5-5. Adjusted neutron excess contained in equilibrium cycle

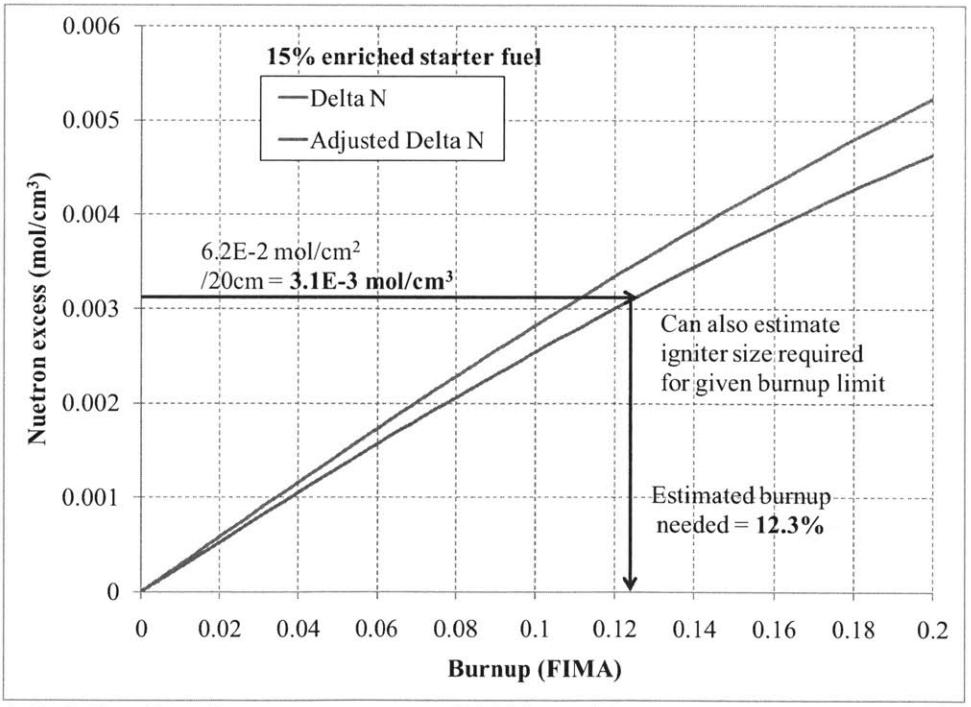

Figure 3.5-6. Predicted neutron excess of 15% enriched starter fuel (infinite-medium approximation)

3.5.3 Example transition model

Starting from 20 cm of 15% enriched starter fuel (4 5-cm zones) and 0.3% enriched feed fuel, the target equilibrium cycle was established by shuffling the fuel according to the sequence given in Table 3.5-2. Only the innermost 20 zones are shown because the zones farther out are effectively isolated neutronically. This model simulates the transition from startup to equilibrium and is referred to as the "example transition model." Details on how the transition sequence was developed are given in Appendix A.2.

Table 3.5-2. Startup shuffling sequence for described equilibrium cycle

Cycle number	Cycle Length (EFPD)	Cycle fuel permutation – position from center of core (only inner 20 zones shown out of 50)																			
0	0	1	2	3	4	5	6	7	8	9	10	11	12	13	14	15	16	17	18	19	20
1	1445.1	1	5	2	3	6	7	4	8	9	10	11	12	13	14	15	16	17	18	19	20
2	977.7	5	4	6	3	7	2	1	8	9	10	11	12	13	14	15	16	17	18	19	20
3	1053	5	4	6	7	3	8	2	9	1	10	11	12	13	14	15	16	17	18	19	20
4	1065.9	5	4	6	7	8	1	9	10	11	2	3	12	13	14	15	16	17	18	19	20
5	1085.7	5	6	7	2	8	9	10	11	3	12	13	1	4	14	15	16	17	18	19	20
6	1121.2	5	6	7	8	9	10	1/3	11	12	13	14	15	16	3/1	4	17	2	18	19	20
7	813.8	9	8	7	6	5	10	11	12	13	14	15	16	17	18	19	20	21	22	23	24
8	900	12	11	10	9	8	7	6	5	13	14	15	16	17	18	19	20	21	22	23	24
9	900	13	12	11	10	9	8	7	6	14	15	16	17	18	19	20	21	22	23	24	25
10	613.6	14	13	12	11	10	9	8	7	15	16	17	18	19	20	21	22	23	24	25	26
11	900	15	14	13	12	11	10	9	8	16	17	18	19	20	21	22	23	24	25	26	27
12	900	16	15	14	13	12	11	10	9	17	18	19	20	21	22	23	24	25	26	27	28

The starter fuel is initially in zones one through four but is shuffled to zones 1, 3, 4, and 7 before the first cycle; its positions are highlighted in Table 3.5-2. Depleted uranium feed fuel occupies all other zones. The starter fuel moves outward with each cycle and is rearranged to keep the lowest burned zones toward the center, while the feed fuel is kept in order of burnup. In cycle 6, the positions of starter fuel materials 1 and 3 are swapped midway through the cycle, to flatten the starter fuel discharge burnup distribution. By cycle 7, the feed fuel is bred sufficiently that the starter fuel zones can be completely discharged while still leaving the reactor in a critical state. At this point, beginning of cycle reactivity is minimized by reversing the order of the five innermost feed zones. At the start of cycle 8, the innermost eight feed zones are reversed, forming a state close to the final equilibrium cycle. After cycle 8, the equilibrium cycle shuffling scheme is used, with spent feed fuel being discharged from zone number 8, and the equilibrium cycle is quickly established.

This transition sequence was designed to satisfy the following goals:

1) Prevent *k*-effective from falling below unity
2) Keep the cycle-average *k*-effective close to $\overline{k_{eq}} = 1.0375$
3) Keep the peak feed burnup close to the required burnup of 11.6%
4) Discharge the starter fuel at roughly uniform burnup (i.e. minimize peaking)

One can also replace the feed and starter burnup goals with goals for total fluence or radiation damage and obtain similar results. Goal number 2 is in place so that the transition cycles have reactivity characteristics similar to the equilibrium cycle; this also minimizes the contribution to neutron excess resulting from reactivity deviations (the right-hand side of Equation 2.4-20). To achieve goal number 2 while minimizing the number of shuffles (or maximizing the cycle length), it is desirable to minimize the beginning of cycle positive reactivity for each cycle. For more realistic systems, additional goals can be added, such as a peak power density constraint, or a goal to minimize the number of fuel shuffling movements per cycle.

The reactivity evolution computed by REBUS and MCNPXT of the Table 3.5-2 shuffling scheme is given in Figure 3.5-7. REBUS results are shown because REBUS was used for rapidly evaluating a large number of different shuffling options. As seen in the REBUS results, the length of the first 7 cycles was chosen to yield the same middle of cycle *k*-effective, corresponding to that of the equilibrium cycle. In Figure 3.5-7, the equilibrium cycle reactivity results given in Table 3.5-1 can be seen for the cycles occurring after about 12000 days. Overall, the beginning of cycle and end of cycle *k*-effectives deviate by less than 1% from their equilibrium cycle values; this variation can be reduced in more realistic systems which have more degrees of freedom for arranging feed and startup fuel.

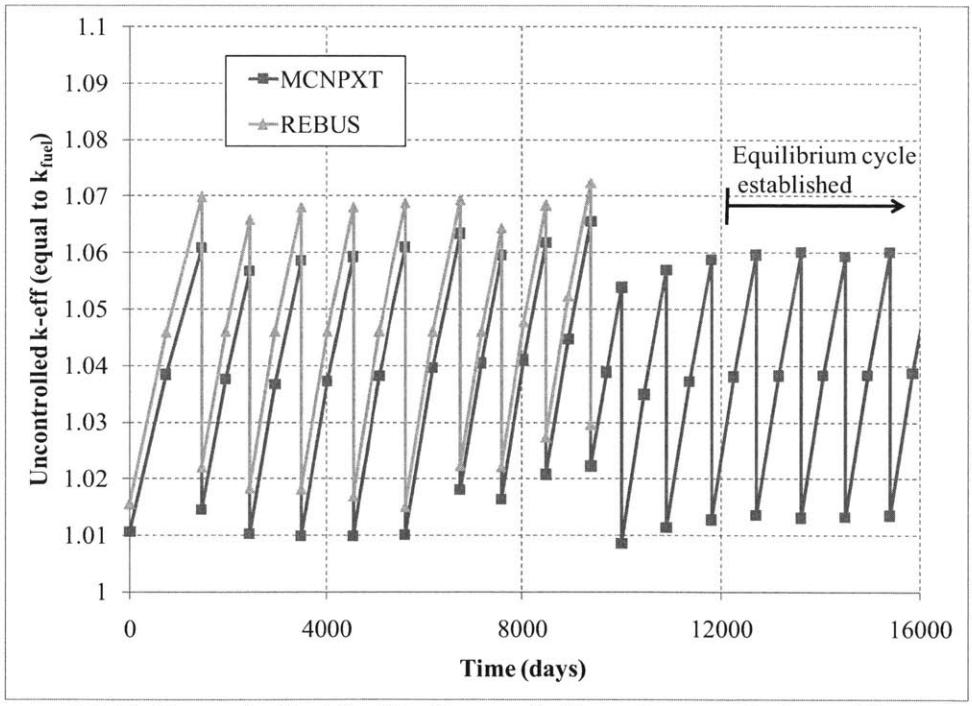

Figure 3.5-7. Uncontrolled *k*-effective evolution of example transition model

The burnup for different fuel zones after 30 cycles for this transition case are given in Figure 3.5-8 (results are from the MCNPXT model). Material numbers 1 through 27 have been discharged, and materials 28 and higher have assumed the equilibrium cycle burnup distribution. This burnup distribution does a good job of satisfying goals 3 and 4. The peak feed discharge burnup is 11.8%, only slightly above the equilibrium cycle value of 11.6%. Meanwhile, the peak starter discharge burnup is 12.1%, very close to the average value of 12.0%.

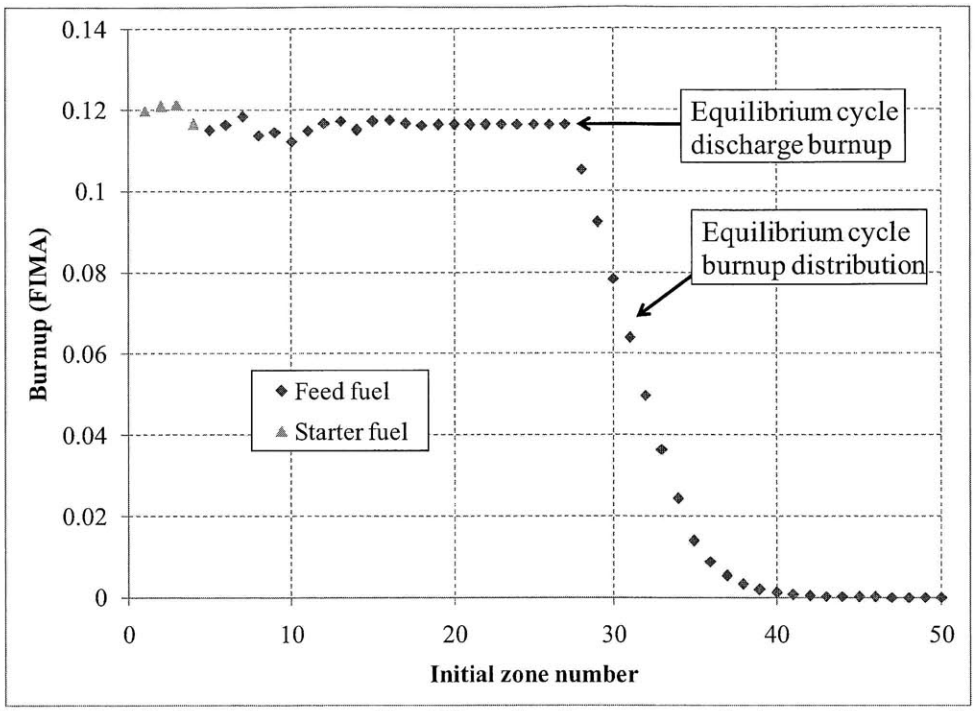

Figure 3.5-8. Fuel burnup after 30 cycles from example transition model

3.5.4 Comparison between transition model and predicted results

There are two contributions to the ΔN_{adj} of a system: first there is contribution or deduction from cycles in which the $\overline{k_{fuel}}$ deviates from $\overline{k_{eq}}$, as given on the right-hand side of Equation 2.4-20. This is referred to as the contribution from "reactivity deviations," because it depends on how much the uncontrolled k-effective deviates from the equilibrium cycle average value. Second, fuel discharged from a system with a non-zero ΔN_{adj} leaves a ΔN_{adj} contribution within the system, which are the second and third terms on the left side of Equation 2.4-20. The contributions due to varying cycle k-effectives are given in Table 3.5-3 and plotted in Figure 3.5-9. When cycle uncontrolled k-effective is high (e.g. cycle 9), more neutrons are lost to control, so the system ΔN_{adj} increases. Conversely, when cycle reactivity is low (e.g. cycle 11), system ΔN_{adj} decreases. Once the equilibrium cycle is established, $\overline{k_{fuel}}$ equals $\overline{k_{eq}}$ (although there is some statistical scatter), and the ΔN_{adj} contribution from reactivity deviations stops accumulating. The total contribution to ΔN_{adj} due to reactivity deviations is approximately **-2.7E-04 mol/cm^2**, which is less than 0.5% of the total neutron cost of the equilibrium cycle, which was calculated earlier to be -6.20E-02 mol/cm^2. This low value is a result of this transition sequence having an average k_{fuel} quite close to that of the target equilibrium cycle.

The contributions to ΔN_{adj} from fuel depletion are summarized in Figure 3.5-10, which also shows the predicted values from the infinite-medium approximation and equilibrium cycle. Figure 3.5-10 shows that the starter fuel yields slightly fewer excess neutrons than in the infinite-medium prediction, since the presence of subcritical feed fuel softens the neutron spectrum it experiences. Meanwhile, transition feed fuel that is bred in the harder spectrum of the starter fuel region ends up being discharged with a small positive reactivity-adjusted neutron excess,

rather than zero as in the equilibrium cycle. These two errors approximately cancel, which is a result of the spectral mixing between the two fuels in the transition model. The total reactivity-adjusted neutron excess from the starter fuel is 5.71E-02 mol/cm^2 and 4.5E-03 mol/cm^2 from the intermediate feed fuel, leaving -6.16E-02 mol/cm^2 behind in the equilibrium cycle feed fuel. Adding the reactivity contribution gives a total of -6.19E-02 mol/cm^2 neutrons to build the equilibrium cycle, very close to the measured value of -6.20E-02 mol/cm^2. The values do not exactly match because there is some statistical scatter in the amount of neutron excess contained in the system at each cycle.

Table 3.5-3. Contributions to ΔN_{adj} from reactivity deviations

Cycle number	$\overline{k_{fuel}}$	$\left(\int_{fuel} dV(\Delta A)\right)\Big\|_{cycle}$ (mol/cm^2)	Contribution to ΔN_{adj} (mol/cm^2)	Cumulative contribution (mol/cm^2)
1	1.0367	0.0962	-7.692E-05	-7.692E-05
2	1.0363	0.0667	-7.855E-05	-1.555E-04
3	1.0352	0.0730	-1.696E-04	-3.250E-04
4	1.0355	0.0748	-1.485E-04	-4.735E-04
5	1.0364	0.0768	-8.092E-05	-5.544E-04
6	1.0381	0.0800	4.406E-05	-5.104E-04
7	1.0391	0.0599	9.546E-05	-4.149E-04
8	1.0402	0.0649	1.740E-04	-2.409E-04
9	1.0437	0.0646	3.993E-04	1.584E-04
10	1.0384	0.0445	4.215E-05	2.006E-04
11	1.0334	0.0652	-2.704E-04	-6.980E-05
12	1.0361	0.0651	-8.888E-05	-1.587E-04
13	1.0367	0.0650	-4.903E-05	-2.077E-04
14	1.0369	0.0650	-4.150E-05	-2.492E-04
15	1.0372	0.0650	-2.191E-05	-2.711E-04
16	1.0374	0.0650	-6.075E-06	-2.772E-04
17	1.0377	0.0650	1.338E-05	-2.638E-04
18	1.0374	0.0650	-6.361E-06	-2.702E-04

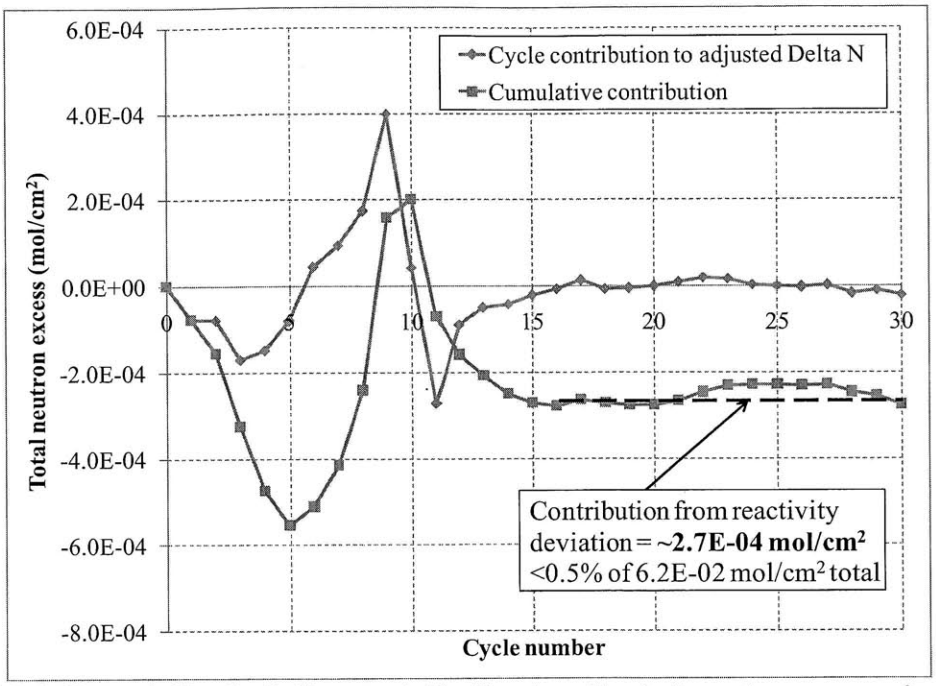

Figure 3.5-9. Reactivity-deviation contribution to adjusted neutron excess in example transition model

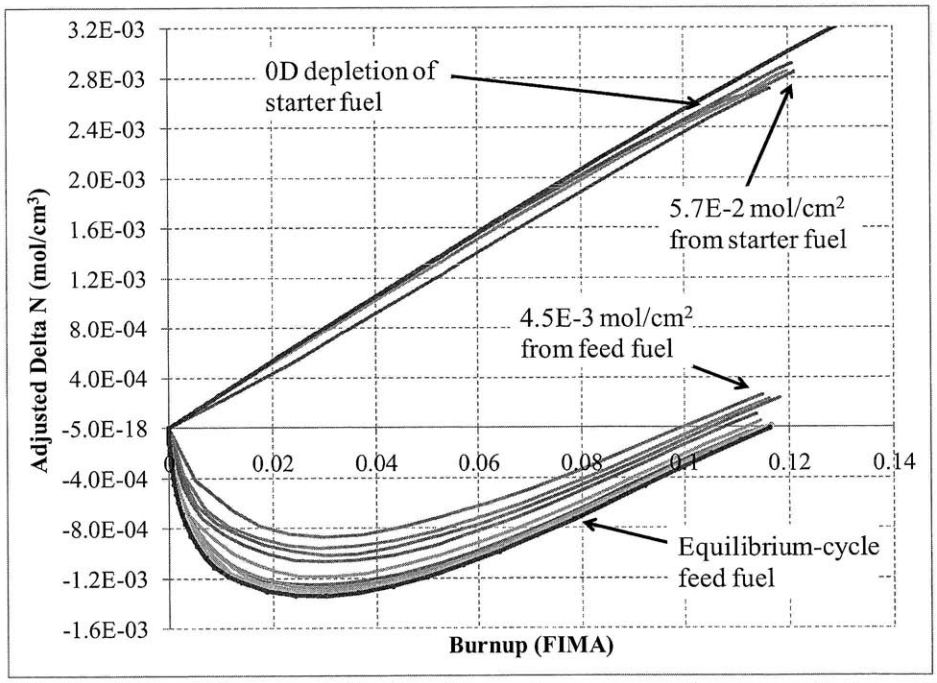

Figure 3.5-10. Fuel depletion contribution to neutron excess in example transition model

The predictions for ΔN_{adj} from the equilibrium cycle for the feed and the infinite-medium depletion for the starter fuel compare well to the actual ΔN_{adj} measured in the transition model. The greater ΔN_{adj} from the feed due to a harder spectrum in the startup model is offset by the lower ΔN_{adj} in the starter fuel due to a softer spectrum. These spectral effects are illustrated in Figures 3.5-11 and 3.5-12, which show the fast flux fraction (>0.1 MeV) as a function of burnup

for the starter and feed fuel respectively. Figure 3.5-11 shows that the starter fuel in the example transition model experiences a slightly softer spectrum than in the infinite-medium depletion approximation, particularly zones that have more fresh feed fuel surrounding them (e.g. starter material 4 over the first cycle). In contrast, transition feed fuel in the example transition model experiences a harder spectrum than equilibrium cycle feed fuel at first, but quickly converge to the equilibrium cycle spectrum history.

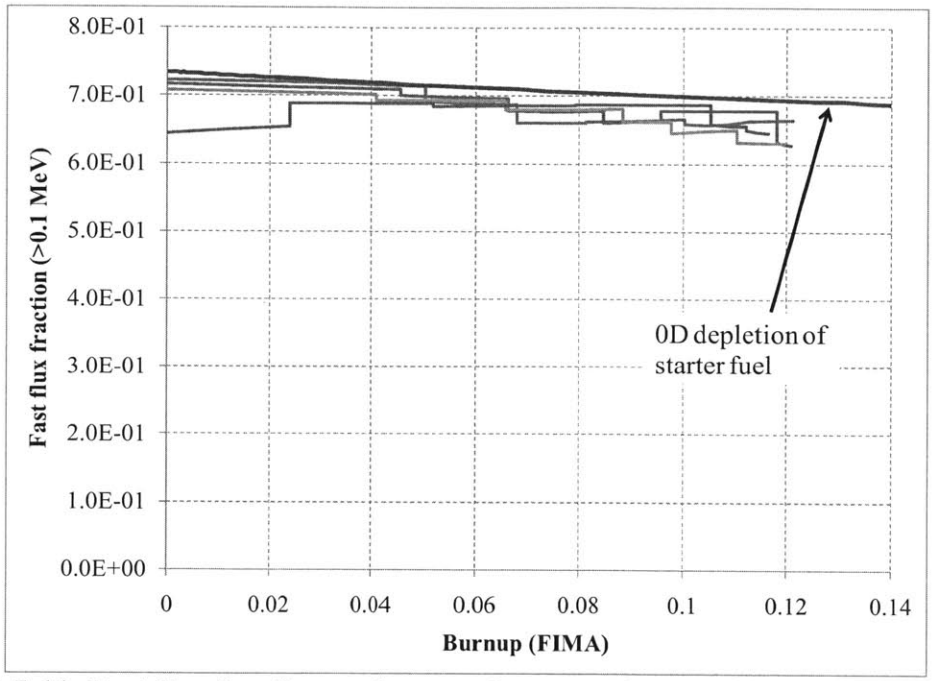

Figure 3.5-11. Fast flux fraction vs. burnup for example transition model starter fuel

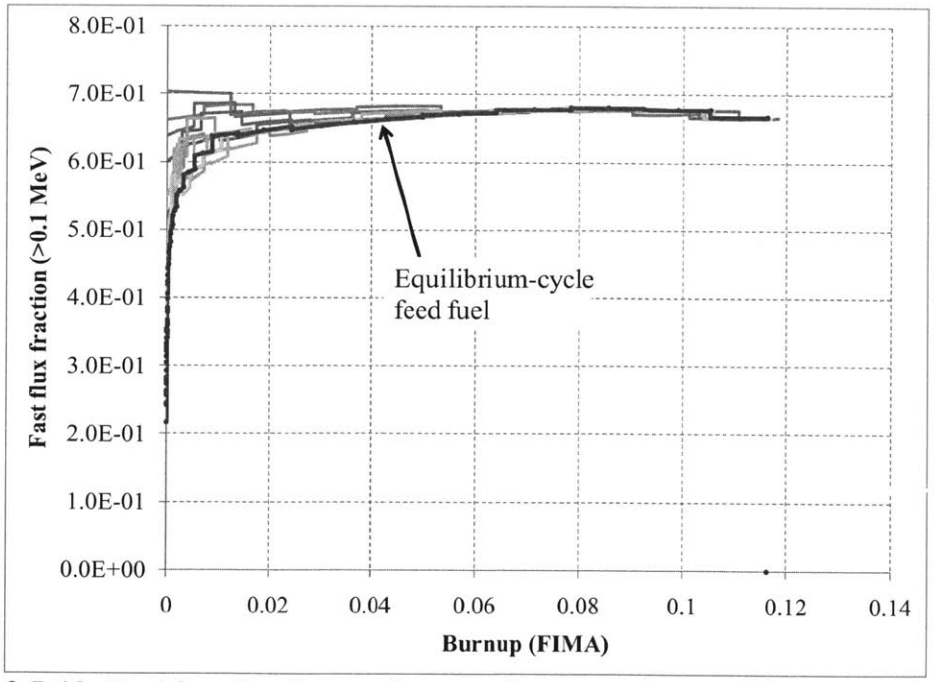

Figure 3.5-12. Fast flux fraction vs. burnup for example transition model feed fuel

The prediction in Subsection 3.5.2 for the required amount of starter fuel is remarkably accurate: the startup model required 20 cm of 15% enriched starter fuel to be burned to an average of 12.0%, while the infinite-medium depletion predicted that the starter fuel needed to be burned to 12.3%, a difference of just three percent. This example shows that it is possible to make an accurate estimate of the starting fissile requirement for a B&B equilibrium cycle without explicitly determining a transition shuffling sequence. The ability to make such an estimate is important, because as this shown in Appendix A.2, determining a transition shuffling sequence even for a simple system can be challenging and computationally expensive. More realistic systems with hundreds of fuel elements and additional constraints would be even more challenging to develop transition sequences for.

Interestingly, the effect that different neutron spectra have on the evolution of neutron excess can be significantly reduced by plotting neutron excess as a function of material damage instead of fuel burnup. Irradiation induced material damage is measured in units of displacements per atom (DPA), and DPA cross sections as a function of material are available in the International Reactor Dosimetry File [IAEA, 2010c]. Additional details about DPA calculations for different materials are provided in Chapter 5. Figure 3.5-13 shows the neutron excess evolution of the different fuel zones as a function of material DPA (measured for HT9 stainless steel) instead of burnup.

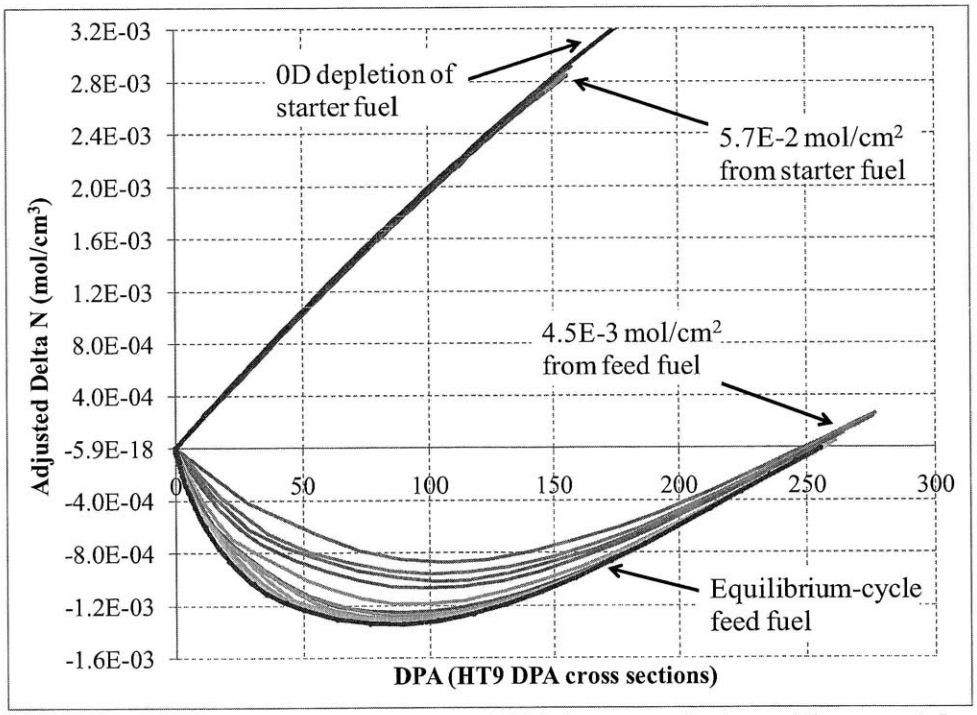

Figure 3.5-13. Neutron excess vs. DPA in example transition model

Figure 3.5-13 shows that plotting neutron excess vs. DPA causes the curves to fall much closer to each other. The curves for the starter fuel deviate by less than 2% from the infinite-medium prediction and all the feed fuel curves cross the x-axis at about the same DPA (255) as the equilibrium cycle feed fuel. The reason neutron excess correlates better with DPA than with

burnup is because DPA cross sections increase as neutron energy increases, so having a harder spectrum causes both neutron excess and DPA to accumulate more quickly.

3.5.5 Additional example transition case using discharged B&B feed fuel as starter

In the previous subsection, it was shown that in a modeled transition from starter fuel to a 1D equilibrium cycle, the neutron excess obtainable from starter and feed fuel closely matched values predicted from an infinite-medium depletion, allowing the amount of starter fuel needed to be accurately estimated. That transition case used 15% enriched uranium as starter fuel and established a convergent-divergent equilibrium cycle. This section describes the results from another transition case that establishes a convergent equilibrium cycle by reburning discharged feed fuel from another B&B reactor. The composition of the starter fuel in this example is exactly the same as the discharged composition from the same equilibrium cycle, including all fission products. Modeling this case is important because the idea of reusing bred-feed fuel from one B&B reactor to start another is central to the idea of a limited-separations fuel cycle. This additional example also provides further verification of the use of the neutron excess concept to estimate starter fuel requirements. This model is called the "second example transition model;" details of the equilibrium cycle and the transition shuffling sequence are given in Appendix A.3.

The most significant result from the second example transition model is the comparison between the neutron excess measured in the transition model and the predicted neutron excess. This comparison is shown in Figure 3.5-14. Again the starter fuel neutron excess is predicted using an infinite-medium depletion model, and the feed fuel neutron excess is predicted using the equilibrium cycle neutron excess curve.

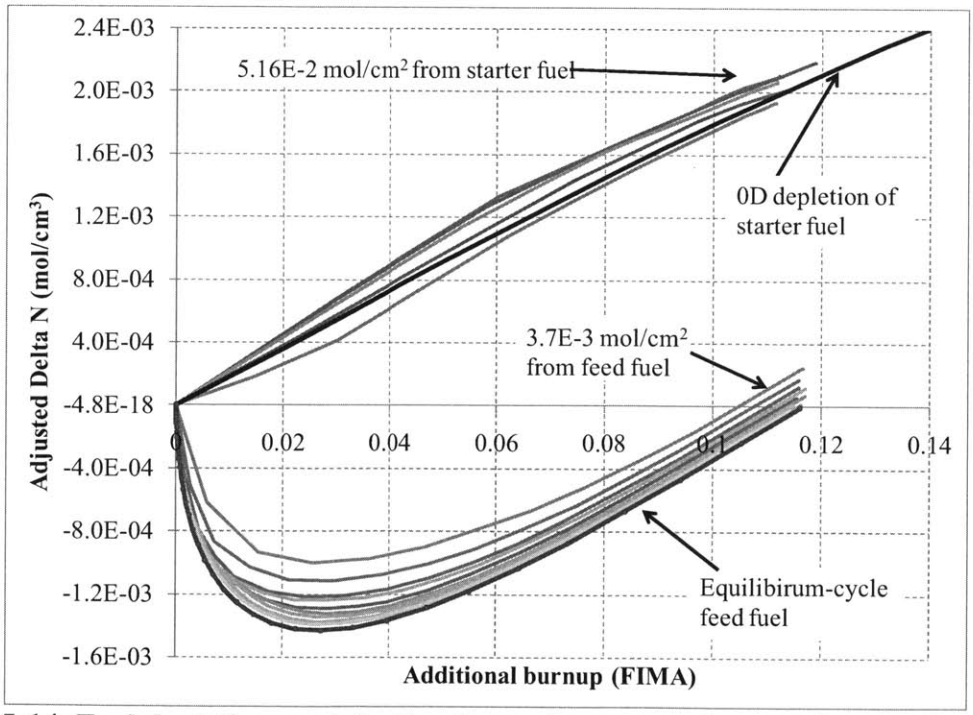

Figure 3.5-14. Fuel depletion contribution to neutron excess in second example transition model

Again, the transition feed fuel in the second example transition model is discharged with a small positive neutron excess, due to being exposed to the harder spectrum present around the starter fuel. The magnitude of this positive neutron excess is smaller than in the first example transition model, because the lower k_∞ of the starter fuel means that less feed fuel can be included in the starter fuel region at startup. At the same time, the fact that there is less feed fuel mixed in with the starter fuel causes the starter fuel to produce slightly *more* neutron excess than predicted by the infinite-medium prediction, versus slightly less with the 15% enriched starter.

To explain this behavior, Figures 3.5-15 and 3.5-16 show the fast flux fraction experienced by the starter and feed fuels as a function of burnup. Figure 3.5-16 is similar to 3.5-12, except the feed fuel is not exposed to quite as hard an initial spectrum in the second example transition model. Meanwhile, in Figure 3.5-15, some of the starter fuel in the transition model is exposed to an initial spectrum that is *harder* than in the infinite-medium depletion. This occurs because in the transition model, the neutron spectrum varies spatially, from harder in the starter fuel to softer in the feed fuel blanket. Meanwhile, in the infinite-medium depletion model, the different neutron energies are mixed together into a single uniform spectrum of intermediate hardness.

The net effect of the differences between the predicted and actual neutron excesses is that the fuel produces 10% more neutron excess than predicted by the infinite-medium depletion approximation. In the second example transition model, the starter fuel is burned to an average of 11.4% FIMA and produces 0.0516 mol/cm^2 neutron excess, while the transition feed fuel produces 0.0037 mol/cm^2, for a total of **0.0553 mol/cm^2**. This is **10%** higher than the infinite-medium approximation prediction of **0.504 mol/cm^2** for when the starter fuel is burned to 11.4% FIMA.

This error is higher than in the first example transition model, which had a total error of less than 3%, also in the conservative direction. The reason the error is higher in the second example transition model is because the lower fissile content in the starter fuel causes the infinite-medium depletion to have a softer spectrum and be more conservative. Also, the neutron spectrum experienced by the starter fuel is particularly significant when the starter is reused fuel, because the spectrum affects how much parasitic absorption occurs in fission products.

As in the first example transition model, plotting neutron excess as a function of DPA (irradiation induced material damage) reduces the error of the predictions, as shown in Figure 3.5-17. In this figure, the starter fuel neutron excess prediction underestimates the actual starter fuel neutron excess by only 2%, and the transition feed fuel has produced nearly zero neutron excess at the equilibrium cycle discharge DPA. Again, this is because DPA correlates more strongly with neutron excess, since DPA and neutron excess are affected similarly by changes in the neutron spectrum present.

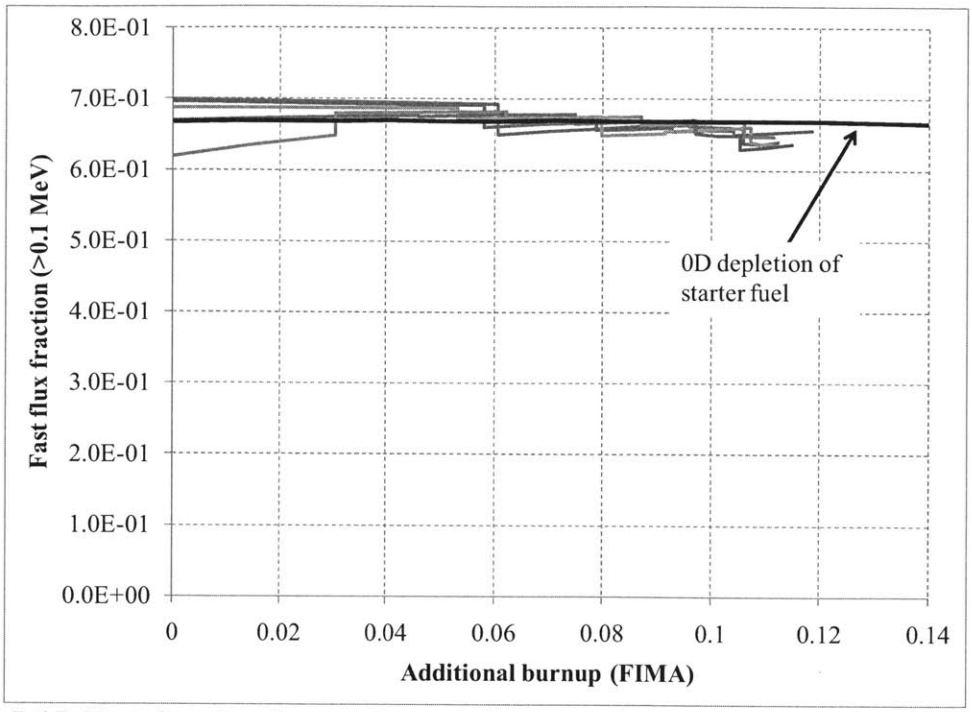

Figure 3.5-15. Fast flux fraction vs. burnup for second example transition model starter fuel

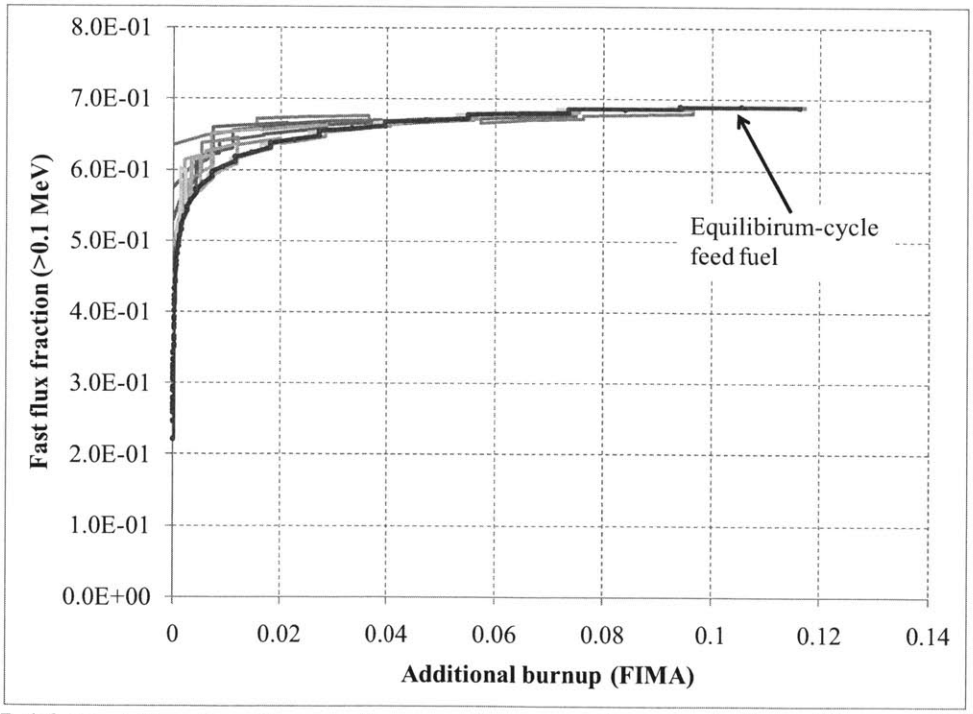

Figure 3.5-16. Fast flux fraction vs. burnup for second example transition model feed fuel

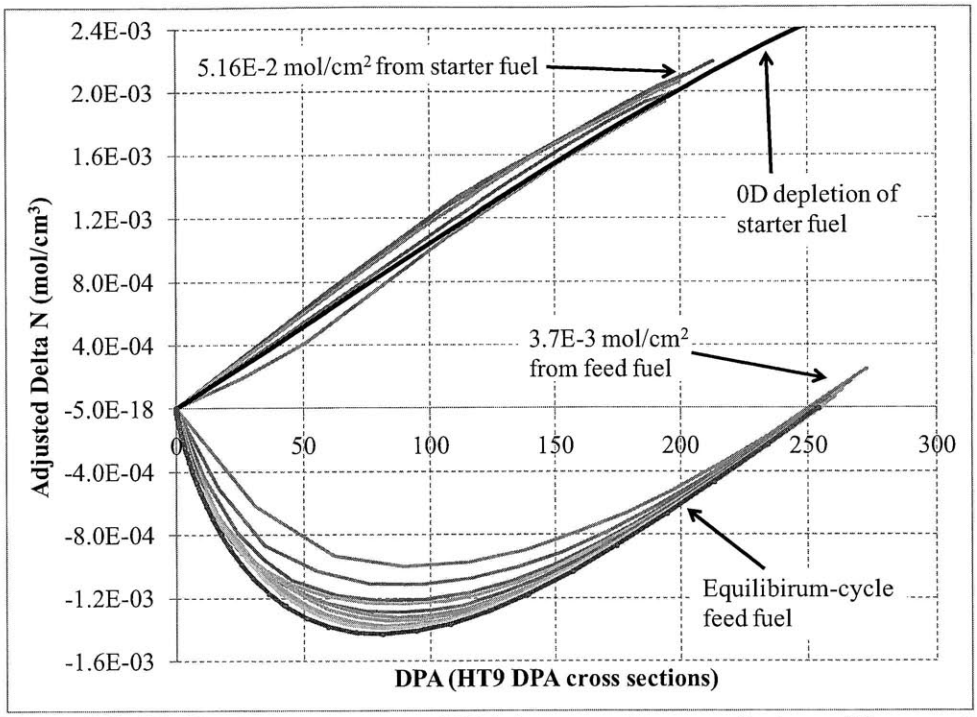

Figure 3.5-17. Neutron excess vs. DPA in second example transition model

3.6 Comparing different starter fuels

Section 3.5 shows that an infinite-medium depletion approximation is able to predict neutron excess for a given composition of starter fuel. The cases considered showed that neutron excess could be predicted as a function of burnup within an accuracy of about 10%, and that accuracy could be improved further by predicting neutron excess as a function of DPA (a measure of material damage due to radiation). One consequence of this conclusion is that an infinite-medium depletion approximation can be used to compare the neutron excess of different starter fuel compositions.

An example of such a comparison is to compare fuel compositions with different enrichments, to determine if there is an enrichment that supplies an optimal amount of neutron excess per unit of fissile material. The results of such a comparison are shown in Figures 3.6-1 and 3.6-2, which plot the adjusted neutron excess (k_{eq} = 1.03) for different enrichment fuels as functions of burnup and DPA. Also shown is a dashed curve that corresponds to the neutron excess obtainable from reusing feed fuel discharged from a B&B equilibrium cycle at 11.6% FIMA

From the two figures, it is clear that higher enriched materials supply more neutron excess at a given burnup or DPA. At high burnup/DPA, the lines become parallel as the U-235 is depleted. The reused feed has an initial k_∞ close to that of 12% enriched material, but its k_∞ drops off faster since reused feed contains more fission products and less U-238 (burnup fraction for the reused feed is in terms of initial HM concentration in the fresh fuel).

Figures 3.6-3 and 3.6-4 show the specific neutron excess (i.e. the adjusted neutron excess divided by the amount of fissile material) of the different enrichment fuels plotted as functions of burnup and DPA. The curves look different when plotted against burnup and DPA because the burnup-DPA relationship is different for the different compositions. Higher enriched material can undergo significant burnup without incurring much DPA, while unenriched material requires a large amount of DPA to first breed in plutonium-239 before it can be burned. (For example, fuel in EBR2 was able to achieve 20% burnup while staying under 200 DPA by using 67% enriched fuel.) Which factor is limiting depends on the fuel design. For high smear density fuel, swelling due to burnup can create fuel-clad mechanical interaction that can cause fuel failure. On the other hand, properly designed fuel can avoid this by allowing enough space for the fuel to swell, so the point at which fuel burnup results in fuel failure can be made to be past that needed to sustain B&B operation. Meanwhile, DPA can result in irradiation induced swelling and creep in the clad and structures of the core, and could also be a limiting factor in reactor operation. For low enrichment (<20%) fuel, the current DPA knowledge limit of ~200 DPA is likely to be more limiting than the burnup knowledge limit of ~20%.

In Figure 3.6-4, one sees that the specific neutron excess vs. DPA curves all cross at the same point at roughly 260 DPA. This behavior is not coincidental. First, the neutron spectrum is similar in all cases because of the same material fractions in each composition (the lower enrichment cases will have somewhat softer spectra, so they accumulate both DPA and neutron excess more slowly with fluence). Second, each composition can be imagined as a linear combination of two compositions: the same core composition with solely U-238 as its fuel, and a fictitious composition consisting of some concentration of U-235 and a negative concentration of U-238. At 260 DPA, the neutron excess contribution from the first composition is zero, while the contribution from the second is exactly proportional to the amount of U-235 present.

The coincident point in Figure 3.6-4 happens to occur at the discharge DPA of the equilibrium cycle, since that point is roughly where depleted uranium just manages to have a positive neutron excess. If the equilibrium cycle discharge DPA is taken as a DPA limit, and a 20% limit is assumed on enrichment (the safeguards limit on U-235 enrichment), then it makes no difference from a fissile material minimization standpoint what enrichment one chooses as starter fuel. Of course, there are other considerations besides neutron excess to take into account. For example, higher enrichment fuel will encounter higher burnup for a given fluence and may result in unwanted fuel clad mechanical interaction. Higher enrichment fuel would also occupy less volume and generate less power for a given power density limit. Lower enrichments would be more efficient if they're burned to a higher DPA or reused, although too low an enrichment may not be able to establish initial criticality. Ultimately, the interchangeability of different enrichments lends a tremendous amount of flexibility when it comes to configuring the starter fuel for a minimum burnup B&B reactor.

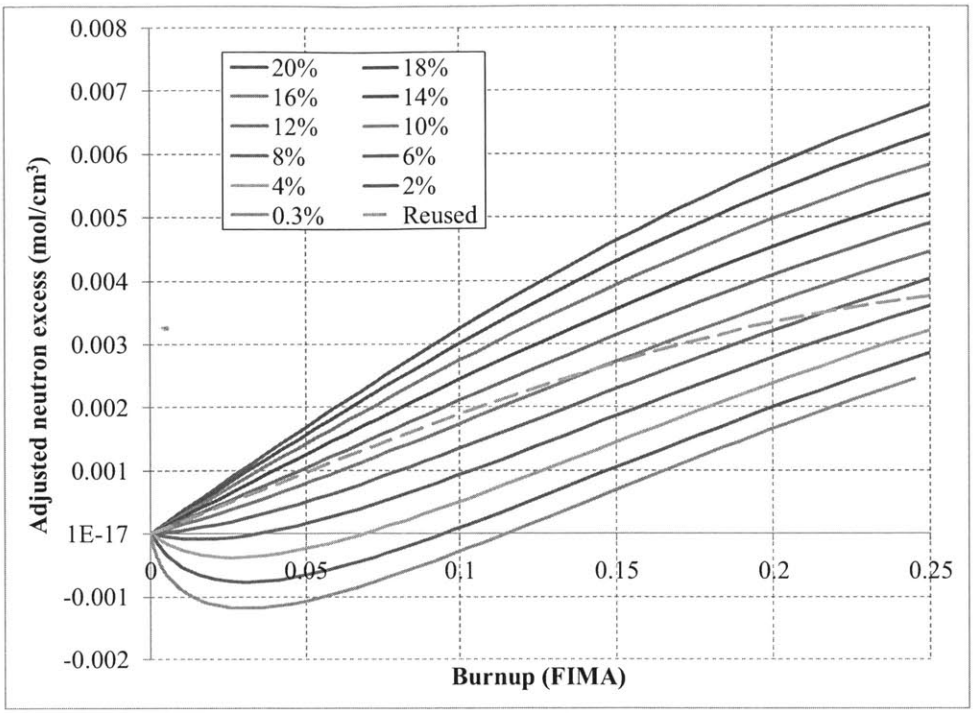

Figure 3.6-1. Adjusted neutron excess vs. burnup for different enrichments from infinite-medium depletion approximation (*k-eq.* = 1.03)

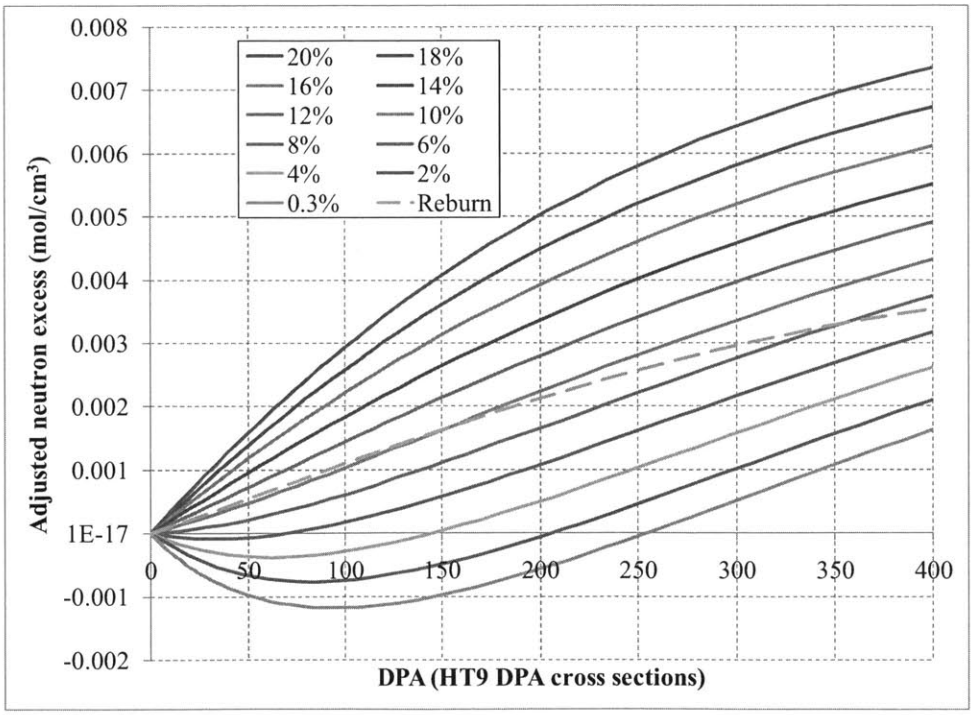

Figure 3.6-2. Adjusted neutron excess vs. DPA for different enrichments from infinite-medium depletion approximation (*k-eq.* = 1.03)

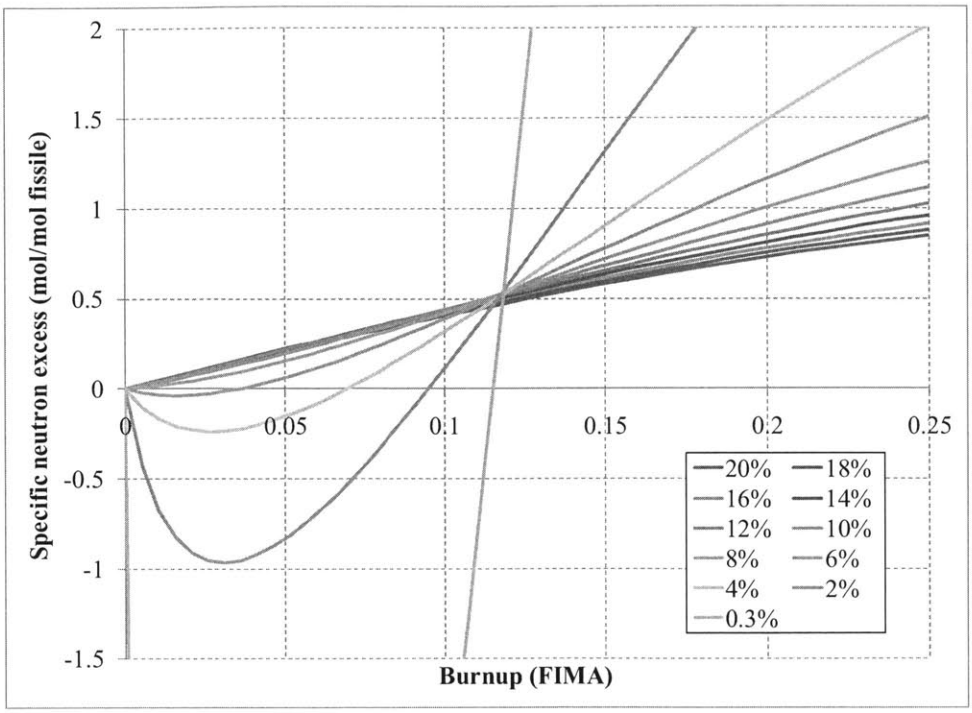

Figure 3.6-3. Specific neutron excess vs. burnup for different enrichments from infinite-medium depletion approximation (*k-eq.* = 1.03)

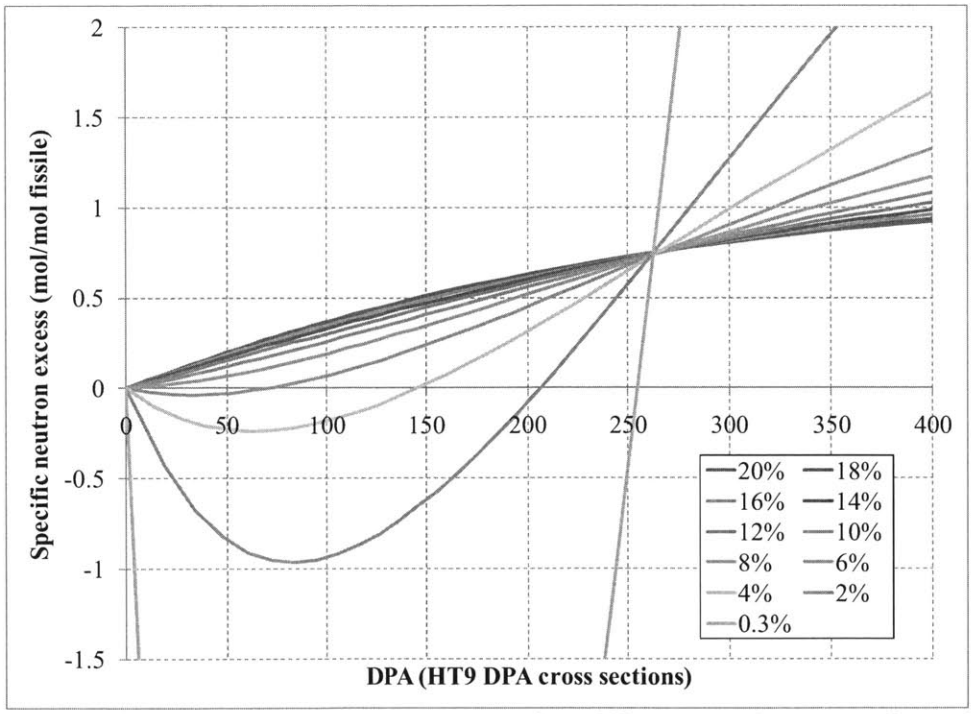

Figure 3.6-4. Specific neutron excess vs. DPA for different enrichments from infinite-medium depletion approximation (*k-eq.* = 1.03)

3.7 Realistic three-dimensional equilibrium cycle configurations

So far, just two equilibrium cycle configurations have been considered that are bounded in three dimensions, composed of spherical shells and stacked cubes (these different geometry cases were introduced in Subsection 3.2.1). The other configurations, made up of infinite slabs and infinite cylindrical shells, are not spatially bounded and cannot be implemented in an actual reactor. While the spherical shell model is spatially finite, the fact that the different zones in that model have different dimensions would make that type of geometry challenging to implement using solid fuel elements (although something similar may be possible using a pebble bed or other granular fuel configuration). The cube model is the closest to being a realistic reactor model, since it consists of congruent polyhedral fuel elements that can be exchanged with one another. In an actual reactor, these polyhedra can be any stackable shape, e.g. rectangular, triangular, or hexagonal prisms.

The cube model considered in Subsection 3.2.1 uses an equilibrium cycle shuffling scheme that converges fuel onto a central point. That choice of shuffling scheme results in a highly peaked flux and power distribution that may not be desirable in an actual reactor. The goal of this section is to investigate additional three-dimensional shuffling schemes that would be more likely to be implemented in an actual reactor. These more feasible models will be important for evaluating the reactor and fuel cycle performance of potential future B&B reactors.

3.7.1 Description of three-dimensional model

For simplicity, a rectangular prism model is considered (instead of hexagonal prisms), with fueled zones 30 cm wide, 30 cm long, and 15 cm high. The height is smaller than the width because for a desirable pancake-shaped power distribution, flux gradients would be steeper in the axial direction. The model consists of 1000 zones arranged in a 10x10x10 rectangular block, with a reflecting boundary condition on the lower z face and either reflecting or periodic boundary conditions on the lower x and y faces. Each of the upper faces has a vacuum boundary condition. The large size represented by the model (6 m wide by 6 m long by 3 m high), is to ensure that leakage is effectively zero in the cases considered.

The composition used in the three-dimensional model continues to be the simplified example core composition of 50% U, 20% Fe, and 30% Na by volume. Like in the previous models, the target equilibrium cycle discharge burnup is set to 113.7 MWd/kg, or 11.6% FIMA, which as simple models showed corresponds to an average k_{fuel} of approximately 1.04. The only differences between the models developed are the equilibrium cycle shuffling sequence used, as well as the number of fuel zones discharged per cycle.

3.7.2 Designing three-dimensional shuffling sequences

As demonstrated for the infinite slab model in Subsection 3.2.2, different equilibrium cycle shuffling paths create different equilibrium cycle power distributions, while having only a minor effect on cycle k-effective. The number of possible equilibrium cycle shuffling paths is immense due to the large number of fueled zones in the system, so rather than considering them at random, shuffling sequences were designed to try and create desirable power distributions.

What is meant by a "desirable power distribution" can be different for different types of reactors. Generally, a good power distribution is one that maximizes power in a core of a given size while staying below some steady-state or transient temperature constraint. The temperature constraint may be for the fuel (to prevent fuel melting) or cladding (to prevent fuel clad chemical interaction or cladding creep). In either case, the constrained temperature is a function of two temperature differences: the temperature rise of the coolant as it passes through the core and the temperature difference between the coolant and the clad/fuel. The first is a function of the coolant flow rate, coolant heat capacity, and the areal power density of the core, defined as the volumetric power density integrated axially. The temperature difference between the coolant and clad/fuel is a function of the local thermal resistance and local volumetric power density. Core thermal hydraulics are described in more detail in Chapter 5 and Appendix A.5.

In liquid-metal-cooled reactors, particularly sodium-cooled reactors, there is a very low thermal resistance between the coolant and clad, due to the high thermal conductivity of liquid metals. As a result, the dominant temperature rise is that of the coolant, so these systems are primarily limited by the peak areal power density in the core, where areal power density is defined as the volumetric power density integrated axially at a particular radial position (i.e., the power produced per unit area of core). The peak clad and fuel temperatures occur close to the core outlet, where the coolant is hottest, and is fairly insensitive to the axial power distribution. In such systems it is desirable to have an axially-short power distribution to allow a smaller coolant pressure drop or higher coolant velocity. A good power distribution for a liquid metal reactor would resemble a pancake: compressed axially and flat radially.

In contrast, in a gas-cooled reactor, the thermal resistance between coolant and clad can be high, especially during loss of flow transients. The local power density becomes much more important, and the peak clad/fuel temperatures occur closer to the power density peak. A good power distribution for a gas cooled system would also strive to flatten the volumetric power density distribution, resulting in a core with a taller aspect ratio than a liquid-metal reactor.

The simplest shuffling sequence is the convergent shuffling sequence considered earlier, where materials are convergently shuffled toward the center of the core. To model such a shuffling sequence, the zones in the 3D model are first ordered according to their distance from the origin[1]. In the equilibrium cycle, the n zones closest to the origin are discharged each cycle, and every other zone is incremented n steps forward. What value of n is chosen depends on the desired cycle length and discharge burnup of the fuel. Each zone in the 3D model has a volume of 13,500 cm^3, containing 128.25 kg of uranium. At the desired discharge burnup of 113.7 MWd/kg, each zone contains 14,580 MWd of thermal energy, or about 40 MW-years. For a desired reactor power rating of 1500 MWth, and assuming one desires a cycle length over one year, one would want to discharge at least 38 zones per cycle on average, or 40 zones per cycle if one wished to maintain 8-fold symmetry.

---

[1] Ties between two zones with the same distance from the origin (centers have the same axial and radial positions) can be sorted arbitrarily. It was found that different instances of random tie-breaking generally do not change the resulting equilibrium cycle state for stable, neutronically connected systems, although there are exceptions which are discussed later on in this section as they arise.

The fact that one can only discharge an integer number of zones may influence decisions regarding cycle length and fuel element volume. For example, consider a hypothetical case in which discharging three sets of 6 hexagonal assemblies corresponds to a cycle length of 300 days, but the desired cycle length is 350 days (allowing 15 days a year for shutdowns). In this situation, one would have to discharge an average of 3.5 sets of assemblies each cycle to obtain the desired cycle length. This could be accomplished by alternately discharging three and four sets of assemblies, which would yield a 2-year multi-stage equilibrium cycle with an overall reactivity swing of a 400 day cycle. To avoid having a multi-stage equilibrium cycle, it may be desirable to change the assembly volume such that a one year cycle corresponds to an integer number of assemblies.

Returning to the case of convergent shuffling, the 3D model was run at a power of 1500 MW with a cycle length of 388.8 days and 5 modeled fuel zones moved per shuffle, which is the equivalent of 40 physical fuel zones when 8-fold symmetry is taken into account. This yields an average discharge burnup of 113.7 MWd/kg, or 11.6% FIMA. The middle-of-equilibrium-cycle k-effective measured from the model is 1.044, and the $\overline{k_{eq}}$ of 1.039 is very close to the result from the 1D convergent infinite slab model (1.041).

The EOEC areal power distribution for one quarter of the core in the convergent shuffling case is shown in Figure 3.7-1. Zone average power density results from MCNPXT are fitted using cubic splines to generate the contour lines shown. The average areal power density in the innermost columns of fuel is approximately 1500 MWd/m^2, with a local peak of close to 1700 MWd/m^2. The power and flux distributions have a spherical shape, as would be expected from shuffling converging to a point. The characteristic dimension of the distributions depends both on the neutron diffusion length and the discharge burnup. A fuel material with a smaller neutron diffusion length will show more compact power and flux distributions, while a higher discharge burnup will mean a larger volume of critical fuel and result in a more spread out distributions. This latter point also means that an end of cycle power distribution will tend to look more spread out than a beginning of cycle distribution, because of the higher burnup contained within the core.

A highly peaked power distribution like that shown in Figure 3.7-1 has several advantages and disadvantages. The primary advantage is that it minimizes the physical size of a B&B system, and has a low neutron excess requirement (i.e. ΔN_{adj} integrated over the core). At the same time, such a system has the most peaked power distribution, meaning that for a given power density limit it would have the lowest power rating. As is discussed in Chapter 5, a reasonable areal power density for a sodium-cooled reactor with a coolant volume fraction of 30% is on the order of 400 MW/m^2, so core power in the convergent case would have to be lowered by about 75% to stay below this value. As discussed in Subsection 3.3.2, a highly peaked system has a large ratio of low-power breeding volume to power producing volume. This is effectively an issue of surface-to-volume ratio since the breeding volume always has a characteristic thickness; smaller systems have a higher surface-to-volume ratio and larger systems have a lower surface-to-volume ratio. As a consequence, even though convergent shuffling minimizes the volume and neutron excess requirements of a B&B core, it would actually have the highest volume and neutron excess requirements per unit power. A table demonstrating this finding is given later as Table 3.7-1.

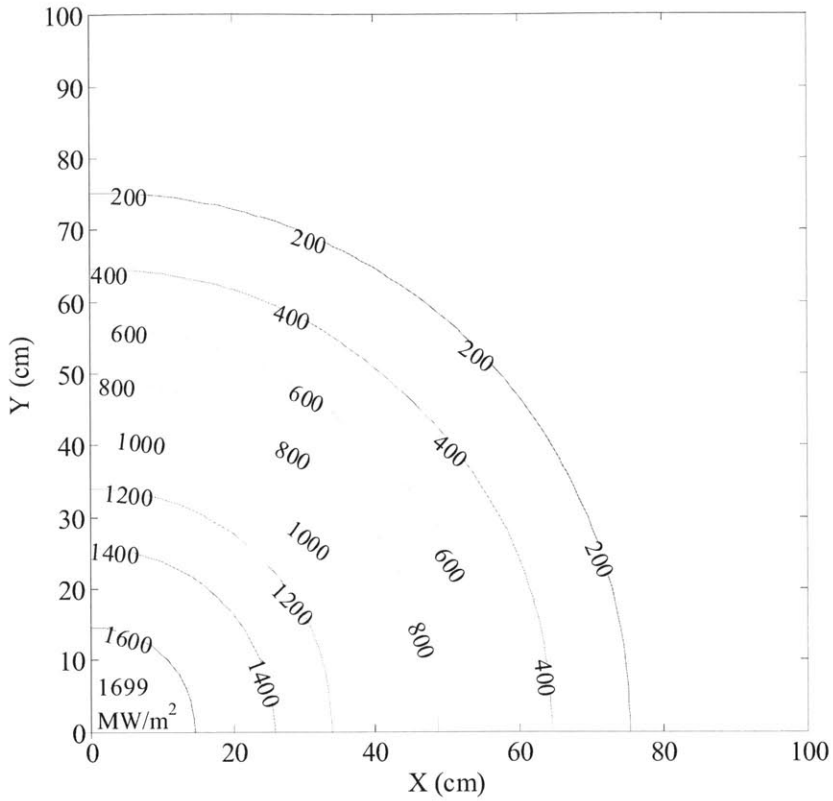

Figure 3.7-1. EOEC areal power density in 1500 MW convergent shuffling case (MW/m^2)

To create flatter, more desirable power shapes, shuffling sequences were created that move more highly bred fuel to regions where power is to be produced. Doing this shifts the power distribution to the desired locations because more highly bred fuel has a higher *k*-infinity and contains more fissile material than fresher fuel. Appendix A.4 goes into detail about how different shuffling sequences were designed and implemented, and shows contour plots of the resulting power distributions. Important analysis and results are presented in this section. Figure 3.7-2 gives an example of a large, uniform power distribution that can be achieved by specifying a particular equilibrium cycle shuffling pattern (this case is referred to as the "flattened power distribution case"). In this case, fuel is shuffled convergently in the axial direction, and in the radial direction it is shuffled from the radial center out to a radius of 180 cm (additional details about the shuffling scheme are given in Appendix A.4). Even though the total modeled power has been doubled from 1500 MW to 3000 MW, the peak areal power density has been reduced from over 1500 MW/m^2 in the convergent case to about 300 MW/m^2. If power is scaled so that the peak areal power densities are equal, the flattened distribution in Figure 3.7-2 would be capable of producing over 10 times more power than the peaked distribution arising from convergent shuffling.

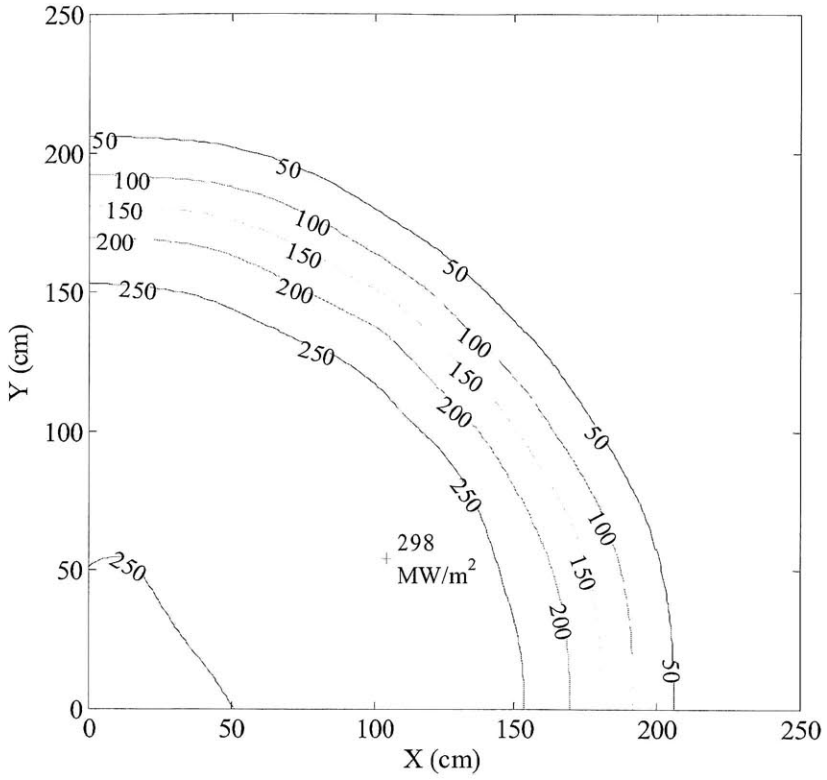

Figure 3.7-2. Areal power density of flattened power distribution case (3000 MW total power)

3.7.3 Periodic vs. reflective symmetry and local breed-burn feedback

One important behavior that arises when designing an equilibrium cycle shuffling scheme is the possibility of local breed-burn feedbacks. These feedbacks occur when there are one or more localized regions of fuel that remain in close proximity over several cycles. Higher flux in such a region causes additional plutonium to be bred there, which in turn concentrates flux even further in that region. This can result in unstable behavior in which the power distribution becomes strongly shifted toward one of these regions. This feedback behavior is unique to B&B reactors because it is a result of fuel k_∞ increasing with burnup.

One example that clearly illustrates this behavior is how the choice of rotational or reflective symmetry (i.e. one's choice of periodic or reflective x and y boundary conditions in the 1/8 core model) can have a profound effect on the equilibrium cycle behavior of a system. The flattened power distribution case shown in Figure 3.7-2 was originally run with periodic boundary conditions, which gives the case rotational symmetry and yields a very flat power distribution. Rerunning the same case with reflective boundary conditions instead produces the equilibrium cycle power distribution seen in Figure 3.7-3. In the two models, the equilibrium cycle shuffling sequence, materials, and geometry are all identical, the only difference is the choice of symmetry used. In the rotational symmetry case, the power distribution is very flat, with no preferential peaking toward either the x or y axis. In the reflection symmetry case, the proximity of more highly bred fuel to itself along the y-axis causes a local peak to form there, which reinforces itself by creating higher flux and breeding in that region. An interesting consequence of this behavior is that the discharge burnup from the reflection symmetry case is bimodal: half the

discharge fuel is burned to twice the average value (~23%) while the other half is hardly burned at all.

The way to avoid positive breed-burn feedbacks that cause locally peaked power and burnup distributions is to design shuffling sequences that can evenly spread out fuel as it is burned. If a group fuel zones spends too much time in spatial proximity, then they can form a stable region of higher power and burnup. This situation occurs in the reflection symmetry case, and is alleviated when the periodic boundary condition effectively divides this stable region into two portions.

Another consequence of local breed-burn feedback is that it is important to be cautious when modeling B&B reactors using symmetries. Imposing a *N*-fold symmetry means that one is perfectly spreading out each material among *N* regions, which may not happen in an non-symmetric model if a breed-burn instability pulls the power and flux distribution toward one of the regions. In order to avoid such instability, one needs to shuffle fuel among the *N* different regions so that no local feedbacks can develop. This means that the way in which this inter-region shuffling occurs is significant, and cannot be fully captured by use of a symmetrical model.

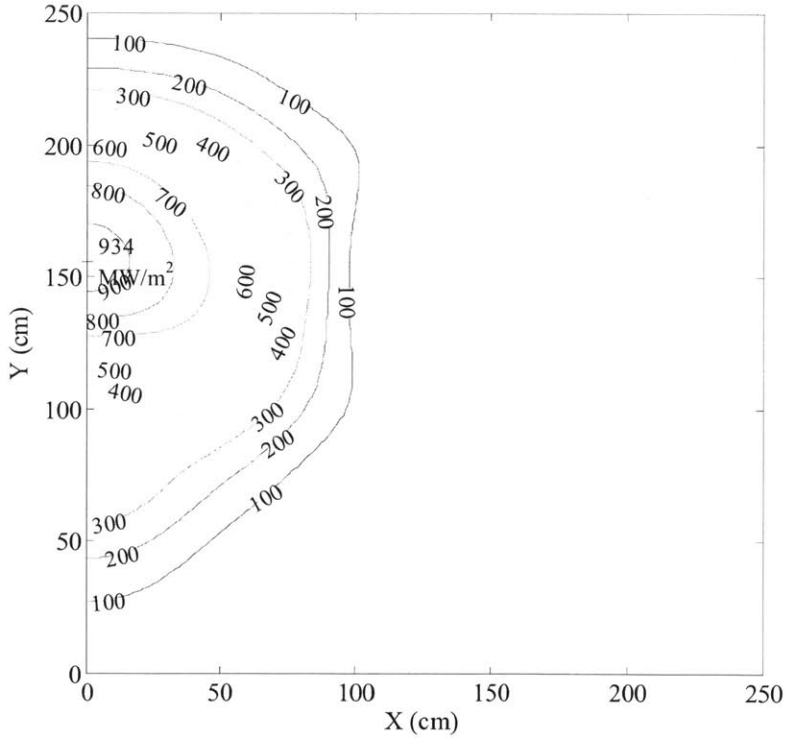

Figure 3.7-3. Areal power density of flattened power distribution case with *reflective* x and y boundary conditions (3000 MW total power)

3.7.4 Oscillatory equilibrium cycle behavior

Another example of the effects of local breed-burn feedbacks is the possibility of oscillatory equilibrium cycle behavior. Such behavior occurs when a local breed-burn region is shuffled such that it moves as a cohesive unit through the core. Examples of such behavior were observed when the "radius" of the flattened power distribution case shuffling scheme was

increased past 180 cm (how "radius" is defined is specified in Appendix A.4). In these shuffling patterns, materials at different axial elevations move nearly in lockstep from the radial center of the core out to the periphery. As a result, fuel at different axial elevations becomes coupled to each other and forms a moving breed-burn feedback region.

The resulting oscillatory behavior is illustrated in Figure 3.7-4. The figure plots the beginning of cycle uncontrolled *k*-effective for three different radius cases. The higher radius cases are offset by 0.1 and 0.2 in the y direction so the three cases can be differentiated in the figure. Increasing radius causes fuel at different axial elevations to be shuffled more synchronously, which increases the stability of the moving breed burn region. In the 180 cm radius case, there is some oscillatory behavior with a period of about 4 cycles that decays to the equilibrium cycle *k*-effective with a characteristic decay time of roughly 20 cycles. When the radius is increased to 210 cm, both the amplitude and period of the oscillations increase, as well as their decay period. Finally, in the 240 cm case, the oscillations assume a period of between six and seven cycles, and do not decay with time.

If one looks at the burnup distribution in the core in the 240 cm case, one finds "waves" of higher burnup material moving from the radial center of the core to the periphery. When the highest burnup material is discharged from the central axial plane at the periphery, the high-burnup material from the axial plane above it is all moved to the center, causing the power peak to move back into the center. This behavior can be seen from the oscillatory behavior of the discharge burnup distribution, shown in Figure 3.7-5. The fact that the each axial plane of material moves almost synchronously in the larger shuffling patterns allows these oscillations to sustain themselves. The smaller radius cases do not exhibit the same behavior because the extra distance around the circumference of the ring disrupts the synchronization of the different layers.

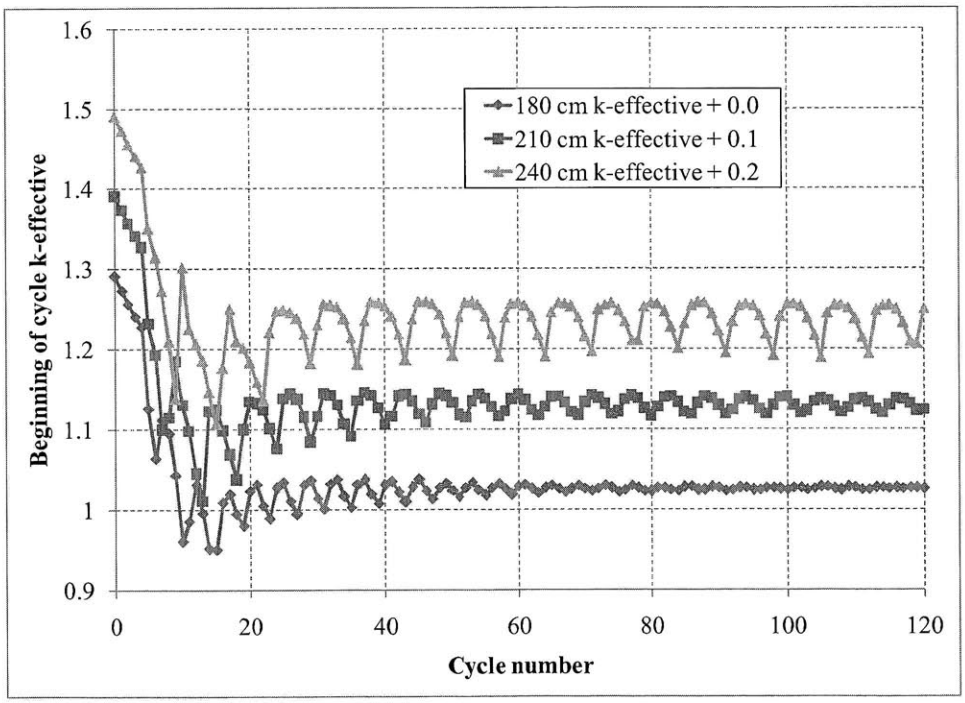

Figure 3.7-4. Oscillatory *k*-effective behavior resulting from synchronously moving fuel regions

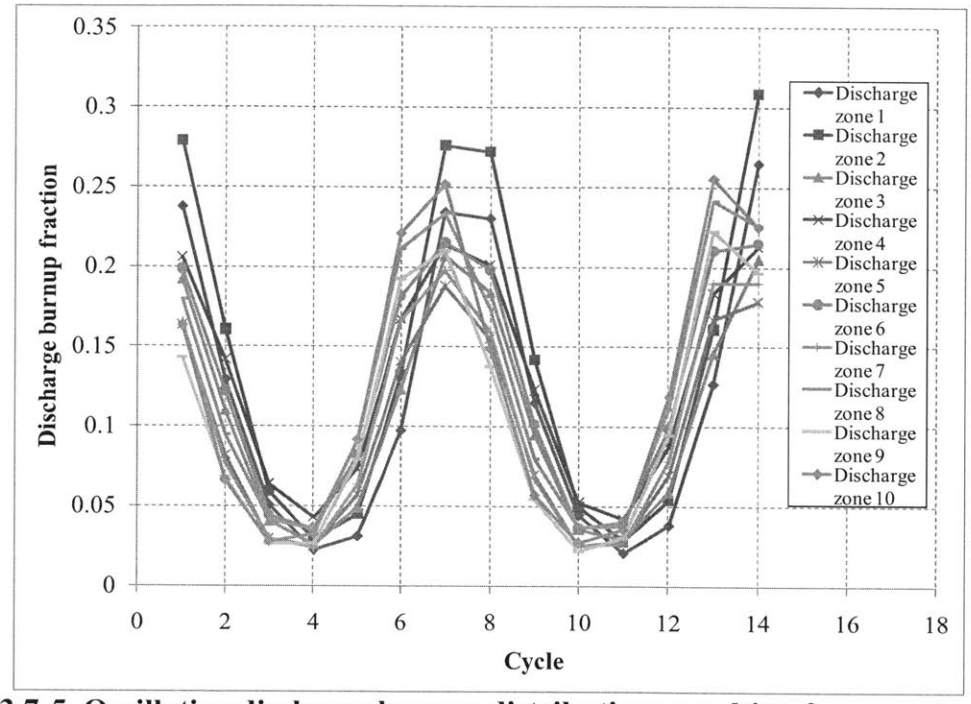

Figure 3.7-5. Oscillating discharge burnup distributions resulting from synchronously moving fuel regions

3.7.5 Summary of three-dimensional shuffling pattern performance

Table 3.7-1 summarizes the important performance parameters of nine three-dimensional shuffling patterns described in Appendix A.4. The patterns selected all have fairly azimuthally-symmetric power distributions and do not exhibit pronounced breed-burn feedback behavior; i.e. no localized power peaks are formed except in the cases where it is expected, e.g. in the convergent shuffling case. Sequence number 9 corresponds to the flattened power distribution case shown earlier. The cases selected represent a wide range of reactor sizes, ranging from 365 MW to over 5300 MW. In each case, power is scaled such that the average areal power density in the highest power assembly is 400 MW/m^2, which is a reasonable limit for a coolant volume fraction of 30%. The equilibrium cycle fuel discharge rate is the rate at which each configuration uses feed fuel, and is proportional to the total power.

One notable result from Table 3.7-1 is that the MOEC k-effective of the different equilibrium cycles is extremely consistent, varying by less than 0.5% across all the cases. The values for $\overline{k_{eq}}$ agree even more closely, varying by less than 0.2%, and they all agree very well with the average equilibrium k-effective of 1.041 predicted by the infinite slab model, and fairly well with the infinite-medium depletion approximation prediction of 1.032.

In terms of reactivity swing, several trends are observed that match the observations from the 1D models in Subsection 3.3.2. Within a given class of shuffling sequences (ring or pinched plane), the change in k-effective per unit energy decreases with increasing power, due to a more spread out flux distribution. Meanwhile, the strictly convergent case has the lowest reactivity swing per unit time, and the larger ring cases and pinched plane cases all have comparable reactivity swing

per unit time. Assuming a maximum cycle change in *k*-effective of 5%, the convergent case is able to have very long 4+ year equilibrium cycles, while the other cases would have more normal cycle lengths between 1.5 and 2 years.

The BOEC critical volume is defined as the volume of fuel with k'_∞ greater than unity. The size of the equilibrium cycle is computed using the same method as presented in Subsection 3.3-1. An example calculation for the three-dimensional case is given in Subsection 3.7.6. Based on the size of the equilibrium cycle, an average areal power density can be computed. The average power densities are fairly low, ranging from 61 MW/m^2 in the convergent case to 194 MW/m^2 for the flattened power distribution case, a factor of two to eight lower than the peak power density of 400 MW/m^2. This is the case because the low power breeding region makes up a large fraction of total core volume and area. Fuel residence time can be computed by dividing the core volume by the fuel discharge rate; as shown in the table, equilibrium cycle residence times can be fairly long for B&B reactors.

The final four rows in Table 3.7-1 contain information that is important for evaluating fuel cycle performance, which is discussed in Chapter 4. The "neutron excess contained in eq. cycle" entry gives the adjusted neutron excess integrated over the volume of each equilibrium cycle, and directly affects how much starter fuel is required to initiate each configuration, as discussed in Section 3.5. The "burnup contained in MOEC" entry is the integral of the fuel burnup in MWd/kg over all the fuel in the core (at MOEC); this number is important because it affects how long a given equilibrium cycle takes to establish. Also given are both these values normalized to the total power; Chapter 4 will show how the smaller the normalized values are, the shorter the reactor doubling time would be in a limited-separations fuel cycle.

Table 3.7-1. Reactor parameters for different shuffling schemes

Sequence number	1	2	3	4	5	6	7	8	9
Shuffling pattern	Convergent	Ring (r=30cm)	Ring (r=60cm)	Ring (r=90cm)	Ring (r=120cm)	Pinched (r=120cm, z.c. =0.5)	Pinched (r=150cm, z.c. =0.5)	Pinched (r=240cm, z.c. =0.5)	Pinched (r=180cm, z.c. =0.98)
Coolable thermal power *P* (MW)	365	459	803	1573	2071	2140	2762	5353	4006
Peak areal power density (MW/m^2)	400	400	400	400	400	400	400	400	400
Eq. cycle fuel discharge rate (m^3/EFPY)	0.123	0.155	0.271	0.532	0.700	0.723	0.934	1.809	1.354
BOEC *k*-effective	1.009	1.010	1.016	1.029	1.033	1.029	1.023	1.030	1.026
MOEC *k*-effective	1.044	1.044	1.043	1.041	1.041	1.041	1.042	1.039	1.042
EOEC *k*-effective	1.061	1.063	1.060	1.053	1.049	1.052	1.059	1.048	1.054
$\overline{k_{eq}}$	1.039	1.040	1.040	1.041	1.041	1.041	1.041	1.039	1.041
Cycle length (MWd)	6.30E6	6.30E6	6.30E6	6.30E6	6.30E6	6.30E6	1.26E7	1.26E7	1.26E7
Cycle length (EFPY)	4.7	3.8	2.1	1.1	0.8	0.8	1.2	0.6	0.9
Reactivity swing per energy (% *k*-eff/GWy)	2.98	3.08	2.57	1.36	0.87	1.38	1.04	0.50	0.80
Reactivity swing per time (% *k*-eff/EFPY)	1.09	1.41	2.07	2.14	1.81	2.95	2.88	2.68	3.21
BOEC critical fuel volume (m^3)	1.30	1.40	2.38	4.10	5.94	4.64	6.26	13.39	8.32
Eq. cycle height (cm)	228	213	204	210	211	198	198	194	193
Eq. cycle area (m^2)	6.00	6.56	8.16	11.96	15.84	13.80	17.55	29.79	20.63
Equivalent radius (m)	1.38	1.45	1.61	1.95	2.25	2.10	2.36	3.08	2.56
Average areal power density (MW/m^2)	60.9	69.9	98.4	131.6	130.8	155.0	157.4	179.7	194.2
Core volume (m^3)	13.7	14.0	16.6	25.1	33.5	27.3	34.8	57.8	39.8
Fuel residence time (EFPY)	111.1	90.1	61.3	47.3	47.8	37.8	37.3	32.0	29.4
Neutron excess contained in eq. cycle (mol)	6.62E3	6.92E3	8.57E3	1.45E4	2.01E4	1.77E4	2.28E4	3.88E4	2.46E4
Burnup contained in MOEC (MWd)	1.13E6	1.19E6	1.79E6	3.07E6	4.19E6	3.49E6	4.89E6	9.36E6	5.74E6
Neutron excess per unit power (mol/MW)	18.12	15.09	10.67	9.24	9.72	8.26	8.24	7.24	6.14
Burnup contained per unit power (EFPY)	8.44	7.13	6.11	5.34	5.54	4.46	4.85	4.79	3.92

3.7.6 Example size calculation for three-dimensional shuffling sequence

The size of the different three-dimensional equilibrium cycle sequences was calculated using the same method introduced in Subsection 3.3.1. First, the neutron absorption rates in each zone of the large 1000 zone model is determined, then the size of the reactor is determined by looking at how many zones comprise 99.5% of all neutron absorptions. In the three-dimensional cases, rather than looking at each zone individually, axial and radial groups of zones are considered together.

Figures 3.7-6 and 3.7-7 show the predicted leakage probability for the flattened power distribution case (using shuffling sequence number 9) as a function of how many radial and axial zones are included. In satisfying the 99.5% neutron absorption criterion in two dimensions, there is a range of solutions in which one can tradeoff between axial and radial leakage. In this example the losses are divided evenly, so the radial and axial zones are cutoff when more than 99.75% of neutron absorptions are accounted for, shown as dashed lines in the figures. The resulting core has ~57 radial zones (5.15 m^2) and 6.4 axial zones (96.6 cm) per octant, so the total core size is ~20.6 m^2 by 193 cm high. For symmetry, the number of radial zones can be rounded down to 56 without incurring much additional loss in *k*-effective. The locations of the inner 56 radial cells together with a 272 cm radius bounding circle are shown in Figure 3.7-8 (each zone is 30 cm along a side).

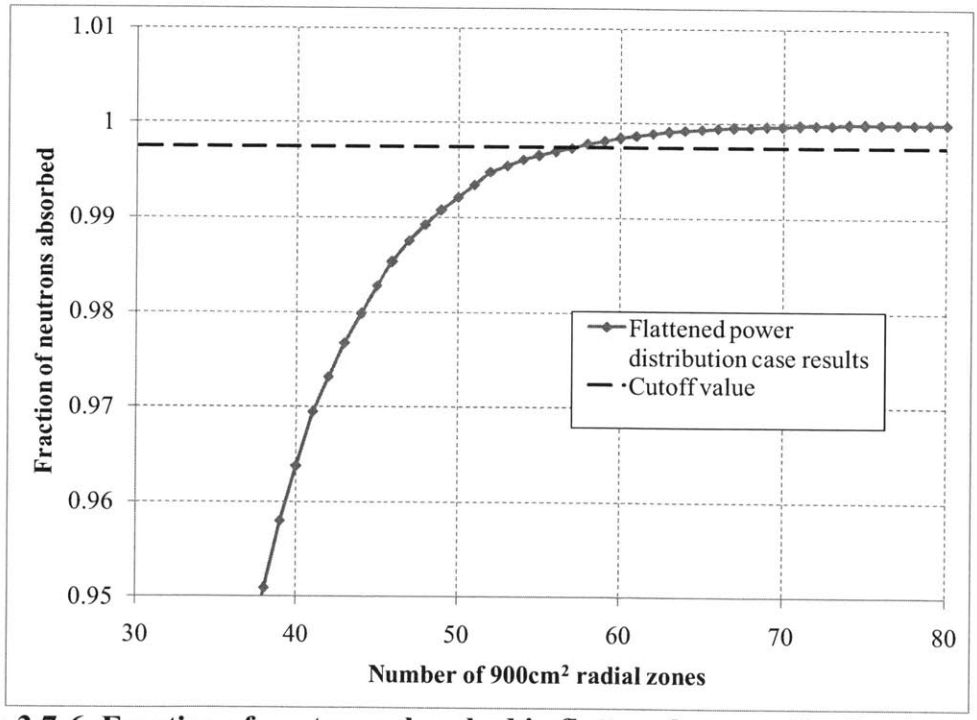

Figure 3.7-6. Fraction of neutrons absorbed in flattened power distribution case vs. number of radial zones

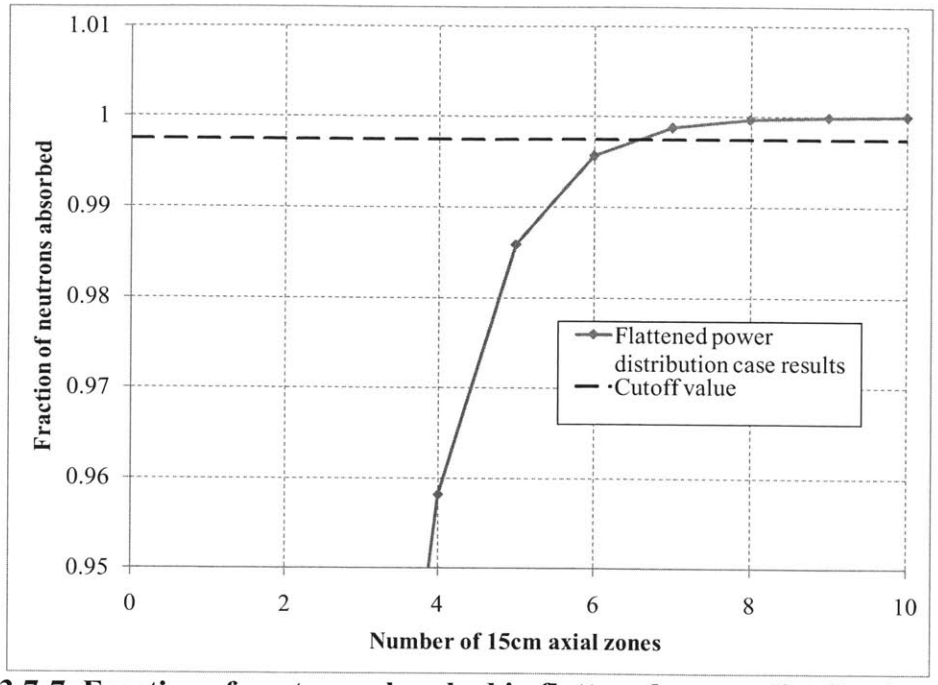

Figure 3.7-7. Fraction of neutrons absorbed in flattened power distribution case vs. number of axial zones

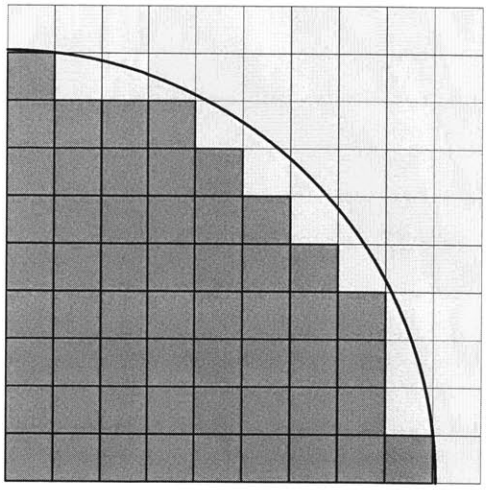

Figure 3.7-8. Radial zones falling within the 99.75% neutron absorption cutoff, with 272 cm bounding circle (each square is 30 cm by 30 cm)

Based on the leakage cutoff criterion, the 3D block reactor has a volume of 20.6 m^2 *1.94 m = 39.8 m^3. This is equivalent to the volume of about 2950 30 cm*30 cm*15 cm fuel blocks. This is a very large number of fuel blocks, and can potentially be reduced through the use of larger fuel elements, or higher burnup allowing for more leakage. Additionally, many of the "corner" zones that are far from the center both radially and axially could be removed or replaced with inert reflector blocks.

Based on core size, the feed fuel residence time during the equilibrium cycle can be computed. For sequence number 9 operating at 4000 MW, the core can discharge an average of 100 fuel

blocks per EFPY, which is a volume of 1.35 m^3. Given a core volume of 39.8 m^3, this corresponds to an average feed fuel residence time of about 29 years. Residence time can affect fuel performance, the decay heat at discharge, as well as fuel cycle economics. Reducing the size of the core and feed fuel residence time also reduces the amount of fuel that needs to be fabricated when the reactor is started.

3.7.7 Axially convergent vs. axially flattened shuffling

The cases of 3D block shuffling patterns considered up to this point have all been convergent in the z-direction: this yields systems with the smallest axial height and lower neutron excess requirements, but also results in high axial peaking. This makes these shuffling designs best suited for liquid metal reactors, which are fairly insensitive to axial power shape. Flatting the axial power distribution in these cases will result in only a small increase of allowable power. On the other hand, in gas cooled systems, there is a high thermal resistance between the coolant and clad/fuel, so the volumetric power density becomes more important. Reducing the axial peaking in gas cooled systems can have a large impact on maximum power.

To demonstrate the ability to design equilibrium cycle shuffling patterns with axially flattened power distributions, five shuffling cases from Table 2.7-1 were rerun with the order of the first and third axial slices reversed. If a block was to be shuffled into the first (centermost) axial slice, it is instead placed in the equivalent position on the third axial slice, and vice versa. The net effect of this operation is to change the axially-convergent patterns from earlier into patterns that are convergent-divergent out to an axial distance of 45 cm from the x-y plane. As shown by sequence 2 in Figure 3.2.2, convergent-divergent shuffling of this type is effective for reducing the power density peak at the core midplane.

The results of the axially flattened shuffling schemes are given in Table 3.7-2, shown alongside results the original shuffling schemes. Once again, a uniform maximum areal power density of 400 MW/m^2 is assumed, even though a flatter axial power distribution could allow a larger power density limit, especially in the case of gas cooled systems. The new shuffling patterns cause peak volumetric power to decrease by 20-33%, while the areal power distributions remain very similar to those from the previous patterns. There is a small increase in axial height (using the 99.75% cutoff criterion) and critical fuel volume due to the axially longer flux and burnup distributions. Equilibrium cycle average *k*-effectives are all very close to those of the axially-convergent cases, while reactivity swing stays about the same.

For the axially flattened cases, there is a small increase in the neutron excess requirement (5-12%), and a larger increase in the burnup contained in an equilibrium cycle (20-40%). For a fixed areal power density limit, such an increase would result in a longer doubling time for the axially flattened cases. However, if one were to instead normalize the power of the different cases to have a fixed peak *volumetric* power density, then the flattened cases would have lower neutron excess requirement per unit power and could therefore achieve shorter doubling times. Therefore, axial power flattening in the manner described could be useful in reactors where volumetric power density is an important constraint, such as gas-cooled reactors. Further flattening could be accomplished by reversing the order of more axial slices than just the inner three considered in this example, or through more complicated axial shuffling arrangements.

Table 3.7-2. Reactor parameters for different shuffling schemes (with axial flattened cases)

Sequence number	4	5	6	7	9	4b	5b	6b	7b	9b
Shuffling pattern	Ring (r=90cm)	Ring (r=120cm)	Pinched (r=120cm, z.c. =0.5)	Pinched (r=150cm, z.c. =0.5)	Pinched (r=180cm, z.c. =0.98)	Ring (r=90cm)	Ring (r=120cm)	Pinched (r=120cm, z.c. =0.5)	Pinched (r=150cm, z.c. =0.5)	Pinched (r=180cm, z.c. =0.98)
Axial sequence	Conv.	Conv.	Conv.	Conv.	Conv.	Conv. Div.	Conv. Div.	Conv. Div.	Conv. Div.	Conv. Div.
Coolable thermal power *P* (MW)	1573	2071	2140	2762	4006	1620	2137	2306	2758	3928
Peak volumetric power density (MW/m^3)	515	508	635	602	657	402	406	451	443	442
Peak areal power density (MW/m^2)	400	400	400	400	400	400	400	400	400	400
Eq. cycle fuel discharge rate (m^3/EFPY)	0.532	0.700	0.723	0.934	1.354	0.547	0.722	0.779	0.932	1.327
BOEC *k*-effective	1.029	1.033	1.029	1.023	1.026	1.027	1.031	1.027	1.021	1.022
MOEC *k*-effective	1.041	1.041	1.041	1.042	1.042	1.040	1.040	1.039	1.040	1.039
EOEC *k*-effective	1.053	1.049	1.052	1.059	1.054	1.052	1.049	1.051	1.056	1.055
$\overline{k_{eq}}$	1.041	1.041	1.041	1.041	1.041	1.040	1.040	1.039	1.039	1.038
Cycle length (MWd)	6.30E6	6.30E6	6.30E6	1.26E7	1.26E7	6.30E6	6.30E6	6.30E6	1.26E7	1.26E7
Cycle length (EFPY)	1.1	0.8	0.8	1.2	0.9	1.1	0.8	0.7	1.3	0.9
Reactivity swing per energy (% *k*-eff/GWy)	1.36	0.87	1.38	1.04	0.80	1.47	1.04	1.43	1.03	0.96
Reactivity swing per time (% *k*-eff/EFPY)	2.14	1.81	2.95	2.88	3.21	2.38	2.22	3.29	2.84	3.77
BOEC critical fuel volume (m^3)	4.10	5.94	4.64	6.26	8.32	5.29	6.91	6.48	8.64	10.80
Eq. cycle height (cm)	210	211	198	198	193	218	219	214	214	212
Eq. cycle area (m^2)	11.96	15.84	13.80	17.55	20.63	12.16	15.95	14.59	18.42	21.23
Equivalent radius (m)	1.95	2.25	2.10	2.36	2.56	1.97	2.25	2.15	2.42	2.60
Average areal power density (MW/m^2)	131.6	130.8	155.0	157.4	194.2	133.2	133.9	158.1	149.7	185.0
Core volume (m^3)	25.1	33.5	27.3	34.8	39.8	26.5	34.9	31.2	39.4	45.0
Fuel residence time (EFPY)	47.3	47.8	37.8	37.3	29.4	48.4	48.4	40.0	42.3	33.9
Neutron excess contained in eq. cycle (mol)	1.45E4	2.01E4	1.77E4	2.28E4	2.46E4	1.53E4	2.10E4	1.98E4	2.47E4	2.71E4
Burnup contained in MOC eq. cycle (MWd)	3.07E6	4.19E6	3.49E6	4.89E6	5.74E6	3.68E6	4.96E6	4.95E6	6.81E6	8.21E6
Neutron excess per unit power (mol/MW)	9.24	9.72	8.26	8.24	6.14	9.43	9.83	8.61	8.96	6.89
Burnup contained per unit power (EFPY)	5.34	5.54	4.46	4.85	3.92	6.22	6.36	5.88	6.77	5.73

3.8 Summary of neutron excess applicability

This chapter confirms the applicability of the theoretical framework developed in Chapter 2, and demonstrates that very simple models can be used to accurately predict the neutron excess quantities of realistic systems. Section 3.1 confirms the relationship between neutron excess quantities and equilibrium cycle average k_{fuel} developed in Chapter 2. It shows that this burnup-reactivity relationship is independent of cycle length and that it is a function of the average discharge burnup of the feed fuel. Section 3.2 shows that the neutron excess evolution in different geometries is nearly identical, meaning that simple one-dimensional models can be used to analyze realistic 3D systems. Different equilibrium cycle shuffling sequences in an infinite slab model can be used to modify the equilibrium cycle power distribution while having only a small effect on the reactivity-burnup relationship; this conclusion is also supported by the more realistic 3D shuffling patterns in Section 3.7.

Section 3.3 shows that there is a unique relationship between size and equilibrium cycle reactivity in B&B reactors: as size decreases, reactivity decreases exponentially from an asymptotic value. This relationship can be determined using a single thick-blanket model by multiplying the asymptotic k-effective by the fraction of neutron absorptions occurring within the reactor size of interest. Section 3.3 also derives an expression that shows how placing fresher fuel in a higher flux region causes the reactivity change per unit time to increase.

Section 3.4 introduces the infinite-medium depletion approximation, which is an extremely fast and fairly accurate method of generating approximate neutron excess curves. The approximation is able to predict average k_{fuel} as a function of burnup or fluence, and is conservative (underestimates k_{fuel}) by less than 1% across a wide range of burnup.

Section 3.5 gives two example models of transitioning between startup and a desired equilibrium cycle. The models demonstrate transition sequences that evenly utilize the chosen starter fuel, do not burn the feed fuel past its equilibrium cycle discharge burnup, and have transition cycle k-effectives close to the equilibrium cycle values. The examples also show how the needed amount of starter fuel can be calculated using an infinite-medium depletion approximation for the starter fuel. In the cases considered, this calculation is accurate to within 10% when fuel burnup is chosen as the limiting parameter; if material irradiation damage (measured in DPA) is used instead then accuracy improves to within 5%. Section 3.6 compares different enrichment starter fuels using an infinite-medium depletion approximation, and concludes that choice of enrichment does not matter from a neutron excess standpoint if the starter fuel is burned to the same DPA as the equilibrium cycle feed fuel.

Section 3.7 shows how more realistic three-dimensional shuffling schemes can be designed with different equilibrium cycle power distributions. It also gives examples of an important consideration in B&B reactors: the possibility of local breed-burn positive feedback, which can lead to highly shifted power distributions as well as oscillatory equilibrium cycle behavior.

4. Limited-Separations Fuel Cycle Analysis

Section 3.5 shows how the neutron excess quantities of different starter fuel compositions can be accurately estimated using an infinite-medium depletion calculation, allowing rapid estimates of the amount of starter fuel needed to start up a B&B reactor. One highly compelling option for starter fuel is the used feed fuel discharged from an operating B&B reactor, which as shown in Section 3.6 can still retain reactivity k_∞ above unity and supply positive neutron excess, even without chemical actinide separation. This possibility allows a single B&B reactor to fan out and establish additional reactors, creating a reactor infrastructure that potentially requires no enrichment or full-separations reprocessing. One critical figure of merit for such a reactor infrastructure is the doubling time with which it can expand. Calculating the doubling time is important for determining if a B&B reactor infrastructure can realistically compete with other fuel cycle options and adequately meet global energy demand. This chapter discusses several limited-separations fuel cycle scenarios and establishes methods for computing their doubling times.

4.1 Description of baseline fuel cycle

In a limited-separations B&B reactor fuel cycle, B&B reactors operating in an equilibrium cycle would discharge used feed fuel at a steady rate. Before this fuel can be used in another reactor, it may need to spend some time undergoing cooling or some form of processing. Processing could be as simple as a physical inspection, or be as elaborate as melt-refining the fuel and casting new fuel elements, which could potentially be used to introduce a different geometry or material composition to the fuel elements. Once sufficient used fuel is available, it can be used to start up a new B&B reactor. Once this new reactor is started up, some time interval is required to burn through the starter fuel and establish the desired equilibrium cycle. The new reactor would then join the existing fleet of equilibrium cycle reactors and begin producing fuel for starting up additional reactors.

Figure 4.1-1 gives a schematic illustration of one possible limited-separations fuel cycle scenario. In this scenario, one or more first-generation B&B reactors are started up using available fissile material, e.g. enriched uranium. Once started, each reactor is capable of running indefinitely using nothing but depleted or natural uranium (or possibly thorium) as feed fuel. Even if a given plant needs to be decommissioned after 60 years, the core can be placed in a new reactor system and continue operating. After a reactor has established an equilibrium cycle, it will begin discharging used feed fuel, which can be used as starter fuel for a new generation of B&B reactors. With each B&B reactor producing fuel to start up new B&B reactors, there is an exponential growth in the number of B&B reactors with a characteristic fleet doubling time.

In this baseline scenario, it is assumed that once starter fuel is used, it is disposed in a geologic repository, rather than used repeatedly. As Figure 4.1-1 shows, there are no closed loops in the fuel cycle; fuel goes through a single path from feed in one reactor, to starter in another reactor, to disposal. Provided that no actinide separations processes are used to convert used feed fuel into new starter fuel, the example scenario is capable of operating with no separated weapons-

material inventory whatsoever, since no uranium enrichment is required after the first generation of reactors is started.

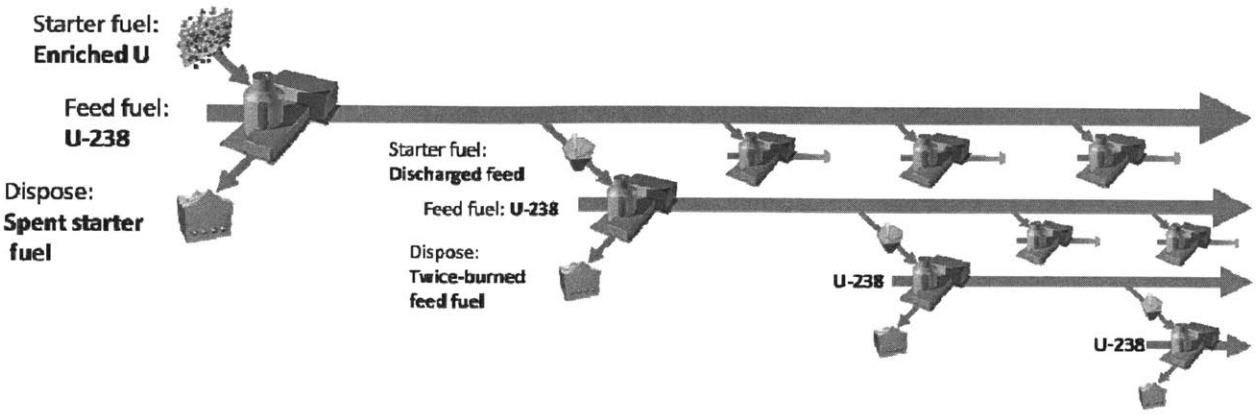

Figure 4.1-1. Schematic illustration of baseline limited-separations fuel cycle

Figure 4.1-2 shows where the two passes through a reactor fall on the schematic neutron excess curve in Figure 2.1-1. The first pass as feed fuel burns the fuel from point A to just past point C, with the slightly positive amount of neutron excess needed to maintain the criticality of the equilibrium cycle. The second pass, where the fuel is now being reused as starter fuel, burns the fuel between point C and point D, which supplies positive neutron excess. Burning the starter fuel past point D would reduce the total amount of neutron excess extracted from the starter fuel.

For core compositions that are very neutronically robust, point D may lie at a total fluence more than twice as high as point C. This creates the possibility of burning fuel for a third pass to extract even more neutron excess. As will be shown later in Chapter 5, the additional neutron excess gained from burning feed fuel to more than double the point C fluence yields only a modest benefit, so fuel cycles in which feed fuel undergoes more than two passes are not explicitly considered.

As depicted in Figure 4.1-2, B&B fuel is in principle capable of supplying positive neutron excess without needing chemical reprocessing to separate actinides or remove fission products. The fuel is not neutronically limited; instead what limits B&B reactor fuel is how much fluence or burnup it can endure before fuel failure. These non-neutronic limits can be raised either through development of advanced fuels, or by using a limited separations process to condition the fuel for further use. Such processes can include replacing the fuel cladding, refabricating the fuel using melt refining (for metal fuel), or a process similar to AIROX (for compound fuels). Removal of some fission products via these processes can increase the amount of neutron excess available from reusing fuel, an option that is discussed further in Subsection 5.3.3. The important feature of a limited-separations fuel cycle is that no process is used which increases the concentration of fissile isotopes, so it is possible to operate this fuel cycle without introducing any weapons-material production capability. Meanwhile, the concentration of fissile isotopes can always be decreased by blending used fuel with additional fertile feed.

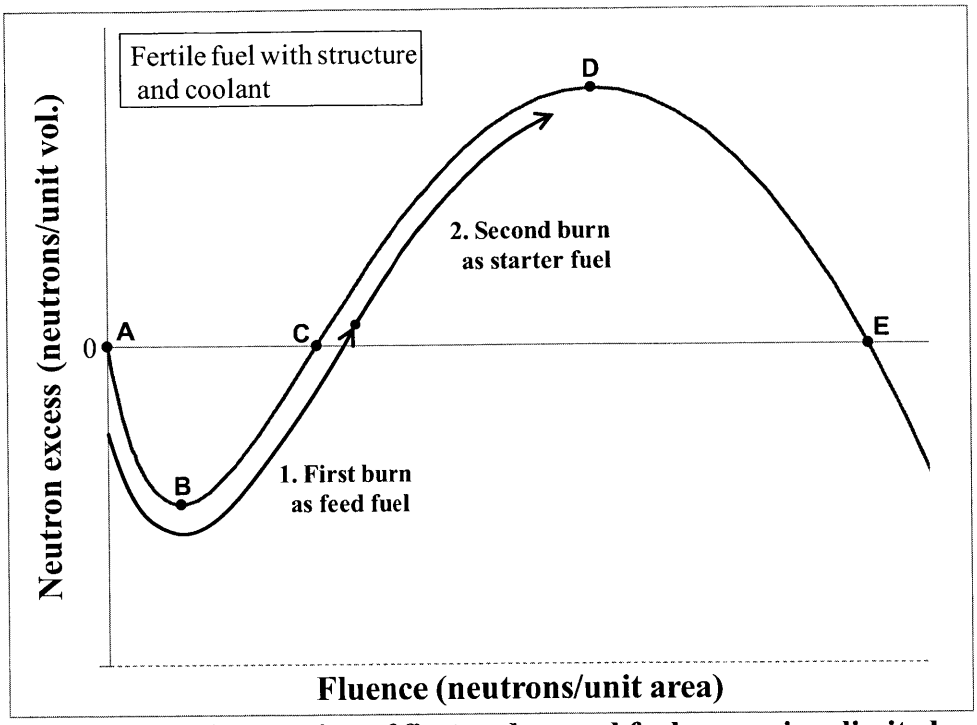

Figure 4.1-2. Schematic illustration of first and second fuel passes in a limited-separations fuel cycle

One possible feature of a limited-separations fuel cycle that is not explicitly depicted in Figure 4.1-1 is the possibility of combining discharged feed fuel from multiple reactors to start up a new reactor. The ability to pool starter fuel in this way is advantageous, since it allows new reactors to be started up earlier in time. For example, assume that an equilibrium cycle reactor requires 10 years to produce enough fuel to start up a new reactor; with 10 such reactors, pooling fuel would allow a new reactor to be started every year, whereas without pooling 10 new reactors would be started at once on year 10.

One important characteristic of the baseline fuel cycle is that each reactor is only fueled once with starter fuel, and the amount of starter fuel is chosen to be sufficient to establish the desired equilibrium cycle, as was done in the two example transition models in Section 3.5. Variations on the fuel cycle are possible in which each reactor is started up using only a partial loading of starter fuel, which can be supplemented later in reactor life with additional starter fuel. These variations on the baseline fuel cycle are described and modeled in Section 4.5.

4.2 Information used in modeling a limited-separations fuel cycle

To model the baseline scenario described, one needs to have several pieces of information:

1) The neutron excess requirement of the equilibrium cycle
2) The neutron excess content of the used fuel
3) Cooling and processing time needed before discharged fuel can be reused
4) The schedule by which used fuel is discharged after the reactor is started

Section 3.5 gives examples of how to obtain items 1 and 2. Item 1, the neutron excess requirement of the equilibrium cycle, can be computed by taking the volume integral of the adjusted neutron excess ΔN_{adj} over the fueled volume of the core at the beginning or end of the desired equilibrium cycle. Item 2, the neutron excess content of the used fuel, can be estimated by performing an infinite-medium depletion calculation of the fuel composition of interest, and then measuring the ΔN_{adj} of the fuel at its burnup or fluence limit. The composition of the reused fuel would depend on its earlier discharge composition as well as any processing it undergoes. The results of such a calculation are given in Subsection 4.2.2.

Item 3, the cooling and processing time, depends on the type of processing used. In principle, used fuel can be directly transferred to another reactor after a very short cooling period if it is transferred within a reactor park using a shielded transfer vessel. Meanwhile, using processes such as AIROX or melt refining could add one or more years to this delay time.

The last item left to calculate is item 4, the used feed fuel discharge schedule: i.e. the amount of feed fuel discharged as a function of time. Subsection 4.2.1 discusses how this discharge schedule can be approximated and compares this approximation to the results from the two example transition models.

4.2.1 Linear approximation for feed fuel discharge schedule

To model a limited-separations fuel cycle, it is important to know how much feed fuel is discharged at what time from each reactor, since discharged feed fuel is used to start additional generations of B&B reactors. To obtain an exact feed fuel discharge schedule, one would have to explicitly model a transition sequence for the reactor, which as demonstrated in Appendices A.2 and A.3 can be challenging and computationally expensive. Fortunately, it is possible to form a very good approximation for the discharge schedule, referred to as the "linear approximation," by using the same information from the minimum starter fuel calculation in subsection 3.5.2.

The linear approximation is based on treating the reactor as a control volume for burnup: the total amount of burnup in the reactor is equal to the total burnup accumulated in the reactor minus the amount of burnup that has left the reactor, as shown in Equation 4.2-1 (it is assumed here that fuel entering the reactor is defined to have zero burnup).

$$BU_{contained\ in\ reactor} = \int dt(BU\ accumulation\ rate) - BU_{discharged\ fuel} \tag{4.2-1}$$

In Equation 4.2-1, the burnup of the discharged fuel is equal to the sum of the burnup of the discharged feed fuel and discharged starter fuel. Solving Equation 4.2-1 for the total burnup of discharged feed fuel yields Equation 4.2-2:

$$BU_{discharged\ feed} = BU_{accumulated} - BU_{contained\ in\ reactor} - BU_{discharged\ starter} \tag{4.2-2}$$

In Equation 4.2.-2, the total burnup accumulated is equal to the total energy produced by the reactor in MWd. Once the equilibrium cycle is established, the other two terms on the right-hand side are known as well, allowing for the total burnup of the discharged feed to be calculated.

The burnup contained in the reactor is equal to the total burnup contained in the equilibrium cycle. The total burnup of the discharged starter fuel can be known from using a neutron excess calculation (described in Subsection 3.5.2) to calculate the required amount of starter fuel, and multiplying this amount by the assumed burnup limit on the fuel. With the three right-hand side terms known, the total burnup of the discharged feed fuel can then be calculated, which is proportional to the total amount of discharged feed since it is discharged at an approximately constant burnup.

For a hypothetical continuous B&B reactor with a cycle length approaching zero, the burnup contained in the equilibrium cycle is constant. Once the equilibrium cycle is established, no more starter fuel is discharged, so the total burnup in the discharged starter fuel is constant as well. The total burnup of the discharged feed *during the equilibrium cycle* can therefore be written:

$$BU_{discharged\ feed}(t) = P_{reactor}t - (BU_{contained\ in\ reactor} + BU_{discharged\ starter}) \tag{4.2-3}$$

Equation 4.2-3 shows that once the equilibrium cycle is established, the amount of discharged feed fuel rises linearly with time. The slope of this rise is equal to the total reactor power $P_{reactor}$, and the y-intercept is negative and equal to the total amount of burnup contained in the equilibrium cycle and starter fuel. The function in Equation 4.2-3 is shown schematically in Figure 4.2-1 as the solid line. Here the amount of burnup is expressed in EFPY by dividing by the reactor power, which makes the slope of the line equal to unity.

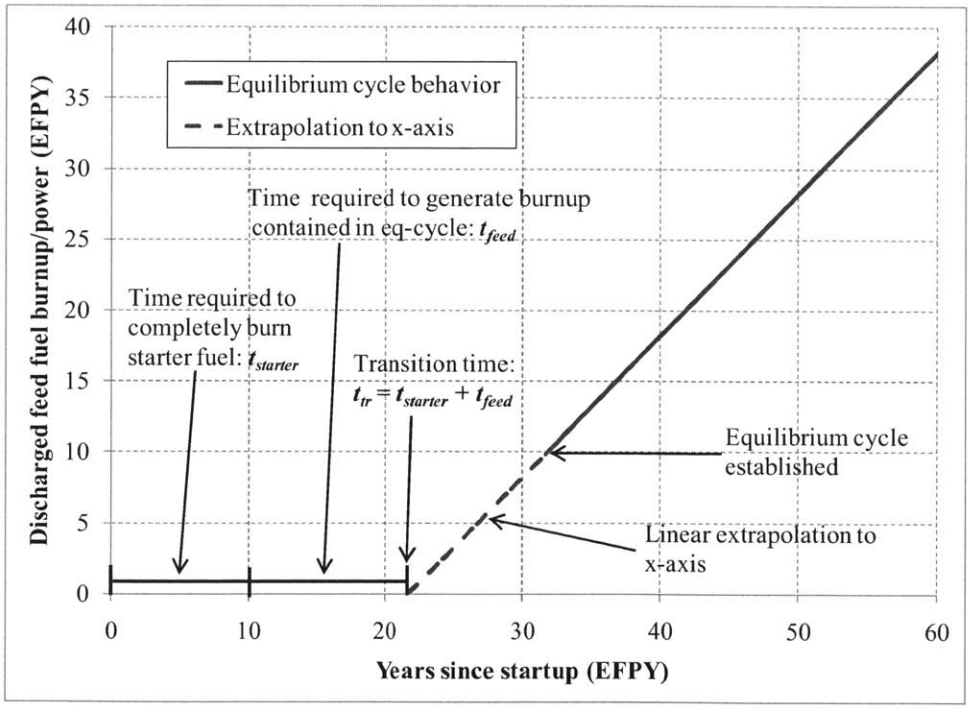

Figure 4.2-1. Linear approximation for feed discharge schedule

If one extrapolates the equilibrium cycle line back to the x-axis (the dashed line in Figure 4.2-1), one obtains the linear approximation for the discharged feed burnup schedule. As shown in the

figure, the x-axis intercept is located at the sum of the time required to completely burn through the starter fuel ($t_{starter}$) and the time required to generate the total burnup present in the equilibrium cycle (t_{feed}). The value of the x-axis intercept in the linear approximation is the "transition time" t_{tr}, so named because it is when feed fuel is first discharged, as well as the minimum amount of time required to transition to the equilibrium cycle. An expression for t_{tr} is given in Equation 4.2-4. The two volume integrals are taken over the starter fuel and the equilibrium cycle respectively, ρ is the density of the fuel in kg/cm^3, BU is burnup in MWd/kg, and P is the total reactor power in MW:

$$t_{tr} = \frac{\int_{starter\ fuel} dV \rho_{starter} BU_{discharge} + \int_{eq\ cycle} dV \rho_{feed} BU_{eq\ cycle}}{P_{reactor}} = t_{starter} + t_{feed} \tag{4.2-4}$$

In an actual reactor, initial discharge of feed fuel can occur before or after the value of t_{tr} given by the linear approximation. This is schematically illustrated in Figure 4.2-2, which shows an example discharge schedule for an early and a late discharge case. The early discharge case would occur if a piece of transition feed fuel is burned to the burnup limit before the transition time t_{tr} is reached, causing some feed fuel to be discharged earlier than assumed by the linear approximation. The late discharge case would result if there were a transitional state containing more feed fuel burnup than the equilibrium cycle of interest. In both cases, the fuel discharge curve would converge to the equilibrium cycle line as the equilibrium cycle is established. A startup sequence that leads to early initial feed discharge is desirable because the discharged feed fuel can be reused sooner.

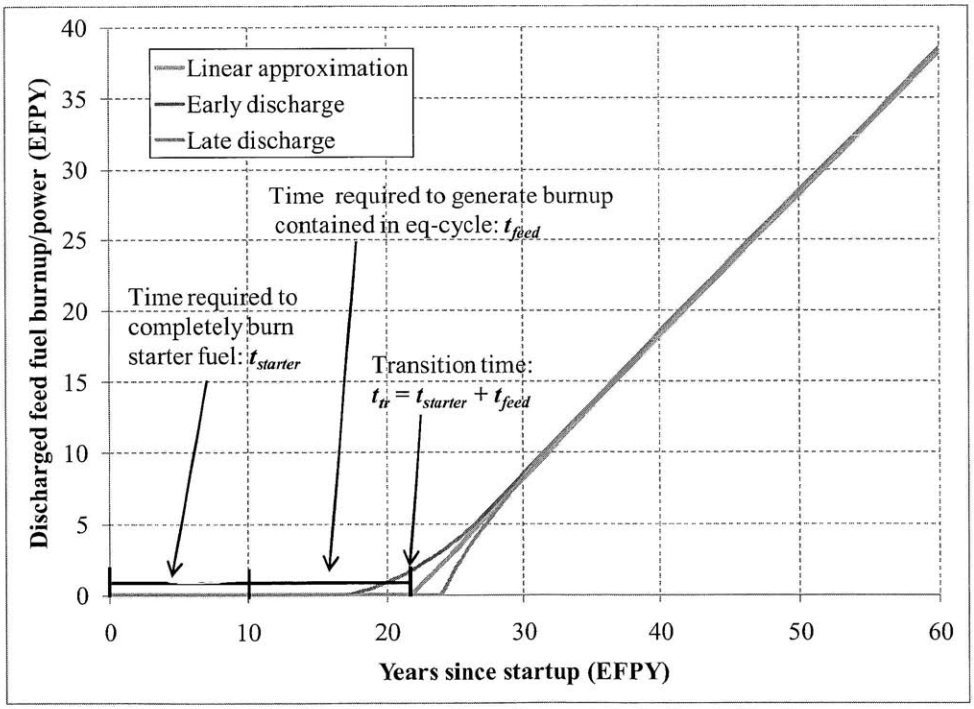

Figure 4.2-2. Examples of early and late feed discharge

In the case of a more realistic system with discrete cycles, fuel is discharged only at the end of a cycle rather than continuously. In this case, the linear approximation can be replaced with a discrete version, which is illustrated in Figure 4.2-3. In the discrete linear approximation, fuel is first discharged half a cycle later than in the linear approximation, since fuel discharge occurs at the end of a cycle rather than continuously from the middle-of-equilibrium-cycle state. The two approximations match each other very closely and would yield equivalent results if used in a fuel cycle simulation (the linear approximation results in doubling times that are shorter by less than 2%, because it discharges fuel slightly earlier than the discrete linear approximation).

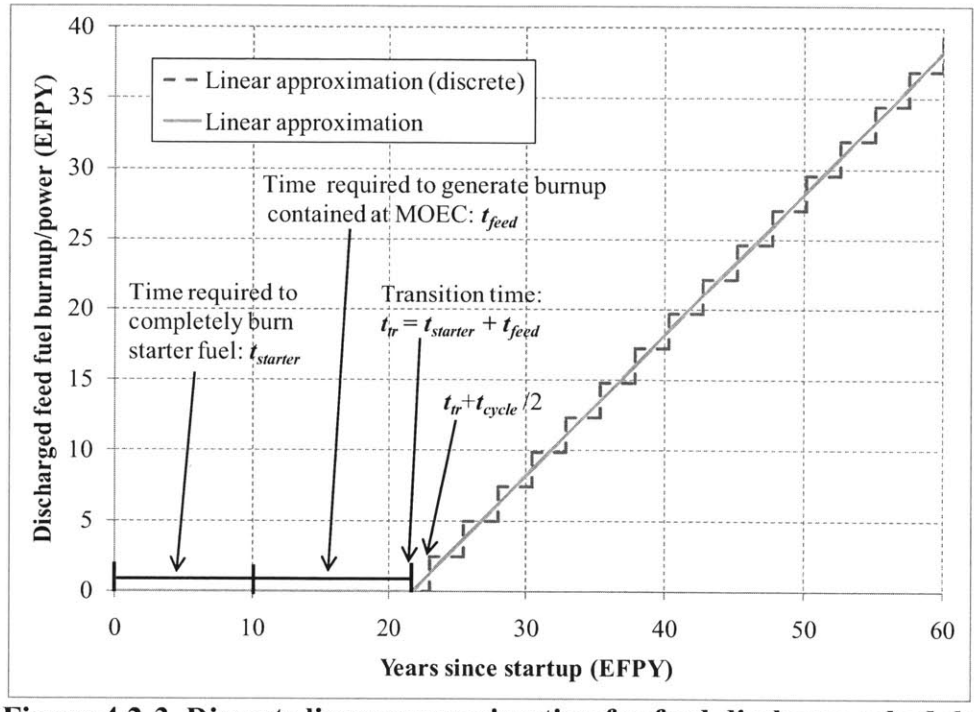

Figure 4.2-3. Discrete linear approximation for feed discharge schedule

Comparison with example transition models

Figures 4.2-4 and 4.2-5 give the actual discharge schedules of the first and second example transition models (described in Section 3.5), along with the corresponding linear approximations. In each case, the linear approximation is based on the *predicted* starter fuel burnup, i.e. it assumes that all the starter fuel is burned to its predicted value, rather than the actual burnup values from the transition models. This means that the linear approximations in these examples were determined solely through the use of neutron excess calculations, without using any of the results from the transition models.

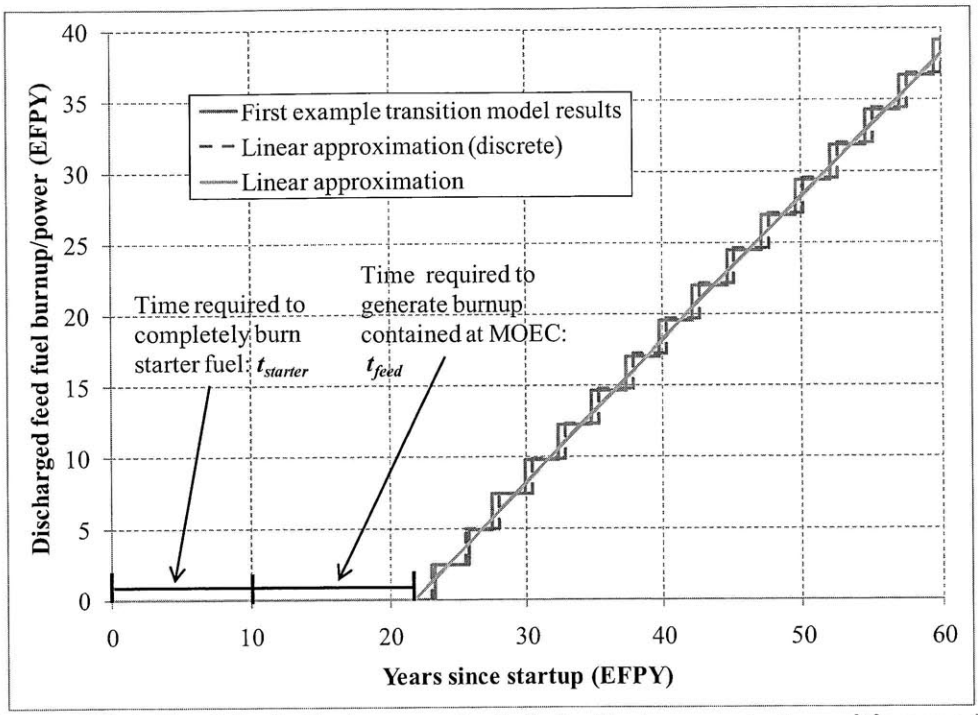

Figure 4.2-4. Feed fuel discharge schedule in first example transition model

The result from the first transition model matches both linear approximations closely, and quickly converges to the expected equilibrium cycle result. It is shifted slightly forward in time compared to the approximations because the average discharge burnup of the starter fuel (12.0% FIMA) is slightly lower than the value predicted by the neutron excess calculation (12.3%).

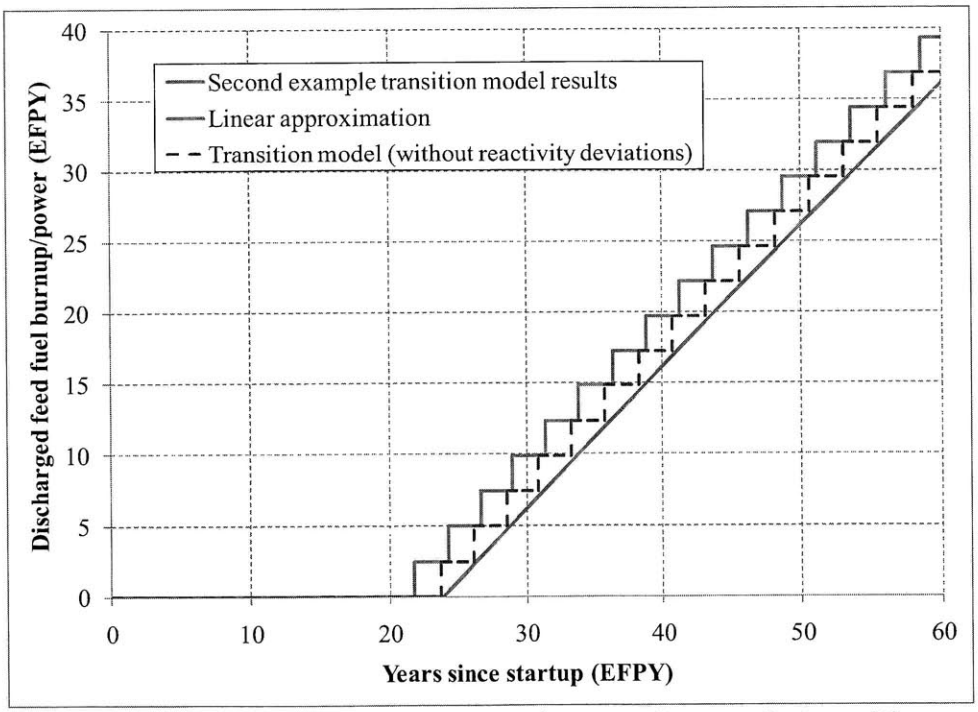

Figure 4.2-5. Feed fuel discharge schedule in second example transition model

In contrast, the result for the second example transition model is shifted forward approximately 3 years compared to the linear approximation. This shift is because the average discharge burnup of the starter fuel (11.4% FIMA) is significantly below the value predicted by the neutron excess calculation (14.6%). A significant portion of the discrepancy is due to the fact that the average k_{fuel} of the second example transition model during the transition cycles falls below the equilibrium cycle average k-effective; this means that fewer neutrons than expected are absorbed in control, reducing the amount of neutron excess needed from the starter fuel (this is shown in Appendix A.3). This portion of the discrepancy is due to the fuel management scheme used, and not due to inaccuracies from the neutron excess calculation. If one assumes that the transition shuffling sequence was chosen so that the average k_{fuel} was the same for each cycle, then one would obtain the dashed curve in Figure 4.2-5. This curve is much closer to the linear approximation, although it is still shifted by about one year forward in time. This remaining discrepancy is a result of the infinite-medium approximation being slightly conservative (by about 10%, discussed in Subsection 3.5.5) in predicting the neutron excess obtainable from the reused feed fuel.

The two examples show that the linear approximation (and the corresponding discrete version) can be used as a good estimate of the feed fuel discharge schedule. The advantage of the linear approximation is that it can be formed based on the starter fuel requirement calculation alone, and doesn't require the development of an explicit transition shuffling sequence. There is very little difference in doubling time results obtained from the linear approximation and from a fuel discharge schedule with discrete cycles; the linear approximation yields doubling times that are shorter by less than 2% because fuel is discharged slightly earlier. The main difference between the linear approximation and actual discharge schedules is error in the transition time t_{tr} prediction (such as in Figure 4.2-5). This error is directly due to the error in the starter fuel requirement calculation, and not a consequence of the linear approximation. Because it is simple and rapid to use and does not introduce significant additional error, the linear approximation is employed in the fuel cycle calculations in this thesis.

4.2.2 Neutron excess from discharged feed fuel

As shown by the fuel neutron excess curves from the example startup cases (Figures 3.5-10 and 3.5-14), not all of the feed fuel undergoes an equilibrium cycle history. The first several zones of discharged feed fuel (referred to as the transition feed fuel) undergo a different history in which they are exposed to a harder initial spectrum from their proximity to the starter fuel; as a result they are discharged with a small positive neutron excess. In the baseline fuel cycle, all of the discharged feed fuel is reused as starter fuel, so one needs to evaluate what neutron excess can be extracted from the transition feed fuel, which can be done using an infinite-medium depletion approximation.

Figure 4.2-6 gives the infinite-medium depletion results for the first nine discharged feed fuel zones from the first example transition model, as well as the result for an equilibrium cycle feed fuel zone. The results assume that the reused core composition does not change from the discharged composition, and there is no fission product removal due to processing. The results for the different feed zones all fall within a narrow band of one another, differing by only about 3% when burned an additional 150 MWd/kgIHM (kg Initial Heavy Metal, defined as the amount

of heavy metal present in the original fuel, instead of the smaller amount in reused fuel). Since the results for the transition feed fuel closely match those from the equilibrium cycle feed fuel, it is reasonable to assume that all discharged feed fuel is able to supply the same neutron excess as the equilibrium cycle feed fuel.

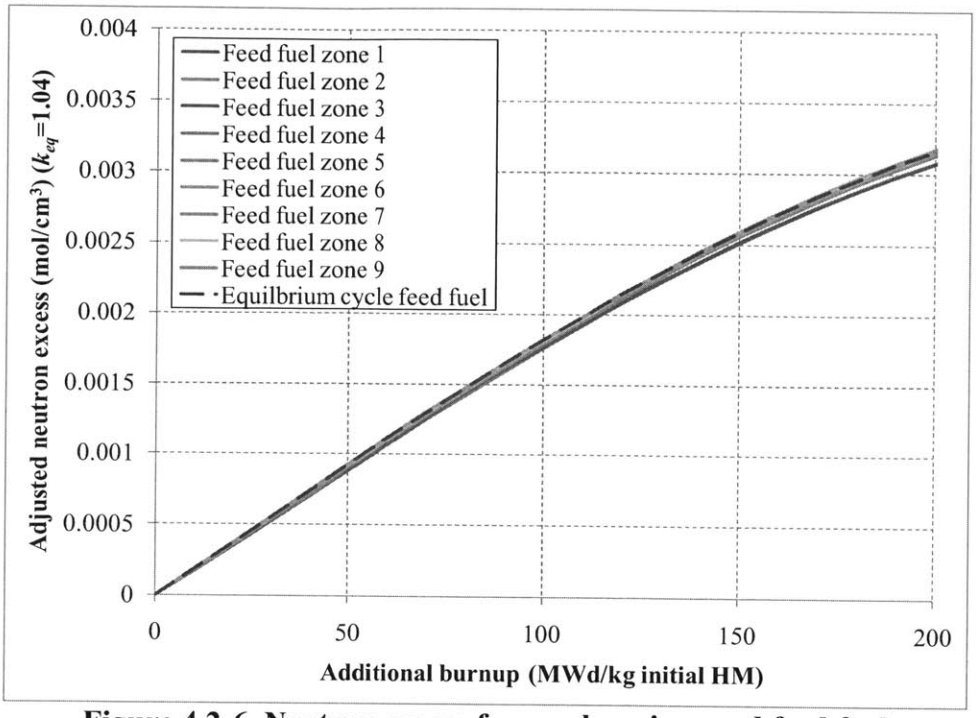

Figure 4.2-6. Neutron excess from reburning used feed fuel

4.3 Example model of baseline limited-separations fuel cycle

The reactor model assumed for this fuel cycle example calculation is the 3D block model using the simplified core composition and the flattened power distribution case shuffling sequence from Section 3.7 (sequence number 9). This shuffling scheme yields a very flat power distribution, which for a peak areal power density of 400 MW/m^2 supplies a total power of roughly 4000 MWt. The relevant reactor parameters for this shuffling scheme and the assumptions used in the fuel cycle model are given in Table 4.3-1.

Discharged fuel from the equilibrium cycle is assumed to be reburned to a total of 260 MWd/kg initial HM, which corresponds to an additional ~260 DPA (as measured on HT9) on top of the ~260 DPA sustained over the first burn to 113.7 MWd/kgHM. It is assumed that fuel cooling/processing between the two burns introduces a *processing time* (t_c) equal to 2 years, although in this example no chemical elements are removed from the fuel during this cooling time. The infinite-medium depletion approximation in Figure 4.2-6 shows that burning the used feed fuel to 260 MWd/kgHM (an additional 146.3 MWd/kgHM) yields an adjusted neutron excess of 2480 mol/m^3. The neutron excess requirement of the selected equilibrium cycle is about 24,600 mol, so a total of 9.93 m^3 of starter fuel is required for each new reactor ($V_{starter}$). At a feed fuel discharge rate (D_{fuel}) of 1.22 m^3/y (factoring in the 90% assumed capacity factor),

an equilibrium cycle reactor will produce enough fuel for a new reactor every 8.15 years. This time period t_s is referred to as the *spawning time* of the reactor. The last timescale of interest is the *transition time* t_{tr}, which as discussed in Subsection 4.2.1 is equal to the amount of time needed to completely burn through the starter fuel added to the amount of time needed to generate the burnup contained in the equilibrium cycle.

Table 4.3-1. Fuel cycle and reactor parameters

Thermal power $P_{reactor}$ (MW)	4000
Peak areal power density (MW/m^2)	400
Capacity factor*	0.9
First burn discharge burnup (MWd/kgHM)	113.7
Heavy metal density ρ (g/cm^3)	9.5
Equilibrium cycle fuel discharge rate, D_{fuel} (m^3/y)	1.22
Second burn discharge burnup (MWd/kg)	260
Neutron excess from second burn (mol/m^3)	2480
Neutron excess discharge rate(mol/y)	3022
Neutron excess required to form eq. cycle (mol)	24,600
Volume of starter fuel required, $V_{starter}$ (m^3)	9.93
Time needed for one eq.-cycle reactor to breed sufficient fuel to start a second $t_s = V_{starter}/D_{fuel}$ (y)	8.15
Cooling and processing time* t_c (y)	2.0
Time required to burn starter fuel $t_{starter}$ (y)	10.48
Time required to establish MOEC burnup t_{feed} (y)	4.36
Total transition time t_{tr} (y)	14.84 (rounded to 15 in the model)

*Capacity factor and required fuel cooling time are assumed, other quantities are calculated

The fuel cycle for this reactor was simulated using a spreadsheet model. Starting from a given number of equilibrium cycle reactors, each reactor would produce fuel at a set rate, which two years after discharge would become usable for starting a new reactor. New reactors would be started up once enough usable fuel has accumulated to start one or more new reactors. Fifteen years after a new reactor is started, it becomes an equilibrium cycle reactor; i.e. it begins to discharge feed fuel at the equilibrium cycle rate. In this example, fuel is used twice, once as feed fuel and then another time as starter fuel, and then disposed.

Results from the model for a case starting with a single equilibrium cycle reactor are given in Figure 4.3-1. The model was run with a time resolution of one year, so new reactors are only started at the beginning of each year. It takes nine years for the equilibrium cycle reactor to produce enough discharge fuel to start a second reactor, and an additional two years before it becomes ready for use, at which point a second reactor is started up. This second reactor transitions to an equilibrium cycle after 15 years, at which point it begins discharging feed fuel as well. It is assumed that the discharged feed fuel from the first and second reactors can be combined to start up a new reactor, which allows this new reactor to be started sooner than if it only accepted fuel from one reactor. For example, if reactor number 5 needed to wait for fuel from one reactor, it would have been started 8 years after reactor number 4, but since it can

accept fuel from both of the first two reactors, it can be started up just 5 years after reactor number 4.

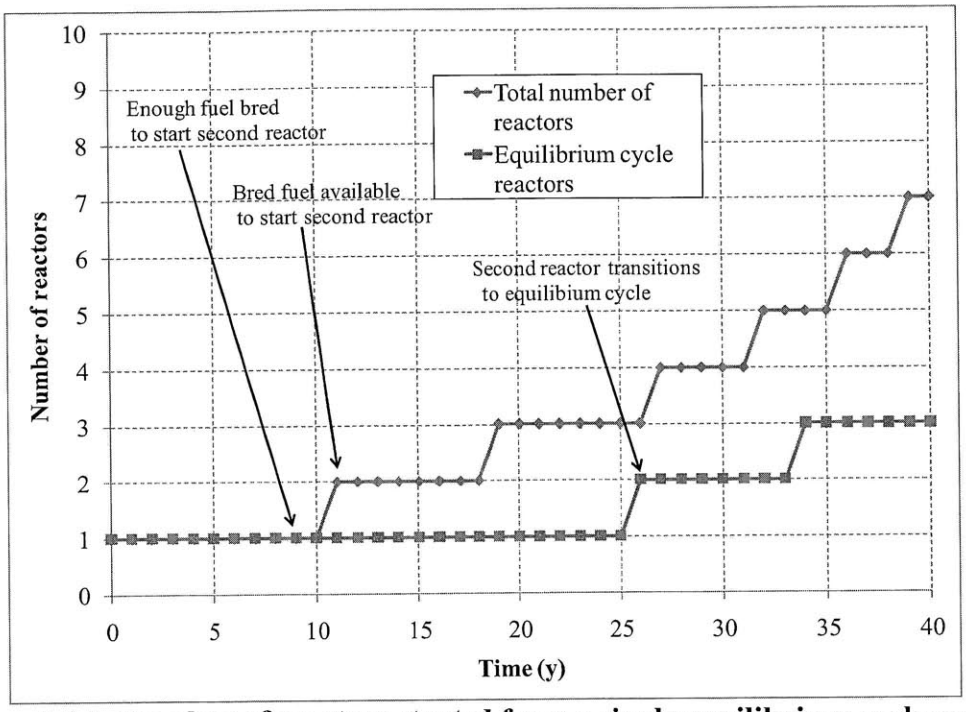

Figure 4.3-1. Number of reactors started from a single equilibrium cycle reactor

The effect of pooling fuel can be seen by modeling a case that starts with a larger number of equilibrium cycle reactors. Figure 4.3-2 shows the result for a case starting with 20 reactors instead of 1. By pooling the fuel discharged from multiple reactors, new reactors can be started sooner (year 3 instead of year 11), and new equilibrium cycle reactors appear sooner. At the end of 40 years, the number of reactors has grown by a factor of nearly 9, in contrast to a factor of 7 in the case starting with a single reactor.

If one extends the results in the two cases out to one hundred years, the trend for each case becomes clear, as shown in Figures 4.3-3 and 4.3-4. The asymptotic behavior of both cases is exponential growth, as seen in the trendlines plotted. In each case, the e-folding time is 19.8 years (1/0.0506), corresponding to a reactor doubling time of 13.7 years. In both cases the total number of operating reactors stabilizes at 2.12 times the number of equilibrium cycle reactors. The non-equilibrium cycle reactors are at different points in their transition stage, and more reactors are constantly being brought online than are reaching their equilibrium cycle.

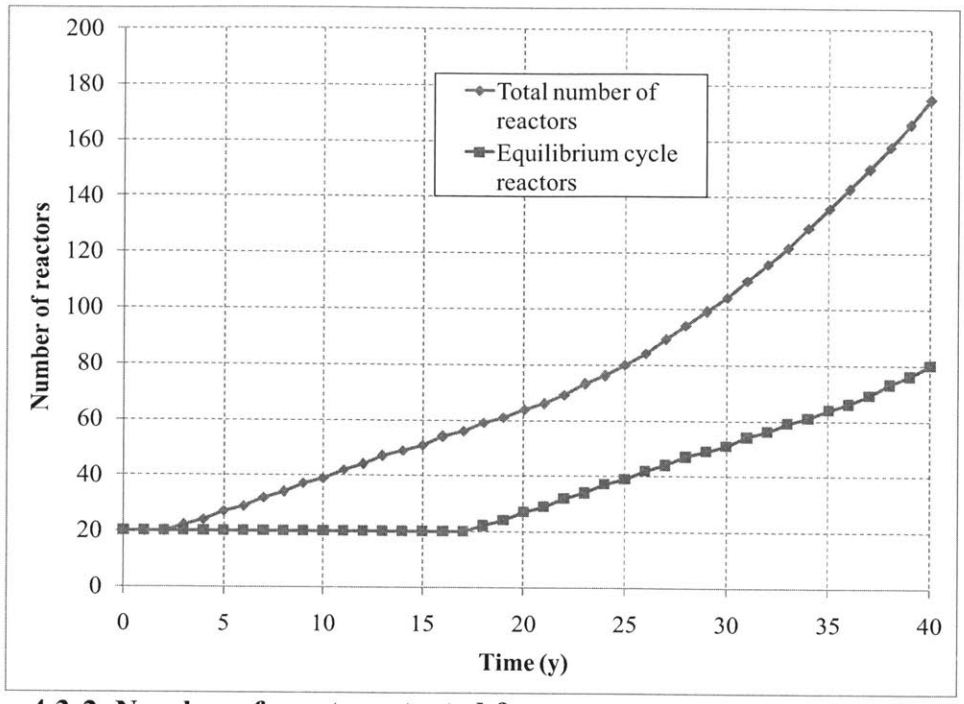

Figure 4.3-2. Number of reactors started from twenty equilibrium cycle reactors

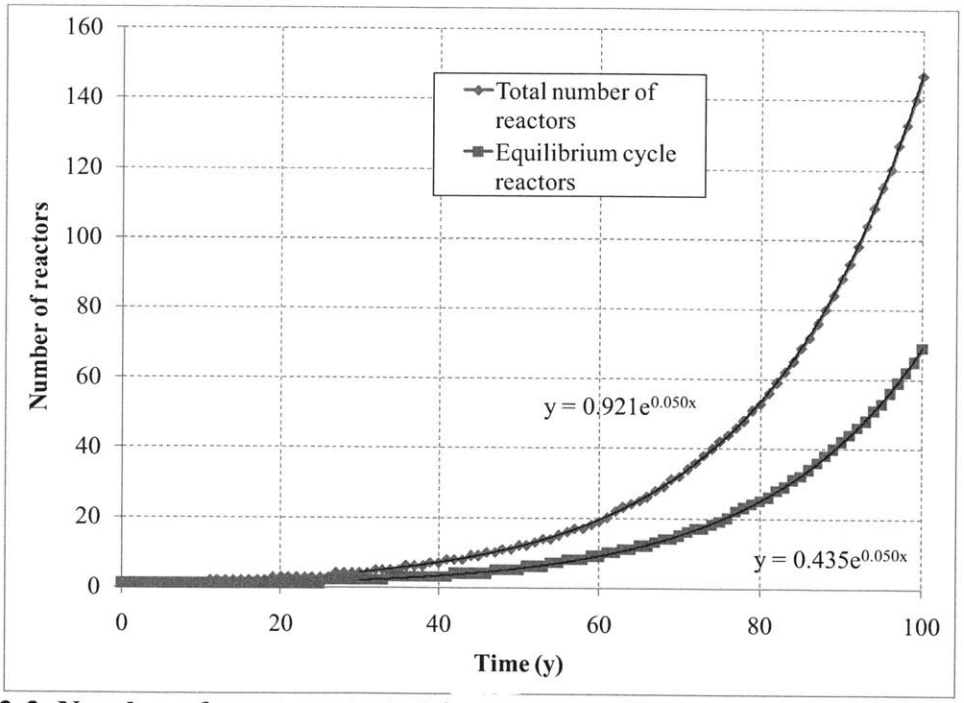

Figure 4.3-3. Number of reactors started from one equilibrium cycle reactor (100 y case)

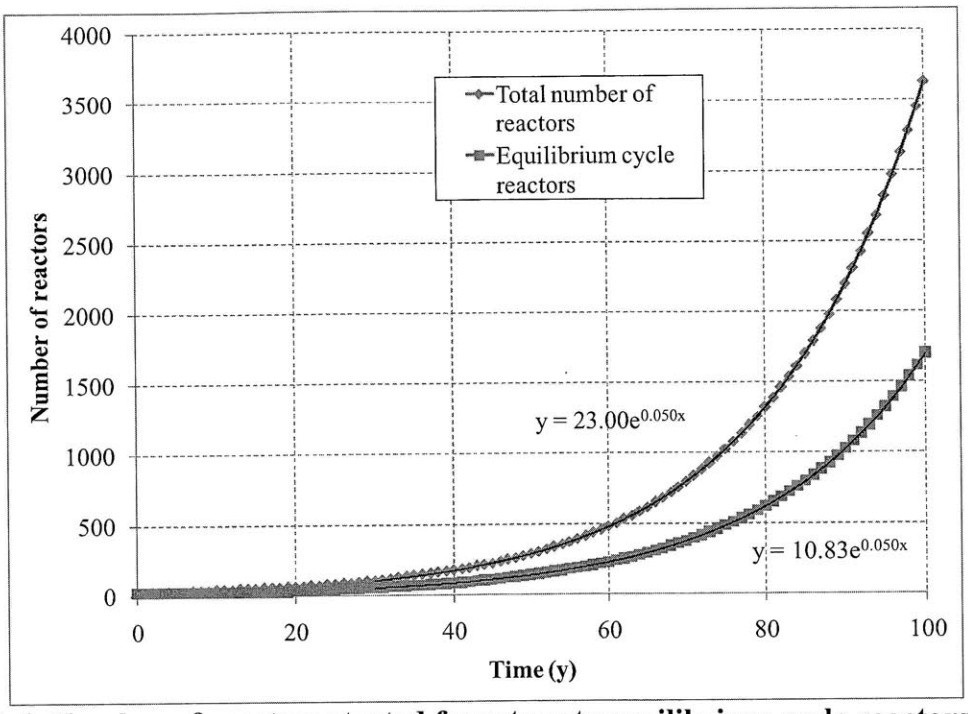

Figure 4.3-4. Number of reactors started from twenty equilibrium cycle reactors (100 year case)

4.4 Calculating reactor doubling time

The doubling time in the example scenario can be computed as a function of the reactor parameters in Table 4.3-1. A set of equations linking the total discharged fuel (F_{tot}), available fuel (F_{av}), the total number of reactors (R_{tot}) and the number of equilibrium cycle reactors (R_{eq}) are given in Equations 4.4-1 through 4.4-4. Each quantity is expressed as a function of time t.

In Equation 4.4-1, D_{fuel} is the fuel discharge rate of an equilibrium cycle reactor. Equation 4.4-1 states that the amount of discharged feed fuel F_{tot} produced is proportional to the number of equilibrium cycle reactors R_{eq} operating. Equation 4.4-2 states the amount of "available" fuel F_{av} is equal to the total amount of fuel F_{tot} shifted back in time by the cooling/processing time t_c, corresponding to when discharged feed fuel becomes available for use.

In Equation 4.4-3, the quantity $V_{starter}$ is the total amount of fuel required to start a new reactor. The equation states that the number of new reactors started is proportional to the amount of available fuel F_{av}. Equation 4.4.4 states that the amount of equilibrium cycle reactors R_{eq} is equal to the total number of reactors R_{tot} shifted in time by the transition time t_{tr}.

The equations above assume that the number of reactors R_{tot} and R_{eq} can be treated as continuous (vs. discrete) quantities, so it would be possible to have for example 2.5 reactors. This approximation is accurate for a mature reactor fleet in which there are a large number of reactors, since there is relatively little difference between N and $N\pm0.5$ reactors when N is large.

$$\frac{dF_{tot}}{dt} = D_{fuel} * R_{eq} \tag{4.4-1}$$

$$F_{av} = F_{tot}(t - t_c) \tag{4.4-2}$$

$$\frac{dR_{tot}}{dt} = \frac{1}{V_{starter}} \frac{dF_{av}}{dt} \tag{4.4-3}$$

$$R_{eq} = R_{tot}(t - t_{tr}) \tag{4.4-4}$$

Let the fraction of total reactors that are in the equilibrium cycle be Y. Then, assume the solutions for R_{tot} and R_{eq} are exponential, where t_e is the e-folding time; this yields Equations 4.4-5 and 4.4-6:

$$R_{tot} = R_0 * e^{(t/t_e)} \tag{4.4-5}$$

$$R_{eq} = Y * R_{tot} = Y * R_0 * e^{(t/t_e)} \tag{4.4-6}$$

In these equations, R_0 is the total number of reactors at time zero. By substituting Equations 4.4-5 and 4.4-6 into Equation 4.4-4, one obtains an expression for Y:

$$YN_0 * e^{(t/t_e)} = N_0 * e^{((t-t_{tr})/t_e)} \tag{4.4-7}$$

$$Y = e^{-t_{tr}/t_e} \tag{4.4-8}$$

Substituting Equations 4.4-5 and 4.4-6 into Equations 4.4-1 through 4.4-3 gives another expression for Y:

$$\frac{dF_{tot}}{dt} = D_{fuel} * Y * R_0 * e^{(t/t_e)} \tag{4.4-9}$$

$$\frac{dF_{av}}{dt} = D_{fuel} * Y * R_0 * e^{((t-t_c)/t_e)} \tag{4.4-10}$$

$$\frac{dR_{tot}}{dt} = \frac{R_0}{t_e} * e^{(t/t_e)} = \frac{D_{fuel} * Y * R_0}{V_{starter}} * e^{((t-t_c)/t_e)} \tag{4.4-11}$$

$$Y = \frac{V_{starter}}{D_{fuel} * t_e} * e^{(t_c/t_e)} = \frac{t_s}{t_e} * e^{(t_c/t_e)} \tag{4.4-12}$$

In Equation 4.4-12, the term $V_{starter}/D_{fuel}$ has been replaced by the spawning time t_s. Setting the two expressions for Y (Equations 4.4-8 and 4.4-12) equal to each other yields an expression for the e-folding time t_e:

$$Y = e^{-t_{tr}/t_e} = \frac{t_s}{t_e} * e^{(t_c/t_e)} \tag{4.4-13}$$

$$e^{((t_{tr}+t_c)/t_e)} = \frac{t_e}{t_s} \tag{4.4-14}$$

Equation 4.4-14 is a transcendental equation that contains the e-folding time t_e and the three timescales from Table 4.3-1: the transition time t_{tr}, the spawning time t_s, and the processing time t_c. A brief description of these timescales is given again below:

Transition time t_{tr}: the time between when a reactor is first started and when it begins to discharge feed fuel at the equilibrium cycle rate

Spawning time t_s: the amount of time it takes for an equilibrium cycle reactor to discharge enough feed fuel to start an additional reactor

Processing time t_c: the amount of time between when feed fuel is first discharged and when it can be reused to start another reactor

Inputting the timescales in Table 4.3-1 into Equation 4.4-14 and solving numerically for t_e yields an e-folding time of 19.4 years, equal to a reactor doubling time of **13.4 years**. Entering this result into Equation 4.4-13 yields an equilibrium cycle fraction Y of 0.465: i.e., the ratio of equilibrium cycle reactors to total reactors. These results from the continuous equations agree very well with those given by the discrete model, which predicts a doubling time and equilibrium cycle fraction of 13.7 years and 0.468 respectively. The small difference between the two results is a consequence of the spreadsheet model having a finite time resolution of one year and assuming a transition time of 15.0 years instead of 14.8 years.

Equation 4.4-14 allows reactor and fuel cycle timescales to be converted into a reactor doubling time, a very important figure of merit. The doubling time solved for by the equation is the asymptotic doubling time for a mature "equilibrium" reactor fleet, in which there is a fixed ratio of equilibrium cycle reactors to reactors undergoing transition. For a "non-equilibrium" reactor fleet, its early growth rate would depend on the reactor mix; i.e. how many reactors are operating in an equilibrium cycle and how many are in transition. Intuitively, a reactor fleet with a higher fraction of equilibrium cycle would have a faster initial growth rate since more fuel is being produced.

4.4.1 Evaluating doubling times of different shuffling sequences

Using Equation 4.4-14, the doubling times of different reactor designs can be evaluated. For example, Table 4.4-1 summarizes different reactor and fuel cycle parameters, including doubling time, for the nine three-dimensional shuffling sequences included in Table 3.7-1. The table introduces a new timescale: the "total starter burn time" (t_{tsb}), which is equal to the sum of the

spawning time (t_s) and the amount of time required to burn through the starter fuel ($t_{starter}$). This timescale represents the amount of time needed to burn the needed amount of starter fuel from zero burnup to its final burnup. The total starter burn time is useful because it is correlates closely with reactor doubling time and is proportional to the neutron excess requirement of the core. The doubling and e-folding time results in Table 4.4-1 assume a capacity factor of 90% and a fuel cooling/processing time of 2 years.

Several trends are evident from Table 4.4-1. First, there is a clear inverse correlation between average areal power density and reactor doubling time. For example, the 90 cm and 120 cm ring cases (as well as the 120 cm and 150 cm pinched plane cases) have very similar average power densities and doubling times, despite having significantly different reactor power levels and sizes. This correlation favors larger reactors, since a larger, higher power reactor will in general be able to have a higher average areal power density by having a higher ratio of power-producing fuel to subcritical breeding fuel. The convergent shuffling scheme, which has the smallest size and the lowest average power density, also has the longest doubling time. Meanwhile, the flattest shuffling scheme (sequence 9) has a larger size and the shortest doubling time. This correlation is shown in Subsection 4.4.2 to be related to a more basic correlation between total starter burn time and reactor doubling time.

Another observation is that the equilibrium cycle fraction is nearly identical across all the cases. This is due to a strong correlation between doubling time and transition time. There is also a strong correlation between the amount of starter fuel required (which affects the time needed to breed the fuel and subsequently burn it) and the burnup contained in the equilibrium cycle per unit power. Subsection 4.4.2 discusses how these correlations can be used to relate the results from these complex three-dimensional cases to those from a much simpler infinite-slab model.

Table 4.4-1. Fuel cycle and reactor parameters for different three-dimensional shuffling schemes

Sequence number	1	2	3	4	5	6	7	8	9
Shuffling pattern	Convergent	Ring (r=30cm)	Ring (r=60cm)	Ring (r=90cm)	Ring (r=120cm)	Pinched (r=120cm, z.c. =0.5)	Pinched (r=150cm, z.c. =0.5)	Pinched (r=240cm, z.c. =0.5)	Pinched (r=180cm, z.c. =0.98)
Coolable thermal power $P_{reactor}$ (MW)	365	459	803	1573	2071	2140	2762	5353	4006
Peak areal power density (MW/m^2)	400	400	400	400	400	400	400	400	400
Capacity factor	0.9	0.9	0.9	0.9	0.9	0.9	0.9	0.9	0.9
Cooling and processing time t_c (y)	2	2	2	2	2	2	2	2	2
Eq. cycle fuel discharge rate D_{fuel} (m^3/EFPY)	0.123	0.155	0.271	0.532	0.700	0.723	0.934	1.809	1.354
N. excess from second burn (mol/m^3)	2480	2480	2480	2480	2480	2480	2480	2480	2480
N. excess discharge rate (mol/EFPY)	306.3	384.6	673.1	1318.7	1736.1	1793.3	2315.3	4486.9	3357.8
Neutron excess contained in eq. cycle (mol)	6.62E3	6.92E3	8.57E3	1.45E4	2.01E4	1.77E4	2.28E4	3.88E4	2.46E4
Burnup contained in MOEC (MWd)	1.13E6	1.19E6	1.79E6	3.07E6	4.19E6	3.49E6	4.89E6	9.36E6	5.74E6
Neutron excess per unit power (mol/MW)	18.12	15.09	10.67	9.24	9.72	8.26	8.24	7.24	6.14
Burnup contained per unit power t_{feed} (EFPY)	8.44	7.13	6.11	5.34	5.54	4.46	4.85	4.79	3.92
BOEC critical fuel volume (m^3)	1.30	1.40	2.38	4.10	5.94	4.64	6.26	13.39	8.32
Eq. cycle area (m^2)	6.48	6.84	8.64	12.6	16.56	14.4	18	30.24	21.24
Equivalent radius (m)	1.44	1.48	1.66	2.00	2.30	2.14	2.39	3.10	2.60
Average areal power density (MW/m^2)	56.4	67.1	92.9	124.9	125.1	148.6	153.5	177.0	188.6
Spawning time per reactor t_s (EFPY)	21.62	18.00	12.73	11.02	11.60	9.85	9.83	8.64	7.33
Volume of starter fuel required $V_{starter}$ (m^3)	2.67	2.79	3.46	5.86	8.12	7.13	9.18	15.64	9.93
Time required to burn starter fuel $t_{starter}$ (EFPY)	27.82	23.17	16.39	14.19	14.93	12.68	12.66	11.12	9.43
Total starter burn time t_{tsb} (EFPY)	49.44	41.17	29.12	25.21	26.53	22.54	22.49	19.77	16.77
Total transition time t_{tr} (EFPY)	36.26	30.30	22.50	19.53	20.47	17.15	17.51	15.91	13.36
E-folding time t_e (y)	53.19	44.54	32.48	28.30	29.67	25.22	25.42	22.78	19.40
Doubling time (y)	36.87	30.88	22.51	19.62	20.57	17.48	17.62	15.79	13.45
Equilibrium cycle fraction Y	0.469	0.470	0.463	0.464	0.465	0.470	0.465	0.460	0.465

4.4.2 Correlating realistic 3D reactor doubling times with 1D doubling times

As shown in the previous subsection, the reactor doubling time of a reactor fleet depends not only on the core compositions of the reactors, but also on the equilibrium cycle configuration chosen. Equilibrium cycles with flatter power distributions are able to achieve faster doubling times, since they are able to produce more power (and therefore more starter fuel) for a given neutron excess requirement and transition time. The larger the reactor physically is, the flatter its power distribution can be, because there is necessarily some width of low-power breeding region around the power-producing region that absorbs excess neutrons. Increasing the size of the reactor increases the perimeter-to-area (and surface-to-volume) ratio of the system, which raises the ratio of power-producing area to breeding area and therefore the average power density. In the limit of an infinite-area reactor, the perimeter-to-area ratio approaches zero and the average areal power density can be made to equal that of an infinite slab case (e.g. picture horizontal planes converging toward the reactor midplane, while being uniformly mixed radially to prevent peaking).

The discussion on designing different three-dimensional shuffling sequences in Section 3.7 and Appendix A.5 also shows the challenges in systematically designing a flattened-power-distribution equilibrium cycle. An identical shuffling sequence can yield different power distributions for different core compositions, which may need to be burned to different discharge burnups to yield the same *k*-effective. The converse is also true: different core compositions will have different optimal shuffling sequences to achieve a target power or average power density. It is therefore difficult to establish fair comparisons between different core compositions using 3D shuffling sequences, since a longer doubling time may be attributed to either a worse core composition or a less optimal shuffling pattern. Fortunately, the performance of different 3D shuffling sequences can be correlated to that of the infinite slab case, allowing the simpler 1D model to be used for fair comparisons between compositions.

As a basis for comparing 3D and 1D models, Table 4.4-2 gives the relevant reactor and fuel cycle parameters for the convergent-shuffling infinite slab model. These results correspond to Table 4.4-1 for the three-dimensional shuffling sequences. Figure 4.4-1 illustrates there is a very strong correlation between the average areal power density of a particular shuffling scheme and its corresponding reactor doubling time. The collection of points with areal power densities between 50 and 200 MW/m^2 are taken from the different axially convergent 3-D shuffling patterns considered, while the point at 400 MW/m^2 represents the value taken from the 1-D infinite slab model. Average areal power density is defined as the total power divided by the area of the core, as determined using the 99.75% radial neutron absorption criteria. The plotted values are in units of inverse EFPY (instead of years), so no cooling time and a 100% capacity factor are assumed for the doubling times shown.

Another way of depicting the results in Figure 4.4-1 is to chart reactor doubling time vs. the radial power peaking factor in the core, where the peaking factor is defined as the peak areal power density over the average areal power density in the core. Such a chart is given in Figure 4.4-2. With the exception of the three cases with the highest peaking factors, the results lie very close to a trend line drawn through the result from the infinite slab model.

Table 4.4-2. Fuel cycle and reactor parameters for infinite slab model

Shuffling pattern	Convergent
Coolable thermal power $P_{reactor}$ (MW/m^2)	400
Peak areal power density (MW/m^2)	400
Capacity factor	0.9
Cooling and processing time t_c (y)	2
Eq. cycle fuel discharge rate D_{fuel} (m/EFPY)	0.135
N. excess from second burn (mol/m^3)	2480
N. excess discharge rate (mol/m^2/EFPY)	335.3
Neutron excess contained in eq. cycle (mol/m^2)	1.24E3
Burnup contained in MOEC (MWd/m^2)	3.65E5
Neutron excess per unit power (mol/MW)	3.11
Burnup contained per unit power t_{feed} (EFPY)	2.50
Spawning time per reactor t_s (EFPY)	3.70
Volume of starter fuel required $V_{starter}$ (m)	0.50
Time required to burn starter fuel $t_{starter}$ (EFPY)	4.77
Total transition time t_{tr} (EFPY)	7.27
Total starter burn time t_{tsb} (EFPY)	8.47
E-folding time t_e (y)	8.61
Doubling time (y)	5.97
Equilibrium cycle fraction Y	0.430

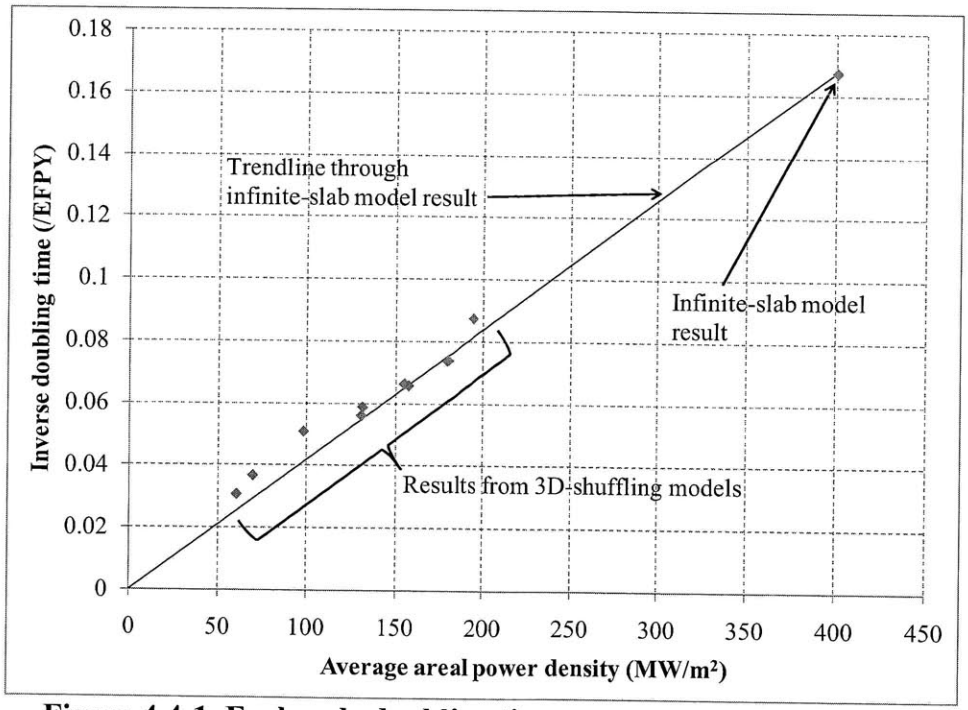

Figure 4.4-1. Fuel cycle doubling time vs. average power density

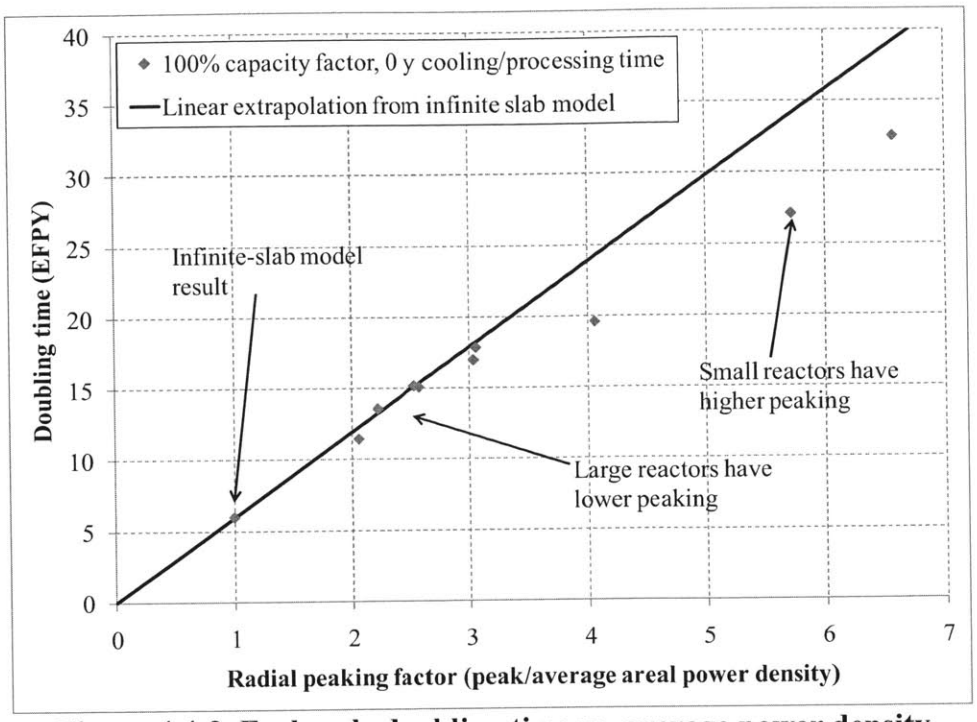

Figure 4.4-2. Fuel cycle doubling time vs. average power density

The reason the correlations in Figures 4.4-1 and 4.4-2 exist is because there are two more basic correlations relating reactor size to the factors that determine doubling time: the neutron excess requirement and the equilibrium cycle burnup requirement. The neutron excess requirement is proportional to the amount of starter fuel required, and determines how long it takes to produce the new starter fuel (the spawning time t_s) and how long it takes to burn the new starter fuel ($t_{starter}$). The equilibrium cycle burnup requirement is how much total burnup is contained in the equilibrium cycle, which determines t_{feed}, the amount of time needed to create this amount of burnup.

The correlation between reactor size and neutron excess requirement is shown in Figure 4.4-3. The figure shows that the reactor size and neutron excess requirement scale approximately linearly with each other. This correlation makes intuitive sense because it follows from the fact that the neutron excess "density" per unit area is approximately constant for all the axially-convergent shuffling schemes. The correlation does deviate somewhat for the more-spherical smaller-size cases (with higher radial peaking factors), for which edge effects become more important.

If the neutron excess requirement is proportional to the area, then the inverse total starter burn time (t_{tsb}) is proportional to the average power density, as shown in Equation 4.4-15.

$$Neutron\,excess\,requirement \sim\propto Area \rightarrow \frac{Total\,power}{Neutron\,excess\,requirement} \sim\propto \frac{Total\,power}{Area} \rightarrow \frac{1}{Total\,starter\,burn\,time} \sim\propto Average\,power\,density \quad (4.4\text{-}15)$$

In Equation 4.4-15 the ~α symbol is used to denote an approximate proportionality, i.e. a correlation. The total starter burn time (t_{tsb}) is defined as the amount of time it would take a B&B core to burn its needed amount of starter fuel all the way from 0 MWd/kg to the ultimate discharge burnup (260 MWd/kg in these examples). With this definition, the total starter burn time is proportional to the neutron excess requirement and inversely proportional to the total reactor power. It is equal to the sum of the reactor spawning time t_s (how long it takes to burn the needed amount of starter fuel from 0 MWd/kg to the first-burn burnup (113.7 MWd/kg in these examples)) and $t_{starter}$ (how long it takes to burn through the starter, i.e. burn it from 113.7 MWd/kg to 260 MWd/kg).

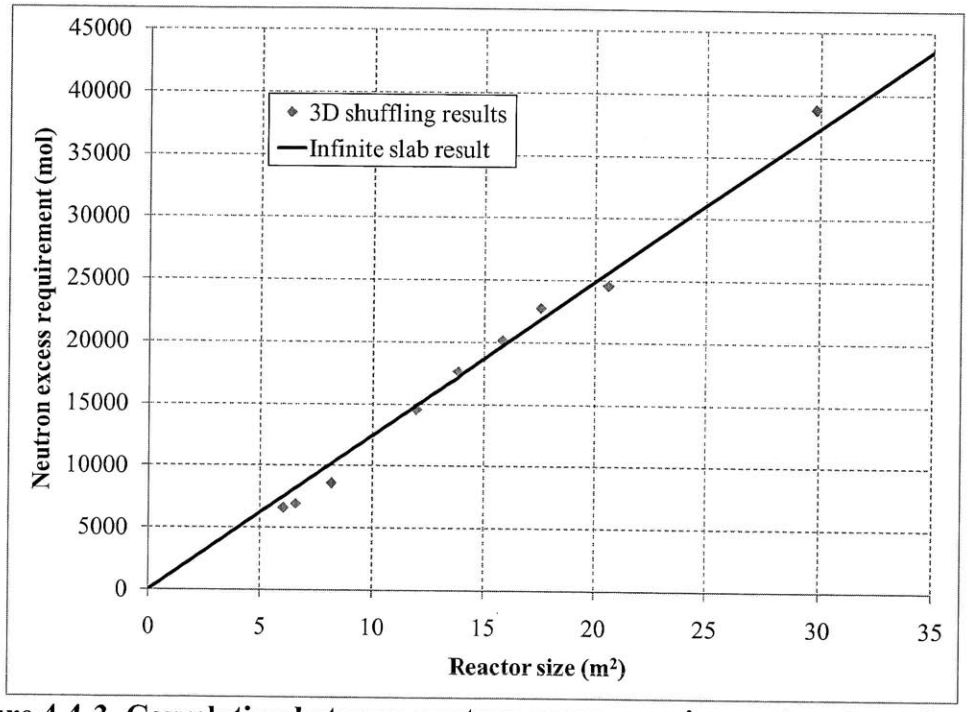

Figure 4.4-3. Correlation between neutron excess requirement and reactor size

The other correlation is between reactor size and equilibrium cycle burnup requirement, which is shown in Figure 4.4-4. The results from the 3D models fall consistently below the infinite slab result, because the 3D reactors all include a low-burnup radial boundary which functions as a breeding region, while the infinite slab model has no radial boundary, since it simulates the axial distribution in an infinite-area reactor.

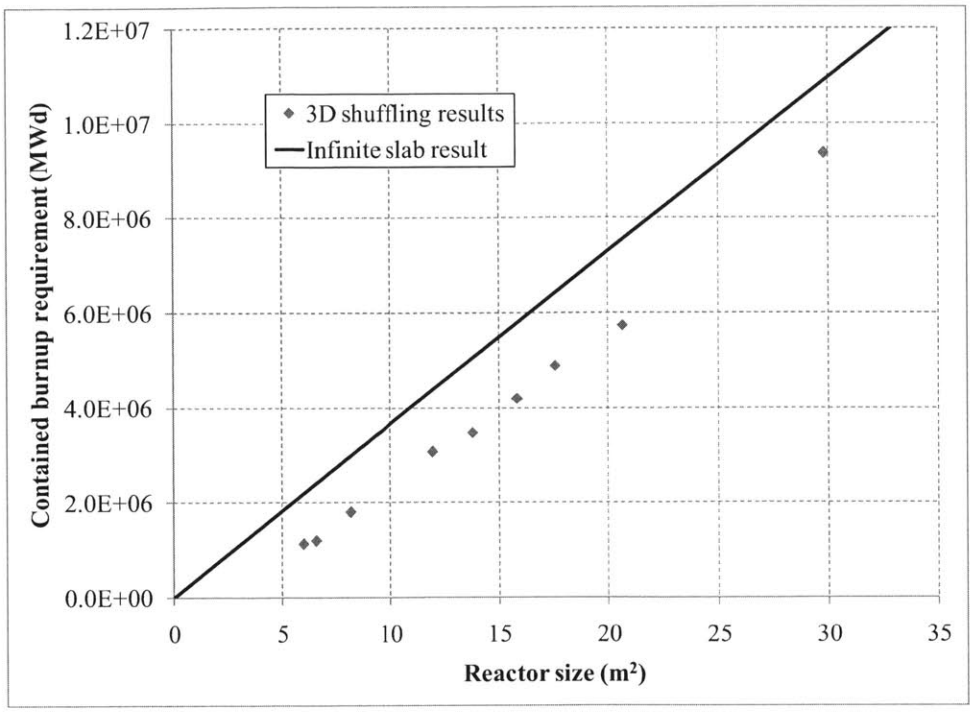

Figure 4.4-4. Comparison of contained burnup requirement versus reactor size

The amount of burnup contained determines the time t_{feed}, a component of the total transition time. If t_{feed} was exactly proportional to the total starter burnup time t_{tsb}, then the reactor doubling time (in EFPY) would be proportional to t_{tsb} as well, since all the timescales would scale uniformly (the cooling/processing time t_c is assumed to be zero for an EFPY calculation). However, Figure 4.4-4 shows that the contained burnup is not quite linear with reactor size, so t_{feed} is not quite proportional to t_{tsb}. It ranges from 17% of t_{tsb} (for the smallest sized case) to 30% (for the largest). The effect this near-proportionality on the relationship between e-folding time and t_{tsb} is quite small: e-folding times range from 95% of t_{tsb} (in the smallest case) up to 102% t_{tsb} (for the largest) , if e-folding time is expressed in EFPY, i.e., assuming zero cooling time and a 100% capacity factor. Therefore, it is reasonable to extend the correlation in Equation 4.4-15 to e-folding or doubling time as well, as given in Equation 4.4-16. In particular, for the cases with flatter power distributions, the ratio between e-folding time and the total starter burn time matches that from the infinite slab model quite well, allowing the correlation in Equation 4.4-16 to accurately link the two.

$$Neutron excess requirement \sim\propto Area \rightarrow \frac{1}{Total\ starter\ burn\ time} \sim\propto Average\ power\ density \rightarrow \frac{1}{Doubling time} \sim\propto Average\ power\ density \quad (4.4\text{-}16)$$

Based on Equation 4.4-16 (and Figure 4.4-2), a good rule of thumb for obtaining the doubling time of a three-dimensional shuffling scheme is to simply multiply the infinite-slab-model doubling time by the power peaking factor of the shuffling scheme. Figure 4.4-2 shows that this rule of thumb applies very well to systems with flatter power distributions and correspondingly shorter doubling times, which are the systems of primary interest in this thesis. The existence of

these correlations is very useful, since it allows the results from very simple 1D models to be applied to more realistic 3D systems.

All the figures so far have assumed a 100% capacity factor and no cooling/processing time, which was done to remove a timescale and make the above analysis simpler. The effects of capacity factor and cooling/processing time can be reintroduced by mapping the 100% capacity factor, 0 year processing time results to another capacity factor and processing time. This is done by dividing the transition and spawning times by the assumed capacity factor, then including the cooling/processing time and re-computing the doubling time using Equation 4.4-14. An example of this is shown in Figure 4.4-5, which maps the results in Figure 4.4-2 to a 90% capacity factor and 2 year processing time. The figure shows that the mapped correlation continues to do a good job predicting the doubling times of the larger 3D shuffling cases.

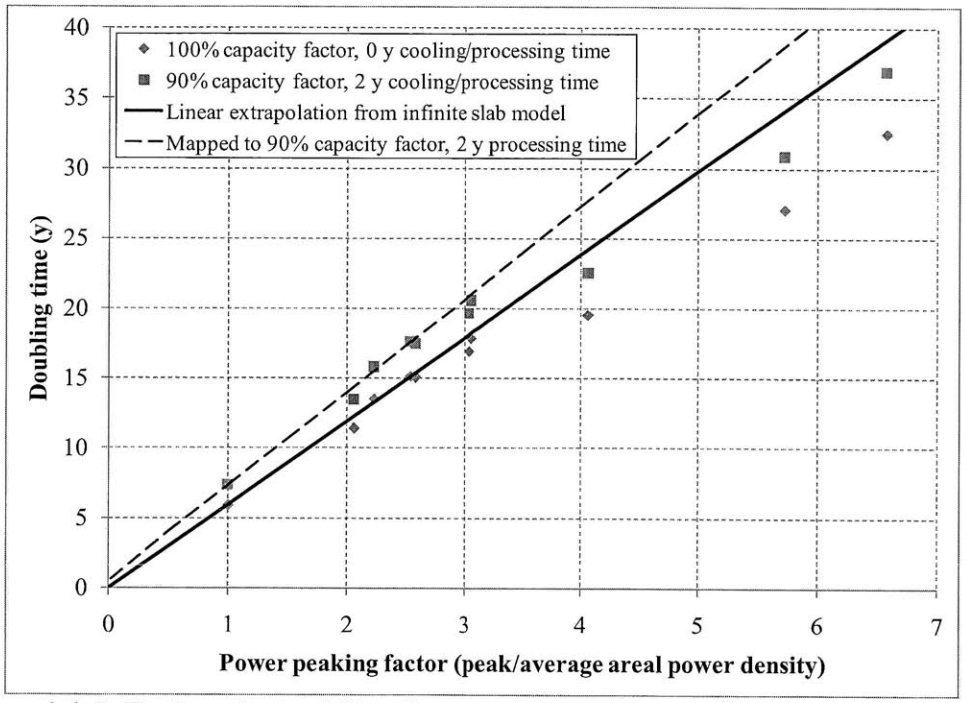

Figure 4.4-5. Fuel cycle doubling time vs. average power density (with capacity factor/processing time mapping)

4.5 Description of advanced fuel cycle options

Section 2.4 identified an important requirement for the startup of a breed-and-burn equilibrium cycle: the positive neutron excess supplied by the starter fuel must be sufficient to offset the negative neutron excess present in the equilibrium cycle. This requirement doesn't specify anything about the time distribution of the starter fuel: one can potentially start up a reactor using some fraction of the required starter fuel load, then introduce the rest of the starter fuel at a later date. This approach would be advantageous because it would delay the cost of some of the starter fuel to a later date, making it cost less in net present value terms. This approach would also allow more reactors to be started up for some amount of starter fuel available at a given time.

The advanced fuel cycle options considered here are based on the idea of being able to start up a reactor with a smaller initial fuel load than specified by the neutron excess requirement.

While the neutron excess requirement doesn't specify how large the initial fuel load needs to be, the initial loading must satisfy other requirements that are basic to reactors in general:

1) Core must be critical
2) Core must remain critical over at least one cycle length
3) Core must be coolable at the rated power level
4) Initial fuel load must fit in reactor core volume

Additionally, there is a requirement specific to B&B reactors:

5) Initial fuel load must be capable of transitioning into the desired equilibrium cycle (with the possibility of additional starter fuel later to satisfy the neutron excess requirement).

Requirement 3 is a thermal hydraulic one; just as the desired equilibrium cycle must satisfy thermal hydraulic limits, so too do the initial and transitional states. This can in general be accomplished by having a sufficiently large volume or area of starter fuel, which encourages use of lower enrichment starter fuel that occupies more space. It also implies having a flat power distribution formed through the use of enrichment grading or internal feed fuel elements. Once an initial state is selected that is coolable at the reactor's rated power, it is generally possible to maintain coolability over the transition to an equilibrium cycle. This is because as the reactor evolves, new feed fuel is bred to become capable of producing power, so the power producing volume of the reactor increases (assuming none of the starter fuel is discharged until transition is complete). This behavior can be potentially be exploited by implementing reactor power uprates during the transition period (discussed in Subsection 4.5.4), which would speed transition and allow more revenue to be generated early on in reactor life.

While requirement 3 encourages high volume, low enrichment initial fuel loads, there is a minimum enrichment stipulated by requirements 1 and 2. Requirement 5 captures the idea that an arbitrary starter configuration or transitional shuffling sequence does not necessarily result in an equilibrium cycle state. For example, one can picture using the neutron excess in the starter fuel to lightly breed a large volume of feed fuel; while doing this preserves neutron excess, the lightly-bred feed is nowhere critical and therefore unable to establish an equilibrium cycle state. This dead-end state could arise as the result of a lower enrichment starter with no internal feed elements, since all breeding would occur uniformly around the large surface of the enriched volume. Having a higher enrichment starter that permits the inclusion of internal blankets makes it easier for feed fuel to become critical and reach the peak equilibrium cycle burnup (i.e. maximum burnup) before the starter fuel is exhausted. Alternatively, an initial starter that's large compared to the equilibrium cycle core size could result in higher neutron leakage during transition, thus increasing the needed starting fissile requirement.

Assuming that a partial starter fuel load can be used, several additional fuel cycle options become available, which are described in the following subsections. The results assume the

flattened power distribution case (three-dimensional shuffling sequence number 9), which is capable of producing ~4000 MWt. The results also all assume that a full power 4000 MW reactor can be initially started up using 2/3 of the total required starter fuel needed to establish the equilibrium cycle.

4.5.1 Early startup fuel cycle

In the previously considered breed-and-burn reactor fuel cycle, reactors were started as enough bred fuel became available to establish a new equilibrium cycle, according to the neutron excess requirement. However, if the amount of starter fuel required to startup a reactor according to requirements 1 through 5 above is smaller than this total amount, then reactors can be started as this lower fuel threshold is reached. Let the fraction of the total starter fuel requirement needed in the initial load be f. This initial load can then be used to build a fractional equilibrium cycle burnup distribution over the time period f^*t_{tr}, where t_{tr} is the equilibrium cycle transition time. At this time, no further operation at full power is possible because the fractional starter load is used up, and the fractional equilibrium cycle created is unable to operate at full power. Therefore, the remaining fraction $1-f$ of starter fuel needs to be added at or before this time to permit the equilibrium cycle transition to be completed.

Results for this fuel cycle are shown in Figures 4.5-1 and 4.5-2, for a case starting with 20 equilibrium cycle reactors. The results in the figures assume the startup fuel fraction f is equal to 2/3, so each reactor is started with 2/3 of its total starter fuel requirement, with the remaining 1/3 added after nine years of operation. Once used feed fuel becomes available as new starter fuel after year 2, a greater number of new reactors can be started up compared to in the baseline case, since the fuel startup requirement per reactor is lower. After nine years of operation, the newly started reactors require additional starter fuel to continue running, meaning fewer new reactors can be started; this coincides with the reduction in reactor growth rate at year 14. However, the fact that reactors can be started sooner means that the doubling time of the reactor fleet is shorter, as shown in Figure 4.5-2. Fitting the curve with an exponential shows that the asymptotic doubling time has been reduced from 13.7 years in the baseline case to **12.7 years** in the early startup case.

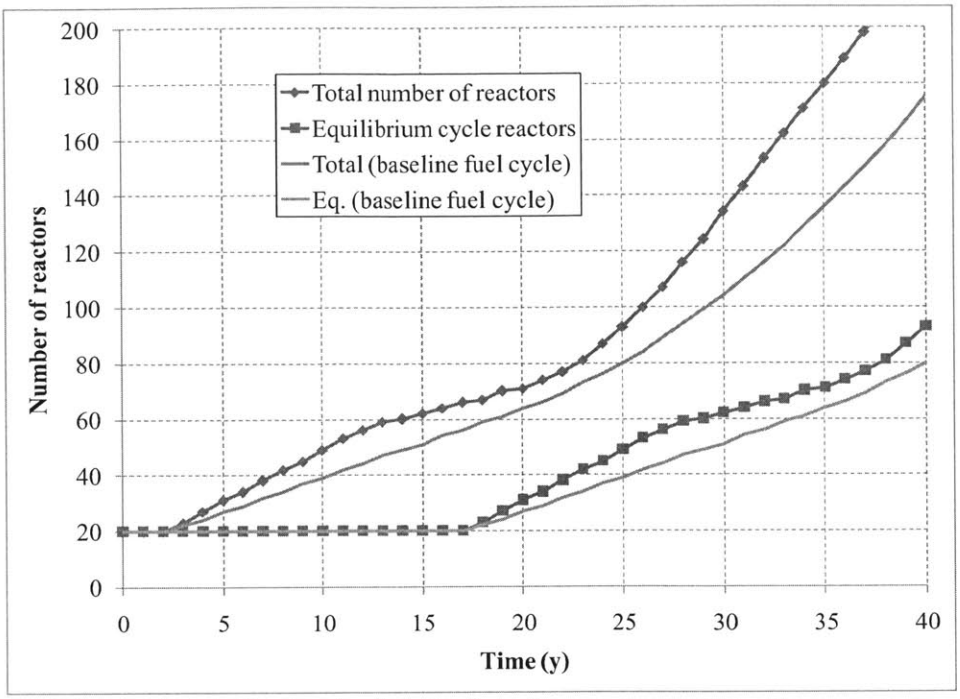

Figure 4.5-1. Early startup fuel cycle reactor buildout scenario

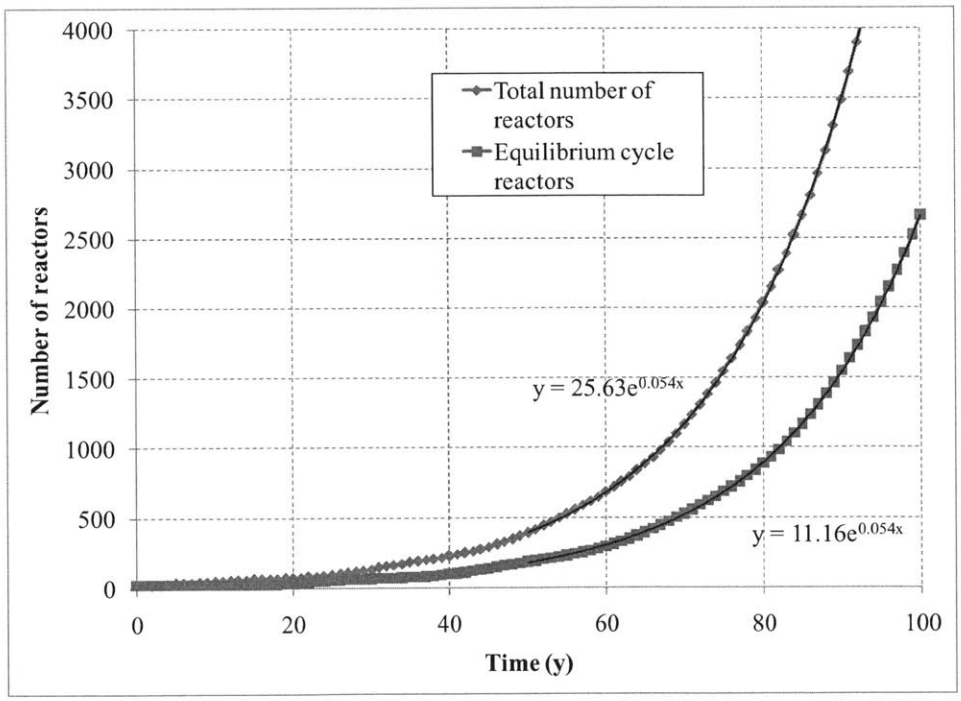

Figure 4.5-2. Early startup fuel cycle reactor buildout scenario (100 y)

There are a couple of issues associated with the early startup fuel cycle. First, if the initial startup fraction (*f*) is less than 0.5, there could be insufficient starter fuel available to finish building the equilibrium cycle in every reactor that is started up. Second, this fuel cycle causes the continued operation of a new reactor to depend on additional fuel input from previous generation reactors, introducing some risk to the new reactor. In the case that sufficient

additional starter fuel is not available, the new reactor would either have to be temporarily shut down or reduced in power, or some substitute starter fuel (e.g. enriched uranium) would have to be added instead.

4.5.2 Reactor merge fuel cycle

The reactor merge fuel cycle is similar to the early startup fuel cycle, except that once the fractional equilibrium cycles are established, they are formed into full equilibrium cycles by being combined with one another, rather than by having additional starter fuel added. So in the case in which each reactor is started with 2/3 of its needed initial fuel load, after the initial startup time of $2/3*t_d$, the 2/3 equilibrium cycles from 3 reactors would be merged to form two full equilibrium cycles. Additional starter fuel from existing equilibrium cycle reactors can be used to restart the third reactor so that it can continue operation. Results for this fuel cycle option are given in Figures 4.5-3 and 4.5-4. Figure 4.5-3 shows that new equilibrium cycle reactors can be established sooner, since starter fuel is being converted to equilibrium cycles in more than one reactor. This reduces the doubling time for this fuel cycle to **11.8 years**, compared to 13.7 in the baseline case. This doubling time is shorter than in the early-startup fuel cycle because the reactor merge fuel cycle shortens the time required for an equilibrium cycle to be established; e.g. in this example 3 reactors are used to establish 2 equilibrium cycles at once.

The reactor merge fuel cycle option introduces several challenges, because it requires that new reactors depend on other reactors to guarantee continued operation. It is more complex than the early startup fuel cycle because it requires fuel to be moved from reactor to reactor up to twice in its lifetime: first during equilibrium cycle merging, then again when it is used as a starter in a new reactor. Also, it requires that new starter fuel be available to restart reactors that have created their fractional equilibrium cycle.

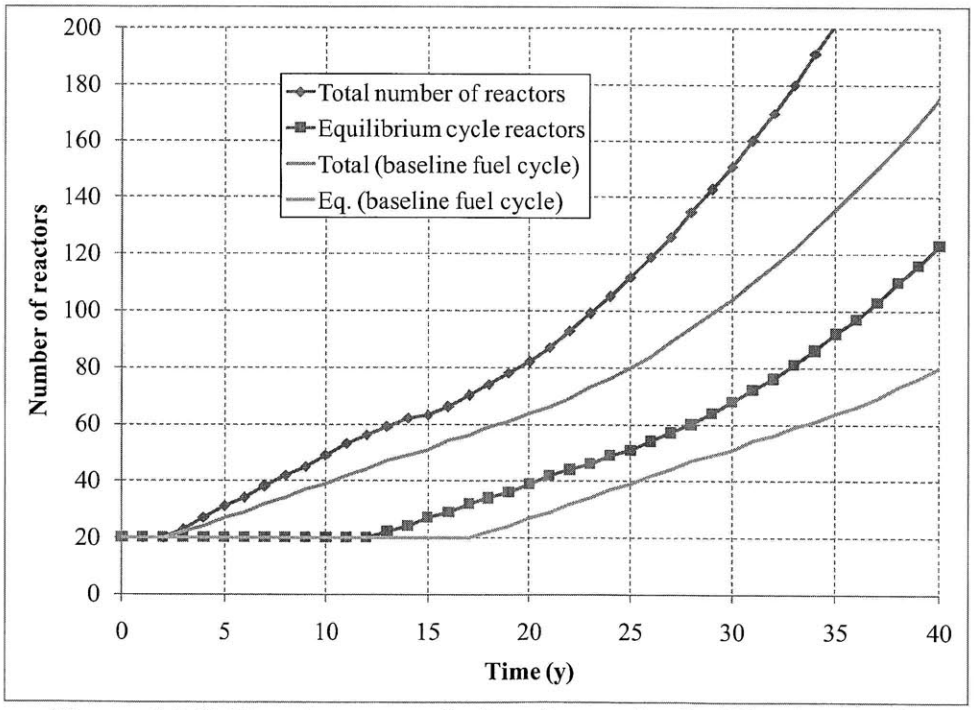

Figure 4.5-3. Reactor merge fuel cycle reactor buildout scenario

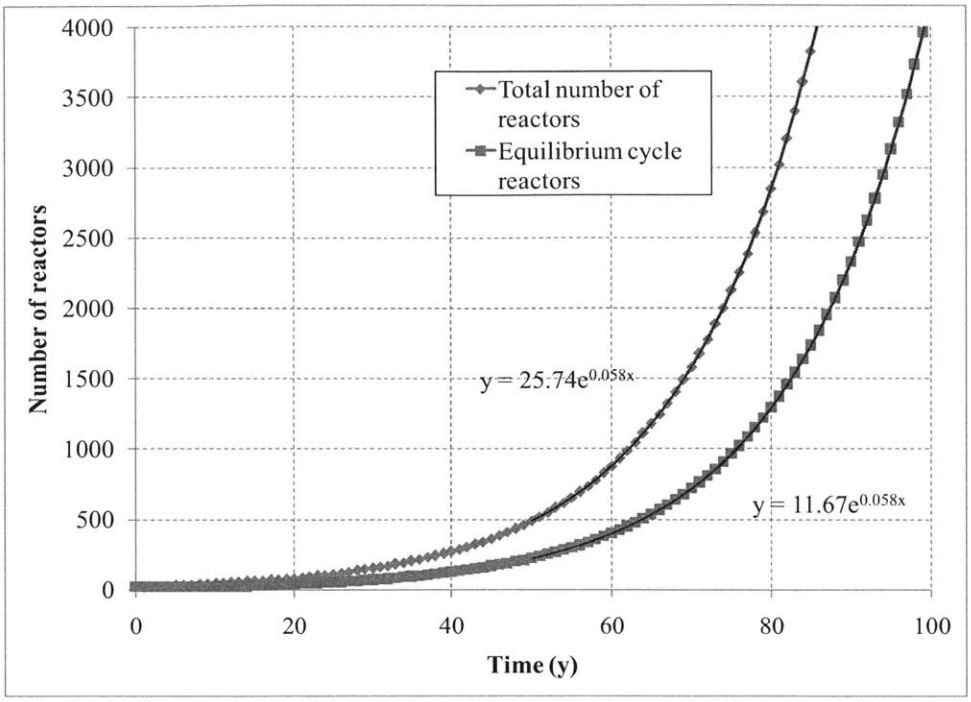

Figure 4.5-4. Reactor merge fuel cycle reactor buildout scenario (100 y)

4.5.3 Reactor growth fuel cycle

The reactor growth fuel cycle also assumes that new reactors can be started using a fractional amount of starter fuel. However, it differs by assuming that the remaining neutron excess can be supplied by the reactor burning its own feed fuel past the neutron-breakeven burnup. This would require either the feed fuel to be refabricated midway through its burn, or to be robust enough to be used straight through without any processing. While this reduces the amount of starter fuel required to initiate an equilibrium cycle, it also increases the transition time to form the equilibrium cycle, since neutron excess must now be supplied by burning feed fuel from zero burnup rather than its intermediate breakeven burnup. Therefore, for this fuel cycle to be effective, the additionally burned feed fuel must be capable of supplying a significant amount of neutron excess. The example shown assumes that the feed fuel can be burned straight through to 260 MWd/kg (~500 DPA), supplying the same amount of neutron excess as the usual starter fuel. In this scenario, a reactor started with 2/3 of the needed starter fuel would have a transition time of 18 years rather than 15 years in the baseline case. Results are shown in Figures 4.5-5 and 4.5-6.

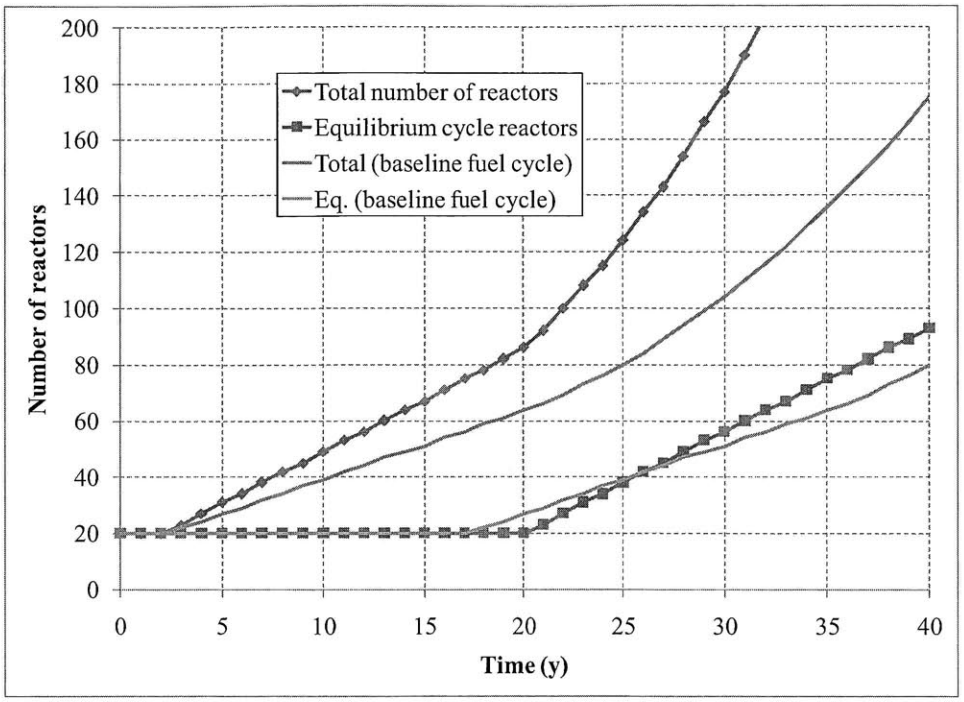

Figure 4.5-5. Reactor growth fuel cycle reactor buildout scenario

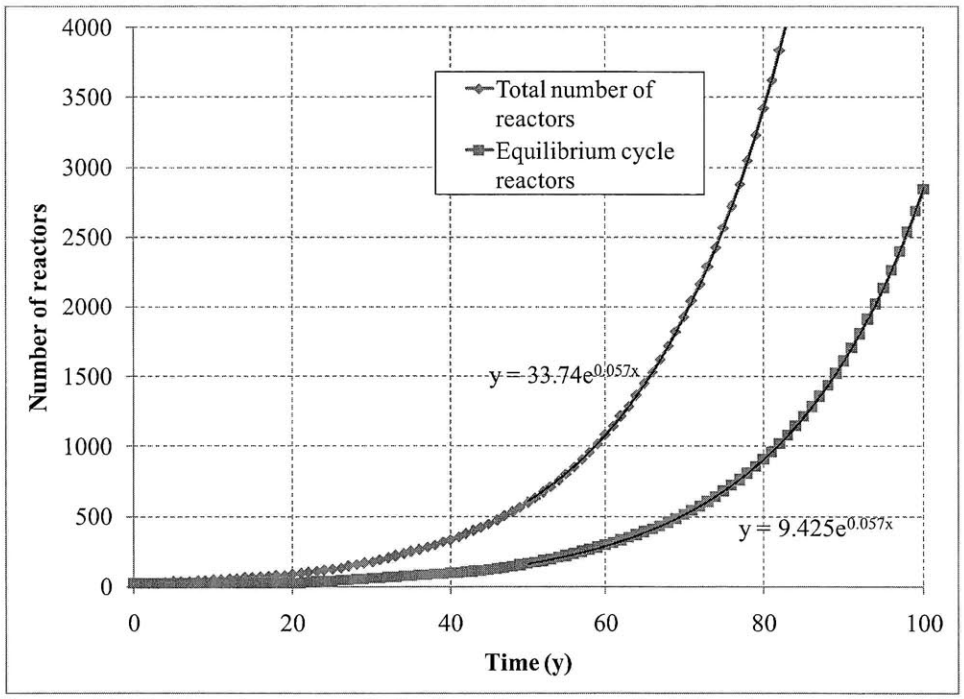

Figure 4.5-6. Reactor growth fuel cycle reactor buildout scenario (100 y)

The reactor growth fuel cycle also has a shorter asymptotic doubling time, **12.0 years**, and is also able to grow faster at the outset from a population of equilibrium cycle reactors. It doesn't have the same disadvantage of the other fuel cycles in requiring fuel from another reactor after startup, but it does require that high burnup can be achieved within a single reactor. In principle the

"free" neutron excess from burning feed fuel past its breakeven point can be used to grow an arbitrary size/power equilibrium cycle from a small amount of starter fuel. Nevertheless, the requirement that the reactor be able to supply its rated power at startup places a minimum on the amount of starter fuel used at the outset.

4.5.4 Possibility of reactor uprates during transition

In addition to the three fuel cycle variations discussed in the previous subsections, another way of shortening doubling times and improving fuel cycle performance would be to allow for reactor uprates during its transition sequence. Such uprates are possible because of the large amount of new fuel that is bred during the transition to the equilibrium cycle.

As an example, consider a hypothetical B&B equilibrium cycle that is capable of providing 2000 MW of thermal power. Suppose that the required amount of starter fuel for this equilibrium cycle can be configured to supply the same amount of power, 2000 MW, at reactor startup. Assume that the transition sequence is designed so that the starter fuel simultaneously reaches its burnup limit at the end of the transition time, so all of the starter fuel is usable throughout transition. In this scenario, as transition proceeds, the amount of power-producing fuel increases with time, since the starter fuel is all usable and an increasing amount of feed fuel is being bred. Right before the end of transition it is in principle possible to have all the starter fuel volume as well as an additional equilibrium cycle worth of feed fuel volume as "usable fuel." At this stage, the fuel would be capable of producing roughly 4000 MW: 2000 MW from the nearly-burned starter fuel and 2000 MW from the equilibrium cycle feed fuel.

In the above scenario, the equilibrium cycle reactor power is 2000 MW, but the potential maximum power during transition ranges from 2000 MW up to 4000 MW. If reactor uprates are possible during transition, then the average transition power could be increased above 2000 MW, which would shorten the transition time and thereby reduce the reactor doubling time. It would also be possible to achieve or enhance this increase in power by using specialized starter fuel with a higher coolant volume fraction and power density limit; e.g. 500 instead of 400 MW/m^2.

The benefits of a shorter doubling time and higher power during transition with a reactor uprate would need to be weighed against the additional cost and complexity of building a reactor system that can be raised and lowered in total power. Because of the more speculative nature of this case and of the other advanced fuel cycle options presented in this section, the baseline fuel cycle in which B&B reactors are only loaded once with starter fuel is used as the standard for the remainder of this thesis.

4.6 Summary of limited-separations fuel cycle findings

This chapter demonstrates how linking B&B reactors in a limited-separations fuel cycle results in an exponentially growing reactor fleet, without any input of fissile fuel after the first generation of reactors is started. Equation 4.4-14 gives a simple expression for computing the reactor fleet doubling time based on reactor and fuel cycle parameters, and several advanced fuel cycle options for shortening doubling time are introduced and investigated in Section 4.5.

Comparison of the doubling times of different equilibrium cycle shuffling options shows that large B&B reactors with flatter power distributions are able to achieve the shortest doubling times.

Section 4.1 describes the baseline limited-separations fuel cycle in which fuel undergoes two passes through different reactors: first as feed fuel in a generation *N* reactor, then as starter fuel to start up a generation *N+1* reactor. Section 4.2 discusses the different parameters from a reactor model that are important for modeling a limited-separations fuel cycle: the neutron excess requirement of a core, the neutron excess content of reused fuel, the discharge schedule of used feed fuel, and the cooling/processing time. A simple and effective method of predicting the feed fuel discharge schedule is the linear approximation, which assumes that feed fuel is discharged at a constant rate after the transition time.

Section 4.3 gives results from fuel cycle models of a growing reactor fleet. It shows that the baseline fuel cycle leads to exponential growth in the number of reactors, with an associated asymptotic doubling time. This doubling time can be computed based on reactor and fuel cycle parameters using a simple analytic expression, derived in Section 4.4. Calculating the doubling times of the different 3D shuffling sequences confirms that larger reactors with flatter power distributions can achieve shorter doubling times, since they require less neutron excess per unit power. Importantly, Subsection 4.4.2 shows that there is a correlation between the doubling times of realistic 3D systems and a simple 1D infinite slab model: the doubling time of a 3D system can be estimated by multiplying its radial power peaking factor by the 1D model doubling time. This allows very rapid comparisons of core doubling times using simple 1D models.

Finally, Section 4.5 models several fuel cycle variations that can be used to shorten reactor doubling times, referred to as the "early startup", "reactor merge" and "reactor growth" options. Assuming that each reactor can be started up using 2/3 of the full starter fuel requirement, the different fuel cycle options are able to achieve between 8 and 14 percent reductions in doubling time. Doubling times become shorter because more reactors can be started using a given amount of available starter fuel. However, Each of the advanced fuel cycle options introduces additional technical complexity, either in the form of increased interdependence among reactors (in the early startup and reactor merge options), or increased fuel burnup requirements (reactor growth option). Subsection 4.5.4 discusses one additional option for shortening doubling times: uprating reactor power during transition. Uprates during transition are in principle always possible, because breeding new fissile material in feed fuel increases the amount of fuel capable of generating power. Uprating reactor power would reduce the time it takes for the reactor to transition to equilibrium and shorten doubling times, but would require a reactor system capable of producing variable power over its lifetime.

5. Evaluation of Different Breed-and-Burn Core Compositions

The goal of this chapter is to use the methods developed in Chapters 2, 3, and 4 to evaluate different core composition options for minimum-burnup B&B reactors (i.e. B&B reactors that are designed to minimize burnup by allowing three-dimensional shuffling). This chapter will consider different possible options for fuel, structure, and coolant, and also consider the effect of different structure/fuel and coolant/fuel ratios. Also considered will be the effect of using natural vs. depleted uranium, the effect of fission gas removal from fuel, and the effect of using a melt refining process to refabricate used fuel.

The primary criteria for judging a given core composition are its minimum required burnup/fluence and its reactor doubling time. Minimum required burnup/fluence is tied to overall neutronic performance: core compositions with lower minimum burnup will have more reactive fuel that is capable of providing more net neutron excess. It is also extremely important for determining which combinations of materials are most promising for near-term implementation of B&B reactors, since high burnup and fluence are currently the limiting factors for B&B reactor design. Meanwhile, reactor doubling time depends on both neutronic performance and on achievable power density, so optimizing for doubling time requires considering the tradeoff between the neutronics and cooling ability of different coolants and different amounts of coolant. Doubling time is an extremely important figure of merit since it determines the ability of a B&B reactor infrastructure to support growing energy demand, especially the growing demand for carbon-free energy.

5.1 Applying the infinite-medium depletion approximation

The infinite-medium depletion approximation, introduced in Section 3.4, is an extremely fast and simple method that provides a fairly good estimate of the reactivity-burnup relationship for a given feed material. Because of these qualities, infinite-medium depletion calculations were used to perform a scoping study of the different reactor fuel, structure, and coolant options available. First, studies were performed on different fuel types alone, since fuel choice has the greatest effect on neutronic performance. A detailed set of calculations is performed on a possible near term core composition consisting of U-2Zr fuel, sodium coolant, and HT-9 structure, to determine the effect that coolant and structure volume fractions have on minimum burnup results. Finally, an overview of a variety of fuel, structure, and coolant combinations is considered to narrow down the number of possible candidate core compositions for the doubling time studies in sections 5.3 through 5.5.

Calculating material damage (DPA)

One quantity that is referenced frequently in this chapter is Displacements Per Atom (DPA), which is a measure of radiation induced neutron damage in a material. To calculate the DPA experienced by a material, one multiplies the energy-dependent fluence experienced by a material with the appropriate DPA cross sections (which also are a function of energy), then integrates over all neutron energies. In MCNPXT, this integral is performed approximately by summing over the 63 energy groups present in the CINDER90 depletion code. DPA cross

sections are obtained from IRDF-2002 [IAEA, 2010c] for elements in steel, and from a PNNL paper [Heinisch, 2004] for silicon carbide. For steel, DPA cross sections were synthesized as a combination of 12% chromium, 0.5% nickel, and 87.5% iron, corresponding roughly to the composition of HT9 stainless steel. The DPA cross sections of different steel compositions are very similar and only differ by a few percent, so the HT9 DPA cross sections are used for all steels considered.

Measuring DPA is important because DPA directly correlates to radiation material damage effects, such as irradiation induced swelling and creep. Other measures such as fast fluence do not accurately capture the energy dependence of neutron damage. Furthermore, DPA is a constraining factor in B&B reactor design: the current DPA knowledge limit for steels is approximately 200 DPA, while a minimum-burnup B&B reactor using natural or depleted uranium as feed is likely to require over 250 DPA or more to operate. Therefore it is important to identify which B&B reactor options are able to minimize DPA and determine what fuel cycle performance is possible as a function of achievable DPA.

5.1.1 Overview of fuel types

The fuels selected are the same as those examined in the MIT breed-and-burn GFR design (Yarsky, 2005), which included a large number of different ceramic and metal fuel options, including many fuels used primarily in research reactors (e.g. U_3Si_2, U-Mo fuels). Two additional fuels are considered in this study: low-weight-percent zirconium alloy fuels (U-2%Zr), and thorium metal fuel. Thorium metal fuel is considered because it is of interest to determine whether B&B reactors operating on thorium feed fuel can be designed.

Low-weight-percent zirconium alloy fuel is considered to determine the effect of metal fuel alloy composition, and as a bounding case for the minimum achievable parasitic absorption in fuel. While pure uranium metal would be the ideal fuel from a neutronics standpoint, it is likely not viable as a reactor fuel because it swells tremendously under irradiation. The swelling behavior of uranium can be greatly improved by alloying it with another metal. There is a great deal of experience using zirconium in metal fuel alloys; zirconium is very good for several reasons: 1) it has a low neutron absorption cross section, 2) it raises the fuel melting point, 3) it inhibits iron-eutectic formation in fuels containing high percentages of plutonium, and 4) it stabilizes the microstructure of metal fuels into a more finely-grained, swelling-resistant form. Past experience with zirconium alloy fuel has mostly consisted of fuels with 10 or more weight percent zirconium. This high percentage was important for fuels with significant loadings of plutonium and minor actinides due to reasons 2 and 3 above. For uranium fuel in a B&B reactor, the total plutonium inventory never rises above 12%, while additional zirconium is produced through fissions as plutonium accumulates, therefore fuel melting temperature and eutectic formation are not limiting. Therefore, reason 4 is the main reason to include zirconium, and past studies have suggested that as little as 2 weight percent zirconium could be sufficient to limit fuel swelling in uranium fuel. [Lagerberg, 1963]

Each fuel composition (with an actinide composition of 99.7% U-238 and 0.3% U-235 by atom fraction, and no structure or coolant present) was depleted in an infinite medium until the neutron excess ratio $\Delta N/\Delta A$ was equal to 0.01, corresponding to an average equilibrium cycle k_{fuel} of 1.01.

Aiming for a k_{fuel} equal to exactly 1.00 is unrealistic because it would require an infinitesimal cycle length and zero losses to control, so 1.01 was chosen as a low value that still allows some margin for startup reactivity and cycle reactivity swing. The ranking order between the different fuel types is generally unchanged for different target k_{fuel} values, although the corresponding needed burnup does rise as the target k_{fuel} rises.

ENDF-B/VII cross sections were used, and over 99.9% of fission products and fission product absorptions were modeled. The burnup (% of total heavy metal atoms), fast fluence (>0.1 MeV) and estimated DPA on stainless steel (HT9) at the reactivity target are given in Table 5.1-1, as well as the theoretical density and melting points of the different fuels investigated. Fuel density does not affect the results of the infinite-medium depletion models, but is factored in later when structure and coolant materials are also included.

Table 5.1-1. Comparison of different fuel compositions without structure or coolant

	Density (g/cc)	HM density (g/cc)	Melting point (°C)	Burnup required (%)	DPA required (HT9 DPA)	Fast fluence req. (/cm^2 s)
Metal fuels						
U-2Zr	18.3	17.9	1160	6.8%	195	4.83E+23
U-2Mo	18.5	18.1	1135	7.1%	202	5.01E+23
U-10Zr	16.0	14.4	1240	8.0%	213	5.26E+23
U-4Zr-2Nb	17.3	16.3	1135	7.9%	216	5.36E+23
U-7Nb	17.0	15.8	1160	9.7%	256	6.35E+23
U-9Mo	17.0	15.5	1135	9.9%	255	6.31E+23
Th	11.7	11.7	1842	19.1%	479	1.19E+24
Ceramic/ compound fuels						
U_3Si_2	12.2	11.3	1650	8.2%	204	4.85E+23
UP	10.2	9.0	2600	10.4%	243	5.94E+23
$U^{15}N$	14.3	13.5	2650	10.6%	214	4.63E+23
UC	13.6	12.9	2400	11.8%	223	4.70E+23
UAl_2	8.1	6.6	1590	12.8%	236	5.23E+23
UO_2	10.9	9.6	2750	15.8%	256	5.11E+23
UCO	12.3	11.0	2400	17.9%	274	5.42E+23
US	10.9	9.7	2475	18.3%	390	8.79E+23
UTe	10.4	6.8	1740	19.6%	441	1.12E+24
USe	11.3	8.5	--	20.9%	429	1.05E+24
UN	14.3	13.5	2650	N/A	N/A	N/A

The fuels in each category are listed in order of ascending burnup requirement. The inclusion of non-uranium elements in fuel reduces neutronic performance in two ways. Additional elements both parasitically absorb neutrons and soften the neutron spectrum; a softer spectrum results in a lower equilibrium concentration of Pu-239 and leads to additional parasitic absorptions, particularly in fission products. Note that the required DPA and fast fluence values are not proportional to the burnup values; for example uranium carbide has a 13% higher required DPA

and 3% *lower* required fast fluence than U-2Zr while needing 74% higher burnup. This is because the different cases involve different neutron spectra, for example the presence of carbon or oxygen atoms results in softer spectra that accumulate DPA and fast fluence at a slower rate with burnup. The required quantities for uranium nitride are marked "N/A" because uranium nitride is never able to return its neutron investment; i.e. its adjusted neutron excess is never positive.

One thing to note in Table 5.1-1 is that despite modest burnup requirements, the DPA and fast fluence levels required to support breed-and-burn operation in depleted uranium fuel are very high, on the order of the experience limit reached in reactors (~200 DPA & 4.0E23 /cm^{2}s). These high values relative to burnup are a result of the hard neutron spectrum as well as the additional fluence required to first breed fissile material before it can be fissioned. Adding materials that soften the neutron spectrum increases both minimum burnup and total fluence, but because of the softer spectrum the minimum DPA and fast fluence scale less than linearly and may even decrease. Since actual reactors require coolant and structure in addition to fuel, both of which would increase the needed burnup and DPA levels, it is clear that many of the worse performing fuels are not near-term candidates for consideration, simply due to their enormous burnups and DPA requirements. Thorium is one of these fuels, considering that even without any alloying materials, coolant, or structure, a fast fluence of over 1E24 is needed to allow breed-and-burn operation. It is in principle possible to operate a B&B system using just thorium as feed fuel, but such a system would be able to include very little structure and coolant, while still requiring very high burnup and DPA levels.

From Table 5.1-1, the most interesting fuels for further study are U2Zr, U10Zr, U_3Si_2, $U^{15}N$, and UC. U2Zr is the best candidate because its neutronic performance is better than any of the other fuels and its high density means that structure and coolant would fractionally absorb fewer neutrons. U10Zr still performs decently well neutronically and is interesting because of the large amount of experience using it as a reactor fuel. U_3Si_2 has the best neutronic performance of the uranium compound fuels, although it does have a fairly low heavy metal density. Uranium nitride using nitrogen-15 offers good neutronic performance and has a high heavy metal density, although the cost of highly enriched nitrogen-15 could be a significant issue, considering the large amount and long residence times of feed fuel in a B&B reactor. Uranium carbide is interesting because it offers a softer spectrum which lowers DPA while maintaining a fairly high heavy metal density and a very high melting temperature.

5.1.2 Investigating a range of U2Zr–Na–HT9 core compositions

By using the infinite-medium depletion approximation, it is possible to quickly investigate the minimum burnup and fluence for a range of core compositions. This is useful for creating a map of what core compositions satisfy desired limits on burnup or DPA. As an example of doing this, an example study was performed for a core composition consisting of U2Zr fuel, HT9 structure, and sodium coolant. HT9 structure and sodium coolant were considered because they represent potential near-term options for a B&B reactor, since there is already experience using them in fast reactor applications. Meanwhile, there is little irradiation data for low zirconium alloys fuels such as U2Zr, so fuel testing would be required to qualify it for use in a reactor.

The composition for HT9 is taken from a paper by Klueh [Klueh, 2005]. Its density at room temperature (7.7924 g/cc) is from a paper by Gelles [Gelles, 94]. Sodium density is assumed to be 0.844 g/cc, corresponding to a coolant temperature of 450°C, a representative average reactor temperature. Room temperature densities are used for fuel and structure materials because their thermal expansion coefficients are small compared to the coolant. In all cases the ENDF-B/VII cross section libraries at 900K are used.

Runs were performed for sodium volumes from 0 to 2 times the fuel volume in intervals of 0.2, and for HT9 volumes from 0 to 1 times in the fuel volume of intervals of 0.1. The target average equilibrium cycle k_{fuel} is 1.01 in all cases. To run the 121 cases, a Python script was written that allows the creation of a large number of infinite-medium MCNPXT input decks from a spreadsheet, allowing a large number of different compositions to be rapidly investigated. Another script was written that allows minimum burnup, DPA, and fast fluence data to be collected from the output files.

Contour plots for minimum required burnup, DPA, and fast fluence for the range of core compositions are given in Figures 5.1-1 through 5.1-3. The plots are fairly linear, which means that a smaller number of runs (e.g. 36 instead of 121) would have been sufficient to yield the same information. The slope of the contours is not uniform among the three plots, reflecting the differences in spectra among the runs. The addition of sodium creates a softer spectrum, so for the same total fast fluence, the composition with more sodium will have a higher DPA and a still higher burnup, due to higher total fluences. Even without sodium or HT9 present, DPA and fast fluence levels are already close to or past current knowledge limits (~200 DPA and 4.0E23 /cm^{2}s respectively). However, if further testing is able to provide a 50% or 100% increase in these experimental limits, the range of possible core compositions expands enormously.

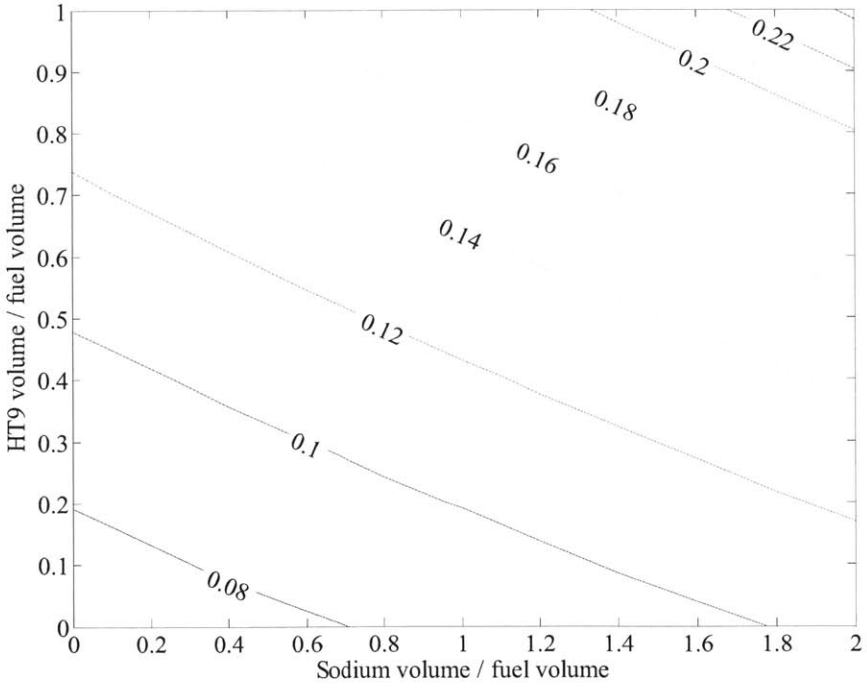

Figure 5.1-1. Minimum burnup for different U2Zr–Na–HT9 core compositions (FIMA)

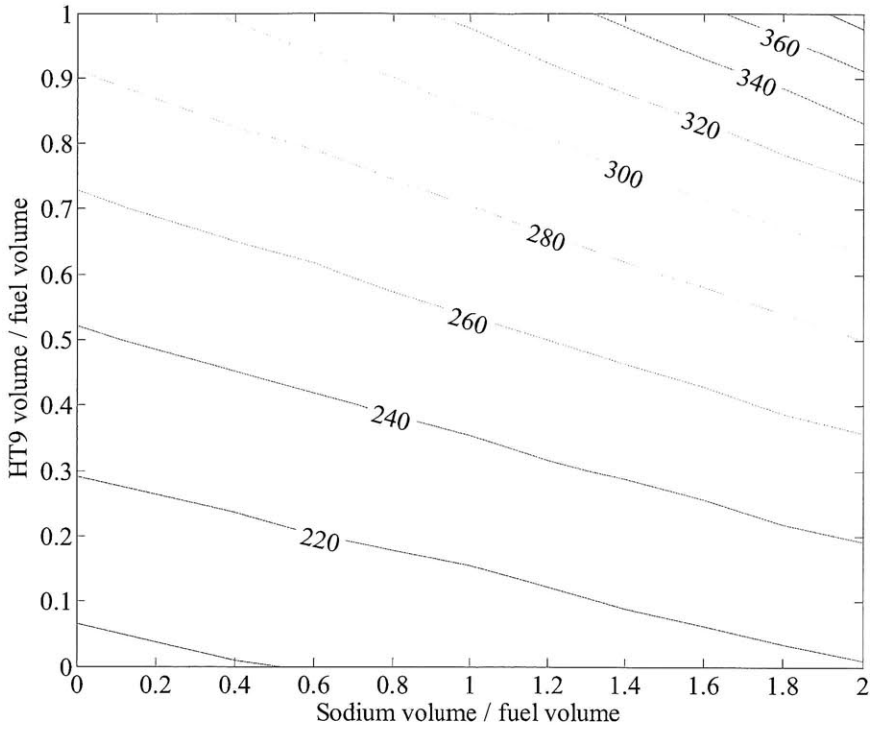

Figure 5.1-2. Minimum DPA for different U2Zr–Na–HT9 core compositions (HT9 DPA cross sections)

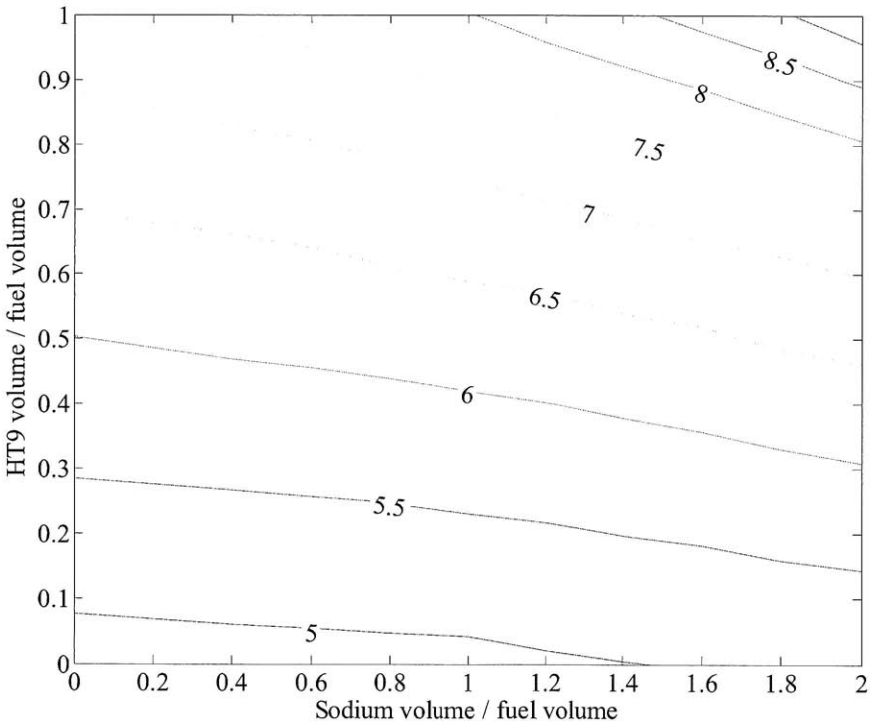

Figure 5.1-3. Minimum fast fluence (>0.1 MeV) for different U2Zr–Na–HT9 core compositions (1E23 /cm^{2}s)

To confirm the results of the infinite-medium depletion approximation, each of the limiting core compositions (at each of the corners) was run using the convergent 5 cm infinite slab model to determine corresponding values for MOEC *k*-effective, burnup, HT9 DPA, and fast fluence. The discharge burnup in MWd/kg was set to be equal to minimum values predicted by the infinite-medium depletion calculation. Results of the comparison are given in Table 5.1-2. The DPA and fast fluence values match very well, showing that a similar discharge fluence spectrum is experienced in the infinite-medium and infinite slab models. Meanwhile, the infinite slab models have MOEC *k*-effectives that are at most 1.2% higher than the predicted k_{eq}, so again the infinite-medium depletion approximation slightly underestimates *k*-effective for a convergent shuffling case. Reactors with non-convergent shuffling schemes would have average *k*-effectives closer to that of the infinite-medium depletion estimate.

As shown in Chapter 3, the results from a simple infinite slab model agree very well with results from more complex and realistic three-dimensional models. Table 5.1-2 shows that the infinite-medium depletion approximation agrees well with results from an infinite slab model for a wide range of core compositions, which in turn means it is suitable for evaluating the performance of more realistic B&B systems.

Table 5.1-2. Comparison of 0D and 5 cm infinite slab model results (0D/1D infinite slab)

Composition volume fractions	100% U2Zr, 0%HT9, 0%Na	33.3% U2Zr, 0%HT9, 66.7%Na	50% U2Zr, 50%HT9, 0%Na	25% U2Zr, 25%HT9, 50%Na
Discharge burnup (MWd/kg)	66.4/**66.4**	101.8/**101.8**	140.5/**140.5**	239.1/**239.1**
Discharge burnup (FIMA)	6.8%/**6.8%**	10.4%/**10.4%**	14.3%/**14.3%**	24.4%/**24.3%**
Discharge DPA (for HT9)	194/**193**	219/**217**	289/**286**	388/**383**
Discharge fast fluence (/cm^{2}s)	4.82E23/**4.76E23**	5.09E23/**5.02E23**	7.33E23/**7.25E23**	9.34E23/**9.22E23**
k_{eq}/MOEC *k*-effective	1.010/**1.022**	1.010/**1.019**	1.010/**1.020**	1.010/**1.015**

5.1.3 Investigating a wide variety of core compositions

The infinite-medium depletion approximation was applied to a wide range of core compositions involving different fuel, structure, and coolant options, in order to obtain a narrowed down list of promising options. Fuels considered are the neutronically promising fuels from the earlier fuels results (U2Zr, U10Zr, U_3Si_2, UN enriched in ^{15}N, and UC). Candidate structural materials for fast reactors are the ferritic/martensitic steels HT9 and T91, oxide dispersion-strengthened steel (ODS) (e.g. MA956, assumed in this study) and silicon carbide. Candidate fast reactor coolants are sodium, lead, lead-bismuth eutectic (LBE), helium, and CO_2.

The assumed densities of the fuel compositions are given in Table 5.1-1 in Subsection 5.1-1. Compositions and densities for the structural materials are given in Table 5.1-3. Silicon carbide is modeled using its stoichiometric composition and its monolithic density; a silicon-carbide composite may have a slightly lower density and include trace elements from its manufacture. The densities for the structural materials are all at room temperature; thermal expansion would

have a small effect on the relative number densities of fuel, structure, and coolant. The sodium, lead, and LBE densities (0.844, 10.52, and 10.13 g/cc respectively) are at a representative core operating temperature of 450°C, while the helium and CO_2 densities (0.0125 and 0.133 g/cc) assume core average temperatures and pressures of 500°C and 20 MPA. The LBE composition is assumed to be at the eutectic point (44.5% Pb, 55.5% Bi).

Table 5.1-3. Compositions and densities for structural materials

Material	HT9	T91	MA956 (ODS)	SiC
Density g/cc	7.79	7.74	7.25	3.21
Element weight %				
Fe	84.55	88.77	73.665	
Cr	12	9	20	
C	0.2	0.1	0.05	30.0
Mo	1	1		
Si	0.4	0.4		70.0
W	0.5			
V	0.25	0.2		
Mn	0.6	0.4	0.15	
Al			4.75	
Ti			0.4	
Y			0.39	
O			0.11	
Ni	0.5		0.25	
P			0.01	
Nb		0.08		
Cu			0.075	
Co			0.15	
N		0.05		

For simplicity, the respective volume fractions of the fuel, structure, and coolant are kept constant, at 1 part fuel, 0.6 parts structure, and 1 part coolant. These fractions are roughly equal to the average values given for fast reactors in the IAEA fast reactor database. For B&B reactors, it would likely be desirable to use smaller amounts of structure and coolant to minimize the total burnup and fluence experienced by the fuel. The IAEA fast reactor database does not give information on the amount of bond material used with metal fuels. Some bond material (a liquid metal such as sodium or lead) is typically used with metal fuels to decrease thermal resistance between the fuel and clad. Bond is not modeled in this study; its effect would be similar to a small amount of the same coolant material, although bond typically gets squeezed out fairly early in the fuel's depletion as the fuel swells.

With 5 fuel types, 4 structure types, and 5 coolant types, a total of 100 different core compositions were studied using the infinite-medium depletion model. Results for the minimum burnup (target average k_{eq} of 1.01), minimum DPA (evaluated using HT9 DPA cross sections in

all cases, and SiC DPA cross sections in the cases with SiC), and minimum fast fluence are given in Tables 5.1-4 through 5.1-8, separated by coolant type.

Because a significant number of compositions did not reach a predicted k_{eq} of 1.01, Tables 5.1-4 through 5.1-8 also give results for the maximum k_{eq} reached by a composition. The maximum k_{eq} corresponds to the point on a neutron excess curve which maximizes the slope of a line connecting the curve with the origin. Figures 5.1-4 and 5.1-5 give schematic illustrations of where the maximum k_{eq} occurs on a neutron excess curve, for cases with the maximum k_{eq} above and below unity. The maximum k_{eq} occurs at a point before the maximum neutron excess when the maximum k_{eq} is greater than unity. The maximum k_{eq} is a good dimensionless figure of merit for the neutronic performance of a fuel composition, and is included in the below tables to give better differentiation of the various cases. It is a better figure of merit than maximum ΔN, since maximum ΔN is a dimensional quantity that depends on factors like the total heavy metal density.

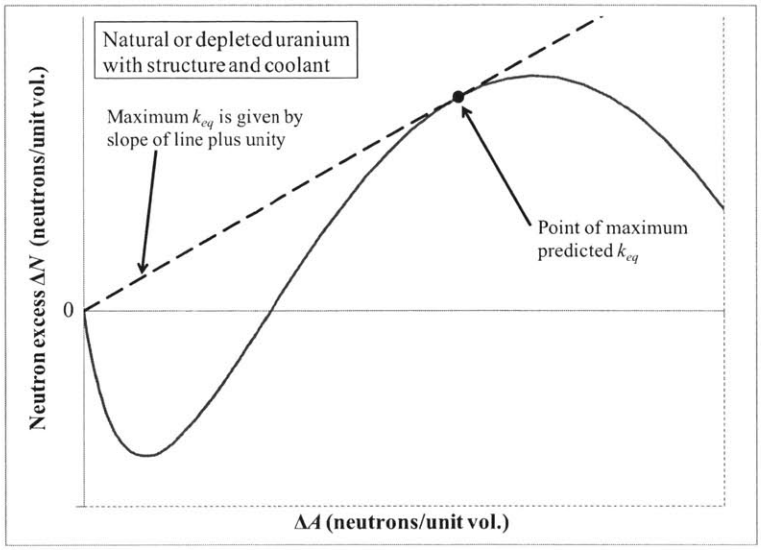

Figure 5.1-4. Schematic illustration of maximum k_{eq} (>1) on neutron excess curve

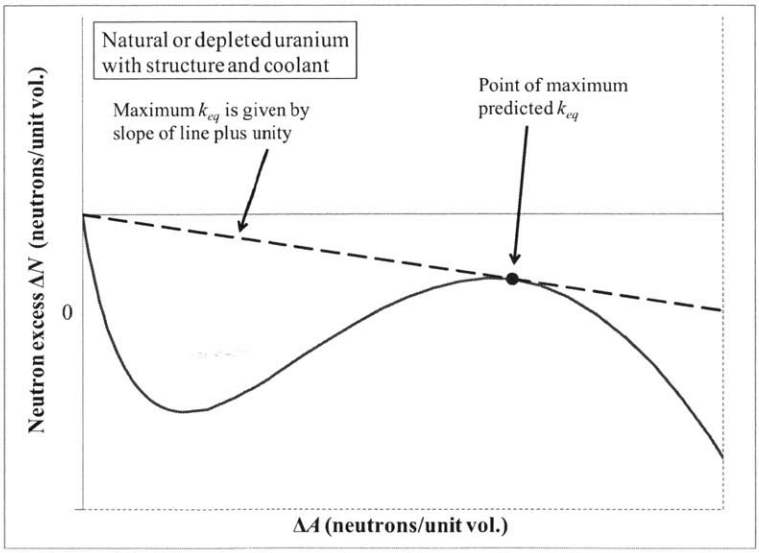

Figure 5.1-5. Schematic illustration of maximum k_{eq} (<1) on neutron excess curve

Table 5.1-4. Minimum burnup for helium-cooled core compositions (for k_{eq} = 1.01)

Fuel	Structure	Coolant	Minimum burnup fraction	Minimum DPA (HT9/SiC DPA)	Minimum fast fluence (/cm^{2}s)(>0.1 MeV)	Maximum k_{eq}
U2Zr	ODS	He	11.2%	245	6.11E+23	1.120
U2Zr	T91	He	11.2%	249	6.28E+23	1.119
U2Zr	HT9	He	11.4%	250	6.30E+23	1.118
U2Zr	SiC	He	12.8%	271	5.09E+23	1.103
U10Z	ODS	He	14.4%	284	7.07E+23	1.080
U10Z	T91	He	14.5%	290	7.30E+23	1.078
U10Z	HT9	He	14.7%	293	7.36E+23	1.076
U10Z	SiC	He	17.2%	322	6.03E+23	1.060
U3Si2	ODS	He	17.3%	302	7.29E+23	1.057
U3Si2	T91	He	17.4%	309	7.58E+23	1.055
U3Si2	HT9	He	17.8%	314	7.67E+23	1.053
U3Si2	SiC	He	20.7%	333	6.31E+23	1.037
UN15	ODS	He	20.8%	326	7.36E+23	1.037
UN15	T91	He	21.3%	336	7.63E+23	1.034
UN15	HT9	He	21.7%	341	7.75E+23	1.032
UN15	SiC	He	23.4%	355	6.59E+23	1.026
UC	ODS	He	26.5%	389	8.61E+23	1.017
UC	T91	He	27.6%	407	9.08E+23	1.015
UC	HT9	He	28.9%	426	9.48E+23	1.013
UC	SiC	He	N/A	N/A	N/A	1.010

Table 5.1-5. Minimum burnup for CO_2-cooled core compositions (for k_{eq} = 1.01)

Fuel	Structure	Coolant	Minimum burnup fraction	Minimum DPA (HT9/SiC DPA)	Minimum fast fluence (/cm^{2}s)(>0.1 MeV)	Maximum k_{eq}
U2Zr	ODS	CO2	11.6%	248	6.07E+23	1.114
U2Zr	T91	CO2	11.6%	251	6.22E+23	1.114
U2Zr	HT9	CO2	11.8%	253	6.25E+23	1.112
U2Zr	SiC	CO2	13.1%	273	5.10E+23	1.099
U10Zr	ODS	CO2	15.1%	290	7.09E+23	1.075
U10Zr	T91	CO2	15.2%	296	7.30E+23	1.073
U10Zr	HT9	CO2	15.5%	299	7.37E+23	1.071
U10Zr	SiC	CO2	17.8%	327	6.10E+23	1.055
U3Si2	ODS	CO2	18.3%	312	7.34E+23	1.050
U3Si2	T91	CO2	18.6%	320	7.65E+23	1.048
U3Si2	HT9	CO2	18.9%	324	7.75E+23	1.046
U3Si2	SiC	CO2	21.7%	340	6.44E+23	1.033
UN15	ODS	CO2	21.8%	337	7.51E+23	1.032
UN15	T91	CO2	22.4%	347	7.81E+23	1.029
UN15	HT9	CO2	22.8%	353	7.93E+23	1.028
UN15	SiC	CO2	24.2%	365	6.72E+23	1.023
UC	ODS	CO2	28.7%	417	9.12E+23	1.013
UC	T91	CO2	31.6%	460	1.01E+24	1.011
UC	HT9	CO2	N/A	N/A	N/A	1.009
UC	SiC	CO2	N/A	N/A	N/A	1.007

Table 5.1-6. Minimum burnup for LBE-cooled core compositions (for k_{eq} = 1.01)

Fuel	Structure	Coolant	Minimum burnup fraction	Minimum DPA (HT9/SiC DPA)	Minimum fast fluence (/cm^{2}s)(>0.1 MeV)	Maximum k_{eq}
U2Zr	ODS	PbBi	13.0%	271	6.83E+23	1.097
U2Zr	T91	PbBi	13.1%	275	7.01E+23	1.095
U2Zr	HT9	PbBi	13.2%	276	7.02E+23	1.094
U2Zr	SiC	PbBi	15.1%	311	5.87E+23	1.079
U10Zr	ODS	PbBi	17.4%	325	8.17E+23	1.056
U10Zr	T91	PbBi	17.6%	333	8.46E+23	1.053
U10Zr	HT9	PbBi	17.9%	336	8.52E+23	1.051
U10Zr	SiC	PbBi	21.6%	390	7.37E+23	1.035
U3Si2	ODS	PbBi	22.4%	368	8.97E+23	1.029
U3Si2	T91	PbBi	22.9%	379	9.38E+23	1.027
U3Si2	HT9	PbBi	23.5%	387	9.56E+23	1.025
U3Si2	SiC	PbBi	33.6%	470	9.89E+23	1.010
UN15	ODS	PbBi	29.4%	435	1.00E+24	1.013
UN15	T91	PbBi	31.8%	473	1.10E+24	1.010
UN15	HT9	PbBi	N/A	N/A	N/A	1.009
UN15	SiC	PbBi	N/A	N/A	N/A	1.002
UC	ODS	PbBi	N/A	N/A	N/A	0.994
UC	T91	PbBi	N/A	N/A	N/A	0.992
UC	HT9	PbBi	N/A	N/A	N/A	0.990
UC	SiC	PbBi	N/A	N/A	N/A	0.986

Table 5.1-7. Minimum burnup for lead-cooled core compositions (for k_{eq} = 1.01)

Fuel	Structure	Coolant	Minimum burnup fraction	Minimum DPA (HT9/SiC DPA)	Minimum fast fluence (/cm^{2}s)(>0.1 MeV)	Maximum k_{eq}
U2Zr	ODS	Pb	13.2%	273	6.86E+23	1.095
U2Zr	T91	Pb	13.3%	277	7.04E+23	1.093
U2Zr	HT9	Pb	13.4%	279	7.09E+23	1.091
U2Zr	SiC	Pb	15.3%	314	5.90E+23	1.077
U10Zr	ODS	Pb	17.8%	330	8.28E+23	1.053
U10Zr	T91	Pb	17.9%	336	8.54E+23	1.051
U10Zr	HT9	Pb	18.2%	340	8.60E+23	1.049
U10Zr	SiC	Pb	22.0%	397	7.46E+23	1.033
U3Si2	ODS	Pb	23.2%	378	9.22E+23	1.026
U3Si2	T91	Pb	23.8%	391	9.68E+23	1.024
U3Si2	HT9	Pb	24.3%	398	9.81E+23	1.022
U3Si2	SiC	Pb	N/A	N/A	N/A	1.008
UN15	ODS	Pb	31.3%	460	1.06E+24	1.011
UN15	T91	Pb	N/A	N/A	N/A	1.008
UN15	HT9	Pb	N/A	N/A	N/A	1.007
UN15	SiC	Pb	N/A	N/A	N/A	1.000
UC	ODS	Pb	N/A	N/A	N/A	0.992
UC	T91	Pb	N/A	N/A	N/A	0.990
UC	HT9	Pb	N/A	N/A	N/A	0.988
UC	SiC	Pb	N/A	N/A	N/A	0.984

Table 5.1-8. Minimum burnup for sodium-cooled core compositions (for k_{eq} = 1.01)

Fuel	Structure	Coolant	Minimum burnup fraction	Minimum DPA (HT9/SiC DPA)	Minimum fast fluence (/cm^{2}s)(>0.1 MeV)	Maximum k_{eq}
U2Zr	ODS	Na	13.4%	262	6.36E+23	1.092
U2Zr	T91	Na	13.5%	266	6.51E+23	1.091
U2Zr	HT9	Na	13.6%	267	6.53E+23	1.089
U2Zr	SiC	Na	15.1%	291	5.48E+23	1.077
U10Zr	ODS	Na	18.5%	321	7.75E+23	1.048
U10Zr	T91	Na	18.8%	329	8.03E+23	1.046
U10Zr	HT9	Na	19.0%	332	8.09E+23	1.045
U10Zr	SiC	Na	22.1%	373	7.05E+23	1.031
U3Si2	ODS	Na	25.3%	387	9.02E+23	1.020
U3Si2	T91	Na	26.0%	401	9.48E+23	1.017
U3Si2	HT9	Na	27.0%	415	9.78E+23	1.015
U3Si2	SiC	Na	N/A	N/A	N/A	1.005
UN15	ODS	Na	N/A	N/A	N/A	1.006
UN15	T91	Na	N/A	N/A	N/A	1.004
UN15	HT9	Na	N/A	N/A	N/A	1.002
UN15	SiC	Na	N/A	N/A	N/A	1.000
UC	ODS	Na	N/A	N/A	N/A	0.988
UC	T91	Na	N/A	N/A	N/A	0.986
UC	HT9	Na	N/A	N/A	N/A	0.984
UC	SiC	Na	N/A	N/A	N/A	0.984

To further verify the results from the infinite-medium depletion approximation, a comparison of the k_{fuel} prediction to the MOEC k-effective from the infinite slab model is shown in Figure 5.1-6, for two core compositions with significantly different spectra and neutronic performance: UC–SiC–He and U2Zr–HT9–PbBi. In all cases, the predicted k_{fuel} is found to be within 1% of the modeled value.

Comparing the results in Tables 5.1-4 through 5.1-8, several conclusions can be drawn. Gas coolants are clearly the best neutronically, with helium being slightly superior to CO_2. The metal coolants all perform similarly, with LBE being slightly better than pure lead. Sodium requires higher burnup than LBE or lead, but creates a softer spectrum that reduces the minimum required DPA and fast fluence. The three different steel structural materials each exhibit very similar performance, with ODS being slightly better neutronically (in terms of minimum burnup and maximum k_{eq}) per unit volume than T91, which is slightly better than HT9. Choice of which to use would likely depend primarily on the materials' irradiation performance at high temperature. Silicon carbide requires a somewhat higher burnup than the steels, but has a moderating effect that reduces the required fast fluence. This allows the core compositions using SiC to experience lower fast fluence, as seen in Figure 5.1-7.

The largest factor in determining neutronic performance is the fuel type. Ceramic fuels perform significantly worse than metal ones, as the softer spectra they cause create additional parasitic absorptions and lower the equilibrium ratio of Pu-239 to U-238. Despite its lower heavy metal density, U_3Si_2 is the best performing compound fuel, although its melting point (1650°C) is lower than that of UC (2400°C) and UN (2650°C), losing some of the benefit of using ceramic

fuels. The poor neutronic performance of compound fuels in B&B systems means that they would only be used in cases where their other properties were important, such as their refractory properties in high temperature applications. The neutronic gain achieved by switching from a liquid metal to a gas coolant is lost if such a switch requires use of a ceramic fuel instead of a metal fuel. Metal fuels show much better neutronic performance, and notably the amount of alloying material also makes a significant difference. The neutronic advantage of metal fuels shown here would be offset somewhat by the fact that metal fuels require a lower smear density (to accommodate fuel swelling) and bond material (to reduce fuel temperatures).

Based on these results, a subset of core composition options was selected for the more in depth doubling time study. The coolant options chosen were sodium, lead-bismuth eutectic, and helium. Each of these coolant options yields significantly different thermal hydraulic performance, while LBE and lead have similar neutronic performance, as do helium and CO_2. For structure, T91 and silicon carbide were chosen. All the steel structural materials have similar neutronic performance, and T91 is a likely near-future choice while having neutronic performance between those of the other two types of steel. Silicon carbide has significantly different neutronic performance from the steels because it causes neutron spectrum softening. For fuels, U2Zr, U10Zr, and U_3Si_2 were chosen. U2Zr and U10Zr were selected to examine the effect of alloy composition in a metal fuel, while U_3Si_2 was selected because it is the best performing compound fuel.

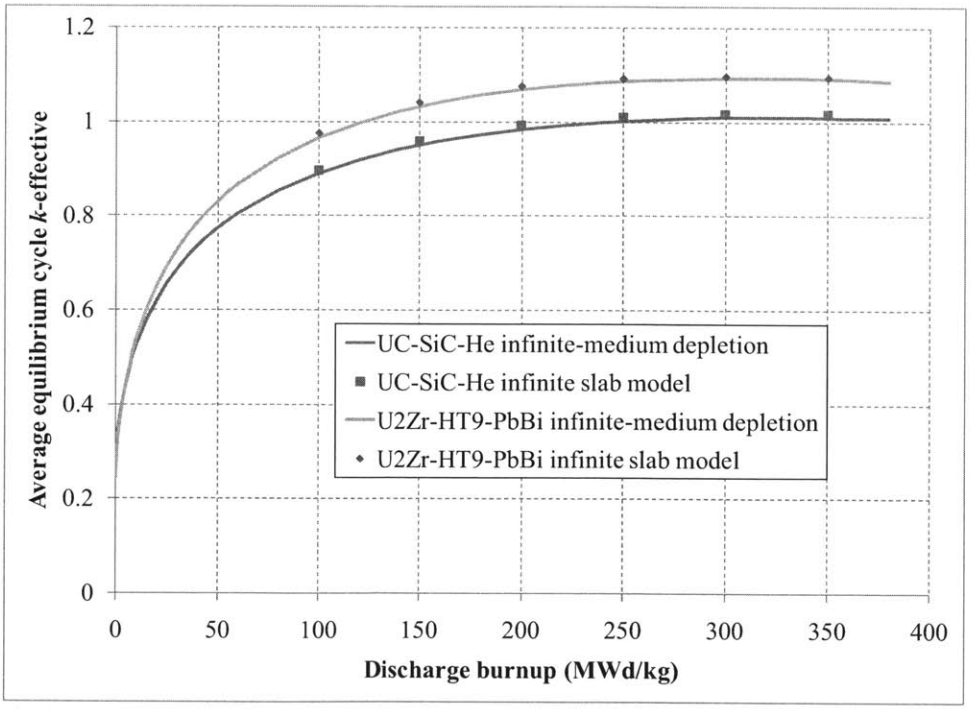

Figure 5.1-6. Comparison of infinite-medium depletion approximation with infinite slab model

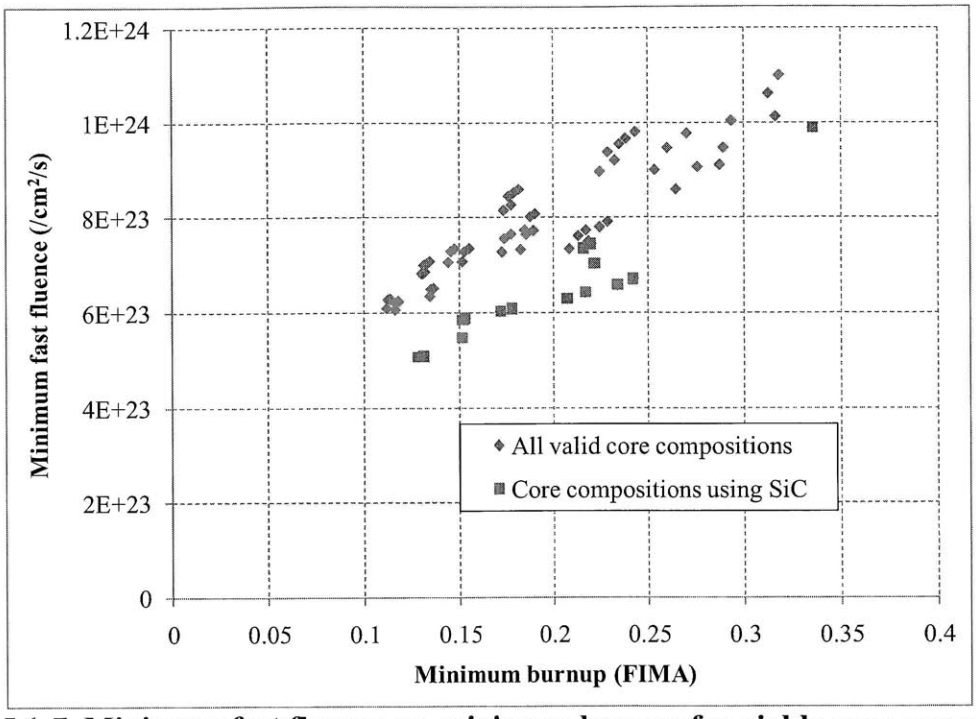

Figure 5.1-7. Minimum fast fluence vs. minimum burnup for viable core compositions

5.2 Assumptions and methodology for comparing core composition doubling times

The asymptotic reactor doubling time of a B&B reactor fleet operating in a limited-separations fuel cycle (as discussed in Chapter 4) depends on a number of different factors, including core composition, power density, capacity factor, reactor size, and several fuel cycle parameters. The most important factor is choice of core composition: compositions with harder neutron spectra and fewer parasitic absorbers will allow shorter doubling times. This is because better core compositions allow reactors to have lower neutron excess requirements and allow reused feed fuel to supply greater amounts of neutron excess.

The thermal hydraulic performance of a core composition is also important, since a higher power density shortens the characteristic reactor timescales that doubling time is based on. Similarly, achievable capacity factor directly influences doubling times as well. As shown in Subsection 4.4.1, the equilibrium cycle shuffling sequence used is also important: a sequence with a large, flat power distribution will have a shorter doubling time than one with a compact, highly peaked power distribution, because larger B&B reactors require less neutron excess per unit power.

In addition to reactor characteristics, fuel cycle parameters also play a role in determining doubling time. As shown in Section 4.4, how long used feed fuel spends cooling or in processing before it can be reused as starter fuel factors into the doubling time. The choice of fuel cycle used is also important, since the baseline fuel cycle and the advanced options discussed in Section 4.5 were shown to have different doubling times. Finally, any fuel processing (such as melt refining or AIROX) that changes the fuel chemistry (e.g. by removal of

volatile fission products) will change how much neutron excess can be extracted from the resulting starter fuel, which would also affect doubling time.

The general procedure for comparing core composition doubling times is to compute the doubling time for an infinite slab model, then use the correlation from Subsection 4.4.2 to translate these doubling times into approximate doubling times for realistic systems. The different neutronic, thermal hydraulic, and fuel cycle assumptions used are given in Subsections 5.2.1 through 5.2.3.

5.2.1 Reactor neutronic models and assumptions

For each core composition studied, two models are used: an infinite-medium depletion model and a convergently-shuffled infinite slab model. First, the infinite-medium depletion model is used to determine the feed fuel discharge burnup that corresponds to an average equilibrium cycle k_{fuel} of 1.02. Then, the infinite slab model is run using this value of discharge burnup, using a convergent shuffling pattern until an equilibrium cycle is reached. This provides values for the total neutron excess requirement as well as the total burnup contained in the equilibrium cycle. To obtain the spawning and transition timescales for this system, the only other information needed is how much starter fuel is required to initiate the equilibrium cycle.

To calculate the amount of starter fuel needed, one needs to know how much neutron excess can be obtained from reusing discharged feed fuel. One approach for doing this is to take the equilibrium cycle discharge composition from the infinite slab model and perform another infinite-medium depletion calculation. This method is flexible because it allows one to change the fuel composition (e.g. remove volatile fission products) before burning it further; however it requires an additional neutronics calculation to implement. A faster but less flexible approach is to simply use the results from the earlier infinite-medium depletion run, starting from the originally calculated discharge burnup. This approach doesn't require an additional calculation, but it also assumes that the fuel composition does not change between when fuel is discharged and when it is reused.

Figure 5.2-1 compares the two approaches for the example core composition from Chapter 3. The figure shows that their results match to within a few percent, which is expected since the composition from the infinite-medium depletion is very close to the composition of the fuel discharged from the equilibrium cycle. For most of the cases studied, the infinite-medium depletion composition is used because it yields equivalent results while reducing the number of computations required; however the equilibrium cycle discharge composition is used in cases investigating the effects of cooling time and processing.

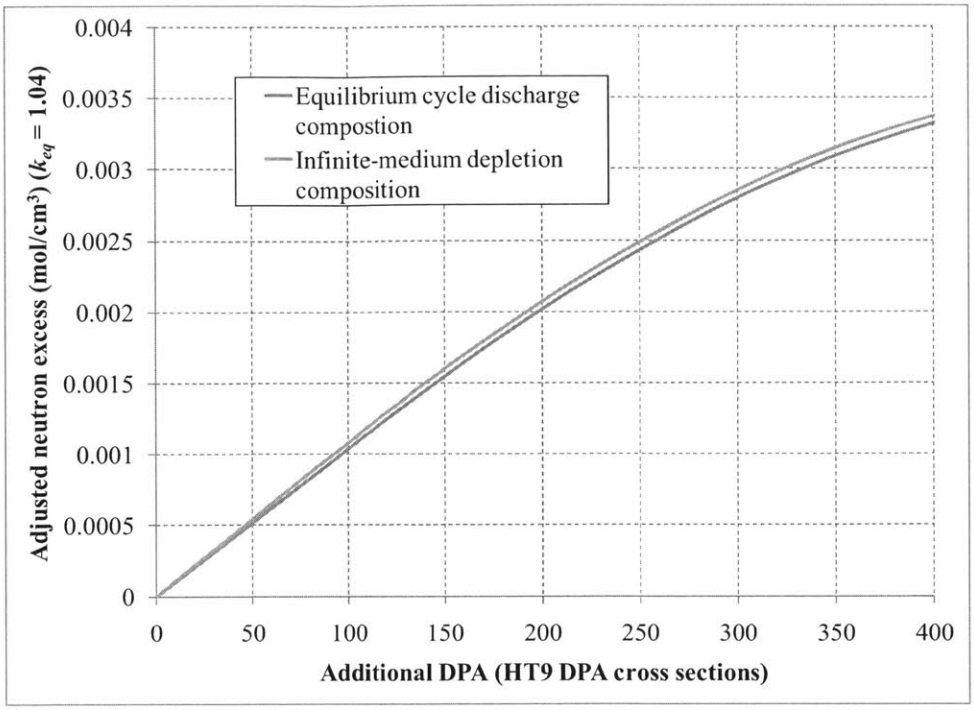

Figure 5.2-1. Neutron excess comparison between discharge feed compositions from infinite-medium and infinite slab models (infinite-medium depletion approximation)

5.2.2 Reactor thermal hydraulic models and assumptions

Based on the results of the infinite-medium depletion model and the infinite slab equilibrium cycle model, it is possible to determine the amount of starter fuel required to start up the equilibrium cycle, as well as the amount of feed and starter burnup that go into establishing the equilibrium cycle. To convert these values into fuel cycle timescales however, it is necessary to know how much power can be extracted from a given core composition: i.e. its thermal hydraulic performance.

Core thermal hydraulics is a highly complex subject in its own right; the amount of power that can be safely removed from a core depends on the fuel design and constraints on fuel and clad temperatures, coolant velocity, pressure drop across the core, and transient performance. Detailed thermal hydraulic calculations are beyond the scope of this thesis; instead, achievable power densities are estimated by assuming a simple model for a fuel pin, then computing maximum power based on two constraints: a coolant velocity constraint and a peak clad temperature constraint. Details about this thermal hydraulic model are given in Appendix A.5.

For sodium, LBE, and helium (at 20 MPa), coolant velocity limits are assumed to be 8 m/s, 2 m/s, and 100 m/s respectively. For sodium, 8 m/s corresponds to a representative value from the IAEA database [IAEA, 2010b]. For lead/LBE coolant, 2 m/s is the limit for preventing excessive corrosion in steel [Samsonov, 1973]. For helium coolant, 100 m/s is an approximate value chosen to limit pressure drop across the core, and is comparable to the values used in the MIT helium-cooled B&B core design [Yarsky, 2005]. The coolant inlet temperature in each case is assumed to be 400°C, and the peak clad temperature is assumed to be 580°C. These

assumptions are only intended to yield approximate realistic power density values for use in scoping calculations, and can be substituted with detailed thermal hydraulic calculations for actual fuel designs.

The output of the thermal hydraulic model is a peak *areal* power density, where areal power density is defined as the volumetric power density integrated axially at a particular radial position. Calculating areal power density is important because the correlation linking the doubling times of different shuffling sequences is based on the radial power peaking factor, which is the ratio of peak to average areal power density.

Figure 5.2-2 shows how the calculated power density limits for sodium-cooled core compositions correspond to the commercial-sized reactor designs from the IAEA database. The squares in the figure correspond to the estimated peak areal power density in the different IAEA database core designs. This is calculated by dividing the total power by the core area, then multiplying by the volumetric power density peaking factor raised to the two-thirds power. Meanwhile, the triangles are the power density results calculated in Appendix A.5 for the different core compositions. These values depend primarily on the coolant volume fraction, and vary slightly due to the different axial power distributions in the infinite slab models (for example, a higher burnup composition would have a more spread-out power distribution and lower axial peaking, so areal power density would be slightly higher). The calculated results agree fairly well with the values for the higher power density designs, confirming that the calculated numbers are realistic.

For both sets of data, there is a clear correlation between higher coolant volume fraction and higher areal power densities, with an approximately proportional relationship between the two for the calculated values. The reason for this proportionality can be seen from the equation linking coolant volume fraction and areal power density, shown in Equation 5.2-1:

$$Q'' = \rho c_p v \Delta T_{coolant} f_{coolant} \tag{5.2-1}$$

Q'': Areal power density, equal to the volumetric power density integrated axially (W/m^2)
ρ: Coolant density, ~844 kg/m^3 at 450°C
c_p: Specific heat capacity, ~1268 J/kgK at 450°C
v: Coolant velocity, maximum assumed to be 8 m/s
$\Delta T_{coolant}$: Coolant temperature rise, less than 180K
$f_{coolant}$: Coolant volume fraction, varies depending on the core composition

In a sodium-cooled reactor, the high thermal conductivity of the sodium and clad means that the peak coolant outlet temperature is close to the peak cladding temperature of 580°C. In the cases modeled, coolant outlet temperature ranges from 555°C to 580°C, meaning that $\Delta T_{coolant}$ only varies from 155°C to 180°C. Since coolant density, specific heat capacity, velocity, and temperature rise are all approximately constant, peak areal power density is therefore approximately proportional to the coolant volume fraction, which explains the result shown in Figure 5.2-2.

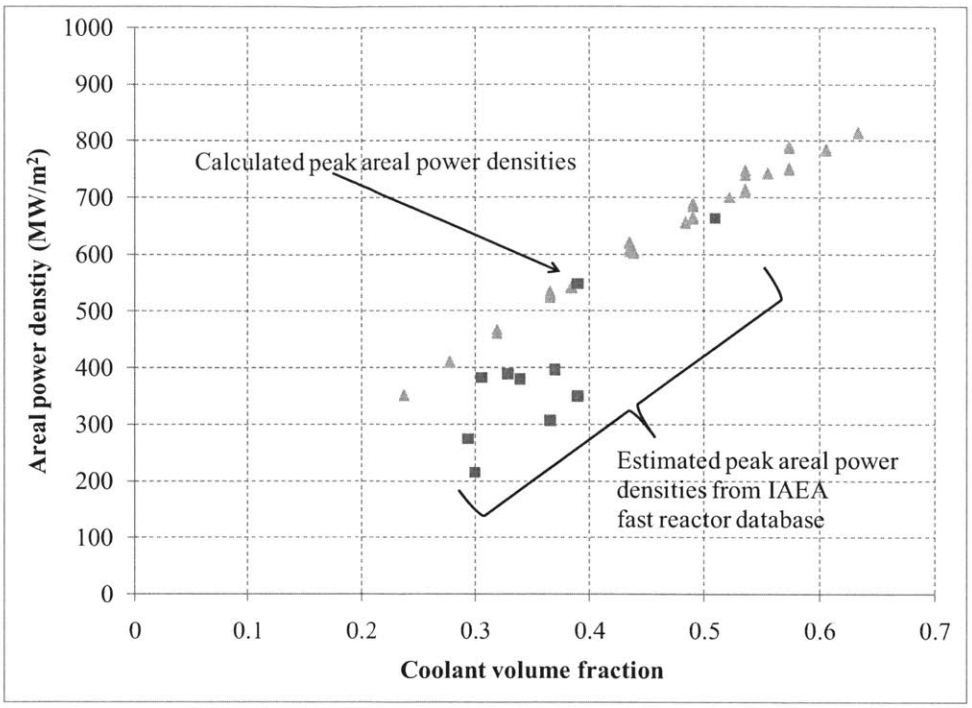

Figure 5.2-2. Areal power density vs. coolant volume fraction for sodium-cooled reactor designs

Similar figures for areal power density will be shown for the LBE- and gas-cooled core compositions in their respective sections. The thermal hydraulic assumptions used in this thesis are not intended to substitute more rigorous analyses of actual fuel designs. Instead, they are intended as a simple means to compare homogenized core compositions that have no specific fuel design associated with them. For a more detailed design of a B&B reactor, one would want to perform detailed thermal hydraulic calculations for the core compositions being studied, and substitute the resulting maximum areal power density results in place of the simple model results used in this thesis. Nevertheless, the simple power density calculations presented in this subsection are useful for providing realistic approximate values for reactor fleet doubling times.

5.2.3 Fuel cycle models and assumptions

With an areal power density limit established, one can use the procedure given in Chapter 4 to calculate the transition time t_d, and spawning time t_s for the infinite slab reactor. The studies in this chapter assume that the baseline fuel cycle is used: i.e. each new reactor is started using a single loading of starter fuel that provides the entire neutron excess requirement for the equilibrium cycle. For the baseline fuel cycle, one can use Equation 4.4-14 to convert the spawning and transition times into a corresponding e-folding time t_e, assuming zero cooling/processing time and a 100% capacity factor. Multiplying t_e by the natural logarithm of 2 (~0.693) gives the doubling time for the infinite slab reactor.

This basic result from the models is referred to as the "infinite-reactor doubling time," since it is the doubling time that could be achieved using a hypothetical infinite reactor with a uniform

power distribution (i.e. a radial power peaking factor of unity). Infinite-reactor doubling times are given in units of EFPY, since a 100% capacity factor is assumed.

To convert the infinite-reactor doubling times to more realistic doubling times, one needs to account for power peaking in finite reactors, as well as reactor capacity factor and cooling and processing time. As shown in Subsection 4.4.2, for a finite core with a reasonably flat power distribution, one can estimate its doubling time by multiplying the infinite-reactor doubling time by the radial power peaking factor of the core. This is equivalent to multiplying the two timescales t_d and t_s by the radial peaking factor. These two timescales can then be divided by the reactor capacity factor to yield timescales in years instead of EFPY. Finally, the two adjusted timescales and the cooling and processing time can be reentered into Equation 3.4-14 to obtain the realistic reactor doubling time.

5.3 Sodium fast reactor core compositions

A total of 96 different sodium fast reactor core compositions are evaluated. Three types of fuel were considered: U2Zr, U10Zr, and U_3Si_2, representing low and high percentage metal alloy fuel and the best performing compound fuel. The metal fuel is assumed to have a smear density of 75% while the compound fuel is assumed to have a smear density of 90%, keeping in mind the relatively high burnup levels required for B&B operation. Two types of structural materials are considered: T91 and SiC. The neutronic performance of different steel alloys (e.g. HT9, T91, and ODS steel) was found to be similar in Section 5.1, so T91 is taken as representative of the other steels. Silicon carbide was found to require higher fuel burnup, but is able to reduce the fast fluence encountered by softening the neutron spectrum.

Compositions in this and the following sections are named using the following convention: fuel type – fuel volume – structure type – structure volume – coolant type – coolant volume. For example, the core composition U2Zr-75-T91-30-Na-100 is a core composition consisting of 75 parts U2Zr fuel, 30 parts T91 structure, and 100 parts sodium coolant by volume. The different volume numbers are normalized so that 100 corresponds to the volume available inside the cladding, or "available fuel volume," so the fuel volume number is equal to the fuel smear density in percent.

Two different amounts of structural material are examined: 30 volume percent of the available fuel volume and 60 volume percent of the available fuel volume. The low amount of structure is similar to that of an inverted-fuel (i.e. coolant channels going though blocks of fuel) gas-cooled fast reactor design [Pope, 2006] which has a structure to fuel volume ratio of 22%. If one assumes that roughly 1 cm of structure is required every 20 cm to form the top and bottom of each fuel subassembly (i.e. 5% of the fuel is replaced by structure), then this ratio increases to 29%, which is rounded up to 30%. The 60% case assumes that much more structure is needed to form the clad, duct, and subassembly coupling structures, or to accommodate a different fuel form (e.g. pins instead of inverted fuel). Here the core is made up of axially-separated "fuel subassemblies" because this analysis pertains to "minimum-burnup" B&B reactors in which fuel can be shuffled in all three dimensions.

For each of the twelve fuel–structure combinations, eight different amounts of sodium coolant are considered, from 50% of the available fuel volume up to 225%, in 25% increments. Bond material between clad and fuel (which may be used with metal fuel) is not explicitly modeled, although some of the sodium in the model can be attributed to bond.

Of the 96 different compositions considered, 52 are capable of reaching the target infinite-medium k_{eq} prediction of 1.02; these compositions are then studied using infinite slab equilibrium cycle models. Equilibrium cycle results for the different compositions are given in Tables 5.3-1 and 5.3-2. The two tables give results for compositions with T91 and silicon carbide structure respectively. The average k_{eq} is the average uncontrolled k-effective over an equilibrium cycle, as defined by Equation 2.2-7. Material radiation damage is represented as the DPA that a sample of HT9 or silicon carbide would experience. Axial length is computed using the 99.75% neutron absorption criterion (presented in Section 3.3), using an exponential interpolation between the 5 cm zones. "MOEC BU contained" is the amount of burnup present at the middle of the equilibrium cycle, and the adjusted ΔN is the neutron excess requirement of the equilibrium cycle. Each bordered section contains a particular fuel and structure combination with different amounts of coolant.

Table 5.3-1. Equilibrium cycle results for sodium-cooled core compositions (T91 structure)

Composition	HM density (g/cc)	Ave. k_{eq}	Discharge burnup fraction	Discharge HT9 DPA	Discharge fast fluence (/cm^2) (>0.1 MeV)	Axial length (cm)	MOEC BU contained (MWy/m^2)	Adjusted ΔN (mol/m^2)
U2Zr-75-T91-30-Na-50	7.47	1.029	11.6%	247	6.07E+23	205	947	1197
U2Zr-75-T91-30-Na-75	6.56	1.028	12.4%	253	6.14E+23	226	980	1209
U2Zr-75-T91-30-Na-100	5.85	1.028	13.3%	261	6.27E+23	246	1034	1233
U2Zr-75-T91-30-Na-125	5.27	1.027	14.2%	268	6.38E+23	261	1082	1249
U2Zr-75-T91-30-Na-150	4.80	1.028	15.4%	278	6.57E+23	277	1145	1276
U2Zr-75-T91-30-Na-175	4.41	1.026	16.4%	287	6.73E+23	296	1207	1287
U2Zr-75-T91-30-Na-200	4.08	1.027	17.7%	299	6.98E+23	308	1295	1318
U2Zr-75-T91-30-Na-225	3.79	1.028	19.2%	314	7.27E+23	324	1400	1345
U10Zr-75-T91-30-Na-50	6.00	1.028	15.1%	291	7.11E+23	227	1143	1287
U10Zr-75-T91-30-Na-75	5.27	1.028	16.6%	304	7.34E+23	247	1231	1314
U10Zr-75-T91-30-Na-100	4.70	1.027	18.2%	318	7.61E+23	269	1336	1350
U10Zr-75-T91-30-Na-125	4.24	1.027	20.2%	338	8.01E+23	290	1476	1389
U10Zr-75-T91-30-Na-150	3.86	1.026	22.6%	363	8.55E+23	310	1677	1426
U10Zr-75-T91-30-Na-175	3.54	1.025	26.0%	402	9.40E+23	334	1991	1466
U3Si2-90-T91-30-Na-50	5.66	1.028	15.9%	286	6.77E+23	236	1180	1301
U3Si2-90-T91-30-Na-75	4.97	1.028	17.6%	302	7.05E+23	257	1288	1335
U3Si2-90-T91-30-Na-100	4.43	1.028	19.5%	320	7.42E+23	279	1420	1373
U3Si2-90-T91-30-Na-125	3.99	1.027	21.8%	343	7.87E+23	302	1595	1406
U3Si2-90-T91-30-Na-150	3.64	1.026	25.0%	378	8.63E+23	326	1886	1456
U2Zr-75-T91-60-Na-50	6.41	1.028	15.5%	295	7.32E+23	217	1202	1337
U2Zr-75-T91-60-Na-75	5.72	1.028	16.7%	306	7.50E+23	233	1270	1358
U2Zr-75-T91-60-Na-100	5.17	1.027	18.2%	320	7.77E+23	252	1366	1385
U2Zr-75-T91-60-Na-125	4.72	1.027	19.8%	335	8.07E+23	267	1479	1409
U2Zr-75-T91-60-Na-150	4.34	1.026	21.6%	354	8.48E+23	285	1632	1441
U2Zr-75-T91-60-Na-175	4.02	1.026	24.0%	381	9.06E+23	305	1840	1478
U2Zr-75-T91-60-Na-200	3.74	1.025	27.4%	422	9.98E+23	326	2203	1514
U10Zr-75-T91-60-Na-50	5.14	1.026	23.2%	394	9.73E+23	242	1796	1502
U10Zr-75-T91-60-Na-75	4.60	1.025	27.9%	452	1.11E+24	270	2300	1560
U3Si2-90-T91-60-Na-50	4.85	1.026	26.2%	414	9.93E+23	256	2084	1538

Table 5.3-2. Equilibrium cycle results for sodium-cooled core compositions (SiC structure)

Composition	HM density (g/cc)	Ave. k_{eq}	Discharge burnup fraction	Discharge SiC DPA	Discharge fast fluence (/cm^2) (>0.1 MeV)	Axial length (cm)	MOEC BU contained (MWy/m^2)	Adjusted ΔN (mol/m^2)
U2Zr-75-SiC-30-Na-50	7.47	1.029	12.6%	279	5.23E+23	192	978	1183
U2Zr-75-SiC-30-Na-75	6.56	1.030	13.4%	288	5.39E+23	213	1023	1196
U2Zr-75-SiC-30-Na-100	5.85	1.028	14.3%	295	5.51E+23	231	1068	1212
U2Zr-75-SiC-30-Na-125	5.27	1.029	15.3%	305	5.68E+23	249	1128	1236
U2Zr-75-SiC-30-Na-150	4.80	1.027	16.3%	314	5.84E+23	267	1189	1248
U2Zr-75-SiC-30-Na-175	4.41	1.028	17.5%	327	6.08E+23	283	1267	1273
U2Zr-75-SiC-30-Na-200	4.08	1.028	18.7%	339	6.28E+23	301	1353	1296
U2Zr-75-SiC-30-Na-225	3.79	1.027	20.0%	354	6.56E+23	318	1446	1314
U10Zr-75-SiC-30-Na-50	6.00	1.028	16.7%	331	6.17E+23	213	1218	1282
U10Zr-75-SiC-30-Na-75	5.27	1.028	18.3%	346	6.44E+23	236	1319	1310
U10Zr-75-SiC-30-Na-100	4.70	1.028	20.1%	365	6.78E+23	258	1448	1347
U10Zr-75-SiC-30-Na-125	4.24	1.027	22.3%	391	7.25E+23	280	1626	1377
U10Zr-75-SiC-30-Na-150	3.86	1.026	25.3%	423	7.82E+23	302	1898	1413
U3Si2-90-SiC-30-Na-50	5.66	1.029	17.3%	315	5.86E+23	223	1261	1291
U3Si2-90-SiC-30-Na-75	4.97	1.028	18.9%	332	6.17E+23	249	1370	1320
U3Si2-90-SiC-30-Na-100	4.43	1.028	21.0%	351	6.50E+23	272	1527	1355
U3Si2-90-SiC-30-Na-125	3.99	1.027	23.4%	378	6.99E+23	297	1724	1384
U3Si2-90-SiC-30-Na-150	3.64	1.026	27.2%	419	7.74E+23	323	2099	1427
U2Zr-75-SiC-60-Na-50	6.41	1.028	18.3%	327	6.01E+23	196	1342	1305
U2Zr-75-SiC-60-Na-75	5.72	1.029	19.8%	342	6.28E+23	213	1447	1337
U2Zr-75-SiC-60-Na-100	5.17	1.027	21.4%	358	6.58E+23	233	1577	1356
U2Zr-75-SiC-60-Na-125	4.72	1.026	23.4%	380	6.98E+23	253	1742	1380
U2Zr-75-SiC-60-Na-150	4.34	1.025	25.9%	409	7.50E+23	274	1991	1412

A few trends can be observed in Tables 5.3-1 and 5.3-2. All the cases show an average k_{eq} between 1.025 and 1.029, consistently slightly higher than infinite-medium prediction of 1.020. This means that some additional core compositions may have been able to reach an average k_{eq} of 1.020, but such core compositions would be barely viable and have extremely long doubling times. The low-structure-fraction SiC cases show higher discharge burnups than the corresponding low-structure T91 cases, but due to their softer spectra have lower fast fluence. The SiC cases exhibit higher DPA because SiC has somewhat (10-20%) higher DPA cross sections than steel in the spectra considered. The shorter neutron mean free paths due to a softer spectrum also reduces the axial length of the SiC cases. Shifting to higher Zr alloy fuel or U3Si2 fuel greatly penalizes neutronic performance, as does going from a low structure fraction to a high structure fraction. Increasing the sodium volume fraction has a more gradual effect.

Starting from the 52 candidate core compositions in Tables 5.3-1 and 5.3-2, several situations are analyzed. First, a case is considered in which fuel is directly transferred from one reactor to another, with no processing or recladding of any kind. In this case, the structural material accumulates DPA over two reactor passes, first as feed fuel in one B&B reactor, then again as starter fuel in an additional B&B reactor. Second, a case is considered in which the fuel can be reclad before it is reloaded into a second reactor, which effectively resets the amount of DPA accumulated on the structural material. The goal in these two cases is to determine reactor doubling time as a function of peak DPA for each of the fuel-structure combinations considered, leaving the amount of coolant as a variable to optimize. Afterward, additional cases are considered to evaluate the effect of using natural vs. depleted uranium, accounting for fission gas escape during irradiation, and the use of melt refining to refabricate metal fuel.

5.3.1 Doubling time vs. DPA without recladding

This first portion of the sodium core composition evaluation considers cases with no fuel refabrication or processing of any kind. It is assumed that fuel and structure can be burned up to an ultimate DPA limit, after which it is disposed. Given a DPA limit, it is assumed fuel discharged from the equilibrium cycles in Tables 5.3-1 and 5.3-2 is then further burned to the ultimate DPA limit when it is reused as starter fuel. The baseline B&B limited-separations fuel cycle is assumed, in which new reactors are started as sufficient starter fuel becomes available. The doubling time can then be computed as shown in Chapter 3. Note that in this no-processing case, it is assumed that fuel is capable of being burned significantly beyond its equilibrium cycle minimum burnup, therefore the "reactor growth" fuel cycle option in Subsection 3.5.3 could potentially be used to reduce reactor doubling times.

For each particular fuel/structure combination, the coolant volume fraction is varied and the infinite-reactor doubling time is calculated as a function of the ultimate DPA limit. Results for U2Zr fuel with a low volume fraction of T91 structure are shown in Figure 5.3-1. The figure shows that there is an optimum coolant fraction that minimizes doubling time. Too low a coolant fraction means lower power density (as shown in Figure 5.2-2), while too high a coolant fraction reduces the neutron excess produced. The curves in Figure 5.3-1 have a minimum near where the coolant volume is equal to 100% of the available fuel volume. The minimum gradually trends toward lower volumes of coolant as the DPA limit decreases, which reduces the neutron excess extractable from a given amount of fuel.

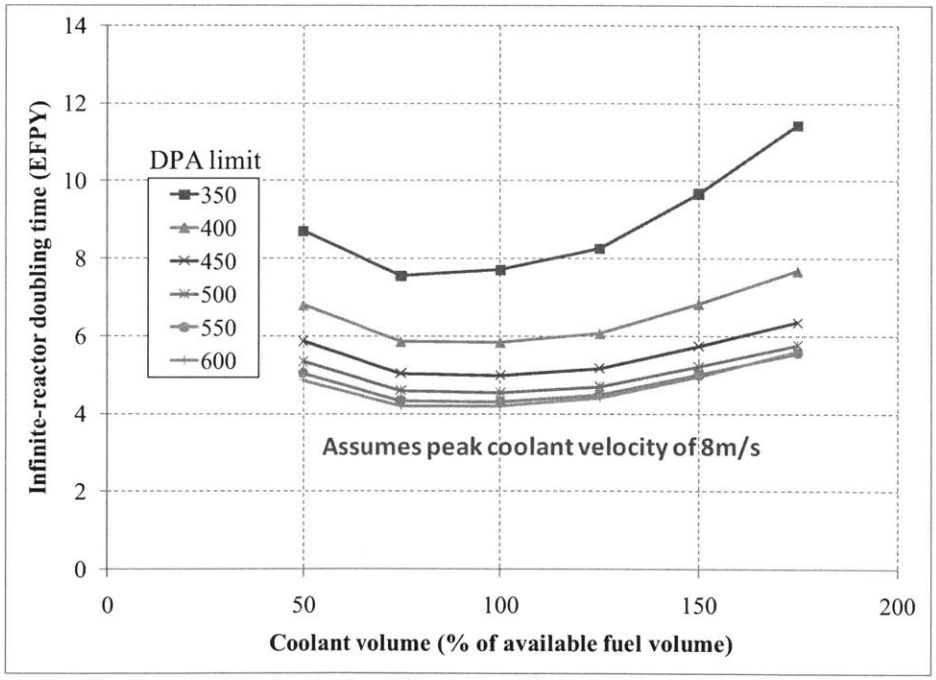

Figure 5.3-1. Infinite-reactor doubling time as a function of coolant volume for different ultimate DPA limits (U2Zr with low structure fraction T91)

A similar optimal doubling time search was performed for each of the fuel/structure combinations considered, yielding the infinite-reactor doubling time as a function of ultimate

DPA limit. An overview of the results for T91 structure is shown in Figure 5.3-2. The legend gives the type of fuel and type of structure, with the numbers being the volume of the fuel/structure relative to the available fuel volume. Each of the points in the figure corresponds to a minimum from a curve like the ones given in Figure 5.3-1.

A log plot is used in Figure 5.3-2 because of the large difference between the best and worst compositions. The multiple-century doubling times for some of the compositions are a result of the very low *k*-infinity in some of the reused compositions, which means that the composition can only supply a small amount of neutron excess. As a result, an enormous amount of starter fuel is required to provide the needed neutron excess for a new equilibrium cycle, which greatly increases both the spawning and transition times. These immense fuel requirements would likely make fuel cycles with such compositions unachievable in practice.

Figure 5.3-2 also shows some that some of the doubling times increase with higher DPA. This is because these compositions have been burned to the point that burning the fuel further begins to cost neutrons instead of supplying them; i.e. the fuel has passed point D on Figure 4.1-2 and has become a neutron absorber.

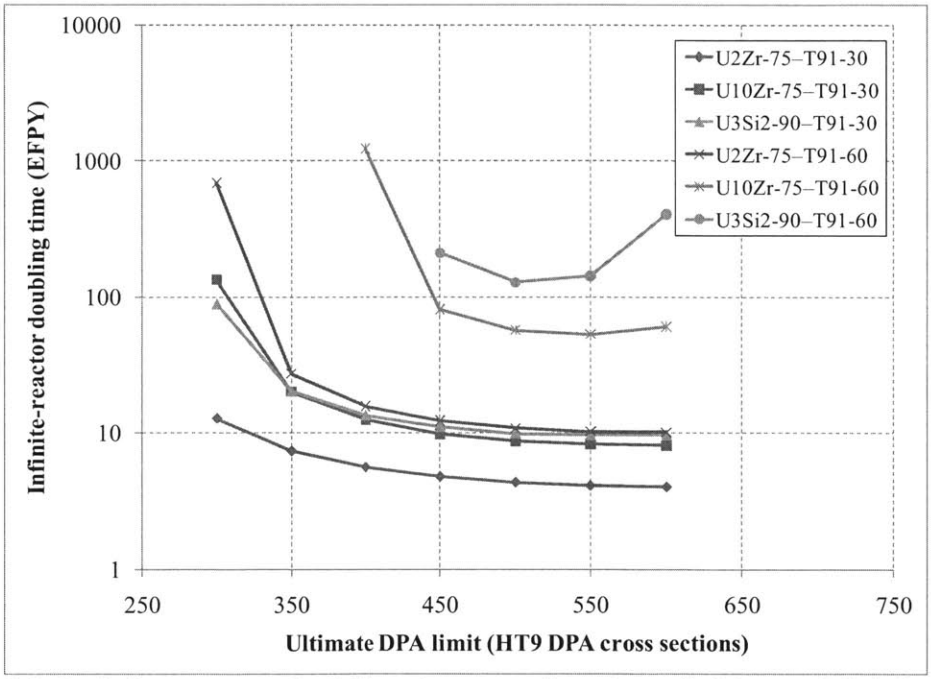

Figure 5.3-2. Infinite-reactor doubling time as a function of ultimate DPA for sodium-cooled core compositions with T91 structure

Figure 5.3-3 shows an expanded view of the best performing compositions using T91, and Figure 5.3-4 gives the corresponding chart for compositions using silicon carbide. The best performing compositions are those with the least non-fuel material: the low structure volume T91 and SiC cases using low alloy percent metal fuels. These can achieve potentially <5 year doubling times in an infinite reactor, corresponding to a ~10 year doubling time in a finite reactor with a radial power peaking factor of about 2.0. The doubling times in these cases plateau at a DPA of about 450-500; burning the core composition further decreases doubling time only slightly.

Any changes from these two best-case compositions greatly worsen doubling time. For example, switching to the higher zirconium fraction fuel U10Zr in the T91 structure case causes the doubling time to approximately double, while switching to the compound fuel U_3Si_2 increases the doubling time even further. Increasing the amount of T91 from 30% to 60% of the available fuel volume also causes doubling times to more than double. Combining two of these changes, e.g. switching to a high-zirconium-fraction metal fuel and increasing the T91 volume fraction causes doubling times to reach close to a century, as shown in Figure 5.3-2. The decrease in performance is even more severe for the SiC clad cases, as the softer spectrum in those cases increases the amount of parasitic absorptions in non-fuel materials. Doubling the amount of SiC present causes infinite-reactor doubling times to rise to over 15 years.

Figures 5.3-5 and 5.3-6 translate these results into realistic reactor doubling times, assuming a radial power peaking factor of 2.2, a capacity factor of 90%, and a fuel cooling time of one year before it can be reused. A 2.2 radial peaking factor is a reasonable value for a large power reactor, as shown in Section 3.7. As discussed in Subsection 5.2.3, the realistic doubling times are computed by multiplying the infinite-reactor timescales by the radial peaking factor and dividing by the capacity factor, then including the cooling time. The figure shows that B&B reactors with no fuel processing can potentially achieve fairly rapid doubling times (~10 years) with no processing, but doing so requires a number of technical advancements. These include demonstrating structural materials at high (400+) DPA, developing low-zirconium-fraction metal fuel, and designing a low-structure-volume-fraction core that allows for high power density operation, high burnup, and three-dimensional fuel shuffling.

The maximum areal power densities assumed for the SiC core compositions in Figure 5.3-4 and 5.3-6 are the same as those for the T91 core compositions. One of the potential advantages of SiC is its potential to operate at higher temperatures and power densities. If SiC can in fact be irradiated to high DPA while enabling higher power densities, then it would be capable of producing shorter reactor doubling times than core compositions using T91. Similarly, if advanced steels (such as oxide-dispersion strengthened steels) are capable of high temperature, high DPA operation, then doubling times would similarly be shorter for those materials.

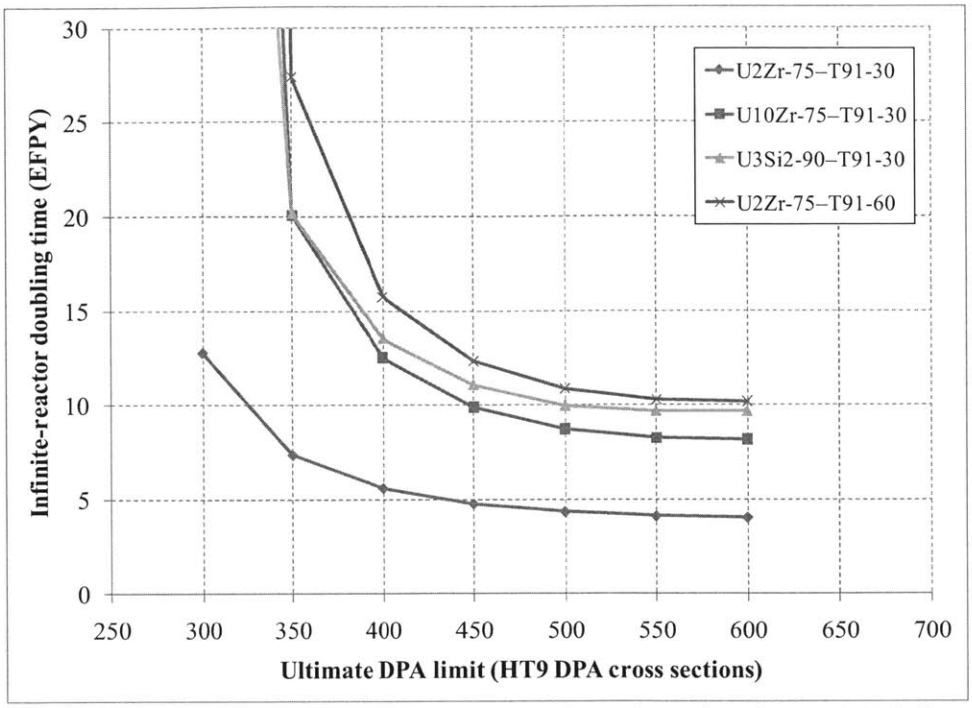

Figure 5.3-3. Infinite-reactor doubling time as a function of ultimate DPA for sodium-cooled core compositions with T91 structure (detail)

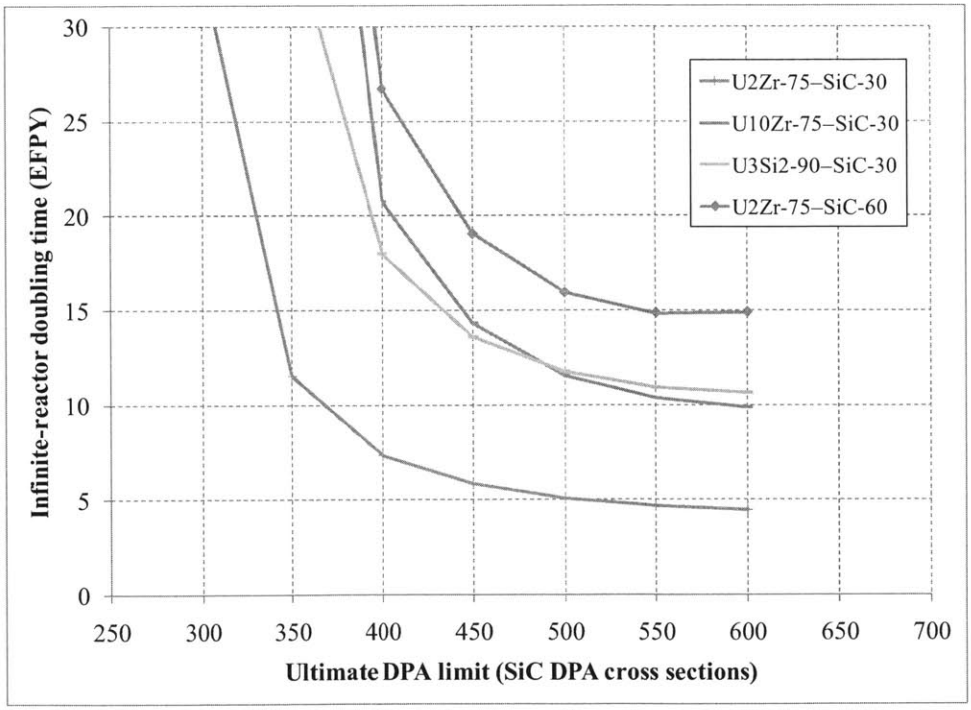

Figure 5.3-4. Infinite-reactor doubling time as a function of ultimate DPA for sodium-cooled core compositions with SiC structure (detail)

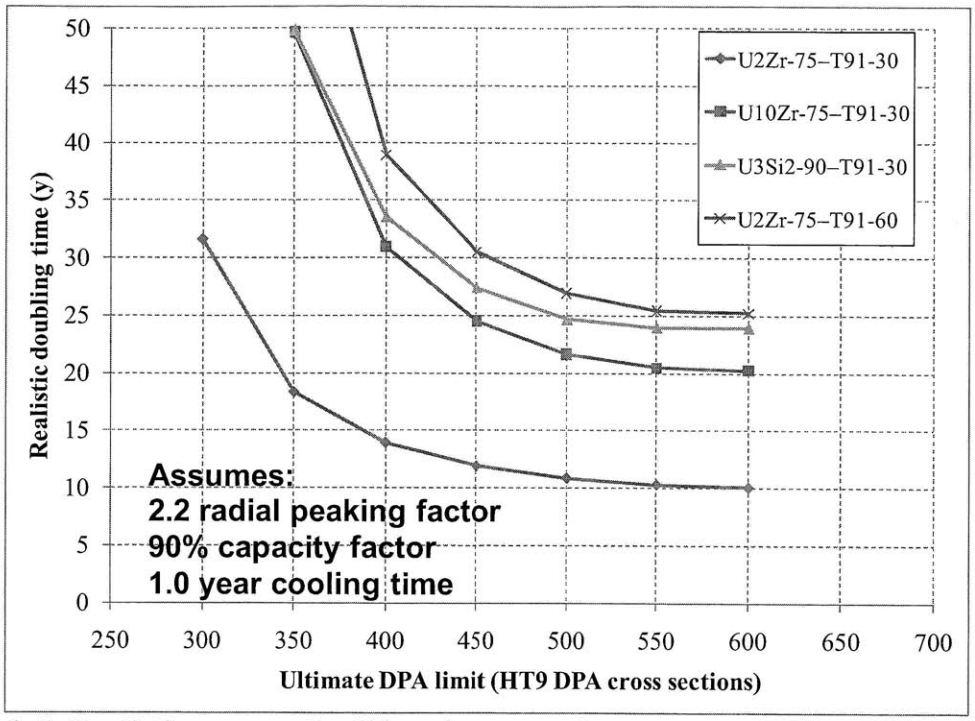

Figure 5.3-5. Realistic reactor doubling times as a function of ultimate DPA for sodium-cooled core compositions with T91 structure (no recladding)

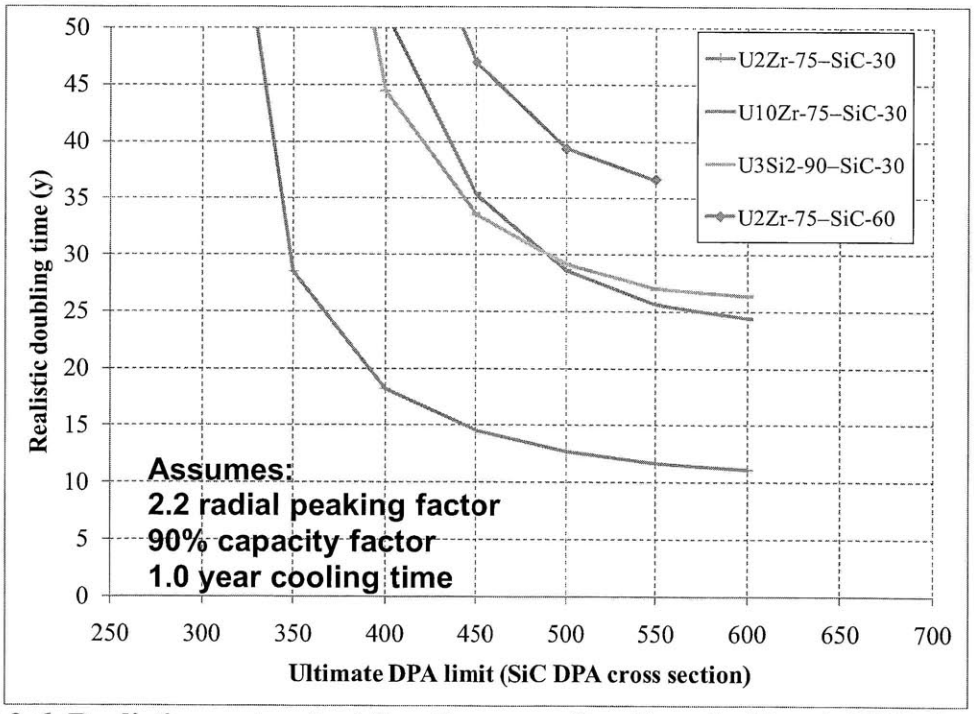

Figure 5.3-6. Realistic reactor doubling times as a function of ultimate DPA for sodium-cooled core compositions with SiC structure (no recladding)

5.3.2 Doubling time vs. DPA with recladding

Subsection 5.3.1 considered sodium-cooled B&B reactors in a fuel cycle with no fuel processing of any kind: used fuel elements would be transferred intact from one generation of reactors to start up the next. The achievable reactor doubling times for a realistic system as a function of ultimate DPA limit are given in Figures 5.3-5 and 5.3-6. With no processing, DPA levels of 400+ are required for realistic reactor doubling times on the order of 10-15 years, and only for the best fuel-structure combinations: low-alloy (2 wt% Zr) uranium-zirconium fuel with a low volume fraction (30% of available fuel volume) of T91 or SiC structure.

In this subsection, an additional analysis is performed in which fuel recladding occurs between the two reactor passes. In this analysis, a core composition is first burned to its equilibrium cycle burnup and DPA in an initial pass, and then undergoes a recladding process that allows the fuel to be irradiated further. This process could consist of just mechanical recladding or also include more complex processes like melt refining. Full chemical reprocessing is an option as well, but is not considered here because the goal of this thesis is to characterize limited-separations fuel cycles that do not use full reprocessing.

In terms of modeling the recladding step, it is again conservatively assumed that no change to fuel chemistry or geometry occurs during processing. With this assumption, a single infinite-medium depletion calculation is sufficient to approximate the behavior of the fuel through both reactor passes, as explained in Subsection 5.2.1. As a result, the only effect of the recladding process is to reset the DPA accumulated by the fuel and structure. This simplified assumption doesn't take into account: a) changes in fuel composition due to radioactive decay during the processing period; b) changes in fuel composition due to processing; and c) changes in fuel geometry during processing. The first two factors, compositional changes during cooling/processing, are considered in more detail in Subsection 5.3.3.

The third factor, changes in fuel geometry, can occur if the fuel smear density, structure fraction, or coolant fraction are changed during fuel processing. In this study, a "direct-transfer" simplification is used, which assumes that there is no change in geometry, and fuel is treated as if it is directly transferred from one reactor to another. However, if the processing step reduces fuel volume through removal of voids and some solid fission products (e.g. through melting and recasting fuel), then it may be possible to put a larger amount of reused fuel into a given fuel element, increasing the amount of neutron excess obtainable. Conversely, if the presence of solid fission products necessitate putting less fuel into each fuel element, then obtainable neutron excess would decrease. The actual smear density and amount of structure needed for the feed and starter fuel would depend on an analysis of fuel performance as a function of fuel burnup, which has not been performed in this case. Similarly, it would be possible during processing of the fuel to change the coolant volume in an assembly, or even the coolant type. Since this study assumes that the new starter fuel is intermingled in three dimensions with the next generation reactor's feed fuel, it is assumed that the coolant volume fraction is kept constant to keep operation simple in subsequent generation reactors.

Infinite-reactor doubling times in EFPY are calculated using the same procedure as in Subsection 5.3.1, using the power density results in Figure 5.2-2. Doubling times are first computed as a

function of second-burn (i.e. starter fuel) additional DPA for each of the 52 core compositions shown in Tables 5.3-1 and 5.3-2. Results for the five different U2Zr-75-T91-30 compositions with different coolant volume fractions are shown in Figure 5.3-7. The DPA accumulated over the first burn is determined by the core composition, corresponding to the breakeven burnup that makes the adjusted neutron excess equal to zero. The black Xs in Figure 5.3-7 correspond to a second (starter fuel) burn that results in the same DPA as the first (feed fuel) burn, so burning up to the black Xs or less does not raise the maximum DPA needed per stage.

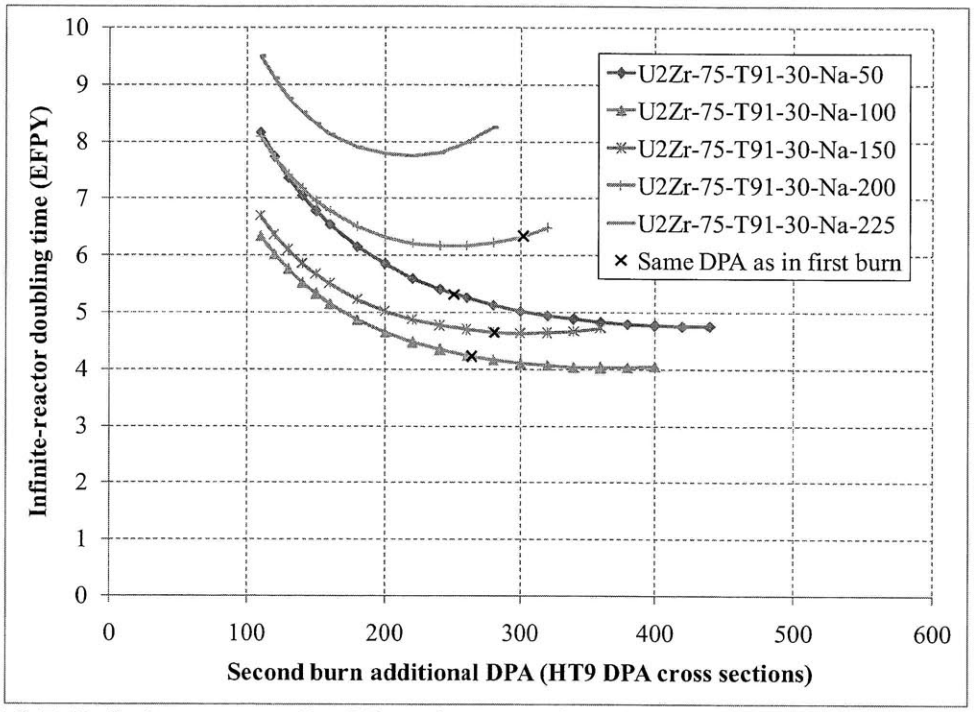

Figure 5.3-7. Infinite-reactor doubling time as a function of second burn DPA for eight U2Zr-75-T91-30 core compositions with different coolant volume fractions

Each of the infinite-medium cases is run to a maximum burnup of 400 MWd/kg, after which the majority of the core compositions have a k_∞ less than unity, such that burning them further would cost neutrons and raise the doubling time. This is seen in Figure 5.3-7 by the fact that most of the curves end shortly after turning upward. Because of the finite DPA simulated, the U2Zr-75-T91-30-Na-225 curve does not have a black X, since it would lie at a DPA higher than the peak burnup simulated.

The results in Figure 5.3-7 can be divided into two sets. The cases with a low minimum burnup (coolant volume from 50-150) have minimum doubling times at second-burn DPA levels *higher* than the first-burn DPA (to the right of the Xs). Meanwhile, the cases with coolant volume from 175-225 have doubling time minima that occur at second-burn DPA *lower* than the first-burn DPA (to the left of the Xs), so they can achieve their lowest doubling times without their second stage burns exceeding the DPA limit established by their original equilibrium cycle.

If one takes the DPA accumulated during the first equilibrium cycle burn as the ultimate DPA limit, then the minimum doubling times for the first set are equal to the doubling times at the black Xs, and the minimum doubling times for the second set are the minimum of the curves in

Figure 5.3-7. Plotting these minimum doubling times for the different T91-structure compositions yields the curves shown in Figure 5.3-8. In each of the curves, the leftmost (lowest DPA) points correspond to the lowest coolant volume (50% available fuel volume) equilibrium cycles, with succeeding points representing increasing coolant volumes. The curves have a characteristic "U" shape, with low coolant fractions having longer doubling times due to lower power densities, and high coolant fractions having longer doubling times due to worse neutronics. The compositions containing less structure and non-uranium fuel material have higher optimal coolant fractions, equal to roughly 100% of the available fuel volume (the third point from the left) in the U2Zr-75-T91-30 case.

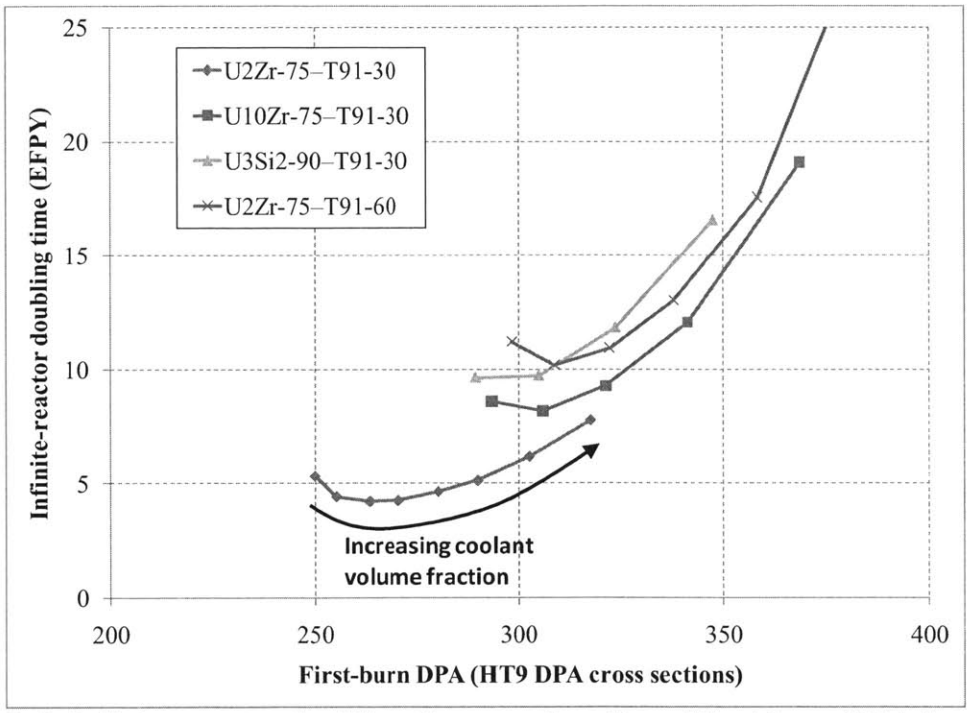

Figure 5.3-8. Infinite-reactor doubling time as a function of first-burn DPA for different sodium-cooled core compositions with T91 structure

As shown in Figure 5.3-8, using a higher DPA limit to include additional coolant and raise power densities only improves doubling time up to a point, after which degradation in the neutron economy causes doubling times to increase. In this case, there is no reason to have a higher-DPA *first* burn, but as Figure 5.3-7 shows, in certain cases going to a higher DPA for the *second* burn can result in an improvement in doubling time. Figure 5.3-9 shows how doubling time can be improved for the U2Zr-75–T91-30 composition by having the second burn go to a higher DPA than the first burn. The figure explicitly shows the amount of coolant present: as the volume of coolant increases, the first burn requires more DPA, and worsening neutronic performance causes doubling time to increase when coolant volume exceeds 125% of the available fuel volume. If one has a higher DPA limit, for example 350 DPA, then the strategy that minimizes doubling time is to use a lower coolant fraction (100% available fuel volume, which corresponds to a coolant volume fraction of 43%), keep the first burn at the same DPA (~265 DPA), and extend the second burn to 350 DPA.

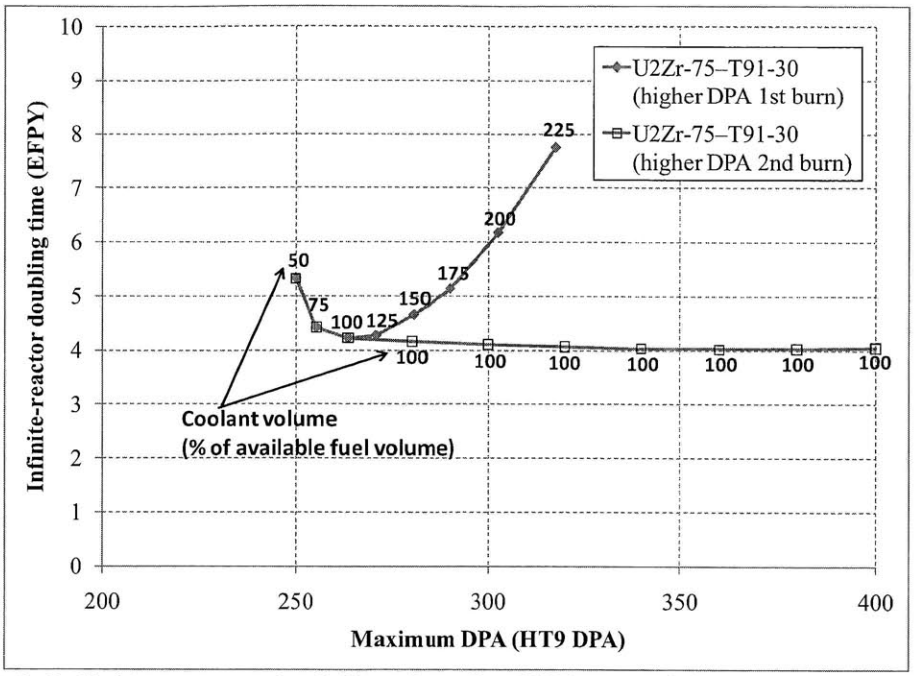

Figure 5.3-9. Infinite-reactor doubling time for U2Zr-75–T91-30 core compositions for higher DPA 1st and 2nd burns

The doubling time improvement from having a higher DPA second burn is quite small, for example, for the U2Zr-75–T91-30 composition, increasing the DPA limit from 265 to 365 decreases the infinite-reactor doubling time from 4.22 years to 4.03 years, an improvement of less than 5% for a 100 DPA increase. In the cases with longer doubling times, there is no reason for the second burn DPA to exceed that from the first, since doing so would extend the second burn to the point that the fuel has k_∞ less than unity, (i.e. past point D on Figure 4.1-2) meaning that no additional neutron excess is supplied.

One important result from Figures 5.3-8 and 5.3-9 is that the infinite-reactor doubling times from the no-recladding case (Figure 5.3.3) are not improved by breaking up DPA accumulation into two burns. This makes sense because the only difference between the two scenarios is whether DPA continues to be accumulated over the first and second burns. The same sensitivity of doubling time to fuel/structure composition can be seen, with U2Zr performing far better than U10Zr and a lower structure volume performing far better than higher. In the case with recladding, once the DPA limit is high enough to allow the optimal coolant volume fraction, being able to burn to higher DPA yields little extra benefit. This is unlike the case without recladding, in which doubling times continue to get shorter even as the ultimate DPA limit exceeds 500.

Figures 5.3-10 and 5.3-11 show the corresponding realistic reactor doubling times for T91- and SiC-structure cases with recladding, assuming a radial peaking factor of 2.2, a 90% capacity factor, and a cooling and processing time of 2 years. Intriguingly, the needed DPA limit for optimal doubling times is quite low for the best performing core compositions, on the order of 265 DPA for T91, or just ~33% higher than the current knowledge limit, and 300 DPA for SiC. Even in the worse performing compositions, ~300 DPA (~325 DPA for SiC) is sufficient to yield

the best-case doubling times, with almost no benefit for going past 300 DPA in a single burn. The materials qualification challenge is therefore surprisingly modest for minimum-burnup B&B reactors that use 3D shuffling; much of the challenge lies instead in the engineering of such a system: how to design a high-power-density, axially-segmented core that minimizes structural and fuel alloying materials.

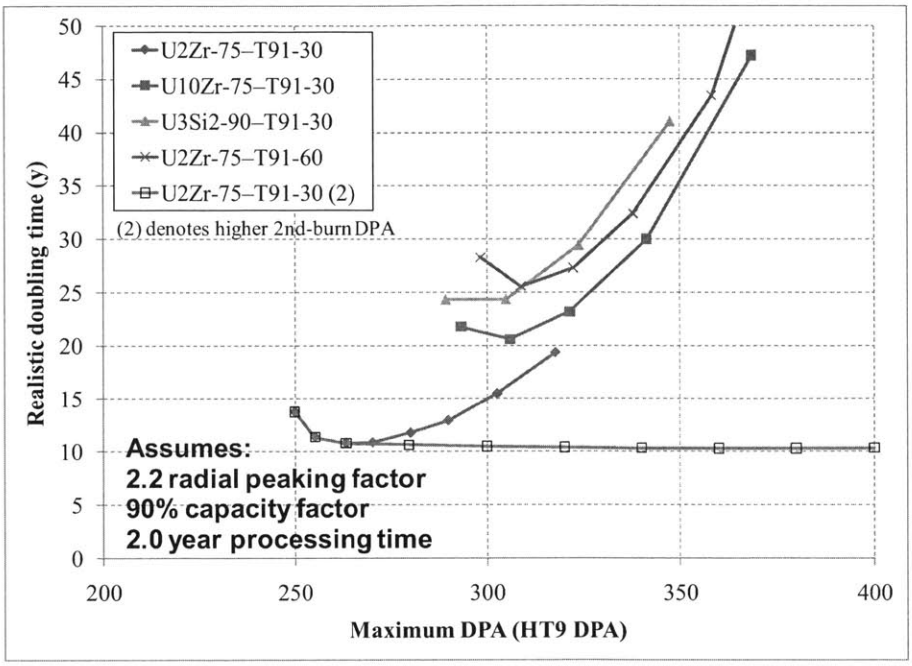

Figure 5.3-10. Realistic reactor doubling times as a function of maximum DPA for sodium-cooled core compositions with T91 structure (with recladding)

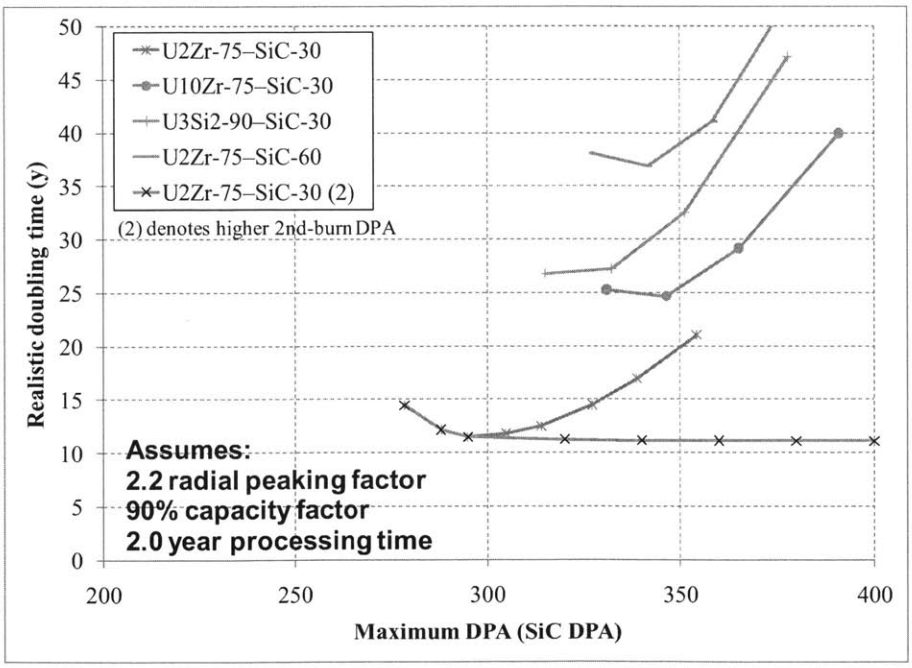

Figure 5.3-11. Realistic reactor doubling times as a function of maximum DPA for sodium-cooled core compositions with SiC structure (with recladding)

5.3.3 Effect of cooling time and melt refining

So far the neutron excess from burning feed fuel a second time has been estimated from infinite-medium depletions of unburned feed fuel. This approach is used mainly because it uses the results from the existing infinite-medium model that had been used earlier to estimate the minimum burnup needed for each core composition. This approach does introduce approximations however: first, the composition of the infinite-medium depletion will not exactly match that of fuel discharged from an equilibrium cycle (although it is close), and second, the effect of any post-discharge cooling time or processing is neglected. A better approximation, and one that would allow the effects of cooling time and processing to be studied, is to perform an infinite-medium depletion of the actual discharge compositions.

Discharged fuel of the core composition with the shortest doubling time (U2Zr-75-T91-30-Na-100) from the convergent infinite slab shuffling case is first allowed to cool for zero years, 2 years, and 20 years. In one set of cases, the composition of the fuel is left unchanged after cooling, while in another a melt refining process occurs which removes volatile and reactive fission products from the fuel mixture. The melt refining process was developed for use with EBR-II and is described in report ANL-6605 [Hesson, 1963]; it is described as removing 100% of noble and volatile fission products (Br, Kr, Rb, Cd, I, Xe, Cs), which escape as gases, and 95% of reactive elements (Sr, Y, Te, Ba, Am, Th, and the rare earths), which react with the zirconia crucibles. It is assumed that the same ratio of original fuel to structure/coolant is maintained, and no additional material (such as makeup uranium) is added. Fuel losses during processing are not modeled, but would be easy to incorporate: for example, 2% process losses would effectively increase the fuel requirement of a reactor by a factor of 1.0/0.98. Whether the refining process occurs at the end or the middle of the cooling period has little effect on the results obtained.

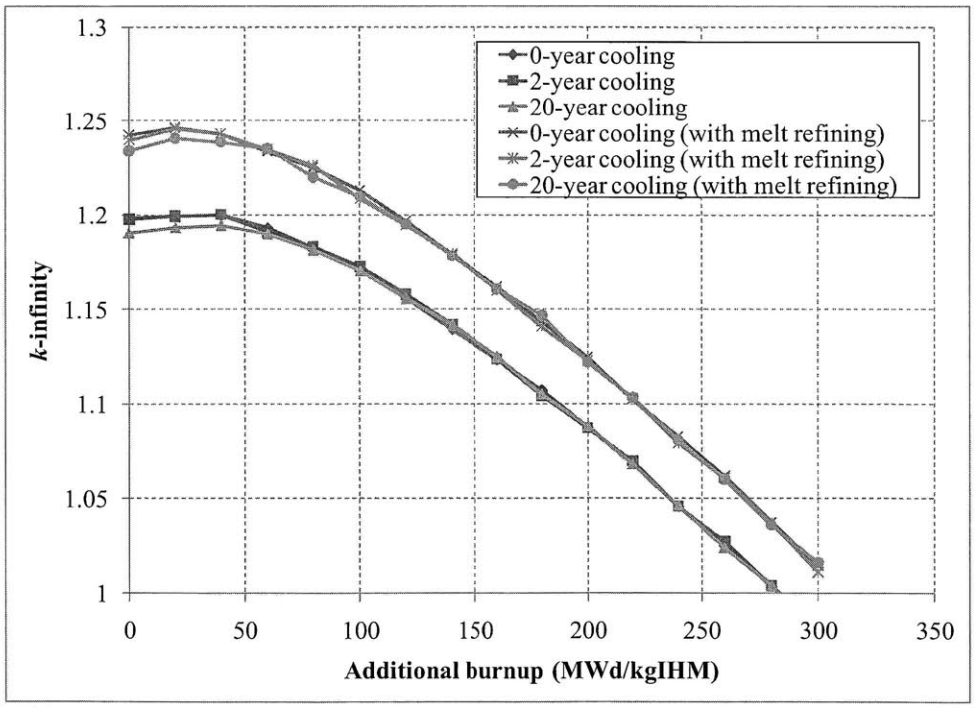

Figure 5.3-12. Fuel k_∞ vs. additional burnup for different cooling and processing scenarios

Figure 5.3-12 shows the fuel k_∞ as a function of depletion for the different cases considered. The zero year and two year cooling cases are nearly indistinguishable, while the twenty-year cooling cases start with a slightly lower k_∞. The k_∞ decrease in the twenty year case is due to the decay of fissile Pu-241 to Am-241, which occurs with a 14 year half life. The difference in k_∞ disappears with additional burnup as Am-241 is converted to fissile Am-242m and Pu-241 is burned. Overall, the effect is small because breed-and-burn reactors rely on a fast neutron spectrum that limits absorptions in Pu-239 and Pu-240, which means only a small amount of Pu-241 is generated. This is illustrated for the two best performing core compositions (U2Zr-75-T91-30-Na-100 and U2Zr-75-SiC-30-Na-100) in Figures 5.3-13 and 5.3-14. The Pu-241/Pu-239 ratio reaches 1.45% in the T-91 case and 1.85% in the SiC case at discharge. The higher ratio in the SiC case is due to a higher discharge burnup and softer spectrum. In worse performing core compositions the Pu-241 fraction can be higher, but in every case even a decade long cooling time has a minor effect on subsequent k_∞.

Figure 5.3-12 also shows that the effect of removing fission products during melt refining is tremendous, as the fuel gains a large and lasting increase in its k_∞. The net effect of this increase on obtainable neutron excess in shown in Figure 5.3-15. The first-burn value of 270 DPA corresponds to an additional burnup of 160 MWd/kgIHM, at which point over three quarters of the available neutron excess has been extracted. At this amount of additional burnup, the cases with a cooling time of twenty years have neutron excesses just 1% below those with zero and two year cooling times, so reactor doubling times would be affected much more by the increased cooling time than by the decreased neutron excess.

Most notably, Figure 5.3-15 shows that with melt refining, 24% more neutron excess can be extracted from a piece of used feed fuel. This means that 19% less feed fuel is needed to initiate an equilibrium cycle, which shortens doubling times by approximately 19%. This would reduce the reactor doubling time of the core composition (from Figure 5.3-10) from 10 years to approximately 8 years. Not only does a melt-refining process give the ability to reset the fluence limit by starting over with new cladding, it also has the potential to greatly improve used feed fuel and the performance of limited-separations fuel cycles.

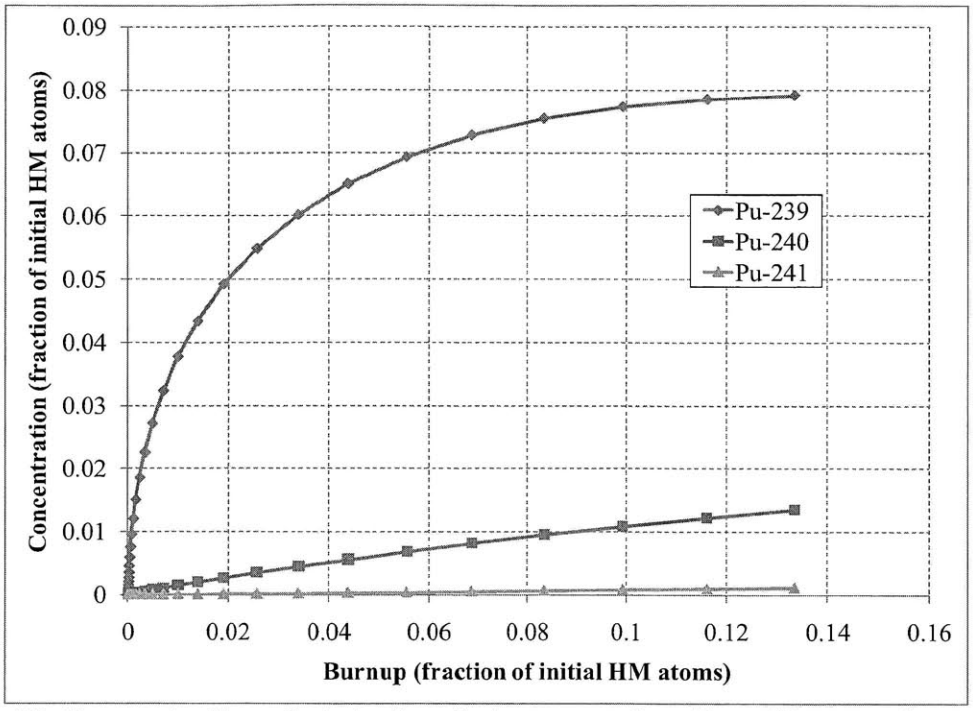

Figure 5.3-13. Concentration of plutonium isotopes as a function of burnup from 1D model (U2Zr-75-T91-30-Na-100 core composition)

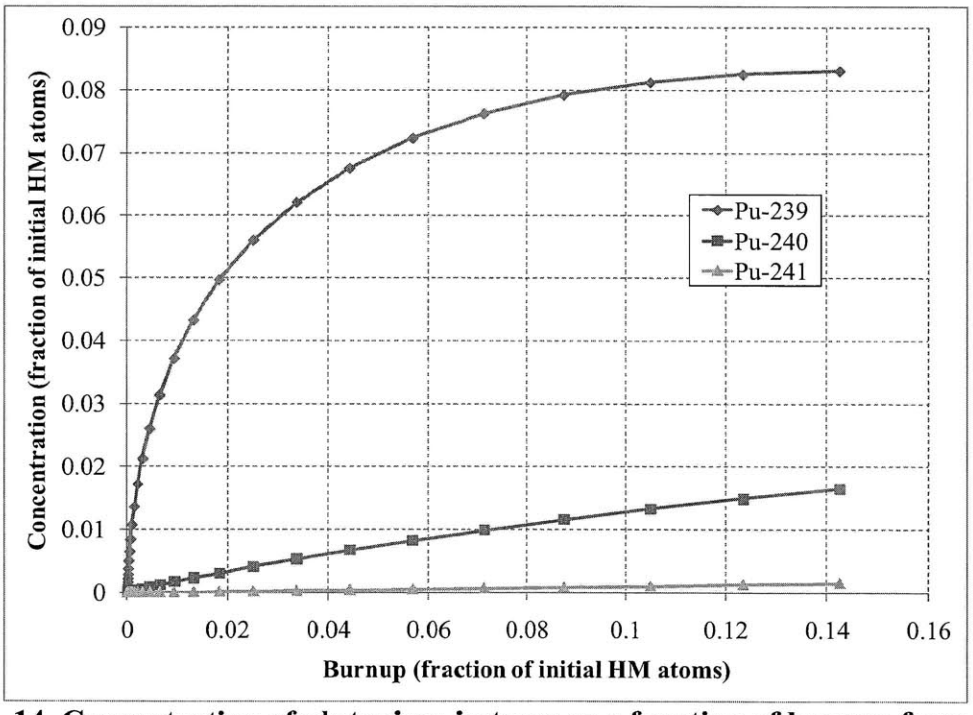

Figure 5.3-14. Concentration of plutonium isotopes as a function of burnup from 1D model (U2Zr-75-SiC-30-Na-100 core composition)

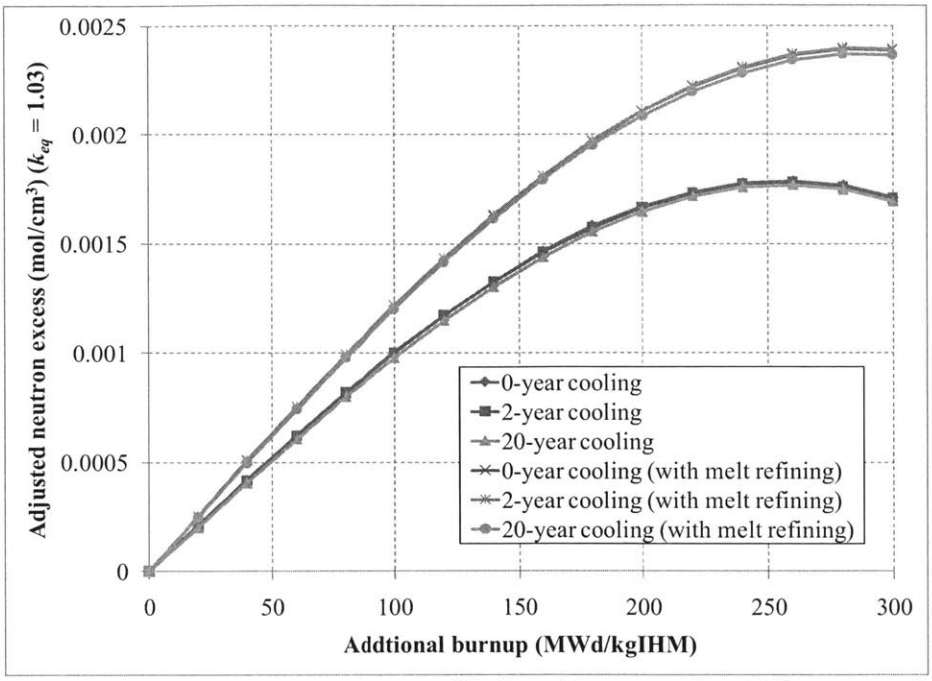

Figure 5.3-15. Fuel neutron excess vs. additional burnup for different cooling and processing scenarios

5.3.4 Effect of fission gas escape

The calculations in the previous three subsections have assumed that all fission products are retained in the fuel and continue to parasitically absorb neutrons through the life of the fuel. In an actual reactor, gaseous fission products would be able to leave the fuel as the fuel is irradiated, either by collecting in a fission gas plenum or by venting from the fuel element completely. This effect is most pronounced for metal fuel, which can develop an open pore structure that allows a significant fraction of fission product gases to escape. Due to the high level of burnup encountered in a B&B reactor (as well as the sensitivity of the B&B neutron economy), it is important to characterize the effect of fission product gas escape.

Fission product gas escape is modeled by assuming that 80% of all noble fission products and fission product decay daughters (Xe and Kr) escape the fuel. This gas escape is assumed to occur exponentially on a 100 second timescale. These values are meant to represent a simple idealized case for metal fuel: the 80% release fraction is a representative value from ANL irradiation tests [Pahl, 1992], and the 100 second timescale is chosen simply so that extremely short lived noble gases do not escape before decaying. The actual escape fraction and escape lifetime of fission product gases would actually be a function of the fuel temperature and irradiation history, and would depend on both the fuel type (ceramic vs. metal) and the gas species considered (e.g. noble Kr vs. volatile Cs).

The doubling time analyses for a minimum burnup B&B core are repeated for sodium-cooled core compositions with T-91 structure, accounting for fission product gas escape as described. Results are given in Figure 5.3-16 for the no-recladding case, and in Figure 5.3-17 for the case in which fuel recladding is allowed. The baseline fuel cycle and depleted uranium feed are

assumed, with no composition changes during discharge due to cooling or melt refining. Since U_3Si_2 is not a metal fuel, it may not release as much fission gas as is assumed (since assumed values are based on a metal fuel release fraction). Therefore, the effect of fission product escape shown in these figures may be non-conservative for the U_3Si_2 composition.

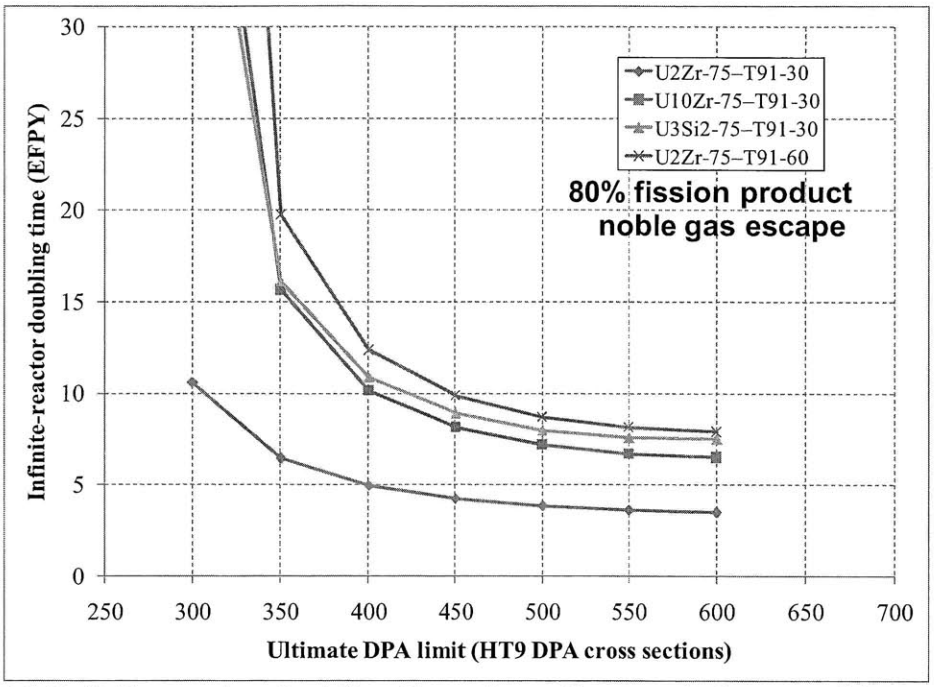

Figure 5.3-16. Infinite reactor doubling times for sodium-cooled compositions with fission product escape (no-reclad case)

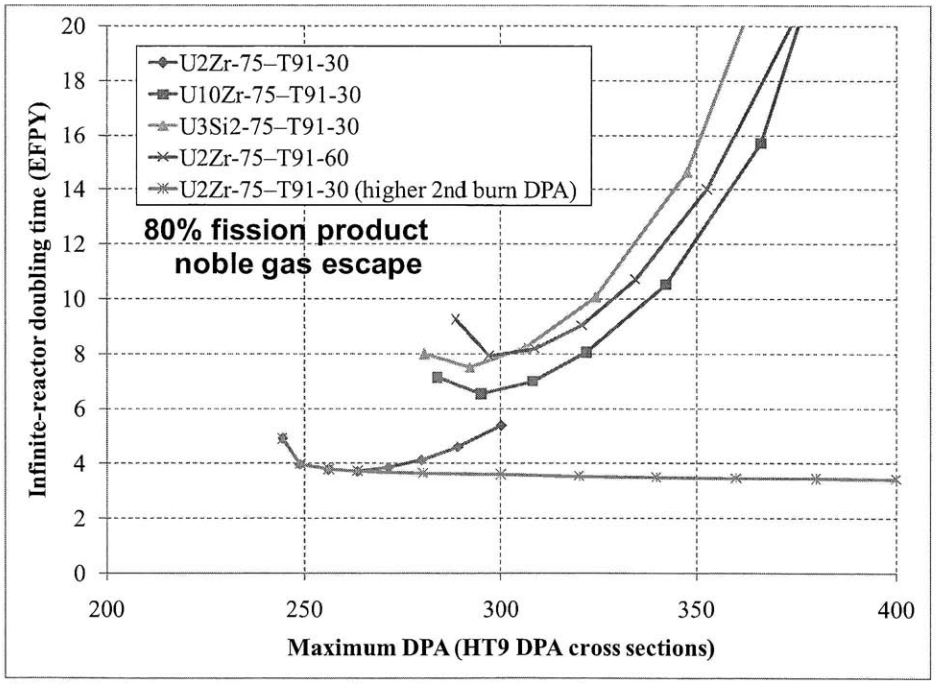

Figure 5.3-17. Infinite reactor doubling times for sodium-cooled compositions with fission product gas escape (with-reclad case)

Figures 5.3-16 and 5.3-17 show that fission product gas escape can potentially make a significant difference in fuel cycle performance. In Figure 5.3-16, the U2Zr-75-T91-30-Na-100 core composition (the third point from the left on the bottommost curve) is shifted from its original position of 263 DPA and 4.22 years with no fission product escape (see Figure 5.3-9), to 256 DPA and 3.78 years with fission product removal, a 10% decrease in infinite-reactor doubling time. The performance improvement for worse core compositions is more pronounced; for example the U2Zr-75-T91-60-Na-75 core composition is improved from 309 DPA and 10.2 years to 297 DPA and 7.9 years. As with other improvements to neutronic performance, accounting for fission product escape shifts the minimum doubling time composition to higher coolant volume fractions.

The benefits of fission product escape become larger as fuel burnup increases. The reason doubling times improve significantly when fission product escape is accounted for is primarily due to increased neutron excess over the second burn, when feed fuel is reused to start a new equilibrium cycle. This is because the fuel contains more fission products over its second burn so removing a fraction of them makes a larger difference. A similar effect was seen in the previous section by modeling melt refining, which allowed roughly 24% more neutron excess from a given amount of fuel by removing a fraction of the fission products. Note that with fission product escape accounted for, melt refining would yield a smaller improvement, since some of the fission products removed by melt refining would have escaped naturally during fuel irradiation.

5.3.5 Effect of natural vs. depleted uranium

All the analyses up to this point have assumed feed fuel compositions containing depleted uranium, consisting of 0.3 atom % U-235 and 99.7% U-238. Using natural uranium (0.71% U-235 by weight) instead of depleted uranium improves the neutronics of B&B reactors, since the additional U-235 is a source of excess neutrons. This leads to a reduction in DPA requirements and a shorter reactor doubling time.

The doubling time analyses for a minimum-burnup B&B reactor were repeated for sodium-cooled core compositions with T-91 structure, replacing the depleted uranium fuel with natural uranium. Infinite-reactor doubling time results are given in Figure 5.3-18 for the no-recladding case, and in Figure 5.3-19 for the case in which fuel recladding is allowed. The baseline fuel cycle is assumed. Fission product escape from the previous subsection is *not* modeled, so that the individual effects of the two changes can be independently characterized.

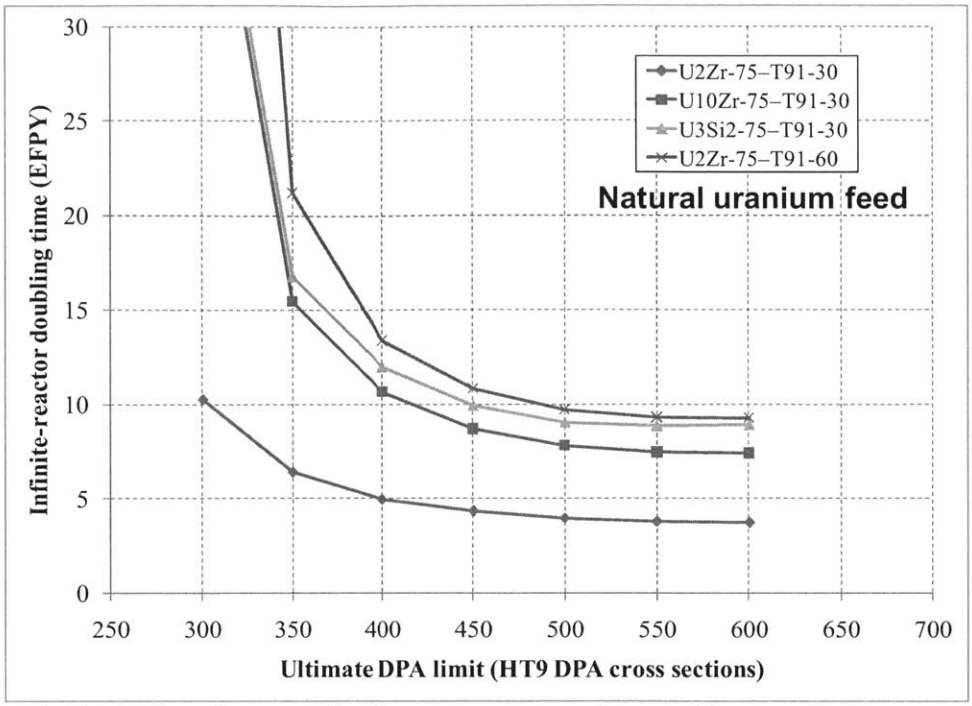

Figure 5.3-18. Doubling time results for natural-uranium sodium-cooled compositions (no-reclad case)

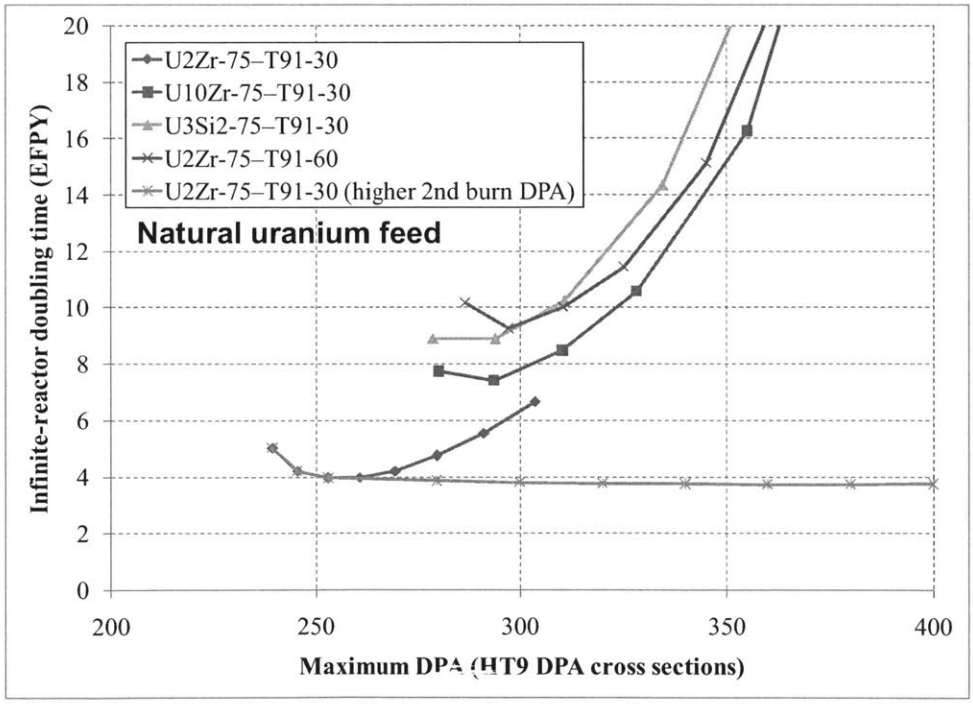

Figure 5.3-19. Doubling time results for natural-uranium sodium-cooled compositions (with-reclad case)

For the U2Zr-75-T91-30-Na-100 core composition (the third point from the left on the lowest line in Figure 5.3-19), the results show an infinite-reactor doubling time of 3.96 years for a minimum of 253 DPA. The corresponding numbers for the depleted uranium case are 4.22 years

and 263 DPA, so there is a 6% improvement in doubling time by using natural instead of depleted uranium. The improvements for the worse performing core compositions are similarly small, about a 5-10% improvement in doubling time and a 10-15 reduction in necessary DPA. Overall the switch to natural uranium may help improve fuel performance margins but would not by itself make a significant change in fluence requirements or system performance. Similarly, going in the other direction to lower U-235 depleted uranium tails would not have a large negative effect.

5.4 LBE-cooled fast reactor core compositions

As discussed in the core composition overview in Section 5.2, lead and LBE coolant have better infinite-medium neutronic performance than sodium if substituted on a per volume basis, on account of their creating a harder neutron spectrum in the core. LBE performs somewhat better than lead neutronically, so it was selected as the basis of a comprehensive core composition overview using infinite slab models. As shown in Subsection 4.4.2, the results from infinite slab models can be used to estimate doubling times for realistic reactor systems.

The same study of sodium-cooled compositions was repeated for LBE-cooled compositions, with the same combinations of fuel and structure options. The structure to fuel volume ratio was either 30% or 60% of the available fueled volume. Equilibrium cycle simulations are run using infinite slab models with convergent shuffling, with the discharge burnup corresponding to an infinite-medium average k_{fuel} prediction of 1.02. Tables 5.4-1 and 5.4-2 show selected characteristics of the 63 different compositions that meet the 1.02 target. Table 5.4-1 gives results for compositions with T91 structure, while Table 5.4-2 gives results for those with SiC structure.

Compared to the same core compositions using sodium, the LBE cases show lower discharge burnup and shorter axial lengths (so smaller overall dimensions), and correspondingly lower neutron excess and contained burnup requirements. The smaller dimensions of the LBE cases are due to a combination of the lower required burnup as well as the shorter neutron mean free path in the LBE system. The performance of the LBE cooled reactor is less sensitive to the amount of coolant present, and is capable of operating with neutronically less robust fuel/structure combinations. Meanwhile, the DPA-to-burnup and fast-fluence-to-burnup ratios are higher in the LBE cases than in sodium, a result of the harder spectrum in the LBE-cooled compositions. Since LBE has less impact on neutronics than sodium, optimum core compositions for LBE-cooled systems include a larger coolant fraction than a corresponding sodium-cooled system would.

Table 5.4-1. Equilibrium cycle results for LBE-cooled core compositions (T91 structure)

Composition	HM density (g/cc)	Ave. k_{eq}	Discharge burnup fraction	Discharge HT9 DPA	Discharge fast fluence (/cm^2) (>0.1 MeV)	Axial length (cm)	MOEC BU contained (MWy/m^2)	Adjusted ΔN (mol/m^2)
U2Zr-75-T91-30-LBE-50	7.47	1.028	11.4%	256	6.47E+23	197	882	1127
U2Zr-75-T91-30-LBE-75	6.56	1.027	12.1%	265	6.71E+23	210	887	1111
U2Zr-75-T91-30-LBE-100	5.85	1.027	12.9%	274	6.97E+23	223	904	1105
U2Zr-75-T91-30-LBE-125	5.27	1.027	13.6%	283	7.19E+23	237	917	1098
U2Zr-75-T91-30-LBE-150	4.80	1.027	14.3%	292	7.45E+23	248	936	1092
U2Zr-75-T91-30-LBE-175	4.41	1.026	15.2%	302	7.71E+23	259	961	1091
U2Zr-75-T91-30-LBE-200	4.08	1.027	16.0%	313	7.99E+23	267	987	1093
U2Zr-75-T91-30-LBE-225	3.79	1.027	17.0%	324	8.28E+23	278	1023	1092
U10Zr-75-T91-30-LBE-50	6.00	1.027	14.5%	297	7.49E+23	216	1035	1195
U10Zr-75-T91-30-LBE-75	5.27	1.027	15.7%	311	7.87E+23	229	1070	1188
U10Zr-75-T91-30-LBE-100	4.70	1.026	16.9%	326	8.27E+23	245	1109	1183
U10Zr-75-T91-30-LBE-125	4.24	1.026	18.2%	342	8.69E+23	261	1157	1183
U10Zr-75-T91-30-LBE-150	3.86	1.026	19.7%	361	9.17E+23	272	1224	1187
U10Zr-75-T91-30-LBE-175	3.54	1.026	21.4%	383	9.76E+23	288	1318	1196
U10Zr-75-T91-30-LBE-200	3.27	1.025	23.4%	410	1.04E+24	302	1437	1205
U10Zr-75-T91-30-LBE-225	3.04	1.024	26.0%	445	1.13E+24	319	1620	1214
U3Si2-90-T91-30-LBE-50	5.66	1.028	15.5%	292	7.15E+23	220	1072	1208
U3Si2-90-T91-30-LBE-75	4.97	1.027	16.7%	307	7.53E+23	236	1104	1194
U3Si2-90-T91-30-LBE-100	4.43	1.027	18.1%	324	7.96E+23	249	1156	1193
U3Si2-90-T91-30-LBE-125	3.99	1.027	19.7%	342	8.44E+23	265	1223	1194
U3Si2-90-T91-30-LBE-150	3.64	1.027	21.5%	365	9.00E+23	280	1312	1201
U3Si2-90-T91-30-LBE-175	3.34	1.025	23.5%	389	9.62E+23	293	1425	1200
U3Si2-90-T91-30-LBE-200	3.08	1.025	26.2%	424	1.05E+24	309	1605	1211
U2Zr-75-T91-60-LBE-50	6.41	1.027	15.0%	299	7.61E+23	206	1101	1248
U2Zr-75-T91-60-LBE-75	5.72	1.026	16.0%	311	7.91E+23	220	1128	1235
U2Zr-75-T91-60-LBE-100	5.17	1.028	17.1%	325	8.28E+23	231	1164	1237
U2Zr-75-T91-60-LBE-125	4.72	1.026	18.1%	337	8.61E+23	245	1206	1229
U2Zr-75-T91-60-LBE-150	4.34	1.026	19.3%	353	9.01E+23	256	1258	1229
U2Zr-75-T91-60-LBE-175	4.02	1.025	20.6%	368	9.43E+23	267	1317	1228
U2Zr-75-T91-60-LBE-200	3.74	1.026	22.1%	388	9.93E+23	278	1398	1236
U2Zr-75-T91-60-LBE-225	3.49	1.025	23.9%	411	1.05E+24	292	1516	1240
U10Zr-75-T91-60-LBE-50	5.14	1.026	21.7%	387	9.81E+23	232	1566	1387
U10Zr-75-T91-60-LBE-75	4.60	1.025	24.2%	420	1.07E+24	248	1731	1392
U10Zr-75-T91-60-LBE-100	4.15	1.024	27.9%	472	1.20E+24	269	2063	1395
U3Si2-90-T91-60-LBE-50	4.85	1.026	24.0%	396	9.78E+23	237	1729	1412
U3Si2-90-T91-60-LBE-75	4.33	1.025	27.8%	448	1.11E+24	259	2048	1410

Table 5.4-2. Equilibrium cycle results for LBE-cooled core compositions (SiC structure)

Composition	HM density (g/cc)	Ave. k_{eq}	Discharge burnup fraction	Discharge SiC DPA	Discharge fast fluence (/cm^2) (>0.1 MeV)	Axial length (cm)	MOEC BU contained (MWy/m^2)	Adjusted ΔN (mol/m^2)
U2Zr-75-SiC-30-LBE-50	7.47	1.028	12.5%	296	5.59E+23	180	912	1123
U2Zr-75-SiC-30-LBE-75	6.56	1.029	13.3%	310	5.85E+23	194	933	1123
U2Zr-75-SiC-30-LBE-100	5.85	1.028	14.1%	323	6.11E+23	205	944	1113
U2Zr-75-SiC-30-LBE-125	5.27	1.028	15.0%	337	6.37E+23	218	969	1113
U2Zr-75-SiC-30-LBE-150	4.80	1.028	15.9%	351	6.63E+23	231	997	1112
U2Zr-75-SiC-30-LBE-175	4.41	1.027	16.8%	366	6.92E+23	241	1021	1108
U2Zr-75-SiC-30-LBE-200	4.08	1.028	17.8%	381	7.20E+23	252	1058	1112
U2Zr-75-SiC-30-LBE-225	3.79	1.027	18.7%	396	7.49E+23	262	1096	1114
U10Zr-75-SiC-30-LBE-50	6.00	1.027	16.4%	347	6.52E+23	198	1113	1210
U10Zr-75-SiC-30-LBE-75	5.27	1.028	17.8%	369	6.93E+23	214	1162	1213
U10Zr-75-SiC-30-LBE-100	4.70	1.027	19.3%	393	7.38E+23	229	1221	1208
U10Zr-75-SiC-30-LBE-125	4.24	1.027	21.0%	420	7.90E+23	243	1304	1218
U10Zr-75-SiC-30-LBE-150	3.86	1.026	22.8%	449	8.44E+23	257	1412	1224
U10Zr-75-SiC-30-LBE-175	3.54	1.025	25.3%	487	9.17E+23	272	1567	1236
U10Zr-75-SiC-30-LBE-200	3.27	1.025	29.1%	550	1.04E+24	291	1858	1249
U3Si2-90-SiC-30-LBE-50	5.66	1.029	16.7%	330	6.18E+23	208	1141	1217
U3Si2-90-SiC-30-LBE-75	4.97	1.028	18.2%	352	6.60E+23	220	1186	1209
U3Si2-90-SiC-30-LBE-100	4.43	1.027	19.9%	376	7.06E+23	236	1256	1210
U3Si2-90-SiC-30-LBE-125	3.99	1.027	21.7%	403	7.58E+23	252	1347	1211
U3Si2-90-SiC-30-LBE-150	3.64	1.026	24.0%	437	8.22E+23	267	1467	1219
U3Si2-90-SiC-30-LBE-175	3.34	1.025	26.7%	478	9.00E+23	284	1691	1230
U2Zr-75-SiC-60-LBE-50	6.41	1.028	18.0%	339	6.27E+23	184	1254	1254
U2Zr-75-SiC-60-LBE-75	5.72	1.029	19.3%	359	6.65E+23	196	1313	1265
U2Zr-75-SiC-60-LBE-100	5.17	1.028	20.7%	380	7.04E+23	209	1375	1262
U2Zr-75-SiC-60-LBE-125	4.72	1.027	22.3%	403	7.48E+23	221	1458	1264
U2Zr-75-SiC-60-LBE-150	4.34	1.026	24.2%	431	8.00E+23	233	1550	1263
U2Zr-75-SiC-60-LBE-175	4.02	1.026	26.7%	468	8.70E+23	249	1763	1277

The better neutronic performance of the LBE core compositions would translate to shorter doubling times than for the sodium cases, if one assumes that the two coolants have the same power density limits. Figures 5.4-1 gives the infinite-reactor doubling times for different LBE core compositions as a function of ultimate DPA limit for a case with recladding allowed. The figure assumes the same power density as in the sodium case, and can be directly compared to the sodium results in Figure 5.3-8. No fission product escape or melt refining is modeled, and depleted uranium is used as feed fuel.

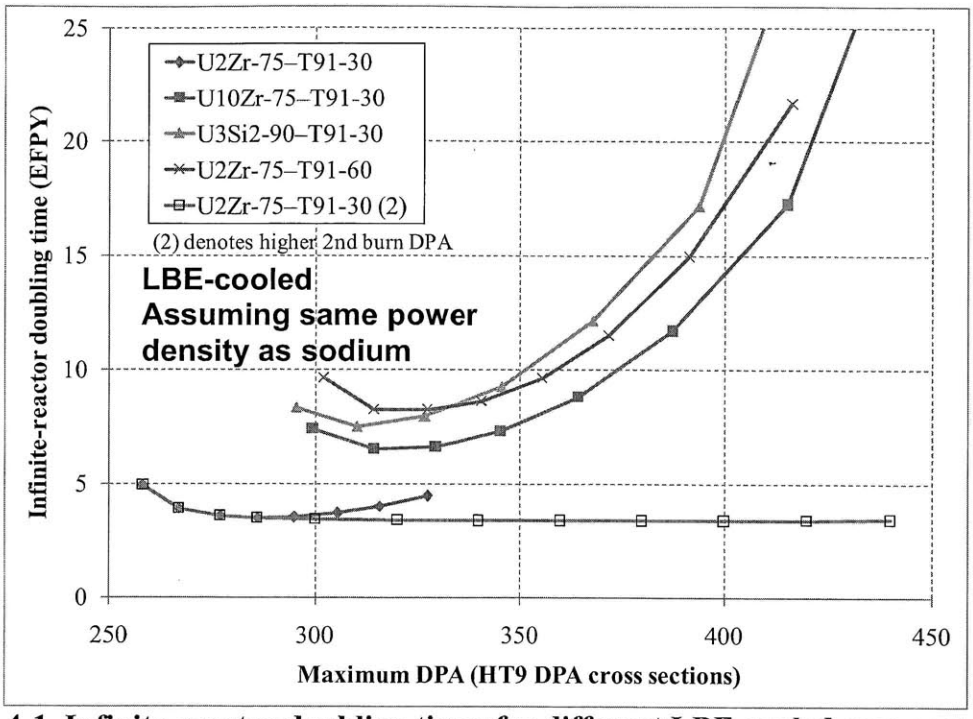

Figure 5.4-1. Infinite-reactor doubling times for different LBE-cooled core compositions (same power density as sodium) (with recladding)

Figure 5.4-1 shows that for the same power density limit, the LBE-cooled core compositions are able to achieve shorter asymptotic doubling times than the sodium-cooled compositions, albeit at a higher DPA: the LBE curves are all shifted downward and to the right relative to the sodium ones.

Even though the better neutronic performance of LBE-cooled core compositions leads to shorter doubling times, this result changes when achievable power densities for LBE are taken into account. Figure 5.4-2 shows how power densities calculated for LBE compare to those for sodium. The LBE power densities are approximately 60-65% lower, which can be explained by looking at Equation 5.3-1. In both the sodium- and LBE-cooled core compositions, the coolant temperature rise is between ~160K and 180K, corresponding to the difference between the coolant inlet temperature and peak cladding temperature. Meanwhile, LBE has a volumetric heat capacity that is ~40% higher than that of sodium, but a coolant velocity limit that is 75% lower (2 m/s versus 8 m/s for sodium). The net effect is that LBE peak areal power densities are approximately 1.4*0.25 = **35%** those of sodium.

The reason for the low 2 m/s velocity limit for LBE is the fact that lead and LBE can both be corrosive to steel at higher velocities, since they are able to strip away steel's protective oxide coating [Samsonov, 1973]. The exact velocity limit depends on the type of steel used and could be raised if an advanced functionally graded composite is used [Short, 2010]. Using a ceramic cladding material such as silicon carbide could also lift this velocity limit and allow much higher power densities.

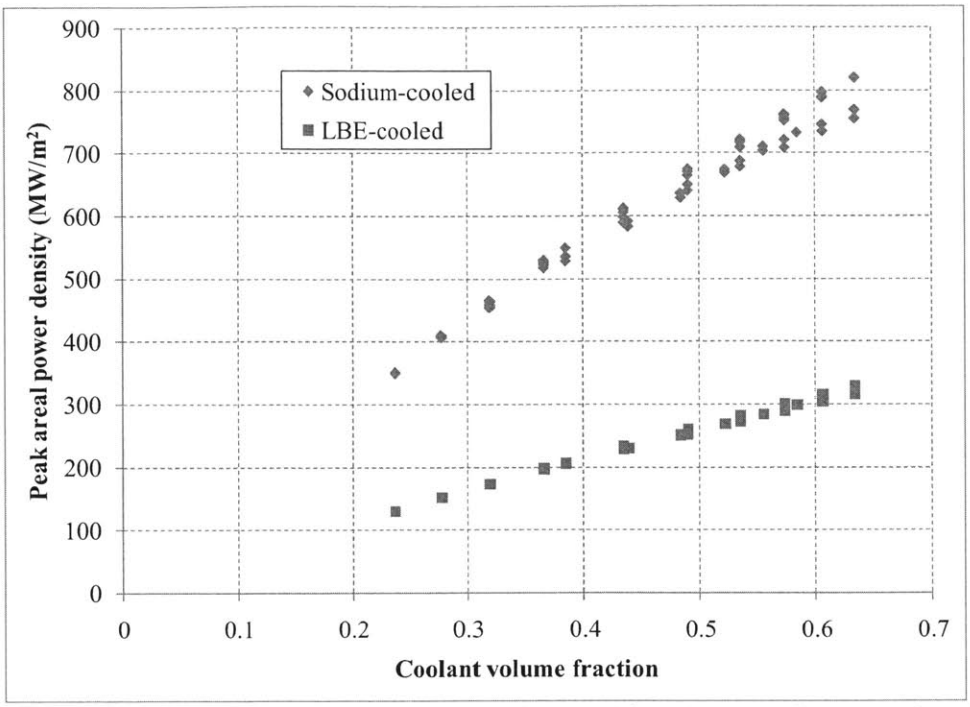

Figure 5.4-2. Comparison of LBE and sodium achievable areal power densities

Figures 5.4-3 and 5.4-4 show the infinite-reactor doubling times for T91-clad core compositions with and without recladding, incorporating the power density limits from Figure 5.4-2. The figures show that the modest doubling time improvements from improved lead or LBE neutronics are completely lost when lower power densities are included: a 20% shorter doubling time vs. sodium due to neutronics in the best case becomes a 150% longer doubling time once power density is factored in. Realistic doubling times would be approximately 2.5 times higher than the infinite-reactor doubling times, on the order of 25 years for the best case core composition. Figures 5.4-5 and 5.4-6 give the corresponding figures for compositions using SiC structure. These figures assume that the SiC compositions have the same power densities as the earlier T91 compositions; if use of SiC structure allows higher power densities in LBE-cooled systems, then shorter doubling times could be achieved. Without a development such as SiC clad or a functionally graded composite to raise power densities, LBE/lead-cooled B&B reactors would have significantly longer doubling times than sodium-cooled B&B reactors, despite their better neutronics.

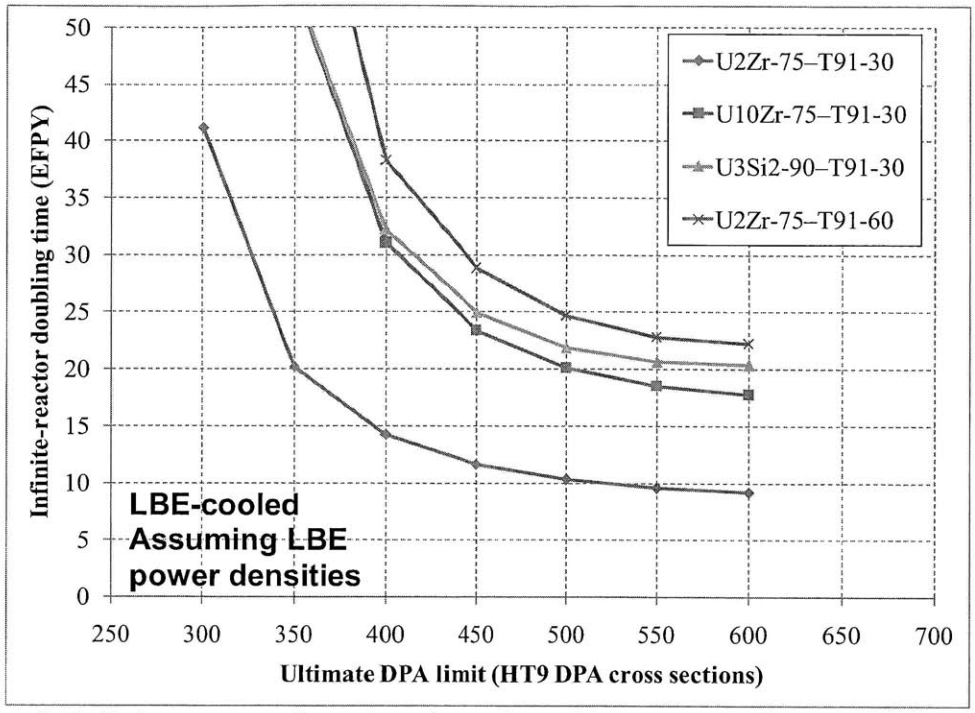

Figure 5.4-3. Infinite-reactor doubling times for different LBE-cooled core compositions with T91 structure (no recladding)

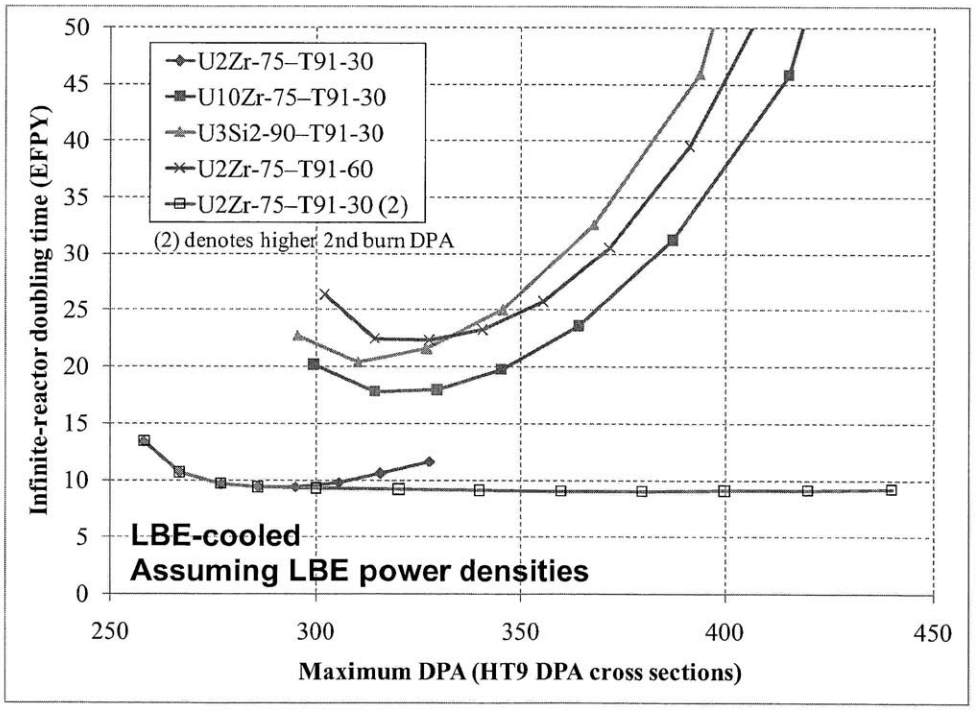

Figure 5.4-4. Infinite-reactor doubling times for different LBE-cooled core compositions with T91 structure (with recladding)

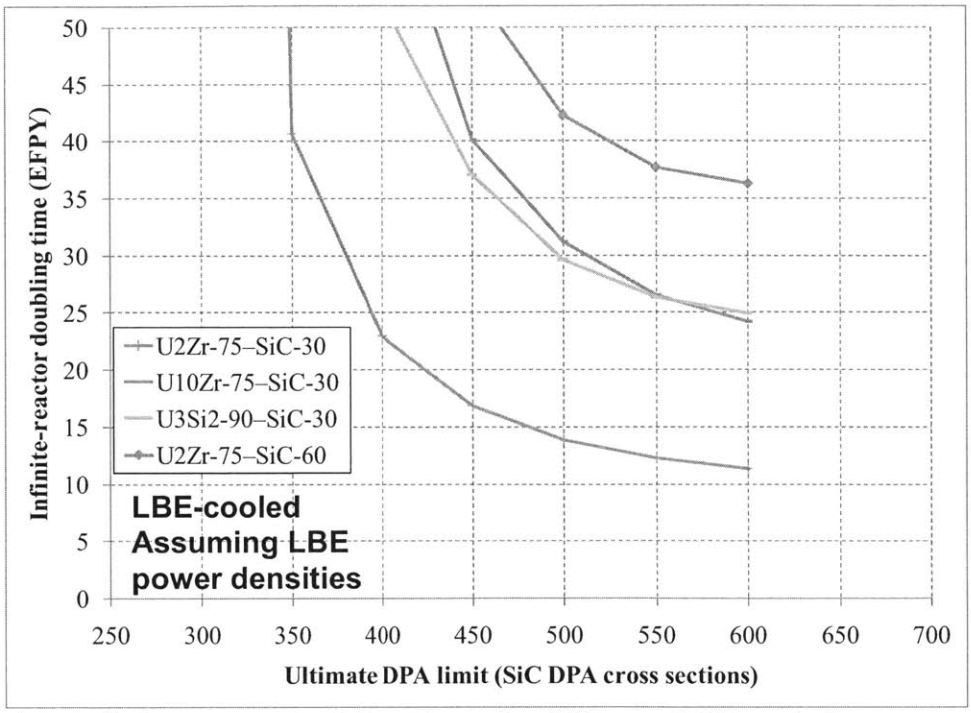

Figure 5.4-5. Infinite-reactor doubling times for different LBE-cooled core compositions with SiC structure (no recladding)

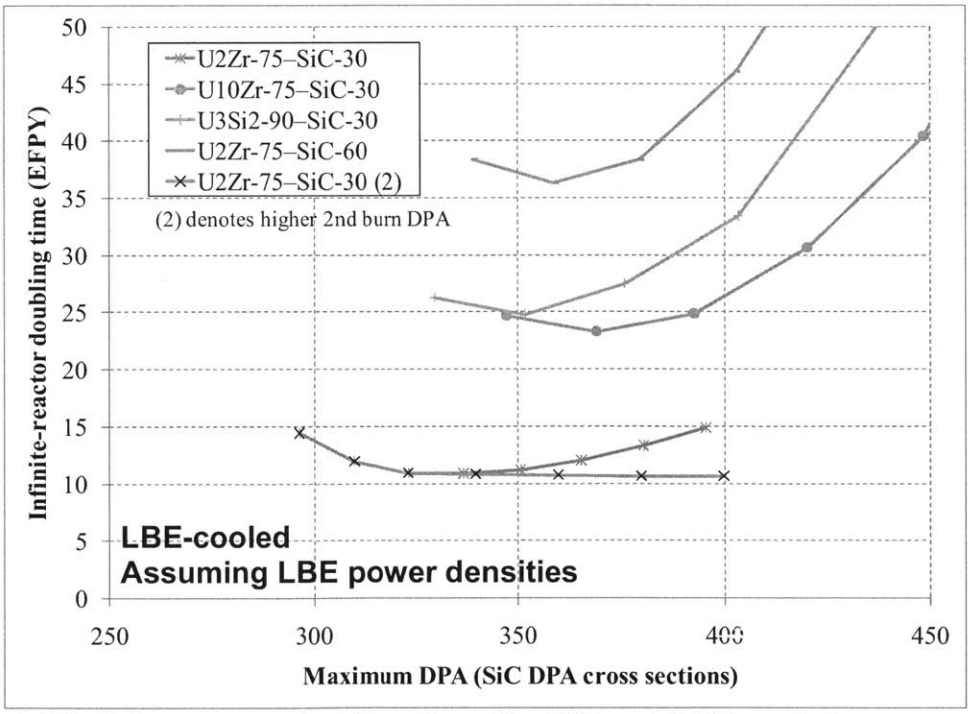

Figure 5.4-6. Infinite-reactor doubling times for different LBE-cooled core compositions with SiC structure (with recladding)

5.5 Helium-cooled fast reactor core compositions

Helium coolant (as well as CO_2 coolant) differs significantly from the liquid metal coolants considered in Sections 4.3 and 4.4. Being a gas, it is almost completely transparent neutronically, while having much worse heat-transfer characteristics than liquid metals. The same core composition evaluation study is performed for helium, assuming a helium density of 0.0125 g/cc, corresponding to helium at 20 MPa and 500°C. The thermal hydraulics calculations (in Appendix A.5) yield lower average helium temperatures, but the density of helium modeled has only a very small effect on neutronic performance.

A total of 96 core compositions are tested, with three fuel types, two types of structure in two different amounts, and eight different amounts of coolant. Since the amount of helium has relatively little effect neutronically, coolant volume is varied from 50%–400% of the available fuel volume, instead of 50%–225% for the liquid metal coolants. Of the 96 core compositions, 90 of them can achieve a predicted k_{eq} of 1.02 in the infinite-medium depletion model, and are rerun in a 1D infinite slab model to obtain equilibrium cycle data. Results for these 90 core compositions are presented in Tables 5.5-1 and 5.5-2, for compositions containing T91 structure and SiC structure respectively.

Table 5.5-1. Equilibrium cycle results for helium-cooled core compositions (T91 structure)

Composition	HM density (g/cc)	Ave. k_{eq}	Discharge burnup fraction	Discharge HT9 DPA	Discharge fast fluence (/cm^2) (>0.1 MeV)	Axial length (cm)	MOEC BU contained (MWy/m^2)	Adjusted ΔN (mol/m^2)
U2Zr-75-T91-30-He-50	7.47	1.028	10.1%	236	5.92E+23	225	879	1165
U2Zr-75-T91-30-He-100	5.85	1.028	10.3%	237	5.94E+23	284	890	1175
U2Zr-75-T91-30-He-150	4.80	1.029	10.6%	239	5.97E+23	342	907	1190
U2Zr-75-T91-30-He-200	4.08	1.028	10.8%	240	6.00E+23	401	924	1202
U2Zr-75-T91-30-He-250	3.54	1.029	11.1%	242	6.04E+23	456	943	1219
U2Zr-75-T91-30-He-300	3.13	1.028	11.3%	243	6.05E+23	512	959	1226
U2Zr-75-T91-30-He-350	2.80	1.029	11.6%	244	6.07E+23	569	975	1241
U2Zr-75-T91-30-He-400	2.54	1.029	11.8%	246	6.11E+23	621	990	1248
U10Zr-75-T91-30-He-50	6.00	1.028	12.7%	270	6.75E+23	246	1007	1235
U10Zr-75-T91-30-He-100	4.70	1.027	13.0%	272	6.80E+23	312	1031	1249
U10Zr-75-T91-30-He-150	3.86	1.028	13.4%	274	6.85E+23	378	1062	1271
U10Zr-75-T91-30-He-200	3.27	1.028	13.8%	277	6.90E+23	442	1087	1285
U10Zr-75-T91-30-He-250	2.84	1.028	14.2%	279	6.95E+23	499	1109	1300
U10Zr-75-T91-30-He-300	2.51	1.028	14.6%	282	7.00E+23	562	1140	1314
U10Zr-75-T91-30-He-350	2.25	1.029	15.1%	286	7.09E+23	621	1174	1337
U10Zr-75-T91-30-He-400	2.04	1.029	15.5%	288	7.14E+23	685	1204	1350
U3Si2-90-T91-30-He-50	5.66	1.028	13.2%	262	6.35E+23	255	1033	1248
U3Si2-90-T91-30-He-100	4.43	1.029	13.6%	265	6.41E+23	322	1052	1264
U3Si2-90-T91-30-He-150	3.64	1.029	14.0%	267	6.46E+23	389	1082	1280
U3Si2-90-T91-30-He-200	3.08	1.028	14.4%	269	6.51E+23	454	1107	1293
U3Si2-90-T91-30-He-250	2.68	1.030	14.9%	273	6.58E+23	518	1137	1314
U3Si2-90-T91-30-He-300	2.37	1.029	15.3%	275	6.63E+23	585	1167	1327
U3Si2-90-T91-30-He-350	2.12	1.029	15.7%	278	6.70E+23	648	1199	1344
U3Si2-90-T91-30-He-400	1.92	1.029	16.1%	281	6.75E+23	707	1226	1361
U2Zr-75-T91-60-He-50	6.41	1.028	13.3%	275	6.96E+23	233	1071	1289
U2Zr-75-T91-60-He-100	5.17	1.028	13.7%	277	7.01E+23	285	1093	1301
U2Zr-75-T91-60-He-150	4.34	1.029	14.0%	280	7.06E+23	339	1117	1320
U2Zr-75-T91-60-He-200	3.74	1.028	14.2%	280	7.07E+23	390	1133	1326
U2Zr-75-T91-60-He-250	3.28	1.028	14.6%	283	7.14E+23	442	1162	1337
U2Zr-75-T91-60-He-300	2.92	1.028	14.9%	285	7.17E+23	490	1183	1352
U2Zr-75-T91-60-He-350	2.64	1.029	15.4%	289	7.26E+23	541	1212	1374
U2Zr-75-T91-60-He-400	2.40	1.030	15.7%	292	7.32E+23	589	1241	1387
U10Zr-75-T91-60-He-50	5.14	1.027	18.2%	336	8.50E+23	256	1385	1411
U10Zr-75-T91-60-He-100	4.15	1.027	18.9%	343	8.66E+23	315	1443	1431
U10Zr-75-T91-60-He-150	3.48	1.027	19.5%	348	8.76E+23	372	1497	1447
U10Zr-75-T91-60-He-200	3.00	1.027	20.2%	354	8.91E+23	433	1555	1468
U10Zr-75-T91-60-He-250	2.63	1.027	20.9%	361	9.07E+23	489	1621	1486
U10Zr-75-T91-60-He-300	2.35	1.027	21.7%	369	9.27E+23	548	1699	1510
U10Zr-75-T91-60-He-350	2.12	1.027	22.5%	377	9.44E+23	604	1774	1537
U10Zr-75-T91-60-He-400	1.93	1.027	23.6%	388	9.71E+23	663	1878	1558
U3Si2-90-T91-60-He-50	4.85	1.027	19.4%	335	8.22E+23	265	1458	1426
U3Si2-90-T91-60-He-100	3.92	1.028	20.1%	341	8.36E+23	326	1517	1453
U3Si2-90-T91-60-He-150	3.28	1.028	20.9%	348	8.53E+23	386	1587	1473
U3Si2-90-T91-60-He-200	2.83	1.028	21.7%	356	8.72E+23	447	1660	1491
U3Si2-90-T91-60-He-250	2.48	1.026	22.4%	361	8.84E+23	510	1729	1501
U3Si2-90-T91-60-He-300	2.21	1.027	23.5%	372	9.10E+23	569	1844	1534
U3Si2-90-T91-60-He-350	2.00	1.027	24.4%	382	9.33E+23	630	1932	1557
U3Si2-90-T91-60-He-400	1.82	1.026	25.9%	398	9.71E+23	691	2084	1575

Table 5.5-2. Equilibrium cycle results for helium-cooled core compositions (SiC structure)

Composition	HM density (g/cc)	Ave. k_{eq}	Discharge burnup fraction	Discharge SiC DPA	Discharge fast fluence (/cm^2) (>0.1 MeV)	Axial length (cm)	MOEC BU contained (MWy/m^2)	Adjusted ΔN (mol/m^2)
U2Zr-75-SiC-30-He-50	7.47	1.029	11.1%	226	5.00E+23	207	905	1150
U2Zr-75-SiC-30-He-100	5.85	1.030	11.4%	227	5.03E+23	262	920	1169
U2Zr-75-SiC-30-He-150	4.80	1.029	11.6%	229	5.06E+23	315	934	1176
U2Zr-75-SiC-30-He-200	4.08	1.029	11.8%	230	5.09E+23	369	948	1184
U2Zr-75-SiC-30-He-250	3.54	1.029	12.0%	231	5.11E+23	426	959	1198
U2Zr-75-SiC-30-He-300	3.13	1.029	12.3%	233	5.15E+23	476	978	1207
U2Zr-75-SiC-30-He-350	2.80	1.029	12.5%	234	5.17E+23	530	997	1220
U2Zr-75-SiC-30-He-400	2.54	1.030	12.8%	237	5.23E+23	579	1017	1237
U10Zr-75-SiC-30-He-50	6.00	1.028	14.2%	259	5.69E+23	226	1061	1233
U10Zr-75-SiC-30-He-100	4.70	1.028	14.6%	262	5.76E+23	286	1087	1252
U10Zr-75-SiC-30-He-150	3.86	1.030	15.0%	266	5.84E+23	349	1123	1268
U10Zr-75-SiC-30-He-200	3.27	1.029	15.4%	269	5.89E+23	410	1151	1286
U10Zr-75-SiC-30-He-250	2.84	1.029	15.8%	272	5.96E+23	467	1181	1301
U10Zr-75-SiC-30-He-300	2.51	1.028	16.2%	275	6.01E+23	524	1208	1314
U10Zr-75-SiC-30-He-350	2.25	1.029	16.7%	279	6.10E+23	583	1244	1329
U10Zr-75-SiC-30-He-400	2.04	1.029	17.2%	283	6.19E+23	637	1285	1349
U3Si2-90-SiC-30-He-50	5.66	1.029	14.4%	251	5.36E+23	240	1070	1237
U3Si2-90-SiC-30-He-100	4.43	1.029	14.8%	254	5.43E+23	304	1102	1253
U3Si2-90-SiC-30-He-150	3.64	1.029	15.2%	257	5.48E+23	368	1131	1269
U3Si2-90-SiC-30-He-200	3.08	1.030	15.7%	261	5.57E+23	433	1168	1292
U3Si2-90-SiC-30-He-250	2.68	1.029	16.1%	264	5.63E+23	495	1198	1303
U3Si2-90-SiC-30-He-300	2.37	1.030	16.5%	267	5.69E+23	559	1225	1320
U3Si2-90-SiC-30-He-350	2.12	1.029	17.0%	271	5.78E+23	619	1267	1338
U3Si2-90-SiC-30-He-400	1.92	1.030	17.5%	275	5.87E+23	685	1314	1356
U2Zr-75-SiC-60-He-50	6.41	1.028	15.8%	264	5.54E+23	204	1170	1259
U2Zr-75-SiC-60-He-100	5.17	1.029	16.1%	267	5.59E+23	252	1198	1275
U2Zr-75-SiC-60-He-150	4.34	1.029	16.5%	270	5.66E+23	299	1224	1290
U2Zr-75-SiC-60-He-200	3.74	1.029	16.9%	273	5.71E+23	347	1255	1306
U2Zr-75-SiC-60-He-250	3.28	1.029	17.3%	276	5.78E+23	393	1291	1315
U2Zr-75-SiC-60-He-300	2.92	1.029	17.7%	279	5.84E+23	441	1313	1329
U2Zr-75-SiC-60-He-350	2.64	1.028	18.0%	282	5.90E+23	484	1346	1340
U2Zr-75-SiC-60-He-400	2.40	1.029	18.4%	286	5.97E+23	532	1379	1358
U10Zr-75-SiC-60-He-50	5.14	1.027	23.7%	351	7.28E+23	231	1763	1426
U10Zr-75-SiC-60-He-100	4.15	1.026	24.7%	362	7.50E+23	286	1866	1444
U10Zr-75-SiC-60-He-150	3.48	1.027	26.0%	375	7.79E+23	341	1982	1467
U10Zr-75-SiC-60-He-200	3.00	1.026	27.3%	390	8.09E+23	403	2158	1492
U10Zr-75-SiC-60-He-250	2.63	1.025	29.3%	413	8.57E+23	459	2400	1523
U3Si2-90-SiC-60-He-50	4.85	1.027	24.1%	344	7.00E+23	246	1811	1420
U3Si2-90-SiC-60-He-100	3.92	1.026	25.4%	357	7.27E+23	305	1943	1441
U3Si2-90-SiC-60-He-150	3.28	1.026	26.5%	368	7.49E+23	365	2058	1466
U3Si2-90-SiC-60-He-200	2.83	1.026	28.3%	389	7.92E+23	423	2277	1491
U3Si2-90-SiC-60-He-250	2.48	1.025	30.9%	420	8.55E+23	496	2626	1521

The two tables show that increasing the amount of helium coolant present has only a very small effect on minimum burnup. The primary effect of increasing the amount of coolant is to increase the axial length of the system, in some cases increasing it to over six meters. On the other hand, the higher reactivity of the helium-cooled core compositions potentially allows fairly short axial heights (on the order of 2 m) to be viable.

A comparison between calculated peak areal power densities for sodium and helium coolant is shown in Figure 5.5-1. Unlike with sodium (or LBE) coolant, the relationship between peak areal power density and coolant volume fraction is no longer linear. This is because the low thermal conductivity of helium causes the temperature difference between the clad and coolant to become much higher, so the coolant temperature rise in Equation 5.3-1 is no longer a nearly constant 170K to 180K. Instead, the coolant temperature rises range from ~50K (for cases with high coolant volume fractions) to ~140K. In cases with higher coolant volume fraction, there is less fuel per unit area, and the linear heat rate of the fuel is higher for a given areal power density. The higher linear heat rate causes the temperature difference between the coolant and clad to become the dominant temperature rise, so the coolant temperature rise (and achievable areal power density) go down.

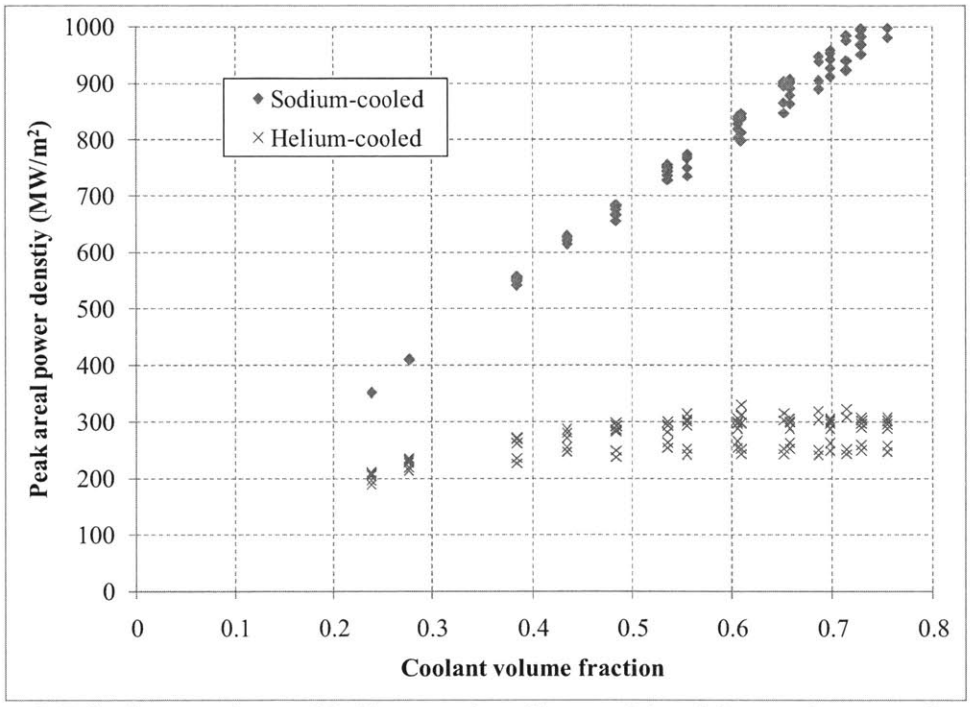

Figure 5.5-1. Comparison of helium and sodium achievable areal power densities

The net effect of the tradeoff between coolant temperature rise and the coolant-clad temperature difference is that increasing the amount of coolant only increases power density up to a coolant volume of about 40% (or ~100% of the available fuel volume). Past this point, diminishing returns set in as the coolant-clad temperature difference becomes larger. Keeping the coolant volume fraction low is also desirable for reducing the size and height of the core, as well as increasing the coolant outlet temperature (thus raising thermal efficiency).

There is some spread among the different points in Figure 5.5-1 because of the different axial power distributions obtained from the different 1D models. Cases with higher axial peaking (shorter axial lengths) will have higher linear heat rates and higher coolant-clad temperature differences, resulting in lower coolant temperature rises and lower areal power densities. This effect is more pronounced for gas-cooled systems because of the much higher thermal resistance between the coolant and clad. As discussed in Subsection 3.7.7, the axial power shape can be

flattened by varying the shuffling sequence used, which can potentially increase areal power densities and reduce doubling times (at the expense of a taller core). Optimizing the axial power distribution would be more appropriately studied with a more detailed thermal hydraulic model, and is not considered in this thesis.

Based on the power densities in Figure 5.5-1, infinite-reactor doubling times are calculated for each of the compositions in Tables 5.5-1 and 5.5-2 as a function of DPA limit. These infinite-reactor doubling times are given for T91-structure cases without and with recladding in Figures 5.5-2 and 5.5-3. Figure 5.5-2 shows that helium coolant does not allow as short doubling times as sodium, due to the factor of ~2 lower power densities with helium coolant. In Figure 5.5-3, the U-shaped curves are all compressed horizontally, because there is almost no change in required DPA when the amount of coolant is increased or decreased. The sharp vertical drop at the beginning of each curve is due to the allowable power density rapidly increasing as the amount of coolant is increased. Increasing the amount of coolant past this point no longer raises power density and gradually degrades neutronic performance, causing the curves to increase again. For helium-cooled systems, doubling times can therefore be minimized by choosing a coolant volume fraction based on thermal-hydraulic performance. Meanwhile, burning starter fuel to a higher DPA on the second burn is able to reduce doubling times to a greater degree with helium than with the other coolants, since the helium-cooled core compositions maintain positive k_∞ to a higher burnup.

Corresponding infinite-reactor doubling time results for SiC-structure cases are given in Figure 5.5-5. As with the other coolants, switching to SiC results in higher DPA (due to higher SiC DPA cross sections) and longer doubling times due to worse neutronic performance.

One final point regarding gas-cooled fast reactors is that the need for a pressure vessel may make it challenging to implement the large core sizes needed by B&B reactors. In particular, the goal of minimizing doubling times favors larger B&B reactors with flatter radial power distributions, with correspondingly large (>5 m) core diameters that may be challenging to achieve in a gas-cooled reactor.

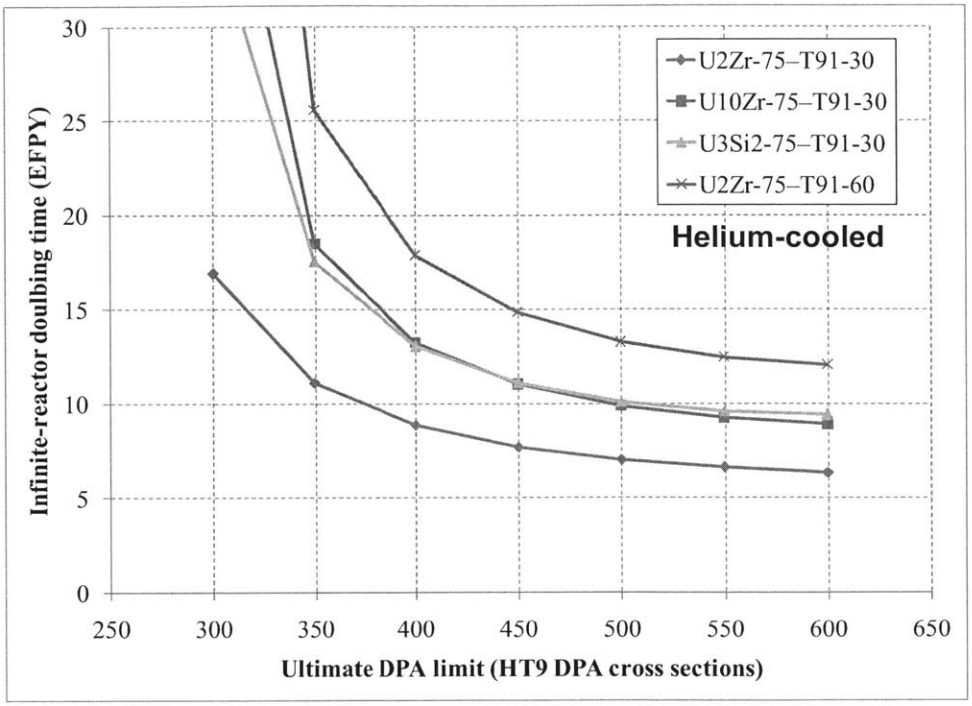

Figure 5.5-2. Infinite-reactor doubling times for different helium-cooled core compositions with T91 structure (no recladding)

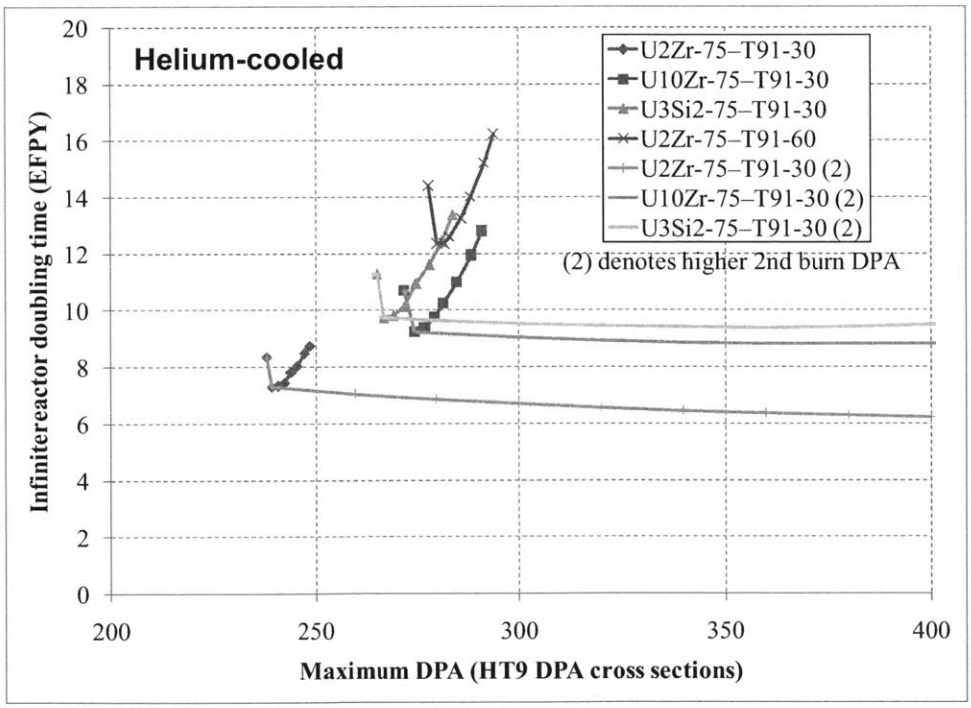

Figure 5.5-3. Infinite-reactor doubling times for different helium-cooled core compositions with T91 structure (with recladding)

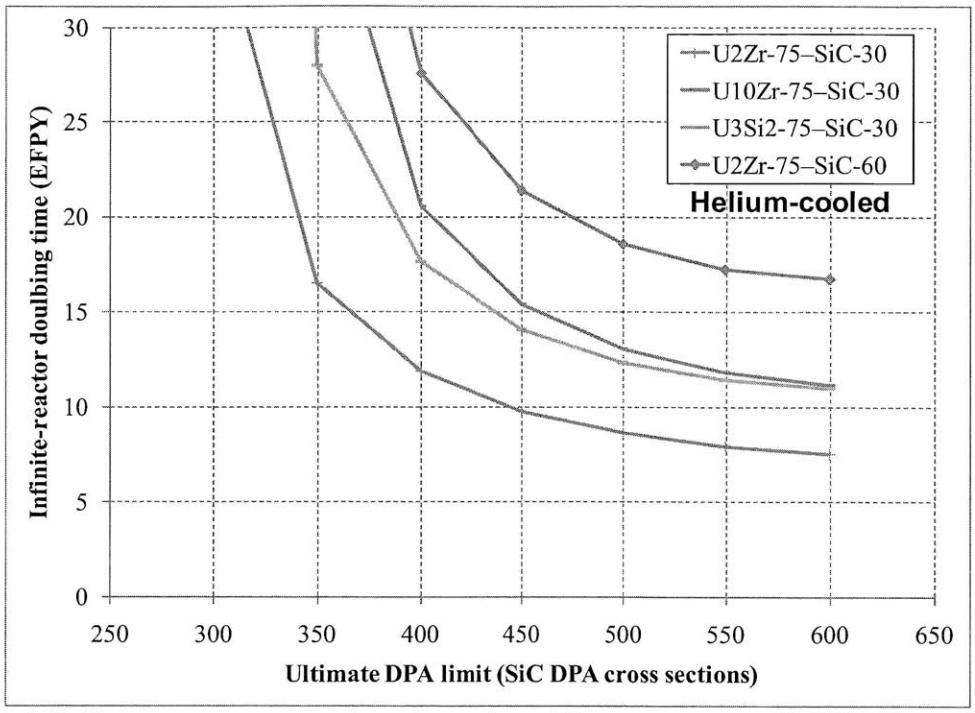

Figure 5.5-4. Infinite-reactor doubling times for different helium-cooled core compositions with SiC structure (no recladding)

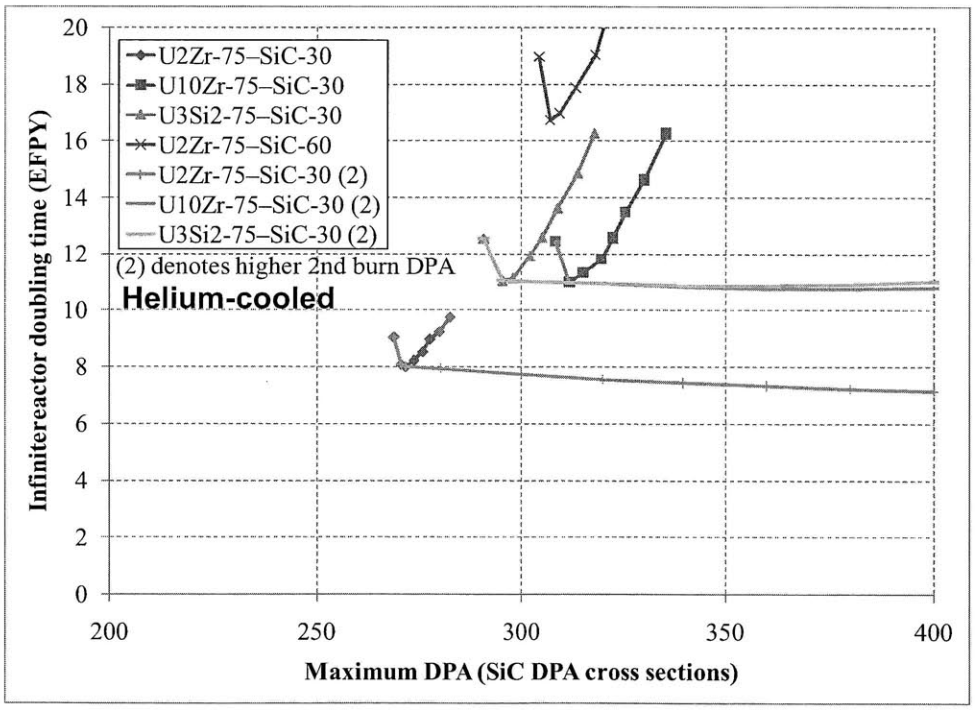

Figure 5.5-5. Infinite-reactor doubling times for different helium-cooled core compositions with SiC structure (with recladding)

5.6 Summary of composition options evaluation

One of the primary conclusions of this core composition study is that B&B reactor performance is very sensitive to core composition. In order to minimize required burnup and DPA and achieve short (sub-decade) doubling times, it is likely necessary to develop fuels with low amounts of alloying material and create fuel designs that minimize the amount of structure used.

To illustrate this conclusion, Table 5.6-1 gives a summary of minimum burnup and DPA results for two types of fuel (U2Zr and U10Zr), two amounts of structure, and two types of coolant (helium and sodium). The results are taken from the more comprehensive data in Tables 5.3-1 and 5.5-1. Switching from U2Zr to U10Zr fuel causes minimum burnup to increase by about 30%, and minimum DPA to increase by about 20%, with the increases being larger for the sodium-cooled compositions. Approximately the same effect is seen if the amount of T91 structure is doubled from 30 parts to 60 parts. Including both changes causes minimum burnup and DPA in the helium-cooled core to increase significantly, and causes the sodium cooled core to no longer be able to sustain critical B&B operation.

Table 5.6-1. Minimum burnup, DPA, and fast fluence for different core compositions

Fuel type	Relative fuel volume*	Structure type	Relative structure volume*	Coolant type	Relative coolant volume*	Minimum burnup (FIMA)	Minimum HT9 DPA	Minimum fast fluence (/cm^2) (>0.1 MeV)
U2Zr	75	T91	30	He	100	10.3%	237	5.94E+23
U10Zr	75	T91	30	He	100	13.0%	272	6.80E+23
U2Zr	75	T91	60	He	100	13.7%	277	7.01E+23
U10Zr	75	T91	60	He	100	18.9%	343	8.66E+23
U2Zr	75	T91	30	Na	100	13.3%	261	6.27E+23
U10Zr	75	T91	30	Na	100	18.2%	318	7.61E+23
U2Zr	75	T91	60	Na	100	18.2%	320	7.77E+23
U10Zr	75	T91	60	Na	100	N/A	N/A	N/A

*Volumes are in parts, where 100 parts corresponds to the total volume (fuel + gap) inside the cladding

Due to the sensitivity to core composition, only a small number of possible fuel types are attractive for use in low-burnup, short-doubling-time B&B reactors. These are high-uranium metal fuels and a very limited selection of compound fuels, of which U_3Si_2 performs the best (roughly as well as U10Zr). For refractory ceramics, uranium nitride fuel using nitrogen enriched in ^{15}N performs best, but would require high burnup (>20%) even in a gas-cooled system.

Compared to the type of fuel used, the types of coolant and structure used have a smaller impact on the neutronic performance of a B&B reactor. All the steels considered (HT9, T91, and ODS) exhibit similar performance, with silicon carbide being slightly worse neutronically, but with the potential to allow higher power densities. Meanwhile, the amount of structure present does have a strong effect on minimum burnup, more so than the amount of any type of coolant.

Type of coolant used has a relatively minor effect on neutronic performance compared to the type of fuel used. Gas coolants perform the best, followed by lead/LBE then sodium. If the goal is to minimize burnup and fluence experienced by the fuel, one would choose helium coolant, metal fuel, and the type of steel that permits the lowest volume fraction of structure, unless a

much smaller volume of silicon carbide can be used. Comparing just liquid metal coolants, lead or LBE require less burnup and DPA than sodium if the volume of coolant is held constant. However, since sodium allows higher power densities than lead or LBE, a smaller volume of sodium is needed to achieve a given power density, so sodium actually has less impact on minimum burnup and DPA than lead/LBE as a function of cooling performance.

The values given in Table 5.6-1 are likely to be bounding values for the amount of burnup and DPA required for a minimum-burnup B&B reactor design. The fuel in such a design is likely to have a composition between U2Zr and U10Zr, and the amount of structure would likely be between 30% and 60% of the available fuel volume. The values show that the levels of burnup required are less than 20%, within current knowledge limits, and the required amount of DPA range from about 240 to 350.

The exact burnup and DPA requirements for an actual system would depend on the fuel, coolant, and structure fractions of an explicit fuel design. The fuel design would need to be capable of sustaining the required amount of fuel burnup and DPA, so consistent neutronic and fuel performance calculations need to be performed for the design. For example, if one increases the thickness of fuel cladding to raise the burnup limit of a fuel design, this would also increase the minimum burnup required for B&B operation.

If fuel performance data show that burnup and DPA limits are sufficient for using sodium coolant, then using sodium instead of a gas coolant would allow a large increase in power density, potentially improving the economics of a B&B system. Because it takes into account both neutronic and thermal hydraulic performance, reactor doubling time can be used as a comprehensive figure of merit for comparing different core composition options.

In terms of minimizing doubling time, the thermal hydraulic performance of the different coolants is more significant than the differences in neutronic performance. With liquid metal coolants, there is a tradeoff between neutronic and thermal hydraulic performance: higher coolant volume fractions allow higher power densities but worsen neutronic performance by softening the neutron spectrum and causing more parasitic absorptions. The optimal sodium coolant volume fraction is on the order of 40%, which corresponds well to conventional sodium fast reactor designs (from Figure 5.2-2). The optimal lead/LBE coolant volume fraction is greater because lead/LBE coolant produces a harder neutron spectrum. In both liquid metal cases, fuel/structure combinations with worse neutronic performance would reduce the optimal coolant volume fraction. Gas coolants are neutronically nearly transparent, so the coolant volume fraction can be optimized on the basis of thermal hydraulics alone.

This chapter computes infinite-reactor doubling times for different core composition options in a number of scenarios. Among the different coolants, sodium can achieve the shortest doubling times, followed by helium/CO_2 then LBE/lead, following the order of their calculated thermal hydraulic performance. Without any recladding, minimizing doubling time requires being able to burn fuel up to approximately 500 DPA. Having the option to reclad fuel between reactor passes allows near-minimum doubling times to be achieved at much more modest levels (<300) of DPA. Fission product escape has a small but non-negligible effect on neutronic performance, and would be important to model in a B&B reactor. The choice of natural versus depleted

uranium for feed fuel makes less of a difference. Fuel composition changes due to a processing step such as melt refining can potentially make a larger (~20%) impact on doubling times, if a significant fraction of fission products is removed during processing.

To summarize the important doubling time conclusions from this chapter, realistic reactor doubling times for different coolants using T91 structure as a function of DPA with recladding are shown in Figures 5.6-1 through 5.6-3. To keep the results conservative, no fission product removal or composition changes due to processing are assumed. The baseline fuel cycle is used, and peak power densities are the ones calculated in Appendix A.5. Other important assumptions are listed on the figures.

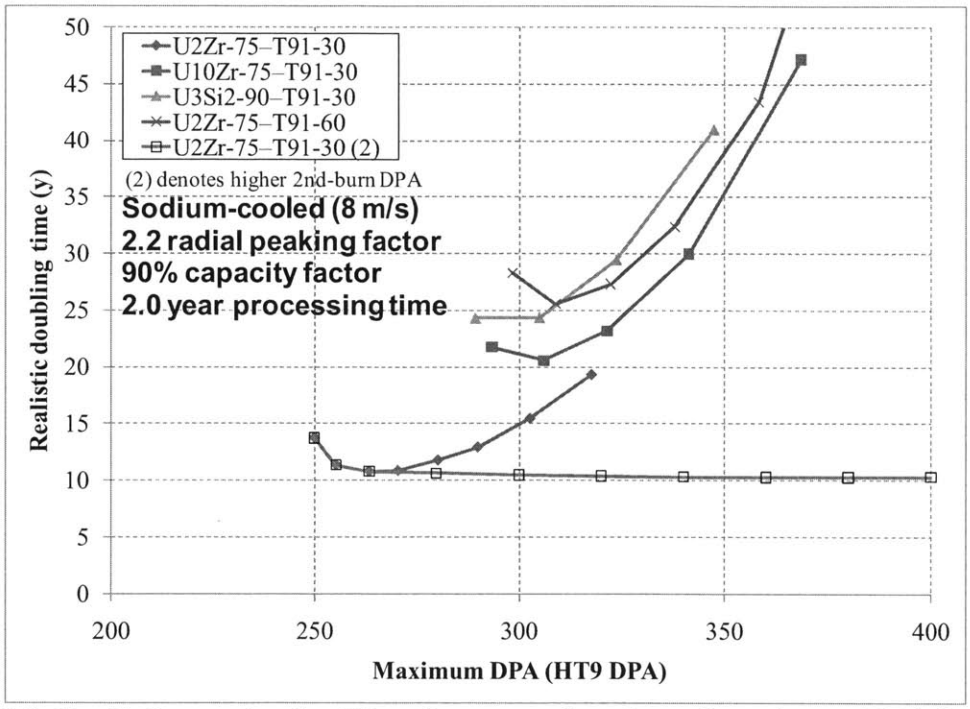

Figure 5.6-1. Realistic reactor doubling times as a function of maximum DPA for sodium-cooled core compositions with T91 structure (with recladding)

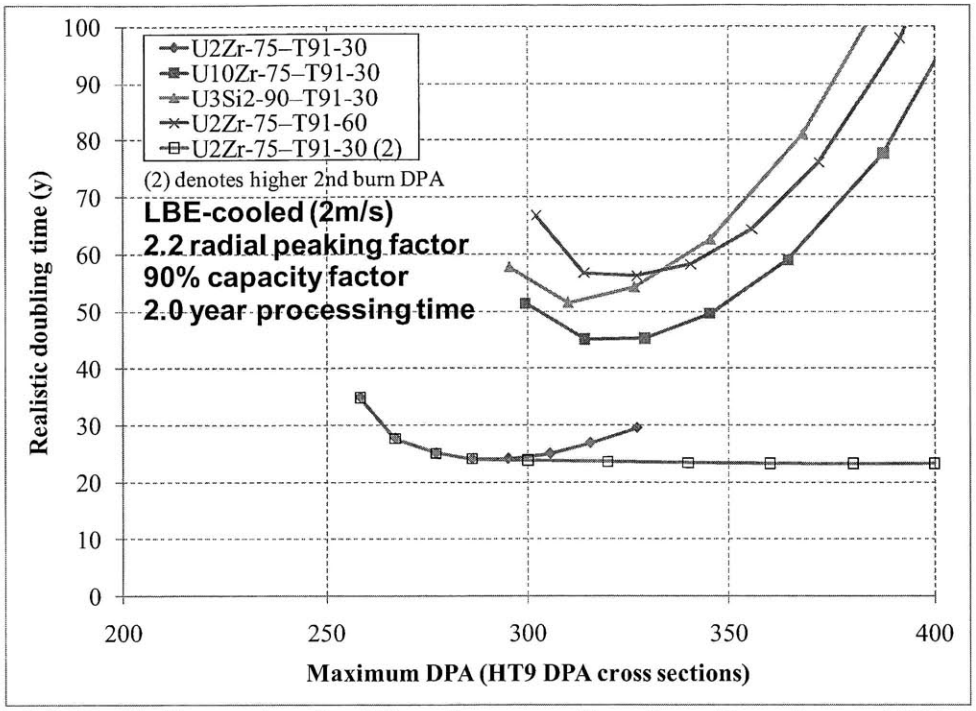

Figure 5.6-2. Realistic reactor doubling times as a function of maximum DPA for LBE-cooled core compositions with T91 structure (with recladding)

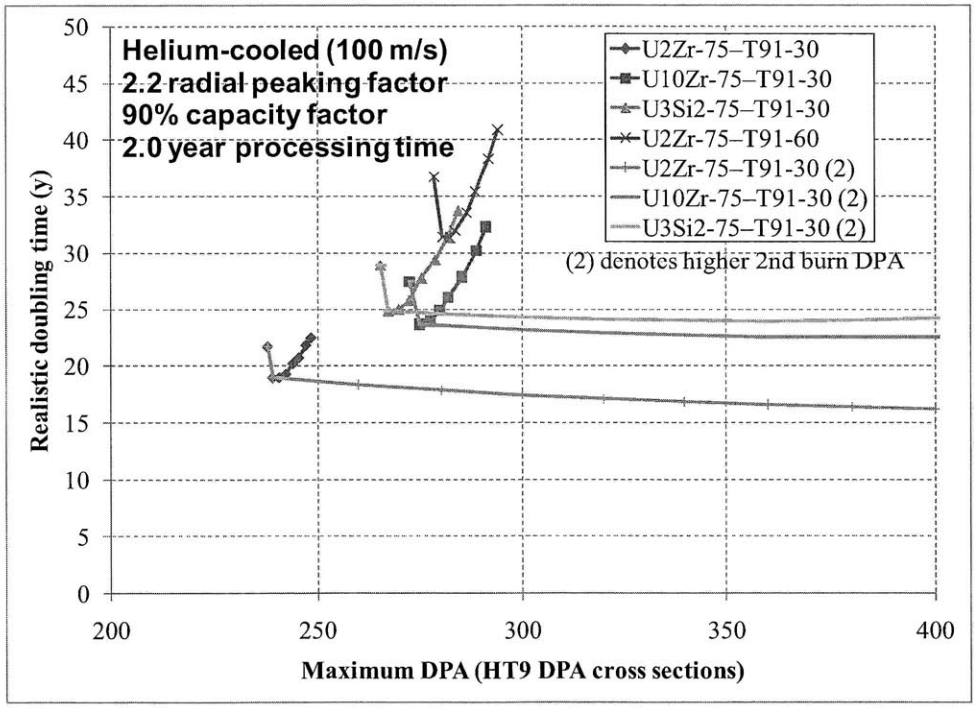

Figure 5.6-3. Realistic reactor doubling times as a function of maximum DPA for helium-cooled core compositions with T91 structure (with recladding)

6. Analysis of Linear-Assembly B&B Reactors

The analyses in the previous chapters have so far all been for minimum-burnup B&B reactors, i.e. reactors that are capable of shuffling fuel in three dimensions to achieve a uniform discharge burnup distribution. Although minimum-burnup B&B reactors represent a best-case scenario for the neutronic performance of B&B reactors, implementing three-dimensional shuffling would require a novel core design using axially-segmented assemblies or a pebble-bed design. Since no existing fast reactor designs allow for three-dimensional shuffling, the possibility of engineering minimum-burnup B&B reactors is speculative, and there may be significant challenges in realizing such a design. Therefore, it is important to also analyze B&B reactors that use conventional, axially-connected linear assemblies that are shuffled radially in two dimensions. Such reactors are referred to as "linear-assembly" B&B reactors in this thesis.

Analogously to Chapter 3, this chapter considers the different applications of the neutron excess concept as they pertain to linear-assembly B&B reactors. First, Section 6.1 describes a two-dimensional cylindrical model that is used to analyze linear-assembly B&B reactors, and outlines some of the unique characteristics of such reactors. Section 6.2 compares the burnup-reactivity relationships of models with different geometries and equilibrium cycle shuffling sequences, and discusses the radius-reactivity relationship of linear-assembly B&B reactors. Section 6.3 describes the unique relationship between reactor height and reactivity, and introduces a simple model that helps explain the axial burnup distributions seen in linear-assembly B&B reactors. Section 6.4 gives an example 2D transition model for establishing a B&B equilibrium cycle, and uses the results to define a new neutron excess quantity, the *twice-adjusted neutron excess*. Section 6.5 uses simple 1D models to explore the neutron excess that can be obtained from different starter fuel configurations. Finally, Section 6.6 integrates the findings in this chapter to develop an example limited-separations fuel cycle using linear-assembly B&B reactors.

6.1 Description of two-dimensional cylindrical model

To model a linear-assembly B&B reactor conceptually, a two-dimensional cylindrical model is constructed that consists of 200 radial zones and 20 axial zones. Each radial zone is a cylindrical shell with an area of 400π cm^2, the same area as four 17.7 cm pitch square assemblies, or six 15.6 cm pitch hexagonal assemblies. The total radius of the model is 283 cm, which is sufficient to prevent nearly all radial neutron leakage. Each axial zone is 12.5 cm long, for a total model height of 250 cm, sufficient to prevent the majority of axial neutron leakage. The axial and radial boundaries are modeled as vacuum boundaries. Instead of using the idealized core composition used in the earlier Chapter 3 models, the composition used is the lowest-doubling-time composition from Chapter 5 (U2Zr-75-T91-30-Na-100) with depleted uranium as feed fuel.

6.1.1 Equilibrium cycle reactivity-burnup relationship

To explore how equilibrium cycle reactivity and burnup are related in a linear-assembly B&B reactor, first a base case is considered that uses convergent shuffling. At each cycle, the innermost three radial zones are discharged, and the remaining zones are shuffled inward, with the three outermost zones replaced with fresh feed fuel. Each radial zone contains 1837 kg of

initial uranium, so 5511 kg are shuffled with each cycle. Average equilibrium cycle discharge burnup is varied from 60 MWd/kg to 200 MWd/kg, corresponding to cycle energies of 330,660 MWd to 1,102,200 MWd. At a total power of 3000 MW, the cycle length varies from 110 to 367 days. As in the one-dimensional cases, moving additional zones per cycle would allow a longer cycle length but would also increase the reactivity swing.

Results for equilibrium cycle uncontrolled *k*-effective in the different cases are given in Figure 6.1-1, as a function of average discharge burnup. The lowest burnup case with a BOEC *k*-effective greater than unity is the one with 120 MWd/kg average burnup, which corresponds to a cycle length of 220.5 days at 3000 MW. If cycle length is shortened to be effectively zero, then there would be no reactivity swing and the minimum burnup needed for a *k*-effective greater than unity would be approximately 100 MWd/kg. The general shape of the curve resembles the equivalent curve for a minimum-burnup B&B reactor (e.g. Figure 3.4-7).

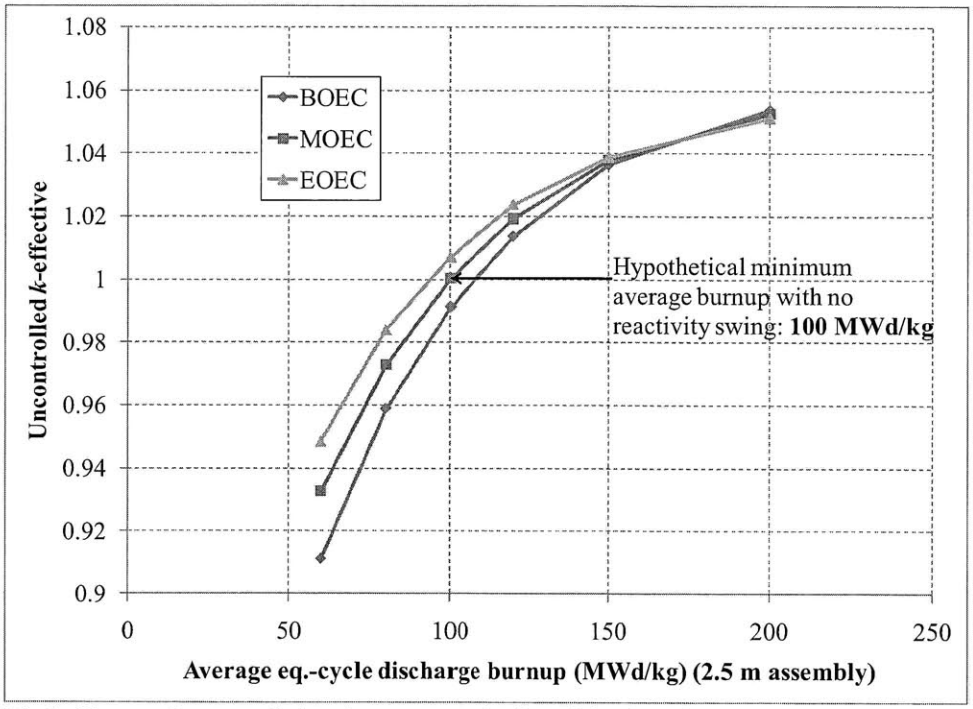

Figure 6.1-1. Example reactivity burnup relationship for linear-assembly B&B reactor

6.1.2 Axial burnup profile

While the average burnup values in Figure 6.1-1 are not very high, the corresponding axial burnup distributions given in Figure 6.1-2 show that there is pronounced burnup peaking. The legend in Figure 6.1-2 gives the total burnup in the assembly expressed as the average assembly burnup (MWd/kg) multiplied by the assembly length (m). The results reported are the average across the 3 zones discharged each cycle. With strictly convergent shuffling, the 3 discharged zones have slightly different burnup distributions since the inner zone is burned further, but the differences among the zones can be eliminated by permuting the zones as they are shuffled through the reactor. Similarly to in a minimum-burnup B&B reactor, averaging a small spread in

discharge burnups in this way would have minimal effect on k-effective, as discussed in Subsection 2.3.2.

The severe burnup peaking seen in Figure 6.1-2 is a result of the positive breed-burn feedback behavior first discussed in Subsection 3.7.3. Better breeding of Pu-239 in the central portion of the fuel further concentrates flux there, leading to the observed burnup peak. This behavior is a consequence of B&B reactor feed fuel having increasing k_∞ with burnup, and is therefore unique to B&B reactors. A more detailed investigation of axial burnup distributions is given in Section 6.3.

As a consequence of the pronounced axial peaking, the minimum burnup required in the linear-assembly case is much higher; with a peak of about 22.5% FIMA (corresponding to 100 MWd/kg average burnup in Figure 6.1-1, or 250 MWd*m/kg for a 2.5 meter assembly), roughly twice as much as the 12.3% required in a minimum-burnup B&B reactor. The DPA corresponding to this peak burnup is also much higher, approximately 430 instead of 250 in the minimum-burnup case.

The fact that the burnup distributions in Figure 6.1-2 extend to the edges of the fuel assembly show that there is neutron leakage from the axial ends of the 2.5 meter fuel. A combination of axial neutron leakage and high peak burnup cause the reactivity swing to get smaller (and become negative) at higher burnup. Fuel at high burnup exhibits less change in k_∞ with burnup, and axial neutron leakage increases over a cycle, effects which are both more significant in the axially-taller high-burnup distributions.

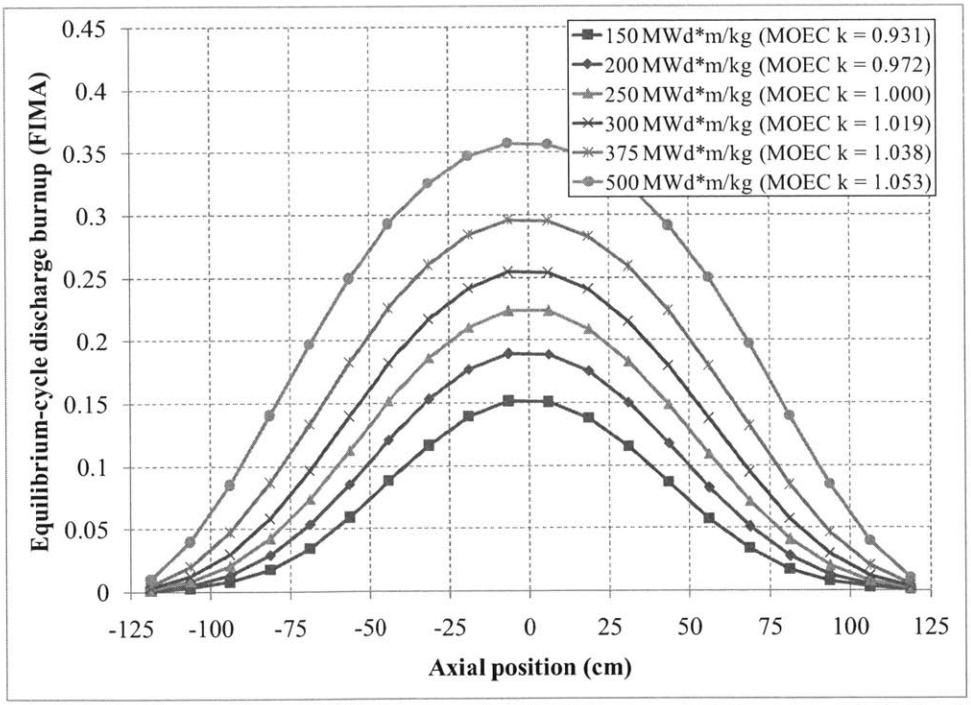

Figure 6.1-2. Example equilibrium cycle discharge axial burnup distributions

Interestingly, even though this example model consists of cylindrical shells, the burnup distribution that develops during convergent shuffling is essentially spherical, as seen in Figure 6.1-3 from the 300 MWd*m/kg case. The radial burnup distribution is taken from the model midplane, while the axial burnup distribution is taken from extrapolating the results for the inner zones to the central axis.

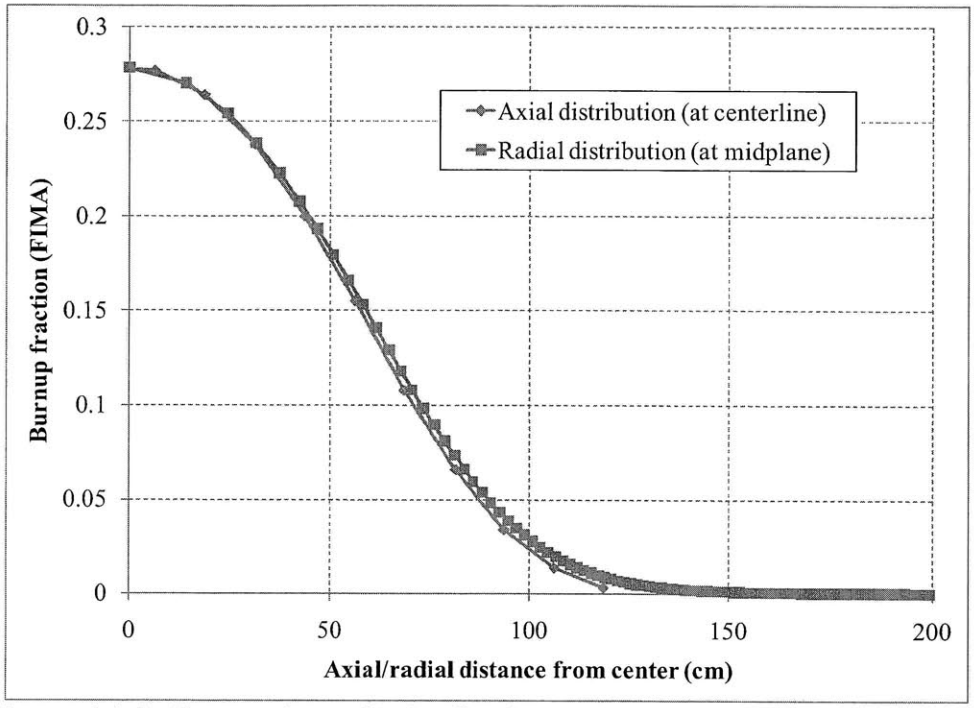

Figure 6.1-3. Comparison of EOEC axial and radial burnup distributions

Beginning-of-equilibrium-cycle radial and axial power distributions for the different burnup cases are given in Figures 6.1-4 and 6.1-5. Power distributions become flatter as burnup increases, due to the larger region of fuel with k_∞ above unity. For this reason, power distributions are also flatter at EOEC than at BOEC. Like in the convergently shuffled one-dimensional models, the power distributions are highly centrally peaked. The core composition in question has a sodium volume fraction of 43%, which corresponds to an areal power density limit of about 600 MW/m^2 (from Appendix A.5). Therefore, in order to satisfy power density limits, the power distribution given by the 250 MWd*m/kg curve (corresponding to the lowest-burnup critical case) would imply de-rating the total core power from 3000 MW to about 950 MW.

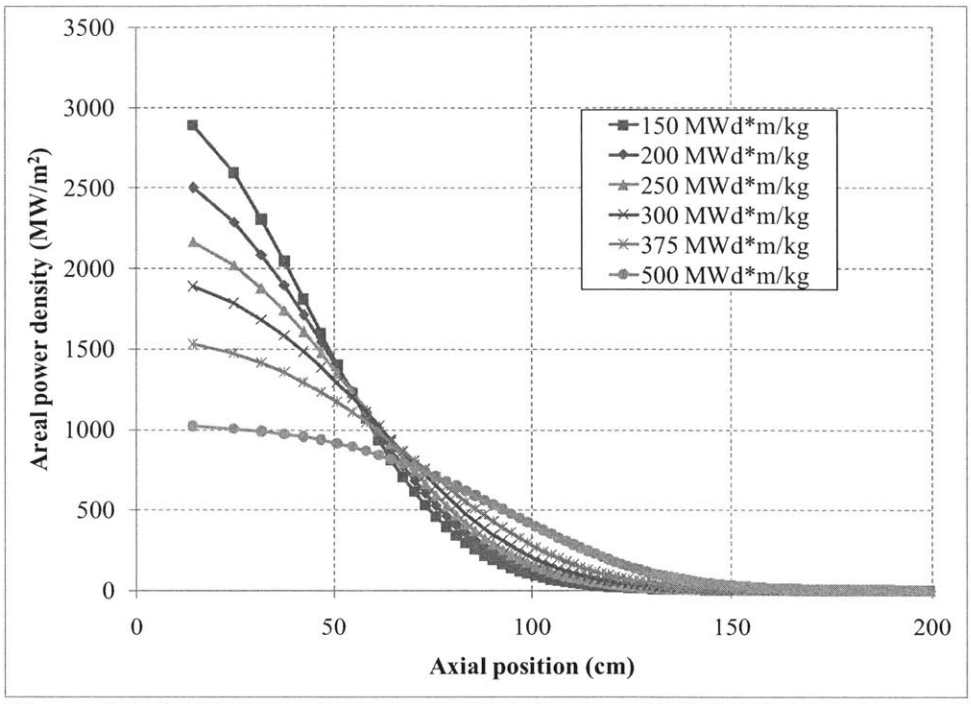

Figure 6.1-4. BOEC radial power distributions (3000 MW total power)

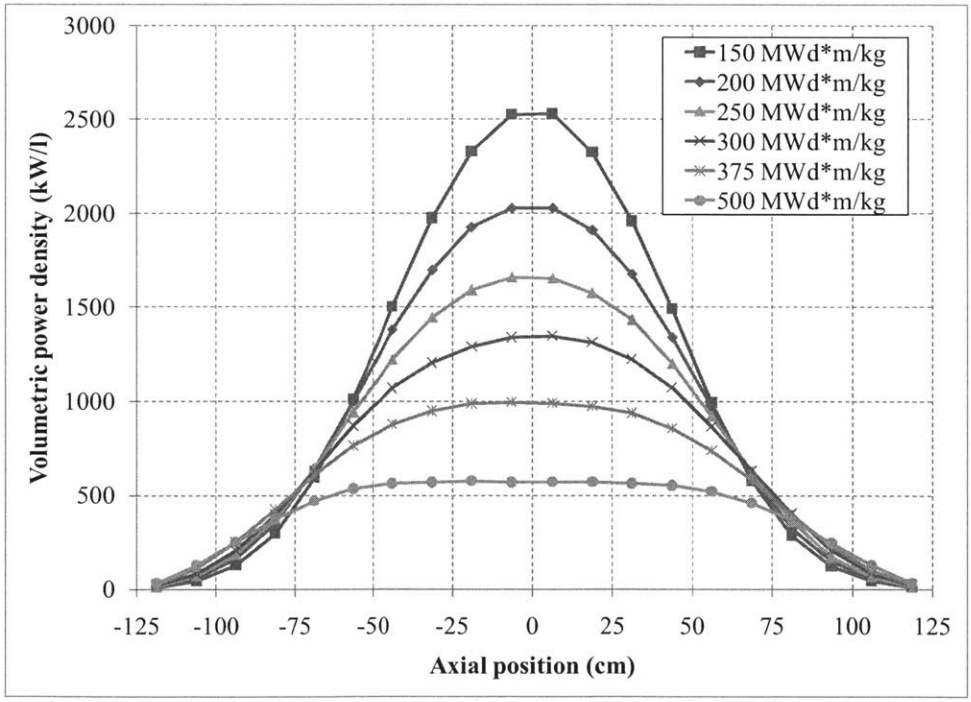

Figure 6.1-5. BOEC axial power distributions (3000 MW total power)

6.2 Effect of different geometries and shuffling sequences

Section 3.2 shows that minimum-burnup B&B reactor models with different geometries and shuffling sequences all have very similar equilibrium cycle reactivity-burnup relationships. This coincident behavior results from the fact that the evolution in neutron excess quantities is similar in all the different cases, forming a link between discharge burnup and equilibrium cycle k_{eq}. The situation for linear-assembly B&B reactors is more complex: instead of discharging fuel at a uniform or close-to-uniform burnup, fuel assemblies are discharged with a highly-peaked non-uniform burnup distribution. At the same time, axial leakage can have an important effect on the k-effective of a linear-assembly B&B reactor. This section investigates different geometry and shuffling-scheme models of linear-assembly B&B reactors and finds that despite these added complexities, the reactivity-burnup relationships of the different configurations still remains essentially constant.

6.2.1 Burnup-reactivity relationships for different geometry models

The previous section introduces a two-dimensional cylindrical model that corresponds to a simplified picture of a linear-assembly B&B reactor. Two other models are constructed using axially-connected assemblies: a two-dimensional planar model and a three-dimensional square assembly model. The planar model is similar to the infinite slab model, except with each planar slab divided into 20 axial zones with vacuum boundaries, the same way the 2D cylindrical model is axially divided. Each "assembly" in the planar model is finite in the vertical direction and the direction of shuffling, but infinite in the dimension transverse to shuffling. The square assembly model is similar to the 3D block models examined in Section 3.7 (30 cm*30 cm*15 cm blocks in a 10x10x10 grid with rotational symmetry), except with the blocks moved as columns instead of independently. Each of these models is shuffled in a convergent manner.

The reactivity-burnup relationships for the three different geometries are shown in Figure 6.2-1. As with the minimum-burnup B&B reactor models, the results for MOEC k-effective are insensitive to the geometry of the model, differing by less than 0.1% between the different models. The output axial burnup distributions are also identical across the different models. This result is useful because it shows that simple two-dimensional planar and cylindrical models can yield the same results as fully three-dimensional models with realistic square or hexagonal assemblies. The non-intuitive behavior shown in Figure 6.2-1 is briefly discussed in the Subsection 6.2.2, and is explained further in the context of neutron excess quantities when axial effects are investigated in Section 6.3.

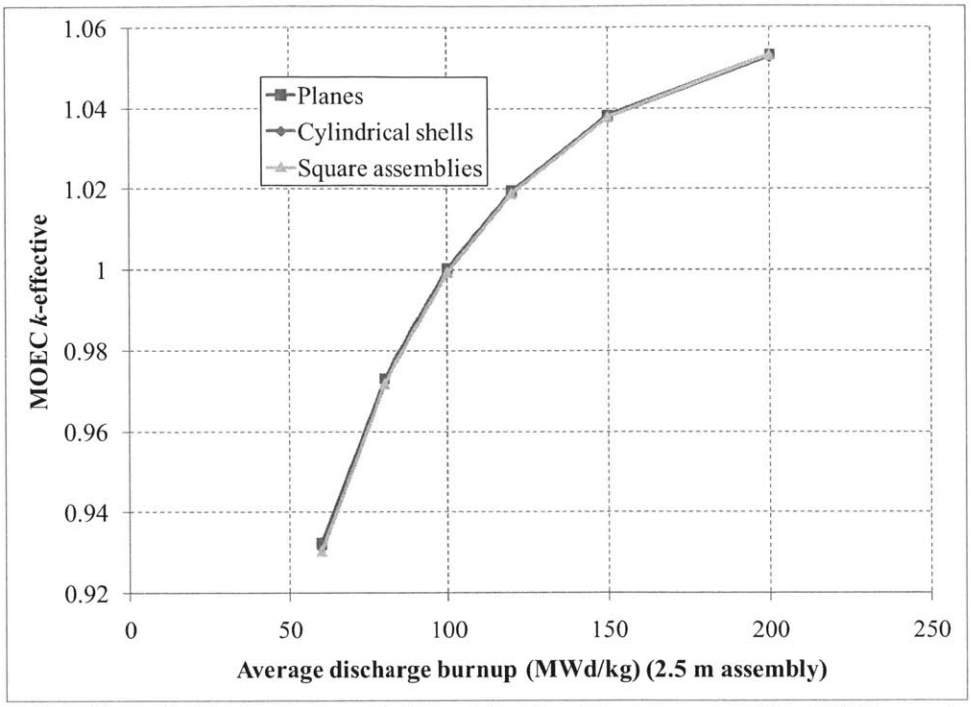

Figure 6.2-1. Reactivity-burnup relationships for linear-assembly B&B reactors with different geometries

6.2.2 Effect of different shuffling sequences in 2D cylindrical model

As with minimum-burnup B&B reactors, the equilibrium cycle power distribution of linear-assembly B&B reactors can be flattened by changing the shuffling scheme used. Two types of shuffling patterns are considered for the 2D cylindrical model in addition to the convergent shuffling: convergent-divergent shuffling, and ring-convergent shuffling.

Convergent-divergent shuffling

One possible shuffling scheme is convergent-divergent shuffling, in which fuel is first shuffled radially inward (converging toward the center) to a specified radius, moved to the center of the core, then shuffled back out to the specified radius (diverging from the center). The EOEC radial burnup distributions for different convergent-divergent shuffling cases are shown in Figure 6.2-2. The numbers in the legend refer to the location of the boundary separating the convergent shuffling region from the divergent shuffling region, with condiv 0 being simple convergent shuffling. For example, in the "condiv 30" case, fuel is first convergently shuffled stepwise from zone 200 to zone 31, skips from zone 31 to zone 1, then is divergently shuffled stepwise from zone 1 to zone 30. Since three zones of fuel are moved at a time, fuel is discharged from zones 28, 29, and 30.

In Figure 6.2.2, the convergent-divergent shuffling pattern can be seen from the fact that fuel is shuffled in order of increasing burnup. The amount of energy per cycle is constant in the different cases, so the average discharge burnup in each case is constant at 120 MWd/kg. The average peak discharge burnup is also the same in each case, about 25.3% FIMA. The case

"condiv 15" gives a good illustration of how permuting the different fuel paths through the core can average the peak burnups of the discharged fuel.

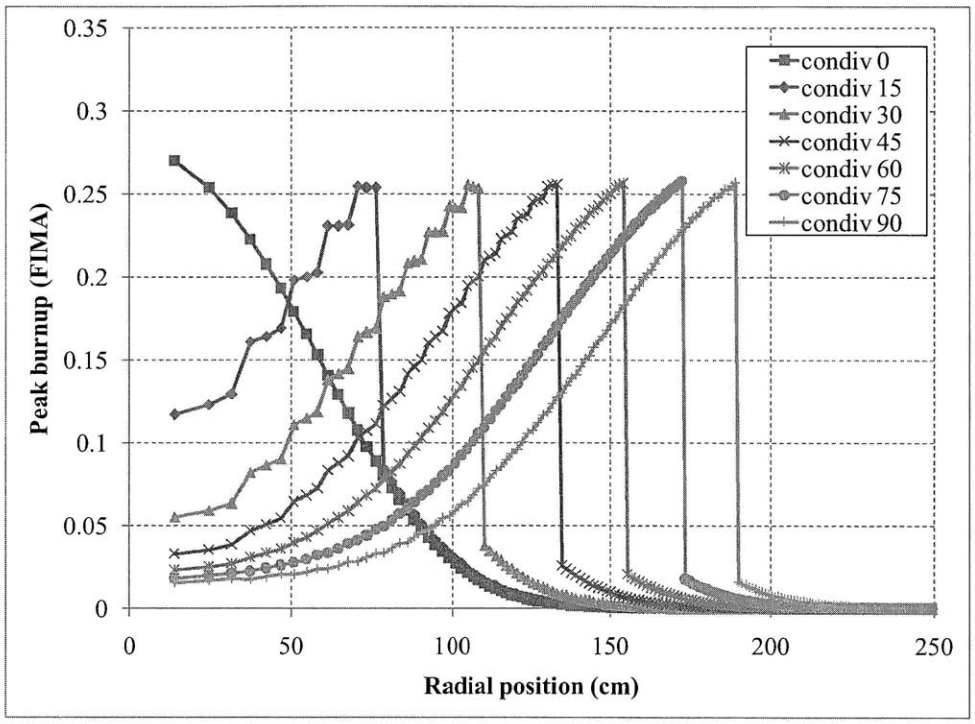

Figure 6.2-2. EOEC radial burnup distributions for convergent-divergent shuffling

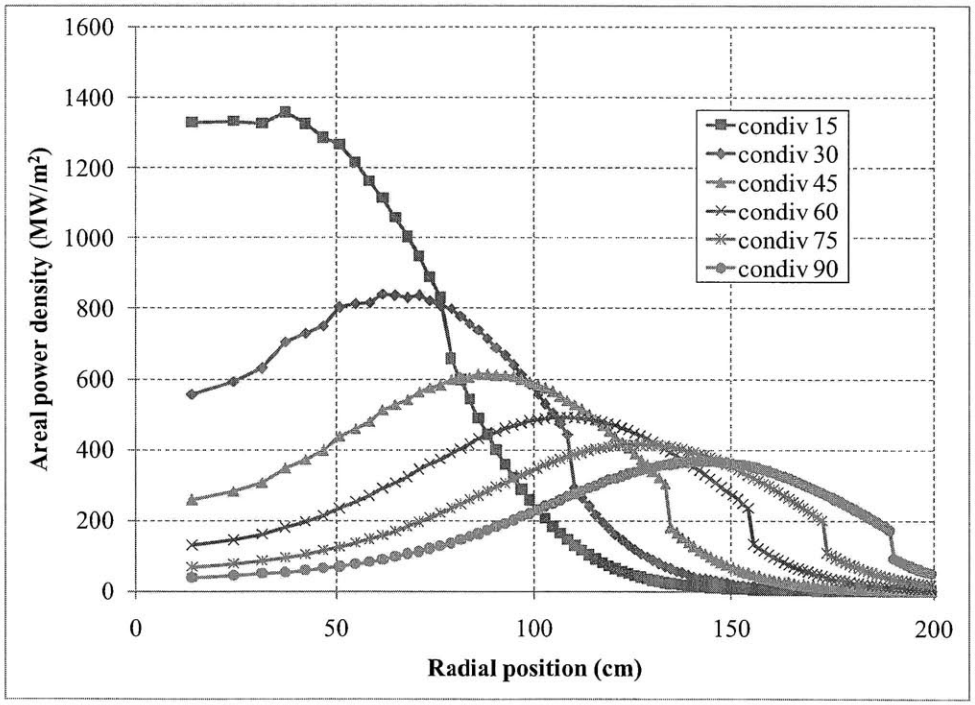

Figure 6.2-3. BOEC radial power distributions for convergent-divergent shuffling cases (3000 MW total power)

The corresponding BOEC power densities are shown in Figure 6.2-3. The figure shows that it is possible to achieve substantial flattening of equilibrium cycle power distributions by changing the shuffling scheme. Cases condiv 45 through condiv 90 have peak power densities below the ~600 MW/m^2 limit and could be operated at 3000 MW. Condiv 90 has a peak areal power density of just 370 MW/m^2, so it could be potentially uprated to over 5000 MW.

In the infinite slab models in Section 3.2 and the 3D block models in Section 3.7, it was found that different shuffling schemes yield very little change in average equilibrium cycle uncontrolled *k*-effective. The same is true for shuffling linear assemblies; Figure 6.2-4 shows the *k*-effective results for the different convergent-divergent shuffling patterns. The MOEC *k*-effective varies by only approximately 0.1%, with the small dip for the condiv 90 case being a consequence of radial leakage from the highly spread out power distribution. Cycle reactivity swing is very low for the strictly convergent case because of the low flux in regions with relatively fresh fuel, and increases for the condiv15 and condiv30 cases as fresher fuel (with greater *k*-infinity swing) is exposed to the high flux central region. Larger condiv cases have progressively lower reactivity swings as the central flux becomes lower and the overall flux distribution expands, reducing the fluence experienced by each region of fuel over a cycle. The low reactivity swing of these cases means that cycle length can be doubled to 441 days at 3000 MW) while still allowing critical operation.

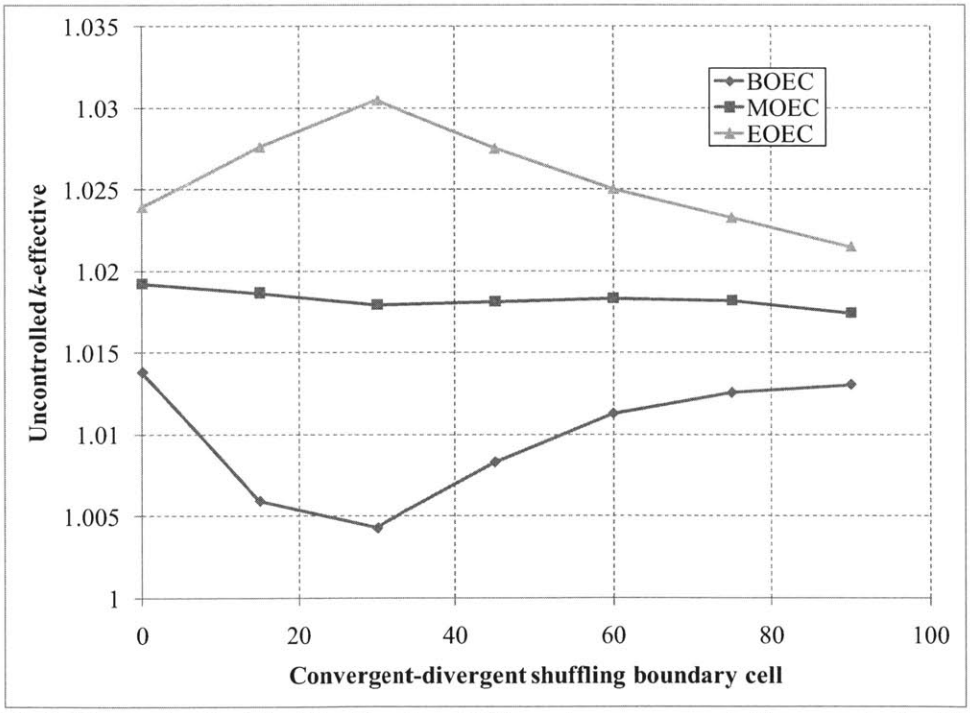

Figure 6.2-4. Uncontrolled *k*-effective for different convergent-divergent shuffling cases

In a minimum-burnup B&B reactor, the discharge fluence spectrum is extremely similar for cases with different shuffling sequences. Similarly, in these linear-assembly cases, the axial burnup distributions of the different cases at discharge are essentially identical. This is shown in Figure 6.2-5, which shows the discharge burnup distributions (averaged among the three discharged zones) for the different convergent-divergent cases. In both cases, this behavior is a

consequence of the low neutron absorption cross sections in the hard spectrum. The average scattering cross section is many times (~40) higher than the average absorption cross section, so each neutron is scattered dozens of times on average. As a result, the distributions in neutron energy and the spatial distribution of flux relative to where neutrons are produced is always roughly the same. Therefore, a given neutron production distribution as a function of axial position (i.e. the ΔP distribution) will result in a specific neutron absorption (ΔA) distribution. The ΔA and ΔP distributions are also linked via depletion history, which means that there exists a unique solution for the two final distributions. This idea is discussed further in the next section in an investigation of axial effects in linear-assembly B&B reactors.

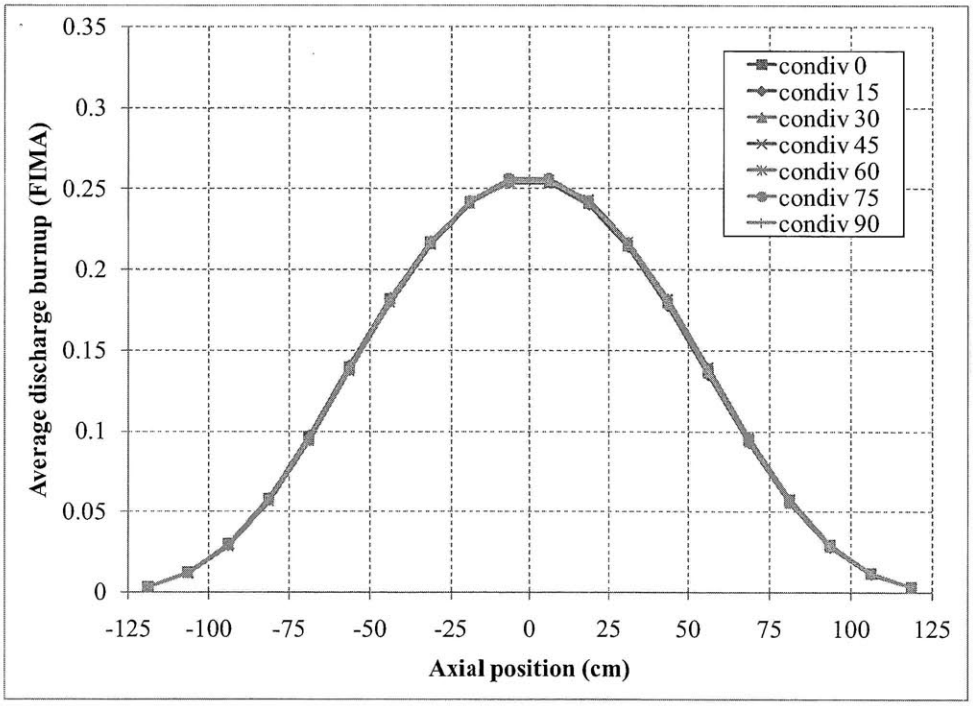

Figure 6.2-5. Discharge axial burnup distributions for convergent-divergent cases

Figure 6.2-6 shows that even though the discharge burnup distributions are the same, intermediate burnup distributions can differ as feed fuel experiences flux with different axial distributions. These differences get evened out as eventually the feed fuel sees flux from assemblies at all burnup levels. This behavior is analogous to how fuel in different minimum-burnup B&B reactors can experience different spectral histories (Figure 3.2-6) but still end up with the same overall fluence spectrum (Figure 3.2-5).

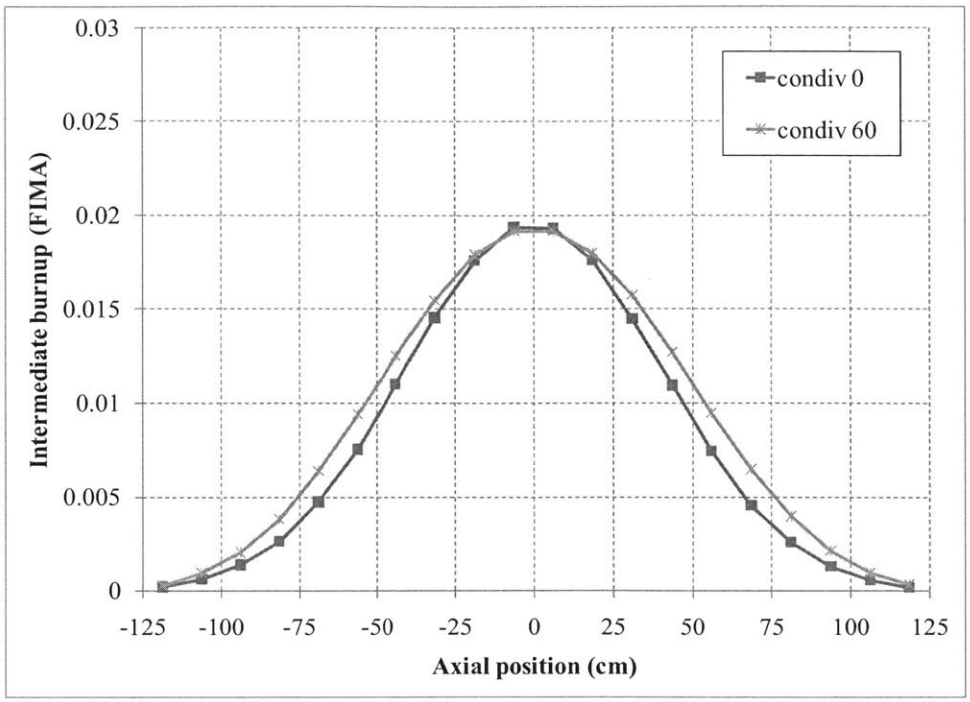

Figure 6.2-6. Intermediate axial burnup distributions for convergent-divergent cases

Ring-convergent shuffling

An alternative shuffling scheme to convergent and convergent-divergent shuffling is considered to further demonstrate that the reactivity-burnup relationship is roughly independent of shuffling sequence. In this shuffling scheme, called "ring-convergent," fuel is first convergently shuffled to a given radial boundary, inside of which the fuel is alternately shuffled between the center of the core and the set boundary. Fuel is eventually shuffled to a "ring" between the center of the core and the boundary, and then discharged. EOEC burnup distributions for ring-convergent shuffling are shown in Figure 6.2-7. In the figure, the shuffling sequences can be seen from the fact that fuel is shuffled in order of increasing burnup. Once again, the number in the legend indicates the radial zone boundary at which there is a switch from convergent to ring-convergent shuffling.

BOEC power distributions for ring-convergent shuffling are shown in Figure 6.2-8. Compared to convergent-divergent shuffling, ring-convergent sequences have smoother power distributions, without an abrupt change in power density at the convergent-divergent shuffling boundary.

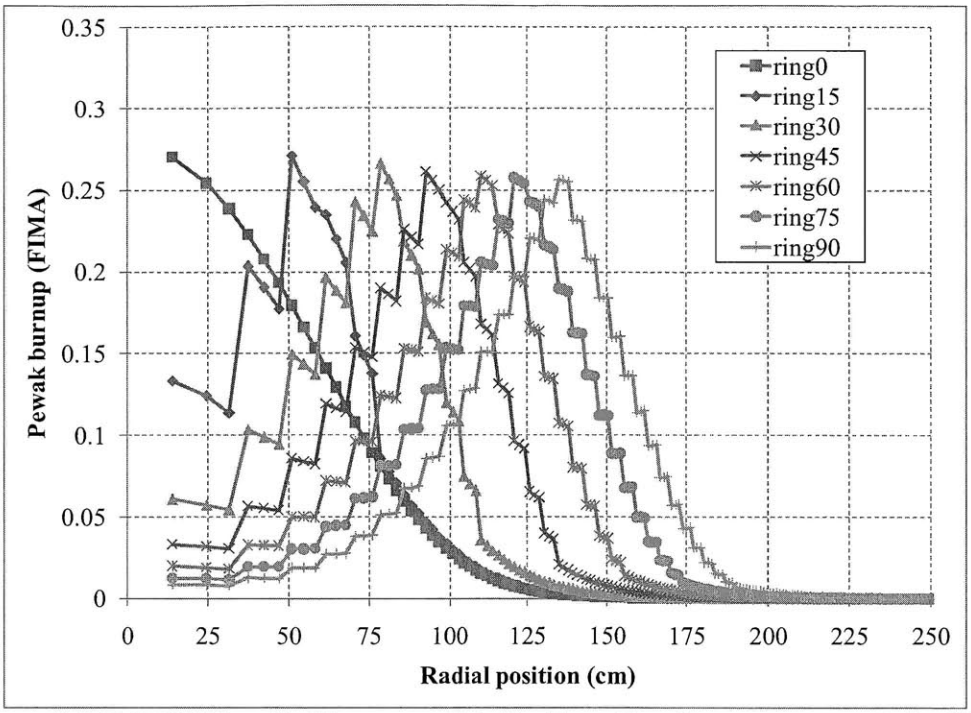

Figure 6.2-7. EOEC radial burnup distributions for ring-convergent shuffling

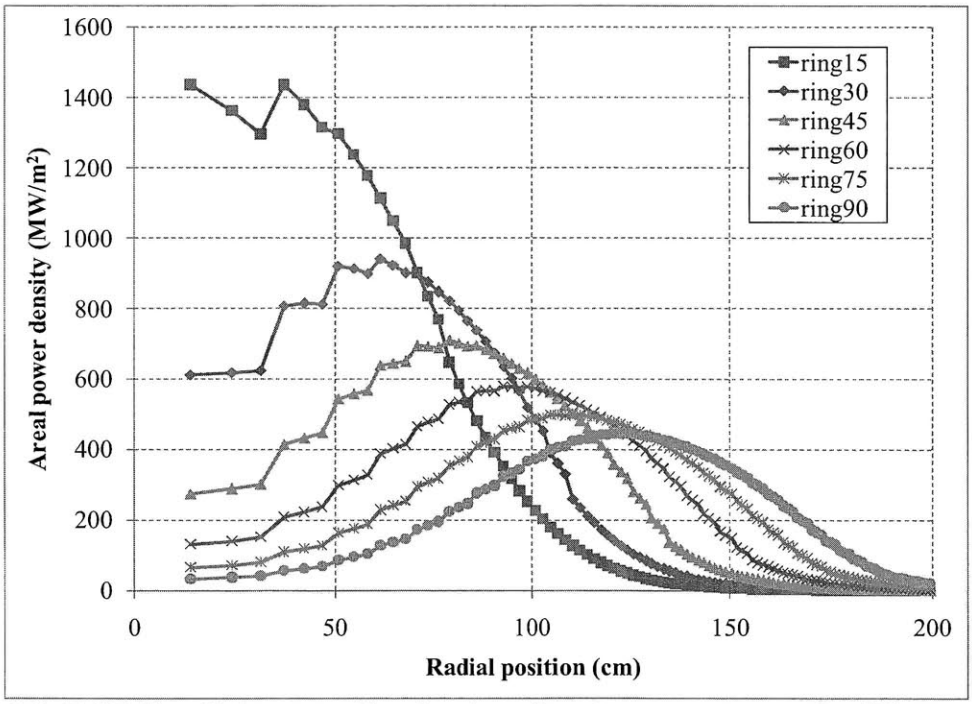

Figure 6.2-8. BOEC radial power distributions for ring-convergent shuffling cases (3000 MW total power)

Figure 6.2-9 shows the equilibrium cycle uncontrolled *k*-effective values for different ring-convergent cases. As with the convergent-divergent cases, the ring-convergent shuffling cases demonstrate extremely small (<0.1%) changes in MOEC *k*-effective for the same average

discharge burnup. Cycle reactivity swing displays the same trends as observed in the convergent-divergent cases.

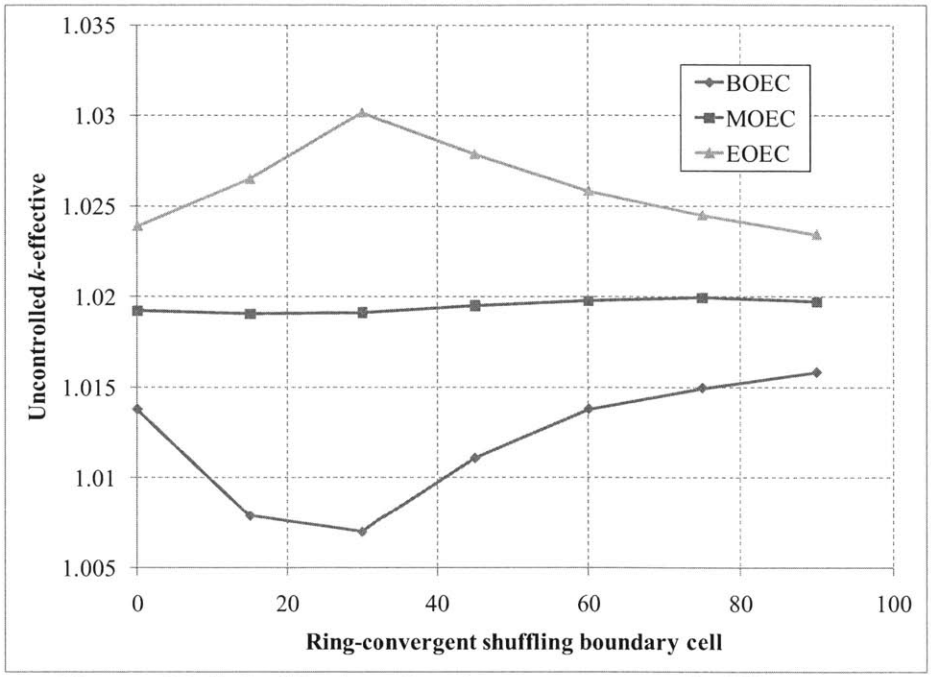

Figure 6.2-9. *k*-effectives for ring-convergent shuffling cases

Like minimum-burnup B&B reactors, linear-assembly B&B reactors also display a fixed burnup-reactivity relationship for cases with different geometries and equilibrium cycle shuffling sequences. Again relatively simple two-dimensional models (like the cylindrical examples in this section) are able to yield the same results as more realistic models. Sections 6.3 and 6.4 discuss how the neutron excess concepts developed for minimum-burnup B&B reactors can be applied to linear-assembly B&B reactors by introducing methods for capturing the effect of non-uniform axial distributions.

6.2.3 Effect of radial size and reflectors on linear-assembly B&B reactors

Subsection 3.3.1 shows how in a minimum-burnup B&B reactor, the relationship between reactor size and equilibrium cycle *k*-effective can be estimated based on the results of a single thick-blanket model with effectively zero leakage. This is done by multiplying *k*-effective from the thick-blanket model by the fraction of neutron absorptions occurring within the desired reactor size. The same approach can be used in a linear-assembly B&B reactor to determine the relationship between *radial* size and *k*-effective. The thick-blanket model in such a case would be a large radius model (with the same axial height) that effectively eliminates radial leakage. The effect of vary axial height is considered separately in Section 6.3.

Figures 6.2-10 and 6.2-11 illustrate the accuracy of this method for the convergent shuffling case and the condiv 60 case, which has a larger minimum radius. The estimated values accurately predict the position and magnitude of the drop in reactivity for more than the first 1.5% in *k*-effective.

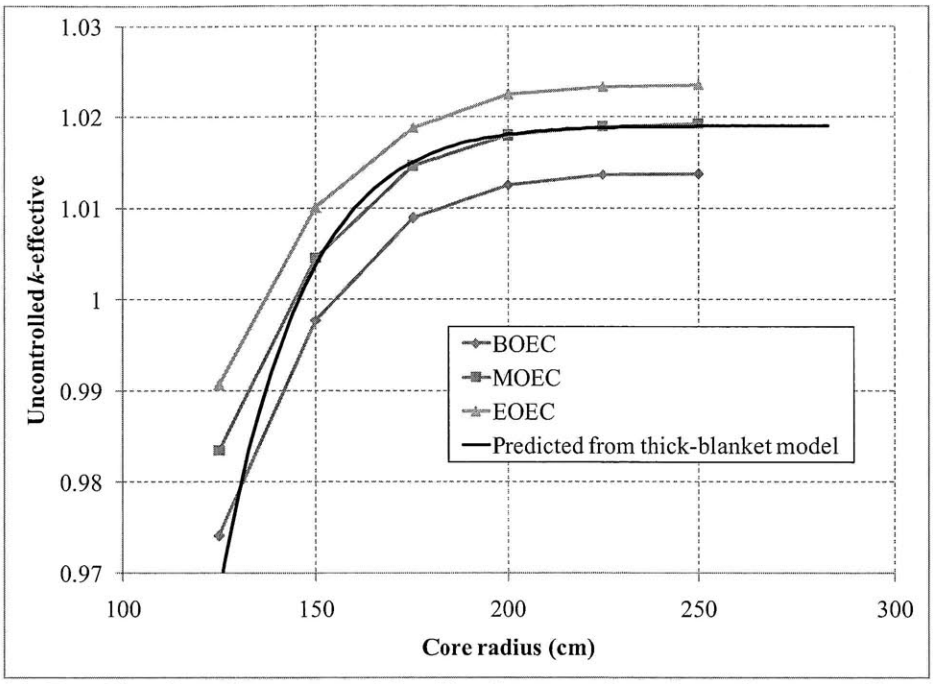

Figure 6.2-10. Predicted and measured k-effective as a function of core radius (convergent shuffling, vacuum boundary)

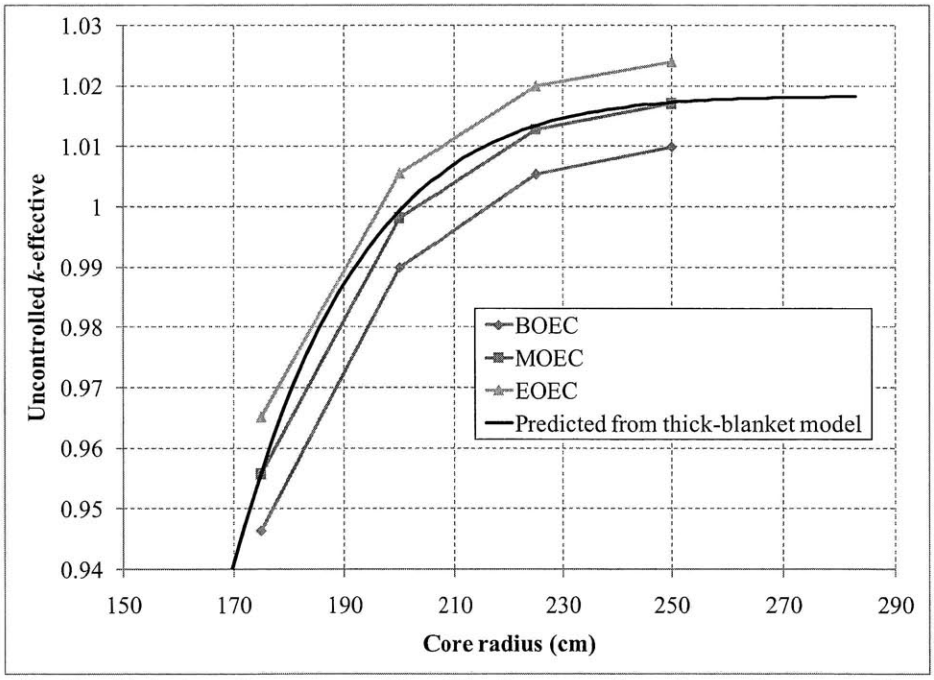

Figure 6.2-11. Predicted and measured k-effective as a function of core radius (condiv 60 shuffling, vacuum boundary)

The presence of a reflector reduces the reactivity deviation from the asymptotic value by a fraction that depends on the reflector efficacy. This is illustrated in Figures 6.2-12 and 6.2-13, which assume a zirconium reflector consisting of the same core composition with zirconium

substituted in place of fuel. The zirconium reflector is able to reduce the drop off in *k*-effective by 50% compared to a vacuum boundary. This reduces the minimum radius of the condiv 60 equilibrium cycle from approximately 220 cm to 200 cm, which reduces the fueled volume and feed fuel residence time by about 20%.

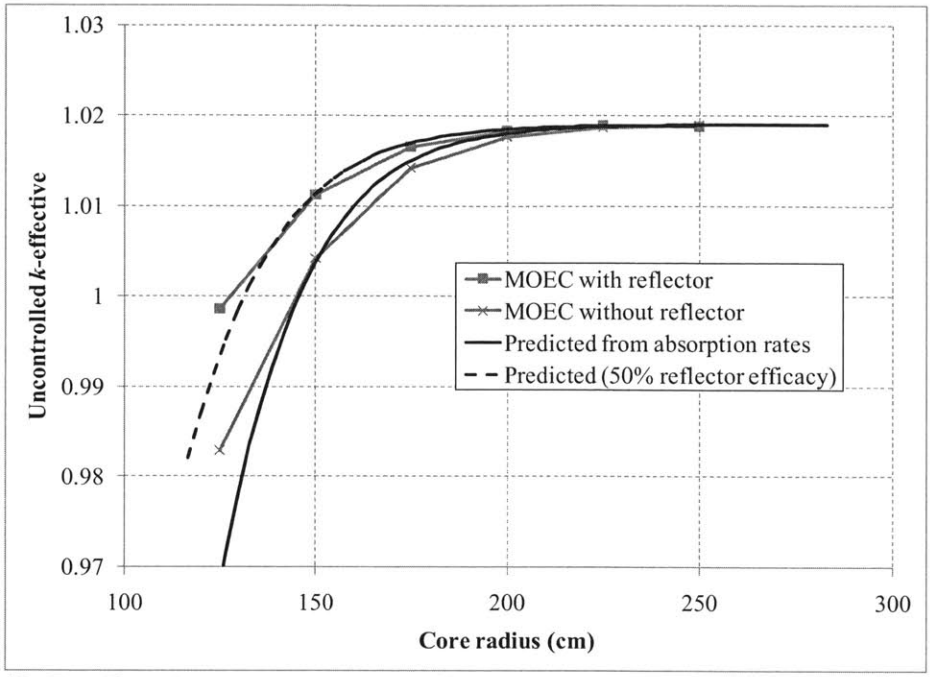

Figure 6.2-12. Predicted and measured k-effective as a function of core radius (convergent shuffling, with reflector)

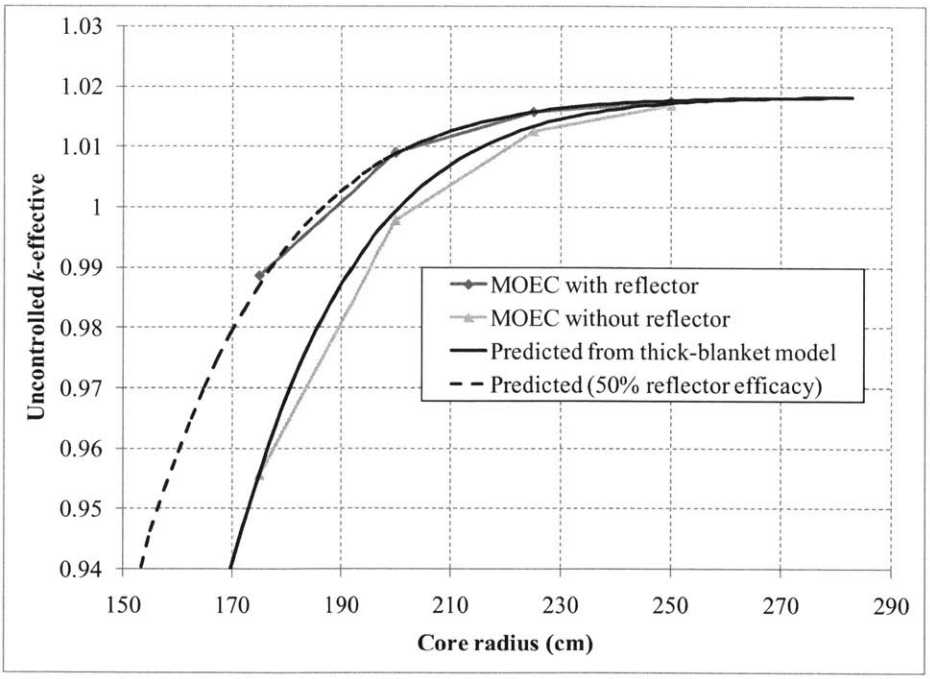

Figure 6.2-13. Predicted and measured k-effective as a function of core radius (condiv 60 shuffling, with reflector)

6.3 Effect of axial length and reflectors

The linear-assembly models presented in the previous two sections have all assumed vacuum boundaries at the ends of the fuel, which act as black neutron absorber. In an actual system, there would be some material present, such as an engineered reflector at the top or bottom of the fuel assemblies (like a section of stainless steel), a gas plenum above the fuel, or an absorbing material used as a shield. This material would not function as a perfect absorber and would cause some neutrons to be reflected back into the fuel.

6.3.1 Reactivity-height relationship in a model with axial reflectors

To model a more realistic reflected case, the 250 cm high convergent-shuffling model is rerun with the vacuum boundary conditions replaced by 1 m of stainless-steel (HT9) filled pins to act as a reflector. The same reflector is modeled on both ends so there is only one value of reflector albedo to consider. The model is run to the same average discharge burnups as the original vacuum-boundary cases. Figure 6.3-1 shows the new burnup-reactivity relationship for the reflected case; peak burnup is shown to illustrate how the reflected cases have lower peak burnup than the vacuum-boundary cases for the same average burnup. Figure 6.3-2 gives the axial burnup distributions for the reflected case.

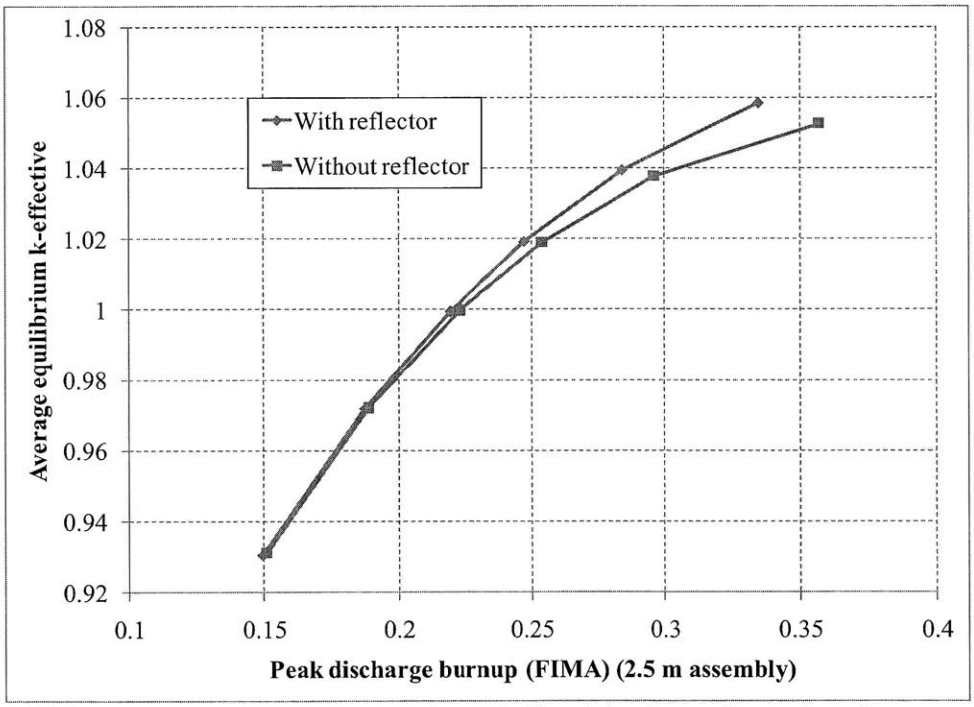

Figure 6.3-1. Peak-burnup vs. reactivity relationship for reflected and non-reflected assemblies

As seen in Figure 6.3-1, at low total burnup, the results for the reflected and non reflected cases match exactly, since the burnup distribution is axially short and doesn't approach the top and bottom of the fuel assembly. At higher burnup, the distribution begins to encounter the edges of the fuel, which causes the reflected case to have a lower peak burnup and slightly higher

reactivity. Figure 6.3-2 shows that in the reflected cases, the burnup distribution of these higher burnup cases begins to flatten back out toward the edges, instead of approaching zero like in the vacuum-boundary cases (Figure 6.1-2). This reduces the peak-to-average ratio of the burnup distribution, resulting in a lower peak burnup for the same total assembly burnup.

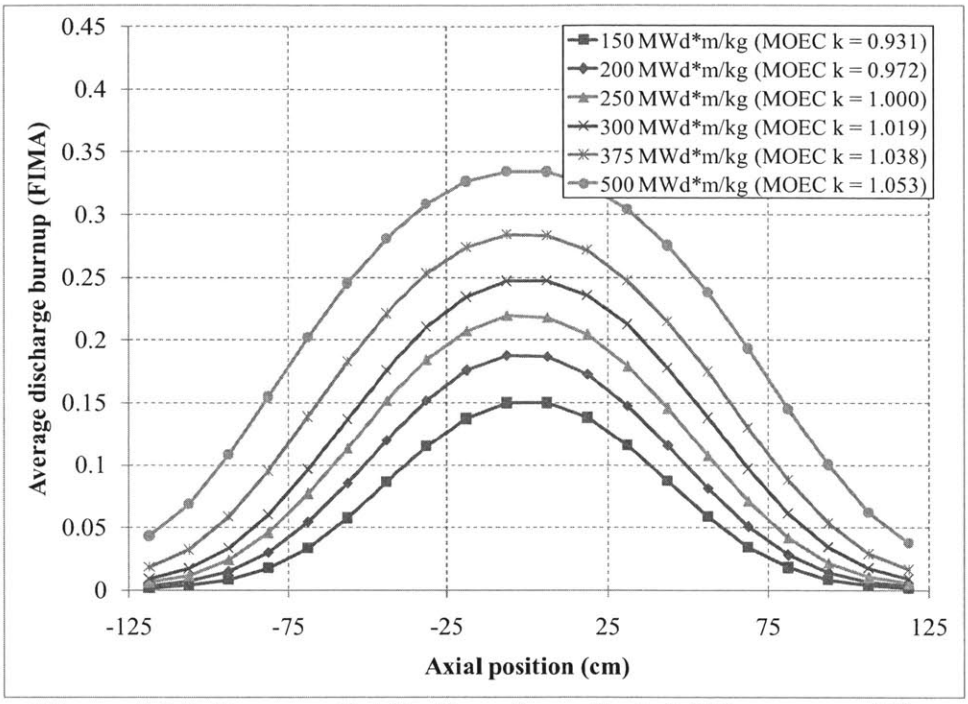

Figure 6.3-2. Burnup distributions for reflected 250 cm assemblies

To determine the effect of axial height in the reflected model, the axial height of the fuel is varied and the burnup specified so that the "average" *k*-effective (as averaged according to Equation 2.3-17) would equal a constant 1.018 in each case. The correct peak burnup value is found by modeling different burnup values and linearly interpolating to the desired *k*-effective. The peak burnup required to achieve the target *k*-effective is plotted as a function of height in Figure 6.3-3.

Figure 6.3-3 shows that for very long assemblies, adding additional fuel to the ends does not change the equilibrium cycle *k*-effective. This is because in a long assembly, the equilibrium cycle burnup distribution does not reach the ends of the fuel, so adding additional fuel to the ends does not change the burnup distribution. This is illustrated in Figures 6.1-2 and 6.3-2 by how the lower-burnup distributions interact minimally with the ends of the fuel. As a result, there is an asymptotic value of peak burnup, displayed as a dashed line in Figure 6.3-3. In a very long assembly, the burnup distribution can potentially shift up and down the assembly while retaining essentially the same shape and *k*-effective, and may do so as a result of axial gradients in the core (e.g. different temperatures at the top and bottom of the assembly).

Interestingly, as the length of the assembly is reduced, the required peak burnup can go down slightly. This is because the very-low burnup fuel at the axial ends of the burnup distribution effectively acts as just an absorber, since it always has a k_∞ much less than unity. Replacing this

fuel with a higher albedo reflector improves the neutron economy, lowering the peak burnup. The burnup savings from the reflector is fairly small, amounting to only about 0.3% peak burnup.

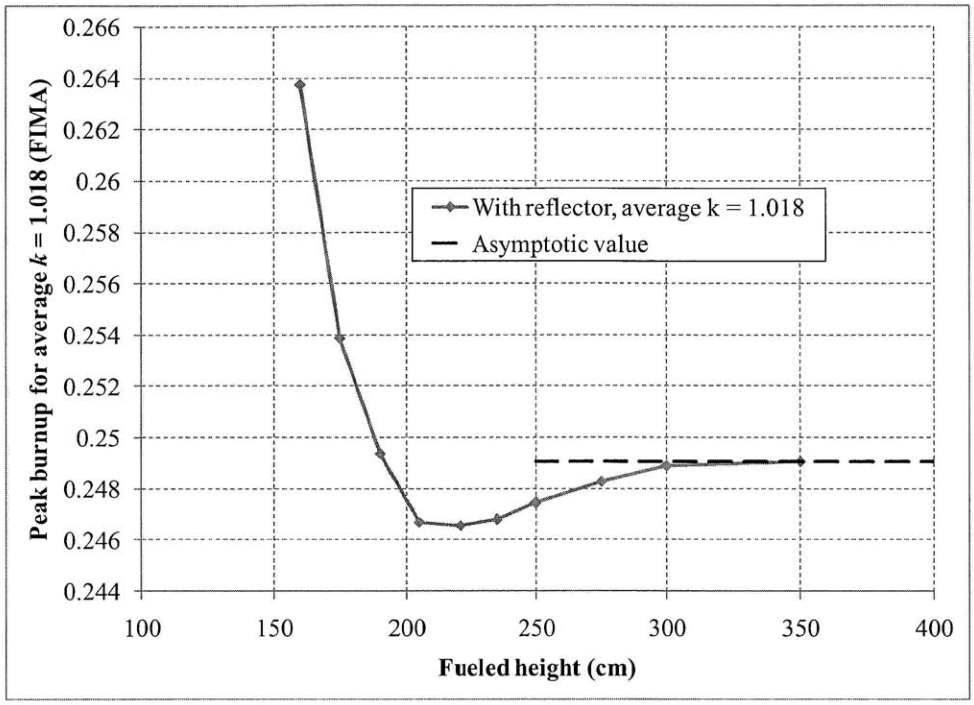

Figure 6.3-3. Burnup required to obtain a reactivity target as a function of axial height

At still shorter assembly lengths (under 205 cm), peak burnup increases as higher-burnup fuel is replaced by reflector. This higher burnup fuel functions better than the reflector since it has absorbed enough neutrons to breed some plutonium and act as a neutron multiplier. The minimum point on the chart is where the fuel at the ends of assembly is equivalent to the reflector; where this point occurs depends on the albedo of the reflector. The rise past this minimum is very fast, with the minimum burnup rising by 1% or more with every 15 cm reduction in fuel height past 175 cm.

Figure 6.3-3 can alternatively be viewed in terms of *k*-effective for a fixed peak discharge burnup; in this case there would be an increase in reactivity centered around 220 cm, and a sharp decrease in reactivity under this value. The relationship between peak burnup and reactivity for a 250 cm high core (as illustrated in Figure 6.3-1) is that every 1.6% increase in peak burnup results in a 1% increase in *k*-effective. This ratio rises to 2.6% burnup for every 1% *k*-effective for the 160 cm assembly, which is a consequence of increased leakage with increasing burnup for the shorter assembly.

6.3.2 Axial distributions in linear assemblies and a simple neutron axial transfer model

An important finding in Section 6.2 is that the axial distribution of discharge burnup is independent of the core geometry and the shuffling path through the core. This means that irrespective of how the assemblies are moved about radially, neutrons are still being generated and absorbed with essentially the same axial distribution. The reason for this behavior is similar to the reason that the equilibrium cycle fuel in a minimum-burnup B&B reactor experiences

essentially the same fluence spectrum, irrespective of how the fuel is shuffled. In B&B reactor fuel, the absorption cross section is much smaller than the scattering cross section and does not change significantly over the life of the fuel. As a result, neutrons tend to be absorbed in a consistent spherical distribution around where they are born. As a result, the axial position at which neutrons are absorbed depends almost entirely on the axial position of where they were created, and not on the radial position, so there is a unique axial mapping of neutron production (ΔP) to neutron absorption (ΔA). This mapping is shown in Figure 6.3-4 for a 350 cm assembly. The ΔP distribution has the same shape as the burnup distribution, since neutrons are created where fissions occur. The ΔA distribution is more spread out than the ΔP distribution because the neutrons migrate from where they are produced. The ΔN distribution shows that the highly burned central fuel acts as a net neutron source while the less burned ends of the fuel are a net neutron sink, with the total ΔN over the assembly being slightly greater than zero to allow for losses to leakage and control.

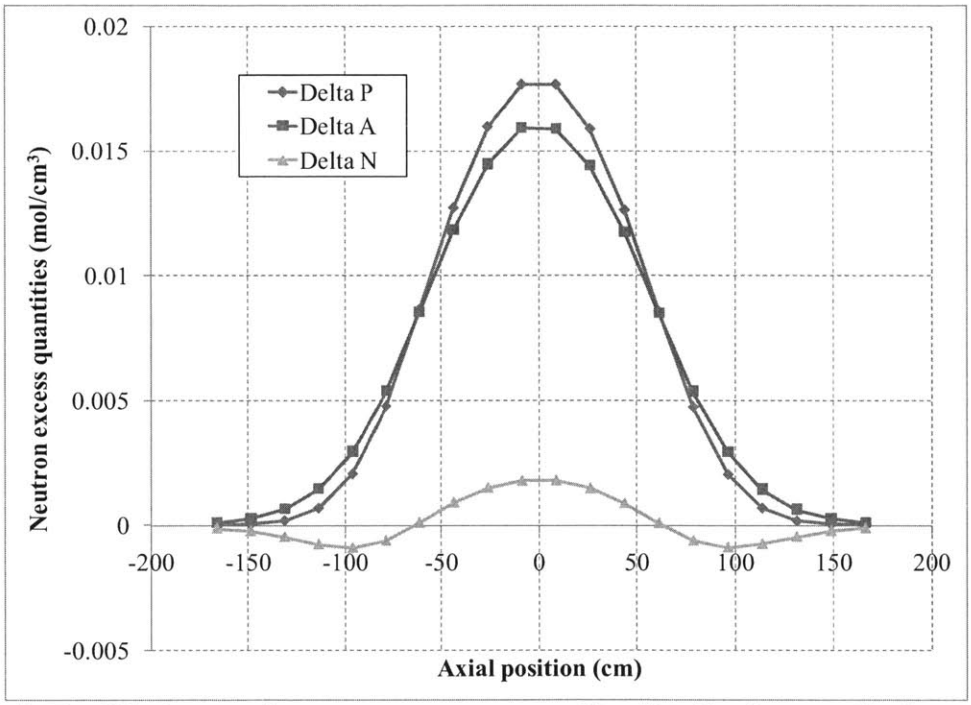

Figure 6.3-4. Equilibrium cycle neutron excess quantity distributions at discharge for a 350 cm assembly

The axial distributions of ΔP and ΔA are related in two ways. First, they are connected as material-dependent neutron excess quantities; a material with a specific depletion history will have specific values for ΔP and ΔA. Therefore, ΔP can be pictured as being a function of ΔA for a particular material's depletion, as written in Equation 6.3-1:

$$\Delta P = f(\Delta A)_{depletion} \tag{6.3-1}$$

The neutron excess curves (ΔN vs. ΔA) for the depletion of the 350 cm assembly are given in Figure 6.3-5. Interestingly, the different curves for the different axial zones all coincide (as might be expected from the spherical symmetry that arises, as seen in Figure 6.1-3), although

they have different endpoints. Also shown are results from the infinite-medium (0D) depletion approximation and the results of a 1D infinite slab model with a discharge burnup equal to the peak discharge burnup of the assembly. Neither the 0D nor 1D neutron excess curves exactly match that from the linear-assembly case, due to different spectral histories over the depletions. However, the linear-assembly neutron excess curves do match those from different geometry models that use linear assemblies (from Subsection 6.2.1), so simple 2D models can still be used to generate the neutron excess curve for a realistic reactor. Interestingly, even though the infinite-medium neutron excess curve does not match the linear-assembly curves exactly, Subsection 6.3.3 describes how an infinite-medium depletion can still be used to provide an estimate of *k*-effective vs. peak burnup.

The other way ΔP and ΔA are connected is through an "axial transfer matrix" (or transform): neutrons born at a certain axial position will have a certain probability of being absorbed at another axial position. One can multiply the ΔP distribution by a transfer matrix (or integrate using a transform) to yield the corresponding ΔA distribution, as expressed in Equation 6.3-2.

$$\Delta A(z_2) = T\Delta P(z_1) = \int dz_1 K(z_1, z_2)\Delta P(z_1) \tag{6.3-2}$$

In Equation 6.3-2, z_1 is the axial position of neutron production, z_2 is the axial position of neutron absorption, and K is the axial transfer kernel linking the two, which creates the axial transfer transform T. Equation 6.3-2 can be rewritten in a discrete form as a matrix multiplication, where **M** is the "axial transfer matrix":

$$\mathbf{\Delta A} = \mathbf{M}\mathbf{\Delta P} \tag{6.3-3}$$

$$\Delta A_j = \sum_{i=1}^{n} M_{j,i}\Delta P_i \tag{6.3-4}$$

In Equation 6.3-4, ΔP_i is the number of neutrons produced in axial zone i, ΔA_j is the number of neutrons absorbed in axial zone j, and $M_{j,i}$ is the probability that a neutron produced in zone i is absorbed in zone j. Because of the low absorption cross section in a fast neutron spectrum, the axial transfer matrix is fairly constant for neutrons produced at different radial positions and in reactors with different shuffling sequences. The presence of radial and axial inhomogeneities in the core (such as streaming channels or control assemblies) would have an effect on how neutrons are redistributed axially, so assuming that the axial transfer matrix is constant is a simplification. The effects of core inhomogeneties are more complex to study and are not covered in this thesis; they are instead left as a topic for future study.

To test the axial transfer idea, an axial transfer matrix is constructed based on simple one-group neutron diffusion theory, assuming constant material properties (absorption and scattering cross sections). The absorption and scattering cross sections are given in Figures 6.3-6 and 6.3-7 as a function of axial and radial position in the convergent shuffling 350 cm case. Absorption (including fission) cross sections increase as a function of burnup due to the accumulation of Pu-239 and fission products, and is also higher far from the center of the core due to the softer spectrum there, but stays near 0.0055 cm^{-1} everywhere (there is statistical scatter in the low flux regions of the core). The elastic scattering cross section is lower where the neutron spectrum is harder (in the center of the core), but doesn't vary much from 0.23 cm^{-1}. Notably, the elastic scattering cross section is approximately 40 times higher than the total absorption cross section.

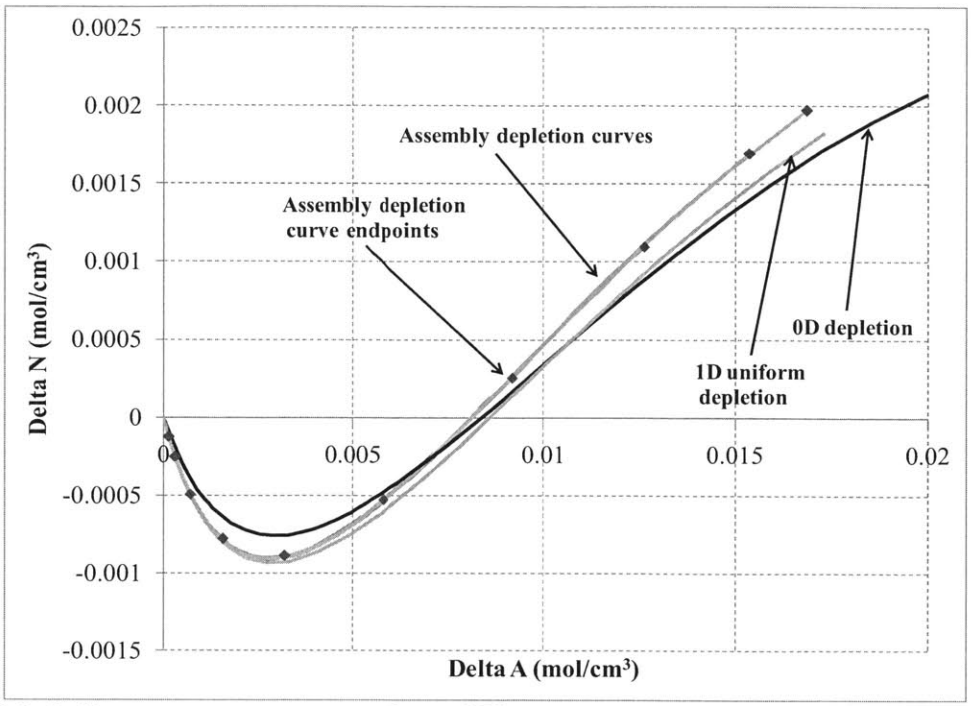

Figure 6.3-5. Neutron excess curves for a 350 cm assembly, 0D and 1D approximations

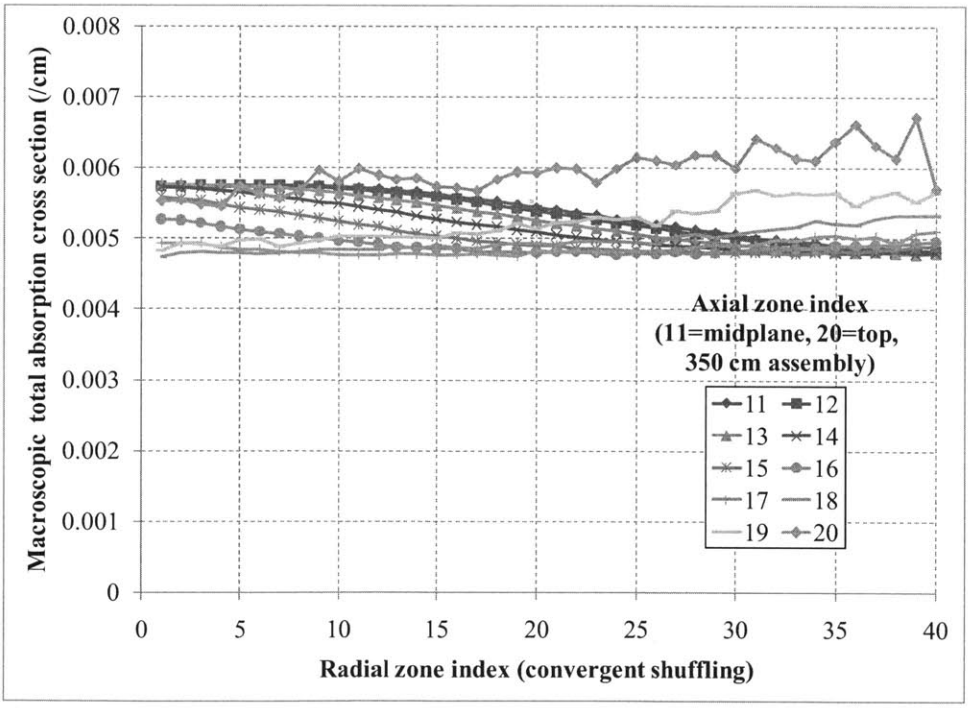

Figure 6.3-6. Absorption (including fission) cross sections in the 2D cylindrical model

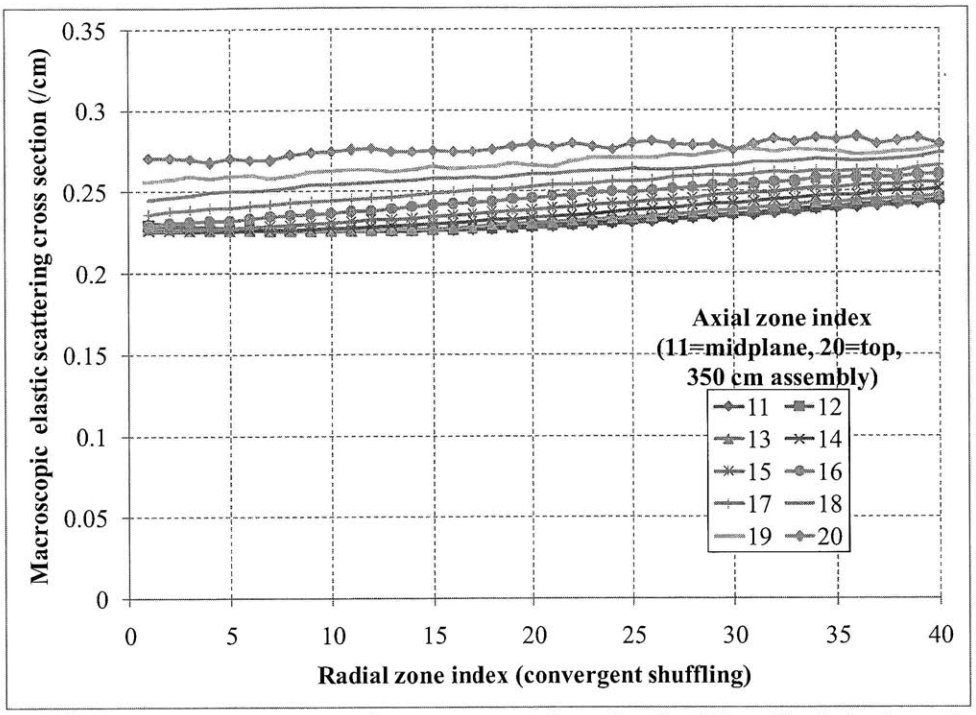

Figure 6.3-7. Elastic scattering cross sections in the 2D cylindrical model

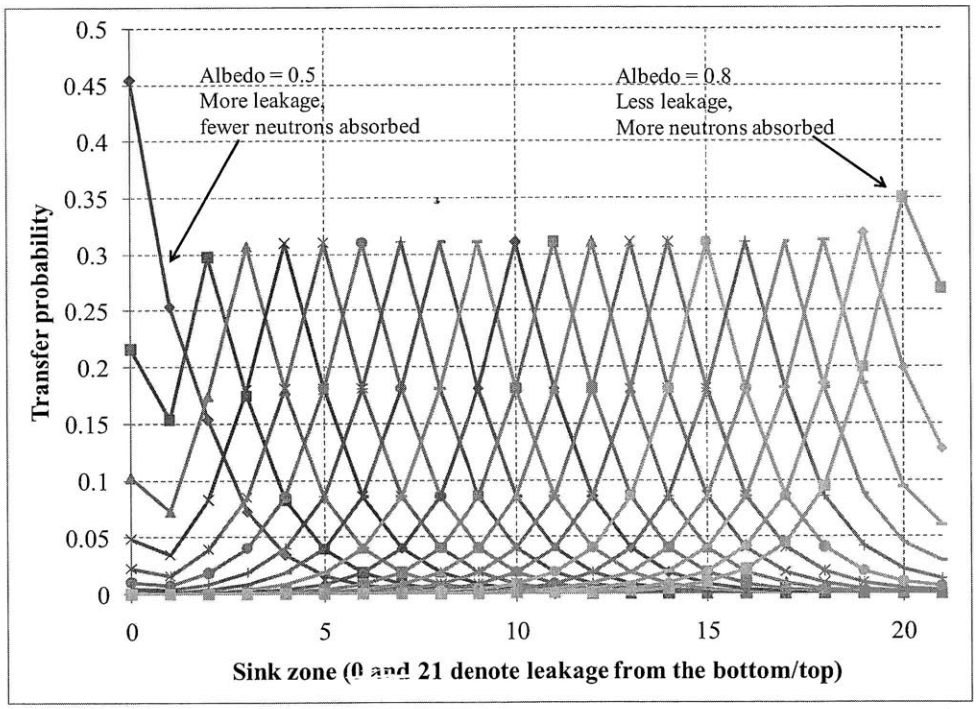

Figure 6.3-8. Graphical depiction of axial transfer matrix, 250 cm assembly, mixed albedos

The mean free path of a neutron (~ 4 cm) is much less than mean absorption distance (~ 2 m), so using diffusion theory is appropriate. Neutrons produced in each of the 20 axial zones is assumed to originate from a plane source at the center of the zone, and the neutron diffusion equation is used to determine the flux and absorption/leakage rates arising from that source.

Details of the neutron diffusion calculations are provided in Appendix A.6. Doing these calculations results in an axial transfer matrix, such as that shown in Figure 6.3-8.

Figure 6.3-8 shows 20 curves, one for neutrons produced from each axial zone. The values of the curves are the probability that neutrons produced in a source zone are absorbed in the specified sink zone; for example the probability that a neutron produced in one of the central zones is absorbed in the same zone is about 31%, and 18% for absorption in each of the adjacent zones. The neutron albedo of the top and bottom boundaries can be specified. A low albedo increases leakage and reduces absorption in that end of the assembly, and a high albedo has the opposite effect (the fuel composition itself has an infinite-thickness albedo of approximately 70%). Neutrons produced in the centermost cells are absorbed before they reach the ends, so their transfer curves are not affected by the boundary albedos. Since this transfer matrix is based on neutron diffusion theory, results near the fuel boundaries are expected to be approximate.

By combining the neutron excess curve (Figure 6.3-5), and the axial transfer matrix (Figure 6.3-8), it is possible to solve for the ΔP and ΔA distributions in an assembly by solving Equation 6.3-1 and 6.3-3 simultaneously. First, one starts with an arbitrary "source" ΔP distribution that is normalized to a target value for total ΔP. Using the axial transfer matrix, the ΔP distribution can be mapped to a ΔA distribution. This ΔA distribution can then be converted back into a ΔP distribution via the neutron excess curve. Repeating this process converges the two distributions to a self-consistent solution, with its average k-effective coming from the normalization factor used at each step. This simple diffusion based model is referred to as the "axial transfer model." By choosing the correct value for the diffusion length (L), it is possible to accurately reproduce the shapes of the ΔP and ΔA distributions from the explicitly modeled reactor, as shown in Figure 6.3-9. A diffusion length of 16.8 cm is used, corresponding to the diffusion length encountered at about 1-2% fuel burnup. The axial transfer model's prediction for average k-effective is also fairly accurate.

One thing that the axial transfer model is useful for is rapidly investigating the effect of assembly length and different reflector albedos, and explaining the results shown in Figure 6.3-3. The results of using the axial transfer model to examine different reflectors and fuel lengths are shown in Figure 6.3-10. Results from the axial transfer model are the smooth curves in the figure. The target average k-effective is set so that the 350 cm assembly case would have the same peak burnup in the predicted and modeled cases. A reflector with an albedo of 0.775 leads to a height vs. burnup curve that matches the measured results in Figure 3 very well. The behavior shown for different albedo reflectors is quite different from that observed in the radial reflector case: reflectors with albedos better than the fuel composition albedo (0.7) can actually allow a small dip in the peak burnup required for a target k-effective. In the limiting case of a perfect reflector, the peak burnup would be the uniform-burnup value (~13%) regardless of length. While a perfect reflector doesn't exist, axial reflectors still can be used to reduce the fueled height in a core by 50 cm or more without causing a decrease in k-effective.

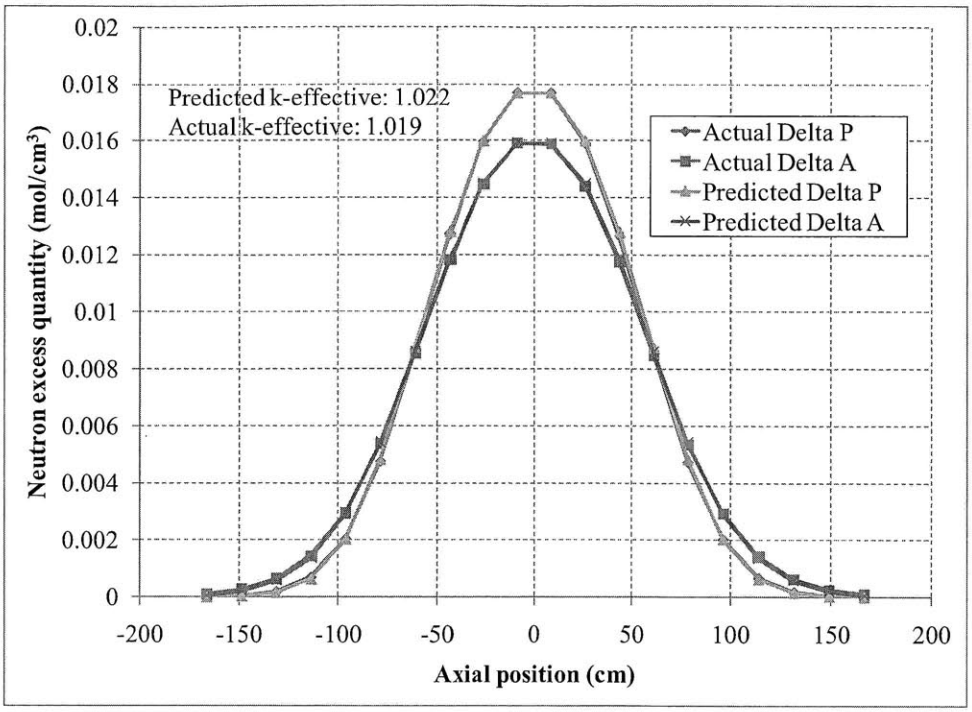

Figure 6.3-9. Comparison of MCNP model results with results from axial transfer model

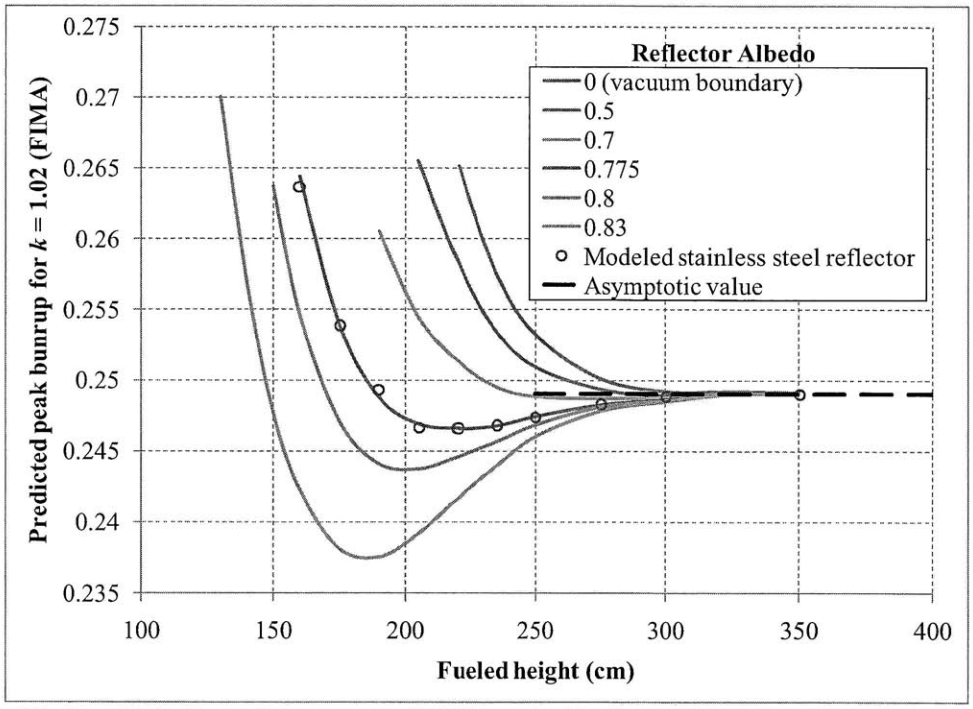

Figure 6.3-10. Predicted performance of different albedo reflectors using the axial transfer model

One other possibility that can be examined is what happens when there are different reflectors at each end of the fuel column; e.g. an engineered reflector/absorber on the bottom and a gas plenum on the top. An example of what occurs in this case is illustrated in Figure 6.3-11: the entire equilibrium cycle burnup distribution shifts somewhat (~10 cm) towards the end with the

higher albedo. This shift is also observed in mixed-reflector MCNPXT models of linear-assembly B&B reactors. Overall, this effect is small and likely only to be significant if one places a strong absorber at one end of the fuel.

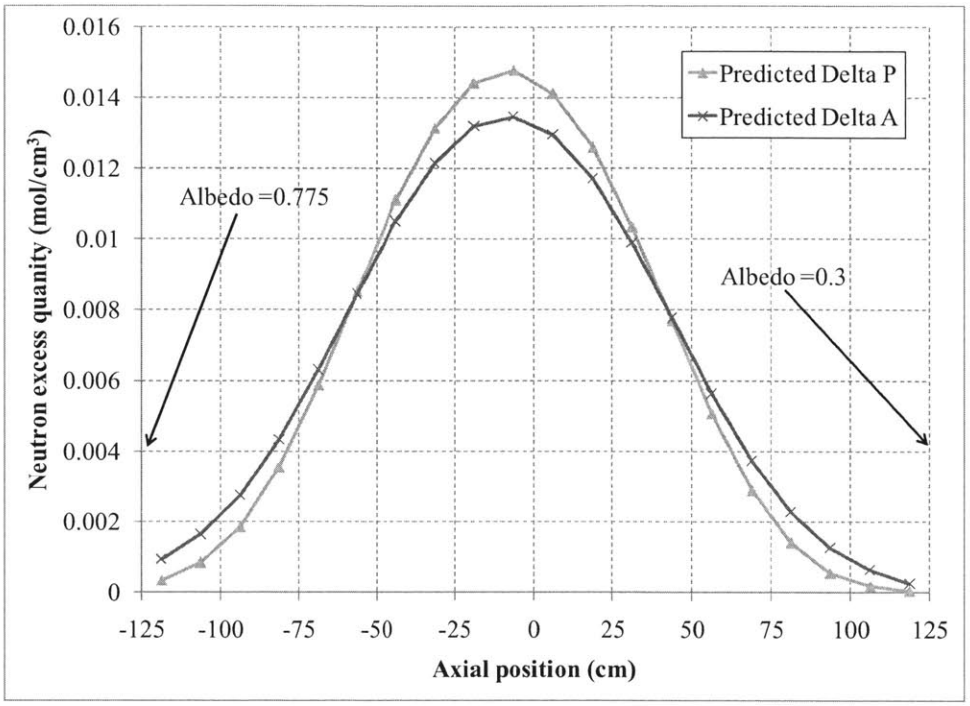

Figure 6.3-11. Predicted performance of mixed albedo reflectors using the axial transfer model

The fact that the axial burnup distribution in fuel only depends on a neutron excess curve and an axial transfer matrix has an important consequence. In a long fuel assembly (i.e. toward the asymptotic burnup in Figure 6.3-10), the axial transfer matrix does not depend on core composition; it is always shaped like a set of exponential drop offs with distance from the neutron source location, like the central curves in Figure 6.3-8. The characteristic length of the exponential drop offs would depend on the diffusion length of the core composition, but this only affects the width of the burnup distribution, not the peak burnup. As a result, the peak asymptotic burnup *only depends on the neutron excess curve of the core composition.* Therefore, the neutronic ranking of the core compositions in Chapter 5 also applies to linear-assembly B&B reactors: core compositions that require higher burnup in a minimum-burnup B&B reactor would also require higher burnup in a linear-assembly B&B reactor. Meanwhile, since a linear-assembly B&B reactor is more demanding neutronically (due to the non-uniform axial burnup distribution), some core compositions that would work marginally in a minimum-burnup B&B reactor would not be able to sustain critical operation in a linear-assembly B&B reactor.

6.3.3 Using the axial transfer model to predict a reactivity-burnup relationship

Interestingly, it is possible to combine the axial transfer model with the infinite-medium depletion approximation neutron excess curve (in Figure 6.3-5) to form rough estimates for average k-effective as a function of peak burnup. This is done in Figure 6.3-12, which shows the

results from Figure 6.3-1 alongside two predicted curves. The predictions as a function of peak DPA instead of peak burnup are shown in Figure 6.3-13.

The shape of the curves and the effect of adding a reflector agree well with the actual results, with the predicted *k*-effectives being approximately 1% lower at higher burnup. The prediction versus DPA is slightly better at predicting when *k*-effective equals unity. The accuracy of the axial transfer model prediction is remarkable considering how many assumptions and simplifications are used. Details about model geometry, flux, and depletion are almost all entirely discarded. Neutron excess properties are estimated using an infinite-medium model, and the axial transfer matrix is approximated using fixed material properties and a one-group diffusion calculation. These assumptions are expected to have greater error at higher values of burnup (due to changing fuel properties at higher burnup values), so such a prediction would not be as accurate for core compositions with poor neutronic performance.

This simple prediction can be used to approximately compare the burnup or DPA requirements of linear-assembly B&B reactors using different core compositions. For example, Figure 6.3-14 shows how the relationship between peak DPA vs. average *k*-effective changes when sodium coolant is replaced with helium. The results given are asymptotic values for average *k*-effective; i.e. axially long assemblies are assumed. For an equilibrium-cycle average *k*-effective of 1.03, switching from sodium to helium coolant reduces the required DPA from 490 to about 430. Therefore, a helium-cooled linear assembly B&B reactor may require on the order of 450 DPA, vs. 500 or higher for a sodium-cooled system.

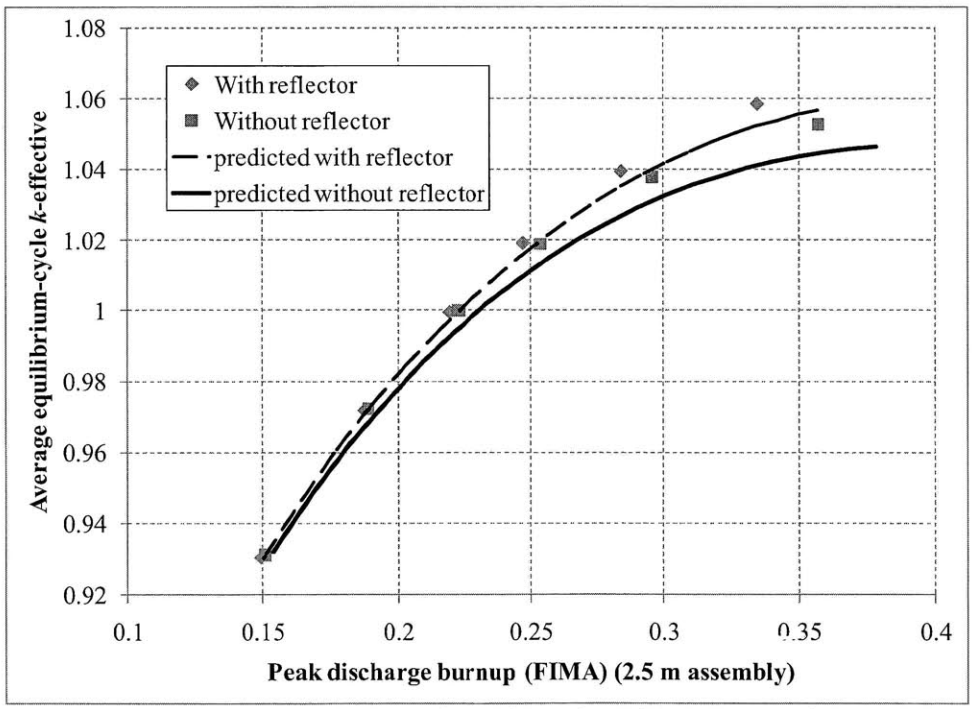

Figure 6.3-12. Predicting *k*-effective as a function of peak burnup using the axial transfer model and an infinite-medium depletion

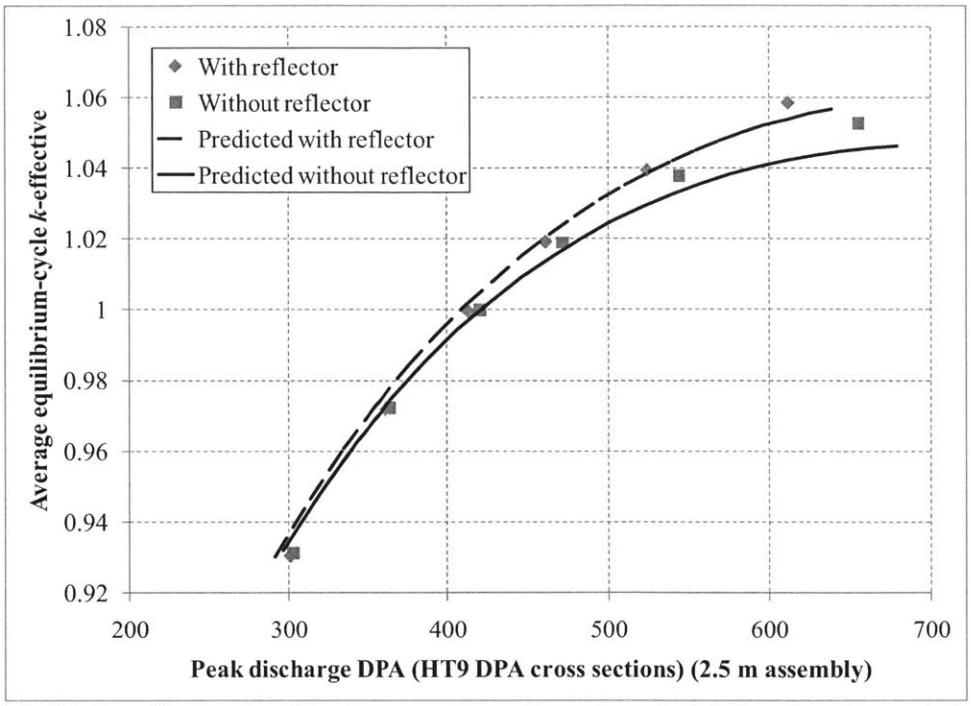

Figure 6.3-13. Predicting k-effective as a function of peak DPA using the axial transfer model and an infinite-medium depletion

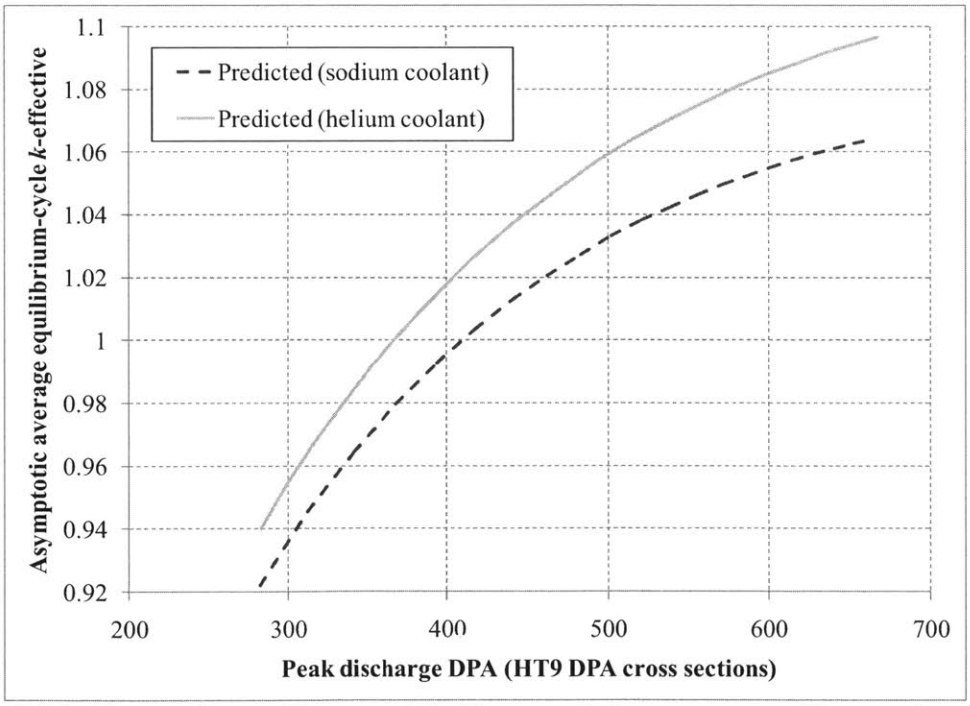

Figure 6.3-14. Comparing sodium- and helium-cooled core compositions using the axial transfer model and infinite-medium depletion prediction

6.4 Neutron excess quantities for linear-assembly B&B reactors

Section 6.3 shows how the combination of a neutron excess curve and an axial transfer matrix can be used to predict the axial distributions in a linear-assembly B&B reactor, as well as the relationships between *k*-effective, length, and peak burnup. The fact that the total absorption cross section is small compared to the scattering cross section means that both the neutron excess curve and axial transfer matrix vary only slightly with different radial geometries and shuffling sequences, so the same reactivity-burnup relationship is present in different reactor configurations. This finding is equivalent to the result for minimum-burnup B&B reactors, which also have reactivity-burnup relationships that do not depend strongly on different geometric and shuffling configurations.

Another important finding for minimum-burnup B&B reactors from Chapter 3 is how the neutron excess concept can be used to calculate the amount of starter fuel needed to start up a desired equilibrium cycle. The goal of this section is to develop a similar set of methods for linear-assembly B&B reactors that can be used to evaluate the neutron excess "cost" of a given equilibrium cycle, and estimate the neutron excess "worth" of a given starter assembly configuration. To accomplish this, several modifications need to be made to the neutron excess concept to account for the effects of having non-uniform axial distributions. First, the "adjusted neutron excess" quantity needs to be modified to account for varying axial leakage, and second, the effect of having different axial distributions of neutron excess needs to be evaluated. To better understand the neutron-excess behavior of linear-assembly B&B reactors, an example linear-assembly transition model is first constructed, described in Subsection 6.4.1.

6.4.1 Example linear-assembly transition model

The linear-assembly transition model consists of 2.0 m tall fuel assemblies with a composition of 75 parts U2Zr fuel, 25 parts void, 30 parts T91, and 100 parts sodium by volume, which is one of the best performing core compositions evaluated in Chapter 5. The model is reflected on the top and bottom by 1.0 m axial reflectors, using the same core composition except with T91 stainless steel substituting fuel and void. The length of the reflectors does not have a large impact on model behavior, so shorter reflectors can be substituted; replacing the top reflector with a fission gas plenum does not have a large effect either. Past the reflector on each end is a vacuum boundary. Fission product escape is modeled by assuming that 80% of noble fission products and fission product daughters (Kr and Xe) escape the fuel with a time constant of 100 seconds.

Axially, the model is divided into 22 axial zones: twenty 10 cm zones for the fuel and two 1 m zones for the reflectors. Radially, the model consists of 100 cylindrical shells, each with an area of $37^2\pi$ cm^2 (~4300 cm^2), corresponding to a total model radius of 3.7 m, which is large enough to eliminate essentially all radial leakage. The radial zones are large in order to reduce the number of degrees of freedom in the problem and permit faster evaluation of different shuffling options. Each radial zone has an area corresponding to 18 hexagonal assemblies with a pitch of 16.6 cm; in an actual system the fuel assemblies in each batch can be permuted so that each assembly would have the same discharge burnup.

Equilibrium cycle description

The equilibrium cycle shuffling sequence is a convergent-divergent pattern in which radial zones 11 and 12 are discharged at each cycle. The fact that two zones are discharged each cycle means that there are two separate but similar histories through the core. This particular equilibrium cycle was chosen so that the areal power density limit of ~600 MW/m^2 for this core composition would be satisfied while yielding a total reactor power of 2400 MW. A cycle length of 660 EFPY was selected, which is equal to about two years assuming a ~90% capacity factor. The ratio of the zone size to cycle length were chosen such that the equilibrium cycle discharge burnup would correspond to a BOEC *k*-effective of about 1.01. Equilibrium cycle *k*-effective values are given in Table 6.4-1. Equilibrium cycle power and DPA distributions are given in Figures 6.4-1 and 6.4-2.

Table 6.4-1. Uncontrolled *k*-effective of linear-assembly transition model equilibrium cycle

BOEC *k*-effective	1.007
MOEC *k*-effective	1.033
EOEC *k*-effective	1.056
"Average" *k*-effective	1.0327
Cycle reactivity swing (Δk-effective)	0.049

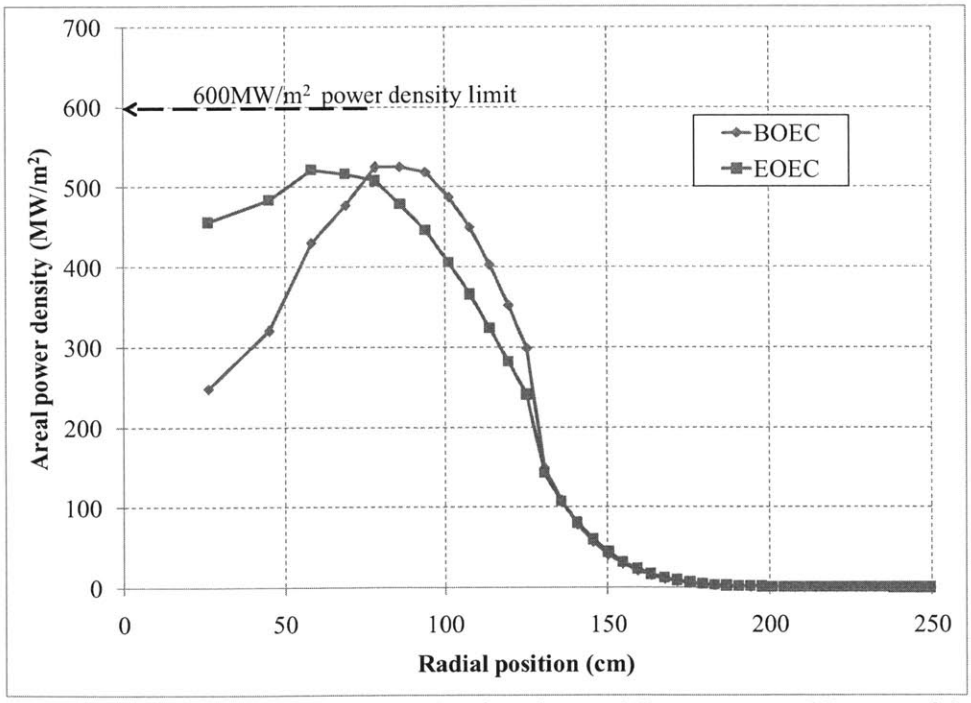

Figure 6.4-1. Equilibrium cycle power distributions of linear-assembly transition model

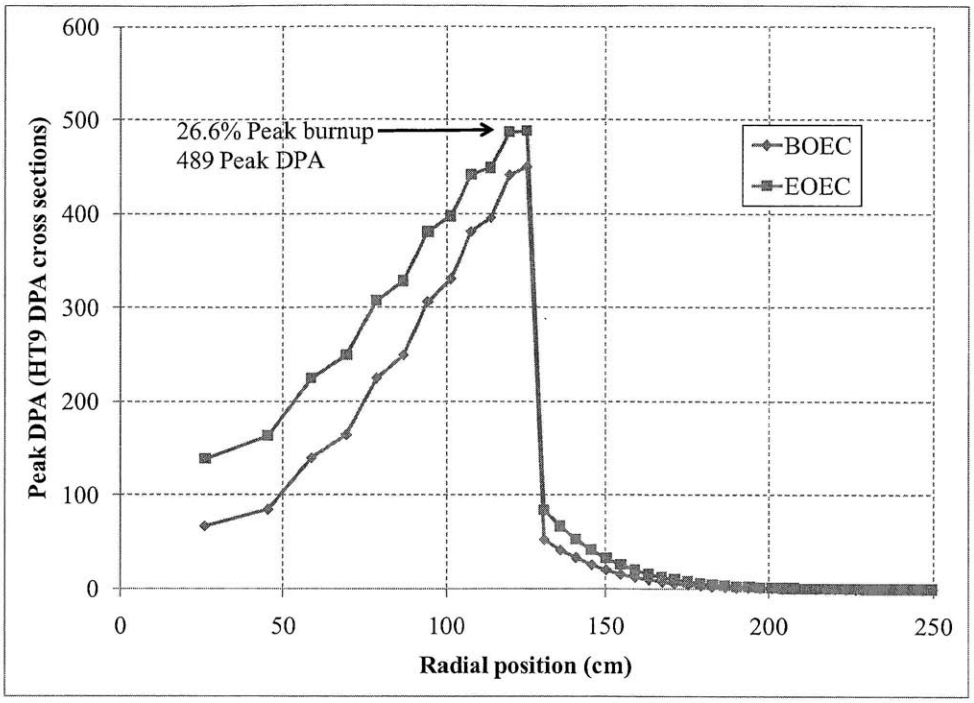

Figure 6.4-2. Equilibrium cycle peak DPA distributions and peak burnup of linear-assembly transition model

In Table 6.4-1, the "average" *k*-effective is obtained using the same neutron-absorption averaging as given in Equation 2.3-14, except integrating absorptions over fueled and axial leakage regions, not just fueled regions. As will be shown later in Subsection 6.4-2, this value of *k*-effective will be used in the definition for twice-adjusted neutron excess. Reactivity swing is large, almost 5%, which is a result of how the equilibrium cycle places fairly fresh fuel in a high flux region, causing it to breed quickly. This also results in the significant power swing seen in Figure 6.4-1. The power and reactivity swings can be reduced by shortening the cycle length; doing this would also allow a lower burnup since a lower average *k*-effective could be accommodated.

Transition sequence model

The starter fuel assemblies have the same composition as the feel fuel, but with 15% enriched uranium along the central 1.0 m of the core and 50 cm of depleted uranium on each end. There are twelve radial zones of starter fuel, corresponding to a starting enriched fissile load of 4.5 MT uranium-235. The number of starting zones is chosen to permit the power density limit of 600 MW/m^2 to be satisfied at the beginning of life. The power distribution of the beginning of life configuration is shown in Figure 6.4-3. Several interior positions are filled with feed fuel to bring the *k*-effective of the BOL state closer to unity, and to flatten the power distribution and facilitate breeding in the feed fuel. The inclusion of these interior blankets causes the BOL power distribution to look significantly different from the equilibrium cycle distribution; radial enrichment grading can be used to make the power distribution more uniform. At the end of the first cycle, the interior feed zones have increased in power after having plutonium bred in them, while the starter assemblies decrease in power, yielding a flatter power distribution.

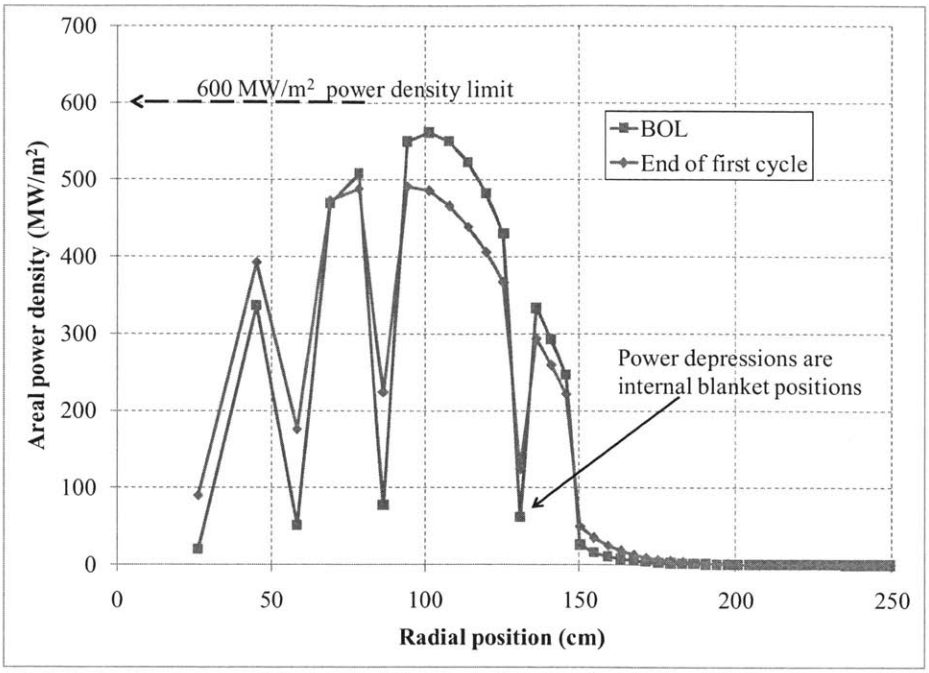

Figure 6.4-3. Linear-assembly transition model beginning of life power distributions

From this starting configuration, shuffles are performed to establish the desired equilibrium cycle. The overall goals of the shuffling sequence are similar to those from the example transition case in Section 3.5: minimize burnup and DPA and keep uncontrolled *k*-effective low to prevent neutron losses to control. Additionally, an areal power density constraint of 600 MW/m^2 was instituted so that the resulting power distributions are thermal-hydraulically coolable. Different shuffling possibilities were manually designed and modeled in MCNPXT, and the ones fitting the criteria given were selected. The selected fuel permutations in the example transition case are shown in Table 6.4-2.

Table 6.4-2. Startup shuffling sequence for linear-assembly transition model

Cycle number	Cycle Length (EFPD)	Fuel material permutation – position from center of core (only inner 20 zones shown out of 100)																			
0	0	1	2	3	4	5	6	7	8	9	10	11	12	13	14	15	16	17	18	19	20
1	660	13	1	14	2	3	15	4	5	6	7	8	9	16	10	11	12	17	18	19	20
2	660	15	12	14	11	16	10	1	9	8	13	2	7	3	6	17	4	18	19	20	21
3	660	15	14	5	16	13	4	12	6	17	3	11	7	2	10	18	1	19	20	21	22
4	660	17	13	16	14	15	18	9	8	1	5	10	19	2	7	11	3	20	21	22	23
5	660	19	18	17	13	16	14	15	20	4	6	12	8	9	3	11	21	22	23	24	25
6	660	21	20	19	18	17	13	16	15	14	22	7	2	10	1	5	23	24	25	26	27
7	660	23	22	21	20	19	12	6	18	17	13	16	14	15	24	25	26	27	28	29	30
8	660	25	24	23	22	21	11	4	20	19	18	17	13	15	26	27	28	29	30	31	32
9	660/462	26	25	24	23	22	21	20	19	18	17	14	16	27	28	29	30	31	32	33	34
10	660	28	27	26	25	24	23	22	21	20	19	18	17	29	30	31	32	33	34	35	36
11	660	30	29	28	27	26	25	24	23	22	21	20	19	31	32	33	34	35	36	37	38
12	660	32	31	30	29	28	27	26	25	24	23	22	21	33	34	35	36	37	38	39	40

In Table 6.4-2, the bold entries highlighted in lighter gray correspond to the positions of the starter fuel materials. The starter fuel zones are always arranged in order of DPA, with the lowest peak DPA closer to the central zone. The un-highlighted entries (in white) and entries highlighted in darker gray are zones containing feed fuel: the un-highlighted entries are lower DPA fuel that is arranged with *higher* peak DPA toward the center, while the highlighted entries are higher DPA feed fuel that are arranged in reverse: with *lower* peak DPA toward the center. The reversed feed allows the equilibrium cycle DPA/burnup distribution (Figure 6.4-2) to be reproduced, which is seen in cycles nine and higher by how the regions with reversed feed correspond to those in the equilibrium cycle.

Table 6.4-2 shows that at different points in the transition sequence, certain fuel materials are removed and subsequently put back; for example in cycle 3 starter fuel materials 8 and 9 are removed from the central 20 zones, then reintroduced at cycle 4. This is done because leaving all of the starter fuel in the central zones would result in a growing power producing area, which would increase the area of the core needing significant cooling. Temporarily removing starter fuel allows the power producing area to remain within the inner 16 zones. Since fuel that is removed in early cycles is at a low level of burnup/DPA, reintroducing it in later cycles allows it to be burned further. After cycle 9, the equilibrium cycle shuffling pattern is adopted.

The uncontrolled *k*-effective evolution of this shuffling scheme is shown in Figure 6.4-4. With a fixed cycle length, the beginning of cycle 9 (when all the starter fuel is removed) has a *k*-effective of about 1.063. To bring this down to ~1.05, and reduce burnup experienced by the fuel, cycle 9 was shortened by 30% from 660 EFPD to 462 EFPD.

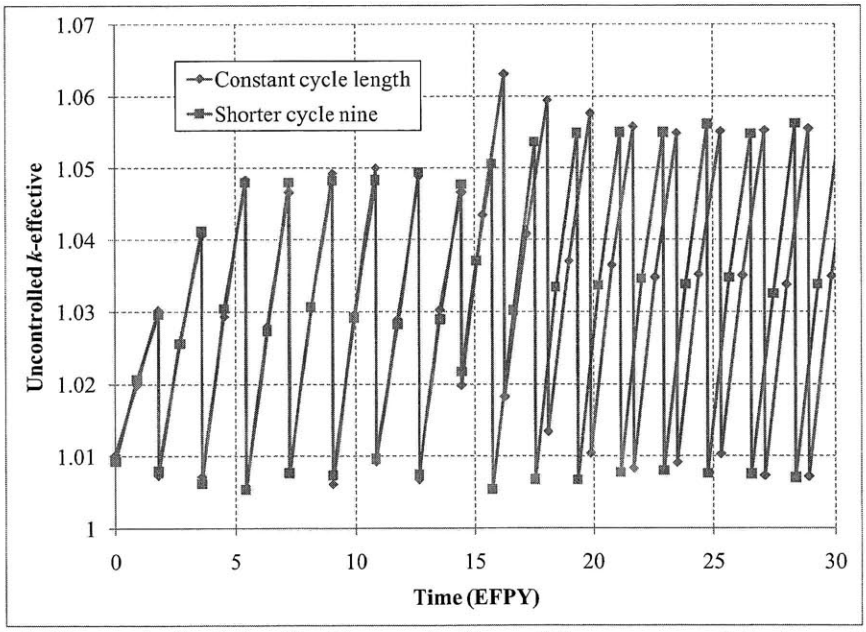

Figure 6.4-4. Uncontrolled *k*-effective evolution of linear-assembly transition model

The peak DPA distribution after twenty cycles is shown in Figure 6.4-5. Clearly, the peak DPA distribution in this example is not optimal: the starter fuel has only been burned to average of around 300 DPA, and some of the feed fuel has been burned past the equilibrium cycle value of 489 DPA to over 560 DPA. However, despite the non-optimal transition, this model still serves

as an example of how starter and feed assemblies deplete during transition. It can therefore be used as a comparison point for simple models designed to predict the worth of different starter fuel configurations. These simple models can then be used to determine a more appropriate starter fuel configuration for the given equilibrium cycle.

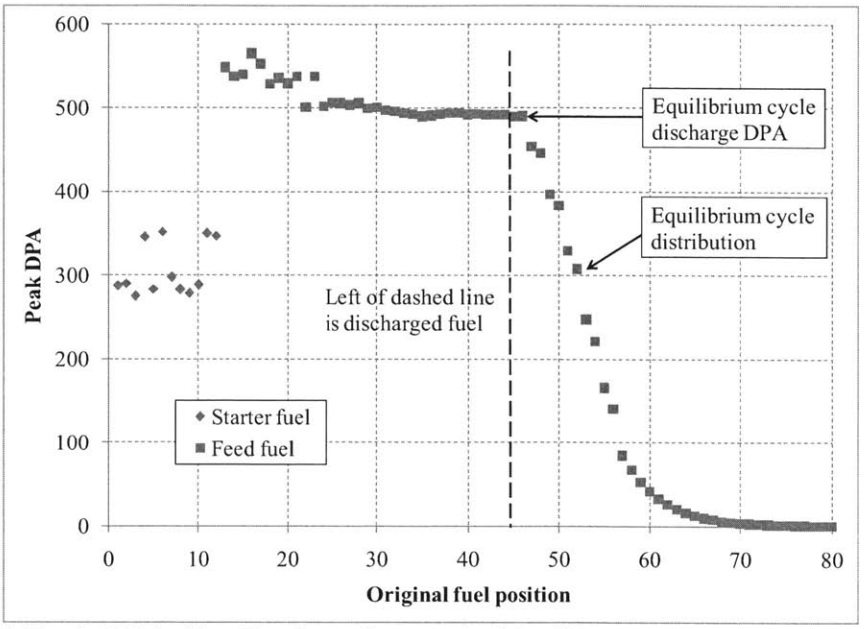

Figure 6.4-5. Peak DPA distribution after cycle 20 of linear-assembly transition model

In Chapter 2, a neutron excess balance expression was developed (Equation 2.4-20) for calculating the amount of starter fuel requirement of a given equilibrium cycle, reproduced here as Equation 6.4-1:

$$\int_{\substack{eq-cycle\\ fuel}} dV\left(\Delta N_{adj}\right) + \int_{\substack{starter\\ fuel}} dV\left(\Delta N_{adj}\right) + \int_{\substack{transition\\ feed\ fuel}} dV\left(\Delta N_{adj}\right) = \sum_{\substack{transition\\ cycles}} \left(\left(\overline{k_{fuel}} - \overline{k_{eq}}\right) \left(\int_{fuel} dV\left(\Delta A\right) \right) \Big|_{cycle} \right) \tag{6.4-1}$$

The right-hand side term corresponds to the deviation between the number of neutrons lost to leakage or control in a cycle and the expected losses based on the equilibrium cycle loss fractions. To explicitly write out $\overline{k_{fuel}}$ and $\overline{k_{eq}}$ in terms of these losses to leakage and control, two new quantities $\overline{F_{ctrl}}$ and $\overline{F_{leakage}}$ are defined in Equation 6.4-2, as the ratio between neutron absorptions in control or leakage and neutron absorptions in fuel over a cycle:

$$\overline{F_{ctrl}} \equiv \frac{\left(\int_{ctrl} dV\left(\Delta A\right) \right) \Big|_{cycle}}{\left(\int_{fuel} dV\left(\Delta A\right) \right) \Big|_{cycle}} \qquad \overline{F_{leakage}} \equiv \frac{\left(\int_{leakage} dV\left(\Delta A\right) \right) \Big|_{cycle}}{\left(\int_{fuel} dV\left(\Delta A\right) \right) \Big|_{cycle}} \tag{6.4-2}$$

As given in Equation 2.4-12, $\overline{k_{fuel}}$ is equal to the ratio of total neutron absorptions over a cycle to absorptions in fuel, which allows one to substitute the expressions in Equation 6.4-2 to obtain Equation 6.4-3. By analogy, $\overline{k_{eq}}$ can also be rewritten in terms of the equilibrium cycle equivalents of $\overline{F_{ctrl}}$ and $\overline{F_{leakage}}$, as given in Equation 6.4-4.

$$\overline{k_{fuel}} = \frac{\left(\int_{fuel} dV(\Delta A) + \int_{ctrl} dV(\Delta A) + \int_{leakage} dV(\Delta A) \right)\Big|_{cycle}}{\left(\int_{fuel} dV(\Delta A) \right)\Big|_{cycle}} = 1 + \overline{F_{ctrl}} + \overline{F_{leakage}} \tag{6.4-3}$$

$$\overline{k_{eq}} = 1 + \overline{F_{ctrl-eq}} + \overline{F_{leakage-eq}} \tag{6.4-4}$$

Substituting Equations 6.4-3 and 6.4-4 into the right-hand side term in Equation 6.4-1 yields Equation 6.4-5:

$$\left(\overline{k_{fuel}} - \overline{k_{eq}}\right)\left(\int_{fuel} dV(\Delta A) \right)\Big|_{cycle} = \left(\overline{F_{ctrl}} - \overline{F_{ctrl-eq}}\right)\left(\int_{fuel} dV(\Delta A) \right)\Big|_{cycle} + \left(\overline{F_{leakage}} - \overline{F_{leakage-eq}}\right)\left(\int_{fuel} dV(\Delta A) \right)\Big|_{cycle} \tag{6.4-5}$$

The two terms on the right side of Equation 6.4-5 are the neutron excess deviations due to control and leakage respectively. In a minimum-burnup B&B reactor, it is possible to approximate both terms as zero: the term due to control can be made close to zero by designing each transition cycle to have the same minimum *k*-effective and maximum *k*-effective, while the leakage in a minimum-burnup B&B reactor is small and fairly constant due to the blanket of feed fuel surrounding the core. Meanwhile, in a linear-assembly B&B reactor, there can be a more significant amount of axial leakage from the core, especially since the ideal assembly length (from Figure 6.3-10) is short enough for the flux distribution to extend into the reflector.

Figure 6.4-6 shows the respective contributions to neutron excess deviation from the linear-assembly transition model. The contribution due to control is significant (890 mol neutron excess, which as will be shown later corresponds to about ~325 kg U-235 worth of starter fuel), and results from the fact that the early cycles have an average uncontrolled *k*-effective closer to unity than the equilibrium cycle. This contribution can be reduced by increasing the length of the early cycles, which would be operationally desirable, or can be traded for a reduction in the required amount of fissile starter fuel.

The neutron excess contribution due to leakage is more than twice the contribution due to control. This occurs because the "leakage fraction" $\overline{F_{leakage}}$ during transition is different from the equilibrium cycle value. Figure 6.4-7 shows how the leakage fraction varies from cycle to cycle in the linear-assembly transition model; it starts at roughly 1% and grows to an equilibrium cycle value of about 3%. The large radial size of the model means that essentially all the leakage is in the axial direction. The leakage fraction changes because the initially short (1.0 m) enriched

region in the starter fuel does not cause much leakage, while the final equilibrium cycle extends farther along the length of the fuel and causes more leakage. Unlike with the contribution due to control, there is no way to reduce the leakage contribution without either changing the length of the fuel or changing the starter fuel design (e.g. making the enriched length longer). Therefore, an alternative formulation is needed that can account for varying neutron leakage, which is introduced in the next subsection as the "twice-adjusted" neutron excess.

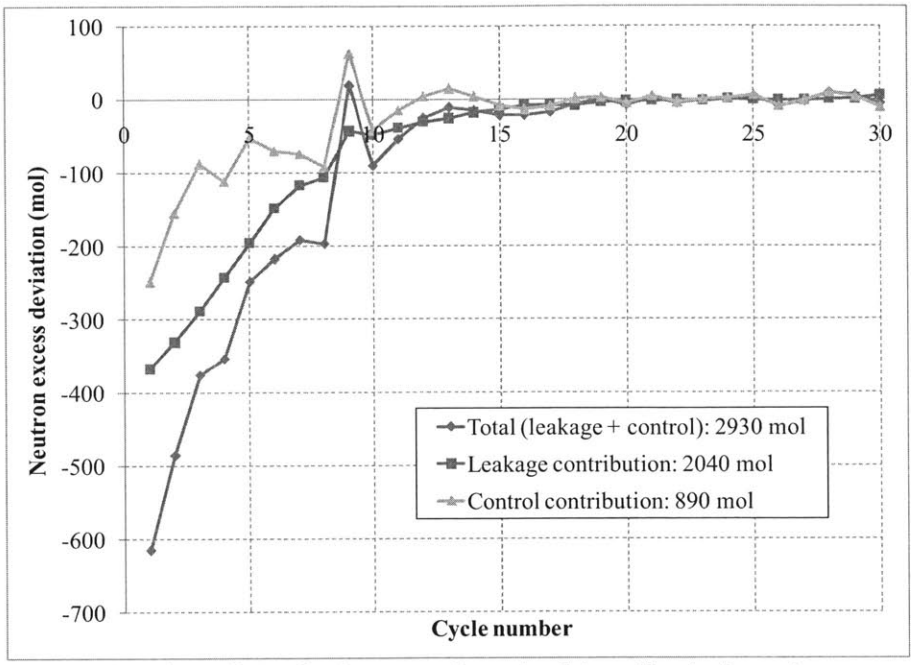

Figure 6.4-6. Contributions from leakage and control to adjusted neutron excess in linear-assembly transition model

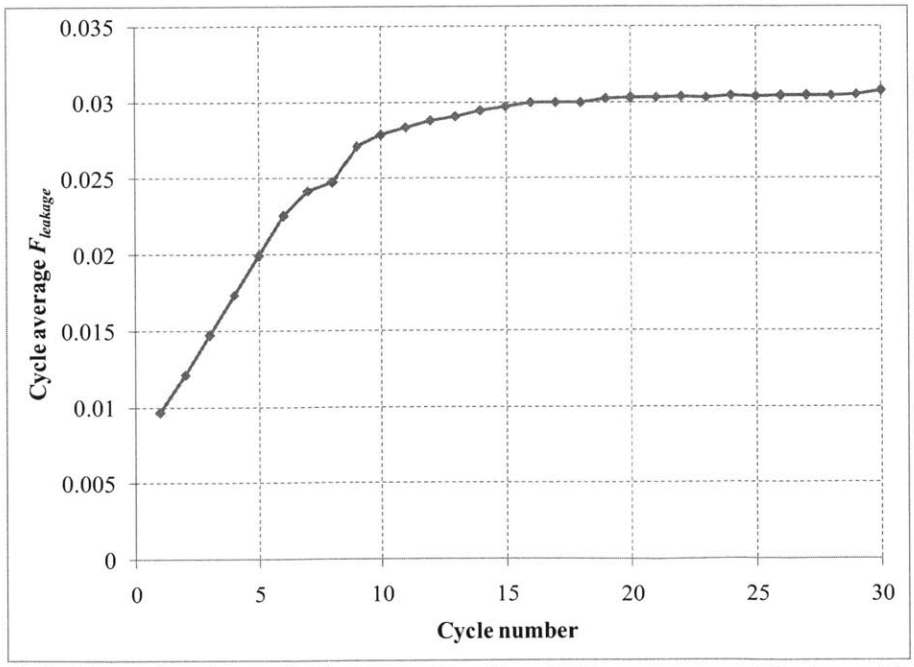

Figure 6.4-7. Variation in cycle leakage fraction in linear-assembly transition model

6.4.2 Definition of twice-adjusted neutron excess

To account for variable leakage, the definitions of $\overline{k_{fuel}}$ and $\overline{k_{eq}}$ are changed to also include neutrons absorbed in axial leakage regions as well. The new quantity, $\overline{k_{fuel2}}$, is defined in Equation 6.4-6, while $\overline{k_{eq2}}$ is the equilibrium cycle value of $\overline{k_{fuel2}}$:

$$\overline{k_{fuel2}} \equiv \frac{\left(\int_{fuel} dV(\Delta P)\right)\Big|_{cycle}}{\left(\int_{fuel} dV(\Delta A) + \int_{axial} dV(\Delta A)\right)\Big|_{cycle}} = \overline{k}\frac{\left(\int_{fuel} dV(\Delta A) + \int_{ctrl} dV(\Delta A) + \int_{radial} dV(\Delta A) + \int_{axial} dV(\Delta A)\right)\Big|_{cycle}}{\left(\int_{fuel} dV(\Delta A) + \int_{axial} dV(\Delta A)\right)\Big|_{cycle}} \tag{6.4-6}$$

In Equation 6.4-6, absorptions in leakage regions have been split into two terms: a "radial" term corresponding to radial leakage and an "axial" term corresponding to axial leakage. The "radial" and "axial" labels do not necessarily have to correspond to radial and axial leakage; instead what differentiates the two types of leakage is that the "radial" component is roughly constant over every cycle while the "axial" component may vary during the transition cycles. Equation 6.4-6 shows that the k-effective of an uncontrolled system with no radial leakage is equal to k_{fuel2}, similar to how in a system with no leakage (radial or axial) the uncontrolled k-effective is equal to k_{fuel} (Equation 2.3-6).

Using these definitions, the neutron excess balance equation (Equations 2.4-17 and 6.4-1) can be rewritten as:

$$\int_{fuel+axial} dV\left(\Delta P - \overline{k_{eq2}}\Delta A\right) = \sum_{\substack{transition \\ cycles}} \left(\left(\overline{k_{fuel2}} - \overline{k_{eq2}}\right)\left(\int_{fuel+axial} dV(\Delta A)\right)\Big|_{cycle} \right) \tag{6.4-7}$$

The derivation of Equation 6.4-7 exactly mirrors that of Equation 2.4-17, except $\overline{k_{fuel}}$ and $\overline{k_{eq}}$ have been substituted with $\overline{k_{fuel2}}$ and $\overline{k_{eq2}}$, and the volume integrals have been extended to include axial leakage regions in addition to the fuel. The axial-leakage terms multiplied by $\overline{k_{eq2}}$ are the same on each side of Equation 6.4-7:

$$\int_{axial} dV\left(\overline{k_{eq2}}\Delta A\right) = \sum_{\substack{transition \\ cycles}} \overline{k_{eq2}}\left(\int_{axial} dV(\Delta A)\right)\Big|_{cycle} \tag{6.4-8}$$

Subtracting the axial-leakage integrals from each side of Equation 6.4-7 and cancelling the terms in Equation 6.4-8 yields Equation 6.4-9:

$$\int_{fuel} dV\left(\Delta P - \overline{k_{eq2}}\Delta A\right) - \sum_{\substack{transition \\ cycles}} \left(\overline{k_{fuel2}}\left(\int_{axial} dV(\Delta A)\right)\Big|_{cycle} \right) = \sum_{\substack{transition \\ cycles}} \left(\left(\overline{k_{fuel2}} - \overline{k_{eq2}}\right)\left(\int_{fuel} dV(\Delta A)\right)\Big|_{cycle} \right) \tag{6.4-9}$$

Since there are no fissions in the axial leakage region, the ΔP term in that region can be omitted. The remaining axial-leakage absorption term can be rewritten by substituting the expression for $\overline{k_{fuel2}}$ from Equation 6.4-6 to obtain Equation 6.4-10:

$$\overline{k_{fuel2}}\left(\int_{axial} dV(\Delta A)\right)\Big|_{cycle} = \frac{\left(\int_{fuel} dV(\Delta P)\right)\Big|_{cycle}}{\left(\int_{fuel} dV(\Delta A) + \int_{axial} dV(\Delta A)\right)\Big|_{cycle}} \left(\int_{axial} dV(\Delta A)\right)\Big|_{cycle} \tag{6.4-10}$$

The right side of Equation 6.4-10 can be simplified by noting that three of the terms (shown in Equation 6.4-11) combine to form the conditional probability (F'_{axial}) that a neutron produced is absorbed in an axial-leakage region, *provided that it does not leak radially or get absorbed in control*:

$$\overline{F'_{axial}} \equiv \frac{\left(\int_{axial} dV(\Delta A)\right)\Big|_{cycle}}{\left(\int_{fuel} dV(\Delta A) + \int_{axial} dV(\Delta A)\right)\Big|_{cycle}} \tag{6.4-11}$$

Combining this expression with Equation 6.4-10 yields Equation 6.4-12:

$$\overline{k_{fuel2}}\left(\int_{axial} dV(\Delta A)\right)\Big|_{cycle} = \overline{F'_{axial}}\left(\int_{fuel} dV(\Delta P)\right)\Big|_{cycle} = \left(\int_{fuel} dV(\Delta P f'_{axial})\right)\Big|_{cycle} \tag{6.4-12}$$

In Equation 6.4-12, f'_{axial} is the cumulative conditional probability that the neutrons created by a given differential volume fuel element dV leak axially from the fuel, provided that they *do not* leak radially or get absorbed in control. For example, suppose at some point in its depletion, a volume of fuel has produced 0.01 moles of neutrons/cm^3, and 5% of these neutrons were absorbed in control, 3% in axial leakage, and the remaining 92% in fuel. At this point in its depletion, f'_{axial} for the volume of fuel is equal to 3%/95% = 3.16%, and $\Delta P f'_{axial}$ is equal to 0.000316 mol/cm^3.

The reason that the *conditional* probability of axial leakage is used rather than the unconditional probability is that the conditional probability is simpler to predict: the fraction of neutrons lost to control or radial leakage has a stronger effect on the unconditional probability than the conditional probability. For example, consider two equivalent reactors with similar flux distributions in which one has none of its neutrons lost to control and the other has 10% of its neutrons lost to control. The latter reactor would have an unconditional axial leakage probability about 91% (=100/110) as large as the former reactor, while both reactors would have similar conditional axial leakage probabilities due to their similar flux distributions.

Substituting Equation 6.4-12 into the left-hand side of Equation 6.4-9 gives a new neutron excess quantity, the *twice-adjusted* neutron excess, defined in Equation 6.4-13:

$$\Delta N_{adj2} \equiv \Delta P(1 - f'_{axial}) - \overline{k_{eq2}}\Delta A \tag{6.4-13}$$

Like, the adjusted neutron excess, the twice-adjusted neutron excess is only defined for fueled regions. Substituting the twice-adjusted neutron excess into Equation 6.4-12 gives Equation 6.4-14, which is the neutron-excess balance equation for linear-assembly B&B reactors:

$$\int_{fuel} dV(\Delta N_{adj2}) = \sum_{\substack{transition \\ cycles}} \left(\left(\overline{k_{fuel2}} - \overline{k_{eq2}}\right) \left(\int_{fuel} dV(\Delta A) \right) \Big|_{cycle} \right) \tag{6.4-14}$$

The definition of twice-adjusted neutron excess includes a variable term (f'_{axial}) for the neutrons that are lost to axial leakage as well as a constant term ($\overline{k_{eq2}}$) those lost to control and radial leakage. Like for the adjusted neutron excess, the quantity contained in a system becomes constant once the equilibrium cycle is established. The total twice-adjusted neutron excess does not change if the fraction of neutrons lost to radial leakage and control over a cycle equals the equilibrium cycle value. The amount of axial leakage can change over transition cycles without changing the amount of twice-adjusted neutron excess in a system, since the definition of twice-adjusted neutron excess accounts for axial leakage through the f'_{axial} term.

In a linear-assembly B&B reactor, the leakage term f'_{axial} depends primarily on the axial position of the fuel where the neutrons were produced, and is fairly constant over the life of the fuel. There are several ways to evaluate f'_{axial}, first, one can customize a transport code to explicitly follow neutron histories and output a measurement of f'_{axial}. Second, one can approximate f'_{axial} using a simplified model, such as the axial transfer model from Subsection 6.3.2. Finally, one can deplete simple models of fuel compositions (e.g. an infinite plane of starter fuel assemblies) and obtain the total axial leakage as a function of depletion.

6.4.3 Applying twice-adjusted neutron excess to the linear-assembly transition model

The twice-adjusted neutron excess satisfies a neutron excess balance equation that has the fuel contribution on one side balanced by the reactivity-deviation contribution on the other, given in Equation 6.4-14. Explicitly writing out the different types of fuel contributions gives Equation 6.4-15:

$$\int_{\substack{cycle \\ fuel}} dV(\Delta N_{adj2}) + \int_{\substack{starter \\ fuel}} dV(\Delta N_{adj2}) + \int_{\substack{transition \\ feed\ fuel}} dV(\Delta N_{adj2}) = \sum_{\substack{transition \\ cycles}} \left(\left(\overline{k_{fuel2}} - \overline{k_{eq2}}\right) \left(\int_{fuel} dV(\Delta A) \right) \Big|_{cycle} \right) \tag{6.4-15}$$

To evaluate the ΔN_{adj2} of fuel, the value of f'_{axial} is estimated using the simple axial transfer model; i.e., a neutron diffusion approximation. This is a valid approximation because as shown in Figures 6.3-6 and 6.3-7, the properties of the fuel do not vary greatly with material depletion. Under this approximation, f'_{axial} is constant with depletion and only depends on the axial position

of the fuel. For a 2.0 m long assembly with boundaries that have an albedo of 0.775 (corresponding to a stainless steel reflector), the value of f'_{axial} as a function of axial position is shown in Figure 6.4-8.

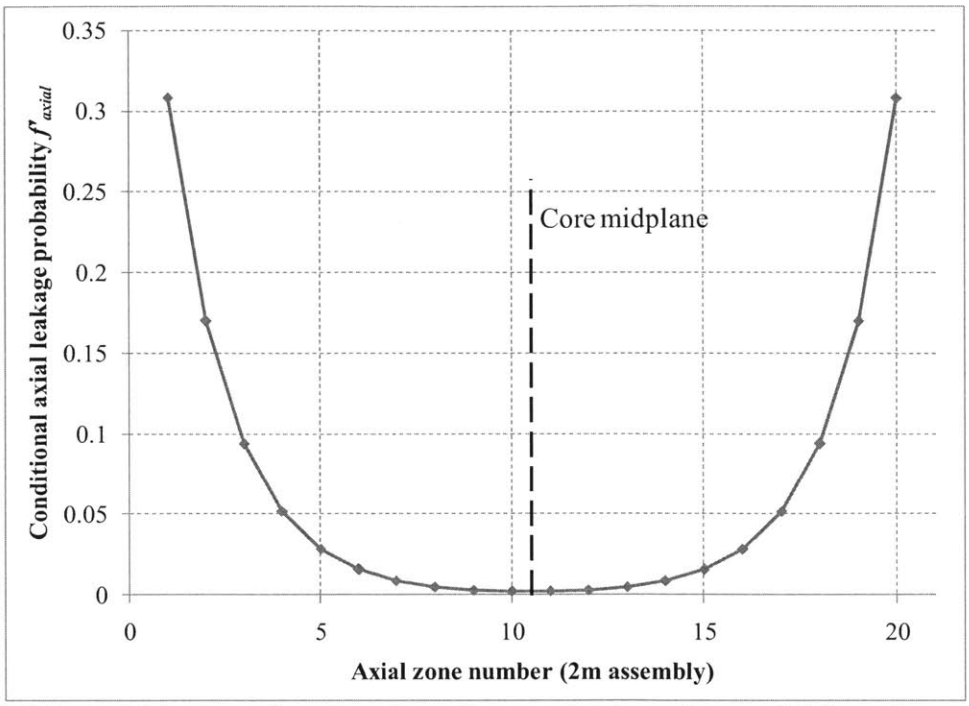

Figure 6.4-8. Axial leakage fraction f'_{axial} from axial transfer model for a 2 m assembly

With the axial leakage function f'_{axial} from Figure 6.4-8, it is possible to evaluate each of the terms in Equation 6.4-15 in the linear-assembly transition model. The leftmost term is the neutron excess contained in the chosen equilibrium cycle. The value of this term is shown in Figure 6.4-9, with each point in the figure being the value of ΔN_{adj2} integrated over a given radial zone (as a result, the units are moles of neutrons since the integral is being taken over a volume). The value of k_{eq2} used to calculate twice-adjusted neutron excess is the average uncontrolled k-effective given in Table 6.4-1. Summing over all the radial zones yields a total neutron excess of **-1.09E4 mol**. Again, the total neutron excess is the same at both the beginning and end of the equilibrium cycle, since the discharged fuel has a total neutron excess of zero.

Figure 6.4-10 shows the value of the rightmost term in Equation 6.4-15. Since the value of twice-adjusted neutron excess assumes that a fixed fraction of neutrons are lost to control each cycle, cycles in which more or fewer neutrons are lost to control cause the total neutron excess of a system to change (deviations due to variations in radial leakage would be included here as well, however the model considered has no radial leakage present). In the linear-assembly transition model, the first eight transition cycles have a lower average k_{fuel2} than the equilibrium cycle, which causes the total neutron excess of the system to become negative. The lower average k_{fuel2} is due to the fact that the starter configuration has a slower rate of reactivity change than the equilibrium cycle, so for a constant cycle length the average k-effective is lower. In total this reduces the neutron excess requirement of the equilibrium cycle by **810 mol**. This can be taken advantage of in two ways: first, the initial reactor cycles can be made longer to improve the capacity factor of the system (which is desirable to increase the revenue stream of a new reactor);

alternately, one can take advantage of the "bonus" neutron excess this provides to reduce the amount of starter fuel needed. In this case, taking the reactivity contribution as zero would be a conservative assumption.

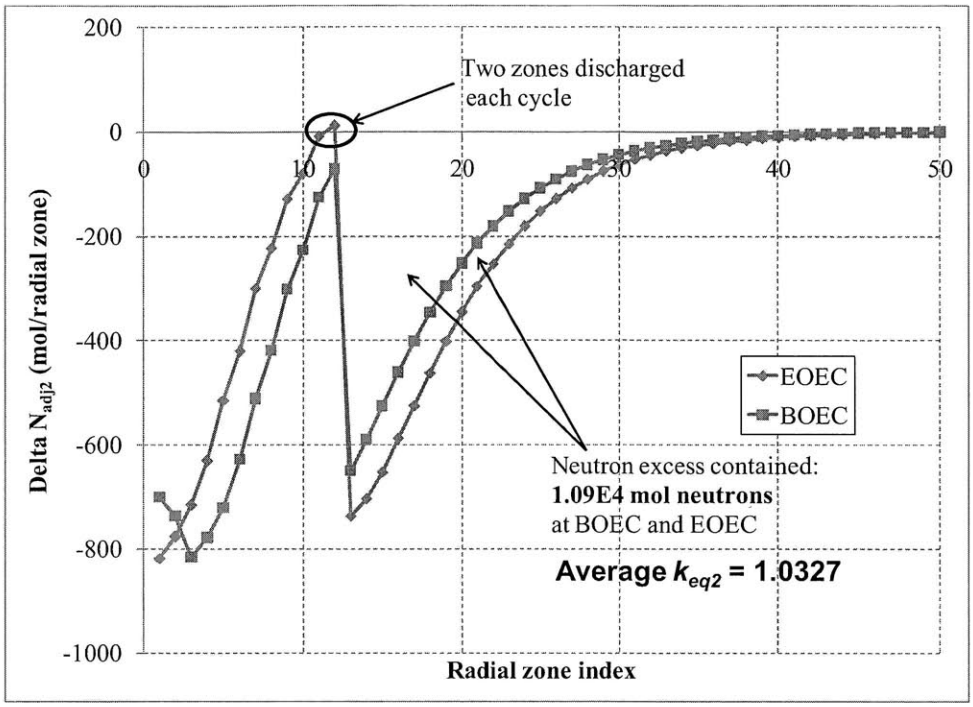

Figure 6.4-9. Twice-adjusted neutron excess of linear-assembly transition model equilibrium cycle

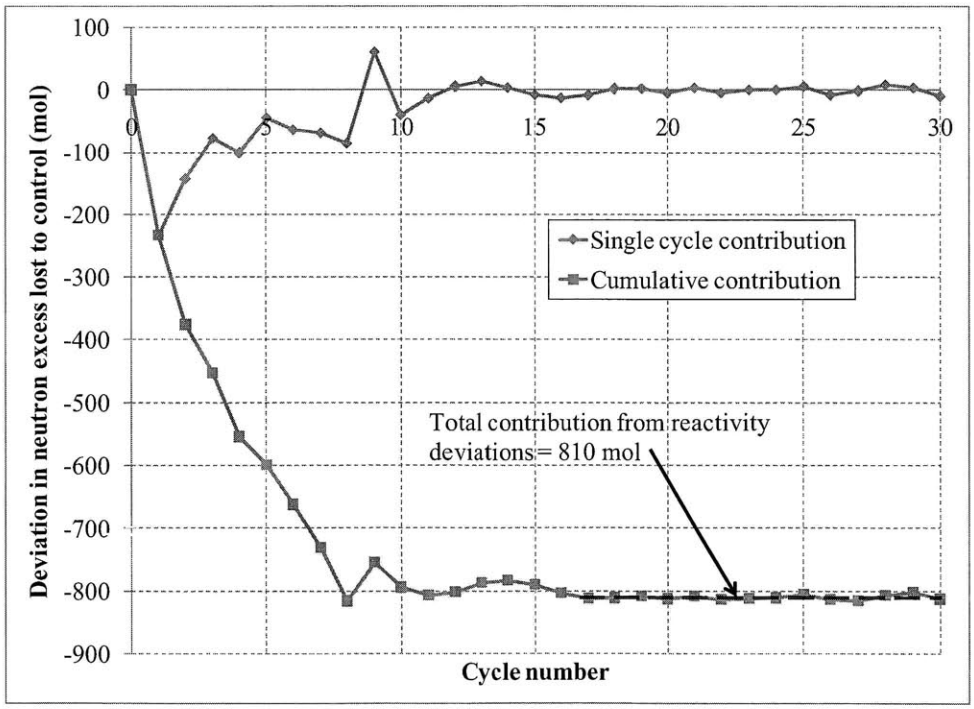

Figure 6-4.10. Contribution of reactivity deviations to system neutron excess in linear-assembly transition model

Finally, the contributions due to the starter and feed fuel are shown in Figure 6.4-11. The starter fuel contributes a total of **9.02E3 mol** to the neutron excess, while the transition feed fuel contributes **1.24E3 mol**. The substantial contribution from the transition feed fuel is mostly a consequence of the fact that it has been burned significantly beyond the equilibrium cycle peak DPA of ~490 DPA; if the transition feed fuel had only been burned to this limit then its contribution would have been much closer to zero.

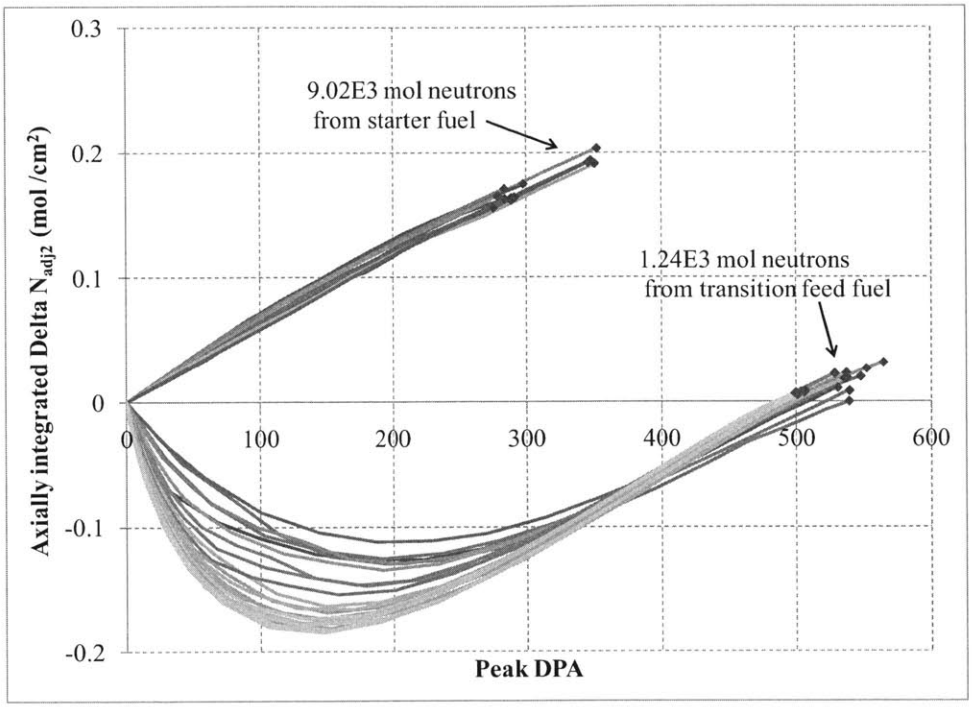

Figure 6-4.11. Contribution of fuel depletion to system neutron excess in linear-assembly transition model

Together, the contribution from the fuel and reactivity deviations yield **1.11E4 mol** neutron excess for establishing the equilibrium cycle, which is slightly higher than the 1.09E4 mol measured as the neutron excess requirement. The ~200 mol neutron excess difference is a result of the error in estimating the number of leakage neutrons. Figure 6.4-12 shows a comparison between the actual number of leakage neutrons each cycle and the amount predicted using the axial transfer model. The axial transfer model tends to underestimate leakage early in core life, when the fuel largely consists of fresh depleted uranium, which is relatively transparent to neutrons. Since there is actually more leakage than predicted, the total twice-adjusted neutron excess of the fuel would be slightly lower than the calculated value. The error from using the axial transfer function to estimate leakage is over an order of magnitude smaller (180 mol vs. 2040 mol, from Figure 6.4-6) than the neutron excess deviation from assuming constant leakage when using adjusted neutron excess instead of twice-adjusted neutron excess.

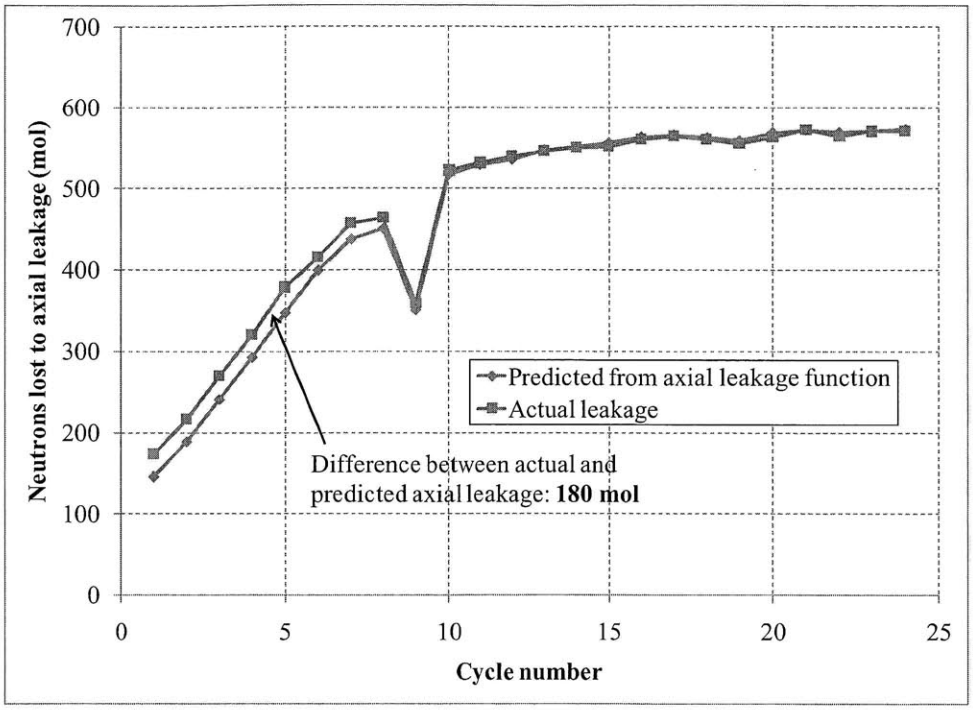

Figure 6.4-12. Comparison of actual axial leakage and prediction from axial leakage model

6.5 Estimating neutron excess for linear-assembly B&B reactors using simple models

Section 6.4 demonstrates how a neutron-excess balance equation (Equation 6.4-15) for the twice-adjusted neutron excess ΔN_{adj2} (Equation 6.4-13) applies to linear-assembly B&B reactors. If it is possible to estimate the twice-adjusted neutron excess for a given configuration of starter fuel, then Equation 6.4-13 allows one to calculate the required amount of starter fuel in the same manner as was done for minimum-burnup B&B reactors in Section 3.5. A simple and fairly accurate method for estimating twice-adjusted neutron excess is to simply deplete an infinite-plane model of the starter assembly configuration, analogous to using an infinite-medium depletion to study different starter fuels for a minimum burnup B&B reactor.

6.5.1 Infinite-plane depletion approximation

The infinite-plane depletion approximation involves taking a starter fuel configuration of interest and extending it radially into an infinite plane with the same axial arrangement (fuel length, distribution of enrichment, and reflector/shield) as the starter fuel. The resulting one-dimensional model (referred to as either the infinite-plane model or 1D model) can be depleted in its own self-consistent spectrum and axial flux distribution, yielding results for axially-integrated ΔN_{adj2} as a function of peak burnup or DPA.

Figure 6.5-1 compares the results in Figure 6.4-11 to the prediction from an infinite-plane depletion calculation. The results compare very well: for the same peak DPA as the discharged starter assemblies, the infinite-plane depletion estimates a total neutron excess contribution of

8.66E3 mol from the starter fuel, just 4% less than the amount measured in the linear-assembly transition model. Figure 6.5-1 also compares the feed fuel neutron excess curves to the equilibrium cycle neutron excess curves. There are two equilibrium cycle histories because two zones are shuffled each cycle, resulting in two separate paths through the core. Feed fuel histories initially differ significantly from the equilibrium cycle histories, but eventually converge to the equilibrium cycle histories.

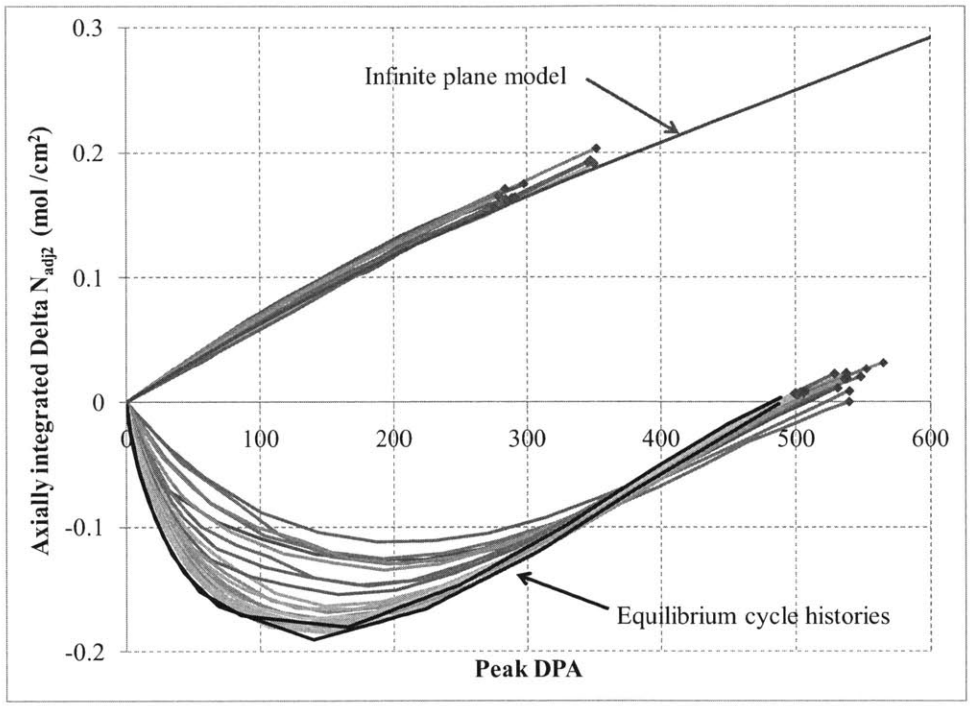

Figure 6.5-1. Comparing neutron excess vs. peak DPA of linear-assembly transition model and infinite-plane model

The differences between the infinite-plane prediction and the results from the transition model are due to the different flux spectral histories and axial profiles encountered during depletion. Figure 6.5-2 compares the axial distribution of DPA from the two different models, and shows that there is relatively little difference in axial fluence distribution. To evaluate the effect of varying axial distributions, the results from the 1D model were made to artificially match the axial distributions from the transition model, by linearly interpolating the neutron excess contribution based on the DPA experienced at each axial node. The results of this comparison are given in Figure 6.5-3. Figure 6.5-3 shows that simply matching the axial shape yields less than a 1% change in neutron excess when compared to the default 1D model, accounting for only a small fraction of the 4% discrepancy observed. Further, the differences in axial distribution do not explain the large spread seen in the different starter fuel assemblies.

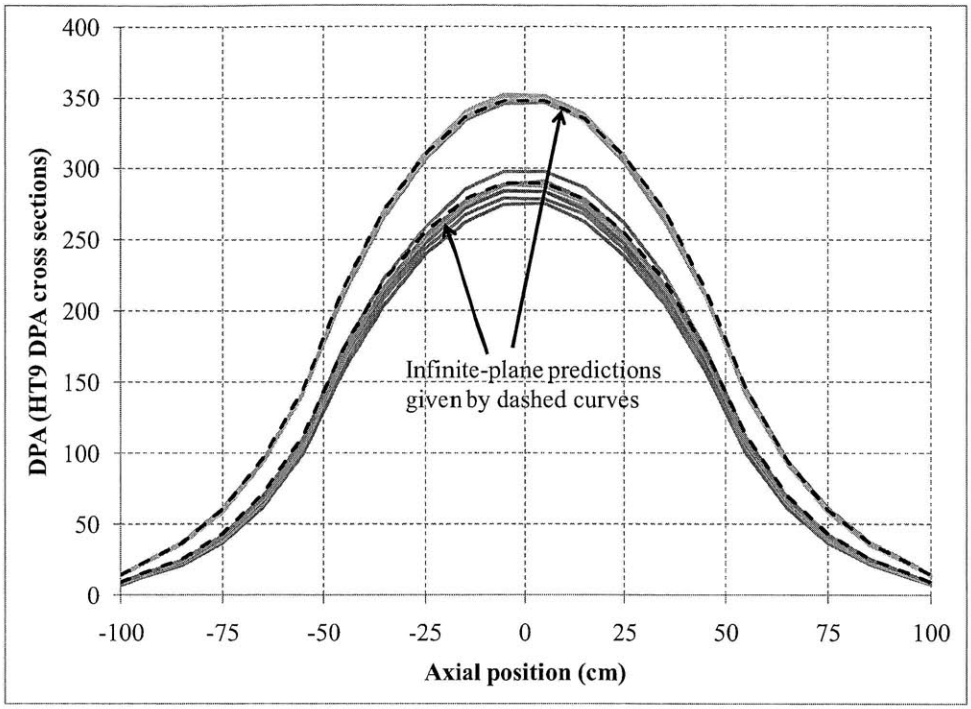

Figure 6.5-2. Comparison between infinite-plane and transition model axial DPA distributions

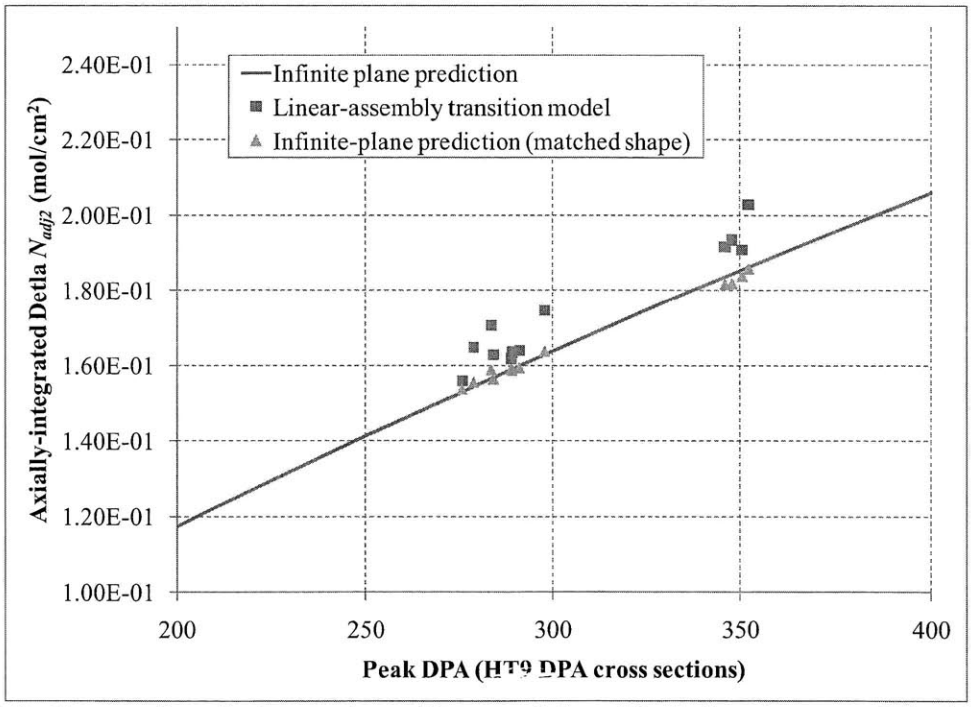

Figure 6.5-3. Comparison between transition model and infinite-plane model with matched axial shape

The other difference between depletion in the two models is the spectral history encountered. The individual spectral histories of the starter fuel can be complex, as starter fuel experiences a range of spectra as it is shuffled from the center of the power-producing region (which has a

harder spectrum) to its periphery (which has a softer spectrum) (for example, see Figures 3.5-11 and 3.5-15). Instead of plotting results for individual starter assemblies, Figure 6.5-4 plots the fast flux fraction experienced at the fuel midplane for the entire group of starter assemblies as a function of peak DPA. The 0^{th} and 100^{th} percentile lines are the minimum and maximum fast flux fraction experienced, and the 15^{th}, 50^{th}, and 85^{th} percentile lines are the minimum fast flux fraction of at least that percentage of the flux experienced by the starter fuel. Meanwhile, the fuel in the infinite-plane model experiences a gradually varying spectrum with a fast flux fraction that roughly approximates that experienced by the transition model fuel.

Figure 6.5-4 shows that on average, the spectrum experienced by the transition model fuel starts slightly softer than in the infinite-plane model, but becomes harder toward the end of irradiation. This harder spectrum at the end of irradiation causes a greater amount of neutron excess to be produced, because fewer neutrons are parasitically absorbed in fission products. Figure 6.5-4 also shows that parts of the starter fuel experiences very soft spectra, for example at the pronounced dip between 90 and 130 DPA; this occurs when the starter fuel is shuffled to a peripheral position in the core. However, the flux experienced at these positions is relatively low, and Figure 6.504 shows that 70% of starter flux has a spectrum within a relatively narrow band around the median fast flux fraction.

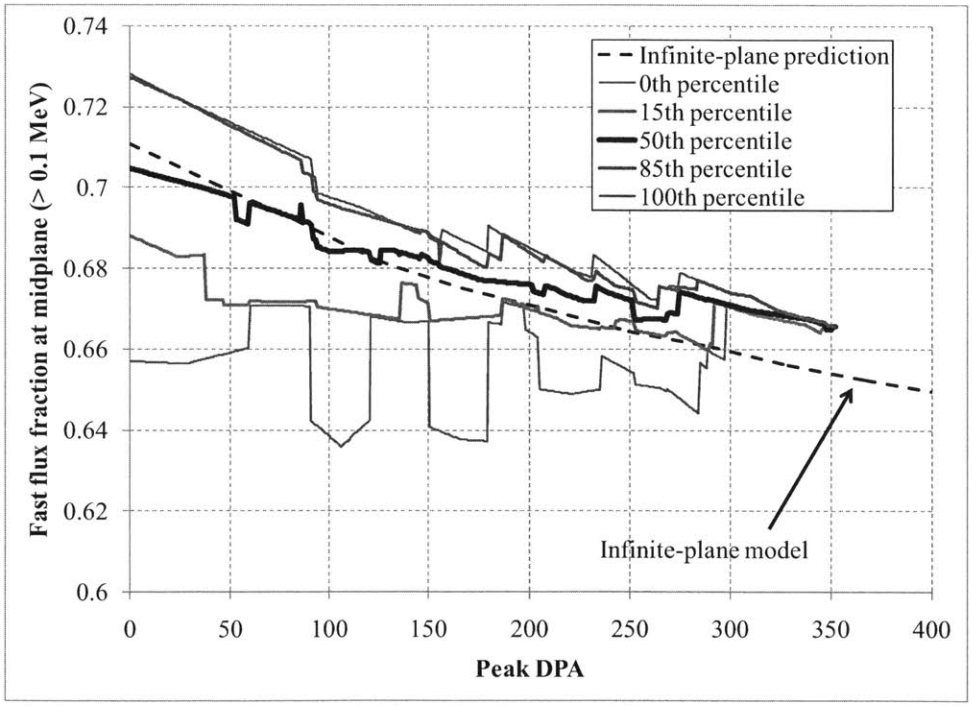

Figure 6.5-4. Comparison of spectral histories in transition model and infinite-plane model

A comparison between midplane fast fluence fraction and the amount of neutron excess obtained is shown in Figure 6.5-5. The y-axis is the ratio of neutron excess produced by a starter fuel assembly in the transition model and that produced by the infinite-plane model when burned to the same peak DPA. The x-axis gives the fraction of fluence composed of >0.1 MeV neutrons experienced over the irradiation history of the midplane of the assembly. Figure 6.5-5 shows there is only a rough correlation between the average hardness of the neutron spectrum

encountered by an assembly and the neutron excess it produces. However, the large scatter among the points in the transition model show that midplane fast fluence fraction does not completely explain the differences in neutron excess, and that the spectral history effects in Figure 6.5-4 are significant as well.

To better capture the neutron spectral effect and yield more accurate starter fuel neutron excess predictions, one possible option is to switch from using an infinite-plane model to modeling a two- or three-dimensional reactor model with a desired starter configuration, then simply depleting the entire reactor model without shuffling. This would better match the initial neutron spectrum in actual reactor models without requiring a complex fuel management scheme to be developed.

The conclusions in this section are also supported by results from an additional transition model described in Section 6.6, which uses discharged feed fuel from a linear-assembly B&B reactor to start up an additional linear-assembly B&B reactor.

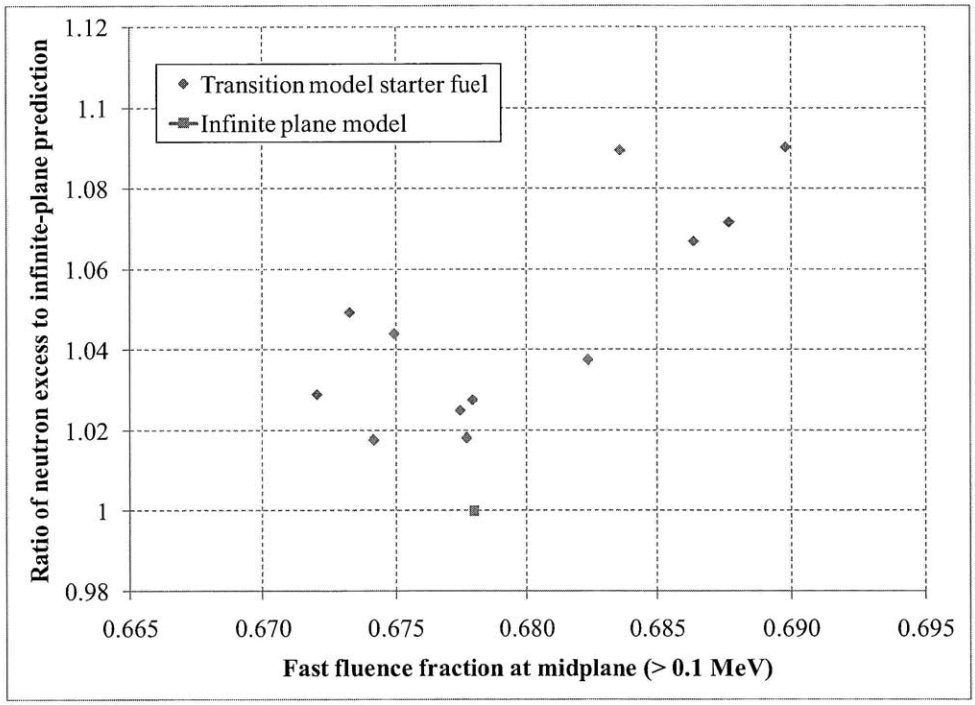

Figure 6.5-5. Effect of spectral histories on neutron excess in transition model

6.5.2 Starter-feed depletion approximation

In addition to approximating starter fuel depletion using the infinite-plane model, one can also use a one-dimensional model to approximate the depletion of transition feed fuel. As shown in Figure 6.4-11, some feed fuel zones have neutron excess curves significantly different from the equilibrium cycle curve. The overall contribution to neutron excess is small: if each feed fuel zone had only been depleted to a peak DPA of 490 (the equilibrium cycle value), then the total neutron excess from the feed fuel would have been approximately **-300 mol**, about 3% of the total neutron excess requirement. Instead, the feed fuel produces 1240 mol of neutron excess

because it is depleted significantly past 490 DPA, something which would be avoided in an optimized transition sequence.

To estimate how much neutron excess is produced or absorbed by the transition feed fuel, the starter-feed depletion approximation is used. The approximation uses a one-dimensional model similar to the infinite-plane model, but with an additional region of feed fuel blended in to yield a starting *k*-effective equal to the desired BOL *k*-effective. Effectively, the starter-feed depletion models the starting fuel configuration of an infinitely large reactor. Because it includes feed fuel, the effect that starter fuel and feed fuel have on each other during their depletion can be investigated.

As an example, assume that a 100 cm tall section of starter fuel with an enrichment of 10% has an infinite-plane *k*-effective of 1.01. To simulate a 100 cm tall starter with 15% enriched fuel, the fair comparison model would be an infinite plane consisting of 2/3 starter fuel and 1/3 depleted feed fuel, to bring the average enrichment down to the needed 10% (this example neglects the small amount of U-235 in depleted uranium). With a 20% enriched starter, the ratio would be 1/2 starter and 1/2 depleted feed. The total composition being modeled in each case is the same, so each model evolves in the same manner, but with a different portion of the model being attributed to the starter fuel.

Results from the starter-feed depletion model are shown in Figure 6.5-6; two curves are shown corresponding to the neutron excess results for the starter and feed fuel respectively. In the starter-feed model, the feed fuel occupies 52.5% of the area of the starter fuel, yielding a starting *k*-effective of 1.01. The starter fuel depletion produces less neutron excess than in the infinite-plane model because the addition of feed fuel softens the neutron spectrum. The feed fuel neutron excess curve from the starter-feed model closely resembles the neutron excess curves from the "interior" feed fuel zones, i.e., the zones inside the starter fuel region at reactor startup (materials 13 through 16 in Table 6.4-2).

Based on the starter-feed depletion model, this transition feed fuel supplies -0.0135 mol/cm^2 of twice-adjusted neutron excess, or -58 mol per 4301 cm^2 fuel zone. Multiplying the amount of starter fuel in the transition model (12 zones) by the ratio of feed fuel to starter fuel in the starter-feed model (52.5%), yields ~6.3 zones of "transition" feed fuel. This number is larger than the number of "interior" feed fuel zones in the transition model (4 zones) because the transition model is finite and has additional leakage to exterior feed fuel zones. Multiplying 6.3 transition feed zones by -58 mol per zone yields approximately **-360 mol** of neutron excess. This estimate is fairly close to the actual neutron excess generated at 490 DPA by the feed fuel of -300 mol, showing that the starter-feed depletion model can be used to approximately characterize the contribution from transition feed fuel.

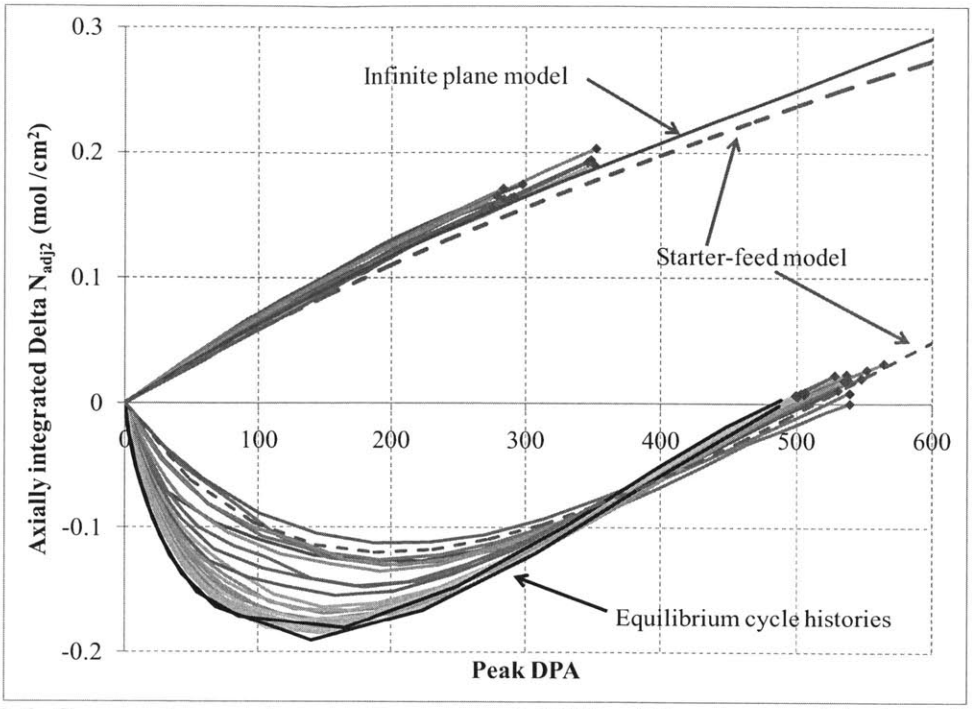

Figure 6.5-6. Comparing neutron excess vs. peak DPA of linear-assembly transition model and starter-feed model

Figure 6.4-7 shows the fast flux fraction (>0.1 MeV) experienced at the fuel midplane as a function of peak DPA in the starter-feed model and the feed fuel in the transition model. Eight representative feed fuel histories from the transition model are shown: four from the interior feed positions (materials starting in zones 1, 3, 6, and 13, interior to the starter fuel) and four from exterior feed positions (materials starting in zones 17, 22, 27, and 32).

The interior feed fuel histories show harder spectrums on average than the equilibrium cycle histories throughout their depletion, because they start inside the power producing region of the core. Early on, exterior feed fuel histories also exhibit harder spectra than the equilibrium history, since they are shuffled into the power producing region fairly early during their depletions. Later transition feed fuel begins to have spectral histories very close the two equilibrium cycle histories.

The starter-feed model is able to approximate the harder spectra experienced by the interior feed fuel zones at the beginning of their depletions, as well as the harder spectra seen by subsequent exterior transition feed fuel zones as they are moved into the center of the core. The exterior transition feed fuel, which has fuel histories lying between the interior feed histories and the equilibrium cycle histories, are roughly accounted for by the larger amount of "transition" feed fuel predicted by starter-feed model (6.3 zones) and the actual number of interior feed zones (4 zones).

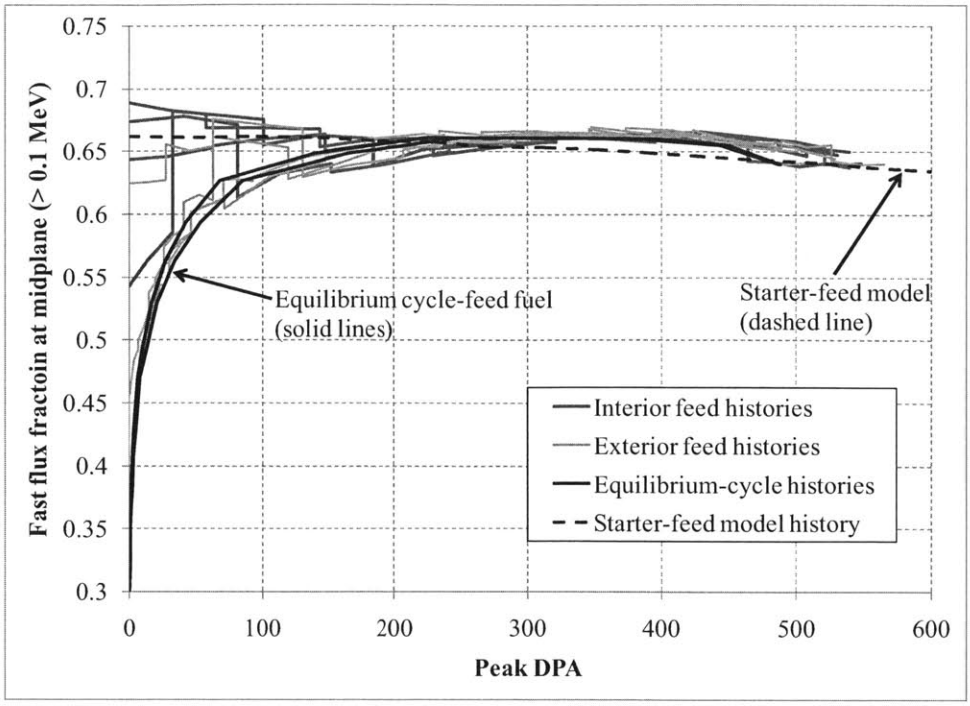

Figure 6.5-7. Comparing fast flux fraction vs. peak DPA of linear-assembly transition model and starter-feed model

6.5.3 Using one-dimensional models to compare enriched starter fuel configurations

For any given equilibrium cycle, it is desirable to create a starter fuel design that accomplishes the following:

1) Is critical upon startup
2) Supplies the necessary neutron excess to establish an equilibrium cycle
3) Supplies full power upon reactor startup
4) Minimizes the total fissile fuel required
5) Allows a transition sequence with a fixed power distribution (allowing fixed orificing)

There are infinite variations in starter fuel design that can be used to accomplish these goals, involving different ways of axially and radially grading enrichments and core compositions. For simplicity, this section will primarily examine starter fuel configurations with uniform enrichment along a given length of the starter (e.g. the 15% uniform enrichment along the central meter in the linear-assembly transition model). Goals 2 and 3 above effectively set the amount of neutron excess required per unit area of starter fuel. This required amount of neutron excess can be achieved using either a shorter length of higher enrichment fuel or a longer length of lower enrichment fuel. The choice of either higher enrichment or longer length can have an impact on goal number 4, the total fissile requirement. How to best accomplish goal 5 is beyond the scope of this study, since finding a starter configuration that matches the equilibrium cycle power distribution would likely require some type of radial enrichment grading.

As shown in Subsection 6.5.1 (and also later in Section 6.6), one-dimensional models consisting of an infinite plane of starter fuel give reasonably accurate results for the actual neutron excess

extractable from the starter fuel, with a ~10% error possible due primarily to spectral differences between the infinite-plane model and the actual transition case. The spectral differences arise because in an actual reactor model, the neutron spectrum is softer in regions farther away from where fissions are occurring, e.g. in the feed blanket region, while in an infinite-plane model, there is no spectral separation and the fuel is depleted at a uniformly "medium" spectrum. How large this error is depends on how well the spectrum in the infinite-plane model matches the spectrum in the starter region of the core.

The actual spectrum in a starter core depends primarily on the core composition and the size of the starter fuel region, and will be approximately constant between different enrichments of starter fuel (since higher enrichment starter fuel would include more interior feed assemblies to have the same starting k-effective). Meanwhile, the spectrum in the infinite-plane model *does* depend on starter enrichment: the higher the enrichment in the starter, the harder the spectrum is in the infinite-plane model. As a result, the error between the infinite-plane model and the transition model is greatest for low enrichment fuels (such as reused feed fuel in Section 6.6). This conclusion mirrors the situation for the infinite-medium depletion approximation used in Chapter 3.

Because of the effect of neutron spectra, the starter-feed model is used to compare different starter configurations. It is a better tool than the starter-only model because it depletes different enrichment starter fuels using a consistent neutron spectrum. As stated earlier, the starter-feed model essentially simulates the starting configuration of an infinite-size reactor. Notably, it is *less* accurate than the starter-only model in terms of predicting neutron excess in an actual core (as seen in Figure 6.5-6), because it uses a softer spectrum than the starter-only model. However, unlike with the starter-only model, the starter-feed model is *uniformly* inaccurate, so better cross comparisons can be made.

Comparison of different starter configurations

Nine different starter fuel configurations are tested, with enriched lengths of 1.0, 1.4, and 1.8 meters at enrichments of 10%, 14%, and 18%. Table 6.5-1 gives the average enrichment and starter area fractions for each of the cases. The remaining area is filled with depleted (0.3% U-235) feed fuel. Neutron excess results from the starter-feed models are given in Figure 6.5-8. Figure 6.5-9 shows the same results as neutron excess per mol of initial U-235. The numbers in the legend entries give the enrichment and enriched length respectively. All the neutron excesses are twice-adjusted with an assumed k_{eq2} of 1.033; the comparisons remain the same if this value of k_{eq2} is changed.

Table 6.5-1. Starter area fractions for different starter fuel configurations

Enriched length *(average enrichment for k-eff = 1.01)*	**Starter enrichment**		
	10%	**14%**	**18%**
100 cm *(9.9%)*	0.99	0.70	0.54
140 cm *(9.0%)*	0.90	0.64	0.49
180 cm *(8.6%)*	0.86	0.61	0.47

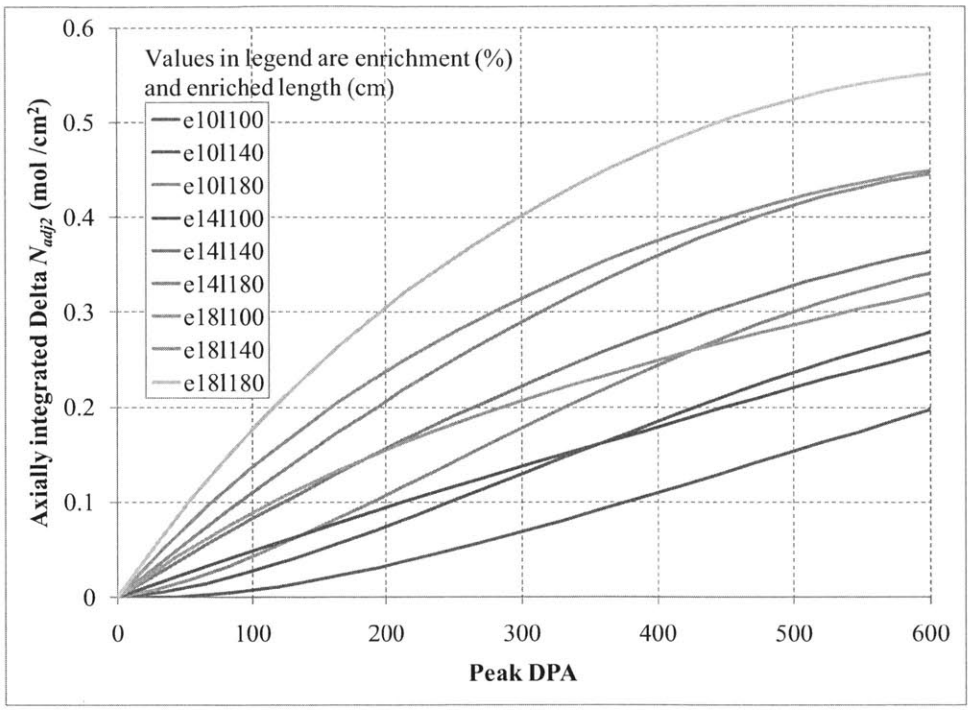

Figure 6.5-8. Twice-adjusted neutron excess per unit area from starter-feed model

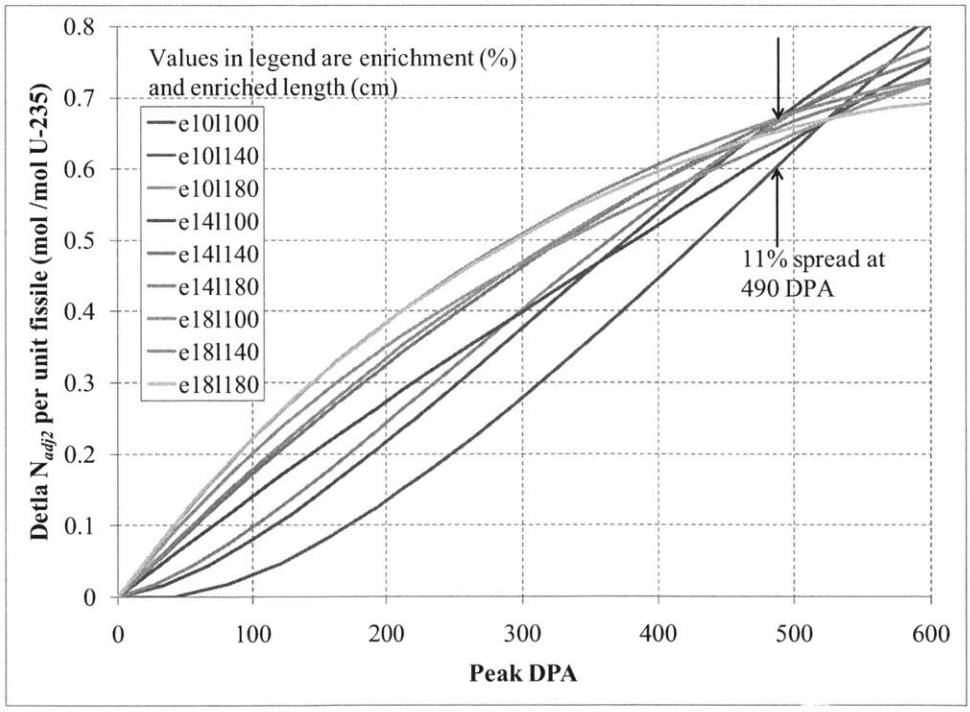

Figure 6.5-9. Specific neutron excess per unit area from starter-feed model

In Figure 6.5-9, one finds that if each configuration of starter fuel is burned to the same breakeven value of 490 DPA, the neutron excess extractable from each is very similar, with the best (tied between the 140 cm cases) and worst case (1 m of 10% enriched fuel) differing by only 11%. The similarity is due to the fact that the fissile U-235 is all utilized to roughly the same

degree in each case, while the fertile U-238 approximately breaks even and yields roughly zero neutron excess at 490 peak DPA. This latter point is more apparent in Figure 6.5-10, which compares the different enrichments with a 140 cm enriched length. Each case in Figure 6.5-10 has the same evolving flux distribution in position and energy, and the crossover point occurs when the fissile U-238 is burned by the flux distribution to yield a zero neutron excess. Since the contribution from the fissile U-235 is directly proportional to the amount of U-235 present, the curves exactly coincide at this point. Before this point, the higher enrichment starter fuel performs better, while after this point the lower enrichment fuel is more efficient. This picture changes somewhat if the starter fuel is burnup limited instead of DPA limited: a limit on burnup (e.g. 30% FIMA) would favor lower enrichment because lower enrichment fuel experiences lower burnup for a given fluence or DPA.

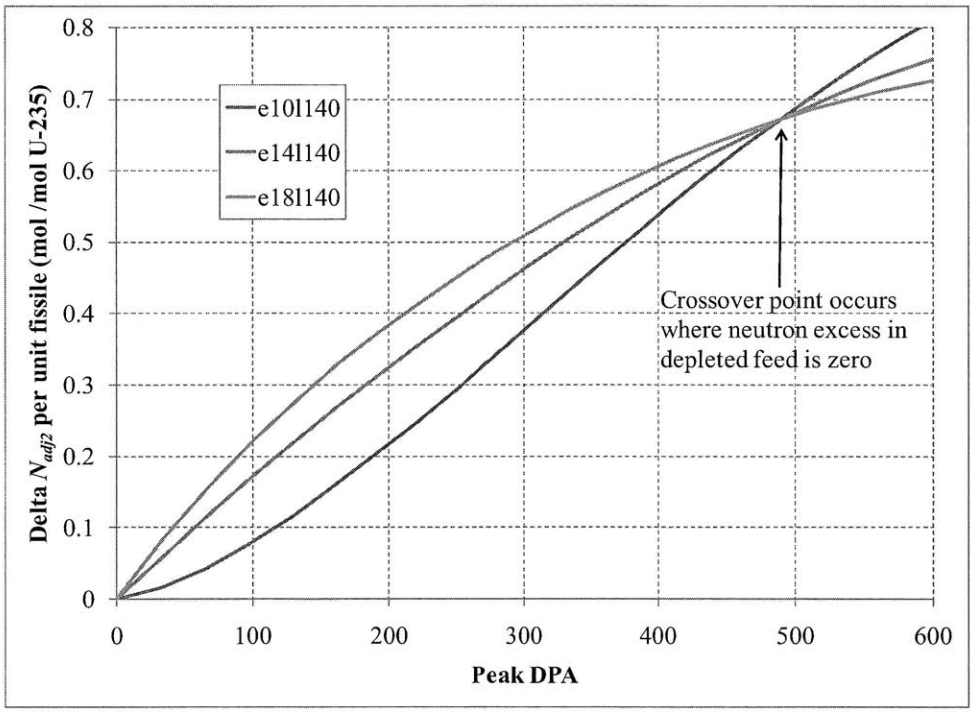

Figure 6.5-10. Specific neutron excess per unit area for 140 cm enriched length cases

Figures 6.5-11 through 6.5-13 give results separately for 10%, 14%, and 18% enriched fuel. For each enrichment, the same pattern is evident: the longer 180 cm enriched length performs best at lower peak DPA, followed by 140 cm at middling values (including 490 DPA), then finally 100 cm for very high peak DPA. The longer enriched lengths are superior at first because a greater portion of neutrons are captured in the enriched fuel versus in the unenriched ends of the fuel. As the fuel burns further and the burnup distributions grow wider, the longer starter configurations become worse because of the increased effect of leakage out of the ends of the fuel. To illustrate this, Figure 6.5-14 gives neutron excess results for the 14% enrichment cases without counting the effect of leakage (i.e. setting f'_{axial} artificially to zero); the longer configuration performs better throughout. The tradeoff between fissile utilization and leakage means that there is an optimal enriched length which maximizes neutron excess obtained from the starter fuel; however as the results here show there is relatively little difference (<11%) between very long and short enriched lengths.

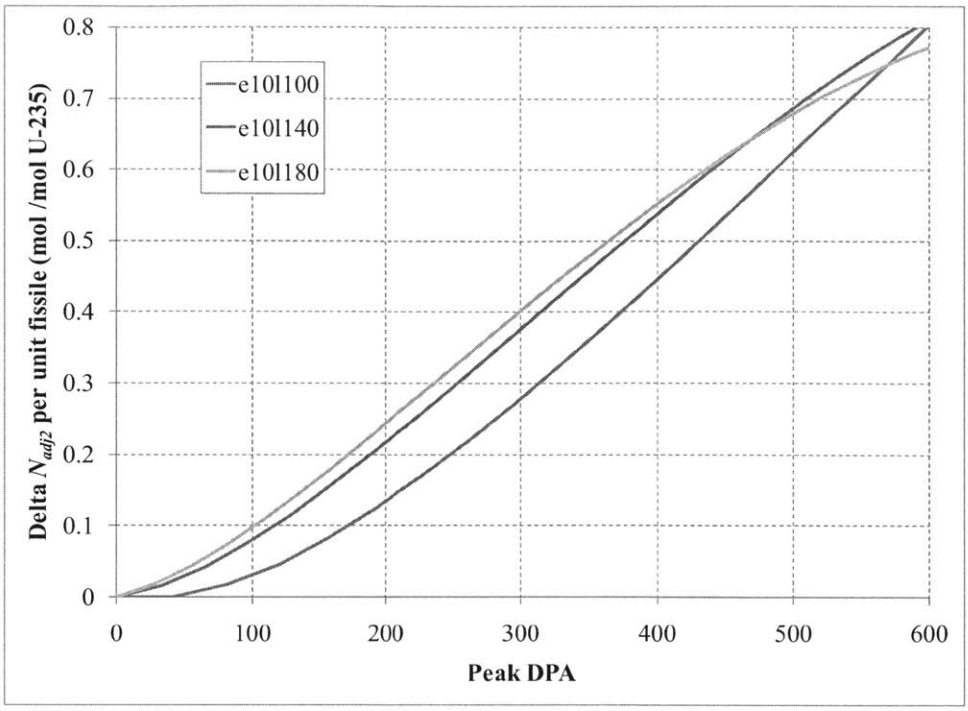

Figure 6.5-11. Specific neutron excess per unit area for 10% enrichment cases

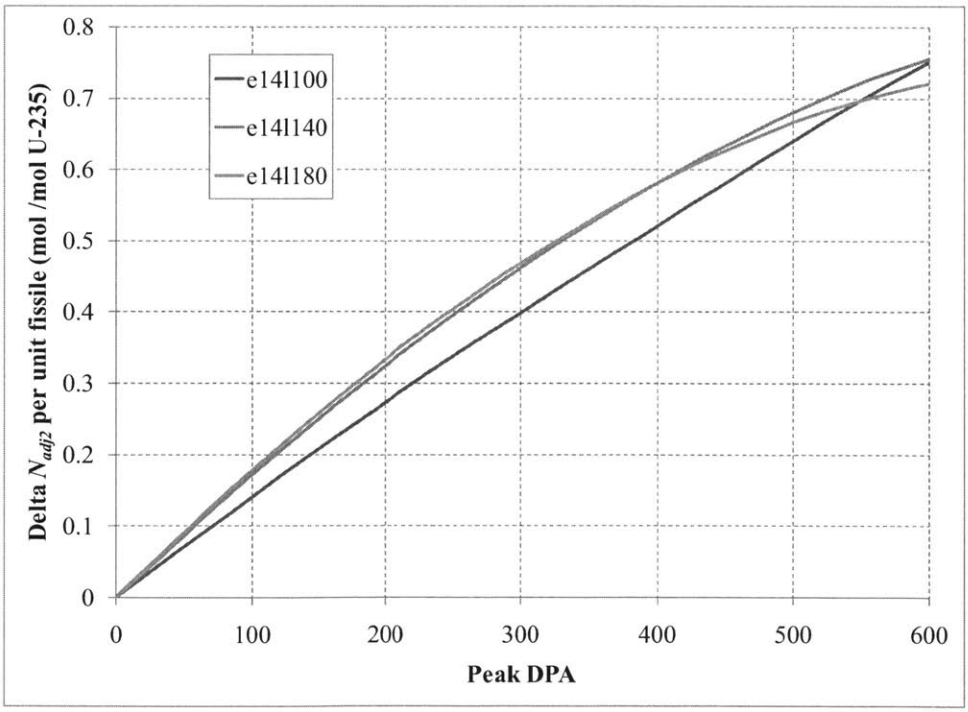

Figure 6.5-12. Specific neutron excess per unit area for 14% enrichment cases

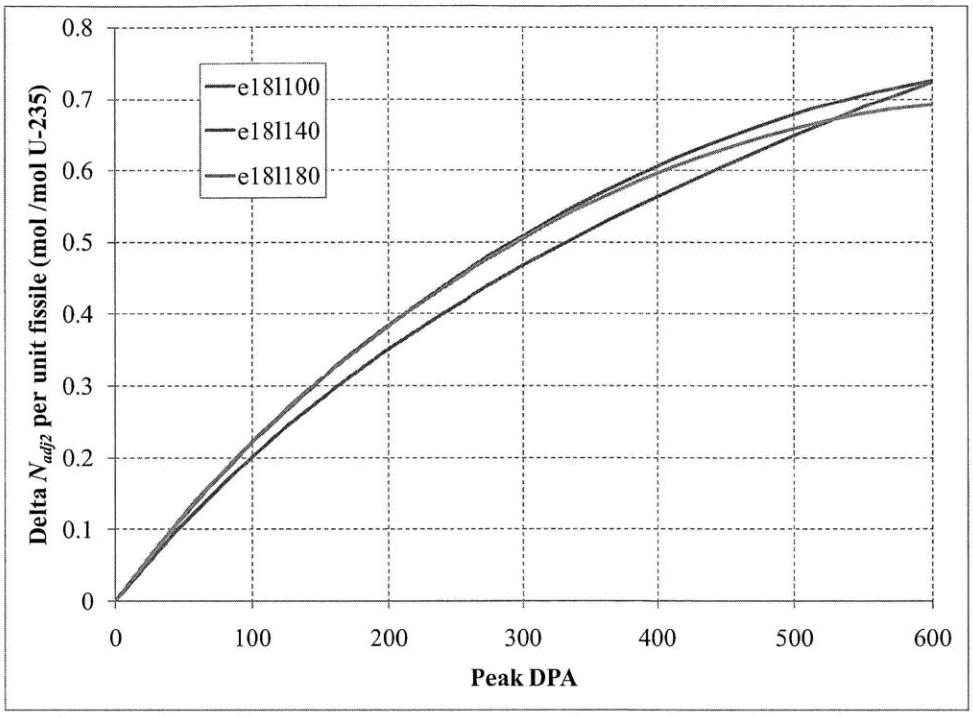

Figure 6.5-13. Specific neutron excess per unit area for 18% enrichment cases

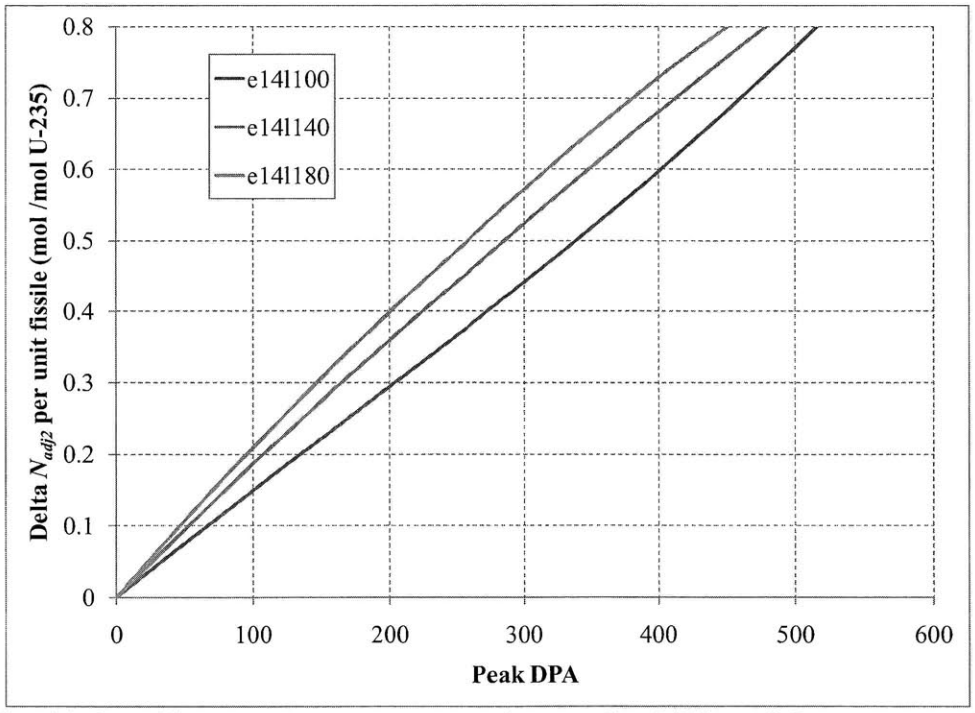

Figure 6.5-14. Specific neutron excess per unit area for 14% enrichment cases (without leakage)

To improve the neutron excess obtainable as a function of peak DPA, one possibility is to reduce the axial peaking of the DPA distribution, so that the enriched starter fuel can be used more uniformly. This reduction in peaking can be accomplished by axially shaping the starter fuel enrichment profile and putting lower enrichment fuel in the center of the fuel. An un-optimized example of such a shaped distribution is shown in Figure 6.5-15: it is enriched to 10% in the central 60 cm, followed by 17% for 40 cm on each side, then finally depleted uranium for the 30 cm on each end. This distribution contains the same amount of fissile U-235 as the starter fuel that is uniformly enriched to 14% for 140 cm.

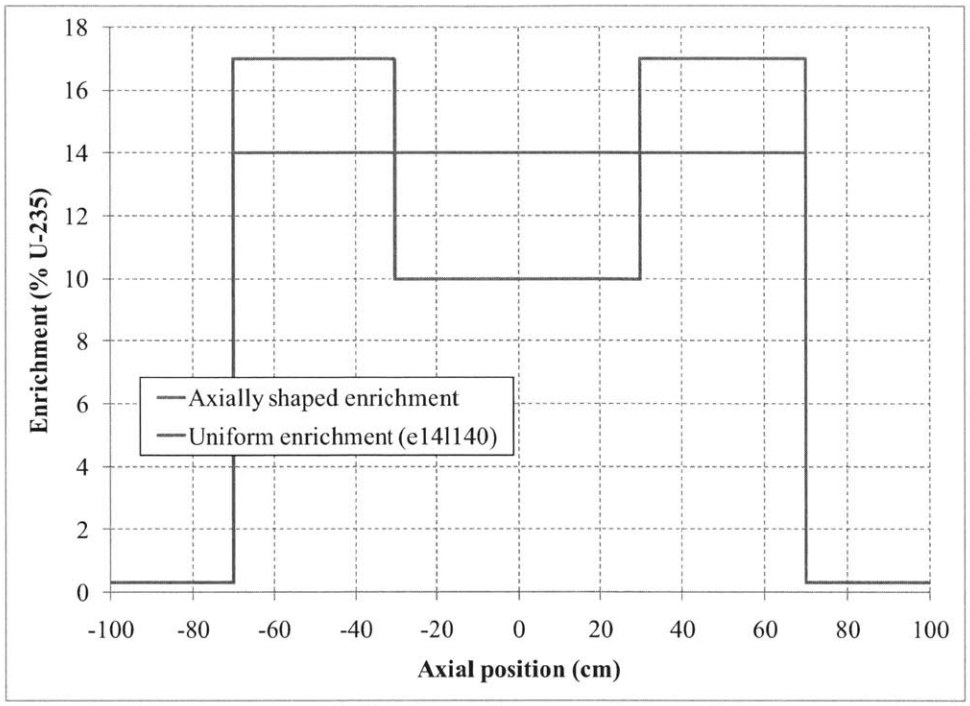

Figure 6.5-15. Example axially shaped starter fuel enrichment distribution

Using a starter-feed depletion model to analyze the axially-shaped starter fuel gives the results shown in Figure 6.5-16. As the figure shows, at the equilibrium cycle peak DPA of 490, the axially-shaped starter is able to provide approximately 5% more neutron excess per unit fissile than the uniform enrichment starter configurations, including the 140 cm 14% enriched case. As shown later in Figure 6.5-19, the shaped starter fuel is able to have a very uniform DPA distribution along its central 60 cm, which nearly maximizes utilization of the 10% enriched central region and improves overall fissile utilization. This result shows that using axially-shaped starter fuel distributions can be used to reduce the amount of fissile fuel required to initiate a desired equilibrium cycle.

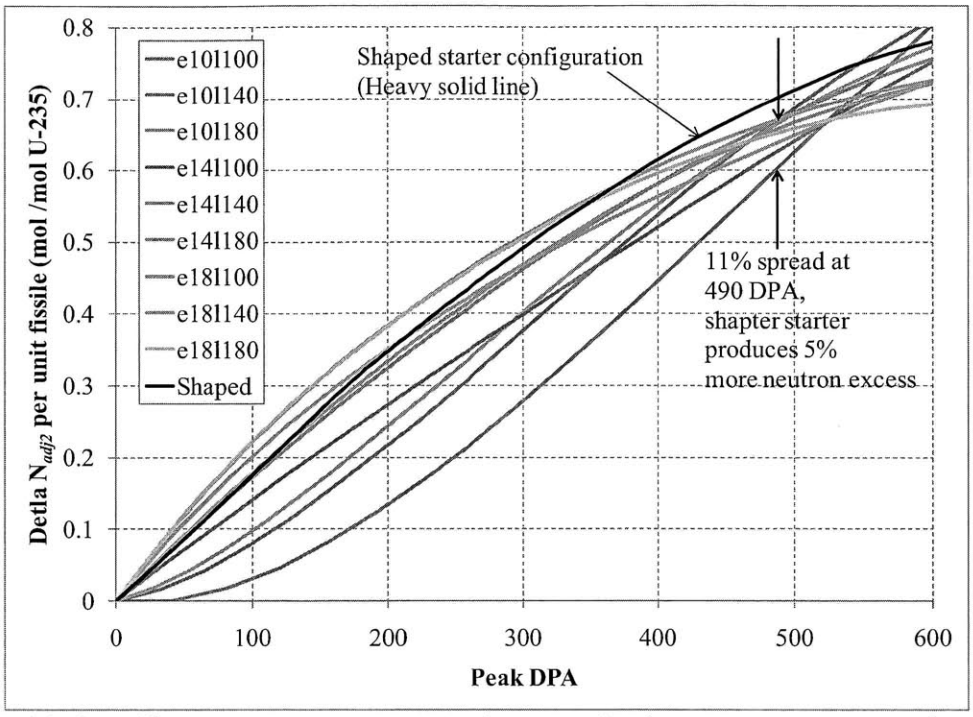

Figure 6.5-16. Specific neutron excess per unit area of axially-shaped starter from starter-feed model

Comparison between starter-only and starter-feed infinite-plane models

Figure 6.5-17 illustrates the differences in predicted neutron excess for a starter-only infinite-plane model and the starter-feed model. Differences between two models are due to the different spectral and axial neutron distributions caused by the presence of feed fuel in the starter-feed model. For the 10% enriched, 100 cm enriched length case, there is very little feed fuel present so the two models agree almost exactly. Meanwhile, as one adds to either enrichment or the enriched length, the amount of feed fuel in the starter-feed model increases, causing the results from the two models to diverge. In the most extreme case, with 180 cm of 18% enriched fuel, the neutron excess result at 490 DPA from the starter-only model is 8% greater than that from the starter-feed 1D model.

The comparison shows that the presence of feed fuel has a relatively small effect on the neutron excess obtainable from starter fuel, so using the starter-feed model instead of a starter-only model to estimate neutron excess does not introduce a large additional error. The comparison also gives a sense how differences in spectra in the starter-only depletion models affect their predictions of neutron excess. Since the starter-feed models have a consistent spectrum between them and would be about uniformly conservative compared to an actual transition model, the starter-only models for shorter, lower-enrichment starter fuel would be a few percent more conservative than starter-only models for longer, higher-enrichment starter fuel.

For example, as seen previously in Figure 6.5-6, results from an actual transition model using 100 cm of 15% enriched starter fuel are 4% greater than predicted by a starter-only model, and 9% greater than predicted by a starter-feed model. Therefore, the starter-only model is slightly

more accurate. Both models would become more accurate as the size of the starter region increases, which would soften the average neutron spectrum in the starter region. In the limit of an infinite-size starter, the starter configuration would be equivalent to the starter-feed model and experience the same initial spectrum.

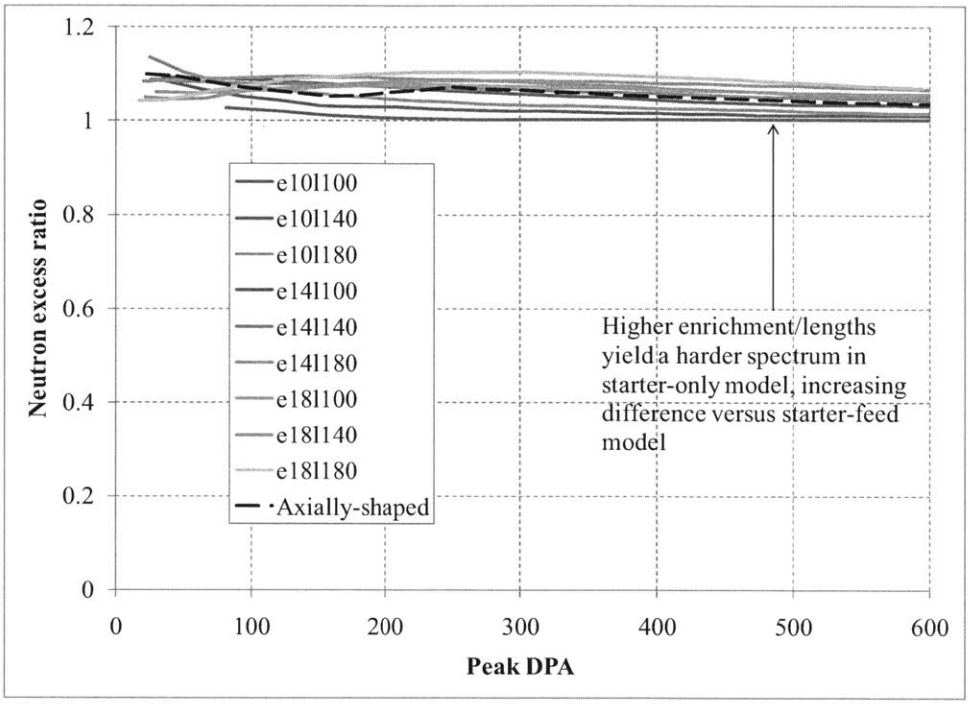

Figure 6.5-17. Ratio of neutron excess measured by basic 1D model and fair comparison 1D model

6.5.4 Effect of starter configuration on transition feed

With the starter-feed models, it is also possible to look at the evolution of feed fuel as it is exposed to flux from the different configurations of starter fuel. With a starter-feed model, changing the enrichment of the starter doesn't change the composition and evolution of the overall problem, so how the feed fuel evolves depends only on the length of the starter. Figure 6.5-18 shows the differences in feed neutron excess evolution for the three enriched lengths studied, and the 140 cm axially-shaped distribution. At the breakeven peak DPA of 490, the case with the uniform enrichment 140 cm starter has a very small positive neutron excess (<0.01 mol/cm^2, compared to a starter contribution on the order of 0.2 mol/cm^2). The 180 cm case and 140 cm axially-shaped cases have slightly higher neutron excesses while the 100 cm case has a slightly lower neutron excess. Correspondingly, the longer cases are able to reach a net neutron excess of zero at lower peak DPA than the shorter cases.

The reason the longer starter fuel configurations cause the feed fuel to have higher neutron excess at 490 DPA is due to the *shape* of the fluence distribution at that point. Just changing the *width* of the neutron distribution only changes the magnitude of the neutron excess: for example lengthening the fluence distribution by 40% would just lengthen the neutron excess distribution by 40%, causing a 40% larger neutron excess. The longer distribution would still be expected to break even and yield zero neutron excess at the same peak DPA. The 180 cm and axially-shaped

distributions have the earliest breakeven points not because they have the *longest* distributions, but because they have the *flattest* shaped distributions, as shown in Figure 6.5-19. The 180 cm starter has a flatter distribution because it has the smallest fraction of neutron absorptions in the exponential-shaped "tails" of the feed region, while the axially-shaped distribution has been specifically designed to lower the axial peaking of the DPA distribution.

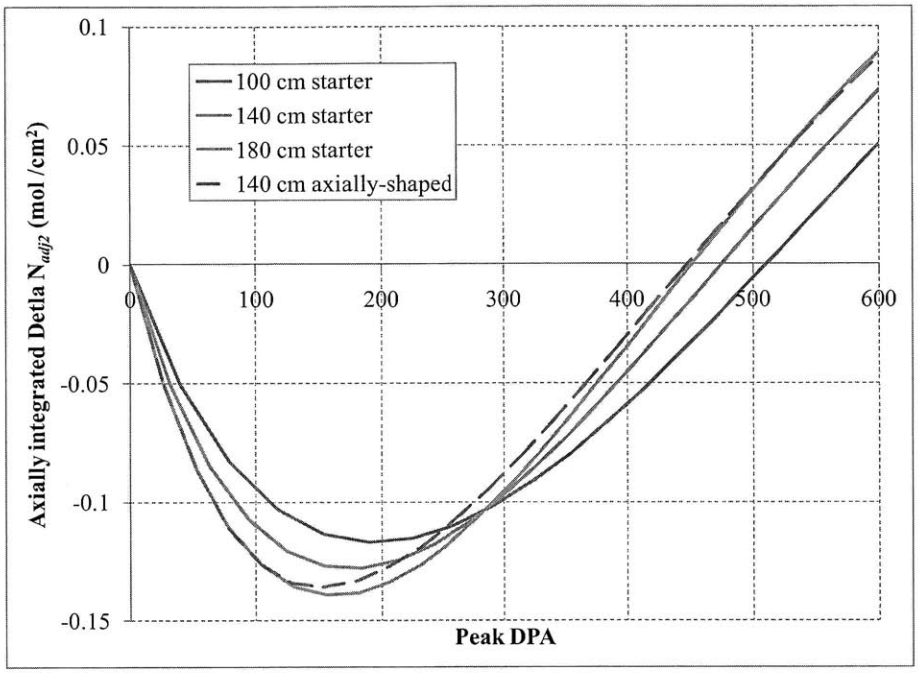

Figure 6.5-18. Feed neutron excess for different length/shaped starters in starter-feed model

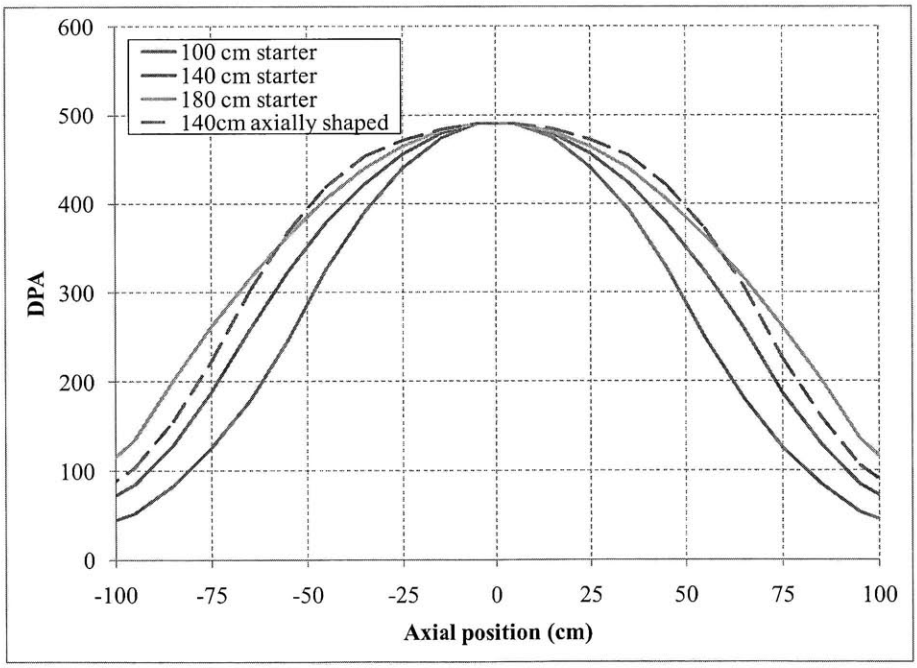

Figure 6.5-19. Axial DPA distributions for different length/shaped starters in starter-feed model

6.5.5 Effect of neutron excess axial distribution

So far, the approach used to estimate the neutron excess obtainable from a given starter configuration has been to first use an infinite-plane model to approximate the neutron excess from the starter fuel, then use a starter-feed model to approximate the neutron excess from the transition feed fuel. The amount of neutron excess obtained from the transition feed fuel depends on the starter configuration; for example Figure 6.5-16 shows that flatter fluence distributions allow more neutron excess to be extracted from feed fuel.

While this approach gives good numerical estimates for neutron excess obtainable from starter and "interior" transition feed fuel, it does not directly address the role played by the *axial distribution* of neutron excess. For example, one can intuitively imagine that a given amount of neutron excess generated near the axial end of the core would not be as effective at launching an equilibrium cycle as the same amount of neutron excess generated at the axial center. The reason that neutron excess toward the ends would be less effective is because the subsequent neutrons produced in nearby feed assemblies would have more losses to leakage, reducing the amount of neutron excess obtainable from the feed fuel. The net effect would be a sub-unity gain term: each unit of neutron excess generated by the starter fuel would contribute less than one unit toward establishing the equilibrium cycle, with the remaining neutron excess being lost in the higher-leakage transition feed fuel.

To gain a better understanding of what effect axial distributions have on neutron gain in feed fuel, the axial transfer model is used to model an idealized scenario. In this idealized case, first one starts with an axial ΔA distribution and depletes feed fuel assemblies using it until the DPA limit is reached. The ΔA distribution is translated into a ΔP distribution by using the equilibrium cycle neutron excess curve. Then, the axial transfer matrix (developed using a diffusion approximation, as described in Subsection 6.3.2) is used to convert the ΔP distribution into a new ΔA distribution. Repeatedly iterating in this way eventually yields the equilibrium cycle distribution. While undergoing these iterations, one can keep track of the total neutron excess gain, i.e. how much additional neutron excess is gained or lost from iteration to iteration. In this manner, one can compare different starting axial distributions and get a sense of the gain obtainable from each. In this scenario, only the equilibrium cycle neutron excess curve is used, so the effect of different neutron spectra is not studied, only the effect of axial distributions.

As an example, first assume a starting neutron absorption distribution that is a 1 m wide square wave; i.e. neutron absorptions occur evenly in the central 1 m and not at all in the 50 cm near each end. Burning the central portion uniformly to 490 DPA (~0.168 mol neutrons absorbed per cm^3) causes 1.116 neutrons to be produced per neutron absorbed, with the same square-wave distribution. The absorption and production distributions have the same shape because neutrons are produced where absorptions cause fissions to occur. Of these neutrons produced, 0.033 are lost to control (assuming equilibrium cycle control losses), and 0.008 are lost to leakage. The remaining 1.076 neutrons are reabsorbed in new feed fuel with a new axial distribution, corresponding to a gain of 1.076 for the zeroth iteration. This means that for each unit of neutron excess invested by starter fuel in this axial configuration, this first generation of feed fuel generates an additional 0.076 units of neutron excess.

Figure 6.5-20 shows the axial distributions resulting from the first 5 iterations, and shows how the initial square-wave distribution converges toward the equilibrium cycle distribution with each iteration. Table 6.5-2 gives the neutron balance results for each iteration, and Figure 6.5-21 plots the values in Table 6.5-2.

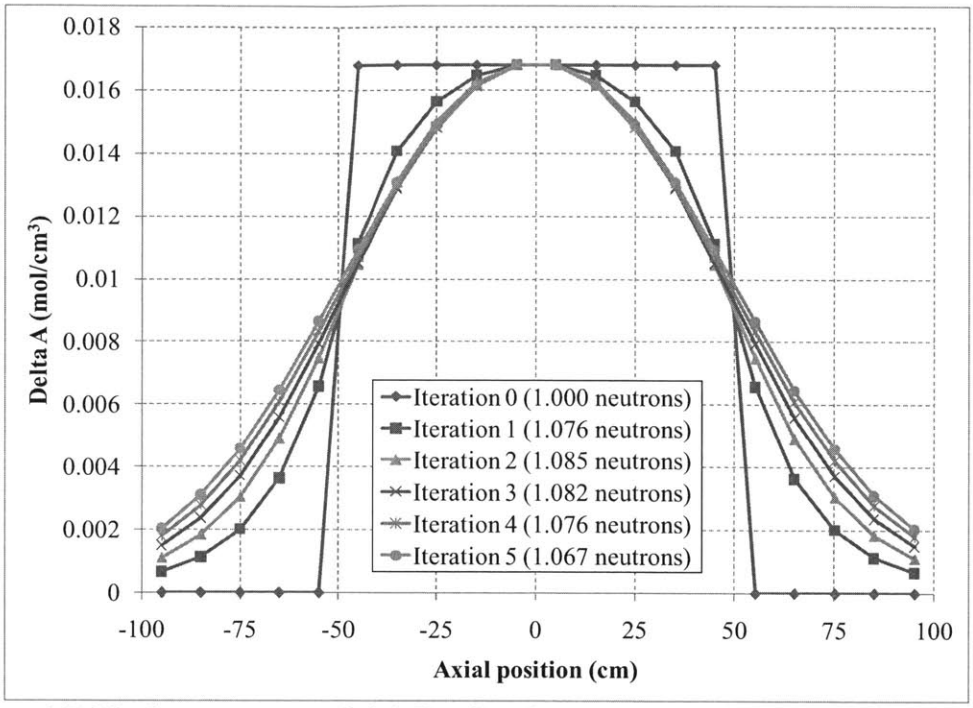

Figure 6.5-20. Convergence of ΔA distributions towards equilibrium cycle shape

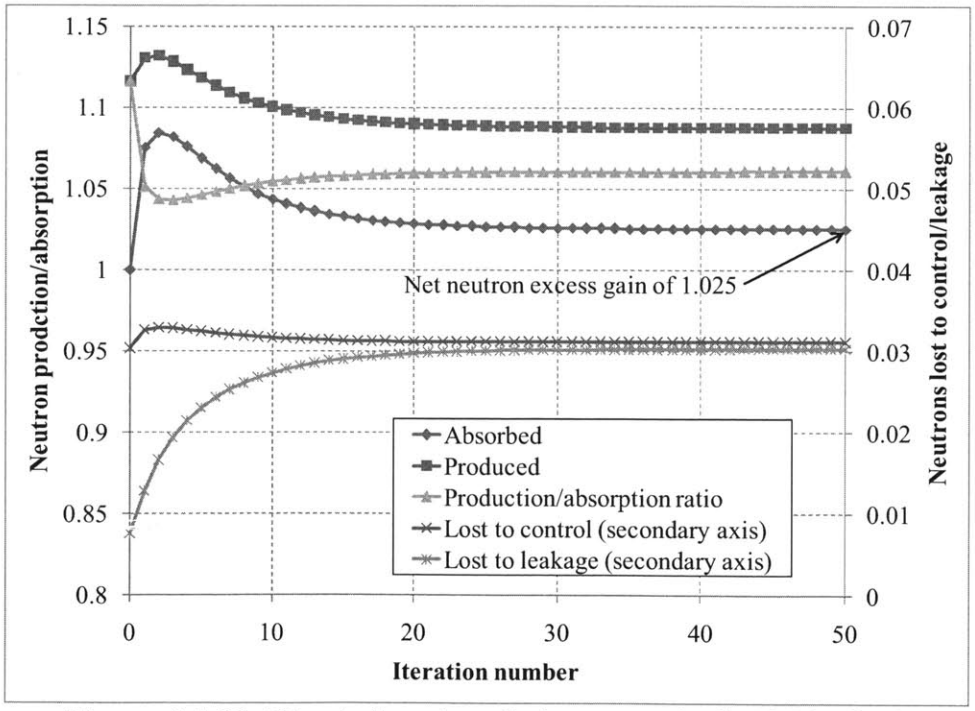

Figure 6.5-21. Chart of neutron balance results in Table 6.5-2

Table 6.5-2. Neutron balance from axial-transfer model iterations

Iteration	Absorbed	Produced	Lost to control	Lost to leakage	Production/ absorption ratio
0	1.0000	1.1161	0.0329	0.0076	1.1161
1	1.0757	1.1306	0.0333	0.0128	1.0511
2	1.0845	1.1319	0.0333	0.0166	1.0437
3	1.0820	1.1284	0.0332	0.0194	1.0429
4	1.0757	1.1232	0.0331	0.0215	1.0442
5	1.0687	1.1181	0.0329	0.0231	1.0462
6	1.0621	1.1134	0.0328	0.0243	1.0483
7	1.0563	1.1092	0.0327	0.0253	1.0501
8	1.0513	1.1057	0.0326	0.0261	1.0518
9	1.0471	1.1028	0.0325	0.0268	1.0533
10	1.0436	1.1004	0.0324	0.0273	1.0545
11	1.0407	1.0984	0.0324	0.0278	1.0555
12	1.0382	1.0967	0.0323	0.0282	1.0563
13	1.0362	1.0953	0.0323	0.0286	1.0571
14	1.0345	1.0942	0.0322	0.0288	1.0576
15	1.0331	1.0931	0.0322	0.0291	1.0581
16	1.0319	1.0923	0.0322	0.0293	1.0585
17	1.0308	1.0916	0.0322	0.0294	1.0589
18	1.0300	1.0910	0.0321	0.0296	1.0592
19	1.0293	1.0904	0.0321	0.0297	1.0594
20	1.0286	1.0900	0.0321	0.0298	1.0597

Figure 6.5-21 shows that while the zeroth iteration results in a large neutron production/absorption ratio (in fact, the largest theoretically possible), subsequent iterations have production/absorption ratios much closer to the equilibrium cycle values as neutron diffusion causes the axial distribution to spread out. Therefore, while the gain after the zeroth iteration is 1.076, the total gain after many iterations is only 1.025, an increase of 2.5%. Once the equilibrium cycle distribution is established, for every neutron absorbed 1.061 are produced, of which 0.031 are absorbed by control and 0.030 are lost to leakage, resulting in a net gain of exactly unity.

The same technique can be used to compare the different initial feed fuel ΔA distributions that result from the three starter fuel configurations considered. These ΔA distributions will look similar to the curves given in Figure 6.5-19, which plots the axial distribution of DPA. Each initial distribution eventually converges to the equilibrium cycle distribution. The 100 cm enriched length starter fuel does so with a total gain of **0.968**, meaning for every unit of neutron excess created by the starter fuel, -0.032 are produced in transition feed fuel, so 0.968 units are invested into the equilibrium cycle distribution. This is consistent with the result from the linear-assembly transition model, in which a 100 cm starter produces 9020 mol neutron excess while the feed fuel produces -300 mol at the equilibrium cycle discharge DPA. The corresponding gains for the 140 cm and 180 cm enriched lengths are **1.010** and **1.045** respectively, and the gain for the 140 cm axially-shaped starter is **1.032**. The 140 cm starter case has an axial distribution very close to the final equilibrium cycle distribution, thus the near unity neutron excess gain factor.

In an actual reactor, neutrons produced in one assembly are absorbed across many other assemblies, rather than in the step-by-step iterations assumed by using the axial transfer model. Therefore, the axial distributions in actual transition fuel will all have varying amount of contribution from the starter fuel distribution and the equilibrium cycle distributions, as opposed to 100% starter fuel (iteration zero) or 100% equilibrium cycle (later iterations). While the two situations are qualitatively different, the axial transfer model represents a simple way of capturing the effect that the starter fuel distribution has on feed fuel. Based on the results from the axial transfer model, different starter fuel axial distributions only have an effect in the several percent range, so once again differences in neutron spectra (which aren't accounted for in the axial transfer model) are expected to have a larger effect on feed fuel neutron excess. While the effect of axial shape is small, it nevertheless favors longer, flatter initial neutron distributions.

One additional phenomenon that can be investigated using the axial transfer model is the effect of axially offset starter distributions, such as if the enriched portion of the starter fuel were not centered on the core midplane. Figure 6.5-22 shows how the neutron balance evolves with successive iterations for a case in which a uniform 140 cm enriched starter is offset 20 cm from the core midplane (i.e. the depleted uranium on both sides of the enriched fuel have lengths of 10 and 50 cm respectively). The figure shows that for each initial neutron initially absorbed by transition feed fuel, only 0.73 neutrons are absorbed in the equilibrium cycle distribution, so about 1/3 more starter fuel would be required than the same starter without an offset, which has approximately unity gain. The sub-unity gain factor is due to increased leakage reducing neutron excess as the axial distribution of neutron absorptions gradually shifts back to the axially-centered equilibrium cycle distribution.

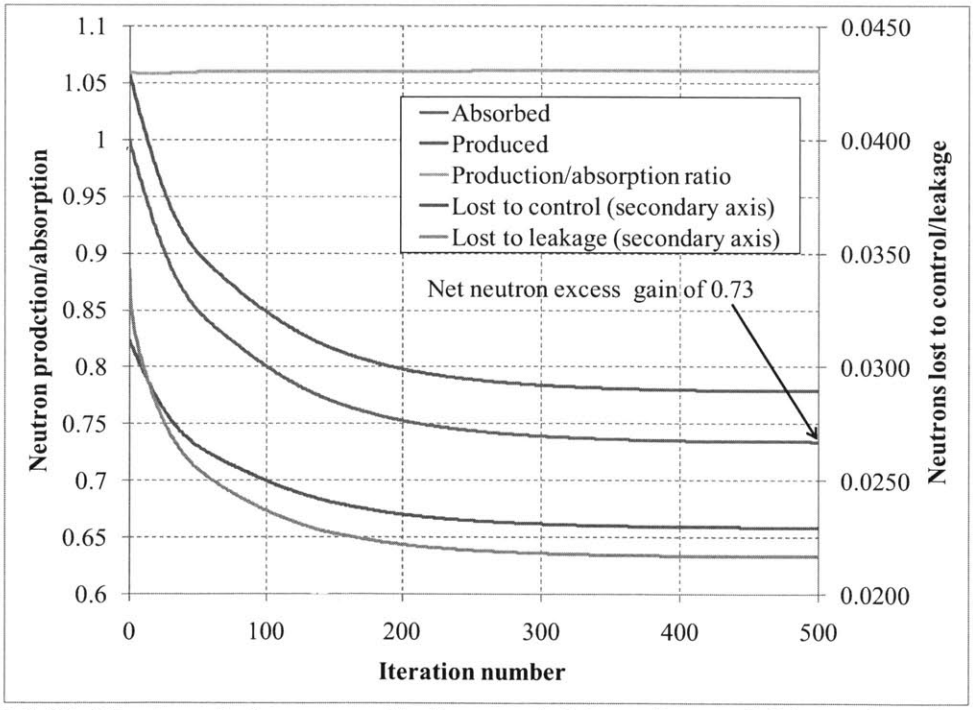

Figure 6.5-22. Neutron balance results from axial transfer model iterations for 140 cm starter offset axially by 20 cm

Another important feature of Figure 6.5-22 is the large number of iterations (~400) required for the equilibrium cycle distribution to form. This behavior occurs because there is only a small difference in leakage between the equilibrium cycle distribution and the axially offset distribution (the leakage probability changes from 3.4% for the axially offset starter to 3.0% for the centered equilibrium cycle), so there is a very weak "restoring force" for creating the centered equilibrium cycle. The implication for an actual reactor is that a B&B reactor with axially-offset starter fuel would require a large number of cycles for the equilibrium cycle axial distribution to become established. Also, this behavior highlights a shortcoming in the starter-only and starter-feed infinite-plane models. If one were to analyze an axially-offset starter configuration in one of the infinite-plane models, the results would be very similar to those for axially-centered starter fuel, with a small difference due to leakage. Meanwhile, the axial transfer model iterations show that the starter fuel configuration can have lasting effects through many generations of transition feed fuel, with the small negative neutron excess of each ultimately summing to a large total effect.

6.5.6 General guidelines for designing efficient linear-assembly starter fuel

In designing starter fuel to establish a desired equilibrium cycle, one important criterion is that the starter fuel must be able to supply the equilibrium cycle's neutron excess requirement. Another important criterion is that the starter fuel configuration must be capable of supplying the reactor's rated power, so there is no need for de-rated reactor operation at startup. This second goal sets a thermal hydraulic requirement on the starter fuel area: the starter fuel must occupy a minimum area in order to supply full power at startup. The combination of thermal hydraulic and neutron-excess requirements for starter fuel combine to give a target valuc of starter fuel "strength" in terms of neutron excess supplied per unit area. To supply this amount of neutron excess, many starter fuel configurations are possible, trading off between enriched length and average enrichment.

If one's goal is to minimize the initial fissile inventory of the starter, several factors work in favor of having a longer, lower-enrichment starter fuel design. First, the neutron excess extractable from the fissile fuel increases slightly with a longer starter, since a larger fraction of neutrons is absorbed within the starter fuel. Second, a longer and flatter starter configuration allows a small amount of extra neutron excess to be extracted from feed fuel. Finally, if one is constrained by peak burnup rather than by peak DPA (which may be likely given the higher burnup experienced in starter fuel), then lower enrichments will experience less burnup and have better fuel performance. The latter two factors also favor the use of starter fuel with axially graded enrichment: i.e. a higher enrichment on the ends and lower enrichment in the middle. Such a configuration leads to a flatter neutron production distribution, while lowering the peak burnup in the center of the fuel.

There is a natural limit on having longer, lower enrichment, and axially-shaped starter fuel: such configurations have lower initial reactivity, so eventually the starter fuel would become unable to initiate criticality. Therefore, a general guideline is to use the longest/lowest-enrichment starter fuel that still allows a critical reactor configuration, while accounting for the inclusion of internal blankets or radially graded enrichment for power flattening.

There is one more consideration for the tradeoff between longer and higher enrichment starter fuels: the longer starter fuel would take longer to burn through and therefore extend the transition time to the equilibrium cycle. This may be less important for B&B reactors started with enriched uranium, but it could have an important effect on the doubling time of a B&B reactor fuel cycle. Reactors in such a reactor infrastructure may favor using slightly less efficient shortened starter fuel in order to reduce transition time and allow new reactors to be spawned more quickly.

6.6 Designing a limited-separations fuel cycle using linear-assembly B&B reactors

One of the goals of this thesis is to demonstrate how fuel discharged from one generation of B&B reactors can be used to start up a subsequent generation of B&B reactors in a limited-separations fuel cycle, and to characterize the reactor doubling times associated with such a fuel cycle. Chapter 5 considers this topic in a general way for minimum-burnup B&B reactors that use axially-segmented assemblies, and examines a large number of different possible core compositions and fuel cycle parameters. For B&B reactors that use more conventional axially-connected assemblies, the situation is more complex because of the introduction of non-uniform axial burnup distributions.

To design and characterize a limited-separations fuel cycle for linear-assembly B&B reactors, the following steps are taken:

1) For a specified core composition, evaluate different equilibrium cycles and select a desired one
2) From the neutron excess cost and power level of the equilibrium cycle, determine an appropriate starter fuel configuration using 1D infinite-plane models of the starter fuel
3) Estimate doubling time in the same manner as for minimum burnup B&B reactors
4) Construct a transition model to verify results from the 1D model and doubling time estimate

In the example in this section, the core composition used is the same as that used previously in this chapter: 75 parts U-2Zr, 30 parts T91, and 100 parts Na by volume, with 25 parts void to represent the fuel expansion volume (fuel-clad gap). In each case, the model has the 2D cylindrical geometry used in Section 6.4, with twenty 10 cm axial zones (total axial height of 2.0 m) and one hundred 4300 cm^2 radial zones (total radius of 3.7 m). Stainless steel reflectors are modeled at both the top and bottom of the fuel; the axial height of 2.0 m represents a minimum height before reactivity begins to drop off (or peak burnup begins to rise). The 3.7 m radius is large enough to effectively eliminate all radial leakage from the core. Each 4300 cm^2 radial zone corresponds to 18 hexagonal assemblies with a pitch of 16.6 cm. These large homogenized zones are used to reduce the number of possible fuel permutations and reduce computational complexity.

6.6.1 Neutron excess cost of different equilibrium cycles

Ten different equilibrium cycle shuffling schemes are modeled in the two-dimensional cylindrical model: the convergent shuffling case, five convergent-divergent cases, and four ring-convergent cases. Examples of convergent-divergent and ring-convergent shuffling were given previously in Subsection 6.6.2. The different convergent-divergent and ring-convergent cases

differ in what radial position fuel is discharged from. For each case, the cycle length modeled is 2400 MW * 660 d = 1584000 EFPD. The target burnup (which corresponds to an average k_{cq2} of 1.034) is 792000 MWd per zone, which is half the energy per cycle, so two zones are discharged at each cycle once the equilibrium cycle is established. A summary of the performance of the ten different shuffling schemes is given in Table 6.6-1. Table 6.6-2 gives results for the same shuffling schemes, except with the cycle length scaled to yield the same BOEC *k*-effective of 1.005 in each case.

In Tables 6.6-1 and 6.6-2, "Conv." refers to the convergent shuffling pattern, CD 1-5 are the convergent-divergent patterns, while RC 1-4 are the ring-convergent patterns. The convergent-divergent and ring-convergent schemes are ordered according to where their fuel is discharged; the higher numbered cases have larger fuel discharge radii and therefore larger power distributions. While each simulation was run at a total power of 2400 MW, the power rating in each case has been normalized so that the peak BOEC power density is 580 MW/m^2, giving a small margin to the assumed power density limit of ~600 MW/m^2. The higher power level cases therefore have correspondingly shorter cycle lengths in EFPY, since each case was modeled with the same cycle length in MW.

Table 6.6-1 gives the twice-adjusted neutron excess contained at the beginning and middle of the equilibrium cycle. These numbers are different because over the first half of an equilibrium cycle, k_{fuel2} is less than k_{eq2}, so neutron excess increases, and the reverse is true over the second half of the cycle. This idea is explained further in Appendix A.7, which shows how the neutron excess requirement depends on cycle length. In all cases, the difference between the two is small (<3%) compared to the total magnitude of neutron excess contained.

Table 6.6-2 gives results for the same equilibrium cycles, but with their cycle lengths scaled to give a BOEC uncontrolled *k*-eff of 1.005, under the assumption that cycle reactivity swing varies linearly with cycle length. The MOEC and average k_{eq2} of the cycles is assumed to remain constant with this scaling. The cycle length multiplier is the amount that both the cycle time and the amount of fuel discharged per cycle are multiplied by to obtain the new cycle. From the scaled results, one sees that one of the advantages of the ring-convergent shuffling schemes is a small reactivity swing, which permits long multi-year cycles. The convergent shuffling case can have the longest cycle length by far, due to its low reactivity swing and low power level.

While increasing the cycle length does have an effect on the BOEC and EOEC power distributions, it is assumed that this effect is small, and that each case would be capable of supporting the same amount of total power, since some power density margin had been assumed for the original cycle length cases. The MOEC neutron excess is kept constant from Table 1, while the difference between the BOEC/EOEC and MOEC neutron excess is scaled according to the square of the cycle length, as explained in Appendix A.7.

Table 6.6-1. Fuel cycle and reactor parameters for different shuffling schemes

Shuffling pattern	Conv.	CD1	CD2	CD3	CD4	CD5	RC1	RC2	RC3	RC4
Fuel discharge radius (cm)	0.0	90.6	128.2	157.0	181.3	202.7	90.6	128.2	157.0	181.3
BOEC *k*-effective	1.018	0.995	1.007	1.016	1.021	1.024	1.011	1.024	1.028	1.029
MOEC *k*-effective	1.034	1.037	1.033	1.033	1.034	1.034	1.034	1.034	1.035	1.035
EOEC *k*-effective	1.042	1.054	1.056	1.048	1.044	1.042	1.055	1.044	1.042	1.040
Average k_{eq2}	1.035	1.036	1.033	1.033	1.033	1.033	1.034	1.034	1.035	1.035
Cycle length (MWd)	1.584E6	1.584E6	1.584E6	1.584E6	1.584E6	1.584E6	1.584E6	1.584E6	1.584E6	1.584E6
Peak Power Density (MW/m^2)	580	580	580	580	580	580	580	580	580	580
Total Power (MW)	948	1600	2647	3613	4439	5231	2365	3748	4781	5624
Cycle length (EFPY)	4.58	2.71	1.64	1.20	0.98	0.83	1.84	1.16	0.91	0.77
MOEC neutron excess (mol)	8777	8818	11111	14403	17797	21459	11646	17761	23135	27657
BOEC/EOEC neutron excess (mol)	8698	8623	10985	14323	17739	21414	11537	17711	23096	27622
MOEC burnup contained (EFPY)	7.56	6.01	5.92	5.88	5.94	5.91	5.87	5.65	5.59	5.55

Table 6.6-2. Fuel cycle and reactor parameters for different shuffling schemes (scaled cycle lengths)

Shuffling pattern	Conv.	CD1	CD2	CD3	CD4	CD5	RC1	RC2	RC3	RC4
BOEC *k*-effective	1.005	1.005	1.005	1.005	1.005	1.005	1.005	1.005	1.005	1.005
MOEC *k*-effective	1.034	1.037	1.033	1.033	1.034	1.034	1.034	1.034	1.035	1.035
EOEC *k*-effective	1.049	1.050	1.058	1.059	1.057	1.060	1.061	1.061	1.064	1.061
Average k_{eq2}	1.035	1.036	1.033	1.033	1.033	1.033	1.034	1.034	1.035	1.035
Cycle length multiplier	1.81	0.77	1.07	1.69	2.34	2.97	1.27	2.82	3.87	4.42
Cycle length (MWd)	2.866E6	1.215E6	1.698E6	2.679E6	3.702E6	4.702E6	2.018E6	4.460E6	7.008E6	8.040E6
Total Power (MW)	948	1600	2647	3613	4439	5231	2365	3748	4781	5624
Cycle length (EFPY)	8.28	2.08	1.76	2.03	2.28	2.46	2.34	3.26	4.02	3.92
MOEC neutron excess (mol)	8777	8818	11111	14403	17797	21459	11646	17761	23135	27657
BOEC/EOEC neutron excess (mol)	8519	8703	10966	14173	17480	21061	11469	17364	22490	26911
MOEC burnup contained (EFPY)	7.56	6.01	5.92	5.88	5.94	5.91	5.87	5.65	5.59	5.55
Core area (m^2)	9.19	10.23	13.18	16.36	19.52	22.82	12.81	17.94	22.59	26.86
Average power density (MW/m^2)	103	156	201	221	227	229	185	209	212	209
Neutron excess per area (mol/m^2)	927	851	832	867	896	923	895	968	998	1005
Neutron excess per power (mol/MW)	8.99	5.44	4.14	3.92	3.94	4.03	4.85	4.63	4.72	4.80
Approx. day-one starter fuel area (m^2)	1.96	3.31	5.48	7.47	9.18	10.82	4.89	7.75	9.89	11.64
Neutron excess per starter unit area (mol/cm^2)	0.434	0.263	0.200	0.190	0.190	0.195	0.234	0.224	0.228	0.232

The total area of the cycle corresponds to the area in which 99.5% of neutron absorptions occur. The average power density of each case is low, similar to the cases using 3D shuffling, since each requires a thick blanket of feed fuel that generates very little power. The average power density increases for larger systems because the ratio of power-generating area to breeding blanket increases. More complex shuffling schemes could potentially flatten the power distribution further and raise the average power density for a given size reactor. Meanwhile, the neutron excess cost per unit area is fairly constant across the cases, ranging from 832 mol/m^2 in the CD2 case to 1005 mol/m^2 in the RC4 case.

One important parameter is the neutron excess cost of the reactor per unit power generated. This factor is important because the fuel discharge rate is proportional to the total power, while the amount of discharged fuel needed to start a new reactor is related to the neutron excess cost. Therefore, the neutron excess cost per unit power is closely related to the doubling time of the system. Since neutron excess cost is roughly proportional to core size, shuffling schemes with high average power densities will have lower neutron excess/power ratios, and therefore shorter doubling times. By this metric, the CD3 shuffling scheme performs the best, requiring 3.92 mol of neutron excess per megawatt generated. Because of its reasonable power level (~3600 MW thermal, comparable to a large LWR) and cycle length (~2 years), the CD3 shuffling scheme is selected as the target equilibrium cycle for additional studies. To make the number of fuel zones discharged at each cycle an integer number, the cycle length is rounded down to 660 EFPD at a power level of 3600 MWth, which corresponds to an equilibrium cycle fuel discharge rate of 3 zones per cycle.

6.6.2 Designing starter fuel made from reused melt-refined feed fuel

The last two rows in Table 6.6-2 relate to design of the starter fuel. The approximate day-one starter fuel area is the area of starter fuel needed for the reactor to achieve full power on day one of operation. It is equal to the reactor total power divided by the maximum equilibrium cycle power density (580 MW/m^2) and multiplied by a peaking factor (1.2) to account for peaking within the starter fuel power distribution. Dividing the total neutron excess cost by the required starter fuel area gives the required amount of neutron excess per unit area of starter fuel, i.e. the required "strength" of the starter fuel.

The neutron excess per unit area of starter fuel is proportional to the neutron excess per unit power, so it is higher for the small, low average power density cases and lower for the large cases with flatter power profiles. For the convergent case, the required starter fuel "strength" of 0.434 mol/cm^2 is too high to achieve using starter fuel made from discharged fuel from a previous generation, therefore a larger area of starter fuel is needed. This can be handled in several different ways: first, one can simply use the large starter fuel area, and operate the fuel at a lower power density. Second, one can opt for starting up the reactor at a higher power level, then de-rating the power to the equilibrium cycle level once the equilibrium cycle is established. Third, one can start with a partial load of starter fuel on day one, then introduce additional starter fuel down the road to finish establishing the equilibrium cycle. This is the same strategy employed in the "early startup" fuel cycle variation, and has the advantage that new reactors can be brought online sooner, without requiring the full amount of starter fuel needed.

A similar set of methods can be used to implement starter fuel that supplies more neutron excess per unit area than required. One could operate the fuel at a higher power density during startup, or operate the reactor at a lower power level during transition. Alternatively, one could partially burn the starter fuel, and use the remaining neutron excess as margin against fuel failure or as fuel for starting additional reactors. These methods involve downsides in terms of lost electricity revenue or increased complexity, so it is advisable to use starter fuel configurations that can provide the necessary amount of neutron excess while also being able to supply full power on day one.

To design starter fuel that supplies the desired amount of neutron excess, infinite-plane models are used to evaluate different starter fuel variations. Irrespective of which equilibrium cycle case is used, the discharge burnup distribution is the one shown in Figure 6.6-1. In this case, the ends of the fuel have been bred sufficiently that k_∞ is greater than unity; i.e. the fuel is a net producer of neutrons. Once way to reconfigure the used fuel is to reverse each half of the assembly such that the ends of the fuel are now in the center, and vice versa. This would be accomplished by separately melt refining different axial sections of fuel. The lower curve in Figure 6.6-2 shows what the reconfigured burnup distribution looks like. This configuration is sensible since it places the least burned, lower k_∞ fuel at the center, which flattens the resulting flux distribution and results in a fairly uniform final burnup distribution. The upper curve in Figure 6.6-2 shows the change in burnup profile predicted by an infinite-plane model of this reconfigured fuel, assuming that the fuel has undergone a melt-refining process (described in Subsection 5.3.3) and a cooling time of two years. Figure 6.6-3 shows the corresponding twice-adjusted neutron excess that the infinite-plane model predicts.

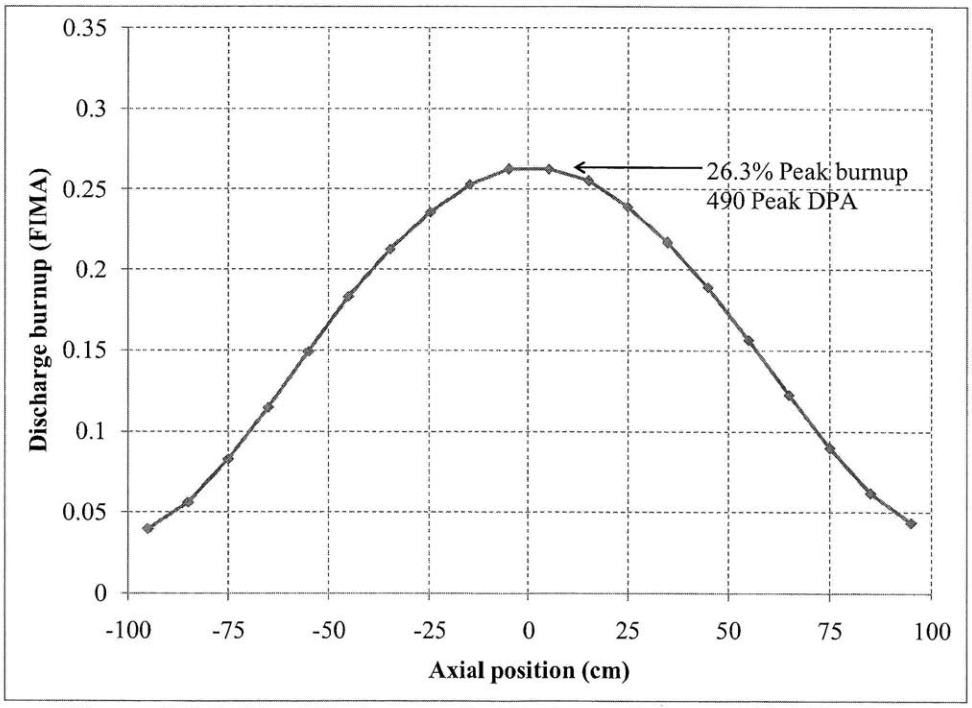

Figure 6.6-1. Equilibrium cycle discharge burnup distribution

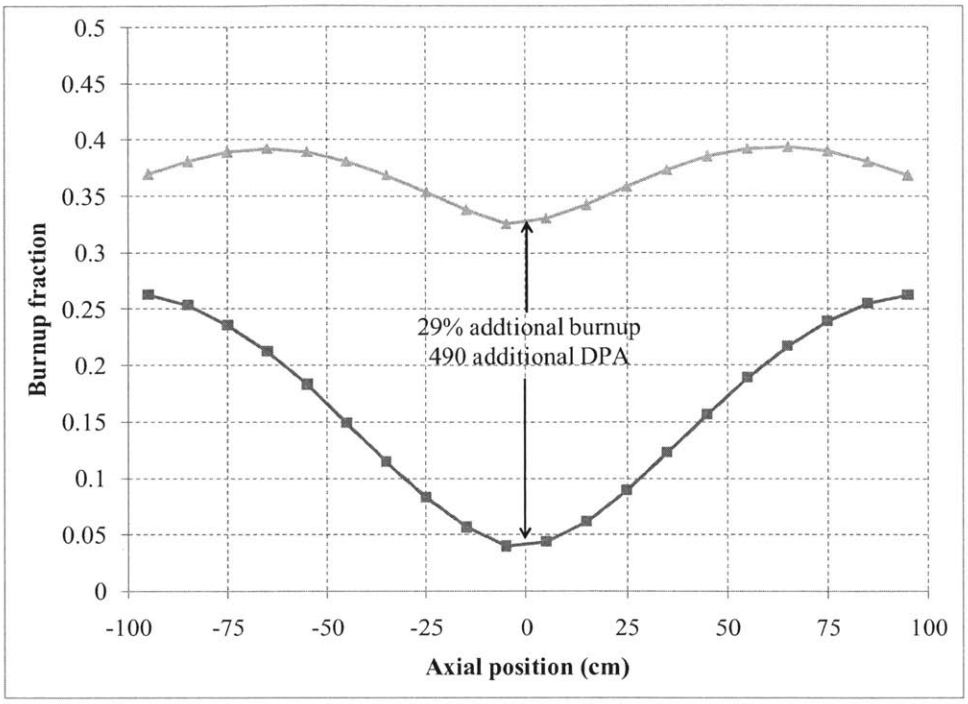

Figure 6.6-2. Initial and final distribution of reconfigured discharged feed fuel

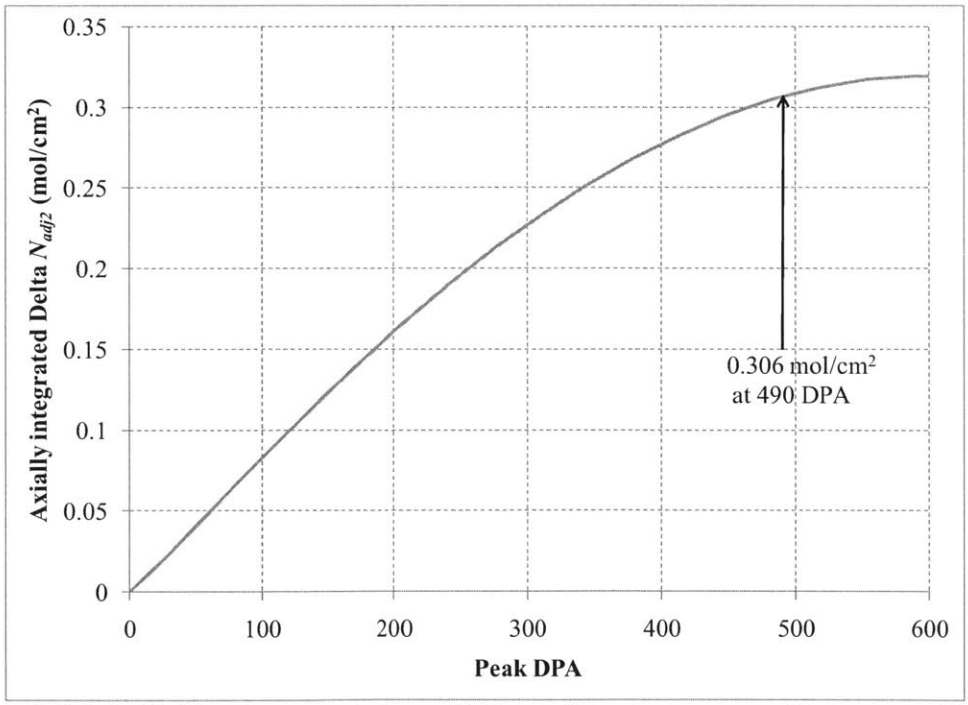

Figure 6.6-3. Infinite-plane model prediction of neutron excess from reconfigured discharged feed fuel

Figure 6.6-3 shows that the infinite-plane model predicts a neutron excess of 0.306 mol/cm^2 from the reconfigured fuel once the 490 DPA limit is reached. This is higher than the 0.190 mol/cm^2 needed for the selected equilibrium cycle (CD3), so it is desirable to find a new starter fuel configuration that uses less discharged fuel while supplying the correct amount of neutron excess.

Two ways of doing this are considered: first, one can uniformly dilute the starter fuel column with depleted uranium; second, one can shorten the starter fuel column and replace the ends with depleted uranium. The neutron excess obtainable from these two alternative configurations is shown in Figure 6.6-4. The percentage given in the legend is the concentration of reused fuel, with the balance made up by depleted uranium, while the length gives the height of the reused fuel column. Figure 6.6-5 gives the same results, except normalized to the amount of reused fuel present. Figure 6.6-4 shows that for a fuel DPA limit of 490, a 140 cm fuel column can supply a neutron excess of about 0.196 mol/cm^2, slightly more than the 0.190 mol/cm^2 required. Figures 6.6-4 and 6.6-5 show that using 200 cm of 70% reused fuel would yield a higher neutron excess at 490 DPA, but that configuration would be subcritical to begin with and therefore wouldn't be usable by itself as starter fuel. Also, the diluted full-length starter configurations would require a longer amount of time to burn through than the shortened configurations, increasing transition time.

For the chosen equilibrium cycle, a starter fuel area of 7.74 m^2 is employed, corresponding to 18 radial zones in the reactor model. The starter fuel configuration is 140 cm of reversed discharged fuel, as pictured in Figure 6.6-6. According to the infinite-plane model, this amount of starter fuel will supply a neutron excess of 15,200 mol, allowing about a 7% margin for the 14,200 mol needed. Thanks to this margin, the starter fuel only needs to supply a neutron excess of 0.183 mol/cm^2, which in the infinite-plane model corresponds to a peak DPA of 430.

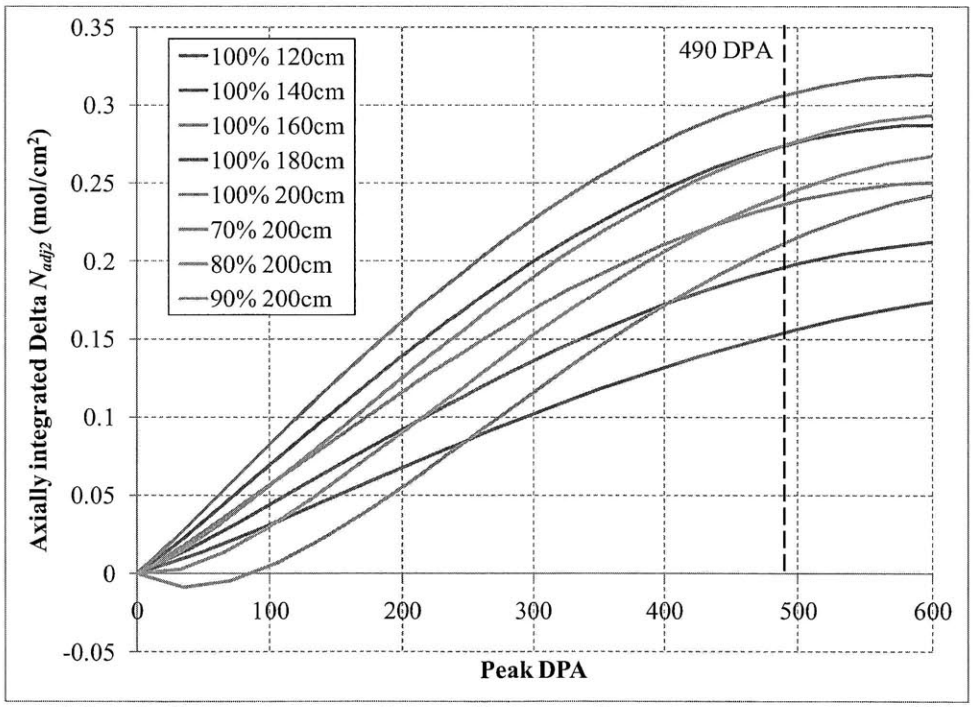

Figure 6.6-4. Infinite-plane model predictions of neutron excess from different configurations of reused feed fuel

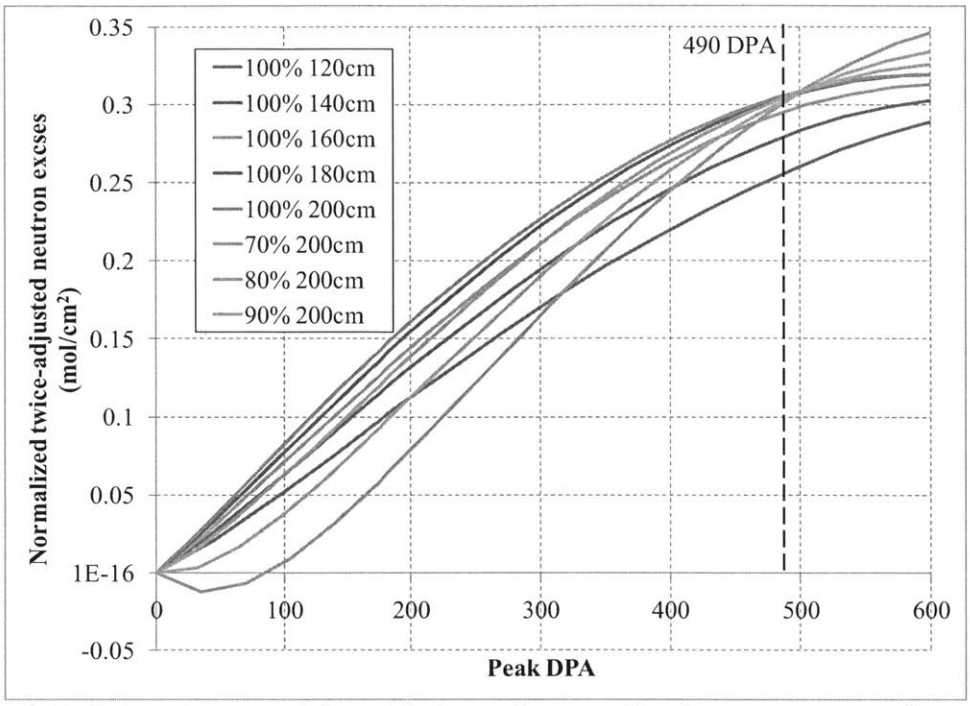

Figure 6.6-5. Infinite-plane model predictions of normalized neutron excess from different configurations of reused feed fuel

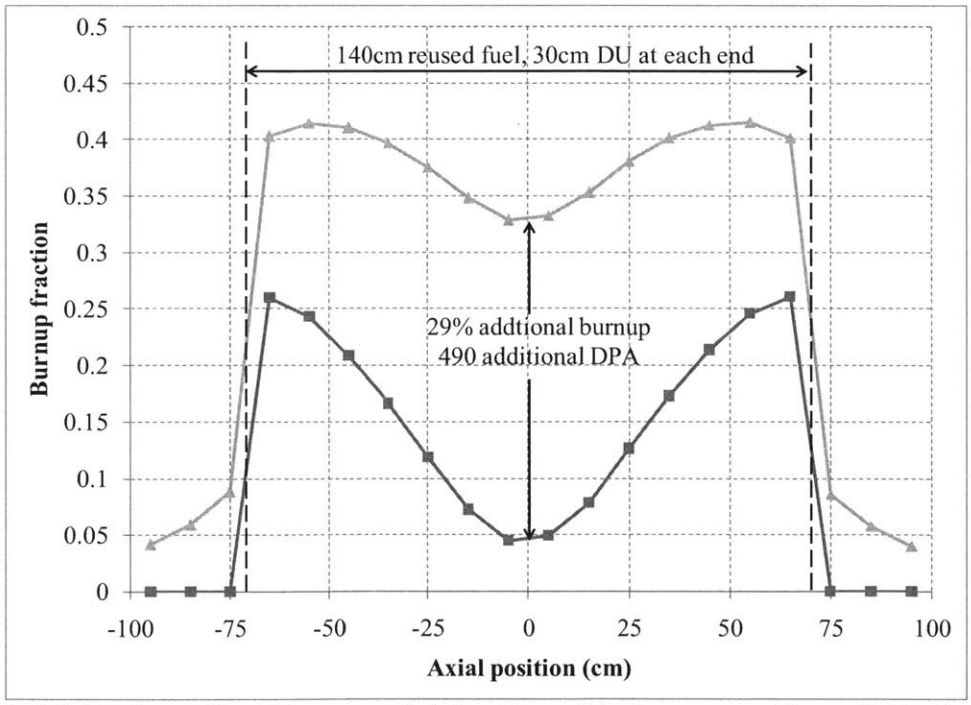

Figure 6.6-6. Initial and final burnup distribution of 140 cm reconfigured discharged feed fuel in infinite-plane model

6.6.3 Initial doubling time estimate

The expression for calculating the doubling time of a B&B reactor fleet was developed in Chapter 4 (Equation 4.4-14), and is reproduced as Equation 6.6-1:

$$e^{((t_{tr}+t_c)/t_e)} = \frac{t_e}{t_s} \tag{6.6-1}$$

In Equation 6.6-1, t_e is the reactor e-folding time, t_c is the cooling/processing time, t_{tr} is the equilibrium cycle transition time, and t_s is the starter fuel spawning time, i.e. the amount of time required for one reactor to produce enough starter fuel to start a new reactor.

If one assumes an average capacity factor equal to 330/365, or 90.4%, and a cooling/processing time of two years, then the terms in Equation 6.6-1 have values calculated as follows. The transition time t_{tr} is the sum of the time needed to finish burning the starter fuel and "burn in" the equilibrium cycle. According to the infinite-plane model, burning the starter fuel to 430 peak DPA requires 176 MWd/cm^2, so burning through 7.74 m^2 would require 1.36E7 MWd, 10.4 EFPY, or 11.5 years. The MOEC state contains 5.9 EFPY worth of burnup, or 6.5 years worth, which summed with 11.5 yields a total transition time of approximately **18.0 years**. Each reactor requires 18 zones worth of starter fuel, which takes 18 * 0.7 / 3 = 4.2 cycles to discharge, corresponding to 7.6 EFPY or **8.4 years**.

Plugging these values into Equation 6.6-1 and solving numerically yields an e-folding time of 21.4 years, corresponding to a doubling time of **14.8 years**. This is about 50% longer than the ~10 year doubling time estimated for the case using the same core composition in a minimum-burnup B&B reactor. Aside from the differences in the two equilibrium cycles, the linear-assembly case has a longer doubling time because it loses more neutrons to leakage and burns fuel to a less uniform level than the minimum-burnup case. Importantly, it also requires a single-pass peak DPA close to 500, versus less than 300 DPA needed for the case with minimum burnup B&B reactors. However, the use of conventional assemblies could greatly simplify reactor design. It is arguable which configuration would allow more neutronically favorable core compositions: a minimum-burnup reactor would require additional axial structure to hold the fuel blocks together, while the case with conventional assemblies may require either more clad or lower fuel smear densities to allow higher fuel burnup.

6.6.4 Example limited-separations fuel cycle transition case using proposed starter fuel design

MCNPXT is used to model the transition between the selected starter fuel design (18 zones with 140 cm of reused fuel) and the selected equilibrium cycle (3600 MWth, with 660 EFPD per cycle). This model is referred to as the "linear-assembly doubling model," since it describes a case in which discharged feed fuel from a B&B reactor is used to start up a second identical reactor. The shuffling sequence is determined using trial and error, with the goal being to find a sequence that would converge to the equilibrium cycle in a reasonable amount of time, while keeping k-effective above unity and the peak areal power density below 600 MW/m^2. The final accepted shuffling sequence is given in Table 6.6-3.

Table 6.6-3. Transition shuffling sequence for linear-assembly doubling model

Cycle Number	*Cycle fuel permutation starting from central zone (Each cycle is 660 EFPD long)*																							
1	19	1	2	20	3	4	5	6	7	8	9	10	11	12	13	14	15	16	17	18	21	22	23	24
2	19	20	18	17	16	15	21	14	1	13	2	12	11	10	3	9	4	8	7	22	23	24	25	26
3	22	19	21	20	5	6	18	23	7	8	17	4	9	16	3	15	14	12	1	24	25	26	27	28
4	25	24	22	26	23	19	11	10	13	2	1	5	6	12	14	15	21	20	3	16	27	28	29	30
5	27	28	25	26	24	22	18	9	17	7	4	8	11	10	23	19	21	20	2	13	29	30	31	32
6	29	28	27	25	26	24	30	16	3	15	14	12	6	22	23	21	19	20	5	1	31	32	33	34
7	32	31	30	29	28	33	27	13	2	8	25	26	24	22	23	19	21	20	4	18	34	35	36	37
8	36	35	34	32	33	31	30	29	28	27	25	26	24	22	23	19	21	20	37	38	39	40	41	42
9	39	38	37	36	35	34	32	33	31	30	29	28	27	25	24	26	23	22	7	40	41	42	43	44
10	41	40	39	38	37	36	35	34	17	32	33	31	9	1	30	29	28	27	5	10	42	43	44	45
11	44	43	42	41	40	39	38	37	36	35	34	11	32	33	31	16	3	30	18	45	46	47	48	49
12	47	46	45	44	43	42	41	40	39	38	37	36	35	34	32	33	31	29	48	49	50	51	52	53
13	50	49	48	47	46	45	44	43	42	41	40	39	38	37	36	35	34	21	51	52	53	54	55	56
14	53	52	51	50	49	48	47	46	45	44	43	42	41	40	39	38	37	36	54	55	56	57	58	59
15	56	55	54	53	52	51	50	49	48	47	46	45	44	43	42	41	40	39	57	58	59	60	61	62

Two shades are used in Table 6.6-3, corresponding to those used in Table 6.4-2. First, the cells filled in with lighter gray are the positions of the starter fuel zones. As more feed fuel is bred, the number of starter assemblies in the power producing region decreases. This is done so that the power producing region remains approximately the same size during transition, reducing the need for complex flow orificing. Some starter fuel is reintroduced in cycles 9 through 11, because in those cycles, some feed fuel has been discharged at its DPA limit, so the starter fuel is needed to maintain a critical system with a sufficiently large power distribution. In each cycle, the starter fuel is ordered so that the fuel with the lowest peak DPA is placed innermost, and the fuel with the highest peak DPA is preferentially left out of the power producing region.

From cycles 2 onward, there is usable starter fuel that is left out of the power producing region. This fuel could potentially be placed back in the power producing region, which would expand the power producing region and allow more power to be produced during transition. Doing this would both speed up transition while allowing revenue from electricity production to be generated sooner, but would require a unique plant configuration capable of supporting a temporary uprate.

The darker gray shade in Table 6.6-3 indicates the feed fuel that has experienced the most burnup and DPA. Furthermore, the feed fuel highlighted in dark gray is arranged in order of lowest DPA toward the center, so the highest DPA feed fuel at a given cycle is the outermost dark gray cell. Meanwhile, the un-highlighted feel fuel (in white) is arranged with the highest peak DPA toward the center. From this coloring, one can see that in cycles 12 and onward, a configuration close to the convergent-divergent equilibrium cycle has been developed, with the highest DPA feed fuel located in zone 18.

The discharge DPA distribution from this startup sequence is given in Figure 6.6-7. The equilibrium cycle peak discharge DPA is 486 DPA when averaged across the three zones discharged per cycle, but due to peaking within the three zones, the peak discharge DPA is 495 DPA. This case does a much better job of limiting the peak DPA in the transition feed fuel than

the earlier linear-assembly transition model. Peak transition fuel DPA is held to 519 DPA, less than 5% more than the equilibrium cycle peak of 495 DPA.

The peak DPA averaged across the 18 starter fuel zones is 376 DPA, with the maximum peak DPA in these zones equal to 406, for a peak-to-average of 1.08. The average of 376 DPA is 88% of the value of 430 DPA predicted by the 1D model. This reason for this discrepancy is illustrated later in the discussion on the neutron excess contribution from the starter fuel.

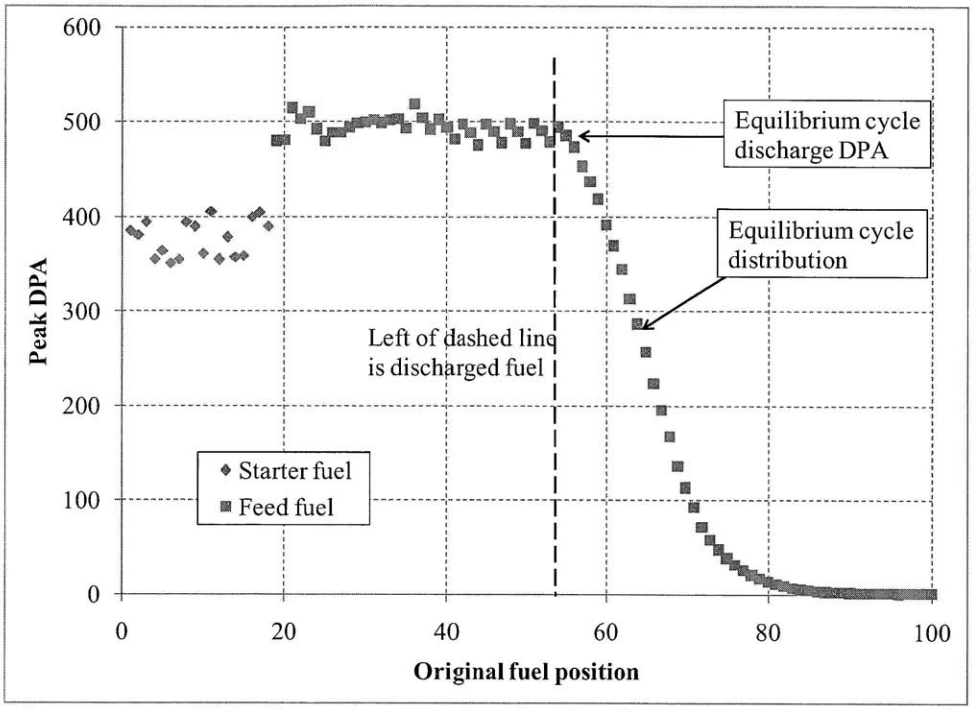

Figure 6.6-7. Peak DPA discharge distribution for linear-assembly doubling model

The evolution of uncontrolled *k*-effective for the linear-assembly doubling model is given in Figure 6.6-8. There is some cycle-to-cycle variation during the early transition shuffles, which quickly settles into the equilibrium cycle *k*-effective evolution by about year 25. The transition sequence does a good job of keeping the uncontrolled *k*-effective close to the average equilibrium cycle value, as well as close to the minimum and maximum bounds set by the equilibrium cycle.

Since there is no radial leakage in this simplified model, uncontrolled *k*-effective in this model is equal to the model's k_{fuel2}, defined in Subsection 6.4.2. The contribution to neutron excess due to deviations in k_{fuel2} is illustrated in Figure 6.6-9. Because the transition sequence does a good job of staying near the average k_{eq2} of the equilibrium cycle, the total contribution is very small (~70 mol), less than 1% of the total amount in the equilibrium cycle (14.2E3 mol) and within the statistical error of the simulation.

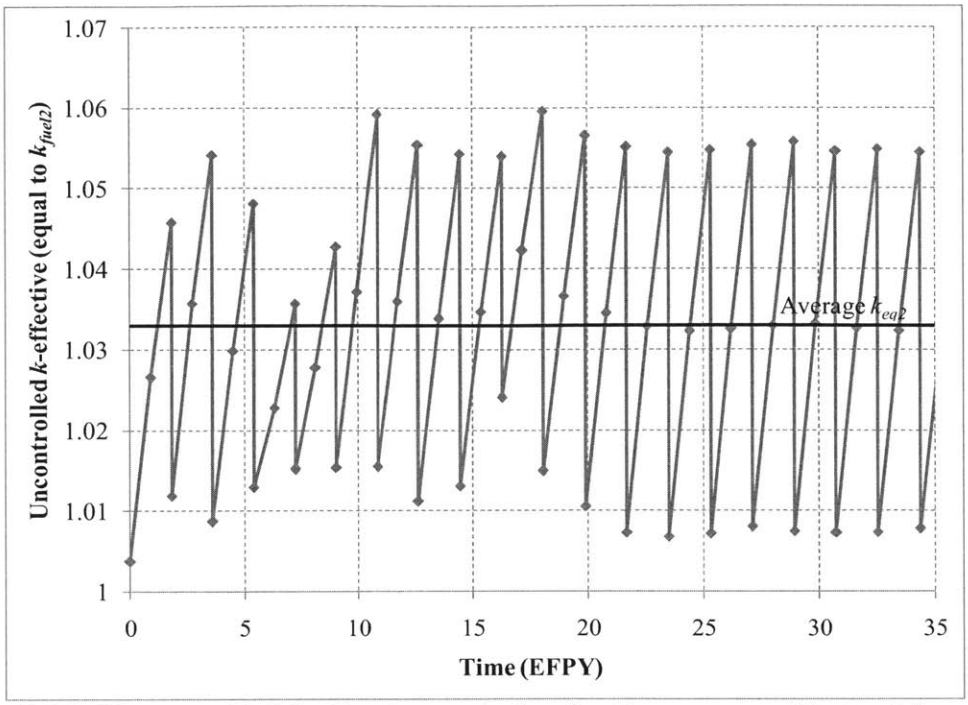

Figure 6.6-8. Uncontrolled *k*-effective evolution for linear-assembly doubling model

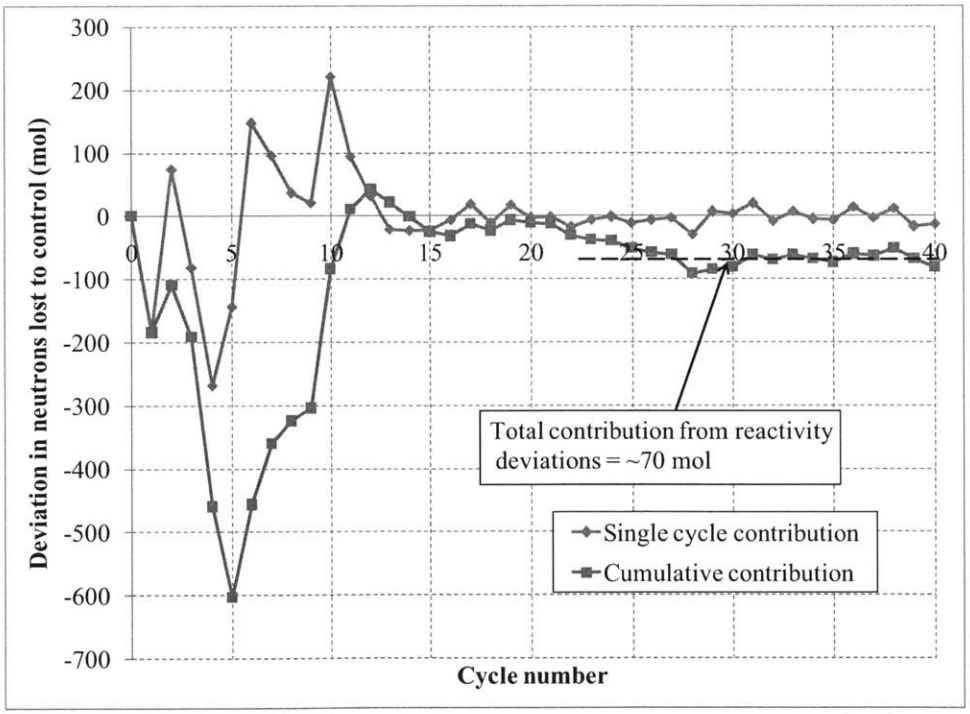

Figure 6.6-9. Contribution of k_{fuel2} deviations to system neutron excess in linear-assembly doubling model

The contributions to neutron excess of the different types of fuel are shown in Figure 6.6-10. Because the peak DPA of the transition feed fuel is successfully kept close to the equilibrium cycle value, the neutron excess contribution of the transition feed fuel is very low, less than 3%

of the total required for establishing the equilibrium cycle. Almost all the required neutron excess is provided by the starter fuel. The infinite-plane prediction of the starter fuel neutron excess agrees well with the results from the actual transition case, but it is slightly conservative: the actual starter fuel neutron excess averages 10% higher than the infinite-plane prediction.

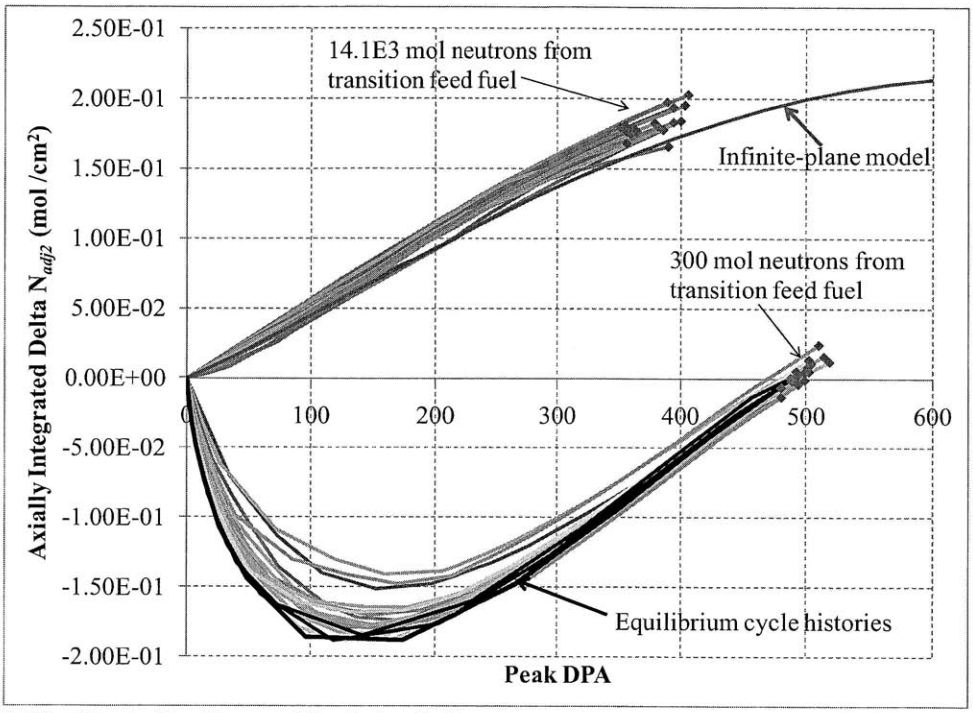

Figure 6.6-10. Contributions of fuel depletion to system neutron excess in linear-assembly doubling model

Aside from the neutron excess results, another significant result from the linear-assembly doubling model is the power distribution of the core over the transition cycles. Figure 6.6-11 shows the maximum areal power density at each radial position over the transition sequence, referred to as the "power envelope" of the transition cycle. Interestingly, the power envelope of the transition sequence contains only 15% more total power than an ideal power envelope that only contains the equilibrium cycle power distributions. This suggests that using a fixed-orificing scheme would be possible for this transition sequence without a large drop in average coolant outlet temperature. Since the transition sequence was not explicitly designed to maintain a constant power shape, it is likely that additional optimization can be performed to shrink the transition sequence power envelope and improve the performance of fixed orificing.

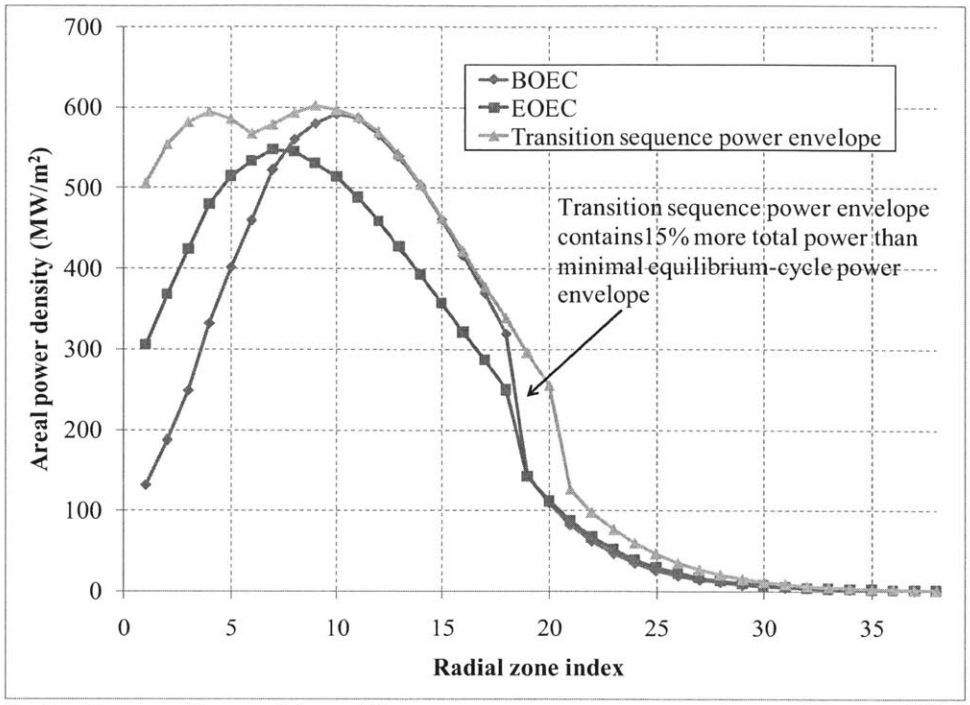

Figure 6.6-11. Comparison of transition sequence power envelope with equilibrium cycle power distributions

6.6.5 Starter fuel depletion comparison between linear-assembly doubling model and infinite-plane model

Like in the linear-assembly transition model, the 10% difference between the axially-integrated neutron excess predicted by the infinite-plane (1D) approximation and the actual results from the doubling model can be attributed to two factors: differences in the axial flux distribution and differences in the flux energy spectra. This is because the neutron excess evolution of a fuel assembly depends only on the axial-position and energy dependent flux histories that the assembly experiences.

Figure 6.6-12 illustrates the differences in axial distribution by comparing the final DPA distributions of the 18 starter fuel zones with curves from the 1D prediction. The 1D model yields slightly flatter distributions than the transition model: for a given peak DPA the 1D model shows higher DPA experienced at the ends of the fuel. The cause for this is the presence of the feed fuel in the transition model: the plutonium breed-burn feedback in the feed fuel results in a more highly peaked flux distribution than that in the 1D model.

There are two expected effects from the difference in the axial distribution. In the 1D model, which has a flatter fluence distribution, there is better utilization of the starter fuel, which fills the middle 140 cm of the fuel assembly. At the same time, the flatter distribution also means there are more neutron losses into the depleted fuel at the end 30 cm of each end and more leakage out the ends of the fuel, both of which offset the gain from better utilization of the starter fuel.

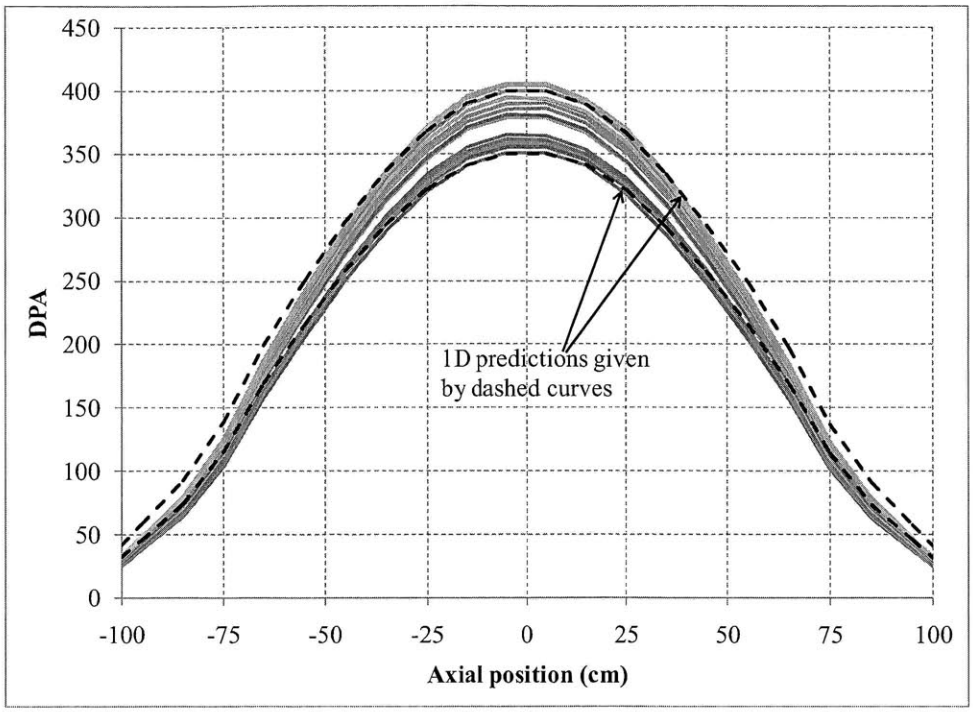

Figure 6.6-12. Comparison between infinite-plane and linear-assembly doubling mode model starter fuel axial distributions

To evaluate the effect of varying axial distributions, the results from the 1D model are made to artificially match the axial distributions from the doubling model, by linearly interpolating the neutron excess contribution based on the DPA experienced at each axial node. The results of this comparison are given in Figure 6.6-13. Figure 6.6-13 shows that simply matching the axial shape only yields about a 2% increase in neutron excess when compared to the 1D model, explaining only a small fraction of the 10% average discrepancy observed. Further, the differences in axial distribution do not explain the large spread seen in the different starter fuel assemblies, confirming the conclusion reached in Subsection 6.5.1 for the linear-assembly transition model.

The remainder of the discrepancy between the doubling and infinite-plane models, as well as the reason behind the spread in the doubling model results, is due to the different spectral histories encountered by the fuel in the different models. The spectral histories at the midplane of the fuel in each model are shown in Figure 6.6-14. Overall, the neutron spectra experienced in the doubling model are harder than that in the 1D model. This is because in the 1D model, there is a uniform spectrum throughout of "medium" hardness, while in the doubling model, the average spectrum is segregated into the "harder" burning region and the "softer" blanket region. Because the starter fuel spends most of its time in within the harder burning region, it experiences a harder neutron spectrum on average than in the 1D model.

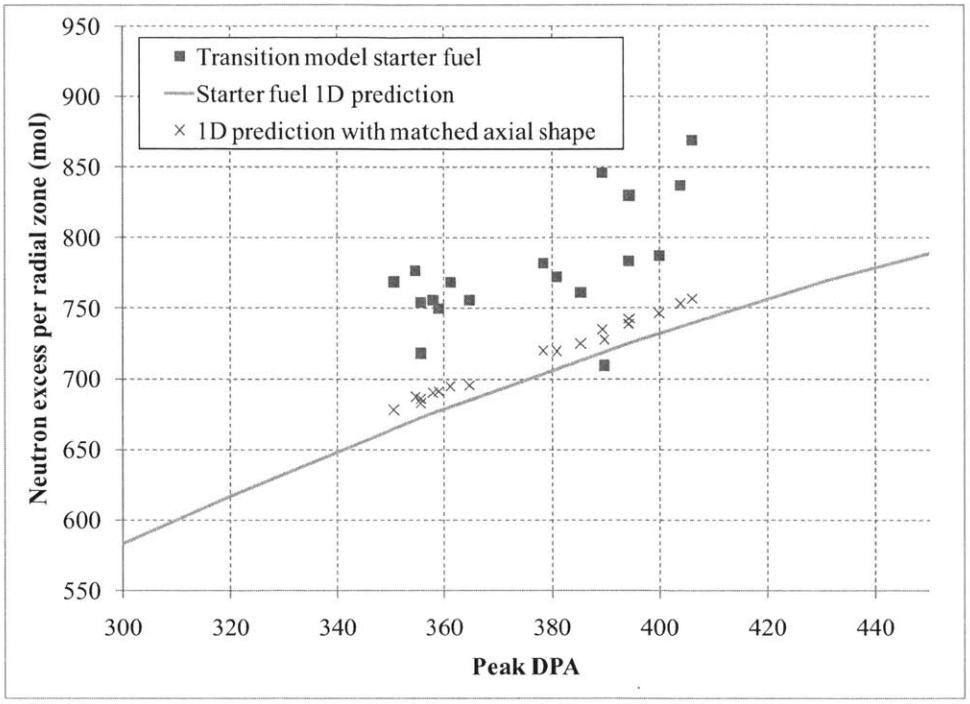

Figure 6.6-13. Comparison between doubling model and infinite-plane model with matched axial shape

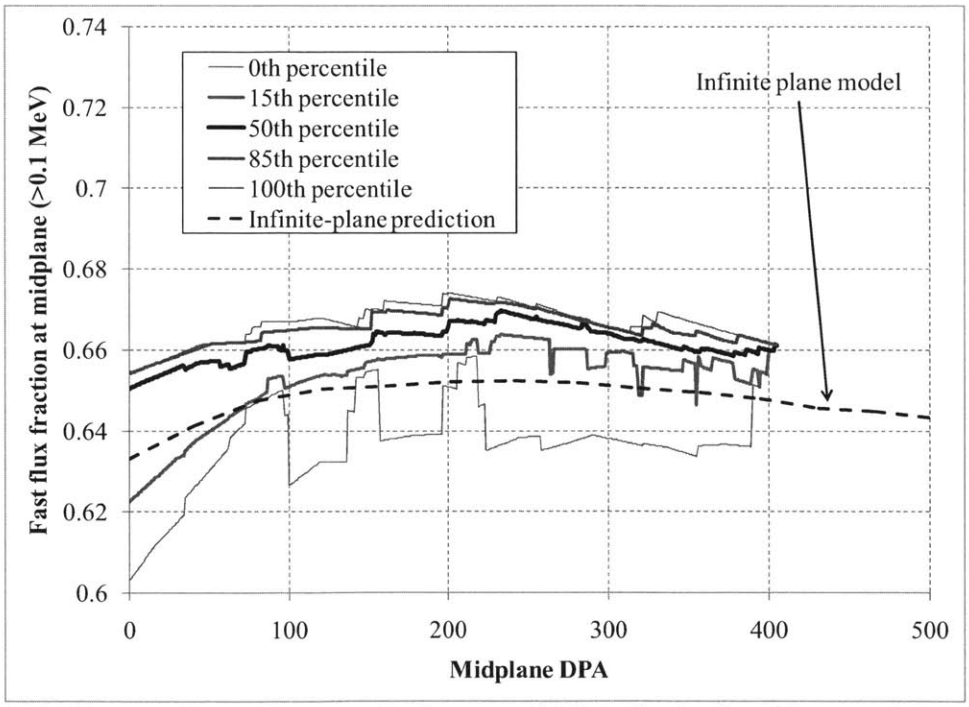

Figure 6.6-14. Comparison of starter fuel spectral histories in doubling model and infinite-plane model

The effect of neutron spectrum on neutron excess evolution is shown in Figure 6.6-15. The y-axis is the ratio of neutron excess produced by a starter fuel assembly in the doubling model and that produced by the 1D model when burned to the same peak DPA. The x-axis gives the

fraction of fluence composed of >0.1 MeV neutrons experienced over the irradiation history of the midplane of the assembly. Figure 6.6-14 shows a clear correlation between the average hardness of the neutron spectrum encountered by an assembly and the neutron excess it produces. There is a much stronger correlation in the doubling model than in the earlier transition linear-assembly model (Figure 6.5-5), because the presence of fission products in the reused feed fuel makes the number of neutron absorptions (thus the neutron excess) more sensitive to neutron spectrum. One can again conclude that the majority of the discrepancy between the doubling model and the 1D model is due to differences in neutron spectra.

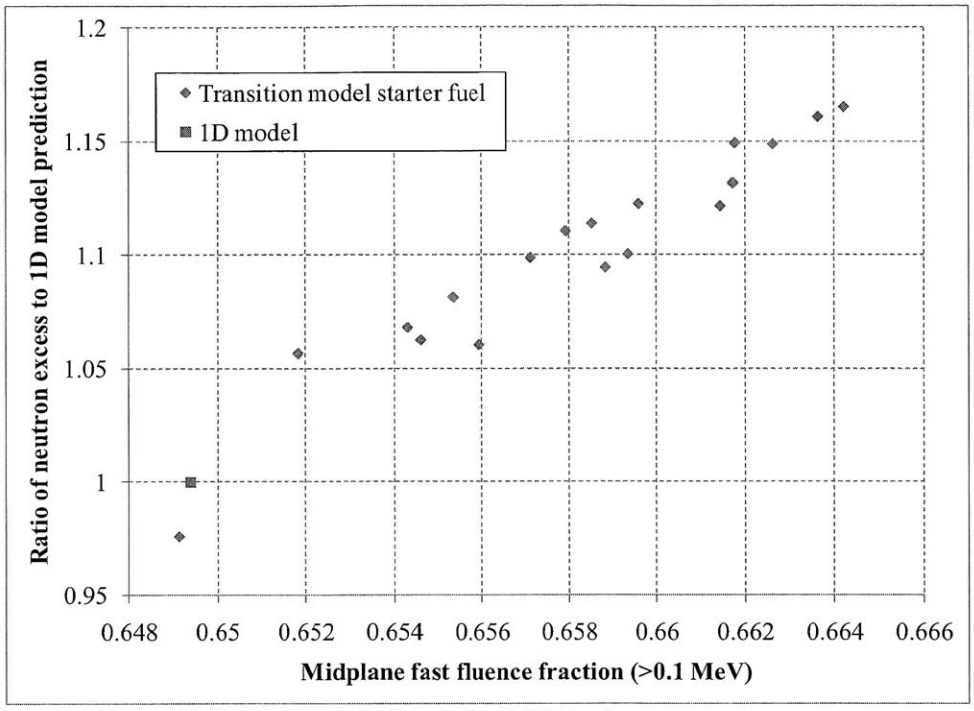

Figure 6.6-15. Effect of spectral histories on neutron excess

6.6.6 Feed fuel depletion and discharge schedule in linear-assembly doubling model

The previous subsection compared the axial DPA distributions and fluence histories of the starter fuel in the transition model with the results from the infinite-plane approximation. It is equally important to make a similar set of comparisons for the transition feed fuel, since the composition of the feed fuel and the timing of when it is discharged directly affects the startup of the next generation of reactors.

Feed fuel discharge schedule

The shuffling sequence given in Table 6.6-3 shows when feed fuel is first discharged from the core, starting with three zones at cycle 9. In two instances (materials 21 and 29), feed fuel is first discharged at a lower DPA then brought back for an additional cycle: material 21 is discharged at cycle 9 and returns for cycle 13, while material 29 is discharged at cycle 10 and returns for cycle 12. Figure 6.6-16 shows the total number of feed assemblies that have been discharged as a function of time. The dashed stepped line corresponds to how many burned feed zones are outside the power producing region at a given time, while the solid stepped line gives how many

burned feed zones have been permanently discharged. In both cases, the number of discharged zones rises at a constant rate of 3 per cycle once the equilibrium cycle has been established.

Also shown is the linear approximation from the earlier doubling time estimate (in Subsection 6.6.3) based on the results from the 1D model. That calculation assumed that the transition period would require 10.4 EFPY to burn through the starter fuel and an additional 5.9 EFPY to establish the equilibrium cycle. After this transition period, the core would be in a configuration similar to the equilibrium cycle and could begin discharging feed fuel at the equilibrium cycle rate. In the actual transition model, the amount of fuel discharged during the equilibrium cycle is ahead of the linear approximation by about one sixth of a cycle, or about 0.3 EFPY. The reason the transition model is slightly ahead is because the starter fuel did not need to be burned as far as predicted by the doubling time estimate (to an average of 380 DPA vs. 430 DPA), so only 10.1 EFPY instead of 10.4 EFPY was required to burn through the starter fuel. The transition model also shows how fuel can be discharged slightly sooner than estimated by the linear approximation, but this behavior only lasts for a few cycles before the equilibrium cycle is established. Figure 6.6-16 shows that the linear approximation serves as an excellent (and slightly conservative) estimate to the actual feed fuel discharge schedule of an explicitly modeled transition sequence.

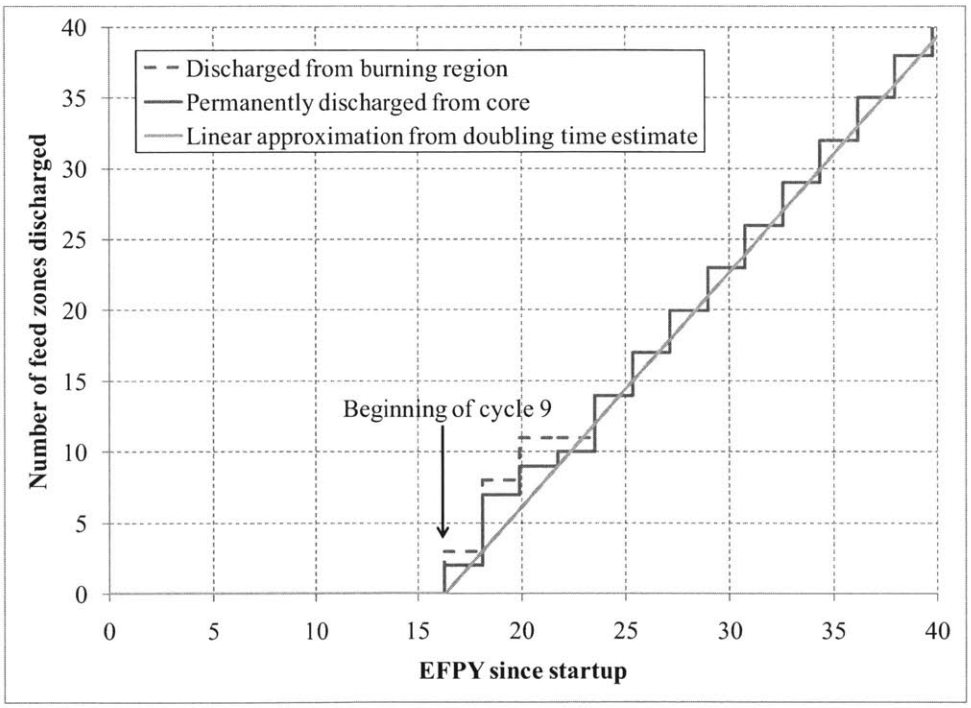

Figure 6.6-16. Discharge schedule for doubling model compared to linear approximation

Composition of discharged transition feed fuel

Figure 6.6-17 shows the axial discharge DPA distributions of the transition feed fuel. Also shown using dashed lines are the equilibrium cycle distribution and the distribution arising from the infinite-plane model. It's interesting to note that the DPA distributions for the transition feed fuel are more centrally peaked than both the equilibrium cycle distribution and the 1D

distribution. This central peaking occurs because the initial configuration of the starter fuel concentrates the flux to within the central ~140 cm of the assemblies. As a result, plutonium is preferentially bred in this central region, creating a short initial flux distribution that gradually spreads into the equilibrium cycle state. Comparing the two dashed curves shows that the burn distribution of the starter fuel is not that different from that of the equilibrium cycle, so the transition between the two is fairly rapid and the transition feed fuel distributions are similar to that from the equilibrium cycle.

Figures 6.6-18 and 6.6-19 show the corresponding burnup and plutonium-239 distributions in the transition feed fuel. Figure 6.6-18 shows a similar result to Figure 6.6-17, but with one outlier: the topmost orange curve shows higher burnup than the others. This is because this curve corresponds to feed fuel material number 21, which spends several cycles in the softer spectrum at the periphery of the burning zone. The softer spectrum it experiences allows it to sustain more burnup for a given amount of DPA. Figure 6.6-19 shows that the lower burnup at the axial ends of the transition feed fuel results in a lower plutonium-239 concentration, which has implications for when the transition feed fuel is subsequently made into new starter fuel.

To determine the neutron excess worth of this feed fuel, each of the transition feed fuel zones is reassembled in the same way as the equilibrium cycle feed is, as shown in Figure 6.6-6. Each of the resulting starter configurations is then depleted in an infinite-plane model. Results for neutron excess as a function of peak DPA for the different transition feed fuel starters are shown in Figure 6.6-20. The figure shows that the different transition feed fuel compositions produce roughly the same amount of neutron excess as the equilibrium cycle feed fuel, with the infinite-plane predictions differing by less than 5%.

The net effect of there being more or less neutron excess available from the transition feed fuel would be a change in the effective transition time. If less neutron excess were available from the transition feed fuel, then the effective transition time would be longer, since producing neutron excess at a slower rate after transition is roughly equivalent to there being a delay in starting to produce neutron excess. If one conservatively assumes that the transition feed fuel discharged during cycles 9-14 (over 9.0 EFPY) are on average able to supply only 95% of the neutron excess of the equilibrium cycle feed fuel, this 5% reduction in neutron excess translates to a 0.45 EFPY increase in the transition time, which would only increase the doubling time by 1.2% (from 14.8 years to 15.0 years). Therefore, the initial doubling time estimate is not significantly affected by the different neutron excess obtainable from transition feed fuel. Instead, the major issue associated with transition feed fuel will likely be characterizing its composition and fuel performance so that a starter fuel configuration and transition sequence can be designed to make use of it.

Overall, the initial doubling time estimate from Subsection 6.6.3 of 14.8 years is remarkably close to what can be achieved according to the linear-assembly doubling model. The primary source of error is again in the starter fuel neutron excess estimate: in the doubling model, the starter fuel produces about 10% more neutron excess than predicted by the infinite-plane model, so the required amount of starter fuel would be about 10% less. This would reduce the reactor spawning and transition times correspondingly and lead to a roughly 10% reduction in doubling time, from 14.8 years to about 13.3 years. This section demonstrates how using the neutron

excess concept allows a variety of equilibrium cycle and starter fuel configurations to be compared, guiding the design of a starter fuel configuration for a limited-separations fuel cycle using B&B reactors.

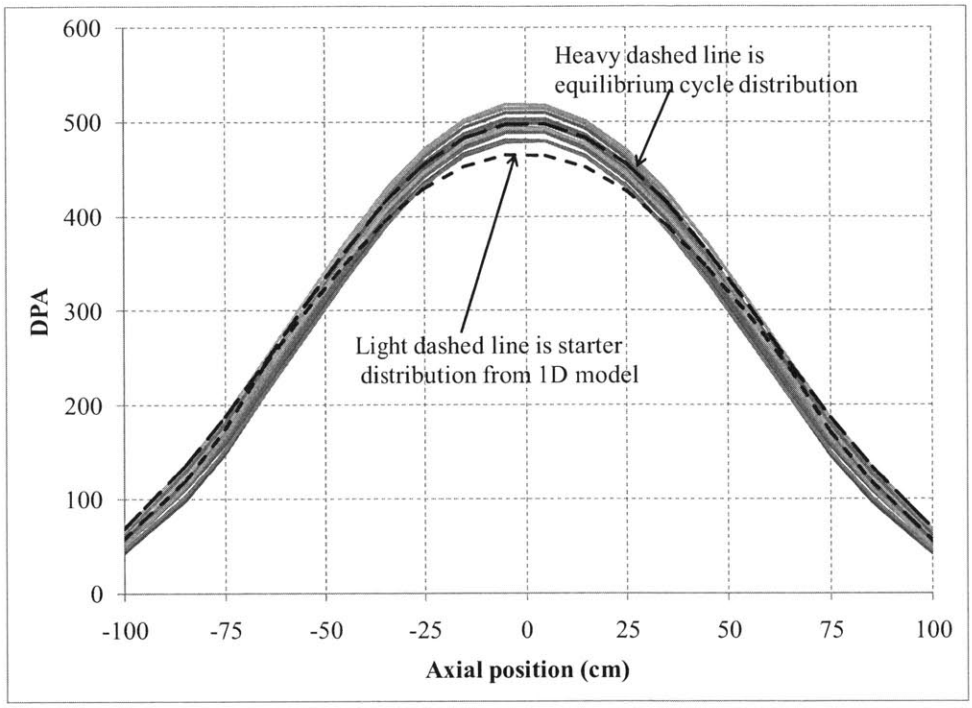

Figure 6.6-17. Discharge axial DPA distributions for transition feed fuel from doubling model and infinite-plane model

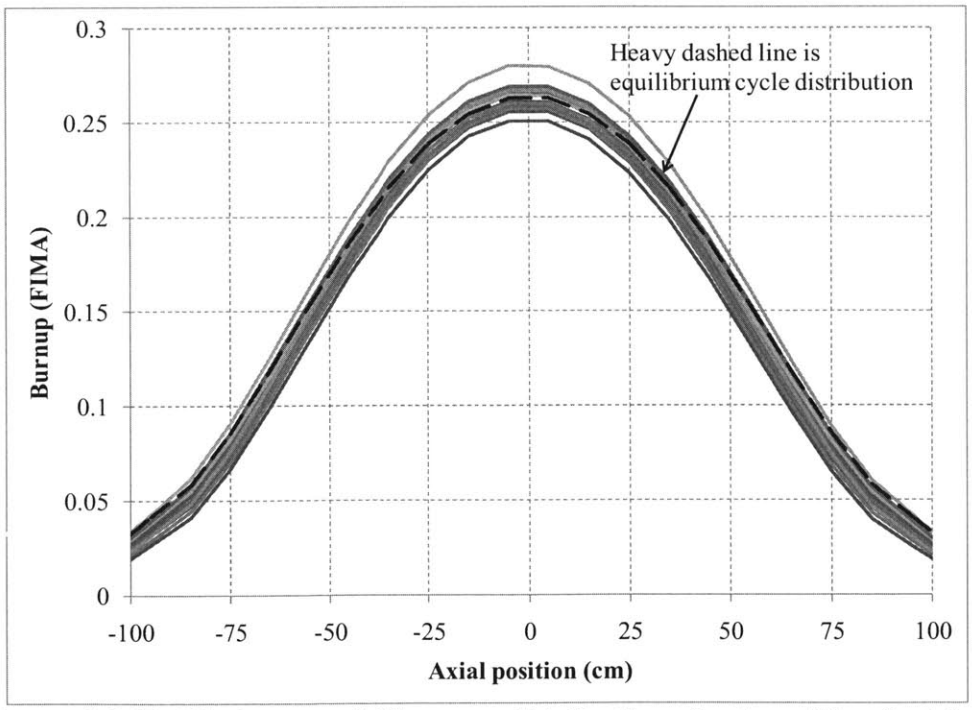

Figure 6.6-18. Discharge axial burnup distributions for transition feed fuel

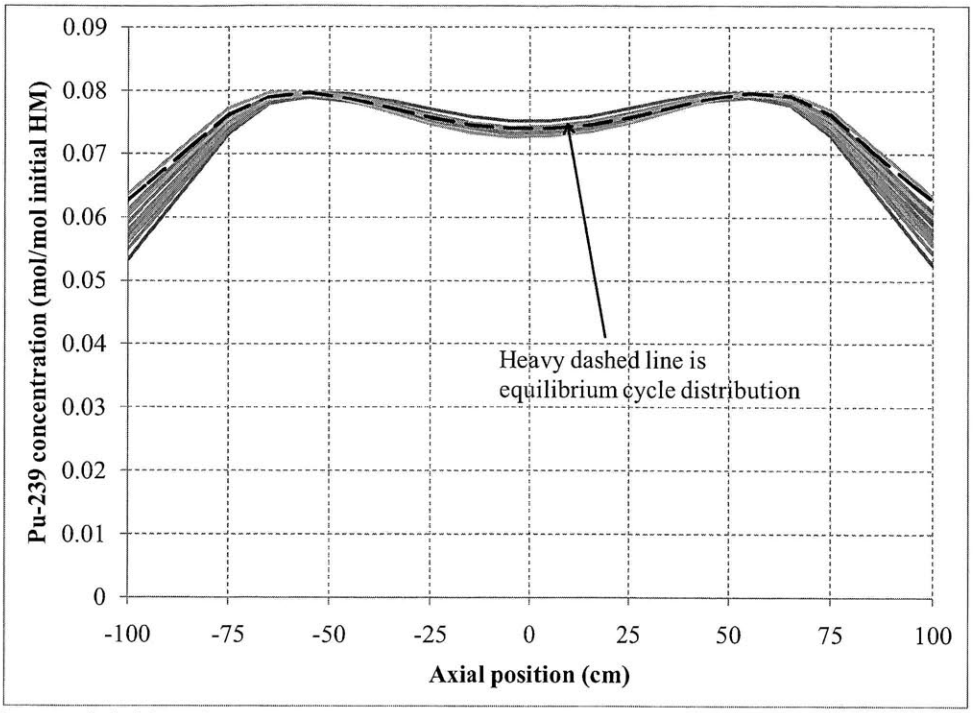

Figure 6.6-19. Discharge axial Pu-239 distributions for transition feed fuel

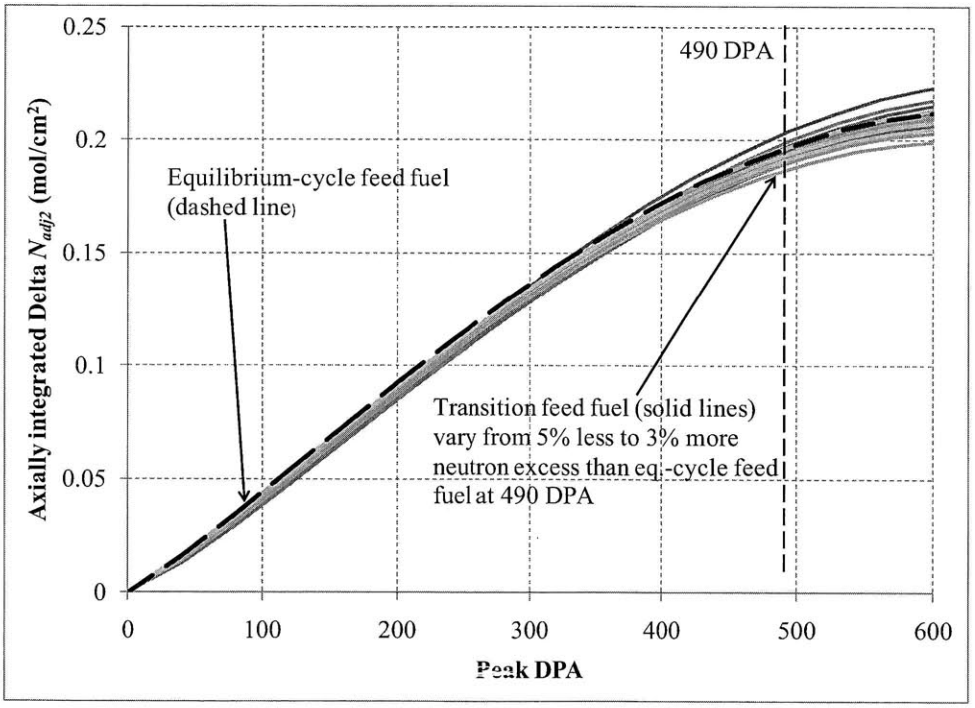

Figure 6.6-20. Infinite plane neutron excess predictions for starter fuel made from transition and equilibrium cycle feed fuel

6.7 Summary of linear-assembly B&B reactor findings

Linear-assembly B&B are much more challenging from a minimum burnup and DPA perspective than minimum-burnup B&B reactors: for example, the lowest-doubling-time core composition from Chapter 5 (U2Zr-75-T91-30-Na-100) requires less than 14% burnup and 270 DPA in a minimum-burnup B&B reactor, but needs approximately 27% burnup and 500 DPA in a linear-assembly B&B reactor. With this core composition and using melt refining to recycle fuel, achievable doubling time increases from 8 years for minimum-burnup B&B reactors to 14 years for linear-assembly B&B reactors. The chief advantage of linear-assembly B&B reactors is that they would be easier to engineer than a minimum-burnup B&B reactor.

Like for minimum-burnup B&B reactors, linear-assembly B&B reactors also have an equilibrium cycle burnup-reactivity relationship that depends almost solely on the reactor core composition, with relatively little dependence on reactor geometry and shuffling pattern. This behavior is again due to the low absorption cross sections in a fast reactor, which means that neutrons scatter many times before absorption and therefore are always absorbed in a similar spatial and energy distribution around where they are produced. The relationship between where a neutron is produced and absorbed axially can be approximated using a simple neutron axial transfer model based on diffusion theory, which can successfully predict the axial burnup distribution as well as the unique height-reactivity relationship in a linear-assembly B&B reactor. The fact that the axial transfer matrix looks the same for different core compositions implies that the neutronic ranking of core compositions from Chapter 5 would apply equally to linear-assembly B&B reactors.

The neutron excess concept developed in Chapter 2 can also be applied to linear-assembly B&B reactors, after it is revised to take into account the possibility of variable axial leakage. The neutron excess concept can be used to compare different equilibrium cycles, and simple infinite-plane models can be used to compare different starter fuel configurations. Section 6.6 integrates these ideas and shows how the neutron excess concept and simple 1D models can be used to design and estimate the doubling time for a limited-separations fuel cycle using linear-assembly B&B reactors.

7. Implications of B&B Reactors and Limited-Separations Fuel Cycles

A nuclear infrastructure consisting of B&B reactors operating in a limited-separations fuel cycle would have broad implications for nuclear proliferation/diversion, uranium resource utilization, and nuclear waste. This chapter provides a qualitative overview of these implications when compared to a standard LWR fuel cycle and a conventional fast reactor fuel cycle with full actinide separations. The comparisons given are qualitative because there is uncertainty about the future performance of these different fuel cycle options, particularly in the case of B&B reactors and limited-separations processes, both of which require further technology development. The base case for the comparison will be the linear-assembly B&B reactor fuel cycle developed in Section 6.6. This case is selected because it is based on a well defined core composition, does not require a large advance in reactor technology (as a minimum-burnup B&B reactor might), and has a reasonable reactor doubling time (~15 years). This chapter also considers some of the additional fuel cycle options that include either B&B reactors or a limited-separations fuel cycle.

7.1 Nuclear proliferation and materials diversion

Both B&B reactors and a limited-separations fuel cycle introduce unique advantages to the proliferation resistance of a nuclear fuel cycle. The main benefit of a B&B reactor is that once it is started, it can operate without input of additional fissile fuel. Unlike an LWR or conventional fast reactor, it is not dependent on either enrichment or reprocessing facilities to supply it with fuel. This benefit overcomes a significant barrier to deployment of nuclear energy in non-weapon states. With a nuclear infrastructure based on LWRs or conventional fast reactors, access to either enrichment or reprocessing capability is required to sustain nuclear generation. This motivates countries to develop their own enrichment/reprocessing capacity, so that their future energy security can be ensured.

With B&B reactor technology, it is possible for a country to guarantee future nuclear energy production without needing to develop its own enrichment/reprocessing capability, or rely on external enrichment/reprocessing capacity from other countries. The natural or depleted uranium required to keep a B&B reactor operating is readily available, and does not carry the proliferation concerns and international policy implications of producing fissile fuel materials. Whether mature B&B reactor technology would be able to reduce a country's desire to develop enrichment or reprocessing capabilities would have to be considered on a country-by-country basis. In any case, the development of B&B reactor technology would add a compelling "third option" other than developing native enrichment/reprocessing capabilities or depending on external supplies of fissile fuel.

The other component of the described fuel cycle with proliferation implications is the use of limited-separations processes to reuse B&B reactor feed fuel. Such processes are defined as ones that are incapable of separating bred fissile actinides from primarily fertile feed fuel, i.e. plutonium from uranium or uranium from thorium. As a front-end component of the nuclear fuel cycle for producing usable fissile fuel, limited separations processes confer proliferation

advantages over full-separations reprocessing and enrichment because no weapons-usable material can be made by the production facility. In order to obtain usable weapons material, used feed fuel would need to be diverted from the limited-separations facility and undergo actinide separations.

The need to divert and reprocess material would give additional opportunities for proliferation safeguards to operate, in detecting either diversion of materials or a clandestine reprocessing facility. Furthermore, in limited-separations processes, all fuel materials are always mixed with a significant inventory of fission products, so the material would be very challenging to divert and diversion would be easy to detect. Importantly, the presence of fission products effectively eliminates the threat of diversion by a sub-national group, since such groups would lack the resources necessary to properly transport and process the highly radioactive material. Conversely, it is also worth noting that the presence of fission products would also make fuel fabrication and transport in a limited-separations fuel cycle more challenging.

Viewed as a back-end component of the nuclear fuel cycle, i.e. as a way of managing used nuclear fuel, limited-separations processes may have a proliferation and diversion *disadvantage* in comparison to an LWR once-through fuel cycle, in which used fuel is stored and then disposed directly after use. Even though a limited-separations process cannot be used to produce weapons materials, a country using such a process would develop the experience and facilities needed to handle radioactive material, so instituting full-separations reprocessing would not pose as great a technical hurdle. Limited-separations processes may also affect the likelihood of materials diversion from the fuel cycle. With direct disposal, diversion of fuel material would likely occur on a discrete assembly-by-assembly basis: i.e. entire assemblies of fuel material would have to be diverted. If a limited separations process involves taking apart a fuel assembly and refabricating the fuel, then this may allow fuel material to be diverted on a incremental basis, i.e. a small fraction of a process flow or of each processed batch could be diverted. This incremental diversion may be more challenging to detect and safeguard against than diversion of complete fuel assemblies.

Meanwhile, compared to an LWR or fast reactor back-end involving chemical reprocessing, limited-separations processes would be better in terms of proliferation and materials diversion, for the same reasons given for the different front-end options. Also, some limited-separations processes may not confer any proliferation disadvantage, such as direct reuse of used fuel that keeps all fuel elements intact.

In terms of the ultimate backend of a limited-separations fuel cycle, i.e. disposal of twice-burned feed fuel, proliferation and diversion resistance should be similar to that of direct disposal of used LWR fuel. One possible difference may be that a B&B reactor fuel form, such as metal fuel, could require processing before it is suitable for disposal in a geologic repository, while used LWR oxide fuel may not need processing. Whether such processing is needed would depend on both the fuel form as well as the disposal technology used. If processing is needed, it would be necessary to develop pre-disposal processing for the fuel form that does not allow separation of actinides. An example of a potential process for disposing different fuel forms without separations is the GMODS process described in a 1994 Oak Ridge paper [Forsberg, 1994]. Use of the pre-disposal process could represent a proliferation disadvantage in the same

manner as other limited-separations processes. Another factor that could affect proliferation and diversion performance is the isotopic composition of disposed plutonium; this is addressed further in Section 7.3 on waste generation and disposal.

The large improvement in uranium resource utilization (discussed in Section 7.2) may also have proliferation implications. With a greatly reduced demand for uranium mining, the fuel cycle in such a scenario would transition from being primarily mining-based to being primarily manufacturing-based. It would become easier to monitor and safeguard the limited number of fuel manufacturing facilities for such a fuel cycle, compared to the large uranium supply chain required to support an LWR infrastructure.

Finally, there are broader anti-proliferation implications for using a limited-separations fuel cycle with fast breeder reactors (which may or may not be B&B reactors). As shown by the example fuel cycle calculations in this thesis, such a fuel cycle is able to grow exponentially and achieve very high uranium utilization rates, and is the only type of fuel cycle that can do so without needing enrichment or actinide separations reprocessing. If technology for such a fuel cycle is developed and becomes widely adopted, gradually replacing current LWR technology, then it is possible to envision a world in which enrichment and reprocessing facilities are no longer needed for nuclear energy production. If enrichment and reprocessing facilities are not needed for civilian nuclear power, then this allows a reduction in the number of dual-use facilities that can be used produce nuclear materials for both civilian and military purposes. This makes it potentially feasible for such facilities to be restricted and controlled internationally in a manner similar to biological and chemical weapons today. Therefore, global adoption of limited-separations fuel cycles with fast breeder reactors provides a potential avenue for future nuclear disarmament.

7.2 Uranium resource utilization

A significant advantage that B&B reactors and other fast reactor systems have over thermal reactors (such as LWRs) is their ability to greatly extend uranium resources by breeding new fissile fuel from U-238, which comprises 99.3% of natural uranium. In a thermal reactor, this breeding is limited, and the majority of fissions occur in U-235, so less than 1% of all uranium mined is fissioned. In a B&B reactor, it is possible to achieve upward of 40% total fuel burnup in natural uranium, even without any fuel processing.

To illustrate how uranium resource utilization is improved, a reactor build-out scenario based on the example transition case in Section 6.6 is modeled. In that case, each 3600 MW reactor has a conservatively estimated transition time of 18 years, after which it produces enough fuel to start a new reactor every 8.4 years. Assuming two years for cooling/processing, the reactor doubling time of this fuel cycle scenario is approximately 15 years. In the example scenario, ten 3600 MWt B&B reactors are built between 2030 and 2040, using enriched uranium as starter fuel. Eighteen years after these reactors are started up, they begin discharging used feed fuel, which after two years of cooling and processing time, can be used to start up additional B&B reactors. The resulting growth in the number of B&B reactors is shown in Figure 7.2-1. The figure shows that additional B&B reactors can be started up using reused feed beginning in 2056, and the total

number of reactors grows to 98 by 2100. These results approximately scale with the number of initial reactors, so if 50 reactors are started with enriched uranium instead of 10, then the number of reactors in 2100 would be about 500.

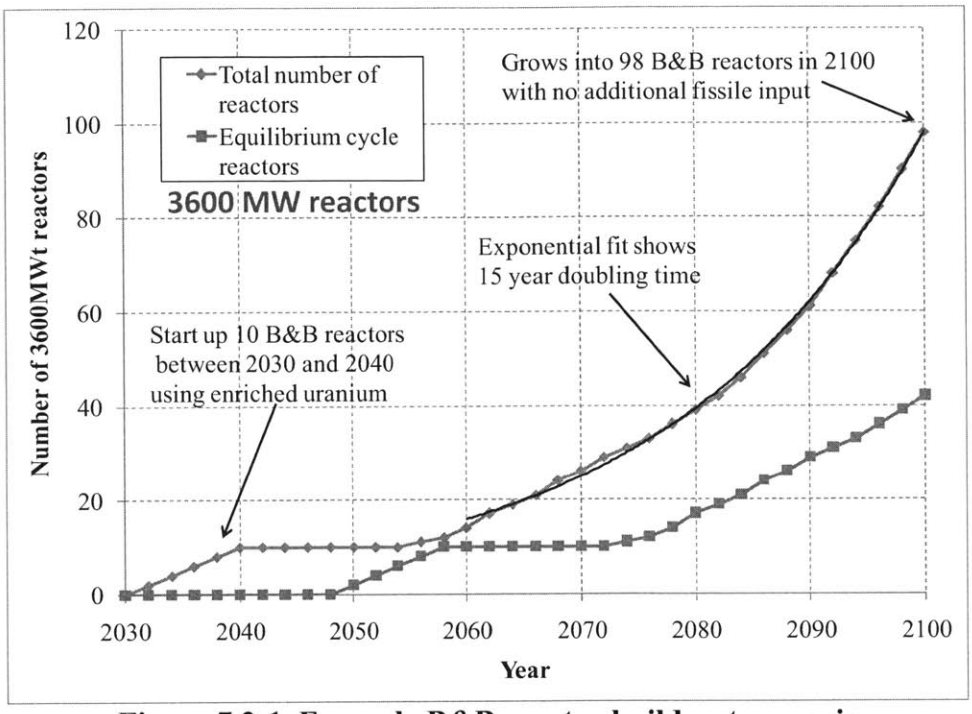

Figure 7.2-1. Example B&B reactor build-out scenario

Using the neutron excess concepts developed in Section 6.4, it is estimated that each reactor requires 54 metric tons of 10% enriched uranium for starter fuel, or 5.4 MT of fissile U-235. The enriched uranium is positioned in the central 120 cm of a 7.74 m^2 starter fuel area (equivalent to 324 hexagonal assemblies with a 16.6 cm pitch). This starter configuration would require less time to burn through than the 140 cm long starter made from reused feed fuel, so the transition time estimate of 18 years is slightly conservative. Assuming a depleted uranium tails composition of 0.2% U-235, this amount of starter fuel corresponds to a natural uranium requirement of 1042 MT per reactor. In addition to the 54 MT of enriched starter fuel, each reactor is loaded with 137 MT of depleted or natural feed fuel at startup.

Eighteen years after startup, at the end of transition, it is assumed that the used starter fuel is discharged and replaced with 90 MT of depleted uranium feed fuel, corresponding to 54 MT of starter fuel and 36 MT of depleted uranium on the axial ends of the starter fuel assemblies. After transition, each reactor discharges used feed fuel at a rate of 15 MT every two years, which is replaced with the same amount of depleted uranium feed fuel. Based on these assumptions, the total uranium requirement of the example build-out scenario is shown in Figure 7.2-2. The total natural uranium requirement between 2030 and 2040 is 10,420 MT; this natural uranium is converted to 540 MT of 10% enriched starter fuel and 9,880 MT of 0.2% U-235 depleted uranium. The monotonically increasing curve in Figure 7.2-2 is the total feed fuel requirement of the reactor fleet, this feed fuel can be either depleted or natural uranium. If the depleted uranium produced during starter fuel production is used as feed, it would be able to supply the feed fuel requirement of the growing reactor fleet until 2083, about 45 years after the initial set

of reactors are deployed. Past this point, either natural uranium or existing stockpiles of depleted uranium can be used as feed fuel. Current stockpiles of depleted uranium (from military and civilian enrichment) are enormous, amounting to approximately 1.5 million metric tons globally, roughly half of which is in the United States. If this depleted uranium is all burned to an average burnup of 28% (the average discharge burnup of the starter assemblies), then it can be used to produce 35,000 quadrillion BTU of thermal energy, or 3900 trillion kWh, enough to satisfy 100% of current global electricity consumption for over 200 years.

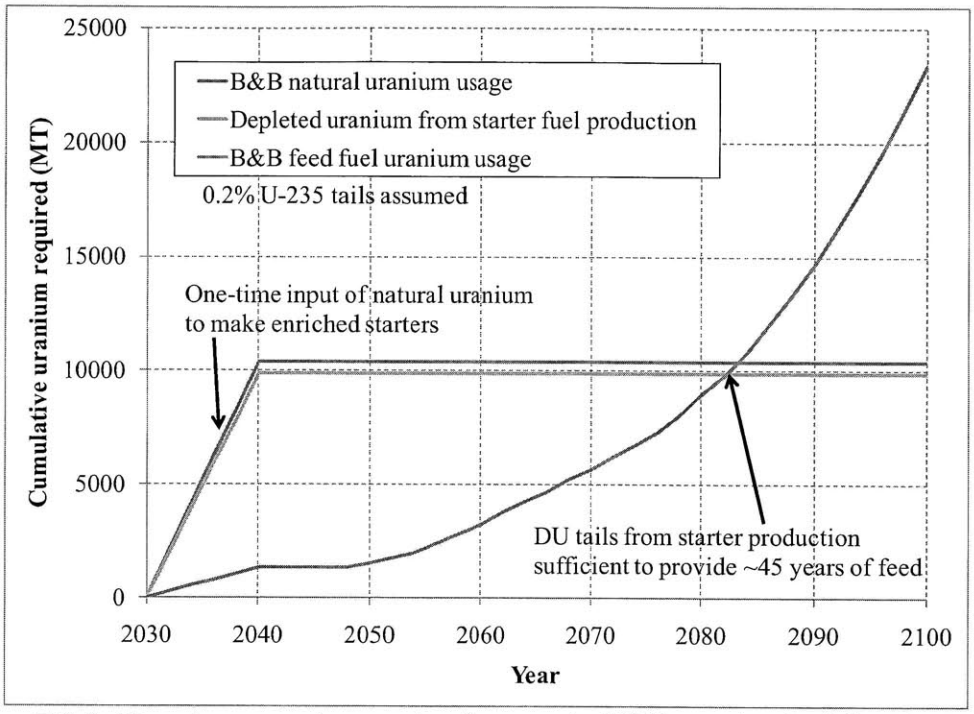

Figure 7.2-2. Uranium requirements of example B&B reactor build-out scenario

The results in Figure 7.2-2 can be compared to the corresponding uranium requirements for an LWR fleet operating in a once-through cycle generating the same amount of thermal energy. This comparison is given in Figure 7.2-3, and assumes an average LWR enrichment of 4.5% (3.75% for the first core) with an average discharge burnup of 50 MWd/kg (33.3 MWd/kg for the first core). Figure 7.2-3 shows that an LWR reactor fleet would require over an order of magnitude more natural uranium to sustain.

The B&B reactor has two advantages in uranium utilization: first, there is a factor of 8.4 improvement from its ability to burn depleted/natural uranium directly, since each kilogram of 4.5% enriched uranium for an LWR requires 8.4 kilograms of natural uranium to produce (assuming a 0.2% U-235 tails composition). Second, the average burnup in a B&B reactor is approximately 5.5 times higher, as the starter assemblies are discharged at an average burnup of 28% FIMA, versus just over 5% in an LWR. (This value of 28% includes the less burned 30 cm sections of depleted uranium at the axial ends of the starter fuel; if this fuel is also reused then the average burnup would be about 38%, the average discharge burnup of the central 140 cm of starter fuel). Multiplying these two factors yields a total advantage of 8.4*5.5 = 46.

In Figure 7.2-3, at the year 2100 the LWR fleet has consumed roughly 20 times more uranium than the B&B reactor fleet. This factor is smaller than the total uranium utilization advantage of 46 because of the longer fuel residence time of B&B reactors: approximately 25 years instead of 4.5 years in the case of an LWR. This means that B&B reactors must be fueled further in advance, which effectively shifts the B&B reactor uranium requirement curve earlier in time.

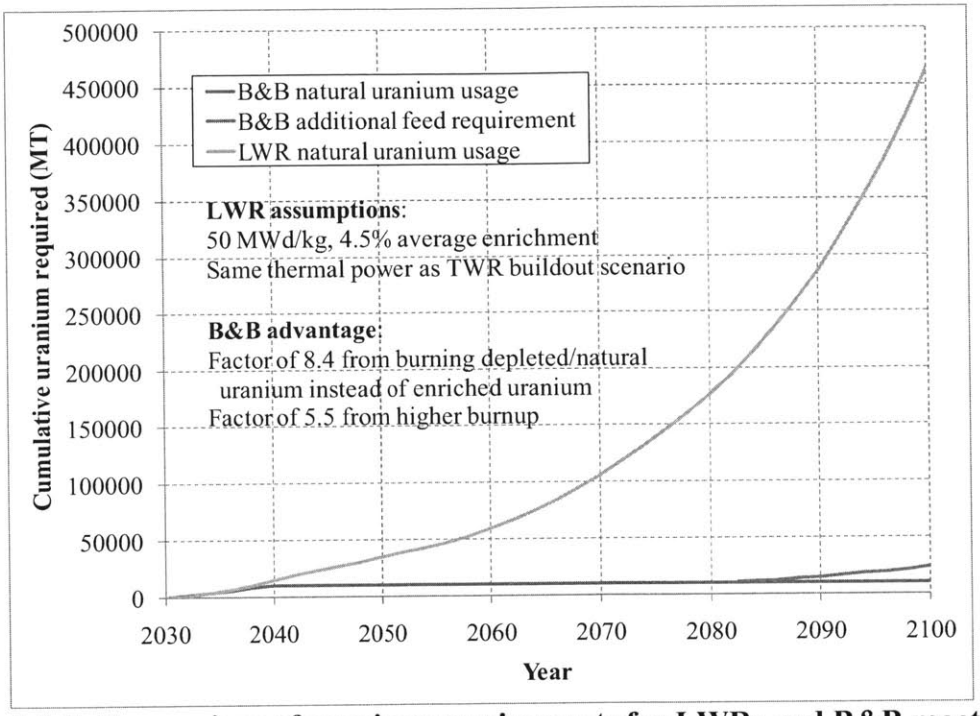

Figure 7.2-3. Comparison of uranium requirements for LWRs and B&B reactors for example build-out scenario

Similarly, a comparison of the enrichment requirements of the two fuel cycle options is shown in Figure 7.2-4. Enrichment is measured in separative work units (SWU), a standard unit of enrichment work. The B&B reactors and LWRs require roughly the same amount of enrichment for the first 10 years, when the B&B reactors are being started up using enriched uranium. After this point, the additional enrichment required by the B&B reactor fleet becomes zero, while it continues to rise exponentially for the growing LWR fleet. The needed enrichment capacity (number of SWU required per year) also rises exponentially.

Both uranium and enrichment requirements for the LWR fuel cycle can be reduced by approximately 1/3 by reprocessing the discharged LWR plutonium into MOX fuel. Even so, B&B reactors would still hold over an order of magnitude advantage in uranium resource utilization. Meanwhile, a conventional fast reactor fuel cycle with full actinide separation reprocessing can achieve uranium utilization rates approaching 100%, roughly a factor of three better than a limited-separations fuel cycle using B&B reactors. Therefore, the advantages in uranium utilization outlined for a B&B reactor would also apply to other fast reactor fuel cycle options that include significant breeding.

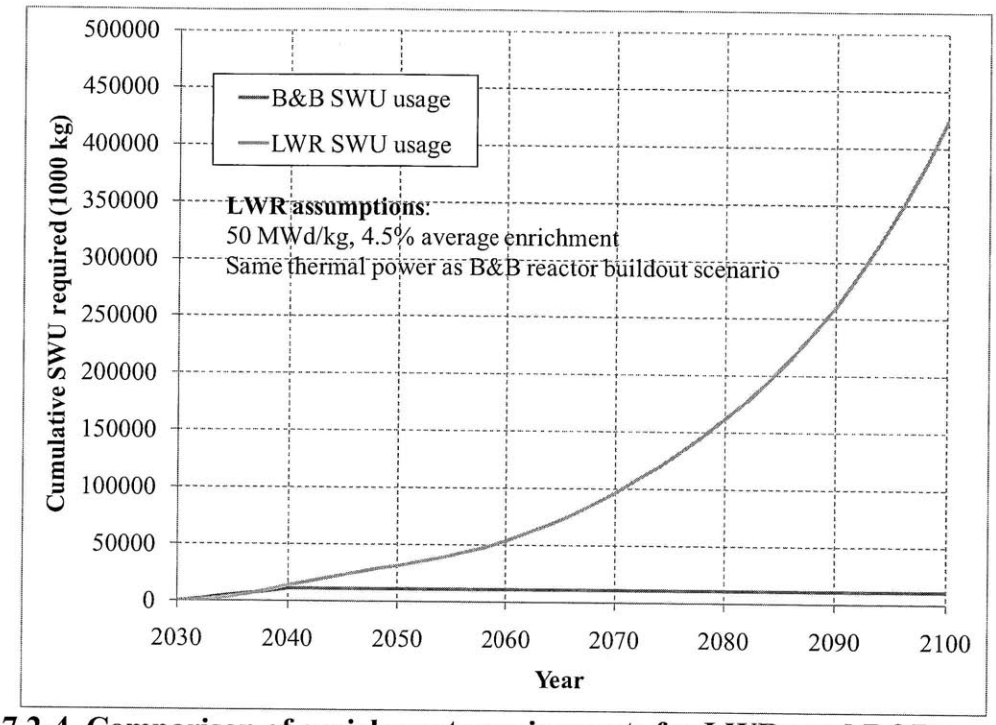

Figure 7.2-4. Comparison of enrichment requirements for LWRs and B&B reactors for example build-out scenario

The implications of greatly improved uranium resource utilization are significant, although they may not be realized until the future, when demand for uranium starts to outpace supply. According to the 2009 IAEA Redbook, there are roughly 5.5 million tons of known and inferred uranium resources that can be recovered at a reasonable cost (<$130 /kg). Meanwhile, each year the world uses around 65,000 metric tons of uranium ore to produce about 15% of its electricity. Therefore, at current usage rates, there is enough uranium available in conventional resources to last for roughly 85 years. Once conventional uranium resources are used up, then uranium will need to be obtained from lower grade ores or potentially seawater, which would be more costly than current uranium mining and would drive up the price of uranium.

While an 80+ year supply would be sufficient for a couple generations, this number assumes that the world's usage rate of uranium stays constant over this interval, which is not likely to be the case. There are currently enough new reactors on order or planned to add 1/3 to total nuclear generating capacity within the next decade, and new reactor proposals worldwide will nearly double nuclear generating capacity within two decades. [World Nuclear Association, 2010] Extrapolating this growth rate (~30% per decade) into the future means that existing uranium resources will last for only 45 years. Therefore, plants being built today may face uranium shortages or price increases within their operating lifetimes. If a more aggressive growth rate of nuclear energy results as a response to global climate change, then this timescale becomes even shorter: for example if nuclear energy were to supply 50% of global electricity demand, then known resources would last under 25 years.

These scenarios all use the IAEA Redbook figures for uranium resource availability. However, values from the Redbook are based on current costs and technology, and therefore represent a lower bound for uranium resource availability. It is possible that more uranium resources could become available with a relatively modest increase in cost. Since uranium only comprises a small percentage (2-4% [MIT, 2010]) of the cost of nuclear electricity, uranium prices would have to increase significantly to affect the competitiveness of nuclear energy. However, increasing uranium extraction costs are not the only implication of depleting uranium resources. For example, uranium resource distribution could become a significant issue if countries begin to use up their domestic uranium supplies. Also, extracting uranium from lower grade ores would increase the environmental impact of nuclear energy.

The issues associated with uranium resource available are all effectively solved through use of a B&B reactor infrastructure. With B&B reactors operating in a limited-separations fuel cycle, it is possible to achieve uranium utilization rates on the order of 60 times higher than current LWR rates (the factor of 45 calculated earlier assumed an equal thermal efficiency and relatively high average LWR burnup). This means that the previous timescales could all be multiplied by a factor of 60; so known conventional uranium resources would be able to supply 50% of current global electricity demand for approximately 1500 years. Including the 1.5 million MT of depleted uranium currently stockpiled brings this number to over 1900 years. The corresponding reduction in uranium mining and enrichment requirements would greatly lessen the environmental impact and carbon dioxide emissions of the nuclear fuel cycle.

Additionally, the fact that B&B reactors can extract a huge amount of energy from uranium means that B&B reactors are extremely insensitive to the price of uranium: uranium prices could increase by a factor of ten and have nearly no effect on the price of B&B reactor electricity. This allows uranium extraction from low grade ores or even seawater to become economically feasible. The addition of these more expensive sources of uranium vastly increases the amount of uranium available; for example it is estimated that 4.6 billion tons of uranium are contained in seawater, a factor of 1000 more than contained in conventional terrestrial sources. The ability of B&B reactors to accept any and all uranium, at practically any cost, and extract roughly 30% of its energy value means that B&B reactors have the potential to provide the entire world's supply of electricity and energy for millennia to come. Under a fast reactor infrastructure, in either a limited-separations or full-separations fuel cycle, nuclear energy becomes truly sustainable.

Higher uranium utilization rates would have similar implications for energy security. For example, the United States uranium demand is about 28% of the world total, while it only possesses 6% of the world's uranium resources. Domestic supplies of uranium would be able to support the current U.S. usage rate for less than two decades. With 60 times higher uranium utilization, domestic supplies would be able to last approximately one thousand years, even without including depleted uranium stockpiles. If one also factors in the ability to economically make use of more dilute sources of uranium, then one concludes that nuclear energy security is all but guaranteed for millennia with the use of fast reactors and either limited or full separations technology. Distribution of uranium resources would never become an issue since countries could still economically make use of plentiful low-grade resources, potentially including uranium from seawater.

7.3 Waste generation and disposal

In a limited-separations fuel cycle, the accumulation of fission products in fuel eventually make it a net neutron absorber, so that it cannot be used to sustain a nuclear chain reaction. Therefore, fuel is disposed after it has reached roughly 30-40% burnup after two passes through a reactor, first as feed fuel, then again as starter fuel to start a new reactor. Disposing used B&B reactor fuel would be in principle similar to disposal of used LWR fuel in a geologic repository, although the waste processing and repository requirements may be different for a B&B reactor fuel form, such as metal fuel. Because of the uncertainty regarding future B&B reactor fuel forms and disposal technologies, the topic of repository performance is not considered here, although it is noted that there exist proposed non-separative methods for processing metal fuel to be suitable for geologic repository disposal [Forsberg, 1994].

Outside of differences due to repository performance, B&B reactors and limited-separations fuel cycles result in other qualitative differences when it comes to waste from the nuclear fuel cycle. First, the ability to reduce or eliminate future uranium enrichment leads to less depleted uranium waste, and the ability to accept depleted uranium as fuel offers an avenue to utilizing existing depleted uranium waste. Meanwhile, using a limited-separations process may lead to the production of additional low and intermediate level nuclear waste as byproducts of the process used. The type and amount of this waste would depend on the process employed, while some processes, such as direct reuse, may produce no additional waste.

In terms of high level waste, i.e. used fuel, the higher burnup achieved with B&B reactors means that the mass and volume of wastes produced would be smaller than from an LWR per unit energy produced. For an average final burnup of 38% (the average fuel burnup of the twice-burned feed/starter fuel), a B&B reactor would be producing about 87% less waste (in terms of initial heavy metal mass and volume) than a typical LWR. Meanwhile, the higher-burnup B&B reactor waste would be more concentrated in both transuranics and fission products. Representative waste quantities for a B&B reactor and an LWR once-through fuel cycle are given Table 7.3-1. Two sets of data are given for B&B reactors, one for a B&B reactor once-through fuel cycle, and one in which all used fuel is burned a second time as starter fuel (including the depleted uranium axial ends of the starter fuel). Table 7.3-2 gives the same quantities, except normalized to total thermal power produced. Note that if a LWR fuel cycle with reprocessing is considered, waste quantities per unit energy would decrease by up to a third due to increased uranium utilization.

The total amount of fission products per unit energy is essentially the same for the different cases, since the total recoverable energy per fission does not vary much between the different reactors. However, the fission products coming from the B&B reactors will have had more time to decay and cool because of the longer core residence time of the fuel, so the short-term decay heat will be lower per unit of energy produced.

Fuel being disposed from a B&B reactor fuel cycle has a smaller amount of minor actinides (neptunium and higher actinides) than fuel from an LWR fuel cycle. In particular, the amount of higher actinides (americium, curium, berkelium, and californium) is higher in LWR discharged fuel (because of the higher neutron capture cross section in a thermal spectrum), which increases

the amount of near term decay heat and spontaneous fission neutrons. The transuranic content of B&B reactor fuel consists almost completely of plutonium, with neptunium-237 (from U-238 (n,2n) reactions) and americium-241 (from decay of plutonium-241) being the highest concentration minor actinides.

Table 7.3-1. Representative used fuel compositions at discharge (g per initial kg HM)

Fuel cycle option	B&B once through	B&B with limited-separations	LWR once through
Discharge burnup (MWd/kg IHM)	157	375	50
Fission products (including gases)	161	384	53
Uranium	746	524	935
Minor actinides	1.0	1.4	~1.5
Plutonium	92	91	10.5
Pu-238	0.4 (0.4%)	0.7 (0.8%)	0.3 (2.9%)
Pu-239	76 (83%)	65 (71%)	5.5 (52%)
Pu-240	14 (15%)	22 (24%)	2.0 (19%)
Pu-241	1.3 (1.4%)	2.6 (2.9%)	1.8 (17%)
Pu-242	0.2 (0.2%)	0.8 (0.9%)	0.9 (8.6%)

Table 7.3-2. Representative used fuel compositions at discharge (kg per GWy thermal)

Fuel cycle option	B&B once through	B&B with limited-separations	LWR once through
Total mass	2320	970	7300
Fission products (including gases)	374	374	387
Uranium	1730	510	6830
Minor actinides	2.3	1.4	~11
Plutonium	214	88	77
Pu-238	0.9 (0.4%)	0.7 (0.8%)	2.2 (2.9%)
Pu-239	177 (83%)	63 (71%)	40 (52%)
Pu-240	33 (15%)	21 (24%)	15 (19%)
Pu-241	3.0 (1.4%)	2.5 (2.9%)	13 (17%)
Pu-242	0.5 (0.2%)	0.8 (0.9%)	7 (8.6%)

LWR used fuel has a very low concentration of plutonium because the Pu-239 fission cross section is much greater than the U-238 capture cross section in a thermal spectrum. Per unit energy, the B&B fuel cycle with limited-separations generates a similar amount of plutonium as an LWR once through cycle, while the once-through B&B cycle generates roughly three times as much. The LWR plutonium isotopic vector contains a greater fraction of heavier plutonium nuclides, whereas the plutonium in discharged B&B fuel is over 95% plutonium 239 and 240. The fraction of fissile plutonium is similar for the B&B fuel cycle with limited separations (74%) and the LWR once through cycle (69%), and is higher for the B&B once through cycle (84%). In linear-assembly B&B reactors and LWRs, there is a distribution of isotopic vectors corresponding to the distributions in discharge burnup, with lower burnup fuel having a higher

fissile isotope fraction, so values above and below these averages will be present in all three cases.

The relatively long transition times and large amount of contained burnup in a B&B reactor also has implications for handling waste from B&B reactors. An LWR must replace roughly one-third of its core every 18 months, meaning that nuclear waste needs to be dealt with almost immediately after an LWR begins operation. In contrast, a B&B reactor is capable of running on its initial load of starter fuel for the duration of transition (18 years in the linear-assembly example) before the starter fuel needs to be discharged to allow room for incoming feed fuel. An equilibrium cycle B&B reactor also contains six or more years worth of contained burnup, which effectively is the average delay between when fuel is loaded and when it is discharged. The significant delay between when fuel is loaded and discharged from the core gives time for fission products to decay, reduces the net present cost of processing and disposal, and allows additional time for development and refinement of fuel cycle back-end technologies.

7.4 Additional fuel cycle options

In addition to the limited-separations fuel cycle with B&B reactors described in this thesis, many other fuel cycle options are possible that take advantage of either B&B reactors, limited-separations processes, or both. Seven interesting options are briefly described here.

7.4.1 Using B&B reactors in a once-through fuel cycle

Even without operating in a limited-separations fuel cycle, B&B reactors can offer significant advantages: namely the ability to achieve high fuel utilization while being able to run indefinitely on fertile fuel. Using B&B reactors in a once-through fuel cycle is appealing because it does not require any used fuel processing technologies to be developed, and will likely be the most cost effective fuel cycle option as long as the price of enriched uranium fuel remains below that of reused fuel. The primary difference between the once-through and the limited-separations fuel cycle is that the once-through cycle would still need enriched uranium to expand, which would mean greater uranium and enrichment requirements.

7.4.2 Using B&B reactors in a full-separations fuel cycle

Instead of using only limited-separations processes to produce starter fuel for new B&B reactors, full-separations processes could also be used if the cost and proliferation risks are determined to be acceptable. Such a fuel cycle could also be analyzed using the concepts developed in this thesis, similarly to how the effect of melt refining was examined in Subsection 5.3.3. By being able to separate out nearly all the fission products, it would be possible to achieve even shorter doubling times than with limited-separations alone. This fuel cycle option would be appealing due to the desirable features of B&B reactors, such as their efficient neutron economies and high single-pass burnup.

7.4.3 Using conventional fast reactors in a limited-separations fuel cycle

If limited-separations technology were to become available before the development of high burnup fuels and materials, then it would be possible to develop a fuel cycle similar to the B&B fuel cycle presented in this thesis, but using a more conventional fast reactor design. These reactors would resemble seed-and-blanket fast reactors, except that the blanket fuel would be turned into new seed fuel using a limited-separations process rather than through full-separations reprocessing. Such a fuel cycle was originally studied at the EBR-II fuel cycle facility, which was then subsequently used to research electrochemical reprocessing.

Another way to picture a reactor in such a fuel cycle is as a generalized B&B reactor in which the feed fuel can be taken out for processing one or more times as it is bred and then burned. Such a fuel cycle would share the same proliferation characteristics of the B&B version, and would also allow an exponentially growing nuclear infrastructure with no weapons material production capacity. This scenario can also be analyzed using the concepts developed in this thesis: to do so one would include the fuel undergoing processing into the neutron excess and contained burnup requirements of the desired equilibrium cycle.

7.4.4 Reusing LWR used fuel as B&B reactor feed fuel

B&B reactors, being able to burn fertile uranium fuel, are also able to use LWR used fuel as feed, which consists of primarily fertile uranium with a relatively small concentration of fission products, plutonium, and minor actinides. Ideally, LWR used fuel would be converted into a fuel form more appropriate for B&B reactor operation, such as metal fuel. While converting and refabricating LWR fuel into B&B feed would certainly cost more than depleted uranium feed, doing so would effectively consume the LWR used fuel since the resulting waste would be equivalent to waste generated from depleted uranium. It would therefore convert the LWR used fuel disposal issue into a B&B reactor used fuel disposal issue, while simultaneously pushing it back in time by several decades.

7.4.5 Reusing B&B reactor used fuel as conventional fast reactor fuel

As demonstrated several times in this thesis, the discharged feed fuel from a B&B reactor has k_∞ above unity even without any processing, so it can be used to start up additional B&B reactors. Instead of being used to start up additional B&B reactors, the fuel can also be used to start up either conventional fast reactors or small modular fast reactors. Doing so displaces the cost of enriched or reprocessed fuel. This is particularly significant in the case of small modular reactors: their low specific power causes their fuel cycle costs to be very high, so having B&B reactors to serve as a source of "free" or reduced-cost fuel can be a tremendous benefit. This option would make sense if further energy growth is no longer needed: conventional fast reactors could be started and sustained instead of continuing to expand the fleet of B&B reactors.

7.4.6 Using B&B reactors to breed LWR fuel

Discharged B&B reactor fuel would *not* have k_∞ above unity in a thermal spectrum; the high concentration of fission products would cause too many parasitic absorptions. However, lightly

bred (~4% burnup) B&B reactor fuel can be used as fuel in an LWR. Converted into an oxide, this fuel would have a similar reactivity evolution in an LWR as low enrichment fuel, while the fission products present would act similarly to a burnable poison. To produce lightly bred fuel in a B&B reactor, it would be necessary to discharge a fraction of the feed fuel after it has produced a positive neutron excess, since the extracted lightly bred fuel carries a negative neutron excess. This would increase the burnup requirement of the B&B reactor, with the size of the increase depending on the desired ratio of fully-burned to lightly-bred discharged fuel.

7.4.7 Using B&B reactors to deeply burn fuel

As depicted in the schematic neutron excess curve in Figure 4.1-2, B&B reactor feed fuel is first burned until it reaches a net positive neutron excess, then burned further as starter fuel to supply neutron excess to starting a new B&B reactor. Instead of using neutron excess of the reused feed fuel to start a new reactor, it is also possible to use it to burn fuel past the point that its k_∞ falls below unity. Doing so could in principle be used to burn fuel up to the maximum theoretical burnup illustrated in Figure 2.1-1. This option would be able to extract additional energy from fuel while further reducing the quantity of waste produced per unit energy.

8. Conclusions and Recommendations

This thesis introduces a general framework for analyzing breed-and-burn reactor systems and limited-separations fuel cycles, based around the newly developed neutron excess concept. The neutron excess concept is a method to account for the neutron economy of a system by tracking neutron absorption and production in the materials of that system. Using the methods developed, it is possible to analyze important B&B reactor parameters, including minimum burnup and irradiation damage, starter fuel requirements, and the transition time required to establish an equilibrium cycle. Together, these parameters can be used to calculate the fleet doubling times for B&B reactors operating in a limited-separations fuel cycle. A primary advantage of the neutron excess concept is that it can be used for extremely rapid characterization of different B&B reactor options, allowing the goals of this thesis to be accomplished.

Section 8.1 summarizes the capabilities of the different B&B reactor analysis methods developed in this thesis, and Section 8.2 gives the important results from the core composition study using these methods. Section 8.3 gives the conclusions from the investigation of linear-assembly B&B reactors. Section 8.4 goes over the results from modeling B&B reactors operating in a limited-separations fuel cycle, and summarizes the implications of such a fuel cycle. Section 8.5 concludes by giving recommendations for future work, in terms of both the neutron excess concept and future design of B&B reactors.

8.1 Summary of B&B reactor analysis methods

Chapter 2 develops the neutron excess formulation and shows how the uncontrolled equilibrium cycle k-effective of a B&B reactor can be evaluated based on the discharge neutron excess of equilibrium cycle feed fuel. Equations are derived that show this relationship for both continuous systems with flowing fuel elements and more realistic discrete systems with finite cycle length. These equations are also able to account for the effect of non-uniform equilibrium cycle discharge burnup.

In addition to predicting equilibrium cycle k-effective, the neutron excess concept can also be used to predict the amount of starter fuel required to establish a desired equilibrium cycle. Such a calculation is possible because neutron excess is conserved in a critical reactor. Conceptually, the calculation is performed by first measuring the negative neutron excess contained in the desired equilibrium cycle, then dividing this result by the amount of neutron excess obtainable per unit volume of starter fuel, thus obtaining the volume of starter fuel that is required. Additional adjustments are made to the calculation if the fraction of neutrons lost to leakage or control during the transition to equilibrium deviates from the equilibrium cycle leakage and control loss fractions. Formulations for this calculation for both continuous and discrete systems are also developed in Chapter 2.

Chapter 3 demonstrates an important feature of neutron excess: it evolves in a similar manner in models with different geometries and equilibrium cycle shuffling sequences. This allows one to use simple one-dimensional models to accurately predict the relationship between burnup and equilibrium cycle k-effective for realistic three-dimensional systems. Furthermore, it was also

found that zero-dimensional infinite-medium depletion models can be used to approximate neutron excess evolution, allowing average *k*-effective to be predicted to within 1%. The infinite-medium depletion approximation was established as an extremely rapid screening tool for comparing different B&B reactor core compositions. It can also be used to estimate the amount of neutron excess obtainable from starter fuel, giving results accurate to within 10% in the cases studied.

Even though changing the equilibrium cycle shuffling sequence has only a small effect on neutron excess evolution, the shuffling sequence used has a large impact on the power and flux distributions in a core. In both idealized infinite slab models and more realistic three-dimensional models, shuffling sequences can be designed which yield a desirable flattened power distribution, capable of producing much more power than simple convergent shuffling. Radial peaking factors are still generally large in B&B reactors because a significant fraction of the core must be devoted to a low power blanket of absorbing feed fuel. Larger sized cores are able to have lower radial peaking factors, because they increase the ratio of power-producing area to low-power breeding blanket area (a perimeter-to-area ratio effect). Consequently, larger sized systems have a smaller neutron excess requirement per unit power and are able to achieve shorter doubling times.

B&B reactors display a unique relationship between *k*-effective and size: as size is reduced, equilibrium cycle *k*-effective falls exponentially from an asymptotic value due to increased neutron losses to leakage. Smaller sized systems with increased leakage therefore require higher feed fuel burnup to maintain critical operation. It is possible to obtain an excellent estimate of the size-reactivity relationship from the neutron absorption distribution in a large sized "thick-blanket" model. This is useful since it means that one does not need to run a large number of different-sized models to determine minimum reactor size.

The neutron excess concept is important because it establishes a useful framework for understanding the neutron economy in a B&B reactor. This framework allows one to draw equivalences between realistic B&B reactor models and greatly simplified models, permitting one to analyze a wide variety of B&B reactor options without having to construct detailed models for each option.

8.2 Summary of core composition comparison study

For a B&B reactor design, minimum burnup and DPA are critical parameters because they determine how challenging fuel and materials qualification would be for that design. Using the methods developed in this thesis, it was possible to compare the minimum burnup and DPA requirements of hundreds of different core compositions. Table 8.2-1 gives a summary of these requirements for selected core options in a minimum-burnup B&B reactor. In a minimum-burnup B&B reactor, the fuel can be shuffled in three dimensions. These values are sensitive to the relative amounts of fuel, structure, and coolant present, so a core using a lower amount of structure would require less burnup and fluence.

Table 8.2-1. Minimum burnup for different core compositions (1 part depleted uranium fuel, 0.6 parts structure, 1 part coolant by volume)

Fuel	Structure	Coolant	Minimum burnup fraction	Minimum DPA (HT9/SiC DPA)	Minimum fast fluence (/cm^{2}s)(>0.1 MeV)	Maximum k_{eq}
U2Zr	T91	He	11.2%	249	6.28E+23	1.119
U2Zr	SiC	He	12.8%	271	5.09E+23	1.103
U10Zr	T91	He	14.5%	290	7.30E+23	1.078
U10Zr	SiC	He	17.2%	322	6.03E+23	1.060
U3Si2	T91	He	17.4%	309	7.58E+23	1.055
U3Si2	SiC	He	20.7%	333	6.31E+23	1.037
U2Zr	T91	PbBi	13.1%	275	7.01E+23	1.095
U2Zr	SiC	PbBi	15.1%	311	5.87E+23	1.079
U10Zr	T91	PbBi	17.6%	333	8.46E+23	1.053
U10Zr	SiC	PbBi	21.6%	390	7.37E+23	1.035
U3Si2	T91	PbBi	22.9%	379	9.38E+23	1.027
U3Si2	SiC	PbBi	33.6%	470	9.89E+23	1.010
U2Zr	T91	Na	13.5%	266	6.51E+23	1.091
U2Zr	SiC	Na	15.1%	291	5.48E+23	1.077
U10Zr	T91	Na	18.8%	329	8.03E+23	1.046
U10Zr	SiC	Na	22.1%	373	7.05E+23	1.031
U3Si2	T91	Na	26.0%	401	9.48E+23	1.017
U3Si2	SiC	Na	N/A	N/A	N/A	1.005

The best core composition options for minimizing burnup and DPA are metal fuel (with a strong dependence on alloy content), the type of steel that allows the lowest structure volume fraction, and helium coolant. If sufficient fuel performance margin exists, sodium coolant can be substituted in place of helium to achieve higher power densities at a modest burnup and DPA penalty. For a minimum-burnup B&B reactor, reasonably achievable minimum DPA values are on the order of 250-350 DPA in steel.

For fuel, it was found that uranium alloy metal fuel performs significantly better than compound fuels such as uranium oxide or uranium carbide. The effect of alloy composition was found to be significant, with hypothetical low-alloy fuels (e.g. uranium-zirconium fuel with 2% Zr by weight) performing much better than more conventional alloy compositions, such as U10Zr. Thorium metal fuel is in principle capable of supporting B&B operation, but requires very high burnup and fluence, leaving very little neutronic margin for including structural or coolant material. The best performing compound fuel was found to be U_3Si_2, which neutronically is comparable to U10Zr. More conventional ceramic fuels such as UC, UO_2, and $U^{15}N$ were found to require significantly higher burnup.

Different structure and coolant materials were also compared to each other. The different types of steel evaluated (HT9, T91, and MA956 ODS) were all found to have a similar effect on required burnup and DPA. The primary reason for choosing a particular type of steel would be its ability to withstand the high fluence needed for B&B operation. Another important factor is which material allows the lowest structure volume fraction, since a smaller amount of structure reduces burnup and DPA requirements. Silicon carbide structure requires slightly higher fuel burnup, but reduces the required fast fluence because it softens the neutron spectrum. Silicon

carbide could potentially greatly improve the thermal hydraulic performance of B&B reactors (and other reactor types) if it allows either higher temperature operation or higher lead/LBE coolant velocities, although there is more uncertainty regarding its ability to withstand high fluence.

Per unit volume, the presence of helium, CO_2, lead, LBE, or sodium coolant has a smaller effect on core neutronics than the inclusion of steel or SiC structural material. The gas coolants have the least impact on minimum burnup and DPA, followed by lead/LBE, then sodium. However, the higher power densities achievable with sodium coolant allow sodium to have a smaller impact on required burnup than lead/LBE for a given core power density.

8.3 Linear assembly breed-and-burn reactor analysis methods

While a minimum burnup B&B reactor is capable of burning natural or depleted uranium at roughly 250-300 DPA in steel, a linear-assembly B&B reactor would require on the order of 500 DPA. This is because there is a positive feedback between breeding and burning that causes a burnup peak to form at the axial center of the assemblies, which results from the fact that B&B reactor feed fuel becomes more reactive (i.e. k_∞ increases) as it is burned. Therefore, while linear-assembly B&B reactors may be more straightforward to engineer, they increase the challenge in qualifying fuels and materials for high burnup and fluence operation.

Similarly to minimum-burnup B&B reactors, linear-assembly B&B reactors display an equilibrium cycle reactivity-burnup relationship that is insensitive to radial geometry and shuffling sequence, assuming a fixed core composition and axial length. The axial burnup distribution of discharged equilibrium cycle feed fuel also does not depend on radial geometry or shuffling sequence. This behavior arises because of the low absorption cross sections in the fast spectrum of a B&B reactor, which causes there to be a nearly constant relationship between the axial positions where neutrons are produced and absorbed. This relationship can be approximated using a one-dimensional diffusion calculation, and the resulting axial transfer matrix can be used to predict the discharge axial burnup distribution, as well as the effects of varying axial length and axial reflector albedo. Combining the neutron excess results from an infinite-medium depletion calculation with an axial transfer matrix allows the minimum peak burnup and DPA for a linear-assembly B&B reactor to be estimated, without ever constructing a reactor model.

As with minimum-burnup B&B reactors, a neutron excess balance equation can be used to compute the starter fuel requirement for a linear-assembly B&B reactor. This is accomplished by introducing an additional term into the neutron excess balance equation that accounts for variable axial leakage. The neutron excess obtainable from a starter fuel configuration can be estimated using an infinite-plane model, analogous to using an infinite-medium depletion approximation for starter fuel in a minimum-burnup B&B reactor. Neutron excess predictions using the infinite-plane model were found to agree to within 10% of the modeled reactor transition cases, with differences due primarily to the differences in neutron spectra between the two models. The effect of different axial distributions in starter fuel is small for axially-centered

starter fuel, and slightly favors the use of starter fuel that yields longer and flatter flux distributions.

8.4 Summary of limited-separations fuel cycle analysis

This thesis demonstrates the feasibility of using limited-separations processes to establish an exponentially growing nuclear energy infrastructure, in which feed fuel discharged from B&B reactors is used to start up subsequent generations of B&B reactors. In a limited-separations fuel cycle, the fuel can be refabricated and the cladding replaced, but there is no chemical separation of actinides from each other or from most of the fission products. There is potential for sodium-cooled B&B reactors in such a fuel cycle to achieve fleet doubling times of less than one decade, although this result is highly sensitive to the reactor core composition employed as well as thermal hydraulic performance.

8.4.1 Fuel cycle analysis methods

Doubling time can be calculated from several reactor and fuel cycle timescales: the transition time t_{tr}, the spawning time t_s, and the cooling/processing time t_c. The transition time t_{tr} is the amount of time between reactor startup and when it can begin discharging used feed fuel at the equilibrium cycle rate: it is equal to the time required to burn through the starter fuel and generate the burnup contained in the desired equilibrium cycle. The spawning time t_s is the amount of time required for an equilibrium cycle reactor to discharge enough used feed fuel to start up a new reactor. The amount of fuel required depends on the amount of neutron excess that can be obtained from the reused fuel and the neutron excess cost of a new reactor. Finally the cooling/processing time t_c is the time between when fuel is discharged from a reactor and when it can be reused in a second reactor. Chapter 4 derives a simple analytic expression for computing the asymptotic reactor fleet e-folding time t_e in terms of these timescales.

Doubling time results from the derived expression were found to agree with the doubling times obtained from an explicit model of the fuel cycle. Using the expression, the doubling time performance of different equilibrium cycle options can be compared. Larger-sized equilibrium cycles with flatter power distributions require smaller amounts of neutron excess and contained burnup per unit power, and therefore have shorter doubling times.

A method of correlating the doubling times of realistic three-dimensional reactors to those of simple infinite slab models was developed. It was found that the neutron excess and contained burnup requirements of different axially-convergent three-dimensional shuffling sequences were approximately proportional to the reactor area. As a result, the relevant reactor timescales (the transition time t_{tr} and the spawning time t_s) are approximately proportional to the reactor radial power peaking factor. This means that the doubling time of a realistic three-dimensional equilibrium cycle can be estimated by multiplying the doubling time computed for an infinite slab model (the "infinite-reactor doubling time") by the radial power peaking factor of the realistic equilibrium cycle (which is around 2.0–2.5 for a large reactor). This method of estimating doubling times allows one-dimensional infinite slab models to be used for very rapid comparisons between the potential doubling times of different core compositions.

Several alternative fuel cycle options were considered, based on the idea of starting up a B&B reactor before its full requirement of starter fuel is available. In these scenarios, the remainder of the neutron excess requirement is supplied either by loading additional starter fuel later in the reactor's life, or by burning feed fuel past its equilibrium cycle required minimum burnup. These fuel cycle options are able to achieve slightly faster doubling times because reactors can be started earlier than in the baseline fuel cycle. If a given B&B reactor can be started up at full power using only 2/3 of the required amount of starter fuel, then the different advanced fuel cycle options were found to reduce doubling time by between 8 and 14 percent. Another option to reduce doubling time is to uprate reactor power as more feed fuel is bred, therefore shortening the reactor transition time. However, this option would require either a larger or a flexible capacity balance of plant, so it may be economically preferable to simply design for a higher-power equilibrium cycle configuration instead.

8.4.2 Core composition doubling time comparison

For liquid metal coolants, there is a tradeoff between thermal hydraulics and neutronics: increasing the coolant volume fraction increases achievable power density but worsens core neutronics. There is an optimal coolant volume fraction that minimizes doubling time, which is on the order of 40% sodium coolant, slightly higher for lead/LBE, and increases with neutronically better fuel/structure combinations. In contrast, the volume fraction of gas coolants has very little effect on neutronics, so doubling time can be minimized by separately optimizing the coolant volume fraction for thermal hydraulic performance.

The doubling times for the different coolants depends primarily on the respective coolant's thermal hydraulic performance. Sodium coolant can support the highest power densities (under the thermal hydraulic assumptions used) and is able to achieve the shortest doubling times. Helium coolant follows, then lead and LBE. Lead and LBE are constrained by a low 2 m/s coolant velocity limit which is needed to avoid cladding corrosion; development of new materials could raise or eliminate this limit. With sodium coolant, it is possible to obtain reactor doubling times on the order of ten years, assuming an optimistic hypothetical core composition of 75 parts U2Zr fuel, 25 parts void, 30 parts T91 structure, and 100 parts coolant. Using a process that removes some fission products, such as melt refining, can improve this doubling time to approximately eight years, assuming a two-year cooling/processing time. With a minimum-burnup B&B reactor and the ability to refabricate fuel and replace fuel cladding between the two reactor passes, achieving this doubling time requires cladding to be irradiated to approximately 270 displacements per atom, only about one-third higher than the current knowledge limit.

The feasibility of a limited-separations fuel cycle was also demonstrated for linear-assembly B&B reactors, by using the neutron excess methods developed to select an equilibrium cycle and design appropriate starter fuel. The doubling time of this fuel cycle was found to be approximately 14 years, versus 8 years for a fuel cycle using minimum-burnup B&B reactors with the same sodium-cooled core composition. Meanwhile material DPA requirements rise considerably, from 270 DPA to about 500 DPA, due to the axial peaking present in linear-assembly B&B reactors.

The doubling time achievable with B&B reactors is strongly dependent on the fuel/structure composition used. Changing the fuel type from U2Zr to either U10Zr or U_3Si_2 causes the achievable doubling time to increase by over 100%, as does doubling the relative amount of structure present. The design of a natural or depleted uranium fueled B&B reactor is more dependent on having a neutronically robust core composition than a conventional fast reactor, because there is no option to raise fuel enrichment to offset reactivity losses from a less robust core composition.

8.4.3 Summary of B&B reactor and limited-separations fuel cycle implications

A nuclear infrastructure consisting of B&B reactors operating in a limited-separations fuel cycle would have broad implications for nuclear proliferation/diversion, uranium resource utilization, and nuclear waste. B&B reactors capable of burning depleted or natural uranium carry a significant proliferation advantage compared to LWRs and conventional fast reactors, because they do not require any additional fissile fuel after startup. They offer a potentially attractive option for countries that desire nuclear energy but do not want to develop their own enrichment capability or depend on other countries for enrichment. Limited-separations fuel cycles offer a way to establish a sustainable and exponentially-growing nuclear infrastructure without the proliferation disadvantages of actinide separations. Notably, the high concentration of fission products in fuel produced by limited-separations processes effectively eliminates the threat of diversion by a sub-national entity.

Since B&B reactors can achieve fast-reactor uranium utilization rates while using depleted or natural uranium as feed, they are able extend uranium resources by a factor of about 50 over an LWR infrastructure. Also, the lower fuel costs of B&B reactors allow lower grade sources of uranium to be economically utilized, which could expand potential uranium resources by several orders of magnitude, allowing B&B reactors to supply effectively limitless energy. Improved uranium utilization would also greatly enhance the energy security of countries using B&B reactors. Low uranium consumption and enrichment requirements would significantly reduce the environmental impact of the nuclear fuel cycle.

B&B reactors are able to produce a smaller quantity of high-level waste for disposal than LWRs, because of the higher average burnup in the B&B reactor. Although B&B reactor used fuel contains a higher concentration of plutonium, the net amount of plutonium generated per unit energy produced is similar to LWRs, again because of the higher burnup of B&B reactor fuel. Used fuel from a B&B reactor would also contain a lower concentration of minor actinides, which would improve suitability for disposal in a geologic repository. However, depending on the fuel form of B&B fuel and the disposal technology employed, used B&B fuel may require additional intermediate processing before it can be qualified for disposal.

8.5 Recommendations for future work

The methods introduced in this thesis will be useful for the future design of B&B reactors and their fuel cycles. This concluding section provides recommendations for future studies in this area, divided into recommendations for theory development and for B&B reactor design.

8.5.1 Further B&B reactor theory development

The neutron excess concept developed in this thesis is extremely useful for evaluating a large number of candidate core compositions, as well as providing a framework for understanding the unique characteristics of B&B reactors. As used in this thesis, it applies a number of simplifying assumptions that would benefit from further refinement. First, the effect of including control is not modeled; modeling control would affect fuel neutron excess curves (since the neutron spectrum would change slightly in the presence of control), and control in a linear-assembly system would alter the axial transfer matrix. Similarly, the presence of axial and radial inhomogeneities (such as neutron streaming channels or a materials test position) would also have an effect on neutron excess curves and the axial transfer matrix. Also, it should be possible to develop better models for predicting starter fuel neutron excess curves than the simple infinite-medium and infinite-plane models. The primary source of error in these simple models is the difference in neutron spectrum in the infinite model and in the actual starter configuration. Therefore, one potential way to obtain a better neutron excess prediction would be to model a candidate starter configuration then simply deplete it without shuffling. Such a model would more accurately predict the initial neutron spectrum experienced by the starter fuel and interior feed fuel.

One of the major challenges in modeling a B&B reactor is fuel management: designing optimal equilibrium cycle and transition shuffling sequences in a computationally efficient manner. One example of a past fuel management study, using genetic algorithms, is given in the referenced 2000 paper by Toshinsky. The neutron excess concept provides new quantities to optimize for – namely neutron excess per unit power and contained burnup per unit power – as well as a way to define the size (and therefore the power peaking) of a given equilibrium cycle shuffling sequence. Other parameters that can be optimized include reactivity coefficients, reactivity swing, and change in power shape over a cycle. In addition to developing optimized equilibrium cycle sequences, it would also be very useful to develop methods to quickly compute transition shuffling sequences for evolving a given starter fuel state into a desired equilibrium cycle state. It would also be very desirable for such transition sequences to satisfy additional constraints, such as maintaining a fixed power shape during transition. The ability to efficiently compute transition sequences would allow more systematic comparisons of transition models to simplified models, so that the ability of the simplified models to predict neutron excess can be more broadly characterized.

One last area that has not been studied is the possibility of starting a B&B reactor using a partial load of starter fuel, as is suggested for the advanced fuel cycle options in Chapter 4. Determining the minimum fuel load at startup and the schedule for later additions of starter fuel will be important for calculating B&B reactor fuel cost and doubling times, as well as whether the advanced fuel cycle options would be worth implementing.

8.5.2 Future B&B reactor and limited-separations fuel cycle design

By far, the greatest obstacle to B&B reactor design is the lack of data for fuel and material performance at high burnup and fluence. This thesis identifies minimum-burnup B&B reactors as a way to minimize this technical risk, but minimum-burnup B&B reactors involve additional

engineering risk because they would require development of a novel reactor configuration. In order to design a B&B reactor, the fuel and structural materials used would need to be tested in a fast reactor to the targeted levels of burnup and irradiation damage. Selection of candidate fuel elements for testing should be made based on their neutronic performance (as evaluated using the neutron excess concept) in conjunction with predictive modeling of fuel and material performance, if available. Since the performance of B&B reactors is very sensitive to core composition, it would be very desirable to determine what the minimum amount of alloying material is for metal fuel, as well as to develop fuel element and assembly designs that minimize the amount of structure used.

In terms of limited-separations processes, such a process would only be viable if it provided enough of a cost and proliferation advantage to be used instead of either enrichment or full-separations reprocessing. It is therefore worthwhile to develop and characterize limited-separations processes to determine what benefits and challenges exist. One notable potential challenge may be characterizing and qualifying the fuel produced in a limited-separations process, since the performance of the reused fuel would be closely tied to the composition of the used fuel being processed. Ultimately, well developed B&B reactor and limited-separations technologies could become the foundation for a nuclear infrastructure capable of providing effectively limitless energy, without the costs and proliferation risks of uranium enrichment and full-separations reprocessing.

A. Appendices

A.1 Example infinite slab model equilibrium cycle shuffling sequences

Subsection 3.2.2 discusses the effect of using different equilibrium cycle sequences on the neutron excess evolution; the different sequences considered are described in more detail here. Ten different shuffling patterns were investigated in the one-dimensional infinite slab model with 5 cm wide zones. The fifty zones in the model are numbered sequentially from 1 to 50 starting from the centermost zone. Each shuffling pattern begins with an inward shuffle from zone 50 to zone 26, followed by the patterns given in Table A.1-1. These sequences were selected to investigate a variety of different behaviors that can occur with varying shuffling sequences.

Table A.1-1. Ten equilibrium cycle shuffle sequences investigated for infinite slab model

Sequence #	**1**	**2**	**3**	**4**	**5**	**6**	**7**	**8**	**9**	**10**
From zone 50	26	26	26	26	26	26	26	26	26	26
	25	25	25	25	25	1	1	25	25	25
	24	24	24	24	24	25	2	24	24	24
	23	23	23	23	23	24	25	23	23	23
	22	22	22	22	22	23	24	22	22	22
	21	21	21	21	21	22	23	21	21	21
	20	20	10	20	20	21	22	19	4	13
	19	19	9	18	18	20	21	17	8	2
	18	18	8	16	16	19	20	5	3	4
	17	17	7	14	14	18	19	18	15	3
	16	16	6	12	12	17	18	8	7	1
	15	15	5	10	10	16	17	14	11	7
	14	14	4	8	8	15	16	9	20	15
	13	13	3	6	6	14	15	3	18	14
	12	12	2	4	4	13	14	11	12	6
	11	11	1	2	2	12	13	4	10	18
	10	1	11	1	19	11	12	1	9	8
	9	2	12	3	17	10	11	20	14	17
	8	3	13	5	15	9	10	15	5	9
	7	4	14	7	13	8	9	13	19	5
	6	5	15	9	11	7	8	10	6	19
	5	6	16	11	9	6	7	2	13	20
	4	7	17	13	7	5	6	16	17	11
	3	8	18	15	5	4	5	12	16	12
	2	9	19	17	3	3	4	6	2	10
Discharge	1	10	20	19	1	2	3	7	1	16

Sequence one is the simple inward convergent shuffle, the same sequence used in the basic example model. Sequence two is inwardly shuffled to zone 11, and then shuffled to zone 1 and back out to zone 10; this is referred to as a "convergent-divergent" sequence. Sequence three skips from zone 21 to zone 10, inwardly shuffles to zone 1, then skips back out to zone 11, where

it is outwardly shuffled to zone 20 and discharged. Sequence 4 shuffles inwardly through alternate zones from zone 20, then shuffles the partly-bred fuel back outward to the lower power feed region. Sequence 5 also shuffles inwardly through alternate zones from zone 20, but it sends partly-bred fuel back out for another inward pass. Sequence 6 and 7 shuffle feed fuel to the center of the model very early, and the still-subcritical partly-bred fuel is then inwardly shuffled starting from zone 25. Sequences 8, 9, and 10 all have a random permutation of the inner 20 zones; the purpose of these sequences is to show that the conclusions drawn can be extended to general shuffling sequences.

Each example problem was run with the same starter fuel distribution as the original example problem in Chapter 3: with zones 1-4 enriched to 15%, zones 5-7 enriched to 8%, and zones 8 and higher containing 0.3% U-235 depleted uranium. After five cycles, fuel is shuffled according to the sequences shown in Table A.1-1. Since there was no effort to tailor the initial starter fuel distribution and transition shuffling sequences to maintain critical operation, in most cases the uncontrolled reactivity falls below unity. Each shuffling sequence was repeated with every cycle, and eventually all shuffling sequences converged to an equilibrium cycle. For this example, the total power (120 MW) and cycle length (450 days) were kept constant, which for a fuel discharge rate of 5 cm per cycle yields an equilibrium cycle discharge burnup equal to 113.7 MWd/kgHM.

Figures A.1-1 through A.1-4 shows the end of equilibrium cycle power distributions for the different shuffling sequences. The figures demonstrate that a great deal of control over the equilibrium cycle power distribution can be achieved by changing the equilibrium cycle shuffling sequence. Sequences 1 through 3 show power profiles that consist of smoothly varying regions in which fuel is moved sequentially one zone at a time. Sequences 4 and 5 show jagged power distributions that result from mixing high burnup and low burnup fuel. Sequences 6 and 7 show a central power depression corresponding to the low-burnup feed fuel that is shuffled there. Sequences 8 through 10 have power density profiles that vary unpredictably from zone to zone as a result of randomly mixing different-burnup fuel.

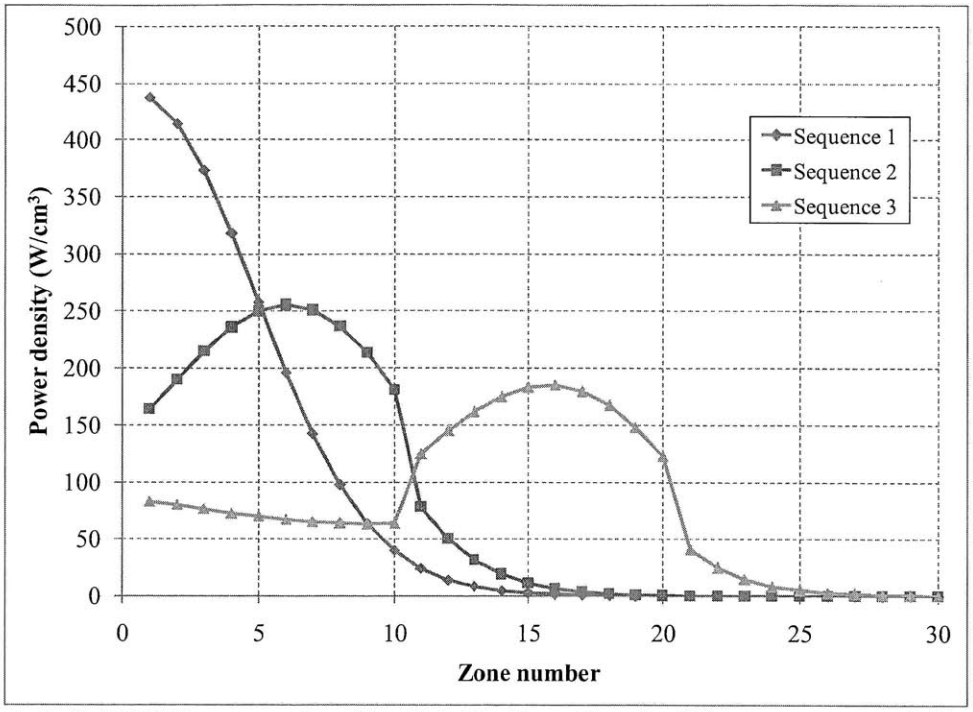

Figure A.1-1. EOEC power density distributions for shuffling sequences 1 through 3

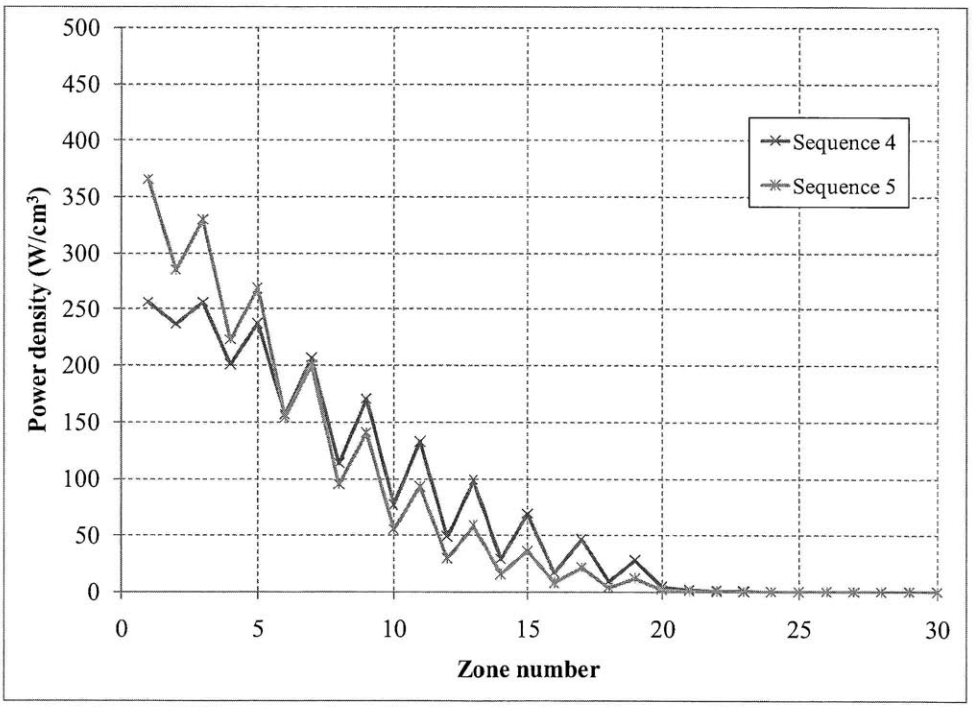

Figure A.1-2. EOEC power density distributions for shuffling sequences 4 and 5

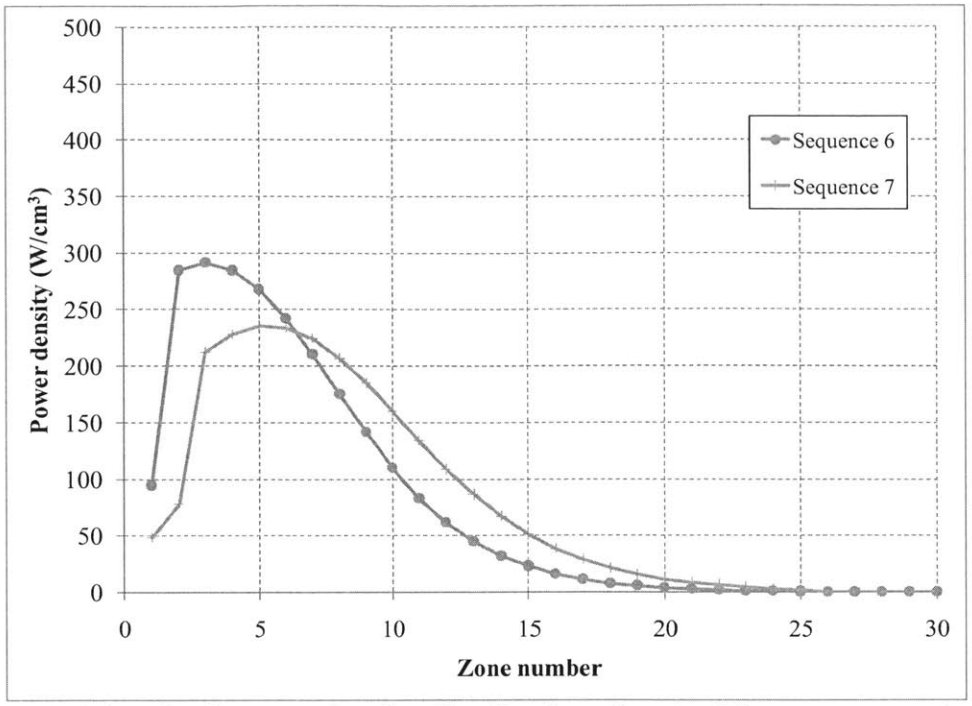

Figure A.1-3. EOEC power density distributions for shuffling sequences 6 and 7

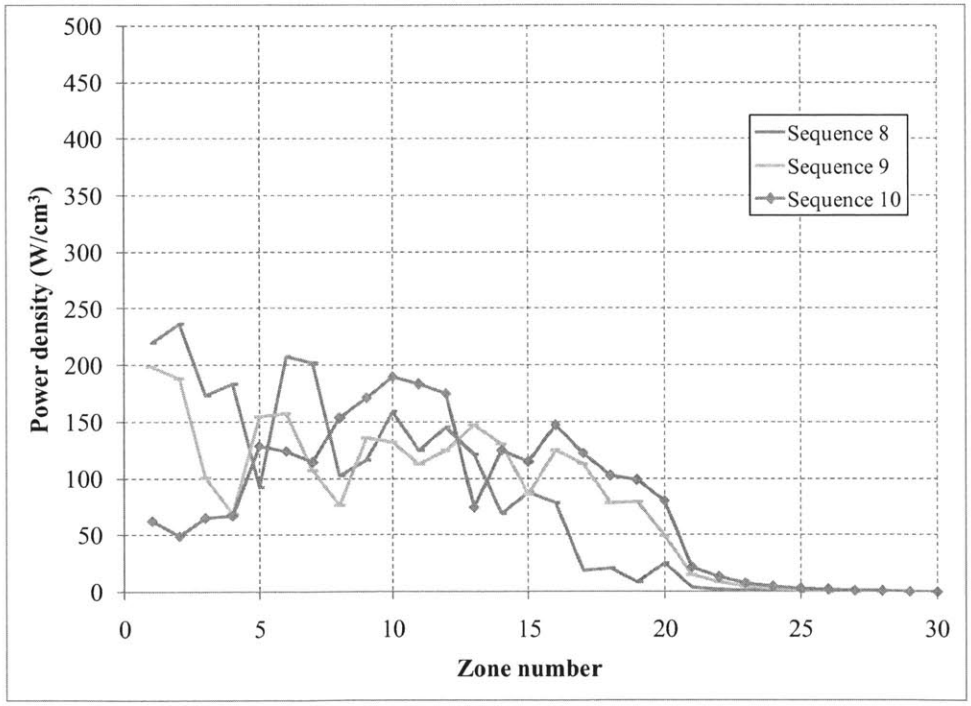

Figure A.1-4. EOEC power density distributions for shuffling sequences 8 through 10

The middle of cycle *k*-effectives for the different shuffling cases are plotted in Figures A.1-5 and A.1-6. Figure A.1-5 shows the transient reactivity behavior as the different cases converge to their equilibrium cycles, and Figure A.1-6 shows how each case settles on an equilibrium cycle value for *k*-effective. Some statistical scatter from the use of a stochastic code is evident in Figure A.1-6. Figure A.1-6 also shows that some shuffling patterns, for example sequence 3,

exhibit oscillating behavior as they approach their equilibrium cycles. This occurs because these shuffling sequences result in delayed feedback. For example, in pattern 3, fuel is shuffled from zone 21 to the center. Higher flux at zone 21 results in better breeding of incoming fuel, which when shuffled to the center causes flux to peak in the center. This central flux peaking reduces the flux at zone 21, resulting in a delayed negative feedback loop. This delayed feedback produces the long-period oscillations seen. This oscillatory behavior, the large number of cycles needed to reach an equilibrium cycle, as well as any subcritical cycles leading up to the equilibrium cycle can all be avoided through having initial conditions closer to the equilibrium cycle state and using more intelligent fuel management to develop the equilibrium cycle state. Doing so is possible in principle because one can imagine starting a reactor preconfigured to closely match the equilibrium cycle state, which would immediately reproduce equilibrium cycle flux and power distributions.

The most remarkable feature of Figures A.1-5 and A.1-6 is how the *k*-effective of each sequence converges to a narrow band. The highest MOEC *k*-effective (1.042) occurs in the convergently shuffled case, and the lowest MOEC *k*-effective (1.029) occurs in case 4, which has its most burned fuel brought out to the softer-spectrum outer cells. The equilibrium cycle *k*-effective data for each sequence is given in Table 3.2-1. Other important conclusions regarding the different shuffling sequences are given in Subsection 3.2.2 and Section 3.3.

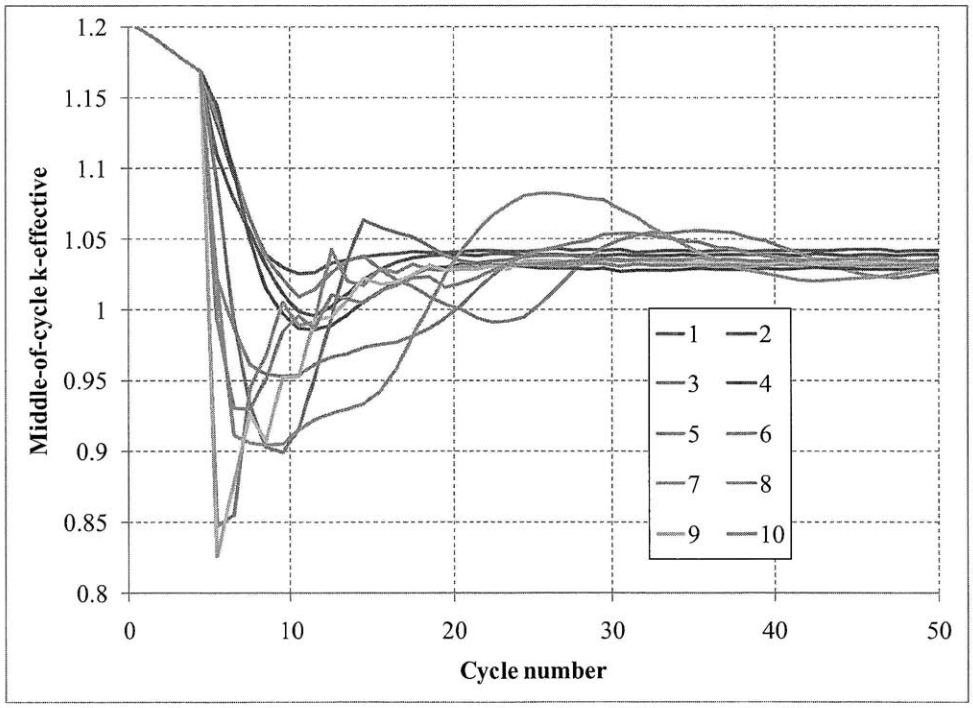

Figure A.1-5. *k*-effective vs. cycle number for different shuffling sequences

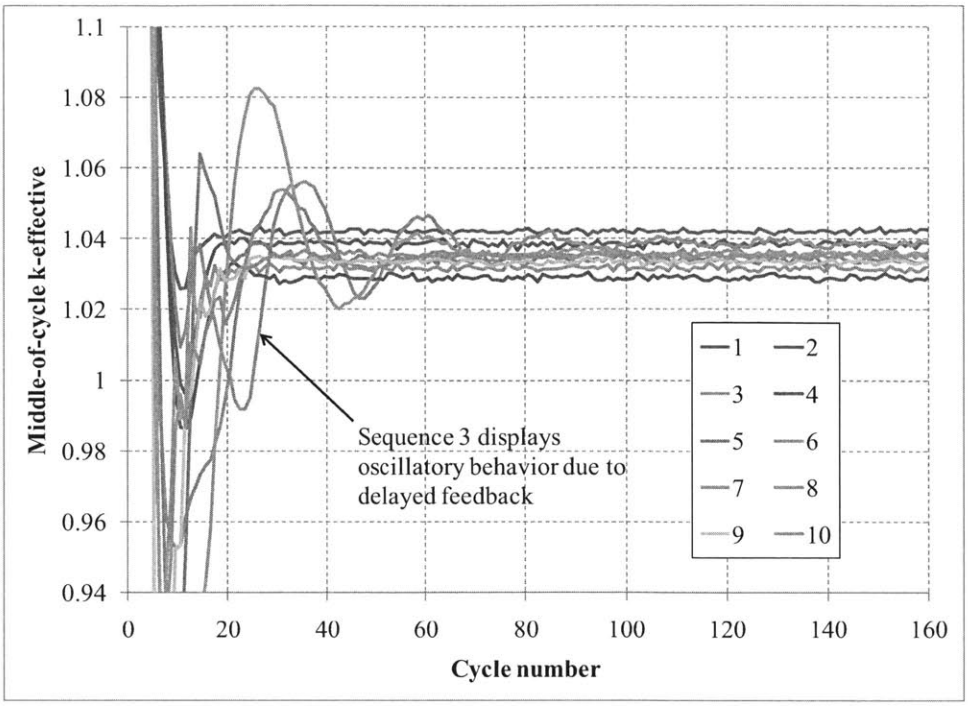

Figure A.1-6. *k*-effective vs. cycle number for different shuffling sequences (eq. cycle)

A.2 Developing the example transition model shuffling sequence

The shuffling sequence for the example transition model in Section 3.5 is given in Table 3.5-2. This shuffling sequence was developed by using rapid deterministic simulations to test a large number of possible shuffling options at each cycle. Only a limited subset of shuffling options could be tested for each cycle because of the enormous number of permutations possible. In the example model, if one assumes that only the innermost 10-20 cells are neutronically significant, there are still a large number of combinations for the starting configuration (at least C(10,4) = 210 combinations) and subsequently an immense number of permutations at later steps, when the feed and starter materials have differentiated themselves (more than 10! ~= 3.6E6 permutations). Given that this number of permutations exists at every cycle, the number of possible fuel histories (spanning many cycles) is enormous, making a brute force approach unreasonable if not impossible. Therefore, an algorithmic approach is used to determine what shuffling options to evaluate.

Starting from a base configuration, different shuffling "moves" are performed then tested using an evaluation function; if the evaluation function increases after a move, then the move is accepted, otherwise it is rejected. This procedure results in the configuration with the highest value for the evaluation function (within the subset of configurations reachable by the specified moves), which is then selected for the following cycle.

The evaluation function used is given in Equation A.2-1:

$$EQM = \sum_i P_i * (BU_{eq,i} - BU_i) \qquad \text{(A.2-1)}$$

EQM stands for Equilibrium Matching function, P_1 is the power in material *i*, BU_i is the burnup in material *i*, and $BU_{eq,1}$ is the equilibrium cycle in material *i*. In Equation A.2-1, the cell indices *i* do not correspond to the physical locations (zone numbers) of the materials, but instead to the feed cells sorted in order of burnup; e.g., BU_2 and $BU_{eq,2}$ are the burnups in the second most burned feed cell and the second most burned feed cell in the equilibrium cycle. The EQM is maximized by preferentially increasing feed power in materials which have burnups far from their equilibrium cycle values. Variations of the EQM can be formed by modifying the exponent of the term in parenthesis in Equation A.2-1, from zero (which would cause EQM to be maximized by maximizing total feed power) to a large number (which would maximize power in the cell with the largest burnup to make up). Instead of using burnup as a criterion, other parameters such as cell *k*-infinity can be used to recreate the equilibrium cycle.

The equilibrium cycle set of burnups used in Equation A.2-1 is actually from an equilibrium cycle with a 10-cell convergent-divergent shuffling scheme, instead of the 8-cell convergent-divergent shuffling scheme that is produced in the example transition model. The reason for this discrepancy is because the shuffling algorithm described is not general enough to produce any desired equilibrium cycle. The lack of generality results from the fact that not all possible configurations are evaluated, only the small subset reachable using the simple type of "move" considered. More generality can be introduced by evaluating a larger number of candidate configurations at each time step, or using shuffling "moves" that more effectively target a desired equilibrium cycle state.

The shuffle "move" considered swaps a piece of starter fuel in zone *i* with an adjacent piece of feed fuel in zone *i+1*. This type of move does *not* swap two adjacent starter materials or two adjacent feed materials, so the overall order of the feed and starter zones is not changed by the moves used.

These swaps are attempted starting from the innermost starter zone, moving outward. If a swap increases the value of EQM while keeping *k*-effective above a specified minimum (1.015 in the REBUS model) then it is accepted, otherwise it is rejected and the swap reversed. If a swap is accepted then swaps are again attempted beginning from the centermost starter fuel cell. Swaps are attempted until none of the possible swaps are accepted. The resulting state where no acceptable swaps exist is the accepted configuration for the next cycle.

A schematic illustration of how these moves proceed is given in the Figure A.2-1. Candidate moves are tested starting from the center of the model (the left side of the figure). The starter fuel in zone one is adjacent to another zone of starter fuel so it is not swapped, and the first candidate move swaps the materials in zones 2 and 3. If the move is accepted (i.e. if it increases EQM while keeping *k*-effective above 1.015), then the algorithm resets, and candidate moves are tested for the new configuration again starting from the center. If the move is rejected, then the original configuration is restored and the next candidate move is tested (swapping materials 4 and 6).

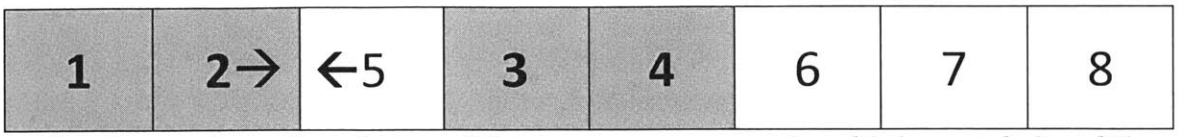

Starting configuration: first candidate move swaps zones 2 and 3 (materials 2 and 5)

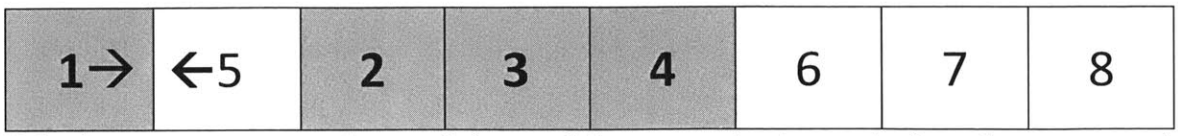

*If the first move is **accepted**: search for candidate moves begins again from the center, so the next candidate move swaps zones 1 and 2 (materials 1 and 5)*

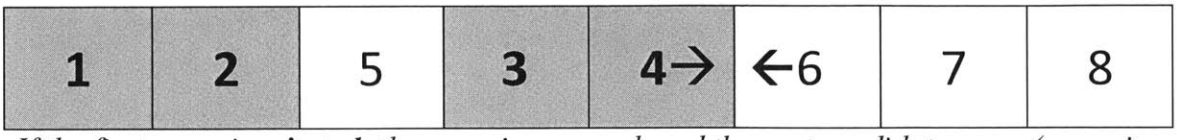

*If the first move is **rejected**: the move is reversed, and the next candidate move (swapping materials 4 and 6) is tested. If all candidate moves are rejected, then state is chosen to be depleted in the following cycle.*

Figure A.2-1. Illustration of shuffling moves used to produce different transition shuffling configurations (boxes highlighted in gray denote starter material)

After this shuffling algorithm is used to determine a configuration for the next cycle, a cycle depletion calculation is performed that targets the same value of average reactivity as the equilibrium cycle. This is done by matching the middle of cycle *k*-effective of the transition cycle with that of the equilibrium cycle (1.046 in REBUS).

After each cycle, the feed materials are sorted from highest to lowest burnup, with the highest burnup materials toward the center. Doing so maximizes the reactivity of the feed configuration in the absence of starter fuel. The starter materials are sorted in the opposite order, with the lowest burnup materials toward the center. This tends to even out the burnup experienced by the starting materials since the zones closer to the center generally experience higher flux. The positions of the feed and starter fuel materials are kept the same during this burnup sorting, so a zone occupied by a feed material before the sorting will still contain feed after sorting.

Even though only a subset of configurations is investigated, the total number of states evaluated is still very large. Therefore, deterministic calculations using REBUS are used in place of slower MCNP simulations. Deterministic calculations are also better for differentiating between similar configurations and for converging on exact reactivity targets. Results from REBUS for the example problem were found to agree reasonably well with those from MCNP in terms of flux and power distributions, except with calculated *k*-effectives roughly 0.5% higher than in MCNP, due to the differences in cross section libraries and models used. The algorithm described above was implemented in REBUS through the use of a Python wrapper. The shuffling sequence obtained by using this algorithm corresponds is the shuffling sequence for the first 6 cycles in Table 3.5-2 and Table A.2-1.

After cycle 6, the feed fuel is bred sufficiently that the starter fuel zones can be completely discharged while still leaving the feed fuel in a critical state. At this point, beginning of cycle *k*-effective is brought close to 1.015 by reversing the order of the innermost feed zones, producing a state similar to the equilibrium cycle. A maximum of five zones can be reversed at cycle 7 while keeping the feed fuel critical. Reactivity increases again over cycle 7, allowing the innermost eight zones to be reversed, forming a state close to the final equilibrium cycle. At cycle 8 and beyond, the equilibrium cycle shuffling scheme is used, with spent feed fuel being discharged from zone number 8, and the equilibrium cycle is quickly established. The resulting shuffling sequence is shown in Table A.2-1.

The sequence in Table A.2-1 and the finalized sequence in Table 3.5-2 differ in two ways. In the final sequence, cycle 10 is shortened from 900 days to 613.6 days, and the starter fuel materials numbered 1 and 3 are swapped midway through cycle 6. Both of these changes were made to improve the discharge burnup distribution of the feed and starter fuel.

The burnups for different fuel zones after 30 cycles of the unaltered shuffling sequence (in Table 3.5-2) are given in Figure A.2-2 (results are from the MCNPXT model). Fuel zones one through twenty seven have been discharged, and zones 28 and higher have assumed the equilibrium cycle burnup distribution. This discharge burnup distribution is improved in two ways. First, shortening cycle 10 from 900 days to 613.6 days reduces the peak discharge burnup of the transition feed fuel from 12.2% to 11.8%, which is only slightly greater than the equilibrium cycle discharge value of 11.6%. As shown in Figure 3.5-7, this cycle length reduction does not cause the core to become subcritical. Second, swapping the most burned starter fuel (material 1) with the least burned (material 3) midway through the sixth cycle reduces the peak starter fuel burnup from 12.6% to 12.1%. With this change, the peak-to-average burnup ratio in the starter fuel is reduced to 1.014. The resulting discharge burnup distribution after the two changes is compared to the original distribution in Figure A.2-3.

Table A.2-1. Startup shuffling sequence for described equilibrium cycle

Cycle number	Cycle Length (EFPD)	Cycle fuel permutation – position from center of core (only inner 20 zones shown out of 50)																			
0	0	1	2	3	4	5	6	7	8	9	10	11	12	13	14	15	16	17	18	19	20
1	1445.1	1	5	2	3	6	7	4	8	9	10	11	12	13	14	15	16	17	18	19	20
2	977.7	5	4	6	3	7	2	1	8	9	10	11	12	13	14	15	16	17	18	19	20
3	1053	5	4	6	7	3	8	2	9	1	10	11	12	13	14	15	16	17	18	19	20
4	1065.9	5	4	6	7	8	1	9	10	11	2	3	12	13	14	15	16	17	18	19	20
5	1085.7	5	6	7	2	8	9	10	11	3	12	13	1	4	14	15	16	17	18	19	20
6	1121.2	5	6	7	8	9	10	1	11	12	13	14	15	16	3	4	17	2	18	19	20
7	813.8	9	8	7	6	5	10	11	12	13	14	15	16	17	18	19	20	21	22	23	24
8	900	12	11	10	9	8	7	6	5	13	14	15	16	17	18	19	20	21	22	23	24
9	900	13	12	11	10	9	8	7	6	14	15	16	17	18	19	20	21	22	23	24	25
10	900	14	13	12	11	10	9	8	7	15	16	17	18	19	20	21	22	23	24	25	26
11	900	15	14	13	12	11	10	9	8	16	17	18	19	20	21	22	23	24	25	26	27
12	900	16	15	14	13	12	11	10	9	17	18	19	20	21	22	23	24	25	26	27	28

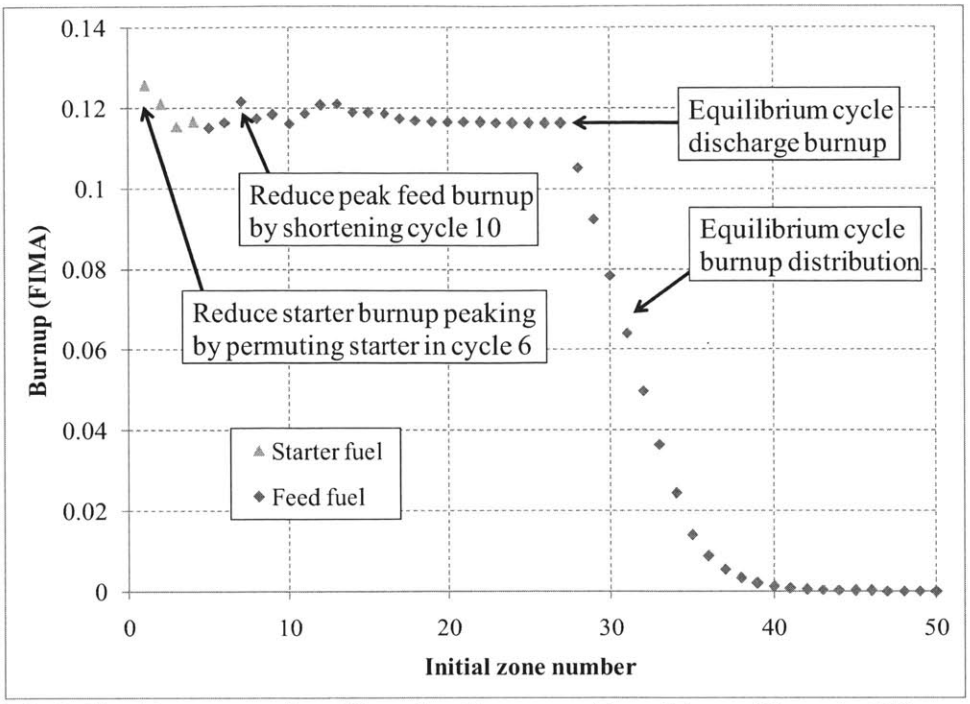

Figure A.2-2. Fuel burnup after 30 cycles from unaltered transition shuffling sequence

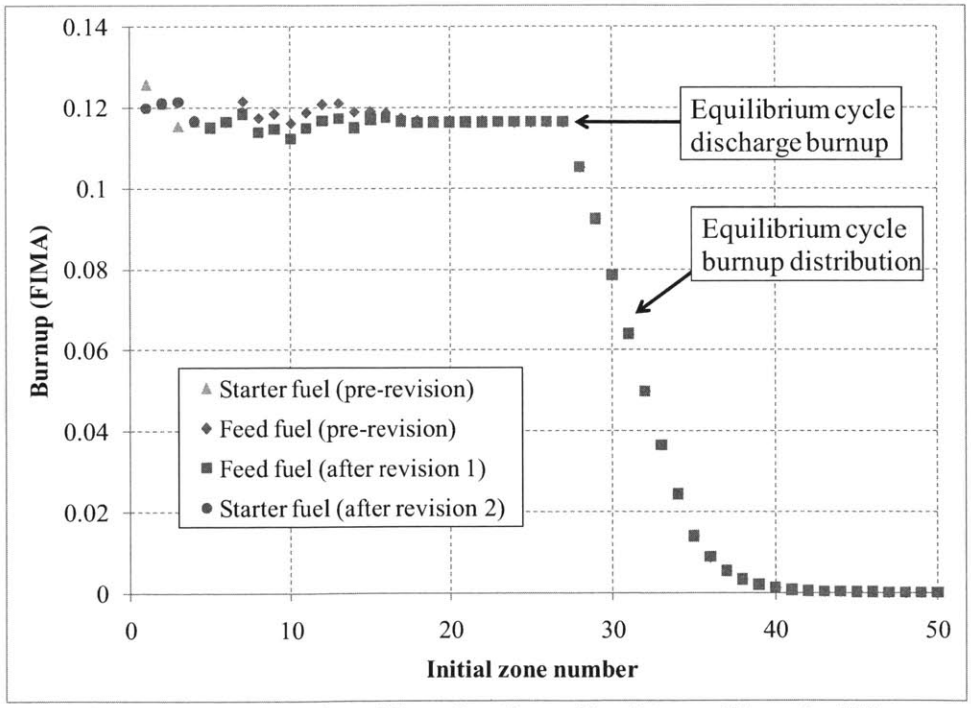

Figure A.2-3. Fuel burnup after 30 cycles from final transition shuffling sequence

A.3 The second example transition model

Subsection 3.5.5 discusses the results from a "second example transition model" that uses feed fuel discharged from an earlier B&B reactor as its starter fuel. This example is important for establishing the potential viability of a limited-separations fuel cycle, and for characterizing the accuracy of the infinite-medium approximation for estimating the neutron excess obtainable from reused-feed starter fuel. Furthermore, it demonstrates that a strictly-convergent equilibrium cycle can be established, which is useful since the three-dimensional equilibrium cycles studied in Section 3.7 are primarily axially convergent. This appendix discusses the equilibrium cycle configuration and transition sequence developed for the second example transition model.

A.3.1 Equilibrium cycle characteristics

The equilibrium cycle considered is the same as that in the "convergent infinite slab model" introduced in Subsection 3.1.1. It uses a simplified core composition of 50% uranium, 20% steel, and 30% sodium by volume, and consists of convergently-shuffled 5 cm infinite slabs. The model is run with a total power of 60 MW/m^2 and a cycle length of 900 days, corresponding to an equilibrium cycle discharge burnup of 11.6%, the same as in previous models. Equilibrium cycle burnup, flux and power distributions are centrally peaked and given in Subsection 3.1.1, and reactivity characteristics are given in Table A.3-1 (these results are also given Tables 3.1-1 and 3.2-1).

Table A.3-1. Equilibrium cycle *k*-effective values for convergent equilibrium cycle

BOC *k*-effective	1.020
MOC *k*-effective	1.042
EOC *k*-effective	1.060
Cycle reactivity swing (Δk-effective)	0.039
$\overline{k_{eq}}$	1.041

Figure A.3-1 shows the adjusted neutron excess of the equilibrium cycle, with a total integral of 6.26E-2 mol/cm^2. This integral is as large as that for the convergent-divergent equilibrium cycle in the first example transition model due to the higher value of average k_{eq} (1.0424 vs. 1.0375) in this example. Because of the lower reactivity of reused feed fuel compared to 15% enriched fuel, five zones of starter fuel are used (instead of four from the first example transition model). Based on an infinite-medium depletion approximation of the starter fuel (shown in Figure 3.5-14, this initial starter fuel loading of 25 cm would need to be burned approximately an additional 15% to supply 2.5E-3 mol/cm^3 of neutron excess.

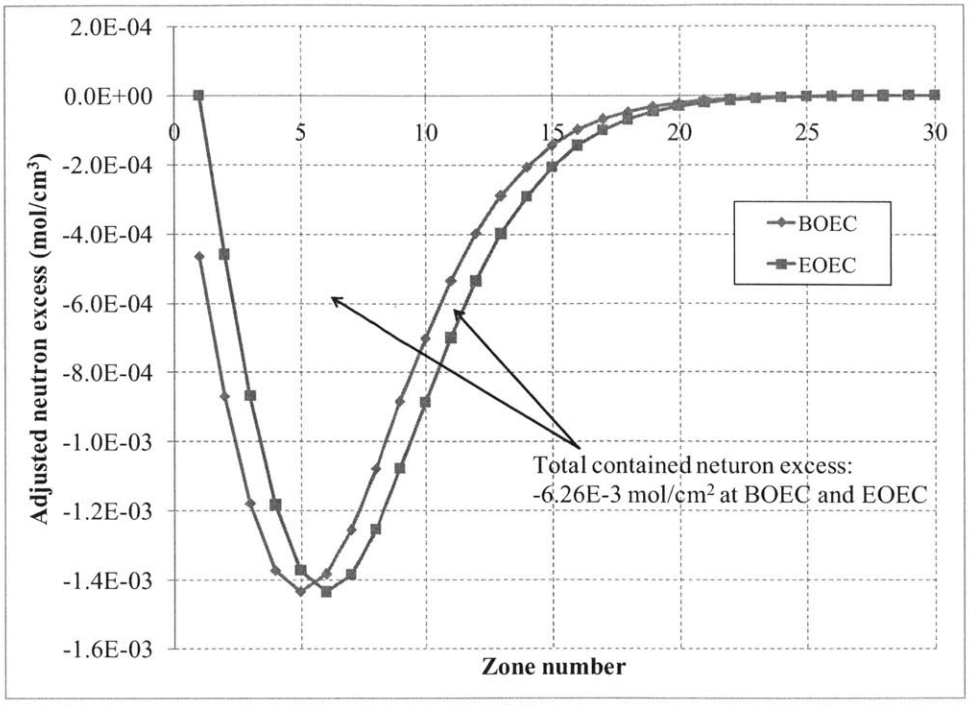

Figure A.3-1. Adjusted neutron excess of convergent equilibrium cycle

A.3.2 Transition shuffling sequence description

The same algorithm described in Appendix A.2 is used to determine the transition shuffling sequence, which is given in Table A.3-1. At cycle 6 and beyond, the fuel is shuffled convergently, and cycle length is adjusted to keep peak feed burnup below 11.8%. The uncontrolled *k*-effective evolution of this transition sequence as computed by REBUS and MCNPXT is given in Figure A.3-2.

Table A.3-2. Transition shuffling sequence for second example transition model

Cycle number	Cycle Length (days)	Cycle fuel permutation – position from center of core (only inner 20 zones shown out of 50)																			
0	0	1	2	3	4	5	6	7	8	9	10	11	12	13	14	15	16	17	18	19	20
1	2195.4	1	2	3	4	6	5	7	8	9	10	11	12	13	14	15	16	17	18	19	20
2	1379.1	5	6	4	3	7	2	1	8	9	10	11	12	13	14	15	16	17	18	19	20
3	1266.6	6	5	7	4	8	1	9	2	3	10	11	12	13	14	15	16	17	18	19	20
4	1165.7	6	7	8	5	9	3	10	11	2	1	4	12	13	14	15	16	17	18	19	20
5	1122.2	6	7	8	9	10	2	11	12	4	13	14	1	5	3	15	16	17	18	19	20
6	807.8	6	7	8	9	10	11	12	13	14	15	16	17	18	19	20	21	22	23	24	25
7	900	7	8	9	10	11	12	13	14	15	16	17	18	19	20	21	22	23	24	25	26
8	900	8	9	10	11	12	13	14	15	16	17	18	19	20	21	22	23	24	25	26	27
9	831.0	9	10	11	12	13	14	15	16	17	18	19	20	21	22	23	24	25	26	27	28
10	900	10	11	12	13	14	15	16	17	18	19	20	21	22	23	24	25	26	27	28	29
11	900	11	12	13	14	15	16	17	18	19	20	21	22	23	24	25	26	27	28	29	30
12	900	12	13	14	15	16	17	18	19	20	21	22	23	24	25	26	27	28	29	30	31

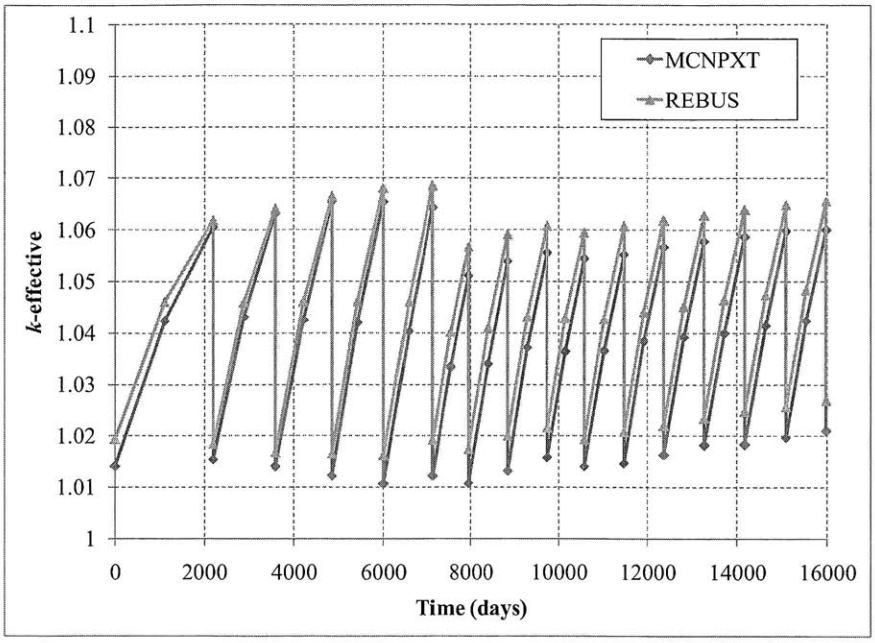

Figure A.3-2. Uncontrolled *k*-effective evolution of second example transition model

Over this transition sequence, average cycle *k*-effective is lower than the equilibrium cycle average *k*-effective, and this acts as a source of adjusted neutron excess since fewer neutrons than expected are lost to control. The magnitude of this contribution for each cycle is shown in Figure A.3-3. While no single cycle contributes more than 1% of the total needed neutron excess, the total contribution is significant, amounting to 11.5% of the equilibrium cycle amount. The contribution would not have been as large had the transition cycle average *k*-effectives matched the equilibrium cycle value more closely.

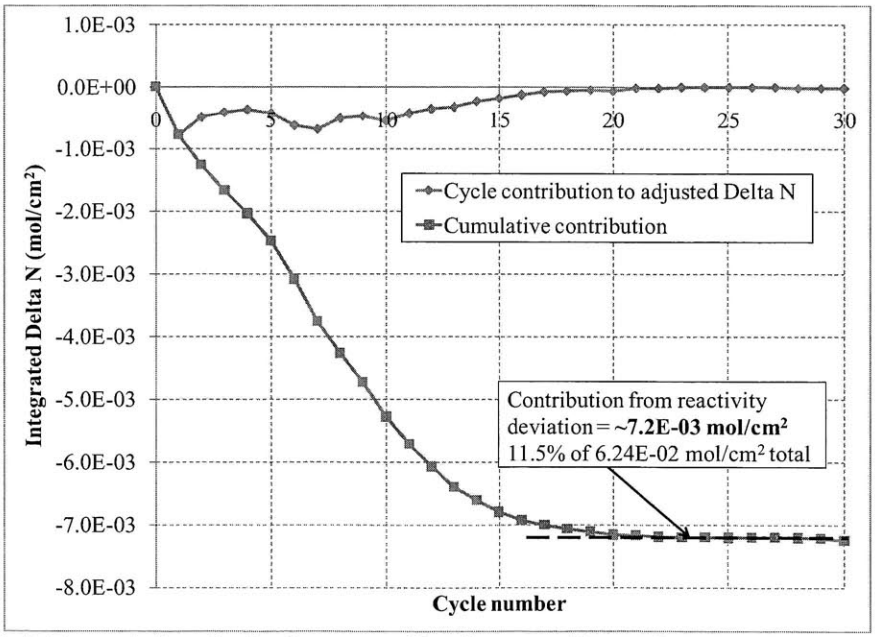

Figure A.3-3. Reactivity-deviation contribution to adjusted neutron excess in second example transition model

The fuel contribution to adjusted neutron excess is given in Figure 3.5-14, along with the infinite medium prediction for the starter fuel. The 5.16E-2 mol/cm^2 from the starter fuel, 3.7E-3 mol/cm^2 from the feed fuel, and 7.2E-3 mol/cm^2 from reactivity deviations add to 6.27E-2 mol/cm^2, within error of the 6.26E-2 mol/cm^2 neutron excess requirement of the equilibrium cycle.

Figure A.3-4 shows the burnup distribution of the starter and feed fuel at cycle 30. All the discharged feed fuel has burnup close to the equilibrium cycle value of just under 11.6%, while the starter fuel discharge burnups are clustered around an average value of 22.9%, corresponding to an additional burnup of 11.4% over the second burn. If one subtracts the reactivity contribution to neutron excess (which is a consequence of the fuel management scheme selected), then one can estimate based on the infinite-medium approximation that the remaining 5.54E-2 mol/cm^2 would require 25 cm of starter fuel to be burned an additional 12.6%. This is a 10% overestimate, with the actual value being lower since the actual transition sequence results in non-zero neutron excess from the feed fuel and additional neutron excess from the starter fuel.

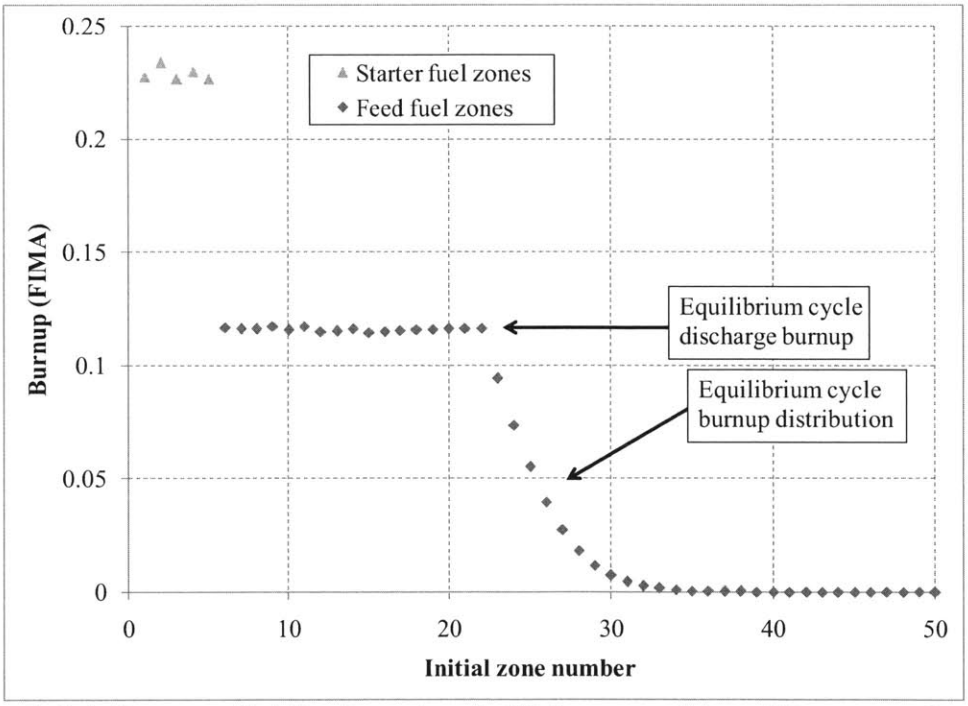

Figure A.3-4. Burnup distribution at cycle 30 for second transition example model

A.4 Designing realistic three-dimensional equilibrium cycle configurations

Section 3.7 gives results for a number of three-dimensional equilibrium cycle shuffling sequences with different physical sizes operating at different power levels. This appendix describes how these shuffling sequences were designed and implemented into the 3D block model. The overall goal was to develop a variety of sequences that yield a flatter, more favorable power distribution than strictly convergent shuffling, which yields the power distribution shown in Figure A.4-1.

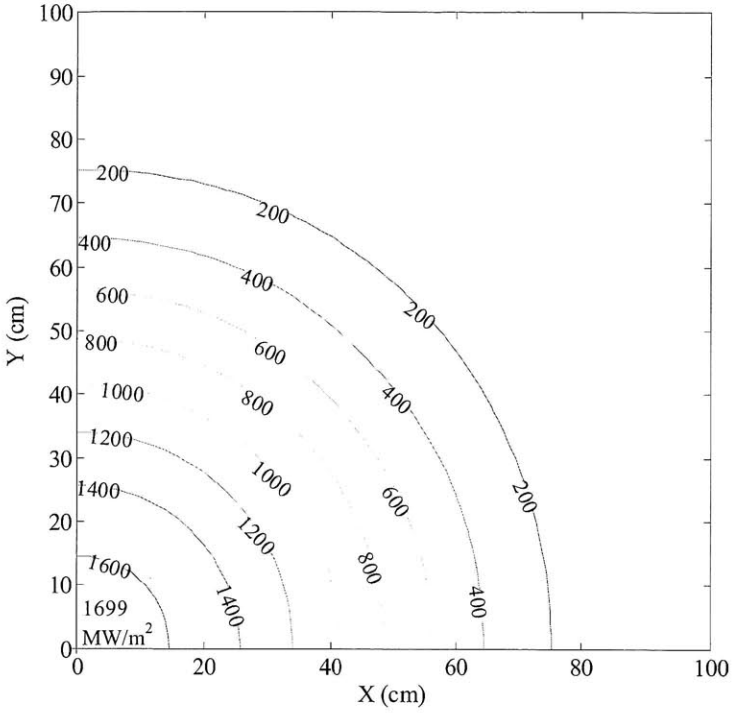

Figure A.4-1. EOEC areal power density in 1500 MW convergent shuffling case (MW/m^2)

The first attempted approach was to shuffle fuel based on its distance from a flat disc, rather than its distance to the origin. Distance contour lines for this approach are shown in Figure A.4-2. The dotted lines in the figure designate the outlines of the fuel blocks in the x-z or y-z planes. While the arrows indicate the net direction of fuel movement, individual fuel blocks would be moved laterally within a given plane several times before being moved to the next plane, because less than one plane is shuffled with each cycle.

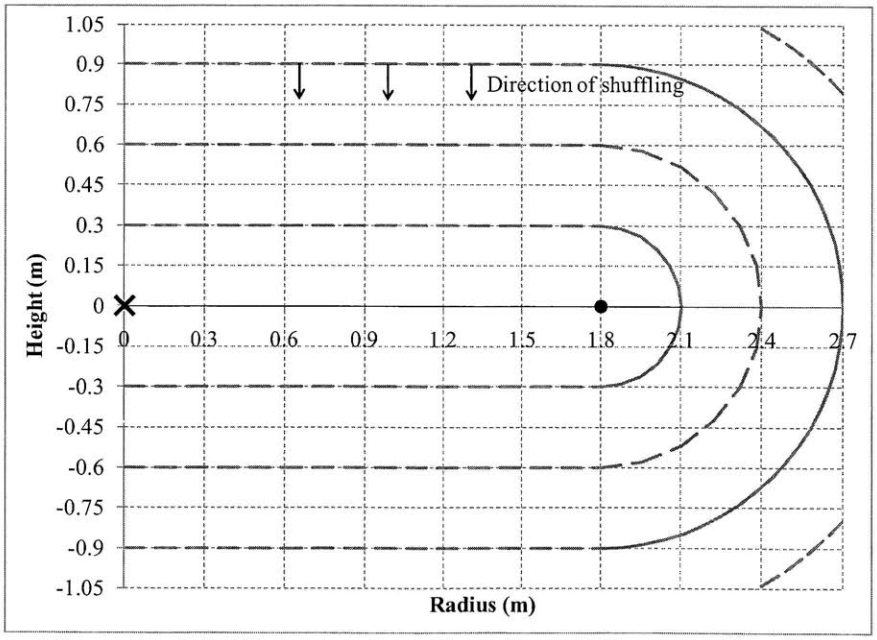

Figure A.4-2. 30 cm contour lines for a 180 cm radius disc

In this case there are a significant number of zones that are the same distance from the plane as one another, so that the method of ordering among these cells is important. If one orders them in a random fashion, then the resulting power distribution would look similar to the one shown in Figure A.4-3. The results in Figure A.4-3 are for a 3000 MW core shuffling 12 zones each 466.56 day cycle, which yields the same discharge burnup (and thus average *k*-effective) as in previous one-dimensional models and the other three-dimensional models considered.

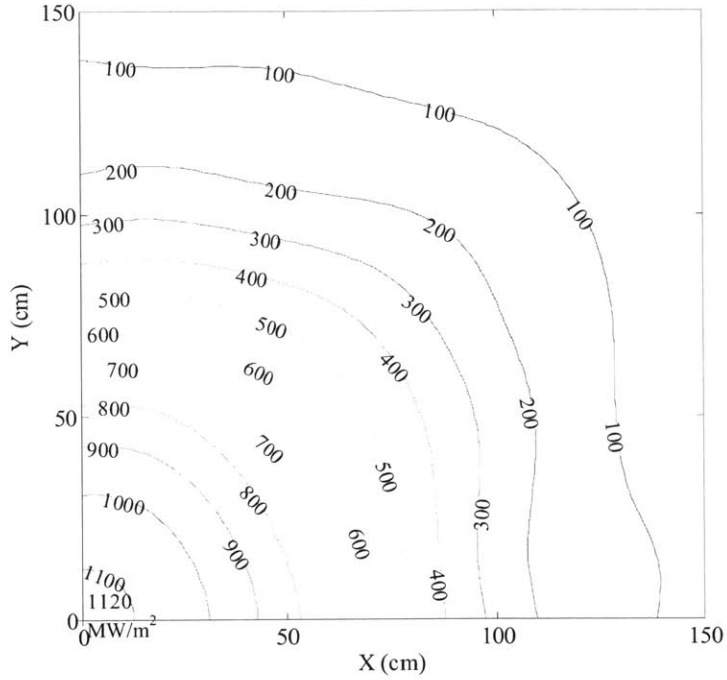

Figure A.4-3. EOEC areal power density in 3000 MW, 180 cm disc shuffling case (MW/m^2)

Figure A.4-3 shows that the power distribution has been spread out significantly; the peak areal power density is 34% lower than in the convergent case even though the total power has been doubled to 3000 MW. Nevertheless, one sees that the distribution is still centrally peaked, and not flat as may be expected from the shape of the contours in Figure A.4-2. This peaking occurs because there is a positive feedback loop between breeding and burning in the power producing region. Higher flux in the center of the core causes more Pu-239 to be bred there, which in turn concentrates the flux further in the center, causing a positive-feedback instability. To avoid this instability, the more highly bred fuel at the center of the core would need to be shuffled away from the center, which would flatten out the flux distribution. However, by randomly ordering the zones on each plane, the more highly bred fuel at the center is not sufficiently spread around the core to prevent flux from continuing to peak there.

Two shuffling patterns were investigated that can successfully create stable and flat power density profiles with a variety of sizes. These patterns, illustrated in Figures A.4-4 and A.4-5, cause fuel to converge to either a ring or a "pinched" plane. The distance contours can also be thought of as being burnup contours, since fuel is burned as it travels from contour to contour. In the ring case, fuel is shuffled convergently toward a ring with radius *r*, so fuel at the origin is less burned than fuel at the ring. The pinched plane is similar to the disc case, except the effective

distance from the x-y plane increases as one approaches the z-axis. The magnitude of this effect is determined by the "z-intercept coefficient"; the illustrated case with a z-intercept coefficient of 0.5 means that a point on the z-axis 15 cm away from the x-y plane is treated as being "30cm away" from being discharged. A z-intercept coefficient just below unity is similar to the disc case in Figure 2.7-2, except fuel traveling through each axial plane is shuffled from the z-axis outward, instead of being shuffled randomly within the plane.

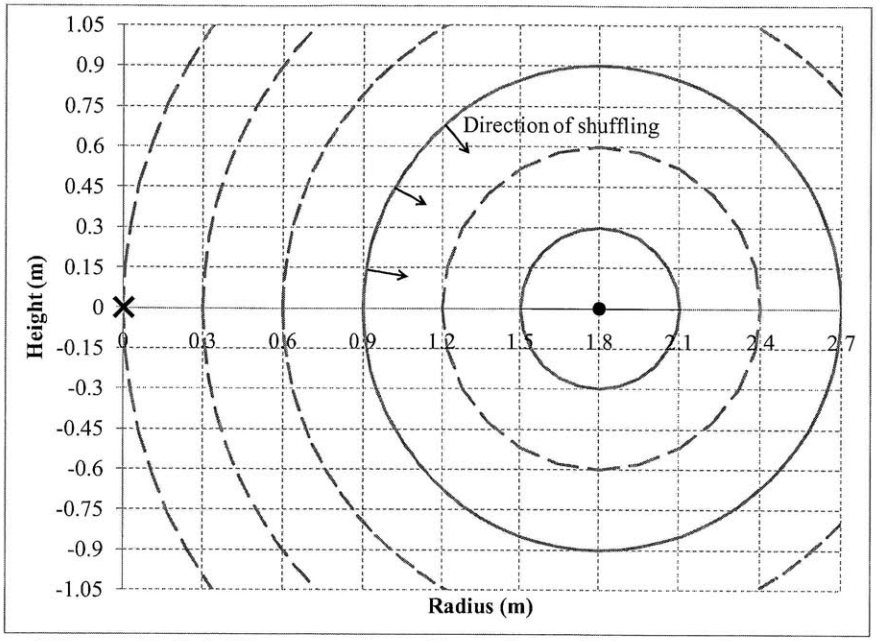

Figure A.4-4. 30 cm contour lines for a 180 cm radius ring

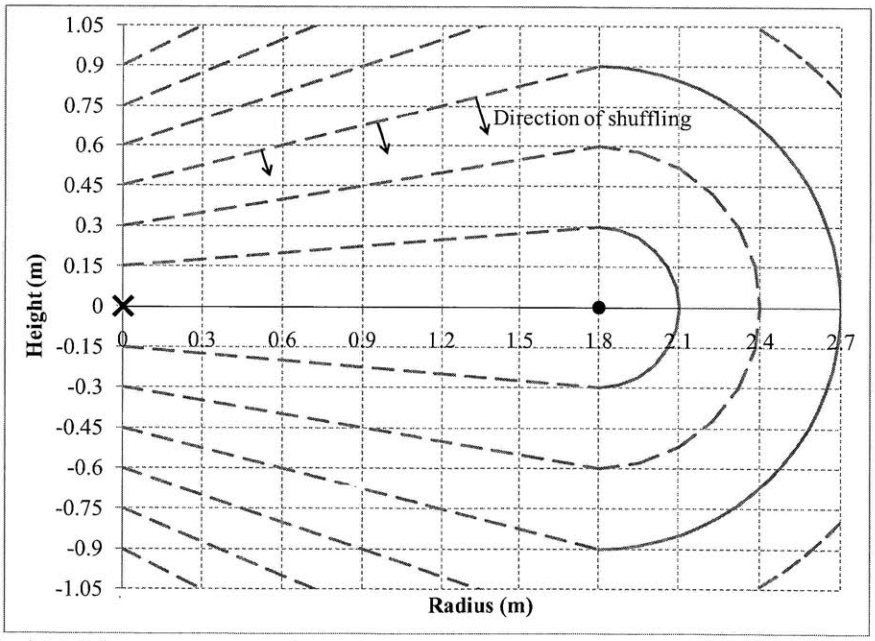

Figure A.4-5. 30 cm contour lines for a 180 cm radius pinched plane (z-intercept coefficient=0.5)

Many other shuffling patterns are possible; for example one can flatten the power profile of the convergent shuffling case by introducing subcritical fresh fuel at the origin. However, as discussed in Subsection 3.3.3, the positioning of fresh fuel in a high flux region can lead to large swings in *k*-effective and power distribution over a cycle. Also, having a region of fresh fuel and highly burned fuel that are spatially near each other can hamper the development of an equilibrium cycle. This is because changing flux and power conditions in the highly burned fuel can alter the evolution of the fresher fuel, which would yield still different flux and power conditions when it eventually replaces the highly burned fuel. An example of this behavior is shuffling sequence 3 in Appendix A.1, which displays long period oscillatory behavior while converging to the equilibrium cycle. The shuffle patterns considered in this section have the advantage of smoothly transitioning in space between fresh fuel and fully burned fuel.

Power density figures for the ring shuffle case for radii from 30 cm to 180 cm are given in Figures A.4-6 through A.4-11. Those with ring radii 120 cm and under were modeled with 1500 MW total power (187.5 MW per core octant), shuffling 40 fuel zones per cycle (5 per octant), while those with ring radii above 120 cm were modeled with 3000 MW total power (375 MW per octant), shuffling 80 fuel zones per cycle (10 per octant). This is done because higher-power distributions require more zones to be shuffled per cycle to maintain the same cycle length. Periodic x and y boundary conditions are used for all cases.

The ring shuffle pattern is good for smaller reactor sizes, and can create a non-centrally peaked power distribution at ring radii above 90 cm. At radii above 120 cm, the burnup distribution is not balanced around the large ring, causing peaked burn areas to form. These peaked areas form because of local regions of breed-burn positive feedback: the shuffling pattern employed does not spread bred fuel evenly enough around the ring to maintain an even annular power distribution. As the size of the power producing region increases, it becomes more challenging to arrange fuel to yield a balanced power distribution.

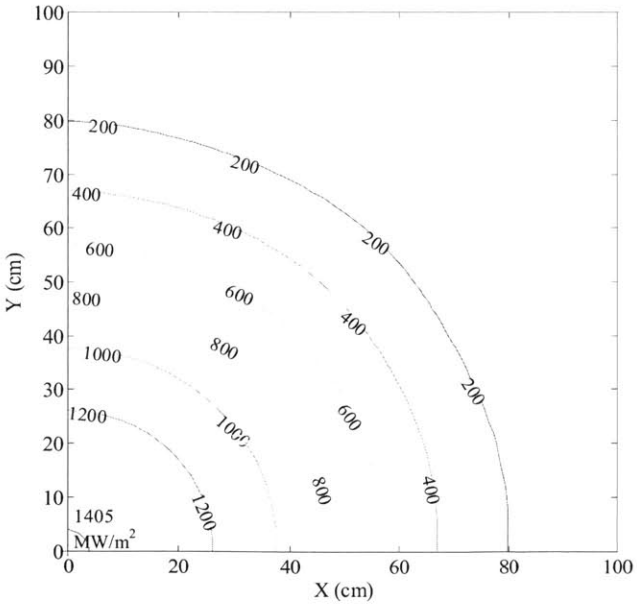

Figure A.4-6. EOEC areal power density for 1500 MW ring (radius = 30 cm)

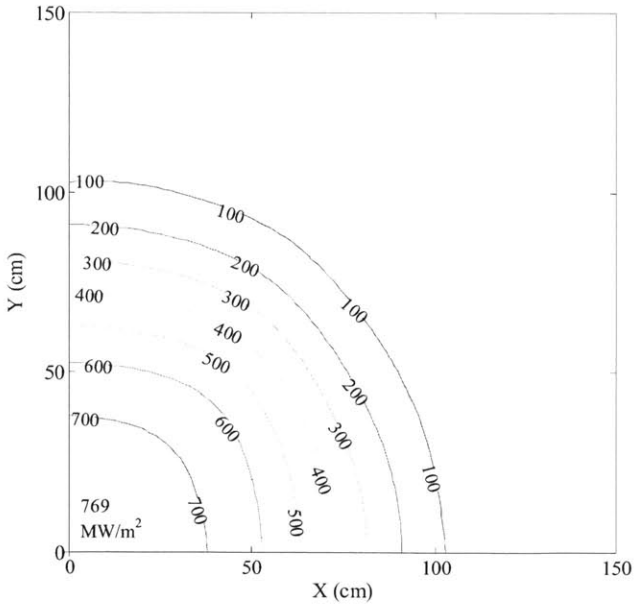

Figure A.4-7. EOEC areal power density for 1500 MW ring (radius = 60 cm)

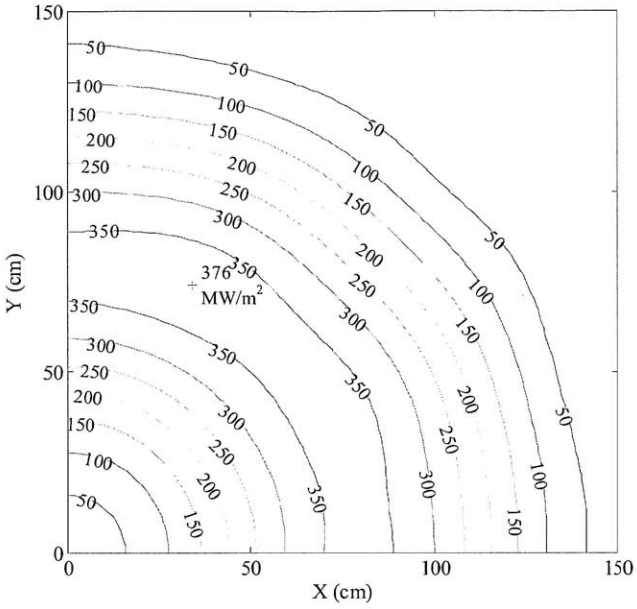

Figure A.4-8. EOEC areal power density for 1500 MW ring (radius = 90 cm)

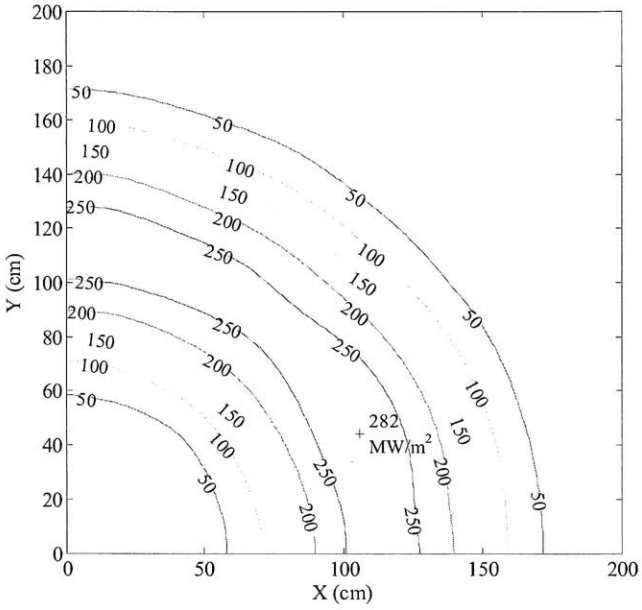

Figure A.4-9. EOEC areal power density for 1500 MW ring (radius = 120 cm)

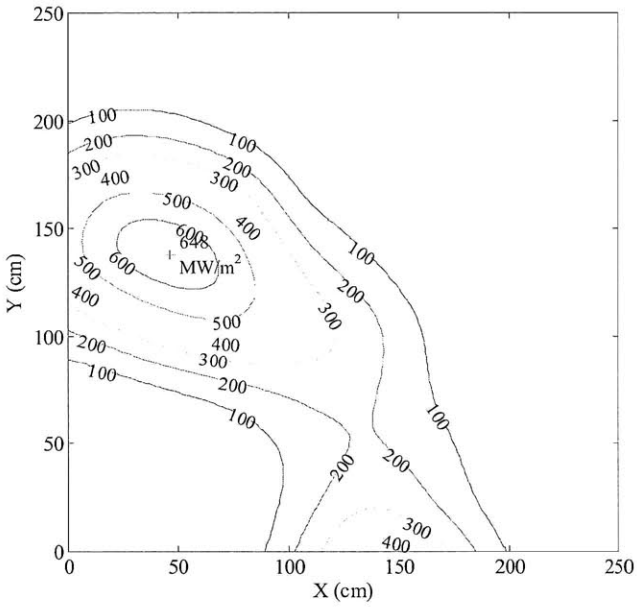

Figure A.4-10. EOEC areal power density for 3000 MW ring (radius = 150 cm)

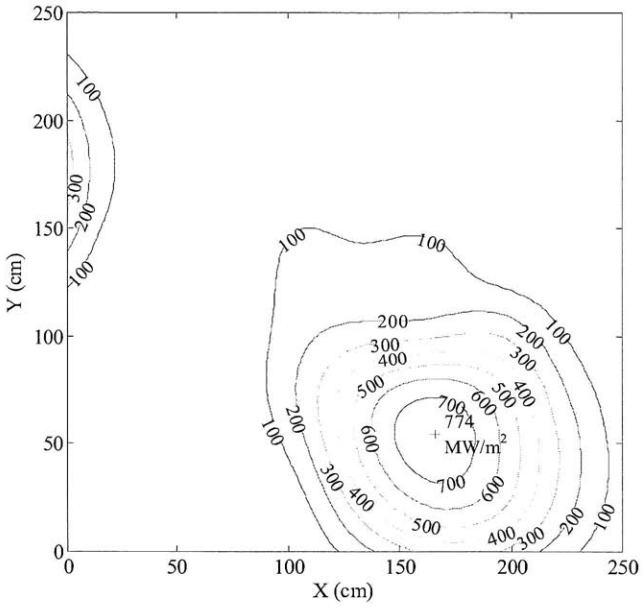

Figure A.4-11. EOEC areal power density for 3000 MW ring (radius = 180 cm)

Using the pinched plane shuffle pattern in Figure A.4-5 with a z-intercept coefficient of 0.5 yields the areal power density distributions shown in Figures A.4-12 through A.4-15. This shuffling pattern fills in the central power depression seen in the ring shuffling cases, and can be extended to larger radii without local power peak formation. Local peaking can be seen in the 180 cm radius case, but it is still possible to establish very large and flat stable distributions, as shown by the 240 cm radius case. At a realistic peak areal power density of 400 MW/m^2, the distribution in Figure A.4-15 corresponds to a very large total power of over 5000 MW.

Additional power distribution flattening can be achieved by adjusting the z-intercept coordinate as a function of shuffling sequence "radius". For example, using a z-intercept coordinate of 0.98 for a radius of 180 cm yields the extremely level power distribution of the "flattened power distribution case" shown in Figure 3.7-2. Trying to extend this shuffling pattern to larger radii yields interesting oscillatory equilibrium cycle behavior, which is described in Subsection 3.7.4.

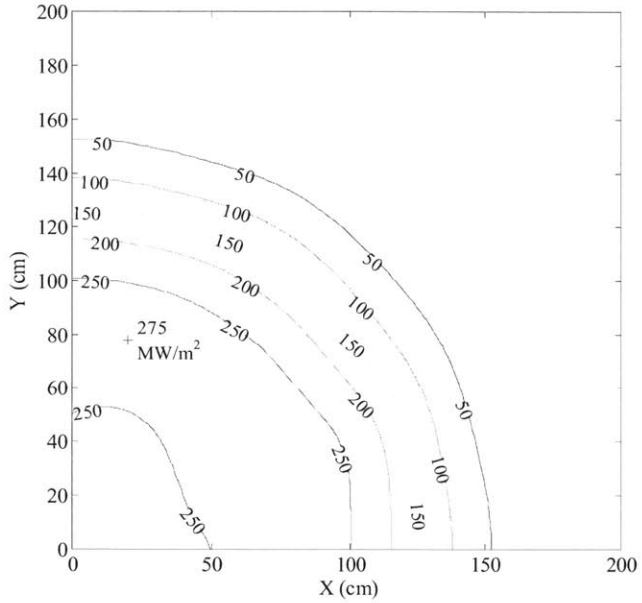

Figure A.4-12. EOEC areal power density for 1500 MW pinched plane (radius = 120 cm, z-int coeff = 0.5)

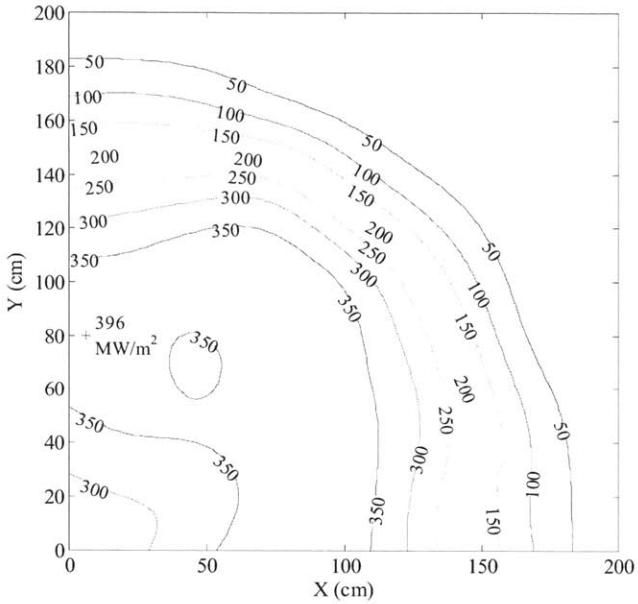

Figure A.4-13. EOEC areal power density for 3000 MW pinched plane (radius = 150 cm, z-int coeff = 0.5)

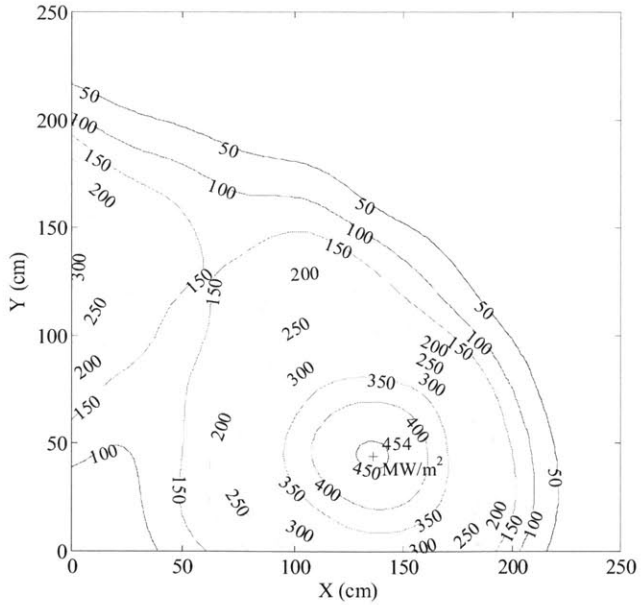

Figure A.4-14. EOEC areal power density for 3000 MW pinched plane (radius = 180 cm, z-int coeff = 0.5)

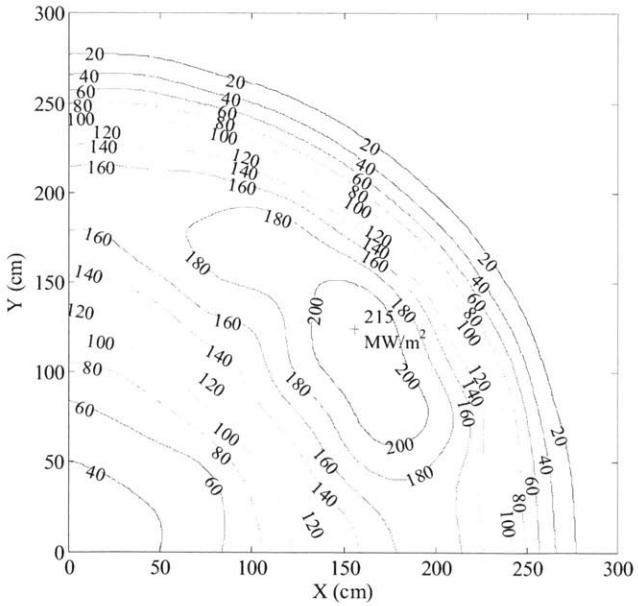

Figure A.4-15. EOEC areal power density for 3000 MW pinched plane (radius = 240 cm, z-int coeff = 0.5)

A.5 Thermal hydraulic assumptions and calculations

Very simple thermal hydraulic calculations were used to compute allowable power density as a function of coolant volume fraction for sodium, lead/LBE, and helium coolant. The thermal hydraulic model consists of a single subchannel calculation for an interior subchannel in a hexagonal array of pins. This subchannel is illustrated in Figure A.5-1.

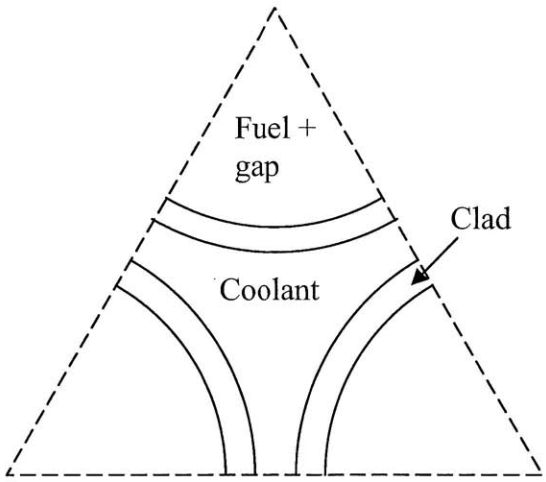

Figure A.5-1. Interior subchannel assumed for thermal hydraulic calculations

The subchannel model assumes a pin geometry with a diameter of 6.6 mm and a clad thickness of 0.4 mm, the same as for BN-800 reactor design. The small size of the fuel pins increases the cladding surface area and reduces the temperature difference between the coolant and cladding, which allows higher power densities. The area of the coolant is set so that the ratio of coolant to fuel+gap area in the subchannel is equal to that of the core composition being studied. For example, for a U2Zr-75–T91-30–Na-100 core composition, the sodium coolant volume is 100% of the volume available inside the clad, which results in a pin pitch of 8.367 mm. The amount of structure present in the subchannel model (29.5% of the fuel+gap area) does not correspond to the amount in the core compositions (30% and 60% respectively); one can account for the actual amount of structure by assuming there is additional volume of structure present outside of the subchannel.

A.5.1 Assumed coolant properties

To simplify calculations, all coolant properties except for density are assumed to be constant and equal to a value at the core average temperature. The assumed coolant properties are given in Table A.5-1. Lead and LBE have similar thermal hydraulic performance, so coolant properties for lead are used to obtain LBE results. Expressions for coolant density are given in Equations A.5-1 through A.5-3 for sodium, lead, and helium respectively [Lyon, 1952; Sobolev, 2008]. The expression for helium assumes that it is an ideal gas at 20 MPa pressure.

Table A.5-1. Assumed coolant properties for thermal hydraulic calculations

	Sodium	Lead/LBE	Helium
Dynamic viscosity μ (Pa·s)	2.46E-4	1.9E-3	3.49E-4
Specific heat capacity c_p (J/kg·K)	1265	145.4	5196
Thermal conductivity k_{cool} (W/m·K)	69	15.4	0.275

$$\rho_{sodium}(kg/m^3) = 950.1 - 0.22976 \cdot T(^\circ C) - 1.46 * 10^{-5} \cdot T^2(^\circ C) + 5.638 * 10^{-9} \cdot T^3(^\circ C) \quad \text{(A.5-1)}$$

$$\rho_{lead}(kg/m^3) = 10673 - 1.2795 * \left(T(^\circ C) + 273.15 - 600.6\right) \quad \text{(A.5-2)}$$

$$\rho_{helium}(kg/m^3) = 4.0 * 20 * 10^6 / \left(8314 * \left(T(^\circ C) + 273.15\right)\right) \quad \text{(A.5-3)}$$

A.5.2 Thermal hydraulic calculation methodology

Conceptually, the thermal hydraulic calculation is carried out by specifying a total mass flux ($\dot{m}$) and areal power density (Q'') such that the maximum clad temperature and coolant velocity limits are exactly met. Given an areal power density Q'' and mass flux $\dot{m}$, the total change in coolant temperature (T_{cool}) between the inlet and outlet can be calculated:

$$T_{cool,outlet} = T_{cool,inlet} + \frac{Q''}{f_{coolant}\dot{m}c_p} \quad \text{(A.5-4)}$$

In Equation A.5-4, $f_{coolant}$ is the coolant volume fraction of the core composition, not the coolant volume fraction in the subchannel model (these are different since the subchannel model does not include the total amount of structure present). The coolant inlet temperature for the different coolants is set to **400°C**. Similar to in Equation A.5-4, the coolant temperature in a particular axial zone i is calculated as:

$$T_{cool,i} = T_{cool,i-1} + \frac{Q'' x_i}{f_{coolant}\dot{m}c_p} \quad \text{(A.5-5)}$$

In Equation A.5-5, x_i is the fraction of total power produced in zone i. This formulation is slightly conservative since it assumes that the coolant temperature in a zone is equal to the temperature at which coolant exits the zone.

Based on the coolant temperature at each zone, the peak cladding temperature in that zone can be calculated as:

$$T_{clad,i} = T_{cool,i} + q'_i \left(R_{clad} + R_{conv,i}\right) \quad \text{(A.5-6)}$$

$$q'_i = \frac{Q'' x_i}{f_{coolant}} \frac{2A_{coolant}}{L_{zone}} \quad \text{(A.5-7)}$$

$$R_{clad} = \frac{\ln(r_{clad,o} / r_{clad,i})}{2\pi k_{clad}} \quad \text{(A.5-8)}$$

$$R_{conv,i} = \frac{1}{2\pi r_{clad,o} h_i} \quad \text{(A.5-9)}$$

In Equation A.5-6, $T_{clad,i}$ is the peak cladding temperature in an axial zone i, q'_i is the linear heat rate in the zone, and $R_{conv,i}$ and R_{clad} are thermal resistance terms. $R_{conv,i}$ represents the thermal resistance between the outer surface of the clad and the coolant bulk temperature, and R_{clad} is the thermal resistance through the cladding.

Equation A.5-7 gives an expression for the linear heat rate in a zone. The term $A_{coolant}$ is equal to the coolant area in the subchannel illustrated in Figure A.5-1. A factor of two is included in the equation because each subchannel only contains half of one pin. In equation A.5-8, $r_{clad,o}$ and $r_{clad,i}$ are the outer and inner radii of the cladding, and k_{clad} is the thermal conductivity of the clad. For stainless steel clad, the clad thermal conductivity is assumed to be 27 W/m·K. No corresponding assumption is made for silicon carbide clad. This is because there is greater uncertainty about the peak operating temperature constraint of silicon carbide, so instead of assuming parameters to calculate power densities for SiC clad systems, the power density values for stainless steel clad are used instead.

In Equation A.5-9, the term h_i is equal to the heat transfer coefficient of the coolant. It is calculated for the different coolants using Equations A.5-10 through A.5-13.

$$h_i = \frac{\mathrm{Nu}_i k_{cool}}{D_H} \quad \text{(A.5-10)}$$

$$\mathrm{Nu}_i(sodium, lead) = 4 + 0.33 * (P/D)^{3.8} * (\mathrm{Pe}_i / 100)^{0.86} + 0.16 * (P/D)^5 \quad \text{(A.5-11)}$$

$$\mathrm{Nu}_i(helium) = \frac{(f_i/8)(\mathrm{Re}_i - 1000)\mathrm{Pr}_i}{1 + 12.7(f_i/8)^{1/2}(\mathrm{Pr}_i^{2/3} - 1)} \quad \text{(A.5-12)}$$

$$f_i = (1.8 * \log(\mathrm{Re}_i) - 1.5)^{-2} \quad \text{(A.5-13)}$$

In Equation A.5-10, Nu_i is the coolant Nusselt number, and D_H is the hydraulic diameter of the subchannel. Equation A.5-11 is the Westinghouse correlation for liquid metals [Kazimi, 1976], and Pe_i is the coolant Peclet number, equal to the product of the Reynolds and Prandtl numbers. Equation A.5-12 is the Gnielinski correlation [Gnielinski, 1976], where Re_i and Pr_i are the Reynolds and Prandtl numbers in zone i, and f_i is a friction factor, defined in Equation A.5-13.

The above equations allow coolant and clad temperatures for the different axial zones to be calculated. The other constraining parameter, coolant velocity, is computed using Equation A.5-14. Since coolant becomes less dense as it is heated, the peak coolant velocity occurs at the outlet of the subchannel.

$$v_{coolant} = \dot{m} / \rho_i \quad \text{(A.5-14)}$$

A.5.3 Example thermal hydraulic calculations

For all thermal hydraulic calculations, it is assumed that the coolant inlet temperature is 400°C with a peak cladding temperature constraint of 580°C; which are representative values for sodium-cooled fast reactors taken from the IAEA fast reactor database. The peak velocity constraint assumed for each coolant is 8 m/s for sodium, 2 m/s for LBE, and 100 m/s for helium.

The axial power distributions x_i are taken from the one-dimensional convergent infinite slab models. These are shown for two core compositions, U2Zr-100-T91-30-Na-100 and U2Zr-100-T91-30-He-100 in Figure A.5-2. The curves do not contain the same area because the model for the sodium-cooled composition uses 5 cm zones while the one for the helium-cooled composition uses 6 cm zones.

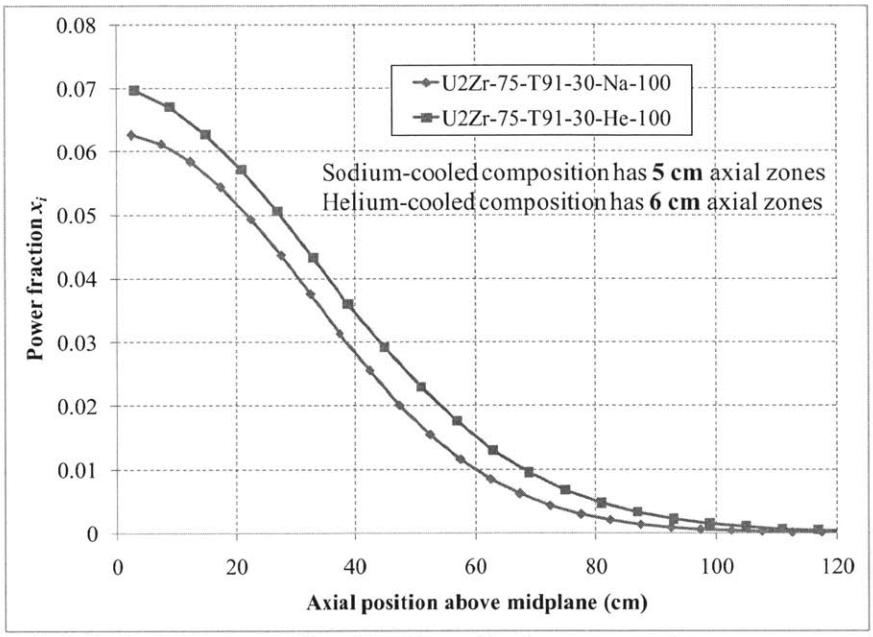

Figure A.5-2. Axial power distributions for two example core compositions

For the sodium-cooled core composition, it was found that an areal power density of **608 MW/m^2** and a coolant mass flux of **6524 kg/m^{2}s** allow the peak cladding temperature and coolant velocity limits to be met exactly. Corresponding values for the helium-cooled core composition are **254 MW/m^2** and **1263 kg/m^{2}s**. Using these input values, it is possible to use the equations in this appendix to solve for the coolant and clad temperature distributions, as well as coolant velocity as a function of axial zone. These results for the two example core compositions are shown in Figures A.5-3 and A.5-4. Only results above the midplane are computed since the peak cladding temperature and coolant velocity occur above the core midplane.

Figure A.5-3 shows that the coolant temperature rise is much higher for sodium coolant than for helium coolant. This is because the excellent thermal conductivity of sodium means that there is only a small temperature difference between the clad and coolant, so the coolant outlet temperature is close to the peak clad temperature. The poor thermal conductivity of helium

coolant causes there to be a large temperature difference between the coolant and clad, so the peak cladding temperature occurs close to the midplane of the core, where the linear heat rate of the fuel is highest. Flattening the power distribution in the helium cooled system (as discussed in Subsection 3.7.7) could improve areal power density and also reactor doubling times.

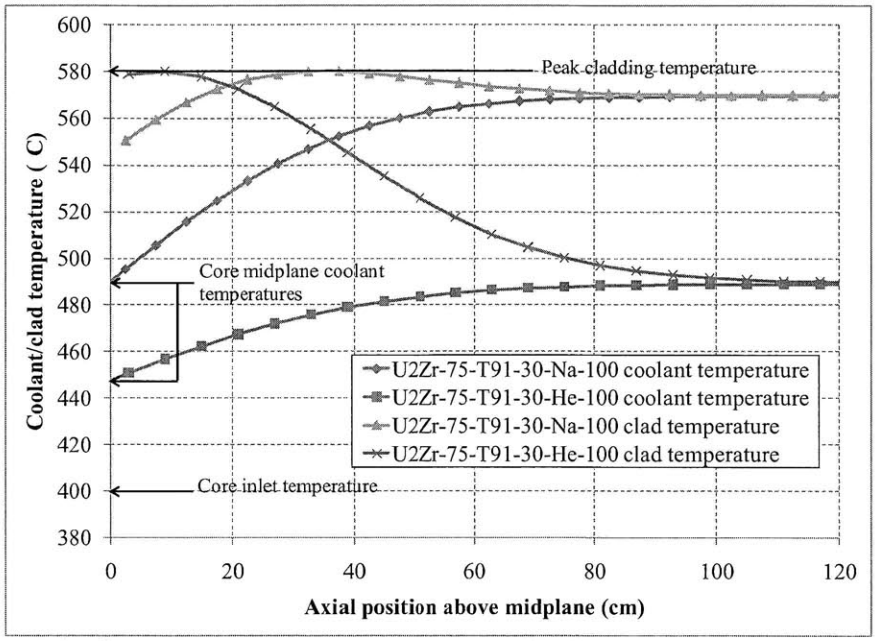

Figure A.5-3. Coolant and clad temperature distributions for two example core compositions

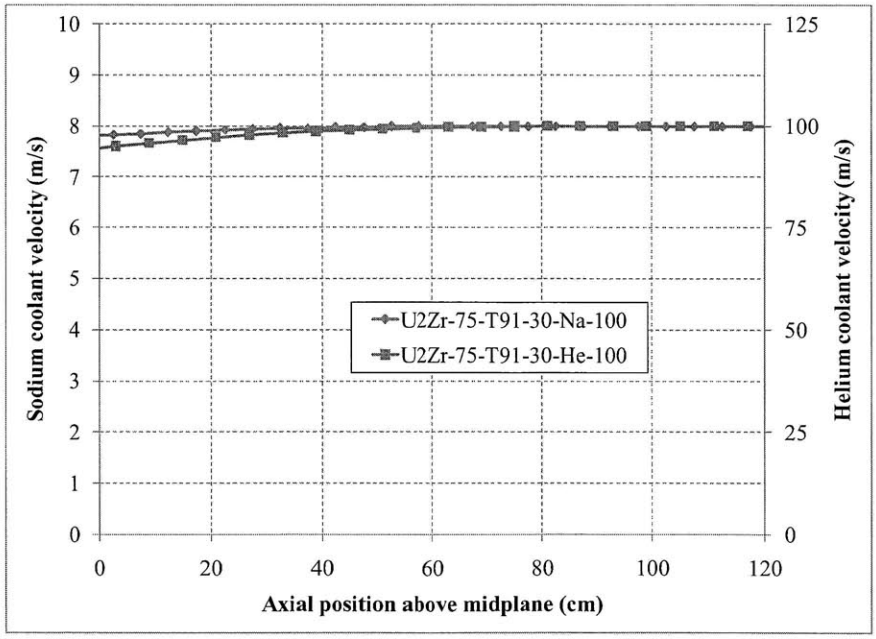

Figure A.5-4. Coolant velocity distributions for two example core compositions

A.6 Details of neutron diffusion approximation for axial transfer model

In Subsection 6.3.2, an axial transfer matrix is used to predict the axial distributions that arise in linear-assembly B&B reactors. This axial transfer matrix gives the relationship between the axial position at which a neutron is produced, and the axial position at which it is absorbed. The axial transfer matrix was computed according to a simple one-dimensional, single-group neutron diffusion approximation, described in this appendix.

In this simple approximation, it is assumed that all neutrons are born at a uniform plane source located at the center of each axial zone. The objective is to compute the shape of the flux distribution as a function of position, taking into account the albedo assumed at the boundary. This situation is depicted schematically in Figure A.6-1, for neutrons produced in the fifth zone from the boundary of the fuel zones. The middle of the neutron production zone is assumed to be at the origin, and the fuel boundary is located at position H, which in Figure A.6-1 is 4.5 zone lengths from the origin. In total, forty of these problems are solved to produce an axial transfer matrix, one for each side of (above and below) each of the 20 axial zones. The general solution to this problem is outlined here.

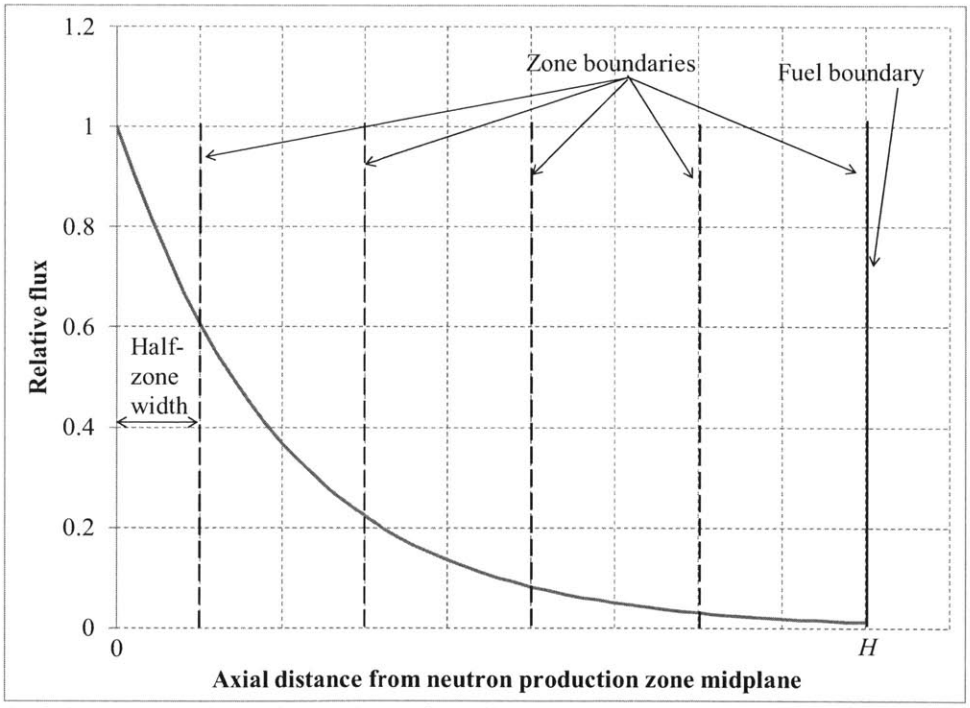

Figure A.6-1. Illustration of problem situation solved with neutron diffusion equation

Based on the neutron diffusion equation in an absorbing medium with constant material properties, flux as a function of position can be written as a linear combination of hyperbolic sine and cosine functions:

$$\phi = C\sinh\left(\frac{z}{L}\right) + \cosh\left(\frac{z}{L}\right) \tag{A.6-1}$$

In Equation A.6-1, z is the axial distance from the neutron production zone midplane, and L is the neutron diffusion length in the material. The value of flux at the source plane (z=0) has been defined to be unity, since only the shape of the flux, not its absolute value, is being solved for. The term C is a coefficient that can be solved for by applying a boundary condition.

Expressions for the forward and backward neutron current are given in Equation A.6-2 and A.6-3, which also follow from neutron diffusion theory.

$$J^{+} = \frac{\phi}{4} - \frac{D}{2}\frac{d\phi}{dz} \tag{A.6-2}$$

$$J^{-} = \frac{\phi}{4} + \frac{D}{2}\frac{d\phi}{dz} \tag{A.6-3}$$

At the boundary, the ratio of the forward to backward neutron currents is set to the neutron albedo of the reflector, A:

$$\frac{J^{-}(H)}{J^{+}(H)} = A \tag{A.6-4}$$

Substituting expressions for flux into Equation A.6-4 gives an equation that can be solved for the coefficient C in Equation A.6-1. First, Equation A.6-4 is rearranged, and expressions for neutron current are substituted in it to yield Equation A.6-5. Rearranging again gives Equation A.6-6.

$$A\left(\frac{\phi}{4} - \frac{D}{2}\frac{d\phi}{dz}\right) - \left(\frac{\phi}{4} + \frac{D}{2}\frac{d\phi}{dz}\right) = 0 \tag{A.6-5}$$

$$(A-1)\left(\frac{\phi}{4}\right) - (A+1)\left(\frac{D}{2}\frac{d\phi}{dz}\right) = 0 \tag{A.6-5}$$

Substituting the flux expression in Equation A.6-1 yields Equation A.6-7:

$$\frac{(A-1)}{4}C\sinh\left(\frac{H}{L}\right) + \frac{(A-1)}{4}\cosh\left(\frac{H}{L}\right) - \frac{(A+1)}{2}\frac{D}{L}C\cosh\left(\frac{H}{L}\right) - \frac{(A+1)}{2}\frac{D}{L}\sinh\left(\frac{H}{L}\right) = 0 \tag{A.6-7}$$

Solving Equation A.6-7 for C yields:

$$C = \frac{-(A-1)\cosh\left(\frac{H}{L}\right) + 2(A+1)\frac{D}{L}\sinh\left(\frac{H}{L}\right)}{(A-1)\sinh\left(\frac{H}{L}\right) - 2(A+1)\frac{D}{L}\cosh\left(\frac{H}{L}\right)} \tag{A.6-8}$$

Substituting this expression for C into Equation A.6-1 yields the flux distribution on one side of the neutron source plane. The flux distribution on the other side of the neutron source plane can be solved for in the same manner, and the two distributions are related by having the same value of flux at the source plane (defined to be unity).

From the flux distribution due to a source plane, the absorption rate in each axial fuel zone is calculated as the integral of the flux over each zone multiplied by the absorption cross section, as written in Equation A.6-9. For absorption within the same zone as the neutron production zone, two of these integrals are added, one for each side of the central neutron source plane.

$$Absorption\ rate = \int_{zone} dz \Sigma_a \phi(z) \tag{A.6-9}$$

The leakage rate out of the fuel region is given by the neutron current at the boundary:

$$Leakage\ rate = -D \frac{d\phi(H)}{dz} \tag{A.6-10}$$

For each source plane, the probability that a neutron produced at that source plane is absorbed in a given sink zone is equal to the absorption rate in that zone divided by the total absorption and leakage rates. Performing this calculation for each combination of source and sink zone yields an axial transfer matrix, which can be used to predict the shapes of axial distributions in a linear-assembly B&B reactor.

A.7 Effect of cycle length on equilibrium cycle neutron excess requirement

Table 6.6-1 gives the twice-adjusted neutron excess contained at the beginning and middle of the equilibrium cycle. These reason these numbers are different is illustrated in Figure A.7-1. During the first half of a cycle, when the uncontrolled k_{fuel2} is less than the average k_{eq2}, there is a net gain in twice-adjusted neutron excess. In the second half of a cycle, the reverse is true and neutron excess goes down, exactly cancelling out the gain from the first half of the cycle. Assuming that the reactivity swing is approximately linear with the number of neutrons absorbed over a cycle, the variation of neutron excess over a cycle would look like a parabola, as shown in Figure A.7-2. The difference between the BOEC and MOEC amount of contained neutron excess therefore scales roughly with the square of the cycle length. This is shown in Figure A.7-3 for the different cycle length infinite slab cases from Subsection 3.1.2.

This scaling law is useful when considering the effects of cycle length: a good approximation is to assume that changing cycle length does not change the MOEC neutron excess (since the MOEC state would remain similar), and scaling the difference between the BOEC and MOEC contained neutron excess as the square of the cycle length. This approach is used in Section 6.6 to scale the cycle lengths of different linear-assembly B&B reactor equilibrium cycles. In all the cases considered, the difference between the BOEC and MOEC neutron excess requirements is small (<3%) compared to the total magnitude of neutron excess contained, since the average k_{eq2} is close to unity.

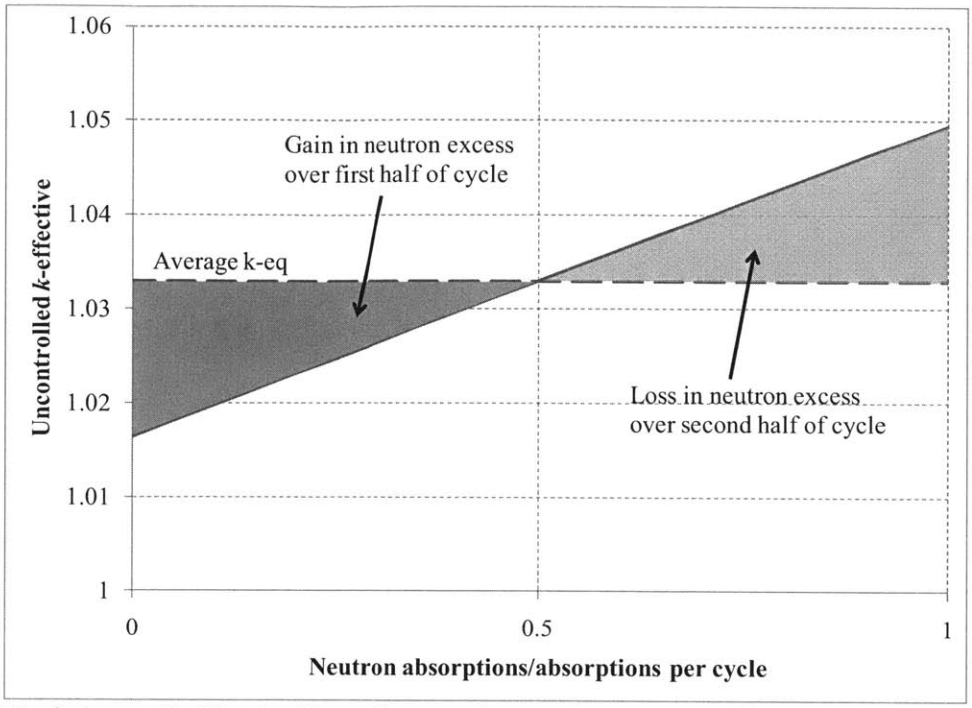

Figure A.7-1. Schematic illustration of cause for neutron excess change over an equilibrium cycle

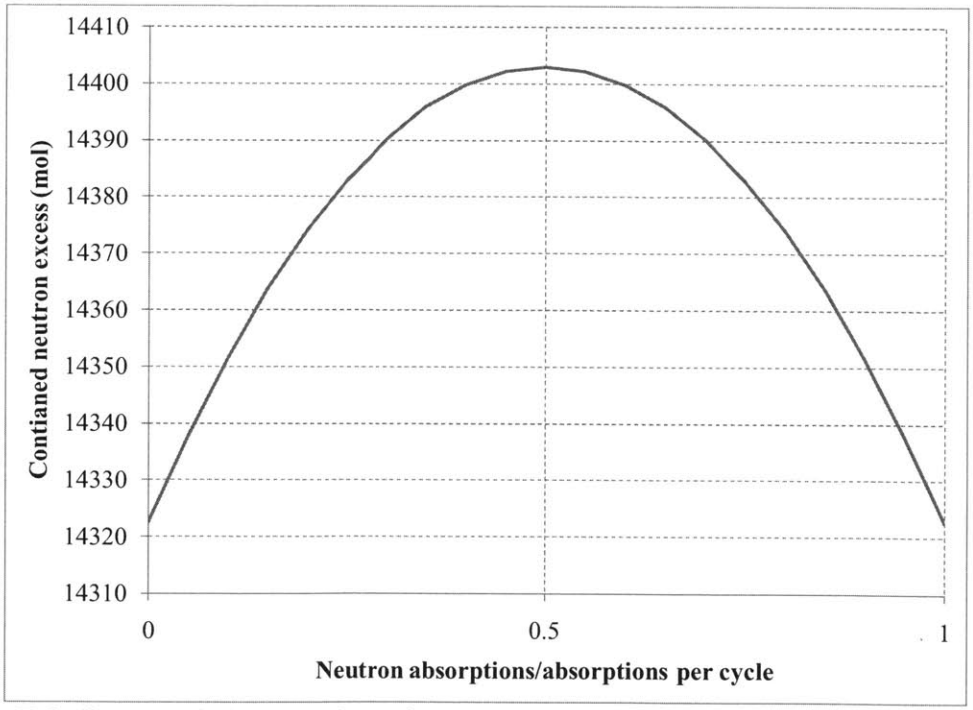

Figure A.7-2. Schematic illustration of neutron excess change over an equilibrium cycle

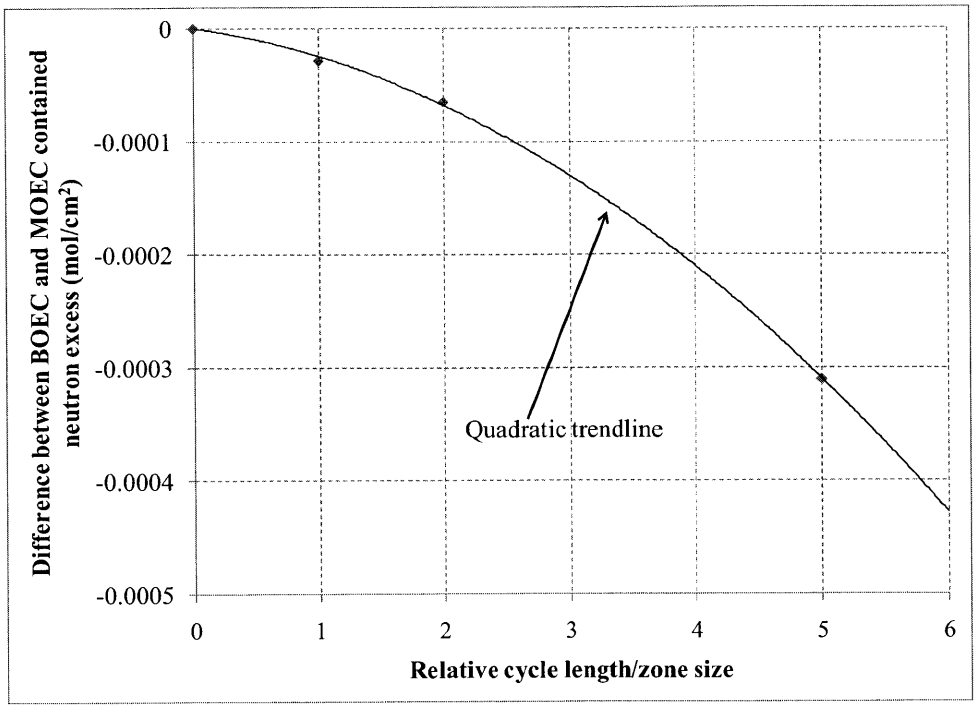

Figure A.7-3. Difference between BOEC and MOEC contained neutron excess in different cycle length infinite slab models

References

Ahlfeld, C., et al., "Cost and Safety Features of 500 MW_e to 1,150 MW_e Traveling-Wave Reactor Plants," *Transactions of the American Nuclear Society* vol.101, 491-492, Washington DC, USA, Nov. 15-19, 2009

Atefi, B.; Driscoll, M.J.; Lanning, D.D., "An Evaluation of the Breed/Burn Fast Reactor Concept," *MITNE-229*, Dec. 1979

Chadwick, M.B., et al., "ENDF/B-VII.0: Next Generation Evaluated Data Library for Nuclear Science and Technology," *Nuclear Data Sheets*, 107(12):2931-3060, 2006

Chen, X-N.; Maschek, W., "Transverse Burckling Effects on Solitary Burn-up Waves," *Annals of Nuclear Energy* 32, 1377-1390, 2005

Choi, H.; Ko, W.I.; Yang, M.S., "Economic Analysis on Direct Use of Spent Pressurized Water Reactor Fuel in CANDU Reactors. I. DUPIC Fuel Fabrication Cost," *Nuclear Technology*, v134, n 2, p110-29, May 2001

Ellis, T., et al., "Traveling-Wave Reactors: A Truly Sustainable and Full-Scale Resource for Global Energy Needs," *International Congress on Advancess in Nuclear Power Plants 2010*, v 1, p 546-558, San Diego, CA, USA, June 13-17, 2010

Feinberg, S.M., "Discussion Comment," *Rec. of Proc. Session B-10,* ICPUAE, No. 2, Vol. 9, p. 447, United Nations, Geneva, Switzerland, 1958

Fischer, G.J., et al., "Physics and Feasibility Study of the Fast-Mixed-Spectrum Reactor Concept," *BNL-25598*, Jan. 1, 1979

Fomin, S.P., et al., "Initiation and Propagation of Nuclear Burning Wave in Fast Reactor," *Progress in Nuclear Energy* 50, 163-169, 2008

Forsberg, C.W., "Single Waste From Repository: Conversion of Miscellaneous Wastes to Glass," *High Level Radioactive Waste Management – Proceedings of the Annual International Conference,* p 512-514, Las Vegas, NV, USA, April 30-May 5, 1995

Gelles, D.S., "Microstructural Development in Reduced Activation Ferritic Alloys Irradiated to 200 DPA at 420°C," *Journal of Nuclear Materials* 212-215, 714-719, 1994

Gnielinski, V., "New Equations for Heat and Mass Transfer in Turbulent Pipe and Channel Flow," *International Chemical Engineering*, v 16, n 2 p 359-368, Apr 1976

Heinisch, H.L, et al., "Displacement Damage in Silicon Carbide Irradiated in Fission Reactors," *Journal of Nuclear Materials* 327, 175-181, 2004

Hendricks, J.S., et al., "MCNPX 2.6.0 Extensions," *Los Alamos National Laboratory report LA-UR-08-2216,* 2008

Hesson, J.C.; Feldman, M.J.; Burris, L., "Description and Proposed Operation of the Fuel Cycle Facility for the Second Experimental Breeder Reactor (EBR-II)," *ANL-6605*, April 1963Yu

IAEA, *Uranium 2009: Resources, Production and Demand,* A Joint Report by the OECD Nuclear Energy Agency and the International Atomic Energy Agency OECD, Paris, ISBN 978-92-64-04789-1, 2010a

IAEA, "Fast Reactor Database - 2006 Update," available http://www-frdb.iaea.org/index.html, 2010b

IAEA, "International Reactor Dosimetry File: IRDF-2002," available http://www-nds.iaea.org/irdf2002/index-crp.html, 2010c

Kazimi, M.S.; Carelli, M.D., "Clinch River Breeder Reactor Plane Heat Transfer Correlation for Analysis of CRBRP Assemblies," Westinghouse, *CRBRP-ARD-0034*, 1976

Kleuh, R.H., "Elevated Temperature Ferritic and Martensitic Steels and Their Application to Future Nuclear reactors," *International Materials Reviews* vol 50, no. 5, 287-310, 2005

Lagerberg, G., "Phase Transformations in a Uranium-Zirconium Alloy," *Journal of Nuclear Materials* 9, No. 3 261-276, 1963

Loh, W.T.; Driscoll, M.J.; Lanning, D.D., "An Evaluation of the Fast Mixed Spectrum Reactor," *MITNE-232*, Feb. 1980

Lyon, R.N., *Liquid Metals Handbook* (2 ed.), Atomic Energy Commission, Dept. of the Navy, Washington, DC, June 1952

MIT, *The Future of the Nuclear Fuel Cycle*, An Interdisciplinary MIT Study, ISBN 978-0-9828008-1-2, 2010

Pahl, R.G., et al., "Irradiation Behavior of Metallic Fast Reactor Fuels," *Journal of Nuclear Materials,* v 188, p 3-9, June 1992

Plaue, J.; Czerwinski, K.R., "Evaluation of Uranium Carbide and Sulfide Fuels for a Gas-cooled Fast Reactor Utilizing Dry Reprocessing," *MIT-GFR-007*, May 2003

Pope, M.A., *Thermal Hydraulic Design of a 2400 MWth Direct Supercritical CO_2-Cooled Fast Reactor,"* Massachusetts Institute of Technology Department of Nuclear Science and Engineering Thesis, 2006

Ryu, K.; Sekimoto, H., "A Possibility of Highly Efficient Uranium Utilization with a Pebble Bed Fast Reactor," *Annals of Nuclear Energy* 27, 1139-1145, 2000

Samsonov, E.G., *The Oxide Handbook*, Plenum Press, London 1973

Schleicher, R.W., et al., "Improved Utilization of U.S. Nuclear Energy Resources Without Reprocessing," *Transactions of the American Nuclear Society* vol.101, 257, Washington DC, USA, Nov. 15-19, 2009

Sekimoto, H.; Ryu, K.; Yoshimura, Y., "CANDLE: The New Burnup Strategy," *Nuclear Science and Engineering* 139, 306-317, 2001

Short, M.S.; Ballinger, R., "Design of a Functionall Graded Composite for Service in High Temperature Lead and Lead-Bismuth Cooled Nuclear Reactors," *MIT-ANP-TR-131*, Oct. 2010

Sobolev, V.P.; Schuurmans, P.; Benamati, G., "Thermodynamic Properties and Equation of State of Lead and Lead-Bismuth Eutectic," *Journal of Nuclear Materials* 376, 358-362, 2008

Teller, E.; Ishikawa, M.; Wood, L., "Completely Automated Nuclear Power Reactors for Long-Term Operation," *UCRL-JC-122708*, Jan. 2006

Toshinsky, G.I., "LMFBR Operation in the Nuclear Cycle without Fuel Reprocessing," *Proceedings of the International Topical Meeting on Advanced Reactors Safety,* 39-44 vol.1, Orlando, FL, USA, 1-5 June 1997

Toshinsky, V.G.; Sekimoto, H.; Toshinsky, G.I., "A Method to Improve Multiobjective Genetic Algorithm Optimization of a Self-Fuel-Providing LMFBR by Niche Induction Among Nondominated Solutions," *Annals of Nuclear Energy* 27, 397-410, 2000

van Dam, H., "Burnup Waves," *Annals of Nuclear Energy* 25, No. 17, 1409-1417, 1998

van Dam, H., "Self-Stabilizing Criticality Waves," *Annals of Nuclear Energy* 27, 1505-1521, 2000

van Dam, H., "Flux Distributions in Stable Criticality Waves," *Annals of Nuclear Energy* 30, 1495-1504, 2003

Wilson, W.B., et al., "Recent Development of the CINDER'90 Transmutation Code and Data Library for Actinide Transmutation Studies," *Los Alamos National Laboratory report LA-UR-95-2181*, 1995

World Nuclear Association, "WNA Reactor Database," available http://world-nuclear.org/NuclearDatabase/, 2010

Yan, M.; Sekimoto, H., "Study on Small Long-Life LBE Cooled Fast Reactor with CANDLE Burn-up – Part 1: Steady State Research," *Progress in Nuclear Energy* 50, 286-289, 2008

Yarsky, P.; Driscoll, M.J.; Hejzlar, P., "Integrated Design of a Breed and Burn Gas-Cooled Fast Reactor Core," *MIT-ANP-TR-107*, Sept. 2005

Yu, K., Driscoll, M.J.; Hejzlar, P., "Neutronic Limits of Breed and Burn Reactor Performance," *Transactions of the American Nuclear Society* 86, 335-366, Hollywood, FL, USA, June 9-13, 2002